SOVIET PHYSICS JETP

VOL. 11, NO. 1 JULY, 1960

A Translation

of the

Journal of Experimental and Theoretical Physics

of the

Academy of Sciences of the USSR

(Russian Original Vol. 38, No. 1, January, 1960)

Published by the

AMERICAN INSTITUTE OF PHYSICS
INCORPORATED

SOVIET PHYSICS
JETP

A translation of the Journal of Experimental and Theoretical Physics of the USSR.

SOVIET PHYSICS—JETP is a monthly journal published by the American Institute of Physics and contains a complete translation of the JOURNAL OF EXPERIMENTAL AND THEORETICAL PHYSICS of the U.S.S.R. Academy of Sciences.

This translating and publishing project was undertaken by the institute in the conviction that dissemination of the results of researches everywhere in the world is invaluable to the advancement of science. The NATIONAL SCIENCE FOUNDATION of the United States has encouraged the project initially and is supporting it in large part by a grant.

The American Institute of Physics and its translators propose to translate faithfully all the material appearing in the original articles. The views expressed in the translations are therefore those of the original authors, and not those of the translators nor of the American Institute of Physics.

Volume 1 of SOVIET PHYSICS—JETP corresponds to Russian Volume 28 (1955). Two volumes are published annually, each of six issues. Each volume contains the translation of one volume of the JOURNAL OF EXPERIMENTAL AND THEORETICAL PHYSICS.

Beginning with Vol. 9 (36), the transliteration of the names of Russian authors follows British Standard 2979, which is being adopted by a large number of scientific journals in the United States. The Library of Congress transliteration is followed in the earlier volumes.

Subscription Prices

Per Year (12 issues)

General:

United States and Canada	$75.00
Elsewhere	79.00

Libraries of non-profit degree-granting Institutions:

United States and Canada	$35.00
Elsewhere	39.00
Back Numbers	$ 8.00

Subscriptions should be addressed to the American Institute of Physics, 335 East 45th Street, New York 17, New York.

SOVIET PHYSICS, JETP is published monthly by the American Institute of Physics, Inc. Second Class postage paid at Ann Arbor, Michigan.

SOVIET PHYSICS

JETP

A translation of the Zhurnal Eksperimental'noĭ i Teoreticheskoĭ Fiziki.

Vol. 11, No. 1, pp. 1-226 (Russian original Vol. 38, No. 1, pp. 3-311, January, 1960) July, 1960

THE RELATION BETWEEN THE TEMPERATURE DEPENDENCE OF ELECTRICAL RESISTANCE AT LOW TEMPERATURES AND THE GALVANOMAGNETIC EFFECT IN STRONG MAGNETIC FIELDS

O. S. GALKINA and L. A. CHERNIKOVA

Moscow State University

Submitted to JETP editor April 6, 1959

J. Exptl. Theoret. Phys. (U.S.S.R.) **38**, 3-6 (January, 1960)

The electrical resistance of nickel-copper alloys with 39.6, 44.55 and 49.6% Cu has been studied between 7 and 30°K. By applying the $T^{3/2}$ law for the temperature dependence of spontaneous magnetization, I_S, the specific resistivity, ρ, can be related to the ferromagnon concentration $n = 1 - I_S/I_0$ (I_0 is the magnetization at $T \to 0$) and the numerical value of the coefficients $(\rho - \rho_0)/n$ derived, where ρ_0 is the residual resistivity. A comparison between this coefficient and the value of $\Delta\rho/\Delta n$ ($\Delta\rho$ and Δn are the changes in ρ and n caused by changes of true magnetization in strong magnetic fields) shows them to be of the same order of magnitude, within the limits of experimental error. This is taken as indirect evidence for the validity of the assumption that the electrical resistance of ferromagnetic alloys at low temperatures is connected with the inhomogeneities in magnetization of the lattice.

WE have previously[1] studied the electrical resistance of nickel, iron, and nickel-copper alloys (up to 25% Cu) in the temperature range from 2 to 78°K, and showed that the temperature variation of resistivity up to about 30°K is well described by the approximate formula

$$\rho = \rho_0 + C\frac{I_0 - I_s}{I_0} = \rho_0 + Cn,$$

where C is a constant and n is the ferromagnon concentration. The existence of a connection between the variation in ρ and the spontaneous magnetization I_S is taken to be a consequence of the scattering of conduction electrons by spin waves. The extra resistance due to this process is described theoretically[4] by formulae containing terms aT^3,[2] bT^2,[3] and $\alpha T + \beta T^2$. As the theory does not give the magnitude of the additional resistance it is not possible to make a quantitative comparison between theory and experiment.

Nevertheless, the present authors, together with Kondorskiĭ, presented indirect evidence of a connection between the temperature dependence of electrical resistivity at low temperatures and inhomogeneities of magnetization in ferromagnetic metals. The change in resistance of iron and nickel between 8 and 30°K was compared with the change of resistance in high magnetic field, i.e., with the magnitude of the galvanomagnetic effect $\rho^{-1}\Delta\rho/\Delta H$, which is proportional to the increase or decrease in true magnetization and is thus related to the increase or decrease in "ferromagnon" concentration. In the previous work[1] the values of the change in $\rho^{-1}\Delta\rho/\Delta H$ and of the susceptibility, $\Delta I_S/\Delta H$, for nickel and iron were determined from data referring to room temperature and were taken from the work of other authors.

The aim of the present work was to obtain reliable experimental data to confirm the relation between the temperature dependence of resistivity

TABLE I. Specimens — Ni-Cu alloys

Cu concentration %	$\frac{\Delta I_s}{\Delta H}\cdot 10^4$, G/Oe	$\rho_T \cdot 10^6$, Ω·cm	$\frac{1}{\rho_T}\frac{\Delta\rho}{\Delta H}\cdot 10^6$, Oe^{-1}	I_0, G	Θ′, °K
39.6	0.54*	34.39	0.26	163	325
44.55	1.0	39.34	0.33	120	210
49.6	2.9	44.48	0.5	87	185

*The susceptibility of the 39.6% Cu alloy was taken from the measurements of Rode and Chang Shou-Kung on the same specimen.

and the galvanomagnetic effect at high fields.

We used nickel-copper alloys with larger copper content: 39.6, 44.55, and 49.6% Cu. These alloys were chosen because of their low Curie temperatures, which makes the low temperature values of $\Delta\rho/\Delta H$ and $\Delta I_S/\Delta H$ larger than in the pure metals (Fe or Ni) and accurately measurable. For the resistivity measurements, specimens were made in the form of wires with diameter d = 0.2 mm and length l = 150 mm, and for the measurement of paraprocess susceptibility they were ellipsoids of revolution with axes 5 and 50 mm. The specimens were annealed in vacuum at 900° C for six hours and then slowly cooled at the rate of 50° per hour. The method of measuring the resistivity was described previously.[1] The paraprocess susceptibility was measured in a field of 5000 oe at 20.4 and 14° K by a ballistic method.

EXPERIMENTAL RESULTS

The electrical resistance of the alloys was measured between 2.2 and 30° K at intervals of 1 — 2°. Table I shows the values of $\Delta I_S/\Delta H$ and of ρ_T at 20.4° K.

Figure 1 shows the dependence of the relative change of electrical resistance, $\Delta\rho/\rho_T$ on the field intensity for the different alloys, at 20.4° K. The values of $\Delta\rho/\rho_T\Delta H$ in the high field region (the linear part of the curves in Fig. 1) are given in the fourth column of Table I. The fifth and sixth columns give the values of I_0 and Θ′ obtained on the same specimens by Kondorskiĭ et al.[5] I_0 is the magnetization at T = 0° K and Θ′ is the parameter in the three-halves law

$$I_s = I_0[1 - (T/\Theta')^{3/2}].$$

The dependence of $\rho - \rho_0$ on $(T/\Theta')^{3/2}$ is plotted in Fig. 2 (ρ_0 is the residual resistance). It can be seen that ρ is linearly related to $(T/\Theta')^{3/2} = n$, and consequently to $(I_0 - I_S)/I_0$, i.e., to the ferromagnon concentration. The calculated values of $(\rho - \rho_0)/n$ are shown in Table II.

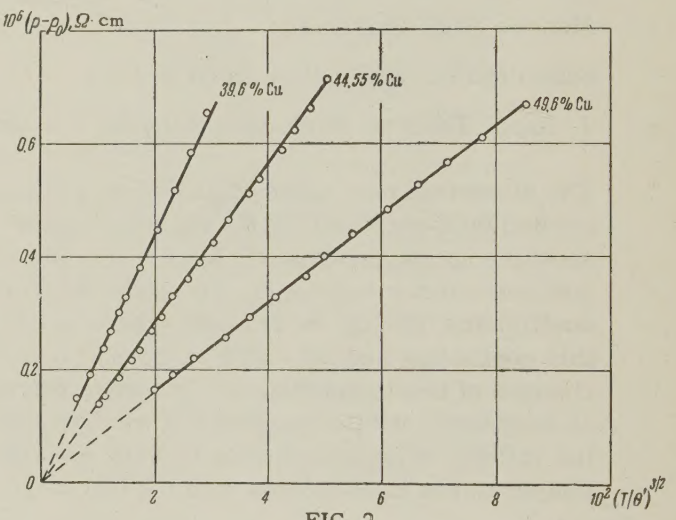

FIG. 2

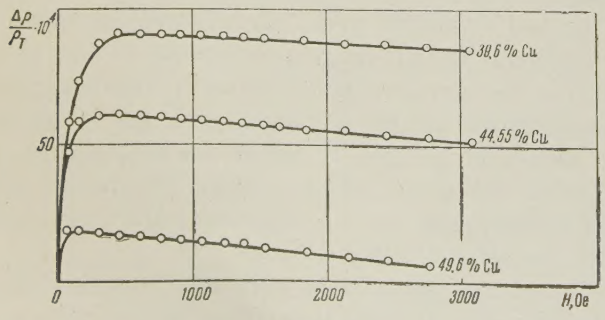

FIG. 1

TABLE II

Cu concentration %	$\frac{(\rho-\rho_0)}{n}\cdot 10^6$	$(\Delta\rho/\Delta n)\cdot 10^6$	
		20,4° K	14° K
39.6	22	27	25
44.55	14	15.6	15.1
49.6	7.9	6.7	7.2

The values of $(\rho - \rho_0)/n$ are compared with $\Delta\rho/\Delta n$, where $\Delta n = \Delta I_S/I_0$ and $\Delta\rho$ is the change in resistivity connected with the change in true magnetization in high magnetic fields. The values of $\Delta\rho/\Delta n$ were derived from the formula

$$\frac{\Delta\rho}{\Delta n} = \left(\frac{1}{\rho_T}\frac{\Delta\rho}{\Delta H}\right)\frac{\rho_T I_0}{(\Delta I_s/\Delta H)}.$$

Values of $\Delta\rho/\Delta n$ calculated from the data of Table I are shown in Table II. Comparison of $(\rho - \rho_0)/n$ and $\Delta\rho/\Delta n$ shows that they agree within the limits of experimental error.

We calculated $\Delta\rho/\Delta n$ for all the alloys at 14° K as well. The values obtained are in the fourth column of Table II. Comparison of the third and fourth columns indicates that $\Delta\rho/\Delta n$ remains constant within the experimental errors.

There is thus a definite connection between the temperature dependence of electrical resistance at low temperatures and the galvanomagnetic effect in high fields. This connection can be explained if it is assumed that in both cases the change in electrical resistance is produced by the scattering of conduction electrons by the inhomogeneities of magnetization.

In conclusion the authors would like to express their gratitude to Professor E. I. Kondorskiĭ for valuable suggestions made during discussion of the results of this work.

[1] Kondorskiĭ, Galkina, and Chernikova, JETP **34**, 1070 (1958), Soviet Phys. JETP **7**, 741 (1958).

[2] S. V. Vonsovskiĭ, JETP **18**, 219 (1948).

[3] A. G. Samoĭlovich and V. A. Yakovlev, JETP **22**, 350 (1952).

[4] E. A. Turov, Izv. Akad. Nauk SSSR, Ser. Fiz. **19**, 474 (1955), Columbia Tech. Transl. p. 426.

[5] Kondorskiĭ, Rode, and Gofman, JETP **35**, 549 (1958), Soviet Phys. JETP **8**, 380 (1959).

Translated by R. Berman
1

REFLECTION OF ELECTROMAGNETIC WAVES FROM A PLASMA MOVING IN SLOW-WAVE GUIDES

O. G. ZAGORODNOV, Ya. B. FAĬNBERG, and A. M. EGOROV

Submitted to JETP editor June 5, 1959

J. Exptl. Theoret. Phys. (U.S.S.R.) **38**, 7-9 (January, 1960)

Electromagnetic wave reflections from a moving plasma were investigated experimentally. It was found that when the wave was greatly slowed down [(1/200) — (1/375) c] the double Doppler effect observed in reflection increased the frequency by 11 — 20%. The measurements were carried out at 24.75 Mcs. The slow-wave structure was a helix. The possibility is indicated of using this effect to amplify microwaves and to multiply their frequencies, to improve the dynamic stability of the plasma, and to perform measurements in plasma.

IT is known that reflection from a moving mirror entails a change in the frequency and amplitude of an incident electromagnetic wave. Under ordinary conditions the magnitude of this effect is negligible. There are two possibilities of increasing this effect — either to increase the velocity of the reflecting surface[1] or to decrease the phase velocity of the wave in the space where the interaction takes place.[2,3] In addition, the effect can be multiplied repeatedly.

Serious difficulties arise in using the first possibility. Naturally, an ordinary macroscopic object cannot acquire a velocity close to c. To produce a reflecting surface one could use an electron beam[1] or a plasma. But to effect the reflection it is essential that the dielectric constant of the reflecting medium be either negative or of sufficiently large absolute magnitude. Since the frequency is much greater in a reference system where the reflecting medium is at rest than in the laboratory system, larger charge densities are necessary if such values of ϵ are to be obtained.* Under these conditions it is impossible to impart relativistic velocities to the plasma.

Another possibility of increasing the effect of reflection becomes available if the velocity of the electron beam of the plasma V_{pl} or even of a macroscopic object remains small, but the phase velocity V_{ph} in the interaction space is considerably reduced. In this case

$$\omega_{ref} = \omega_{inc} \frac{1 + V_{pl}/V_{ph}}{1 - V_{pl}/V_{ph}}, \qquad V_{ph} = \frac{c}{\sqrt{\epsilon}}. \tag{1}$$

Therefore, if the beam velocity or the plasma velocity are close to the phase velocity of the wave, the change in frequency can be quite considerable.

*Reflection takes place also at large plasma conductivities.

It can be shown that in this case the energy reflected from the moving plasma of the wave also increases considerably. The gain in this case is[2,4]

$$R = \left|\frac{1 + V_{pl}/V_{ph}}{1 - V_{pl}/V_{ph}}\right|^2 \left|\frac{1 - m}{1 + m}\right|^2, \qquad V_{ph} < c, \tag{2}$$

where

$$m = \left[1 - \alpha_n \frac{1 - \varepsilon\beta^2}{(1 - \beta^2)\varepsilon}\right]^{1/2}, \qquad \alpha_n = \frac{p^2}{1 - (-1)^n h},$$

$$p^2 = \frac{4\pi n e^2}{m_0 \omega^2}, \qquad h = \frac{eH_0}{m_0 c\omega}.$$

Relation (2) allows us to determine the plasma density and the intensity of the magnetic field at which effective reflection is ensured at a given frequency. The increase in frequency and amplitude can be considerable if the effect considered is repeated many times.

In the present work we have investigated the effect of reflection from the plasma moving in a medium where $V_{ph} < c$. The phase velocity can be reduced by using waveguide systems of the helix type or other slow-wave structures, or else by using the waveguide properties of a low-density plasma produced in the interaction space. If an external magnetic field is applied to such a system, its phase velocity can be varied over a very wide range.

To observe the foregoing effect experimentally, we constructed the setup whose block diagram is shown in Fig. 1. The electromagnetic wave was slowed down by means of a helical waveguide, comprising a porcelain tube 40 mm in diameter on which a helix of 0.4 mm copper wire was wound at a pitch of 0.8 mm. The experimentally measured value of the first velocity of the wave in the helix was $V_{ph} = 1/200$, which was somewhat less than the calculated value $V_{ph} = 1/150$, obviously

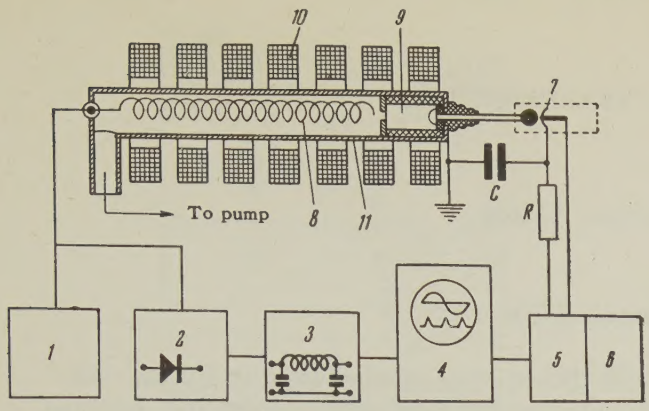

FIG. 1. Block diagram of the setup. 1 – generator, 24.75 Mcs, 2 – mixer, 3 – low-pass filter, 4 – pulse oscillograph, 5 – triggering device, 6 – rectifier, 7 – discharge gap, 8 – slow-wave system, 9 – discharge chamber, 10 – magnetic field coils.

as the result of the effect of the layer of glue between the turns. The phase velocity was measured by the standing-wave method, i.e., the wavelength λ was determined in such a waveguide by measuring the distance between neighboring minima of the standing wave with subsequent recalculation $V_{ph} = \lambda f$. The plasma piston was produced by discharging a capacitor bank of total capacitance 750 μf, charged to 4.5 kv across the discharge gap. The shape of the electrodes, their dimensions, and the distances between them were suitably chosen to produce a maximum velocity of the plasma piston.[5] To make use of the high plasmoid velocity, the plasma source and the slow-wave system were placed as close to each other as possible on a common longitudinal axis, and a longitudinal magnetic field of approximately 600 oe was applied to the entire system.

A generator operating at $f = 24.75$ Mcs was coupled weakly to the helix through a transmission line and a matching device. In order to separate the frequencies of the incident and reflected waves, a nonlinear element (a mixer connected through a low-pass filter to the pulse oscillograph) was added to the transmission line. When the wave was reflected from the leading front of the plasma piston, the incident and reflected frequencies, f_{inc} and f_{ref}, were mixed in the nonlinear element. The resultant outputs of the element were the frequencies f_{inc}, f_{ref}, $f_{inc} + f_{ref}$, and $f_{ref} - f_{inc}$, but the low-pass filter allowed only the lowest (difference) frequency to be applied to the oscillograph. All the higher frequencies were blocked by the filter, the cutoff frequency of which was 8 Mcs.

Figure 2 shows one of the oscillograms obtained. According to the sweep time scale, the difference frequency is 2.75 Mcs, corresponding to a reflected-wave frequency 11% higher than that of the incident wave. A series of experiments was then performed

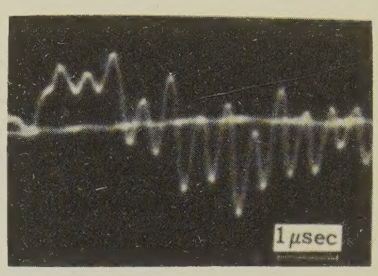

FIG. 2. Oscillogram of the difference frequency $f_{ref} - f_{inc}$.

with the helix, in which the first velocity was reduced to $^1/_{375}$ of the velocity of light. This led to a corresponding increase in the frequency of the reflected wave and the increase of this frequency amounted to 20%.

These changes in the frequency of the reflected wave correspond to a plasma-piston velocity of 8.45×10^6 cm/sec, which agrees with the work of Josephson, whose data were used to construct a plasmoid source. An independent measurement of the velocity of the front of the plasma piston with the aid of piezoelectric elements yielded $V_{pl} = 6 \times 10^6$ cm/sec.

We can therefore take it for granted that the Doppler frequency shift is greatly increased in reflections in the region where the phase velocity of electromagnetic waves is greatly reduced, $V_{ph} \ll c$.

We note that the reflection of the electromagnetic wave from the moving plasma is used by Hey, Pinson, and Smith to measure the velocity of a plasma.[6] However, since the reflection did not take place in a retarding medium, this effect was very small. The frequency shift amounted to 10^{-5}, i.e., it was 50,000 times smaller than in the case considered here: reflection from a plasma moving in a retarding medium.

This effect can be used to amplify and generate microwaves, to accelerate particles, and to perform various measurements in plasma, and also to ensure dynamic stability of a plasma.

In conclusion, I express my gratitude to A. I. Akhiezer, K. D. Sinel'nikov, and L. I. Bolotin for a discussion of the results.

[1] K. Landecker, Phys. Rev. **86**, 852 (1952).

[2] Ya. B. Faĭnberg and V. S. Tkalich, J. Tech. Phys. (U.S.S.R.) **29**, 491 (1959), Soviet Phys.-Tech. Phys. **4**, 436 (1959).

[3] M. Lampert, Phys. Rev. **102**, 289 (1956).

[4] Ya. B. Faĭnberg, Атомная энергия (Atomic Energy) **6**, 431 (1959).

[5] V. Josephson, J. Appl. Phys. **29**, 1, 30 (1958).

[6] Hey, Pinson, and Smith, Nature **179**, 1184 (1957).

Translated by J. G. Adashko

THE CAPACITANCE OF p-n JUNCTIONS AT LOW TEMPERATURES

B. M. VUL and É. I. ZAVARITSKAYA

P. N. Lebedev Physics Institute, Academy of Sciences, U.S.S.R.

Submitted to JETP editor, June 22, 1959

J. Exptl. Theoret. Phys. (U.S.S.R.) **38**, 10-17 (January, 1960)

The capacitances of p-n junctions in germanium and silicon were studied down to helium temperatures. It was established that at very low temperatures the capacitance of the p-n junction itself is not observed because of the small series capacitance of the base between the p-n junction and the electrodes. It was shown that all the observed phenomena could be explained using a simple equivalent circuit. The additional difference of potential affecting the value of the p-n junction capacitance was determined, and its connection with the screening effect of the inversion layer and the contact difference of potential was established.

AN electron-hole or p-n junction occurs in a semiconductor in one portion of which there is a surplus of donor impurities and in another portion a surplus of acceptor impurities.

For the elements of the third and fifth groups, which are commonly used as impurities, the ionization energy W_i is ~ 0.01 ev in germanium and ~ 0.04 ev in silicon.

At sufficiently high temperatures, when $kT \gg W_i$ (k is the Boltzmann constant, T is the absolute temperature), the impurity atoms are almost completely ionized. The surplus ionized impurities not compensated by electrons in the one part and by holes in the other part of the semiconductor, form the space charge of the p-n junction.

At sufficiently low temperatures, when $kT \ll W_i$, the concentration of ionized surplus impurities becomes very small in the homogeneous parts of the semiconductor far from the p-n junction; but the junction itself remains, and the contact or diffusion potential difference U_k in it tends to the value corresponding to the difference in position of the donor and acceptor impurity energy levels:[1]

$$U_k = \frac{E_F - E'_F}{q} = \frac{E_d - E_a}{q} + \frac{kT}{q} \ln \left[\frac{N_d - N_a}{N_a} \right] \left[\frac{N'_a - N'_d}{N'_d} \right] \quad (1)$$

where E_F, E'_F are the Fermi levels in the n-type and p-type germanium, respectively; E_d is the energy level of the donor impurity; E_a the energy level of the acceptor impurity; N_d, N_a are the concentrations of donor and acceptor impurities in the n-type germanium; N'_d, N'_a are the concentrations of donor and acceptor impurities in the p-type germanium; q is the electronic charge.

It is apparent that the large decrease of the electrical conductivity and the increase of the contact potential difference occurring at low temperatures should significantly alter all the properties of a p-n junction, including the differential capacity which typifies the space charge distribution in it. It is, therefore, of interest to study the properties of p-n junctions at low temperatures, particularly their capacitance, especially as recently intensive work has started on the use of p-n junctions as non-linear capacitors, as proposed by one of us several years ago.*

1. EXPERIMENTAL PROCEDURE

The measurements of p-n junction capacitances were made using an MLE-1 bridge at audio-frequencies, a Q-meter in the range of frequencies ν from 50 kcs to 1 Mcs and a special bridge at a fixed frequency of 100 kcs. The amplitude of the measuring signal during measurements with the bridges was about 1 — 5 mv, but for measurements with the Q meter at high Q factors it went as high as 2 v. The biasing voltage was supplied by a battery and measured directly.

The measurements were carried out in liquid helium, hydrogen and nitrogen at atmospheric or reduced pressure of the vapors. Intermediate temperatures from 4.2 to 14° K and from 20 to 65° K were obtained by heating the assembly in the vapors of the corresponding liquid.

The assembly consisted of a copper case inside which were the specimen to be studied and the thermometers (carbon and copper). The

*B. M. Vul. Inventor's Certificate No. 02407/460177, dated June 29, 1954.

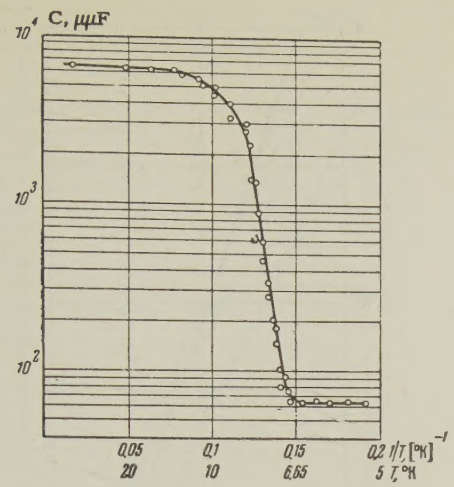

FIG. 1. The capacitance of a germanium diode (specimen no. 1) as a function of temperature. Bias voltage U = 0, frequency of measuring signal $\nu = 10^5$ cps, diode area S = 1.88 cm², thickness d = 0.4 mm.

lead to the specimen consisted of a coaxial cable, the capacity of which (12 μμF) remained constant when the device was moved in the cryostat. The heating rate could be varied from 0.5 to 5° K per hour.

The measurements were made on alloyed germanium and silicon diodes of various dimensions fabricated in the All-Union Electro-Technical Institute[2] and in the P. N. Lebedev Physics Institute of the U.S.S.R. Academy of Sciences. For equivalent types of specimens, very similar results were obtained.

2. CAPACITANCE AT VERY LOW TEMPERATURES

The results of capacitance measurements on germanium and silicon diodes as a function of temperature are given in Figs. 1 and 2. As is seen from these, the capacitance of the diodes is practically constant over a wide temperature range, but diminishes sharply for germanium diodes around helium temperatures and for silicon diodes around hydrogen temperatures. The temperature interval in which the sharp change of capacitance occurs will be referred to below as the "transitional."

On further decreasing the temperature, the capacitance does not decrease further. Having attained definite small values, the capacitances become again almost constant quantities, determined only by the geometrical dimensions and dielectric permittivity of the specimens — a fact which was confirmed by additional measurements on specimens without p-n junctions.

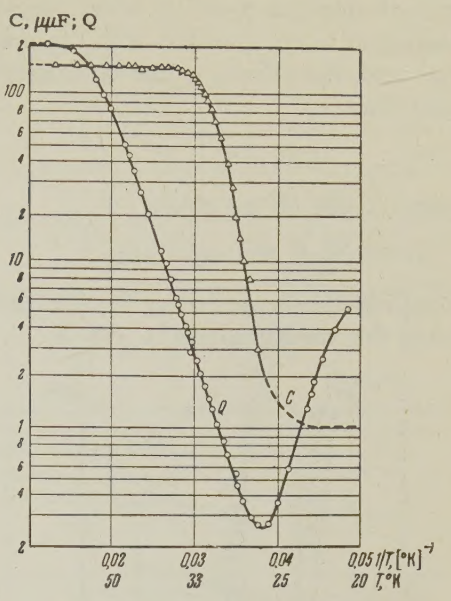

FIG. 2. The capacitance C and Q-factor of a silicon diode (specimen no. 6) as a function of temperature. U = 0, $\nu = 7.3 \times 10^4$ cps, S = 0.04 cm², d = 0.3 mm.

The apparent disappearance of the p-n junction at very low temperatures would seem to be connected with the fact that under these conditions the capacity of the p-n junction itself does not affect the measured capacity. This fact, and also the fact that at very low temperatures the differential real part of the conductivity of the germanium is very small in comparison with the imaginary part, allows the simple equivalent circuit shown in Fig. 3 to be used to calculate the capacitance in the intermediate range.

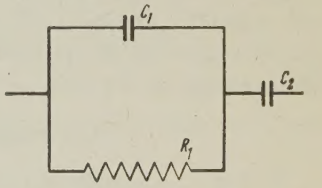

FIG. 3. Equivalent circuit; C_1, R_1, are the capacitance and resistance of the n-type part of the specimen; C_2 is the capacitance of the p–n junction.

For this circuit the measured capacitance is

$$C = C_2 (1 + \omega^2 R_1^2 C_1^2) / (1 + \omega^2 R_1^2 C_1 C_2 + \omega^2 R_1^2 C_1^2) \qquad (2)$$

where C_2 is the capacitance of the p-n junction; C_1 and R_1 are the capacitance and resistance of the n-type part of the semiconductor. The effect of the p-type part can be neglected, because its thickness is small in comparison with the n-type. Since $C_2/C_1 \gg 1$, then at very low temperatures, when $\omega^2 R_1^2 C_1 C_2 \gg 1$, it follows from (2) that

$$C / C_2 = (1 + \omega^2 R_1^2 C_1^2) / \omega^2 R_1^2 C_1 C_2$$

or

$$C - C_1 = 1 / \omega^2 R_1^2 C_1. \qquad (3)$$

The change of electron mobility with temperature can be neglected in comparison with the concentration change and, therefore, it can be considered approximately that

$$1/R_1 \sim n, \tag{4}$$

and therefore from (3) we obtain

$$C - C_1 \sim n^2 \quad \text{for} \quad \omega = \text{const}.$$

This is confirmed by calculating the ionization energy from the results given in Fig. 4.

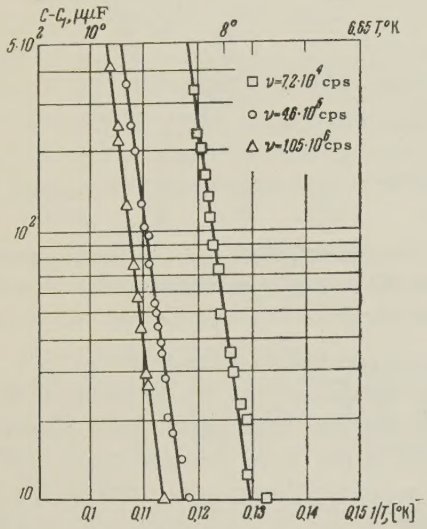

FIG. 4. The temperature dependence of the capacitance $C - C_1$ of a germanium diode (specimen no. 4) in the "transitional" temperature interval for various frequencies of the measuring signal ν. $C_1 = 67\ \mu\mu F$, $S = 2\ cm^2$, $d = 0.4$ mm.

From Eq. (2) it follows that if $C = \text{const}$, then $\omega R = \text{const}$, or $\omega \sim 1/R \sim n$. Since it can be taken in this region of temperature that $n \approx \exp(-W_i/kT)$, then, using (4) we find

$$\ln \omega = \text{const} - W_i / kT.$$

In Fig. 5 a graph is presented of the dependence of $\ln \omega$ on $1/T$ for fixed capacitance of the germanium diode $C = 2C_1$. The ionization energy of the donor impurity atoms in germanium determined from the slope of the line in Fig. 5 is 1.1×10^{-2} ev, which agrees well with known values.[3] From analogous measurements on silicon diodes the value $W_i \approx 0.046$ ev was obtained.

To verify the equivalent circuit in the "transitional" region in addition to the capacitance measurements, the Q-factor was also measured. For the circuit given in Fig. 3 the Q-factor is

$$Q = (1 + \omega^2 R_1^2 C_1 C_2 + \omega^2 R_1^2 C_1^2) / \omega C_2 R_1. \tag{5}$$

It follows from (5) that, due to the change of R with temperature, the Q-factor has a minimum. The minimum Q-factor is

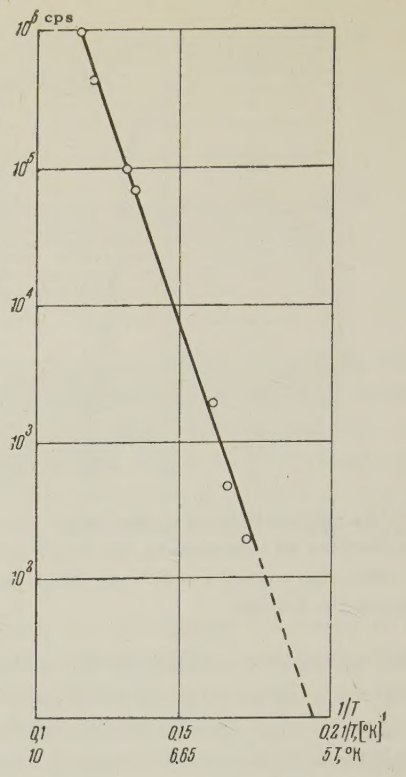

FIG. 5. The relationship between the temperature and the frequency of the measuring signal in the "transitional" temperature interval for constant capacitance $C = 2C_1$ – germanium diode (specimen no. 4)

$$Q_{min} = 2\,[(C_1C_2 + C_1^2)/C_2]^{1/2} \approx 2\,(C_1/C_2)^{1/2},$$

since $C_1 \ll C_2$. The results of Q-factor measurements on germanium and silicon diodes are given in Figs. 2 and 6. The measurements were made with zero bias voltage. For the germanium power rectifier the values $C_1 = 67\ \mu\mu F$, $C_2 = 6750\ \mu\mu F$ were obtained, and correspondingly by calculation $Q_{min} = 0.2$. The character of the change of Q with temperature, the presence of the minimum, and its value, show that the equivalent circuit used is a sufficiently close approximation under our conditions.

Since in actual devices the thickness of the p-n junction (δ) is much smaller than the base thickness (h), then $C_2 \gg C_1$ always and

$$Q = (1 + \omega^2 R_1^2 C_1 C_2) / \omega C_2 R_1.$$

If $\omega^2 R_1^2 C_1 C_2 \ll 1$, which is true at high temperatures, then

$$Q \approx 1/\omega C_2 R_1 \sim n.$$

The slope of the curve Q(1/T) (Figs. 2 and 6) to the left of the minimum corresponds to the temperature dependence $Q \sim n$. If, on the other hand, $\omega^2 R_1^2 C_1 C_2 \gg 1$, which is true at reduced temperatures, then

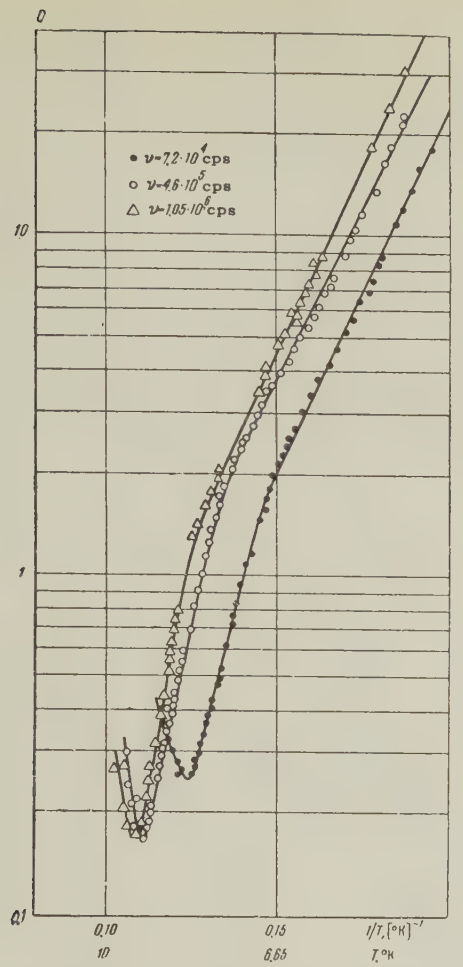

FIG. 6. Q-factor of a germanium diode (specimen no. 4) at low temperatures for various frequencies of the measuring signal ν. Bias voltage U = 0.

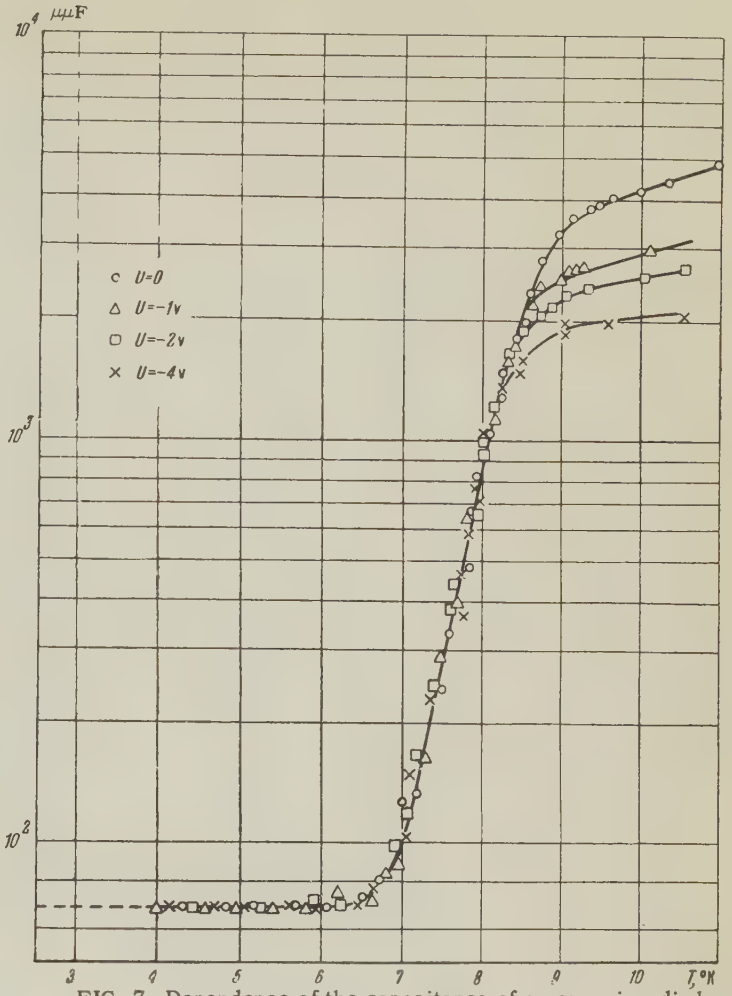

FIG. 7. Dependence of the capacitance of a germanium diode (specimen no. 1) on temperature in the "transitional" region for various bias voltages.

$$Q \approx \omega R_1 C_1 \sim 1/n.$$

The results given in Figs. 2 and 6 confirm that Q ~ 1/n to the right of the minimum, for small alternating signals.

For large signal amplitudes this dependence is destroyed because of the effect of the signal electric field on the quantity n (see reference 4).

As follows from (3), the capacitance C measured in the "transitional" region does not depend on C_2. Whence it follows that in this temperature interval it should not depend on the bias voltage; this is confirmed by the results given in Fig. 7 (common portion of the curves). On increasing the temperature R_1 gets smaller and then it is no longer possible to consider that $\omega^2 R_1^2 C_1 C_2 \gg 1$. In these conditions the measured capacity C becomes a function of C_2, and consequently depends on the applied bias voltage (divergence of the curves in Fig. 7). In some temperature intervals R is still sufficiently large, and thus relaxation effects appear. It is apparent that the nonlinear properties of p-n junction capacitances are fully displayed under the condition $\omega^2 R_1^2 C_1 C_2 \ll 1$ or

$$\gamma \rho \varepsilon (h/\delta)^{1/2} \ll 1.8 \cdot 10^{12}, \qquad (6)$$

where ρ is the specific resistance of the semiconductor.

3. VARIATION OF CAPACITY WITH BIAS VOLTAGE

For a step p-n junction

$$1/C^2 = 8\pi (U_0 - U)/S^2 q \varepsilon N_d \qquad (7)$$

where S is the area of the diode, U_0 is the additional potential difference, U is the applied voltage, ϵ is the dielectric permittivity, N_d the surplus concentration of ionized impurity.

If the concentration N_d remains unchanged during changes of temperature, then, as follows from (7), the straight lines $1/C^2 = \varphi(U)$ should be parallel and the intersections they make on the abscissa axis should be U_0. As is seen from the

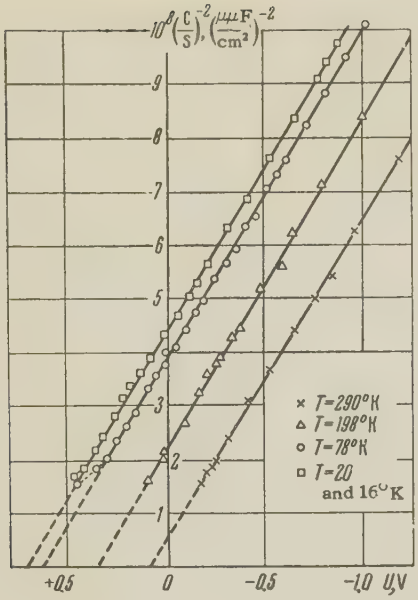

FIG. 8. Dependence of the inverse square of the capacitance of a germanium diode (specimen no. 1) on bias voltage for various temperatures; $\nu = 1.05 \times 10^5$ cps.

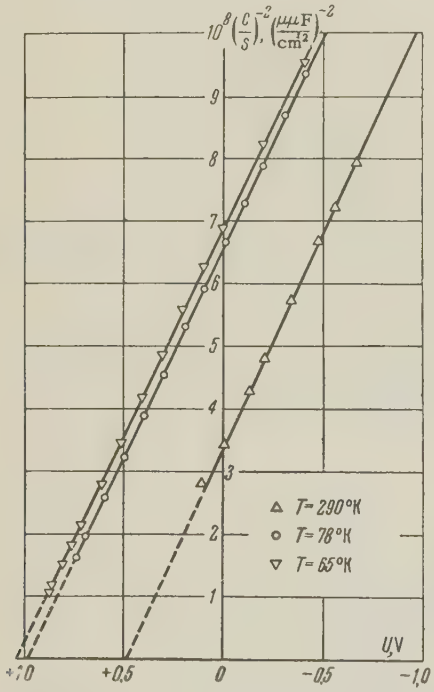

FIG. 9. Dependence of the inverse square of the capacitance of a silicon diode (specimen no. 6) on the bias voltage for various temperatures; $\nu = 1.05 \times 10^6$ ps.

results in Figs. 8 and 9, the slope of the straight lines remains constant. The linear variation of $1/C^2$ on voltage is retained almost to breakdown. If the measurements are made at lower frequencies, the slope is preserved to lower temperatures. This proves that the quantity N_d in (7) can be taken to be independent of temperature. For our germanium specimens $N_d = 8 \times 10^{13}$.

It is apparent that in a specimen of homogeneous n-type germanium, the concentration of surplus ionized impurities decreases sharply on going to low temperatures. However, as follows from the results quoted, in the immediate neighborhood of the boundary between the p-type and n-type parts of the semiconductor, the donor and acceptor impurities remain almost completely ionized, as they are at room temperature. This is also confirmed by the fact that at helium temperatures p-n junctions sustain large reverse voltages while germanium itself breaks down even in field strengths of several v/cm, owing to impurity ionization. Since the impurities in the region of the p-n junction are already ionized, breakdown can only occur when the germanium atoms are ionized, for which field strengths of the order of hundreds of thousands of v/cm are required.

The values of U_0 obtained by extrapolating the straight lines in Figs. 8 and 9 do not, as is well known,[5] agree with U_K—the contact or diffusion potential difference—but at low temperatures the difference between them is insignificant. As follows from (1), at low temperatures U_K is almost the difference between the energy levels of acceptor and donor impurities, and depends little on temperature. This is confirmed by the results given in Fig. 10.

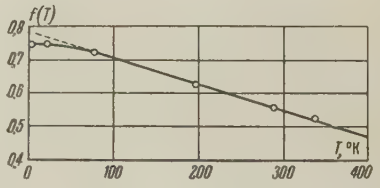

FIG. 10. Dependence of $f(T) = U_0 + (3kT/q) \ln T$ for a germanium diode (specimen no. 1).

It is impossible to measure directly the variation of p-n junction capacity on voltage at helium temperatures. Therefore, by this means [using formula (7)] it is impossible to determine the value of the additional potential U_0. But it can be evaluated by measuring the forward branch of the voltage-current characteristic. The forward current through a p-n junction at low temperatures is

$$J \approx \exp\left\{-\frac{1}{kT}(G - Uq - W_i)\right\},$$

where G is the width of the forbidden gap. As is seen, a sharp increase of current occurs at the voltage $U \approx G/q$ (for germanium $U \approx 0.8$ v), when the external voltage exceeds the contact potential difference at the p-n junction. For our specimen at $T = 4.2°K$, the current increased from 10^{-8} to 10^{-4} amp on changing the voltage from 0.82 to 0.89 v. Under these condi-

tions the base resistance plays an insignificant role, since for its breakdown 0.1 — 0.2v is required in all.[6]

The difference between U_0 and U_K is known to be explained by the inversion layer in the space-charge region.[7] Since the potential drop in the inversion layer has no influence on the field on the p-n junction, it can be considered that the additional voltage is:

$$U_0 = U_к - U_i. \tag{8}$$

To evaluate U_i, the inversion layer can be taken to be of finite thickness in which the concentration of holes $p_n = \beta N_d$, where $\beta > 1$.[8] Then

$$U_i = (kT/q) \ln (N_a'/\beta N_d). \tag{9}$$

The contact potential difference is

$$U_к = (kT/q) \ln (N_a' N_d/n_i^2), \tag{10}$$

where

$$n_i^2 = AT^3 e^{-G/kT} \tag{11}$$

For germanium $A = 3.1 \times 10^{32}$ cm^{-6}/(deg K)^3, G = 0.785 ev; for silicon $A = 1.5 \times 10^{33}$ cm^{-6}/(deg K)^3, G = 1.21 ev.[9] Using (8) and (11) we obtain

$$U_0 + \frac{3kT}{q} \ln T = \frac{G}{q} - \frac{kT}{q} \ln \frac{A}{\beta N_d^2}. \tag{12}$$

In Fig. 10 the quantity $U_0 + (3kT/q) \ln T$ is plotted as a function of temperature; the experimental values U_0 were determined by extrapolating the straight lines $1/C^2 = \varphi(U)$ in Fig. 8. The agreement of the data given in Fig. 10 with (12) is good for $\beta = 4$.

A consideration of data quoted in the literature[5] for p-n junctions fabricated from germanium with surplus donor impurity concentrations from 10^{14} to 10^{17} gives values of β between 4 and 5. The capacity and potential distribution in a p-n junction at low temperatures has been calculated by Vul.[10]

In conclusion, the authors consider it a pleasant duty to express their deep gratitude to Academician P. L. Kapitza for permission to carry out the investigation in the Institute of Physical Problems, and to Prof. V. P. Peshkov for constant interest in the work.

[1] W. Shockley, Electrons and Holes in Semiconductors, Van Nostrand, N.Y. 1951; Russ Transl. IIL, M., 1953.

[2] S. B. Yuditskiĭ, Материалы Всесоюзного совещания по применению комплексных полупроводниковых выпрямительных установок в промышленности (Proceedings of the All-Union Conference on the Use of Complex Semiconductor Rectifying Devices in Industry), TsBTI, M. (1959).

[3] J. A. Burton, Physica **20**, 845 (1954).

[4] S. H. Koenig and G. R. Gunther-Mohr, J. Phys. Chem. Sol. **2**, 268 (1957); É. I. Abaulina-Zavaritskaya, JETP **36**, 1342 (1959), Soviet Phys. JETP **9**, 953 (1959).

[5] D. R. Muss, J. Appl. Phys. **26**, 1514 (1955).

[6] N. Sclar and E. Burstein, J. Phys. Chem. Sol. **2**, 1 (1957).

[7] Harten, Koch, Rath, and Schultz, Z. Physik **138**, 336 (1954).

[8] É. I. Adirovich and E. M. Kuznetsova, Радиотехника и электроника (Radio Engineering and Electronics) **4**, 1708 (1959).

[9] H. J. Fan, Usp. Fiz. Nauk **64**, 333 (1958); H. J. Fan, Coll. Solid State Physics **1**, N.Y. (1955).

[10] B. M. Vul, Dokl. Akad. Nauk SSSR **129**, 61 (1959), Soviet Phys.-Doklady, in press.

Translated by K. F. Hulme
3

POLARIZATION OF HIGH ENERGY μ^+ MESONS IN COSMIC RAYS

N. M. KOCHARYAN, Z. A. KIRAKOSYAN, É. G. SHAROYAN, and A. P. PIKALOV

Physics Institute, Academy of Sciences, Armenian S.S.R.

Submitted to JETP editor June 26, 1959

J. Exptl. Theoret. Phys. (U.S.S.R.) **38**, 18-21 (January, 1960)

The polarization of 2 Bev cosmic ray μ mesons has been measured to be $P = 0.23 \pm 0.12$, which indicates that in the upper layers of the atmosphere most μ mesons come from the decay of π mesons. Our data show that the number of μ mesons from $K_{\mu 2}$ decays can be no greater than 15% of the total number of μ mesons.

In previous investigations[1,2] which have been carried out in our laboratory on the composition of cosmic rays, differential spectra for μ^+ and μ^- mesons have been obtained which show that for momenta $p \gtrsim 2$ Bev/c the ratio of the number of positive μ mesons to negative ones is about 1.3.

The papers mentioned above discuss one possible mechanism which could lead to such a surplus of positive μ mesons. Gol'dman has suggested another,[3] that the surplus might be due to $K^+_{\mu 2} \rightarrow \mu^+$ decays. The purpose of this paper is to report an experimental check on this hypothesis. In order to do this it is enough to measure the asymmetry in $\mu^+ \rightarrow e^+$ decays. It is well known that parity non-conservation leads to an asymmetry in the angular distribution of decay products from a polarized particle.[4] The degree of asymmetry depends on the degree of polarization of the initial particle and is a maximum for polarization equal to one.[5,6] Assuming that the whole current of μ^+ mesons results from the two decays $\pi^+ \rightarrow \mu^+$ and $K^+_{\mu 2} \rightarrow \mu^+$, in our case we will have a mixture of μ^+ mesons with various degrees of polarization. According to data in the literature,[3,7,8] the polarization of μ^+ mesons from the first decay is about 25%, while that from the second decay is $\sim 90\%$. This allows one to infer the relative weights of the two decays from a measurement of the average polarization of the μ^+ meson current.

To study 2 Bev μ mesons at the surface of the earth, we made our measurements 5 m below the surface. At this depth, a detector counting the particles stopping in a copper plate sees mostly μ mesons from the upper layers of the atmosphere.[9]

EXPERIMENTAL ARRANGEMENT

The figure shows a schematic diagram of the experiment. $C_1 - C_5$ are rows of Geiger-Müller

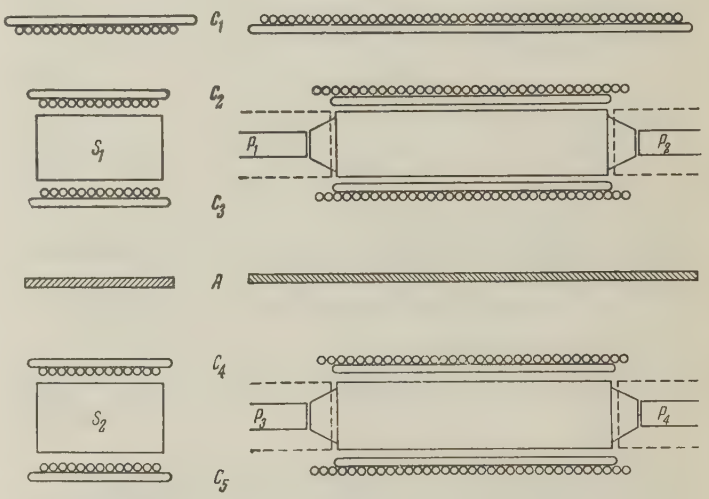

Arrangement of experiment to measure polarization of μ^+ mesons.

counters. Each row has two layers of counters, each of diameter 1 cm, the axes of the two sets being perpendicular, so that the place where a particle crosses the plane of the counters could be found. S_1 and S_2 are scintillation counters $400 \times 150 \times 100$ mm^3 and filled with a solution of p-terphenyl (2 g/l) and αNPO (0.05 g/l) in benzene. Each scintillator fed two photomultipliers (P_1, P_2) and (P_3, P_4), so that it did not matter where along the length of the scintillator the light flash occurred.

The μ^+ mesons were absorbed in a copper plate A with dimensions $600 \times 200 \times 10$ mm^3, and placed between the two scintillation counters.

Each counter in the rows $C_1 - C_5$ fed a neon bulb which lit when a particle passed through the counter. Counts in the scintillation counters were registered in the same way. μ^+ meson decays were identified by delayed coincidences. Only those delayed coincidences were counted in which the time lag between the pulse from the initial μ^+ meson and the pulse due to the decay electron was

0.7 to 6 μsec. The scintillators S_1 and S_2 were periodically exchanged, and the counting system checked regularly. The background due to μ meson decays in the scintillators themselves was obtained from measurements with the copper plate removed and also the delayed coincidence circuit switched off. Each of the decay events observed was plotted on a scale drawing of the apparatus. From the constants of the hodoscope, the trajectory of the primary particle could be obtained, together with the place where the decay occurred, and the direction of travel of the decay electron checked. Such checks eliminated accidental coincidences and verified that the scintillation counter channels were working properly.

RESULTS

A total of 563 decays in copper were observed. In 298 of these the electron was ejected into the upper hemisphere, i.e., the pulses from both the initial μ meson and the decay product came from the upper scintillator. In the remaining 265 cases the decay electron was detected by the lower scintillator. The ratio of the number of electrons going up to those going down is thus $k = 1.12 \pm 0.06$. The uncertainty quoted is the probable error. This takes into account the fact that if the decay electron is ejected at a small angle with the direction of the primary particle, the efficiency of the Geiger counters in detecting one going up is different from the efficiency for one going down. In the first case, both particles can go through one and the same counter. To exclude such an asymmetry, we considered only cases where the secondary particle was counted $\gtrsim 2$ counters away. From the asymmetry we calculated the polarization of the μ^+ mesons, as in reference 10, and found

$$N = c[1 \pm 0.27\xi P_1], \qquad (1)$$

where c is a constant, ξ is a parameter in the two-component neutrino theory, and P_1 is the degree of polarization of the μ mesons in the absorber.

To obtain the true polarization P of the μ mesons, it is necessary to take into account depolarization in the atmosphere and the layer of earth above the apparatus, and also the solid angle of the apparatus. Both effects together give a correction to P_1 of about 8%. The final expression for P is then

$$\frac{N_{up} + N_{down}}{2N_{down}} = \frac{1}{1 - 0.25\,\xi P}. \qquad (2)$$

Substituting the experimental values for N_{up} (the number of electrons ejected upward) and N_{down} (the number of electrons going downward) we get

$$\xi P = 0.23 \pm 0.12; \qquad (3)$$

Since $|\xi| \approx 1$, then $P = 0.23$. This is quite different from the result obtained by Dolgoshein and Luchkov,[12] who got $0.98^{+0.02}_{-0.32}$ for a kinetic energy of 1 Bev.* If this large polarization is due to $K_{\mu 2} \rightarrow \mu$ decays, then according to the data of Gol'dman,[3] not less than 60% of the total number of μ mesons at high altitudes must be due to such decays. Our result $P = 0.23$ agrees with that calculated on the assumption that the mesons come essentially only from $\pi^+ \rightarrow \mu^+$ decays and that the power of the π meson spectrum is $\gamma = 2.5$. Hence it follows that in the upper layers of the atmosphere, even though there are large numbers of energetic protons capable of giving $K^+_{\mu 2}$ mesons, $K^+_{\mu 2} \rightarrow \mu^+$ decays do not contribute significantly to the number of μ^+ mesons formed.

Lohrmann and Teucher[11] have used nuclear emulsions at an altitude of 30 km to measure the relative number of strange particles made in stars where the energy of the primary particle was $10^{12} - 10^{14}$ ev. According to their data, the number of charged K mesons, baryons and antibaryons is about 9^{+8}_{-6}% of the total number of secondary charged particles. The number of $K_{\mu 2}$ particles will be at least less than half the total number of strange particles. Hence, the number of $K_{\mu 2}$ particles will be about 5% of the number of charged π mesons.

Our measurements on the asymmetry in μ^+ meson decays under the earth have thus shown that the μ^+ mesons in cosmic rays come primarily from π^+ meson decays and only to an insignificant extent from decays of $K^+_{\mu 2}$ mesons.

The authors would like to thank G. S. Saakyan for discussion of their results.

[1] Kocharyan, Aĭvazyan, Kirakosyan, and Aleksanyan, JETP **30**, 243 (1956), Soviet Phys. JETP **3**, 350 (1957).

[2] Kocharyan, Aĭvazyan, Kirakosyan, and Aleksanyan, Dokl. Akad. Nauk Arm. SSR **20**, 169 (1955).

[3] I. I. Gol'dman, JETP **34**, 1017 (1958), Soviet Phys. JETP **7**, 702 (1958).

*At the 1959 International Conference on Cosmic Rays in Moscow, Johnson reported results on measurements of μ meson polarization at 540–593 Mev. He obtained 0.21 ± 0.03, which agrees well with our result. He notes that there was no significant contribution from $K_{\mu 2} \rightarrow \mu$ decays.

[4] T. D. Lee and C. N. Yang, Phys. Rev. **104**, 254 (1956).

[5] Garwin, Lederman, and Weinrich, Phys. Rev. **105**, 1415 (1957).

[6] Coombes, Cork, Galbraith, Lambertson, and Wenzel, Phys. Rev. **108**, 1348 (1957).

[7] S. Hayakawa, Phys. Rev. **108**, 1533 (1957).

[8] Fowler, Primakoff, and Sard, Nuovo cimento **9**, 1027 (1958).

[9] G. M. Garibyan and I. I. Gol'dman, JETP **26**, 257 (1954).

[10] G. W. Clark and J. Hersil, Phys. Rev. **108**, 1538 (1957).

[11] E. Lohrmann and M. W. Teucher, Phys. Rev. **112**, 587 (1958).

[12] B. A. Dolgoshein and B. I. Luchkov, JETP **36**, 640 (1958), Soviet Phys. JETP **9**, 445 (1959).

Translated by R. Krotkov
4

ELECTRICAL CONDUCTIVITY OF DIELECTRICS IN STRONG SHOCK WAVES

A. A. BRISH, M. S. TARASOV, and V. A. TSUKERMAN

Submitted to JETP editor, July 4, 1959

J. Exptl. Theoret. Phys. (U.S.S.R.) 38, 22-25 (January, 1960)

The electrical conductivity of air, water, and certain solid dielectrics subjected to strong shock waves has been measured by an electrical contact method. The measured values of the specific conductivity in the shock front are as follows: air, $0.5\,\Omega^{-1}\,cm^{-1}$; water, $0.2\,\Omega^{-1}\,cm^{-1}$. At shock front pressures of approximately 1×10^6 kg/km^2 it is found that the electrical conductivity of Plexiglas or paraffin reaches 1 to $2 \times 10^2\,\Omega^{-1}\,cm^{-1}$, a value which approximates the conductivity of a metal.

INTRODUCTION

In an earlier work[1] we have shown that there is a zone of high electrical conductivity in the front of the shock wave caused by the detonation of a high explosive. It is of great scientific and practical interest to investigate this effect in inert media which are subjected to strong shock waves. Present-day explosives provide a convenient means of producing transient pressures of several millions of atmospheres.[2] It is to be expected that at the high compressions and densities corresponding to these pressures there will be radical changes in the electrical properties of materials.

In 1948 — 1949 the present authors measured the electrical conductivity of air, water, paraffin and Plexiglas in strong shock waves produced by the detonation of charges of high explosives (HE). Under these conditions it is found that the electrical conductivity (in the shock front) is many orders of magnitude greater than the conductivity of the original material. Below we present the experimental data which have been obtained and discuss possible physical mechanisms for the formation of a zone of high electrical conductivity in dielectrics subject to strong shock waves.

EXPERIMENTAL METHOD AND DATA

The rapidly varying electrical resistance in inert media subject to strong shock waves is measured by means of the electrical-contact method which has been described in reference 1. A shock wave in air is produced by placing an aluminum plate P, 2 mm thick, on the end face of the charge Ch (Fig. 1a). This plate prevents the explosion products from striking the measurement contacts K_1. On the far side of the plate there is a supplementary set of contacts K_2; the closing of these contacts is observed on an oscilloscope and denotes the time at which the shock wave passes the free surface of the plate.

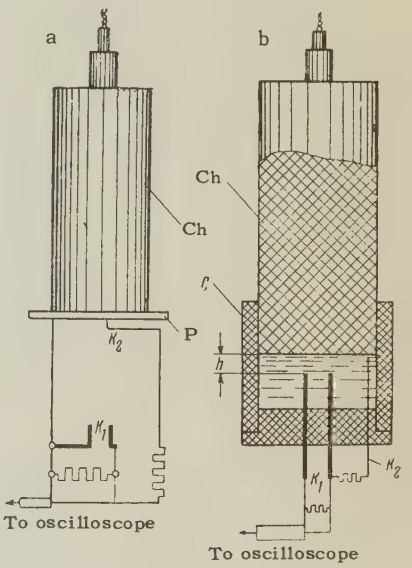

FIG. 1. Arrangement of the charges and contact devices used to measure the electrical conductivity in shock waves: a) in air, b) in water.

When the charge is detonated, the air shock wave, whose velocity is 10 — 15% greater than the velocity of the aluminum plate, reaches contact K_1 first; the oscilloscope is used to determine the electrical resistance in the shock front of the air wave. After a small time interval the contacts are closed briefly by the metal plate. The reference mark denoting the time at which the aluminum plate is set in motion and the marks denoting the change in electrical resistance are then used to measure the mean velocity of the aluminum and air shock wave.

A typical oscillogram obtained with the experimental arrangement of Fig. 1a is shown in Fig. 2. The numbers 1, 2, and 3 denote respectively the time at which the plate is set in motion, the arrival of the air shock wave at the contacts, and closure of the contacts by the metal plate. Analysis of such oscillograms indicates that the mean veloc-

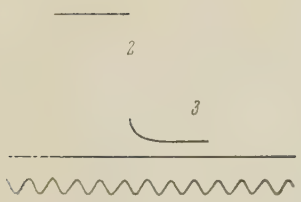

FIG. 2. Oscillogram of the contact measurements of the electrical conductivity in air (arrangement used in Fig. 1a). The frequency of the sinusoidal time markers is 1 Mcs.

ity of the air shock wave is 4.9 km/sec when the distance from the plate to the contact device is 5 to 10 cm. Under these conditions the velocity of the metal is 4.5 km/sec while the resistance of the air in the shock wave front is 2.2 to 2.6 Ω.

To measure the electrical conductivity of water, a large container C filled with distilled water is located at the face of the charge Ch (Fig. 1b). As in the experiments with the air wave, contacts K_1 are used to measure the resistance in the shock front while the closing of the contacts serves to mark the time at which the shock wave is excited in the water. The measurements are carried out with the distance h set at 10, 30, and 50 mm. The functional relation is shown in Fig. 3. With h = 10 mm the resistance of the contact gap is 6.5 to 7.0 Ω; this value increases to 46 to 47 Ω when h = 50 mm.

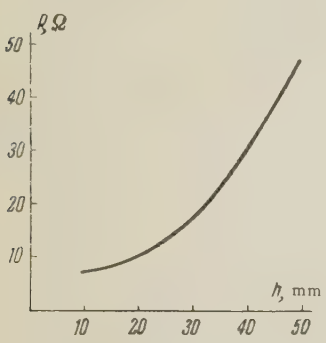

FIG. 3. The resistance R in a shock front in water as a function of the distance h.

The mean velocity of the shock wave in water under these conditions varies from 4 to 6 km/sec.

The measurements described here were carried out with distilled water (specific resistance, approximately 10^5 Ω). In order to evaluate the effect of the initial resistance of the water similar experiments were repeated with ordinary water (initial specific resistance 7.5×10^2 Ω). Although the initial resistance is two orders of magnitude smaller, the electrical resistance in the shock front is the same as when distilled water is used.

The most interesting results have been obtained in measurements of the resistance of solid dielectrics subjected to the effect of strong shock waves. These experiments were carried out with paraffin and Plexiglas in the pressure range $1 \times 10^5 - 1 \times 10^6$ kg/cm^2. The results of these measurements are shown in Fig. 4. In the paraffin case an appreciable reduction in resistance is observed at pressures of $6 - 7 \times 10^5$ kg/cm^2. When the pressure in-

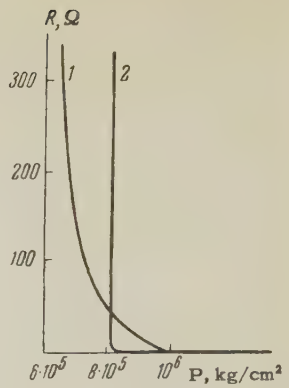

FIG. 4. The resistance R in a shock front as a function of pressure: curve 1 is for paraffin and curve 2 for Plexiglas.

creases to $9 - 10 \times 10^5$ kg/cm^2, the resistance drops rapidly to values of the order of hundredths of an ohm. In Plexiglas the reduction in resistance is observed at higher pressures than in paraffin (8×10^5 kg/cm^2). In this case the resistance vs pressure curve drops suddenly; at a pressure of 8.2×10^5 kg/cm^2 the resistance is of the order of hundredths of an ohm.

The reduced data on electrical conductivity in the shock fronts for air, water, paraffin, and Plexiglas are shown in the table. Electrolytic-model measurements were used to convert the resistance of the contact gap to specific electrical conductivity γ. For shock waves of relatively small intensity in air and water the values of γ lie in the range $0.2 - 0.5$ Ω^{-1} cm^{-1}. For paraffin and Plexiglas in the pressure range $6 - 10 \times 10^5$ kg/cm^2 the specific electrical conductivity increases to $100 - 200$ Ω^{-1} cm^{-1}.

DISCUSSION OF THE RESULTS

There are two possible mechanisms which can be responsible for the appearance of a region of high electrical conductivity in a strong shock front in dielectrics: thermal ionization, and enhancement of electronic transitions, resulting from the combined effects of high pressure and high temperature. An approximate calculation made on the basis of the Saha formula for the case of a shock wave in air gives values of the electrical conductivity which correspond, in order of magnitude, to the present experimental data. However, it is difficult to explain by thermal ionization alone the increase by 15 or 20 orders of magnitude of the electrical conductivity of such perfect dielectrics as paraffin and Plexiglas. The values obtained for these materials at shock pressures of approximately 10^6 kg/cm^2, i.e., 1 to 2×10^2 Ω^{-1} cm^{-1} are only two orders of magnitude smaller than the electrical conductivity of metals.

The effect of high and ultra-high pressures on electrical conductivity of dielectrics has been discussed at length in the literature. For example,

Material	Initial density, δ_0 g/cm³	Initial electrical conductivity γ_0, $\Omega^{-1}cm^{-1}$	Pressure in the wave front P, kg/cm²	Electrical conductivity in the wave front γ, Ω^{-1} cm^{-1}
Air	0.0012	—	$3 \cdot 10^2$	0.5
Water	1	10^5	$1 \cdot 10^5$	0.2
Paraffin	0.8	10^{-18}	$1 \cdot 10^6$	10^2
Plexiglas	1.18	10^{-15}	$8.2 \cdot 10^5$	$2 \cdot 10^2$

Bridgman[3] has shown that at pressures of 12 or 13 $\times 10^3$ kg/cm² and temperatures of 200° yellow phosphorus becomes black phosphorus. This new form has a density 1.4 times greater than the original form, and has an electrical conductivity characteristic of a metal, whereas yellow phosphorus is an insulator. Similar transformations, characterized by an increase in density and the appearance of a high electrical conductivity, are observed in tin and arsenic.

In 1944, Zel'dovich and Landau,[4] in analyzing the transition of metals into the gaseous state, reached the conclusion that at sufficiently strong compression any material will exhibit metallic properties. One of the latest theories concerning the structure of our planet proposes that the core of the earth consists of olivine, and not iron and nickel, as had been thought earlier. At the pressures of 1.4×10^6 kg/cm² which exist at the boundary of the earth's core, olivine has a density of about 10 g/cm³, becomes metallic, and should have a high electrical conductivity.

In 1956, Alder and Christian[5] applied shock waves to CsI crystals and pressed samples of I_2, CsBr, $LiAlH_4$ and certain other dielectrics and found that the resistance in the shock front of the wave was reduced to several hundred ohms (the original resistance of the samples was higher than 10^8 Ω). The shock pressure in these experiments was approximately 2.5×10^5 kg/cm². For this reason the "metallization" of the dielectrics was relatively weak. In the present experiments with paraffin and Plexiglas the pressure in the shock front is four times greater and the values of the electrical conductivity are found to be four orders of magnitude greater than those obtained by Alder and Christian.[5]

The general nature of the phenomena which occur in a strong shock front in dielectrics may be explained as follows. The high temperature and compression in the wave front stimulates atomic interactions and "squeezes" the electronic levels. These effects enhance electronic transitions, and materials which are originally dielectrics acquire an electrical conductivity characteristic of the metal state.

The temperature in the shock front has a strong influence on this effect. It is hoped that further work will make it possible to delineate the individual effects of high pressures and temperatures in the formation of a region of high electrical conductivity in dielectrics. However, the experimental data which are already available indicate that the strong shock waves produced by high explosives offer a convenient way of studying the transformation of dielectrics into "metals" under laboratory conditions.

[1] Brish, Tarasov, and Tsukerman, JETP **37**, 1543 (1959), Soviet Phys. JETP **10**, 1095 (1960).

[2] Al'tshuler, Krupnikov, and Brazhnik, JETP **34**, 886 (1958), Soviet Phys. JETP **7**, 614 (1958).

[3] P. W. Bridgman, Physics of High Pressures, Macmillan, New York, 1935, Russ. Transl. ONTI, 1935.

[4] Ya. B. Zel'dovich and L. D. Landau, JETP **14**, 32 (1944).

[5] B. J. Adler and R. H. Christian, Phys. Rev. **104**, 550 (1956).

Translated by H. Lashinsky

ELECTRON CAPTURE AND DETACHMENT IN COLLISIONS OF FAST HELIUM, BORON, AND FLUORINE ATOMS WITH GAS MOLECULES

Ya. M. FOGEL', V. A. ANKUDINOV, and D. V. PILIPENKO

Submitted to JETP editor July 4, 1959

J. Exptl. Theoret. Phys. (U.S.S.R.) **38**, 26-32 (January, 1960)

Results are reported for measurements of the cross sections σ_{0-1} and σ_{01} for electron capture and detachment in collisions of fast He, B, and F atoms (10 — 60 kev) with inert gas atoms. It has been established that the behavior of the $\sigma_{0-1}(v)$ curves and the position of the maxima on these curves can be explained by the Massey adiabatic hypothesis. The admixture of metastable He atoms in the primary beam has an effect on the $\sigma_{0-1}(v)$ curve for He atoms. The Massey adiabatic hypothesis does not apply to the electron detachment process in fast atoms.

INTRODUCTION

In earlier work[1,2] we have measured the cross sections for electron capture and detachment in collisions between fast H, C, and O atoms and gas molecules. A number of conclusions follow from an analysis of the experimental results obtained in that work. In order to evaluate the generality of these conclusions we have also measured the cross sections for electron capture and detachment for He, B, and F atoms. In addition, the measurements for H atoms in argon and krypton have been extended to energies of 3 to 8 kev in order to determine the positions of the maxima on the $\sigma_{0-1}(v)$ curve.

The present measurements were carried out with the apparatus which was used earlier for studying electron capture and detachment for H, C, and O atoms.[1] The atomic beam is obtained by neutralizing accelerated positive ions in a mercury-vapor target; when this method is used the atomic beam may contain an admixture of particles in excited metastable states. The presence of this admixture affects both the shape of the cross section vs velocity curve and the value of the cross section at a given velocity. Because of the presence of excited atoms in the beam, the thickness of the target in which the ions are neutralized affects the value of the measured cross section.[3]

We have investigated the cross sections σ_{0-1} and σ_{01} as functions of the thickness of the mercury-vapor target for He, B, C, O, and F atoms. With the exception of He, in all cases σ_{0-1} and σ_{01} are independent of target thickness. Thus, only the He atomic beam contains particles in excited states.

RESULTS OF THE MEASUREMENTS AND DISCUSSION

1. Electron Capture by H, He, B and F Atoms

The electron capture cross section has been measured for H atoms in the energy range 3 — 8 kev in argon and krypton, for He atoms in the energy range 10 — 50 kev in neon, argon, krypton, and xenon, and for B and F atoms in the energy range 10 — 60 kev in helium, neon, argon, krypton, and xenon. The value of σ_{0-1} for each energy was obtained by averaging the results of two measurements. In the region of the maxima of the $\sigma_{0-1}(v)$ curves for He the values of σ_{0-1} were obtained by averaging the data of five or six measurements. The random error of the measurements varied from ±7%, for cross sections of the order of 10^{-16} cm^2 to ±30% for cross sections of the order of 10^{-18} cm^2. The error in the measurement of the energy of the atoms was ±3%.

Curves showing σ_{0-1} as a function of the energy and velocity of the H, He, B and F atoms are given in Figs. 1 — 4. Examination of these figures shows that just as in the case of electron capture in H, C and O atoms, which we have investigated earlier, σ_{0-1} for He, B and F is strongly affected by the nature of the gas atom. This dependence is found not only in the numerical value of the cross section for a given velocity, but also in the shape of the $\sigma_{0-1}(v)$ curve. In the light gases (helium and neon) σ_{0-1} increases monotonically with increasing velocity;* in the heavier gases it goes through a maximum or reaches a plateau at the end of the investigated velocity range. Sometimes (boron in krypton and

*The reason the $\sigma_{0-1}(v)$ curves for He atoms are not monotomic is discussed below.

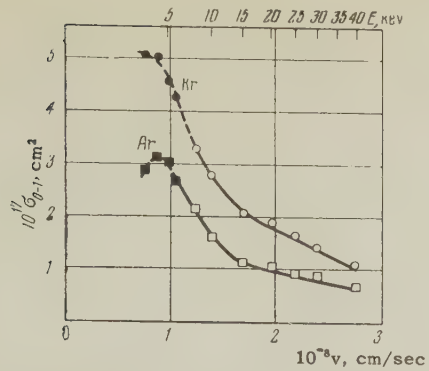

FIG. 1. Cross sections for electron capture by H atoms in argon and krypton. The dark points refer to the present work and the light points refer to the data of reference 1.

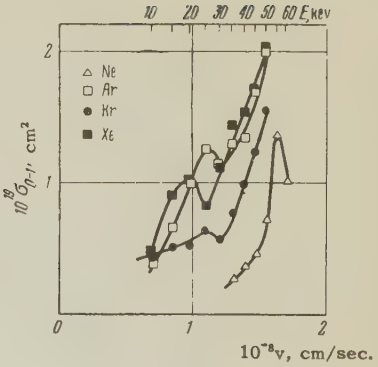

FIG. 2. The process $He^0 \rightarrow He^-$.

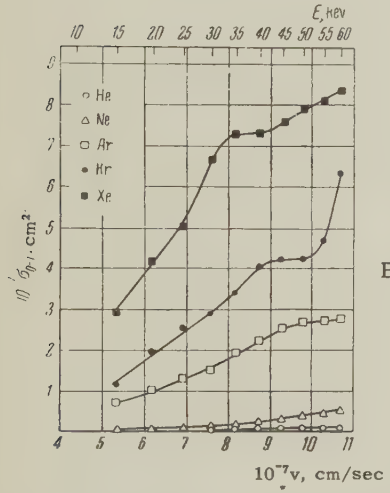

FIG. 3. The process $B^0 \rightarrow B^-$.

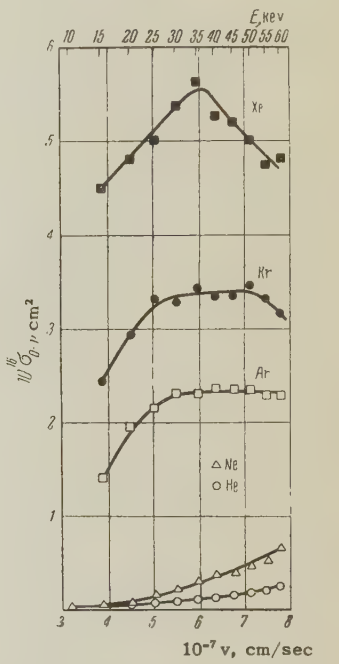

FIG. 4. The process $F^0 \rightarrow F^-$.

xenon) $\sigma_{0,-1}$ increases with increasing velocity after the plateau is traversed. The cross section for He in argon, krypton and xenon ($\sigma_{0,-1}$) exhibits a further increase in velocity after passing through a maximum.

An analysis of the measurements for H, C, and O indicates that the Massey adiabatic hypothesis can explain the features of the $\sigma_{0,-1}(v)$ curves.[4] As will be seen in the analysis given below, the experimental data of the present work support the conclusion that the Massey adiabatic hypothesis can be applied in electron capture by fast atoms.

The resonance defect for electron capture by fast atoms $A + B \rightarrow A^- + B^+$ (process I) can be written in the following form, if we assume that all participating particles are in the ground state:

$$\Delta E = S_A - V_B^I, \qquad (1)$$

where S_A is the electron affinity of particle A and V_B^I is the first ionization potential of particle B. Because excited particles can also undergo a process in which an electron is captured by a fast atom, the following channels are available for the process:

$$A^* + B \rightarrow A^- + B^+, \qquad \Delta E = (S_A + E_A) - V_B^I; \qquad (II)$$

$$A + B \rightarrow A^- + B^{+*}, \qquad \Delta E = S_A - (V_B^I + E_{B^+}); \qquad (III)$$

$$A^* + B \rightarrow A^- + B^{+*}, \quad \Delta E = (S_A + E_A) - (V_B^I + E_{B^+}). \qquad (IV)$$

(E_A and E_{B^+} are the excitation energies of particles A and B^+).

In analyzing the shapes of the $\sigma_{0,-1}(v)$ curves for He, B, and F atoms we assume that the maxima or plateaus on these curves are to be associated with process I for B and F and with process II for He (metastable helium atoms in the $2s^3S$ state). Processes II and IV are excluded for B and F because the fact that $\sigma_{0,-1}$ is independent of the thickness of the mercury-vapor target indicates that there are no excited atoms in the primary beam. It may be assumed that the

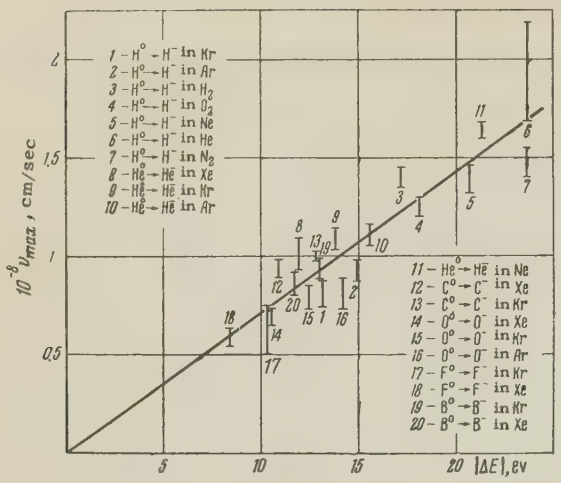

FIG. 5

maxima and plateaus on the $\sigma_{0-1}(v)$ curves for F and B correspond to III, corresponding to the excitation of the lowest level of the slow B^+ ion.

Under this assumption, the constant a which appears in the adiabatic criterion has approximately the same value for all atom-atom pairs for which the maxima on the $\sigma_{0-1}(v)$ curves are observed at 1.2 A. The maxima on the $\sigma_{0-1}(v)$ curves for H, C, and O may also be assigned to III, in which case a has a value which is only slightly different from the value 1.2 A for B and F atoms. However, the $\sigma_{0-1}(v)$ curves obtained indicate that the maxima on these curves cannot be assigned to III. If these maxima are assigned to III, there should be maxima corresponding to I in the low energy range and maxima corresponding to III in the high energy range, due to excitation of higher levels of the slow ion (up to the ionization level). For example, in the case of the pairs B-Ar, B-Kr, and O-Ar there should be maxima due to I near 11.8, 12, and 17 kev. However, no such maxima are observed for these pairs. In the case of H-Ar there are two maxima in the range 4.5 — 10 kev due to processes which are associated with excitation of the slow ion. Consequently, it is reasonable to expect that the $\sigma_{0-1}(v)$ curve will have a broad maximum in this energy range. Actually for H-Ar σ_{0-1} falls off rather rapidly with increasing energy in the range 4 — 10 kev.

The findings given above, which can be supplemented, force us to reject the assumption that the maxima on the $\sigma_{0-1}(v)$ curves for H, B, C, O, and F atoms are due to III. The only remaining explanation is that these maxima are to be associated with electron capture processes in which all participating particles are in the ground state. The value of a is approximately the same (3 A) for all atom-atom pairs for which a maximum is observed on the $\sigma_{0-1}(v)$ curve. The degree to which this quantity remains constant is apparent from Fig. 5, in which the dependence of v_{max} on $|\Delta\epsilon|$ is shown. If a is a constant all points should lie on a straight line. As is apparent from Fig. 5, the experimental points are well grouped about a straight line whose slope corresponds to a = 3 A. The maxima on the $\sigma_{0-1}(v)$ curves for the $He \rightarrow He^-$ process in neon, argon, krypton, and xenon fall on this line if it is assumed that these maxima are to be associated with the capture of the electron by metastable helium atoms in the $2s^3S$ state. This assumption is supported by the experiments in which the cross sections σ_{0-1} and σ_{01} are found to be functions of the thickness of the mercury-vapor target, indicating the existence of metastable helium atoms in the primary beam.

The further increase in σ_{0-1} beyond the maximum on the $\sigma_{0-1}(v)$ curves for $He \rightarrow He^-$ or beyond the plateau for the $B \rightarrow B^-$ process is due to maxima at high velocities, which are to be associated with I and III in the first case and with III in the second case.

It is of considerable interest to examine the factors which affect the maximum value of the cross section for inelastic processes. In processes such as $A \rightarrow A^-$ one of the factors which determines the value of $(\sigma_{0-1})_{max}$ may be the binding energy of the captured electron in the negative ion which is formed, i.e., the electron affinity. Curves showing $(\sigma_{0-1})_{max}$ as a function of electron affinity for krypton and xenon are given in Fig. 6. In plotting these curves we have taken the electron affinity values for H, C, O, F atoms from the survey paper by Branscomb[5] and the electron affinity of He and B from the work of Holpien and Midtal,[6] and Ginsberg and Miller,[7] respectively.

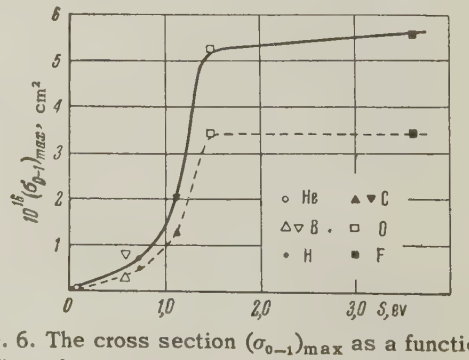

FIG. 6. The cross section $(\sigma_{0-1})_{max}$ as a function of electron affinity for Kr (dashed line) and Xe (solid line).

It is apparent from Fig. 6 that the electron affinity has an important effect on $(\sigma_{0-1})_{max}$ up to the atom O (S ≈ 1.5 ev). However, there is al-

most no change in $(\sigma_{0-1})_{max}$ between O and F although the electron affinity increases by approximately a factor of 2.5. This result indicates that the electron affinity is not the only factor which determines the maximum value of σ_{0-1}. Apparently the structure of the electron shell of the negative ion which is formed is also of great importance.

In B and F, just as in H, C, and O, $(\sigma_{0-1})_{max}$ falls off monotonically as the first ionization potential of the target atom increases. This feature is not found in the He case, apparently because of the admixture of metastable atoms in the He beam.

A comparison of the values of σ_{0-1} for He, B, and F, as measured in the present work, with the data for the cross sections σ_{10} for He^+ ions[8] and σ_{1-1} for He^+, B^+, and F^+ ions[9-11] leads to the same conclusion as for H, C, and O atoms and ions: $\sigma_{10} > \sigma_{0-1} > \sigma_{1-1}$ for helium particles and $\sigma_{0-1} > \sigma_{1-1}$ for B and F ions and atoms.

2. Electron Detachment in H, He, B, and F Atoms

The electron detachment cross section σ_{01} for H, He, B, and F atoms was measured in the same energy range and for the same gases as the cross sections σ_{0-1}. Curves showing the dependence of σ_{01} on energy and velocity for H, He, B, and F are shown in Figs. 7 — 10. The electron detachment cross section for He in helium, neon, argon gases have also been measured by Barnett and Stier[3] by a beam-attenuation technique. The He data of the present work are compared with the data obtained by Barnett and Stier in Fig. 11.

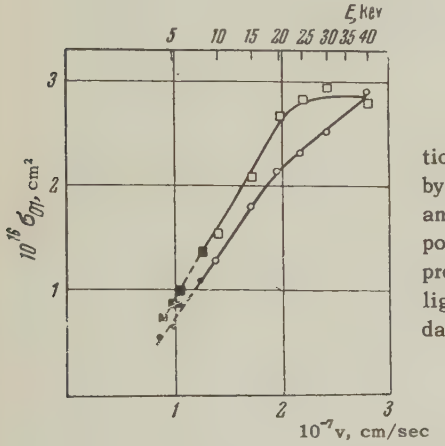

FIG. 7. Cross sections for electron loss by H atoms in argon and krypton. The dark points refer to the present work and the light points to the data of reference 1.

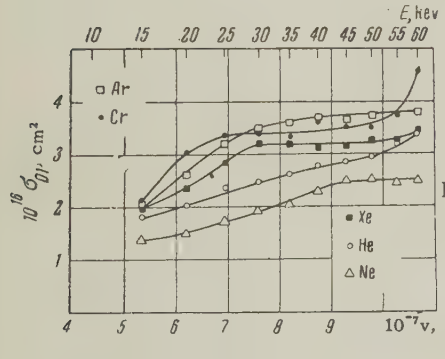

FIG. 9. The process $B^0 \rightarrow B^+$.

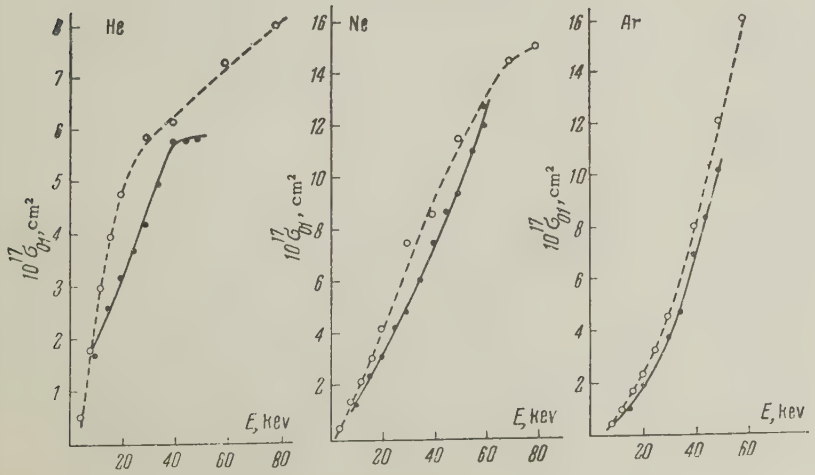

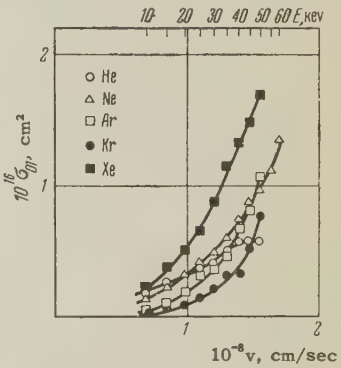

FIG. 8. The process $He^0 \rightarrow He^+$.

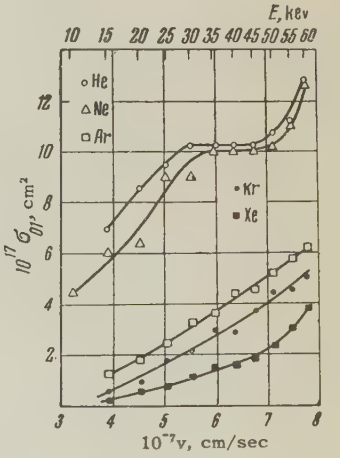

FIG. 10. The process $F^0 \rightarrow F^+$.

FIG. 11. The process $He^0 \rightarrow He^+$; ●) data of the present work, ○) data of reference 3.

An analysis of the values of σ_{01} obtained in the present work and in our earlier work[1,2] reveals that the effect of the gas target-atom on the magnitude of σ_{01} is a function of the atomic number of the fast atom. For H, He, B, and C the dependence of σ_{01} on the atomic number of the gas atom is non-monotonic, whereas for the heavier atoms, O and F, σ_{01} increases monotonically as the atomic number of the target-atom decreases. Thus, σ_{0-1} and σ_{01} change in opposite directions for fast O and F atoms as the atomic number of the gas atom changes. It should also be noted that the gas atom has a stronger effect on σ_{0-1} than on σ_{01}. For example, for O atoms with a velocity of 6×10^7 cm/sec, σ_{0-1} increases by a factor of 120 between helium and xenon whereas σ_{01} is reduced by a factor of 4.

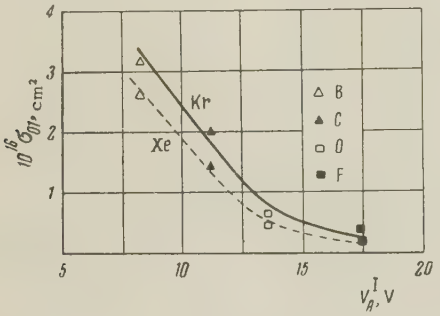

FIG. 12

On the basis of the present work and our earlier work[1,2] certain conclusions may be drawn as to the effect of the fast atom on σ_{01}. For B, C, O, and F, in which the detached electron comes from the same subshell (2p), there is a reduction in the cross section as the first ionization potential of the fast atom increases. This effect is seen in Fig. 12, which shows the dependence of σ_{01} (for the same velocity, 6.5×10^7 cm/sec) on the first ionization potential for B, C, O, and F atoms in the gases krypton and xenon. Presumably the same feature obtains in other atoms in which the detached electron comes from the same subshell. In particular, in the atoms H and He, in which the detached electron comes from the 1s subshell, for all gases except xenon we find $(\sigma_{01})_H > (\sigma_{01})_{He}$. This exception should not occasion surprise since the admixture of metastable atoms, with ionization potentials considerably lower than that of He atoms in the ground state, means that the measured value of σ_{01} is higher than the true value for He atoms in the ground state.

The value of σ_{01} is not determined exclusively by the binding energy of the detached electron. This result follows from the fact that σ_{01} for the O atom is larger than for the H atom, although both atoms have approximately the same ionization potential. Thus it would seem that in this case the electron comes from different electron shells. The number of electrons in the shell from which the electron is detached may also be of importance.

In conclusion we may note that the general behavior of the $\sigma_{01}(v)$ curves and the behavior of these curves for the same fast atom in different target atoms leads to the conclusion that the Massey adiabatic hypothesis does not apply to electron detachment in fast atoms.

In these measurements we were assisted by B. T. Nadykto and V. P. Antonov.

We are indebted to Professor A. K. Val'ter for his continued interest in this work.

[1] Fogel', Ankudinov, Pilipenko, and Topolya, JETP **34**, 579 (1958), Soviet Phys. JETP **7**, 400 (1958).

[2] Fogel', Ankudinov, and Pilipenko, JETP **35**, 868 (1958), Soviet Phys. JETP **8**, 601 (1959).

[3] C. F. Barnett and P. M. Stier, Phys. Rev. **109**, 385 (1958).

[4] H. S. W. Massey, Rep. Progr. Phys. **12**, 248 (1948).

[5] L. M. Branscomb, Advances in Electronics and Electron Physics, Vol 9, Academic Press, New York 1957.

[6] E. Holpien and J. Midtal, Proc. Phys. Soc. (London) **A68**, 815 (1955).

[7] A. P. Ginsberg and J. M. Miller, J. Inorg. Nucl. Chem. **7**, 351 (1958).

[8] J. B. Hasted and J. B. H. Stedeford, Proc. Roy. Soc. (London) **A227**, 466 (1955).

[9] Dukel'skiĭ, Afrosimov, and Fedorenko, JETP **30**, 792 (1956), Soviet Phys. JETP **3**, 764 (1956).

[10] Fogel', Mitin, Kozlov, and Romashko, JETP **35**, 565 (1958), Soviet Phys. JETP **8**, 390 (1959).

[11] Fogel', Kozlov, Kalmykov, and Muratov, JETP **36**, 1312 (1959), Soviet Phys. JETP **9**, 929 (1959).

Translated by H. Lashinsky
6

INFLUENCE OF THE MEDIUM DENSITY ON BREMSSTRAHLUNG IN ELECTRON-PHOTON SHOWERS IN THE ENERGY RANGE $10^{11}-10^{13}$ *ev*

A. A. VARFOLOMEEV, R. I. GERASIMOVA, I. I. GUREVICH, L. A. MAKAR'INA, A. S. ROMANTSEVA, and S. A. CHUEVA

Submitted to JETP editor July 4, 1959

J. Exptl. Theoret. Phys. (U.S.S.R.) **38**, 33-45 (January, 1960)

Fifteen electron-photon showers in the energy range $10^{11}-10^{13}$ ev recorded in emulsion stacks were examined. The energies of the primary γ rays initiating the showers were determined by measuring the energy spectrum of cascade electrons at the depth of 2.5 — 3 radiation units, and from the screening effect on the first pairs. The energy spectrum of pairs produced at a depth of up to 1.5 radiation units was measured. The results are in agreement with calculations carried out taking into account the influence of multiple scattering and of the polarization of the medium on the bremmsstrahlung of high-energy electrons.

1. INTRODUCTION

IT has been stated earlier[1,2] that it is possible to test experimentally the effects of the medium on the bremsstrahlung[3,4] through a study of the energy spectrum of electrons in electromagnetic cascades of sufficiently high energies ($\gtrsim 10^{12}$ ev). The polarization effect (Ter-Mikaelyan[3]) should be felt in the emulsion for the γ-ray frequency range satisfying the condition $\hbar\omega \ll 7\times10^{-5}E$, where E is the electron energy. Moreover, the expression for the radiation intensity J is then $dJ \sim \omega^2 d\omega/E^2$ instead of the Bethe-Heitler relation $dJ \sim d\omega$. The multiple scattering effect (Landau and Pomeranchuk[4]) should be felt in the emulsion for the frequency range $7\times10^{-5} \ll \hbar\omega/E \leq 2\times10^{-8}E/mc^2$, which leads to an expression for the intensity $dJ \sim \sqrt{\omega}\, d\omega/E$.

The foregoing conditions show (see also Fig. 1 of reference 2) that, for $E = 5\times10^{11}-10^{12}$ ev, the influence of the medium should lead to a markedly decreased radiation probability of γ rays with energy $\hbar\omega \lesssim 10^9$ ev. It is evident that this fact will influence the energy spectrum of cascade electrons and electron-positron pairs, this influence being the stronger the greater the cascade depth t.

Special calculations of electromagnetic cascades in nuclear emulsions have been carried out by us earlier using the non-asymptotic cross sections for the elementary electromagnetic processes.[1,2] In one variant of the calculations (B-H), we used the Bethe-Heitler formulas for the radiation processes, while, in the other variant (M), the radiation of high-energy electrons was calculated according to the formulas of Migdal,[5] which take both effects of the medium into account. The calculations have shown that, under certain conditions, the study of the energy spectra of cascade particles at small depths in electron-photon showers in the energy range $10^{11}-10^{12}$ ev makes it possible to determine the form of the bremsstrahlung spectrum of primary electrons. Let us mention some of these conditions:

First, the energy of primary particles producing the showers should be measured with maximum possible accuracy, since the difference between the Bethe-Heitler and Ter-Mikaelyan-Landau-Pomeranchuk spectra depends very strongly on this energy.

Second, the detection efficiency for low-energy electrons and pairs should be sufficiently high, since the difference between the B-H and M spectra is especially pronounced in the soft part of the spectrum.

The experimental results should be compared with calculations carried out using the true (non-asymptotic) cross sections for the bremsstrahlung and pair production. In the interpretation of the results, one should take the large fluctuations in the number of cascade particles, leading to large statistical errors, into account.

In recent years, electron-photon showers in the energy range $10^{10}-10^{12}$ ev have been detected in nuclear emulsions in the course of many experiments.[6-14] In several of the showers, the development in the initial stages was considerably different from the average behavior predicted by the usual cascade theories for showers produced by single γ rays. In particular, anomalies were ob-

served in the number and in the energy spectrum of cascade particles. The hypothesis that these anomalies are characteristic for high-energy processes has been proposed.[15] The most detailed study of a high-energy shower ($\sim 7 \times 10^{11}$ ev) at small depths has been carried out by Miesowicz et al.,[11] who was the first to attempt to explain the experimental results on the spectrum of cascade pairs by means of the influence of the effects of the medium on the bremsstrahlung.

However, similar anomalies have not been detected in later experiments[12-14] in which the showers were studied more systematically. Thus, the published results on the spectrum of cascade particles in high-energy showers are contradictory. The majority of the published material can, unfortunately, not be used in examining the problem of the shape of the bremsstrahlung spectrum of high-energy electrons, since the basic conditions stated above have not been satisfied.

In the present article, the results of a systematic study of 15 electron-photon showers in the energy range $10^{11} - 10^{13}$ ev are presented. Preliminary results on five showers in the energy range $3 \times 10^{11} - 2 \times 10^{12}$ ev have already been published earlier.[16]

2. GENERAL CHARACTERISTICS OF THE SHOWERS

In the course of the experiment, six emulsion stacks with a total volume of about 10 liters were used. The stacks were irradiated at 20 — 27 km altitude. General data on the four stacks analyzed up to 1958, and on the position of the five investigated showers in the stacks, have been reported in references 16 and 17. The two new stacks (α and β) were composed of layers with dimensions $10 \times 20 \times 0.04$ cm^3, and had a volume of 1.4 and 3.1 liters respectively.

The R-NIKFI emulsion was mainly used. The grain density in relativistic electron tracks amounted to 30 — 35 grains per 100 μ, i.e., considerably greater than in the Ilford G-5 emulsion. This facilitated greatly the detection and analysis of the showers.

Showers with energy of $\sim 10^{12}$ ev were usually detected in scanning the plates with the naked eye on white background, along the well-developed part of the cascade at a depth of 2 — 3 radiation lengths. Only those showers produced by single isolated (not connected with jets) photons, and which had a path in one layer not less than a few millimeters, were selected for analysis.

The energy E_γ of the primary photons producing the showers was determined from the number of cascade electrons with energy higher than $\epsilon_c = 300$ Mev at the depth of $2.5 - 3\,t_0$, where $t_0 = 29$ mm is the radiation length in the emulsion. The method used was analogous to that described by Pinkau[13] and Miesowicz et al.[11] (For details, see references 16 and 17.) The lateral electron distribution function of Guzhavin and Ivanenko[18] was used for the calculation of the number of particles traveling within a circle with radius ρ (in contrast with experiments 11, 13, 16, and 17, in which the calculations of Eyges and Fernbach[19] were used).

Numerical integration of the results of Guzhavin and Ivanenko[18] yielded the function $\eta(s, \rho/t_0)$ (where s is the "age" parameter determined by the energy of the primary electron E_0 and the values of ϵ and t), which gives the ratio of the number of electrons with energy $> \epsilon$, whose tracks are inside a circle with radius ρ around the shower axis, to the total number of electrons $N_\beta(\epsilon, E_0, t)$ with energy $> \epsilon$ at a given depth t (see Table I).

Values of the energy E_γ (for 12 out of 15 showers) determined from the curves $N_\beta(\epsilon, E_0, t)$ for electrons, calculated by the Monte Carlo method[2] and from corresponding curves of Janossy,[20] are given in Table II. The difference between the results for the five showers[16,17] presented previously and the data in Table II is due mainly to a change in the lateral corrections inherent in the function η. In addition, those curves $N_\beta(\epsilon, E_0, t)$ which have been used in the present analysis are based on greater statistical material[2] and are somewhat different from the corresponding curves used earlier.[16]

In finding E_γ from the calculated curve $N_\beta(\epsilon, E_0, t)$, the errors in E_γ were determined

TABLE I. Fraction of the total number of electrons with energy $> \epsilon$ falling inside a circle with radius ρ (s — cascade parameter, $x = \epsilon\rho/E_s t_0$, $E_s = 21$ Mev)

x	$s = 0.4$	$s = 0.5$	$s = 0.6$	$s = 0.7$	x	$s = 0.4$	$s = 0.5$	$s = 0.6$	$s = 0.7$
0.01	0.51	0.40	0.31	0.23	0.10	0.84	0.79	0.72	0.66
0.02	0.61	0.51	0.42	0.34	0.15	0.89	0.85	0.80	0.74
0.04	0.71	0.63	0.54	0.46	0.20	0.92	0.89	0.84	0.80
0.06	0.77	0.70	0.63	0.55	0.60	0.99	0.98	0.97	0.95

TABLE II. Results of the measurement of energy E_γ (in 10^{11} ev)

Shower	From Monte-Carlo method	According to Janossy	From Eq. (3)	From Eq. (4)
β-213			$219\ ^{+161}_{-100}$	260
β-212			$96\ ^{+110}_{-50}$	149
D-84	$16.5\ ^{+143}_{-7.0}$	$1.2\ ^{+6}_{-4.5}$	$15.7\ ^{+17.5}_{-8.2}$	24.0
O-209	$8.4\ ^{+4.8}_{-2.7}$	$6.3\ ^{+1.8}_{-1.6}$	$18.4\ ^{+18.1}_{-9.3}$	26.1
E-53	$6.8\ ^{+68}_{-3.8}$	$5.3\ ^{+2.8}_{-2.6}$	$20.2\ ^{+27.2}_{-13.1}$	31.1
α-79	$3.1\ ^{+1.1}_{-1.0}$	$2.3\ ^{+0.7}_{-0.6}$	$12.3\ ^{+12.8}_{-6.2}$	17.9
I-109	$3.1\ ^{+2.2}_{-0.9}$	$2.4\ ^{+0.7}_{-0.6}$	$0.7\ ^{+1.2}_{-0.4}$	1.5
D-44	$2.9\ ^{+2.3}_{-0.9}$	$2.2\ ^{+0.7}_{-0.5}$	$1.4\ ^{+2.2}_{-0.8}$	2.3
β-344	$2.4\ ^{+2.3}_{-0.8}$	$1.8\ ^{+0.5}_{-0.4}$	$2.3\ ^{+4.5}_{-1.8}$	8.4
β-165	$1.9\ ^{+1.1}_{-0.5}$	$1.5\ ^{+0.3}_{-0.3}$	$3.9\ ^{+6.7}_{-3.0}$	13.0
E-78	$1.5\ ^{+1.7}_{-0.5}$	$1.2\ ^{+0.4}_{-0.3}$	$1.1\ ^{+2.2}_{-0.9}$	4.2
D-89	$1.3\ ^{+1.5}_{-0.5}$	$1.0\ ^{+0.4}_{-0.3}$		
O-317	$1.3\ ^{+1.1}_{-0.5}$	$0.9\ ^{+0.3}_{-0.2}$		
E-29	$1.1\ ^{+4.8}_{-0.6}$	$0.8\ ^{+0.5}_{-0.4}$	$2.6\ ^{+5.4}_{-2.1}$	10.0
E-39			$1.5\ ^{+3.2}_{-1.2}$	5.9

from the number of shower electrons according to the calculated distribution functions[2] for showers initiated by two primary electrons with energy $E_\gamma/2$. (See reference 17 concerning the determination of errors E_γ from the curves of Janossy.)

3. MEASUREMENT OF THE ENERGY OF PRIMARY PAIRS FROM THE SCREENING EFFECT

The energies of the primary pairs for $E_\gamma > 3 \times 10^{11}$ ev were also determined from the decrease in the grain density in the pair tracks near the vertex, due to the mutual screening of the electron and positron fields. This screening effect had first been calculated by Chudakov[21] using purely classical considerations, and was then treated by other authors,[22,23] among them Burkhardt[23] using quantum mechanics. The possibility of using the screening effect for the determination of the energy of separate pairs of $E_\gamma \gtrsim 3 \times 10^{11}$ ev was confirmed experimentally by Wolter and Miesowicz,[24] by Varfolomeev et al.,[17] and by Iwadare,[25] who, in addition to the measurement of the ionization energy losses of the pairs, carried out independent measurements of the pair energy. Since the various available theoretical formulas for the ionization due to pairs, as given by different authors, differ considerably from each other in the numerical values of the constants, it is reasonable to determine these from experimental results.[17,24,25]

In a classical treatment, the ratio of the specific ionization losses of a pair I to the losses of two separate electrons $2I_{pl}$ can be written in the form

$$R = A + B \ln r^2, \tag{1}$$

where I_{pl} is the ionization at the plateau of the ionization-loss curve, r is the distance between the trajectories of the electron and the positron, and A and B are constants (at least for $R < 0.9$) which depend on the medium.

The distance r is determined by the initial opening angle of the pair θ and by the multiple scattering of the electron and positron over a distance x from the pair vertex. The angle θ and the deflection due to multiple scattering, and consequently also R, depend statistically on the pair energy E_γ.

For the mean value of R, we can write $\bar{R} = A + B\,\overline{\ln r^2}$, where the averaging, in general, should be carried out taking into account the distribution of the energy E_γ between the components of the

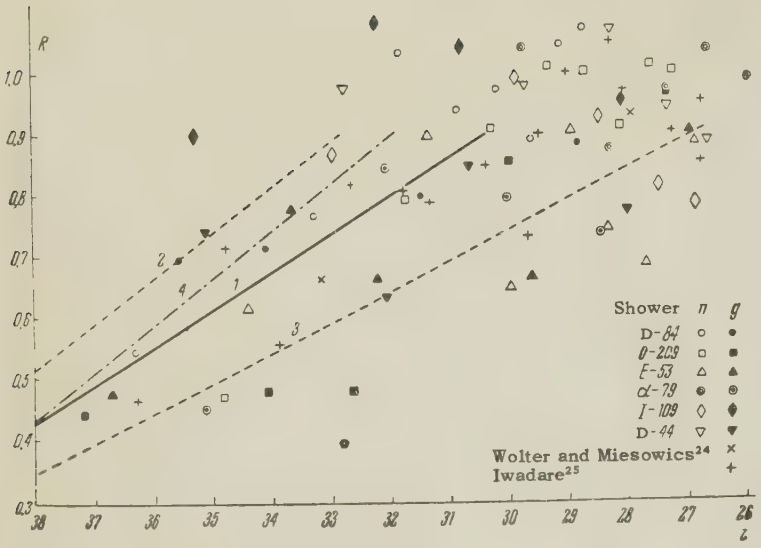

FIG. 1. Ratio of the ionization loss of a pair to that of two separate relativistic electrons R_i: 1 – curve calculated according to Eq. (3); 2 and 3 – curves corresponding to standard deviations of R from curve 1; 4 – curve calculated according to Eq. (4).

pair, the distribution of the multiple scattering deflection at a given distance x, and the distribution of the angle θ for a given energy distribution E_γ. Sacrificing some accuracy, we assume that the average value of $\ln r^2$ can be replaced by $\ln \overline{r^2}$. We furthermore write

$$r^2 = \theta^2 x^2 + \frac{k^2 x^3}{E^2}\left[\frac{1}{a^2} + \frac{2}{(1-a)^2}\right],$$

where a is the ratio of the energy of one of the electrons of the pair to the total pair energy E_γ, and k is the multiple scattering constant determining the mean-square deflection of the electron in space after traversing a path of length x from the tangent to its trajectory at the point x = 0. From the data of Rossi[26] and of Pickup and Voyvodic,[27] it can be assumed that k = 6.15 Mev rad/$cm^{1/2}$.*

If we are interested in the most probable value of R for a given value of E_γ, it is not necessary to average over all possible angles θ, but it is sufficient to consider the angle θ equal to the most probable angle $\vartheta = (4mc^2/E_\gamma)\,F(a)$.[28] After averaging the expression for r^2 over a in the limits of 0.5 – 0.1, using the pair distribution function with respect to the variable a for the case of full screening[26] and the values F(a) from the article by Borsellino,[28] we obtain

$$\overline{r^2} = 1.6\,(2x/E_\gamma)^2\,(1 + 140x),$$

where x is given in centimeters, and E_γ in Mev. For the mean value of R, we can therefore write

$$\overline{R} = A' + B \ln [(2x/E_\gamma)^2\,(1 + 140x)], \qquad (2)$$

where A′ and B, as before, are constants.

Experimental values of R_i are shown in Fig. 1 as a function of $z = \ln [(2x/E_\gamma)^2(1+140x)]$ (where x is given in cm, and E_γ in Mev). Data of references 17, 24, and 25, and results of measurements of the pair α-79 have been used. The constants A′ and B have been determined from experimental points in the range $R \leq 0.9$ by the least-squares method, and the following expression has been obtained as a result

$$\overline{R} = \frac{1}{16.1}\{45.0 + \ln [(2x/E_\gamma)^2\,(1 + 140x)]\}. \qquad (3)$$

The standard deviation of experimental points R_i from the corresponding values $\overline{R}$ given by Eq. (3) is ~20%. It has been assumed that the statistical distribution of the ratio $R_i/\overline{R}$ is independent of $\overline{R}$. The curves for $R_{max} = 1.20\,\overline{R}$ and for $R_{min} = 0.80\,\overline{R}$, where $\overline{R}$ is given by Eq. (3), can be used for an estimate of the errors in the determination of the energy E_γ of individual pairs by means of Eq. (3).

It is evident that the errors in the determination of E_γ from the experimental values of R_{av}, averaged over an interval of x, depend also on the length of this interval x. An increase in the interval length leads to a decrease in the relative statistical fluctuations of the ionization losses of the pair, and thus to a decrease in the error of R_{av}. On the other hand, with an increase of x, the statistical spread of the values R_{av} around the curve C increases. Unfortunately, the ex-

*The deflection from the tangent is, by a factor of $\sqrt{2}$, smaller than the deflection determined by the second differences measured by the sagitta method (see, e.g., reference 26). Moreover, taking into account that the mean absolute value is smaller than the mean square value by a factor of $\sqrt{\pi/2}$, and that the deflection in space is greater than the deflection in a plane by a factor of $\sqrt{2}$, we find that $k = \sqrt{\pi/2}\,k'$, where k′ is a constant corresponding to the mean absolute values of the second differences measured by the sagitta method in a plane. According to Pickup and Voyvodic,[24] k′ = 4.9 Mev rad cm^{-2}.

perimental material presently available is, so far, insufficient for choosing an optimal value of x.

The pair energy E_γ found from ionization measurements is given in Table II. For the first eight pairs, the values of R_{av} were determined by measuring both grain (n) and gap (g) density.[17] For each pair, and for each variation of the ionization measurement method (n and g), two intervals were used, $0-x_1$ and $0-x_2$. The values of x_1 and x_2 were chosen from the conditions $\bar{R}(x_1) = 0.4-0.6$ and $\bar{R}(x_2) = 0.8-0.9$. Thus, for each of the eight pairs, four values each of $E_i(\alpha)$, of $\max E_i(\alpha)$, and of $\min E_i(\alpha)$, were obtained, where $\alpha = n, g$ indicates the method of measurement, and $i = 1,2$ the interval x_1 or x_2. The results were averaged and the errors calculated in the way described below.

First, the mean logarithmic values of E_i, $\max E_i$ and $\min E_i$, were determined separately for the first and second segments of the pair track (logarithmically averaged over the symbol α). Then, by averaging the values of E_i over i, the average values of E_γ given in Table II were obtained. The errors E_γ were determined as standard deviations of $\max E_i$ and $\min E_i$ from E_i. The described method of averaging was chosen since the results of the measurements by the various methods over the same segments are not independent. The deviations $\max E_i$ and $\min E_i$ from E_i are basically due to multiple scattering and not to errors in measuring n and g. On the other hand, the measurements over various segments can be regarded as only weakly correlated.

For the remaining five pairs given in Table II ($E_\gamma \sim 10^{11}$ ev), only the measurements of n over one segment x_2 were used.

For comparison, the values of E_γ are also given in Table II, as determined by the relation

$$\bar{R} = \frac{1}{12{,}9}\left\{43.6 + \ln\left[\left(\frac{2x}{E_\gamma}\right)^2(1+140x)\right]\right\}, \qquad (4)$$

which follows from the calculations of Burkhardt,[23] if one takes the multiple scattering into account and averages the results by the same method as described above.

Comparison of the data given in Table II shows that, in the majority of cases, a satisfactory agreement is obtained between the values of E_γ as determined from the shower development, and from the screening effect using Eq. (3).

The measurements of n and g on the first pairs of the showers β-212 and β-213 are shown in Figs. 2 and 3. The energy of these showers was determined from the screening effect only. This was, first of all, because of the lack of calculated cascade curves for energies $E_\gamma \sim 10^{13}$ ev. For

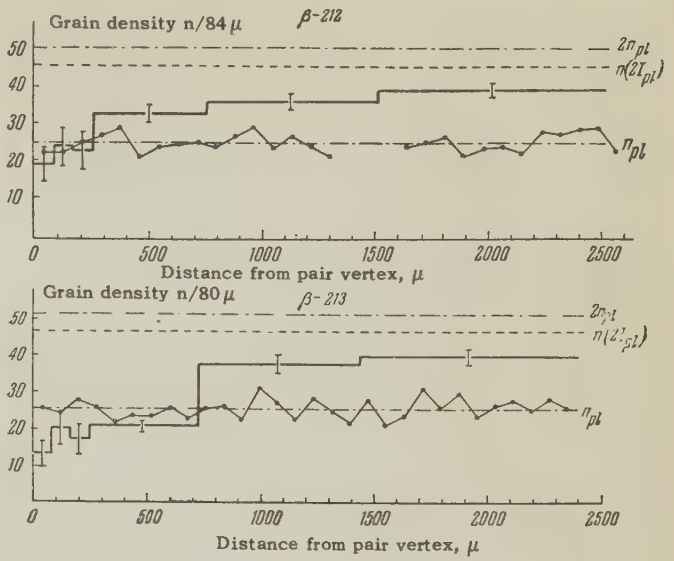

FIG. 2. Grain density n in tracks of electron-positron pairs β-212 and β-213: n_{pl} – grain density on the plateau of a track of a relativistic electron, $n(2I_{pl})$ – grain density in the track of particles with double losses $2I_{pl}$.

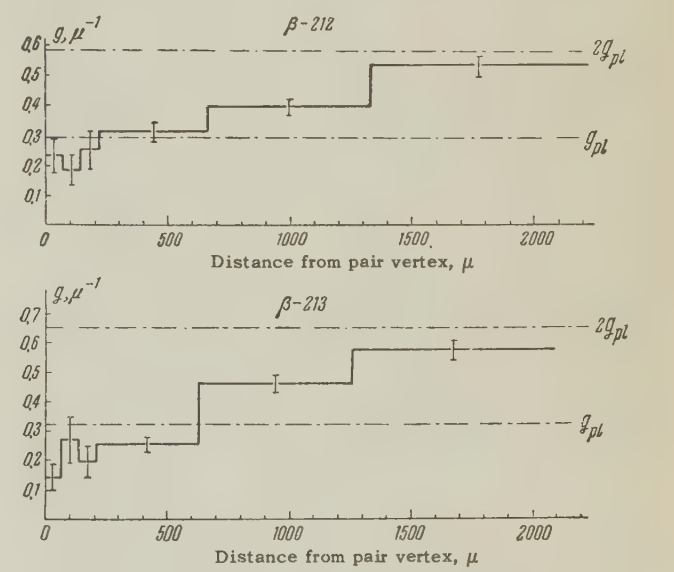

FIG. 3. Gap density g in tracks of the pairs β-212 and β-213.

such high energies, the influence of the medium can already be felt on the spectrum of cascade electrons with energies of $\sim 10^8 - 10^9$ ev (especially at small depths t). The usual cascade curves can, therefore, not be used. In addition, especially large fluctuations in the number of cascade particles at high E_γ lead to very large errors in the determination of E_γ from the shower development by the method described above.

4. MEASUREMENT OF THE ENERGY SPECTRA OF THE PAIRS

Further analysis of the showers consisted of the following: the vertices of the pairs produced

at the depth $\leq 1.5\,t_0$ were carefully searched for. The region inside the radius $\rho = 150\,\mu$ around the shower axis was investigated.* In the majority of cases, the search was repeated several times by various observers in order to reduce to a minimum the possibility of overlooking low-energy pairs.

The pairs lying outside the radius $\rho = 150\,\mu$ or at an angle greater than $10\,(mc^2/E_\gamma) \times \ln(E_\gamma/mc^2)$ to the shower axis, where E_γ is the pair energy, were regarded as part of the background and thus not related to the shower.†

After the spatial position of the shower had been reconstructed, the energy of the pair electron was measured from multiple scattering.

Measurements of the multiple scattering angle were carried out using a MBI-8M microscope with a glass guiding rail insuring low table noise. Additional head isolation of the light source made it possible to lower the thermal noise. During the measurements, the binocular attachment was rigidly connected to the base of the microscope by means of a metal frame. A guard shield was placed between the observer and the photographic plate. The microscope table was placed on rubber shock absorbers, and was loaded with a ballast of about 200 kg. As a result, the general noise in the measurements of the mean absolute values of second differences amounted to $0.13\,\mu$ over a cell of $250\,\mu$, and to $0.20\,\mu$ over a cell of $500\,\mu$. (The noise was measured on proton and electron tracks of $\sim 10^{12}$ ev.) A cell of $250\,\mu$ was mainly used. For a number of cells $n = 15-20$, the relative error in the determination of the electron energy is, according to Expong,[30] given by the expression

$$\sigma = \frac{1.12}{\sqrt{n}}\left[\frac{9}{16} + \frac{2}{3}\lambda^{-2} + \frac{35}{36}\lambda^{-4}\right]^{1/2},$$

where λ is the ratio of the measured second difference to the value of the general noise, amounting to $\sim 20-30\%$ up to an energy of $(5-7)\times 10^8$ ev, which, for the purpose of the present work, was fully satisfactory. In separate cases, either a cell of $500\,\mu$, or the relative multiple scattering method, was used for a determination of the pair energy. In several cases, because of unfavorable conditions for multiple scattering measurements, the pair energy was determined from the opening angle according to the Borsellino formula.[28] In any case, it can be assumed that the pair energy was measured with a sufficient accuracy up to 10^9 ev.

*In fact, the region inside $\rho = 400-500\,\mu$ was inspected, but only the region up to $\rho = 150\,\mu$ was investigated in a systematic and accurate way.

†The angle $\sim (mc^2/E_\gamma)\ln(E_\gamma/mc^2)$ is roughly equal to the mean square angle between the γ ray producing the pair and the track of one electron of the pair.[29]

The showers β-212 and β-213 appear as solid strands of electron tracks over a relatively long path length (up to $\sim 1\,t_0$). In their analysis, our aim was to determine the number of pairs with energy > 1 Mev produced at the depth $\leq 1.0\,t_0$ and $\leq 1.5\,t_0$ respectively.

5. RESULTS AND DISCUSSION

The influence of the medium should make itself strongly felt in the total number of pairs produced at small depths. The total number of pairs N $(>\epsilon)$ with total energy greater than $\epsilon = 1.5$ Mev,* produced at depths $\leq 1.0\,t_0$ and $\leq 1.5\,t_0$ is shown in Figs. 4 and 5 as a function of the primary electron energy. The calculated curves (1 and 2)

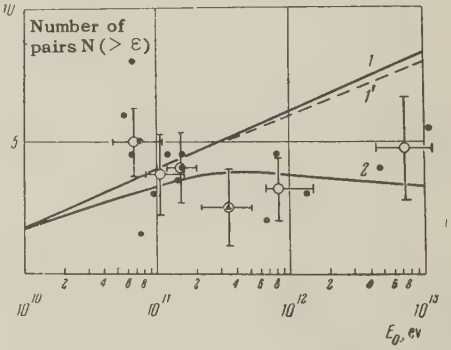

FIG. 4. Number of pairs N(> ε) with energy greater than $\varepsilon = 1-2$ Mev produced on the average at a depth $\leqslant 1.0\,t_0$ per primary electron with energy E_0. 1 – calculated curve for the average of N in the B-H variant; 1′ – calculated curve for the median value in the B-H variant; 2 – calculated curve for the average value of N in the M variant; ● – experimental values for showers listed in Tables II and III; ▲ – results of Miesowicz et al.[11] ○ – experimental data averaged over several showers.

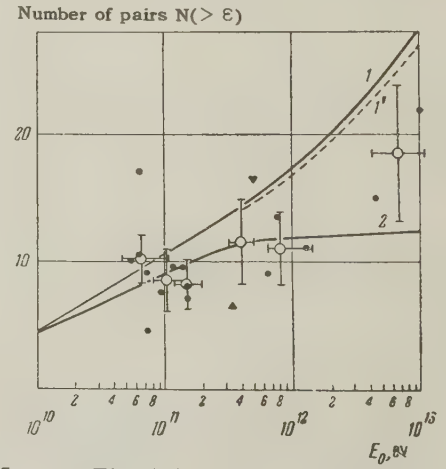

FIG. 5. Same as Fig. 4, but for pairs produced at the depth of $\leqslant 1.5\,t_0$. ▼ – data from the Feynves et al. shower.

have been obtained, respectively, with and without considering the influence of the medium on the radiation for showers produced by an electron with

*Both the experimental and the theoretical numbers of pairs with energy 1–5 Mev are relatively small. The value of ε can, therefore, be taken as 1–2 Mev.

energy E_0. The experimental points give the average number of pairs per primary electron.

The shower E-53 is assumed to be produced by one electron since it develops along the track of one electron. The energy of the second electron of the primary pair is $< 10^{11}$ ev.

In addition to the experimental results on 15 showers investigated in the present experiment (round points in Figs. 4 and 5), the data of Miesowicz et al.[11] on one shower with energy of $\sim 7 \times 10^{11}$ ev (Figs. 4 and 5), and data on one shower with energy of $\sim 10^{12}$ ev analyzed by the Budapest and Prague groups* (Fig. 5), have also been used.

As has already been mentioned above, the values of $E_\gamma = 2E_0$ determined only from the screening effect (Table II) have been used for the showers β-213 and β-212. The energy of shower E-39 has been estimated only from the screening effect because of the unfavorable position of the shower in the stack.

At energies $E_\gamma \sim 10^{12}$ ev, one can consider both methods of measurements of E_γ equally accurate, and the final values of the energy of showers D-84, O-209, and E-53 were therefore determined by averaging the results from Table II.

Because of large statistical errors both in the number of pairs N and in the values of the shower energy E_γ, it was advisable to average the results over separate groups with close values of E_γ. In Figs. 4 and 5, the results for the showers with energy $E_\gamma > 1.8 \times 10^{11}$ ev, collected in six groups, are represented as large light circles. In view of the fact that, according to curves 1 and 2, the number of pairs N depends almost linearly on $\ln E_0$, the averaging has been done in coordinates N, $\ln E_0$. The errors indicated in Figs. 4 and 5 (similarly to other figures in the present article) are statistical errors.

An analysis of the calculations[1,2] showed that the distribution of showers produced by two electrons with energies E_0 with respect to the number of pairs $Q(2E_0, t)$ at a depth t can be described by Poisson's law with an average value of k if, for the independent variable, we take the value $Q(2E_0)/N(2E_0)$, where $N(2E_0) = \bar{Q}(2E_0)$ is the average number of pairs with energy $> \epsilon$. The factor k depends, in general, on E_0, ϵ, and t. For $\epsilon = 1 - 10$ Mev, and $E_0 = 10^{10} - 10^{13}$ ev, we can take $k = 3$ for the depth $1.0\,t_0$ and $k = 6$ for the depth $1.5\,t_0$.

The standard deviations of the number of pairs at the depth t in a shower produced by two electrons can, therefore, be calculated from the relation $\sigma = N/\sqrt{k}$.

The integral energy spectrum of pairs produced at a depth $\leq 1.5\,t_0$ in the three showers D-84, O-209, and E-53 is shown in Fig. 6. In the calculation, the data have been averaged for one primary electron. Theoretical curves correspond to a logarithmic mean energy of primary electrons $E_0 = 8.3 \times 10^{11}$ ev. Analogous results for three showers with energy $E_\gamma \sim 3 \times 10^{11}$ ev (D-44, I-109, and α-79) are given in Fig. 7. Theoretical curves are calculated for the energy $E_0 = 1.5 \times 10^{11}$ ev.

The comparison of experimental and theoretical results has been carried out only for the number and energy spectra of pairs, but not for electrons. This was because of the following reasons: according to the calculations carried out by us,[1,2] the difference between the two variants of the calculations

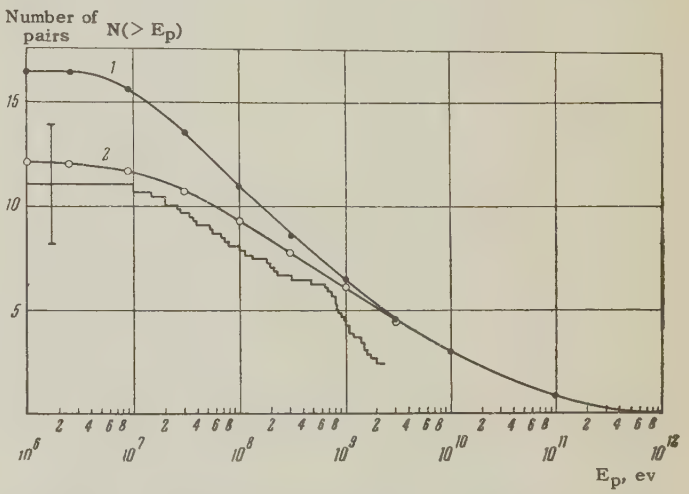

FIG. 6. Integral energy spectrum of electron-positron pairs produced on the average at a depth $\leq 1.5\,t_0$ in showers D-84, E-53, and 0-209 per primary electron. 1 – calculated curve in the B-H variant for $E_0 = 8.3 \times 10^{11}$ ev; 2 – the same in the M variant.

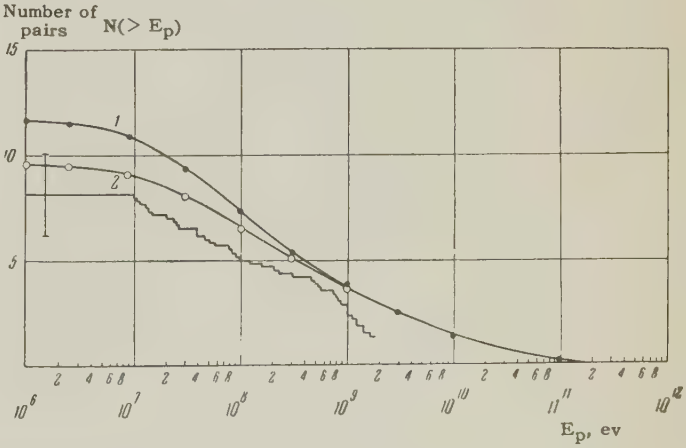

FIG. 7. Same as Fig. 6, but for showers α-79, I-109, and D-44; $E_0 = 1.5 \times 10^{11}$ ev.

*The authors are grateful to Dr. E. Fenyves and Prof. V. Petrzilka for supplying data on this shower.[31]

B-H and M is markedly greater for the spectrum of pairs than for the spectrum of electrons, at the same finite depth.

Moreover, more reason exists for using the results of the one-dimensional calculations for pairs rather than for electrons. As a result of scattering, the length of the low-energy electron path can be substantially different from the path along the shower axis t, which has not been taken into account in the calculations.[1,2] Finally, experimental errors in detecting pairs are much smaller than for single electronic tracks in the section t_i. Slow electrons reaching a given depth can, because of scattering, be found at considerable distances from the shower axis. As a result, the tracks may be missed in scanning. The probability of such omissions is considerably lower when detecting pairs. It is also much simpler to exclude background tracks which are not related to the shower in scanning for pairs.

It follows from the study of the radial distribution of pair vertices in showers that the pairs are mainly concentrated in the region of small ρ ($\lesssim 10\mu$). The mean value of ρ decreases with increasing E_γ. Consequently, the largest experimental errors due to the omission of pairs belonging to the shower should occur in the study of showers with the smallest values of E_γ (in our case $\sim 10^{11}$ ev). However, the number of pairs satisfying an accepted selection criterion in five showers with energy of $\sim 10^{11}$ ev (see Figs. 4 and 5), are at least not smaller than the theoretically expected number. This indicates the absence of systematic negative experimental errors. One can consider that the experimental errors are at least such that they do not lead to a marked lowering of the total number of pairs as compared with statistical errors.

As can be seen from Figs. 4 — 7, the experimental points are concentrated close to curve 2, which takes the effect of the medium on radiation into account. A statistical analysis of the results shown in Figs. 4 and 5 has been carried out in order to obtain some quantitative estimate of the deviation of the experimental data from curves 1 and 2, using various significant criteria. Only the data for showers with energy $E_\gamma > 1.8 \times 10^{11}$ ev have been used. In the first type of analysis, the sign of the deviation of the experimental points from curve 1′ in Figs. 4 and 5 has been taken into account. The values of the probabilities that, for a given point distribution, the curve 1′ is really the median curve, is given in Table III.

The deviations have been assessed by the χ^2 criterion. The statistical distribution of the compared values around theoretical averages y should, in such a case, follow a normal law. In order that this condition be satisfied, it is necessary to compare the experimental values N_i averaged over groups of two to three showers (see Figs. 4 and 5).

TABLE III. Results of a statistical analysis of the data on the number of pairs in showers (in percent)

Method of analysis and criterion	Neglecting errors in E_0		Taking errors in E_0 into account	
	B-H	M	B-H	M
Analysis of the error sign				
$1.0t_0$	32	—	—	—
$1.5t_0$	3.9	—	—	—
$1.0t_0 + 1.5t_0$	3.1	—	—	—
χ^2-criterion				
$1.0t_0$	3.5	90	4	90
$1.5t_0$	6.7	83	11	86
$1.0t_0 + 1.5t_0$	1.2	96	4	96
U-criterion				
$1.0t_0$	0.4	—	0.7	—
$1.5t_0$	1.1	—	1.3	—

In the beginning, let us assume that the errors of the measurements of E_γ can be neglected. The results for each of the showers are independent of each other, and we can therefore consider them as samples from a general set of theoretically possible values N for chosen (fixed) values $x = \ln E_0$. According to the addition theorem for the χ^2 distribution for m experimental (group) values of N_i, the sum of χ^2 can be written as

$$\chi^2 = \sum_{i=1}^{m} \left(\frac{N_i - y(x_i)}{\sigma_i} \right)^2,$$

where N_i is the average experimental group value of the number of pairs, $y(x)$ is the theoretical curve, and σ_i are the standard deviations of the theoretically possible values N_i from $y(x_i)$. Since $y(x)$ and σ_i are known, the sum has m degrees of freedom.

In order to take the errors in the measurements of E_0 into account, the results of the confluent analysis[32] carried out by Klepikov and Sokolov[33] have been used. The errors of E_0 and N_i can be regarded, in first approximation, as non-correlated. The theoretical curves $y(x)$ can, with good accuracy, be approximated over each segment by a straight line, so that $y'' = 0$. The sum of χ^2 can then be represented as

$$\chi^2 = \sum_{i=1}^{m} \frac{[N_i - y(x_i)]^2}{\sigma_i^2 + (y'\delta_i)^2},$$

where δ_i are the errors of $(\ln E_0)_i$. The probability that the resulting value of the sum of χ^2 is not smaller than the observed value, assuming the

correctness of the curves 1 and 2, respectively, is given in Table III.

Finally, an analysis was carried out averaging the results at one point (U-criterion[32]). The averaging was carried out in coordinates N, ln E_0. Data on the number of pairs in 11 showers at the depth of $1.0\,t_0$ and in 12 showers at the depth of $1.5\,t_0$ ($E_\gamma > 1.8 \times 10^{11}$ ev) have been used. The relative deviations $u = [\bar{N} - y(\bar{E})]/\sigma_{av}$ were determined, and corresponding deviations calculated taking into account the errors of E_0

$$u = \frac{\bar{N} - y(\bar{E})}{\sqrt{\sigma_{av}^2 + (\delta_{av} y')^2}},$$

where σ_{av} is the statistical error of the average number of pairs $\bar{N}$, $y(\bar{E})$ is the theoretically expected value of the average, and δ_{av} is the statistical error of the average value of ln E_0. Data given in Table III represent the probability that, in the present experiment, the values of u will not be smaller than the observed values.

The above statistical analysis of the results, carried out using three significant criteria, points to the incorrectness of curve 1. At the same time, a contradiction with curve 2 is not discovered. Thus, one can assume that at least a qualitative proof of the influence of the medium on bremsstrahlung has been obtained. For a quantitative test of the Migdal formulas, it is necessary to increase the statistical material. The experimental possibilities, together with the results of the calculations,[2] justify considering the above-described method of analyzing electron-photon showers as one of the most suitable ones for a further study of the effects of the medium on bremsstrahlung of high-energy electrons.

In conclusion, the authors express their gratitude to D. M. Samoĭlovich and her collaborators for developing the emulsion stacks, to I. A. Svetlolobov for help in reducing the calculated data, and to laboratory assistants A. A. Kondrashina and V. S. Balova for taking part in the scanning and analysis of the showers.

[1] Varfolomeev, Golenko, and Svetlolobov, Dokl. Akad. Nauk SSSR **122**, 785 (1958), Soviet Phys.-Doklady **3**, 977 (1959).

[2] A. A. Varfolomeev and I. A. Svetlolobov, JETP **36**, 1771 (1959), Soviet Phys. JETP **9**, 1263 (1959).

[3] L. D. Landau and I. Ya. Pomeranchuk, Dokl. Akad. Nauk SSSR **92**, 535, 735 (1953).

[4] M. I. Ter-Mikaelyan, Dokl. Akad. Nauk SSSR **94**, 1033 (1954).

[5] A. B. Migdal, JETP **32**, 633 (1957), Soviet Phys. JETP **5**, 527 (1957); Phys. Rev. **108**, 1811 (1956).

[6] Schein, Haskin, and Glasser, Phys. Rev. **95**, 855 (1954).

[7] Debenedetti, Garelli, Tallone, Vigone, and Wataghin, Nuovo cimento **12**, 954 (1954); **2**, 220 (1955).

[8] M. Koshiba and M. F. Kaplon, Phys. Rev. **97**, 193 (1955); **100**, 327 (1955).

[9] A. Debenedetti, C. M. Carelli, et al., Nuovo cimento **3**, 226 (1956).

[10] Barbanti-Silva, Bonacini, de Petri, Jori, Lovera, Perilli-Fedeli, and Roveri, Nuovo cimento **3**, 1465 (1956).

[11] Miesowicz, Stanisz, and Wolter, Bull. Acad. Polon. Sci. CLIII **4**, 811 (1956); Nuovo cimento **5**, 513 (1957).

[12] Debenedetti, Garelli, Tallone, and Vigone, Nuovo cimento **4**, 1151 (1956).

[13] K. Pinkau, Nuovo cimento **3**, 1285 (1956).

[14] H. Fay, Nuovo cimento **5**, 293 (1957).

[15] G. Wataghin, Proc. of the Sixth Rochester Conf. **9**, 24 (1956).

[16] Varfolomeev, Gerasimova, Gurevich, et al., Proc. of the 1958 Ann. Rochester Conf. on High Energy-Physics at CERN, Appendix I, p. 297.

[17] Varfolomeev, Gerasimova, Makar'ina, Romantseva, and Chueva, JETP **36**, 707 (1959), Soviet Phys. JETP **9**, 495 (1959).

[18] V. V. Guzhavin and I. P. Ivanenko, Dokl. Akad. Nauk SSSR **115**, 1089 (1957), Soviet Phys.-Doklady **2**, 407 (1958); Nuovo cimento **8**, Suppl. 2, 749 (1958).

[19] L. L. Eyges and S. Fernbach, Phys. Rev. **82**, 23, 287, 288 (1951).

[20] L. Janossy and H. Messel, Proc. Roy. Irish Acad. **A54**, 217 (1951).

[21] A. E. Chudakov, Izv. Akad. Nauk SSSR, Ser. Fiz. **19**, 651 (1955), Columbia Tech. Transl. p. 589.

[22] G. Yekutieli, Nuovo cimento **5**, 1381 (1957); I. Mito and H. Ezawa, Progr. Theor. Phys. **18**, 437 (1957).

[23] G. H. Burkhardt, Nuovo cimento **9**, 375 (1958).

[24] W. Wolter and M. Miesowicz, Nuovo cimento **4**, 648 (1956).

[25] J. Iwadare, Phil. Mag. **3**, 680 (1958).

[26] B. Rossi, High-Energy Particles (Prentice Hall Inc., New York, 1952), Russ. Transl. IIL 1955.

[27] L. Voyvodic and E. Pickup, Phys. Rev. **85**, 91 (1952).

[28] A. Borselino, Phys. Rev. **89**, 1023 (1953).

[29] M. Stearns, Phys. Rev. **76**, 836 (1949).

[30] A. G. Expong, Ark. Fysik **9**, 49 (1955).

[31] Pernegr, Petrzilka, Sedlak, and Vrana, Proc.

of the Working Meeting on Physics of High-Energy Particles in Liblice (near Prague), 1958.

[32] A. Hald, Statistical Theory with Engineering Applications (John Wiley and Sons, Inc., New York, 1952), Russ. Transl. IIL 1956.

[33] N. P. Klepikov and S. N. Sokolov, Теория вероятн. (Theory of Probability) 2, 470 (1957).

Translated by H. Kasha
7

MAGNETIC STRUCTURE OF SMALL MONOCRYSTALLINE PARTICLES OF MnBi *ALLOY*

Ya. S. SHUR, E. V. SHTOL' TS, and V. I. MARGOLINA

Institute of Metal Physics, Academy of Sciences, U.S.S.R.

Submitted to JETP editor July 16, 1959

J. Exptl. Theoret. Phys. (U.S.S.R.) **38**, 46-50 (January, 1960)

The magnetic structure of particles of manganese-bismuth alloy of various sizes (from 100 down to a few microns) has been studied by the powder-pattern method. It was observed that with decrease of particle size, the magnetic structure changed in a systematic manner. In particles of a few microns or less in size, single-domain magnetic structure was observed.

1. INTRODUCTION

LANDAU and Lifshitz[1] showed theoretically that in ferromagnetic crystals there should exist a multidomain magnetic structure, with the magnetization vectors in different domains oriented along axes of easy magnetization. Furthermore this deduction has been verified experimentally. From very general theoretical considerations it follows that in small monocrystalline ferromagnetic particles, a single-domain magnetic structure is to be expected.[2,3] This single-domainedness should set in when the dimensions of the ferromagnetic crystal are such that a breaking up into domains no longer produces a decrease of the energy of the crystal. In the study of ferromagnetic powders, trends have in fact been observed that could be explained only on the assumption that on passage to fine particles, a single-domain structure comes into existence.[4] However, the single-domain structure has not hitherto been observed by a visual method. The aim of the present work was the observation and study of single-domain magnetic structure by the powder-pattern method.

According to the theoretical estimates of Kittel[2] and Kondorskiĭ,[3] in the common ferromagnetics a single-domain structure should appear at particle dimensions of order 10^{-5} to 10^{-6} cm. In the study of magnetic structure by the powder-pattern method, however, it is desirable to make the observations on comparatively large particles. The critical particle size, below which single-domain structure occurs, depends on the values of the magnetic anisotropy constant and of the magnetic saturation. Specifically, this size increases with increase of the magnetic anisotropy constant, since the latter contributes to increase of the wall energy and consequently to increase of the difficulty of wall creation by breaking up the ferromagnetic into domains. Decrease of the critical size with increase of the value of the magnetic saturation comes about because of the increase of the magnitude of the magnetic charges, whose energy is decreased upon creation of a domain structure. On the basis of these relations, we chose for study the alloy MnBi. This alloy possesses, at room temperature, the largest value of the anisotropy energy among all known ferromagnetics and a comparatively small magnetic saturation; consequently, the single-domain structure in this alloy should occur at comparatively large particle sizes.

2. SPECIMENS STUDIED AND OBSERVATION METHOD

The specimens studied had a cylindrical shape and were obtained by sintering pressed powders of manganese and bismuth at temperatures from 280 to 360° C. At the time of sintering there were formed separate (and mostly monocrystalline) grains of MnBi alloy, isolated from one another by layers made up of bismuth and manganese that had not reacted. The size of these grains varies with the conditions of preparation (temperature and duration of sintering) from a few microns to hundreds of microns. The specimen surface to be studied was prepared by mechanical grinding and subsequent polishing with velvet. To obtain powder patterns, a magnetic suspension prepared by Elmore's[5] method was used. Observations of the powder patterns were made with a type MP-5 microscope. Magnetization of the specimen was accomplished with an electromagnet, at fields up to 24,000 oe. In the observation of the powder patterns, and especially when they were being photographed, it proved necessary that the microscope, specimen, and electromagnet form a single unit. Therefore the specimen was clamped between the

poles of the electromagnet, and the microscope tube was attached to the core of the electromagnet by means of a horizontal movable platform. Since the observations were made in strong magnetic fields, all metal parts of the optical apparatus (microscope, opaque-illuminator, and condenser) were made of nonferromagnetic materials.

3. RESULTS OF THE OBSERVATIONS AND THEIR ANALYSIS

a) Multidomain magnetic structure. In observations of powder patterns on the surfaces of the majority of the crystals, with various crystallographic orientations of the surface, it was observed that in particles of size greater than 50 μ, as a rule, multidomain structure was present. The form of the powder patterns was related in a systematic way to the crystallographic orientation of the specimen surface. The alloy MnBi, as is known, has a hexagonal structure at room temperature; it is therefore a uniaxial ferromagnetic. Consequently, if the hexagonal axis (the axis of easy magnetization) of a crystal of MnBi alloy was parallel to the surface of the specimen or made a small angle with it, then walls were formed on the surface between domains with antiparallel orientations of the magnetization. A view of such a magnetic structure is shown in Fig. 1a. The orientation of the magnetization in the domains is shown by arrows. On application of a magnetic field parallel to the axis of easy magnetization and on increase of it, the process of wall displacement is observed; domains in which the magnetization vector is parallel to the direction of the field absorb domains with antiparallel orientation of the magnetization (Figs. 1b and 1c). In a sufficiently strong field the regions with antiparallel orientation of the magnetization disappear, and the whole crystallite is magnetized uniformly (Fig. 1d). On diminution of the magnetic field, there appear regions with magnetizations oriented antiparallel to the field, and their volume increases. When the external field is zero, the domain-structure picture shown in Fig. 1a is observed; that is, the particle is demagnetized (its remanent magnetization is very small). The further process of reverse magnetization proceeds by wall displacement; that is, by diminution of the volume of regions with unfavorably oriented magnetization.

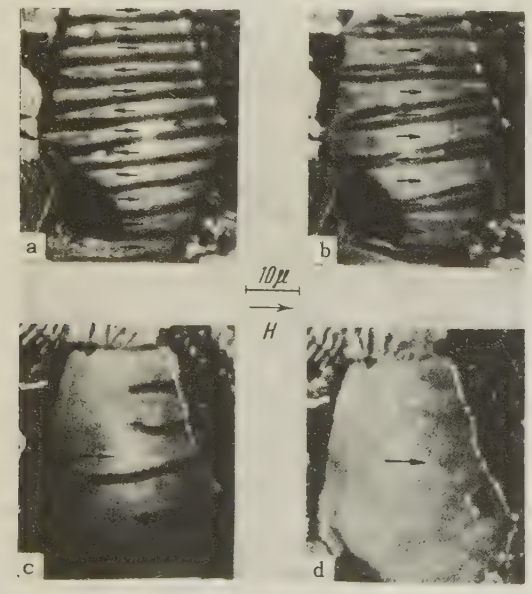

FIG. 1. Powder patterns on a particle with multidomain structure, in magnetic fields: a) H = 0; b) H = 1400; c) H = 3200; d) H = 7400 oe. The hexagonal axis makes a small angle with the observation plane.

If the specimen surface is close to the surface perpendicular to the hexagonal axis, then there appears a magnetic structure in the form of "stars" (Fig. 2). It may be assumed that the "stars" appear at points of termination of basic and closure domains on the crystal surface.

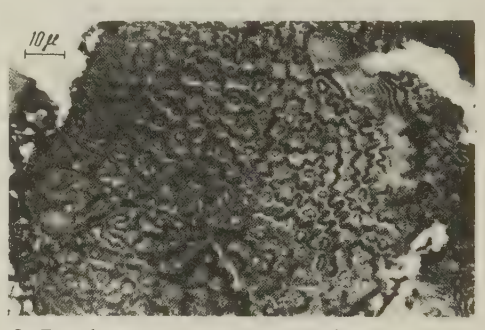

FIG. 2. Powder patterns on a particle with multidomain structure. The hexagonal axis makes an angle of nearly 90° with the observation plane.

The magnetic structures shown in Fig. 1a and in Fig. 2 have been observed in all uniaxial ferromagnetic crystals that have been studied (cobalt,[6] manganese antimony,[7] barium ferrite[8]). Thus in comparatively large crystals of MnBi alloy, there is observed a magnetic structure that is present in all magnetically uniaxial ferromagnetics.

b) Single-domain magnetic structure. In the investigation of the form of the powder patterns in finer monocrystalline particles of the MnBi alloy, it was established that in particles of size a few microns and below, the presence of a single-domain structure could sometimes be observed. The emergence of this structure could be shown by the peculiar form of the powder deposit and its behavior under the influence of a magnetic field. In such particles, for arbitrary changes of the magnetic field, it is impossible to observe a breaking up of the particle into separate domains. If the hexagonal axis of the crystal (the direction of easy magnetization) lies in or makes a small

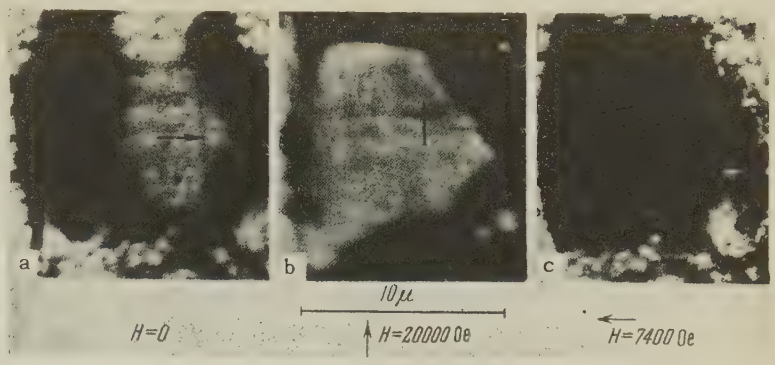

FIG. 3. Picture of the powder deposition on a particle with single-domain structure in a magnetic field. The hexagonal axis makes a small angle with the observation plane.

angle with the specimen surface, then the magnetic powder collects at the edge of the particle where the poles are located. A view of such a magnetic structure is shown in Fig. 3a, where the powder collects at the left and right edges of the particle. If the particle under study is placed in a magnetic field oriented perpendicular to the direction of easy magnetization, then there is observed a displacement of the powder collected at the crystallite edges, in proportion to the strength of the field; this indicates a rotation of the magnetization vector under the influence of the magnetic field. In a strong field, as is clear from Fig. 3b, the powder collects at the upper and lower edges of the particle. This shows that the magnetization vector J_S in the particle is directed parallel to the external field. The property of single-domain structure is displayed also when the particle under study undergoes magnetization reversal in a direction parallel to the axis of easy magnetization (or its projection on the specimen surface). Thus on application of a field oriented antiparallel to the direction of the J_S of the particle, and on gradual increase of it, the powder, which in the initial state was at the edge of the particle, begins gradually to spread over the whole surface of the crystal. In Fig. 3c is shown a view of such a powder distribution in a demagnetizing field of 7400 oe. On further increase of the field, there occurs an instantaneous displacement of the powder to the edges of the crystal. The powder behavior described is caused by the fact that under the influence of the field, there occurs a rotation of the magnetization vector through 180°. In the course of this rotation there appears a vertical component of magnetization, which causes a spreading of the powder over the whole surface of the crystal. The field at which there occurs a displacement of the powder from the middle to the edges of the crystal corresponds to an irreversible rotation of the magnetization vector and is close to the coercive force of the particle. In the present case it amounts to thousands of oersteds. (In the case of the displacement process, the coercive force amounts to hundreds of oersteds.) Thus in MnBi alloy, in particles of the size of a few microns and below, there can occur a single-domain magnetic structure which is preserved in the process of magnetization reversal of the crystal.

c) Intermediate magnetic structure. Of considerable interest are particles of MnBi alloy whose size is a little larger than the critical size. In this case it is possible to produce either conditions under which the process of magnetization reversal of a particle will be accomplished by the usual method, i.e., by formation of nuclei of reversed magnetization and by wall displacement, or other conditions such that the process of magnetization reversal will occur by rotation of the vector magnetization (cf. Fig. 3). Thus, for example, in one of the crystals studied, by choice of the size of the magnetic field* used for initial magnetization of the particle, conditions were produced under which the process of magnetization reversal proceeds variously as follows:

1. The particle is magnetized in a field of 5000 oe. In this field the whole powder collects at the edges of the crystal, which indicates a uniform magnetization of the particle (particle magnetized to saturation). On diminution of the field, closure domains appear; they grow and are converted to domains with antiparallel orientation of the magnetization. In the state of remanent magnetization, the crystal is broken up into several regions with antiparallel orientations of the magnetization. On change of sign of the field, the process of magnetization reversal of this particle occurs by wall displacement, as in an ordinary ferromagnetic with multidomain structure.

2. The particle is magnetized in a field of 20,000 oe. In this case the single-domain magnetic structure is preserved both on diminution of the field and on change of its sign. In a field of 20,000 oe, the magnetic powder collects at the edges of the crystal. Decrease of the field causes a movement of the powder on to the whole surface of the crystal.

*A similar case was treated in detail in reference 9.

After change of the sign of the field and increase of it to 4000 oe, the whole surface is uniformly covered with powder. Upon a further small increase of the field, there occurs an instantaneous clearing of the particle surface, as the powder again collects near the particle edges. Such a movement of the powder is possible if the magnetization-reversal process under observation occurs by rotation of the magnetization vector.

Thus a strong magnetic field can in some cases completely eliminate the possibility of formation of nuclei of reversed magnetization in the process of change of magnetization around a hysteresis loop. Nuclei of reversed magnetization can be formed anew by certain treatments of the crystal, for example by commutation of a constant magnetic field of decreasing amplitude.

The intermediate magnetic structure under consideration is apparently not the only one possible. However, it may be assumed that in all intermediate magnetic structures, the conditions for formation and growth of nuclei of reversed magnetization play a large part.

d) Irreversible reorganization of the magnetic structure on change of temperature. On change of temperature there is to be expected a reorganization of the magnetic structure, and this may be in part irreversible. This irreversibility of the change of magnetic structure shows up especially graphically in crystals of MnBi alloy whose sizes are close to the critical. At room temperature such a crystal has a single-domain structure (Fig. 4a), which is shown by accumulation of the powder at the edges of the crystal in zero field. If the crystal is cooled to the temperature of liquid nitrogen ($-196°$ C) and then heated to room temperature, thereafter a multidomain structure is observed on its surface. In Fig. 4b can be seen the deposition of powder at the walls between domains and on the edges of the crystal.

The result obtained can be understood if we take into account that the MnBi alloy at room temperature has a very large anisotropy constant, whose value decreases rapidly upon lowering of the temperature. The value of the saturation magnetization meanwhile changes very little. From this it follows (cf. Sec. 1) that on lowering of the temperature, there must be a decrease of the critical particle size at which the single-domain structure sets in. In consequence of this, the particle can become multidomain at a low temperature and can retain this structure on heating to room temperature. Irreversible reorganization of the domain structure on lowering of the temperature is also observed in crystals of MnBi alloy with multidomain and intermediate magnetic structures.

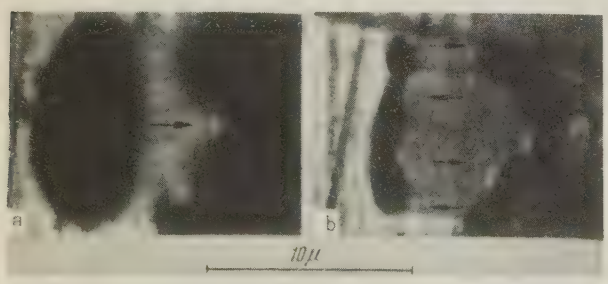

FIG. 4. Picture of the powder deposition on a particle: a) in the state of remanent magnetization; b) after a temperature cycle (+20, −196, +20 °C). The hexagonal axis makes a small angle with the observation plane.

4. CONCLUSION

Study of the magnetic structure of MnBi alloy has shown that crystals of size greater than 50μ are multidomain. The process of magnetization reversal in them occurs in the same way as in all magnetically uniaxial ferromagnetics.[6-8] In particles of the same alloy of size 15 to 10μ, it is possible in a number of cases to detect an intermediate magnetic structure. Magnetization reversal of such crystals, depending on the magnitude of the maximum magnetizing field, can occur either by wall motion or by irreversible rotation of the magnetization vector. In this case the single-domain structure, produced by a large field and retained on magnetization reversal, can be destroyed by commutation of a magnetic field of diminishing amplitude. In small particles of MnBi alloy (a few microns and below), a single-domain magnetic structure is observed. Such particles at room temperature do not break up into domains under any changes of the magnetic field. This single-domainedness can be destroyed by lowering the temperature, which causes a decrease of the critical size for the transition to single-domainedness at low temperatures. Thus the results presented in our work show that in monocrystalline particles of MnBi alloy, upon passage to small sizes, there occurs an essential change of form of their magnetic structure: instead of the multidomain structure, there appear an intermediate and a single-domain magnetic structure.

[1] L. D. Landau and E. M. Lifshitz, Physik. Z. Sowjetunion **8**, 153 (1935).

[2] C. Kittel, Phys. Rev. **70**, 965 (1946); Revs. Modern Phys. **21**, 541 (1949).

[3] E. I. Kondorskiĭ, Dokl. Akad. Nauk SSSR **70**, 215 (1950); **80**, 197 (1951); **82**, 365 (1952).

[4] E. V. Shtol'ts and Ya. S. Shur, Dokl. Akad.

Nauk SSSR **95**, 781 (1954); Ya. S. Shur, E. V. Shtol'ts, and G. S. Kandaurova, Izv. Akad. Nauk SSSR, Ser. Fiz. **21**, 1215 (1957), Columbia Tech. Transl. p. 1205; E. V. Shtol'ts, Ya. S. Shur, and G. S. Kandaurova, Физика металлов и металловедение (Physics of Metals and Metal Res.) **5**, 412 (1957).

[5] W. C. Elmore, Phys. Rev. **53**, 757 (1938).

[6] W. Andrä, Ann. Physik **15**, 135 (1954).

[7] R. Perthel and W. Andrä, Ann. Physik **19**, 265 (1957).

[8] Sixtus, Kronenberg, and Tenzer, J. Appl. Phys. **27**, 1051 (1956); C. Kooy, Philips Tech. Rev. **19**, 286 (1957-8).

[9] Ya. S. Shur, E. V. Shtol'ts, G. S. Kandaurova, and L. V. Bulatova, Физика металлов и металловедение (Physics of Metals and Metal Res.) **5**, 234 (1957).

Translated by W. F. Brown, Jr.
8

DETERMINATION OF MICROSCOPIC PARAMETERS OF ALUMINUM FROM ITS OPTICAL CONSTANTS AND ELECTRIC CONDUCTIVITY

A. I. GOLOVASHKIN, G. P. MOTULEVICH, and A. A. SHUBIN

P. N. Lebedev Physics Institute, Academy of Sciences, U.S.S.R.

Submitted to JETP editor July 17, 1959

J. Exptl. Theoret. Phys. (U.S.S.R.) 38, 51-55 (January, 1960)

The optical constants of aluminum were measured in the $0.8 - 9\,\mu$ range at room temperature and at liquid-nitrogen temperature. The static conductivity and density of the same specimens were also measured. The data obtained were evaluated by using a theory based on the quantum kinetic equations, which takes into account the electron-electron collisions. The concentration of the conduction electrons, the electron velocity on the Fermi surface, and the electron collision frequency were determined.

In the present investigation, which should be considered as a continuation of our research on metal optics,[1-3] we measured the optical constants of aluminum in the spectral region $0.8 - 9\,\mu$ at room temperature and at liquid-nitrogen temperature.

The present status of the theory, which relates the microscopic parameters of the metals with their optical constants,[4-6] calls for accounting for the electron-electron collisions and quantum corrections for the frequency of electron-phonon collisions. The method for reduction of the experimental data is detailed in a paper by one of the authors.[7] According to this method, the measurements of the optical constants must be supplemented by measurements of the specific static conductivity σ_0 at various temperatures.

The optical constants were determined at room temperature by the polarization method, described previously,[1] and at liquid-nitrogen temperature with the apparatus described in reference 8. Measurements were made on an aluminum layer obtained by evaporation in vacuum from a tungsten helix on polished glass. The initial aluminum was 99.99% pure. The measurements were made on mirrors with external reflection within the first few hours after sputtering. Specimens for the measurement of σ_0 and the density ρ were sputtered simultaneously with the mirrors.*

In measuring the quantities σ_0 and ρ, the thickness of the layer was determined by an interference method accurate to 1.5×10^{-6} cm. It has been found that by evaporation in vacuum it is easy to obtain aluminum layers with $\sigma_0 \approx 1.6 \times 10^{17}$ cgs esu* and $\rho \approx 2.0$ g/cm^3. With special choice of the distance from the sputterer to the specimen, of the temperature, and of the sputtering rate, it is possible to obtain mirrors with $\sigma_0 \approx 2.2 \times 10^{17}$ cgs esu and $\rho \approx 2.4$ g/cm^3. For bulk metal $\sigma_0 = 3.1 \times 10^{17}$ cgs esu and $\rho = 2.7$ g/cm^3.

The measurement of the optical constants of the mirrors with different σ_0 and ρ have shown that a reduction in σ_0 and ρ leads to a reduction in κ and to an increase in n, where $n - i\kappa$ is the complex index of refraction; the change in κ is small, but the change of n is considerable.†

Table I shows the results obtained for the optical constants of aluminum mirrors, characterized by values $\sigma_0 = 2.2 \times 10^{17}$ cgs esu and $\rho = 2.4$ g/cm^3. The table also lists, for comparison, the data of Beattie,[9] obtained at room temperature. A comparison of these data shows that our values of n are lower than those of Beattie. Apparently this discrepancy is explained by the lower value of the conductivity of the mirrors used by Beattie ($\sigma_0 = 1.5 \times 10^{17}$ cgs esu). A comparison of our values of κ with those of Beattie[9] shows that these data are in good agreement up to $5\,\mu$. In the further region Beattie's values of κ are somewhat lower, and they still can be explained by the lower values of the conductivity. Unfortunately we could not

*The density ρ does not enter into the calculation formulas. It is needed, however, for evaluating the number of conduction electrons per atom.

*The low value of σ_0 is not due to the small thickness of the aluminum layers. The layers used for the measurements were of the order of 0.45μ, which is 30 times greater than the mean free path of the electrons. In all probability, this is due to the more finely dispersed structure of the sputtered layers compared with the ordinary polycrystalline materials.

†Aluminum exhibits an anomalous effect in the region of the spectrum we have investigated. In this case n and $\varkappa$ must be taken to mean their effective values;[3] we shall leave out the subscripts "eff."

TABLE I. Optical constants of aluminum*

λ μ	n			κ			$10^3 \cdot 4n/(n^2+\kappa^2)$		$10^2 \cdot 4\kappa/(n^2+\kappa^2)$		$\lambda \cdot 4\kappa/(n^2+\kappa^2)$	
	T=295		78	295		78	T=295	78	295	78	295	78
	P.W.	B	P.W.	P.W.	B	P.W.						
0.8	1.12	—	0.83	6.0	—	6.0	12.0	10.9	64.2	65.5	0.514	0.524
0.9	1.05	—	0.75	7.0	—	7.0	8.4	6.0	55.8	56.4	0.504	0.507
1.2	0.95	—	0.63	9.6	—	9.6	4.09	2.72	41.4	41.5	0.495	0.500
1.5	1.14	—	0.78	12.1	—	12.1	3.09	2.12	32.8	32.9	0.492	0.494
2.0	1.75	2.30	1.30	16.1	16.5	16.1	2.67	2.00	24.5	24.6	0.490	0.492
2.5	2.4	3.22	1.7	19,8	20.3	19.8	2.41	1.72	19.9	20.0	0.497	0.500
3.0	3.2	4.41	2.2	23.5	24.2	23.5	2.28	1.58	16.7	16.8	0.500	0.506
4.0	4.8	5.97	3.2	30.0	30.3	30.1	2.08	1.40	13.0	13.1_5	0.520	0.526
5.0	6.7	8.19	4.4	37.6	36.8	37.8	1.84	1.22	10.3_5	10.4	0.520	0.520
6.0	9.5	11.0	6.5	44.4	42.4	44.9	1.84	1.26	8.6	8.7	0.516	0.522
7.0	12.6	14.6	9.1	51.0	49.0	52.0	1.83	1.31	7.4	7.5	0.518	0.524
8.0	15.6	17.0	—	58.1	55.0	—	1.73	—	6.4	—	0.515	—
9.0	21.1	21.1	—	62.1	61.3	—	1.95	—	5.7_5	—	0.517	

*The symbols used here are: λ – wavelength of light in microns, P.W. – present work, B – data of Beattie.[9] The temperature is in degrees Kelvin.

make an analogous comparison with the results of Hodgson,[10] since it does not contain numerical values of n and κ.

A comparison of the data at room temperature and temperature of liquid nitrogen shows, as expected, that κ remains almost constant with temperature, whereas n is substantially reduced.

The reduction of the experimental data, obtained both at room temperature and at liquid-nitrogen temperature, was based on formulas (3) and (11) of reference 7 and the method of successive approximations. It was found here that the third approximation differed from the second by less than 1%.

TABLE II. Microscopic characteristics of aluminum

T, °K	295	78
$N \cdot 10^{-22}$, cm^{-3}	7.4	7.1
N/N_a	1.3_8	1.3_3
$\nu_0^{ee} \cdot 10^{-12}$, sec^{-1}	3.8	0.19
$\nu_0^{ef} \cdot 10^{-13}$, sec^{-1}	6.3	1.2
$\nu^{ef} \cdot 10^{-13}$, sec^{-1}	7.7	3.9
$\nu^{imp} \cdot 10^{-13}$, sec^{-1}	1.3	1.3
$v \cdot 10^{-8}$, cm/sec	2.8	2.5

The results of the reduction of our experimental data are listed in Table II. Here N is the concentration of the conduction electrons, N_a the concentration of the aluminum atoms, ν_0^{ee} the classical frequency of the electron-electron collisions for $\hbar\omega \ll kT$, ν_0^{ef} the classical frequency of the electron-phonon collisions for $\hbar\omega \ll kT$, ν^{ef} the frequency of collisions between electrons and phonons for the near infrared region, ν^{imp} the frequency of electron-impurity collisions, and v the electron velocity on the Fermi surface.

According to the results obtained by Gurzhi[4] $\nu^{ef} = \nu_0^{ef}\varphi(T)$. The function $\varphi(T)$ was also calculated by Gurzhi.[11] For aluminum, the Debye temperature is $\Theta = 398°K$,[12] and therefore $\varphi(T) = 1.22$ when $T = 295°K$. When $T = 78°K$, the value of ν^{ef} reaches its practical limit, 1.2×10^{13} sec^{-1}. Since a further reduction in temperature does not change ν^{ef} for aluminum, we did not deem it necessary to perform measurements at lower temperatures.

The error in the determination of microscopic characteristics of aluminum was 5% for N, 10% for ν_0^{ee}, 30% for v at room temperature, and 20% for v at liquid-nitrogen temperature. The great error in v is due to the fact that aluminum is subject to a weakly pronounced anomalous skin effect and the role of surface losses is small compared with that of volume losses. It must be noted that v should be determined from the value of σ_0 of the investigated mirrors. If the tabulated values are used, the resultant values of v are greatly overestimated.*

Comparison of the results for the microscopic parameters of aluminum, obtained at room temperature and at liquid-nitrogen temperature, shows that N and v hardly change with temperature. The temperature variation of ν_0^{ee} is much faster than the theoretically expected dependence, which is proportional to T^2.

As shown by Gurzhi,[5] the frequency of electron-electron collisions for a frequency ω is

$$\nu^{ee} = \nu_0^{ee}[1 + (\hbar\omega/2\pi kT)^2],$$

*In our earlier investigations[1,2] we did not measure the σ_0 of the sputtered specimens, but used the tabulated values. The values of v given in reference 2 are therefore overestimated.

and therefore the effective electron-collision frequency $\nu_{eff} = \nu^{ef} + \nu^{ee} + \nu^{imp}$ depends on the wavelength of the incident light λ. For $\lambda \approx 5\mu$ we have $\nu_{eff} \approx 0.9 \times 10^{14}$ sec^{-1} at T = 295°K and $\nu_{eff} \approx 0.6 \times 10^{14}$ sec^{-1} at T = 78°K.

Using the values obtained for ν_{eff} and v, we can estimate the mean free path of the electron l and the relaxation time τ.

For T = 295°K

$$l = v/\nu_{eff} \approx 3 \cdot 10^{-6} \text{ cm}, \quad \tau = 1/\nu_{eff} \approx 1.1 \cdot 10^{-14} \text{ sec},$$

for T = 78°K

$$l \approx 4 \cdot 10^{-6} \text{cm}, \qquad \tau \approx 1.7 \cdot 10^{-14} \text{ sec}.$$

The depth of the skin layer for aluminum, in the wavelength interval used by us, is $\delta = \lambda/2\pi\kappa \approx 2 \times 10^{-6}$ cm for both temperatures. We see that $l \sim \delta$, i.e., at both temperatures there is a weakly pronounced anomalous skin effect for aluminum.*

The expressions we employed to relate the optical constants of the metal with its microscopic parameters hold if the inequalities $v/\omega\delta \ll 1$, $\nu_{eff}/\omega \ll 1$, and $\omega \ll \omega_0$ are satisfied, where ω_0 is the limit of the internal photoeffect. That the first two inequalities are satisfied is readily verified. For $\lambda = 5\mu$ we have $v/\omega\delta \approx 0.37$ and $\nu_{eff}/\omega \approx 0.24$ at T = 295°K; and $v/\omega\delta \approx 0.33$ and $\nu_{eff}/\omega \approx 0.16$ at T = 78°K. That the third inequality is satisfied can be verified from the character of the λ-dependence of the quantities

$$N = 1{,}79 \cdot 10^{22} (1 + p^2 G)^2 / \lambda^2 \left(\frac{4\varkappa}{n^2 + \varkappa^2}\right)^2,$$

$$M = \frac{4n}{n^2 + \varkappa^2} + p^2 \beta D.$$

Figures 1 and 2 show the dependence of these quantities on λ in the interval $1.2 - 9\mu$ (the notation of reference 7 is used here). It is seen from the figures that N is independent of λ, and that the dependence of M in this interval coincides with the calculated curve, obtained when the electron-electron collisions are taken into account.

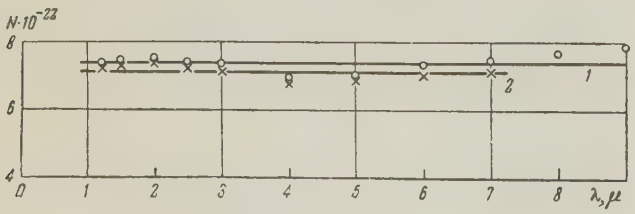

FIG. 1. Plot of N(λ): o – for T = 295°K, × – for T = 78°K.

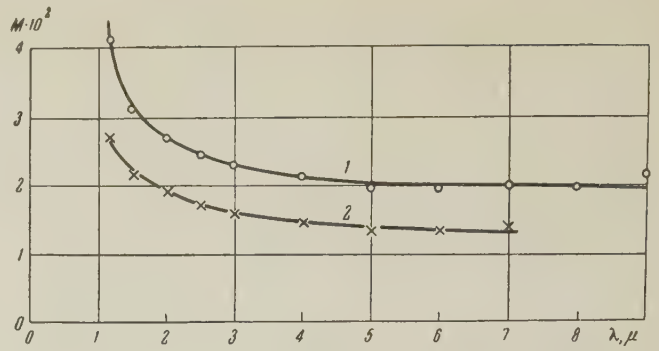

FIG. 2. Plot of M(λ): o – for T = 295°K, × – for T = 78°K.

We can therefore say that the measurements were carried out in the region where the third inequality is also satisfied.*

In the aforementioned paper by Beattie[9] no account was taken of the theory that allows for electron-electron collisions in the processing of the experimental data. Therefore Beattie reaches the erroneous conclusion that aluminum has in the region $2 - 5\mu$ an additional absorption, connected with the internal photoeffect. This conclusion has led Beattie to determine the microscopic parameters only from the results obtained in the $6 - 12\mu$ region. In this region the correction terms already become substantial: at $10 - 12\mu$ the correction terms reach 20 – 30% (the values of $v/\omega\delta$ and ν_{eff}/ω are close to unity). Therefore the accuracy of the corresponding formulas is reduced. Our own measurements and their reduction with allowance for the electron-electron collisions show that there are no additional absorption sources in this region, with the exception of those indicated above.

The value of ν_0^{ee} given above was obtained from optical measurements. This quantity cannot be determined with sufficient accuracy from the temperature dependence of σ_0, since the condition $T \gg \Theta$ cannot be realized.

Although there are no data at present on measurements of the electronic specific heat and surface impedance at radio frequencies, carried out on specimens identical with those used in the optical methods, there is nevertheless a certain interest in the comparison of the results known to us.

Measurements of the electron specific heat yields[13]

$$v/\sqrt{N} = (3{,}7 \cdot 10^{-3} - 4{,}1 \cdot 10^{-3}) \text{ cm}^{5/2} \text{ sec}^{-1}.$$

From optical measurements we obtain

$$v/\sqrt{N} = 9{,}8 \cdot 10^{-3} \text{ cm}^{5/2} \text{ sec}^{-1}.$$

*The values of v and ν^{imp} allow us to estimate the dimensions of the individual crystals of aluminum, obtained in thermal evaporation of the metal: $L \approx v\nu^{imp} \approx 3 \times 10^{-6}$ cm.

*As can be seen from Table I, M increases sharply in the region 0.8 – 0.9 μ. The corresponding absorption band is probably connected with the internal photoeffect.

Measurements of the surface impedance in the radio-frequency range yield[14]

$$v/N = 4.5 \cdot 10^{-15} \text{ cm}^4 \text{ sec}^{-1}.$$

Optical measurements for the same quantity yield

$$v/N = 3.7 \cdot 10^{-15} \text{cm}^4 \text{ sec}^{-1}.$$

In conclusion, the authors are deeply grateful to I. L. Fabelinskiĭ for a discussion of the present work.

[1] G. P. Motulevich and A. A. Shubov, Оптика и спектроскопия (Optics and Spectroscopy) **2**, 633 (1957).

[2] G. P. Motulevich and A. A. Shubin, JETP **34**, 757 (1958), Soviet Phys. JETP **7**, 520 (1958).

[3] V. L. Ginzburg and G. P. Motulevich, Usp. Fiz. Nauk **55**, 469 (1955).

[4] R. N. Gurzhi, JETP **33**, 660 (1957), Soviet Phys. JETP **6**, 506 (1958).

[5] R. N. Gurzhi, JETP **35**, 965 (1958), Soviet Phys. JETP **8**, 673 (1959).

[6] L. P. Pitaevskiĭ, JETP **34**, 942 (1958), Soviet Phys. JETP **7**, 652 (1958).

[7] G. P. Motulevich, JETP **37**, 1249 (1959), Soviet Phys. JETP **10**, 1770 (1960).

[8] Golovashkin, Motulevich, and Shubin, Приборы и техника эксперимента (Instrum. and Meas. Engg.), in press.

[9] J. R. Beattie, Phil. Mag. **46**, 235 (1955); Physica **23**, 898 (1957).

[10] J. N. Hodgson, Proc. Phys. Soc. **B68**, 593 (1955).

[11] R. N. Gurzhi, Dissertation, Phys.-Tech. Inst. Acad. Sci. Ukr. SSR, 1958.

[12] C. Kittel, Introduction to Solid State Physics, Wiley, N. Y., 1953.

[13] J. Eisenstein, Revs. Modern Phys. **26**, 277 (1954).

[14] E. H. Sondheimer, Adv. in Physics **1**, 1 (1952).

Translated by J. G. Adashko
9

CIRCULAR POLARIZATION OF INTERNAL BREMSSTRAHLUNG ACCOMPANYING K-CAPTURE IN Fe^{55}

V. P. PARFENOVA

Institute of Nuclear Physics, Moscow State University

Submitted to JETP editor July 17, 1959

J. Exptl. Theoret. Phys. (U.S.S.R.) 38, 56-59 (January, 1960)

The circular polarization of the internal bremsstrahlung accompanying K-capture in Fe^{55} was measured by scattering in magnetized iron. The technique of the measurements was based on the azimuthal dependence of the Compton scattering cross section of gamma quanta on polarized electrons. Within the limits of error 100 percent polarization of the bremsstrahlung quanta was obtained independent of the radiation energy.

INTRODUCTION

A consequence of parity nonconservation in beta decay is that internal bremsstrahlung accompanying electron capture must be circularly polarized.[1,2] The degree of circular polarization according to the two-component neutrino theory must be 100 percent independent of the energy of bremsstrahlung quanta (for not too low energies).[2] It can now be considered established that the beta-decay interaction has primarily the character of the V-A interaction.[3,4] The possible admixture of S-T interaction would reduce the degree of circular polarization of bremsstrahlung. This circumstance makes it possible to discover the admixture of S-T components in the beta-decay interaction.

Experiments measuring the circular polarization of internal bremsstrahlung accompanying K-capture were done with Ge^{71} and A^{37} in references 5 to 7. In the first case the degree of polarization was found to be much less than 100%, which, in the opinion of the authors, was connected with the presence of admixtures of extraneous radiation from the source. In measurements with A^{37}, 100% polarization of bremsstrahlung was obtained within the limits of error, and for the quantity $|C_T|^2/|C_A|^2$, characterizing the admixture of the T invariant, Miskel and Mann[6] give an upper limit of 8%. The present work measures the circular polarization of internal bremsstrahlung of Fe^{55} ($T_{1/2}$ = 2.6 years, transition energy 220 kev).

EXPERIMENTAL SETUP AND MEASUREMENTS

a. Polarimeter. The azimuthal dependence of the Compton scattering cross section of circularly polarized gamma quanta on polarized electrons was used for measuring the circular polarization. This method was first proposed by Beard and Rose[8] and used for investigation of circular polarization of gamma rays by Beltrametti and Vitale in reference 9. It is based on the fact that during scattering of circularly polarized gamma quanta on electrons whose spins are perpendicular to the direction of gamma ray propagation, anisotropy arises in the scattering cross section, depending on the direction of electron spin orientation. The scattering cross section for this case ($\mathbf{k}_0 \perp \mathbf{s}$, where $\mathbf{k}_0$ is the impulse of the primary photon and $\mathbf{s}$ is the electron spin) is

$$\sigma(\vartheta, \varphi) = \sigma_0 - P\frac{r_0^2}{2}\frac{k^2}{k_0^2}(1-\cos\vartheta)\,sk\sin\vartheta\cos\varphi$$
$$= \frac{r_0^2}{2}[\Delta_0 - P\Delta\cos\varphi].$$

Here ϑ is the scattering angle, φ is the angle between the planes $(\mathbf{k}_0\mathbf{k})$ and $(\mathbf{k}_0\mathbf{s})$, σ_0 is the usual Klein-Nishina cross section, and P is the degree of circular polarization ($P > 0$ for right circular polarization and $P < 0$ for left circular polarization[10]). Maximum relative azimuthal anisotropy was observed with the optimal angle of scattering ϑ_{max} which was obtained from the maximum condition Δ/Δ_0.[8-10]

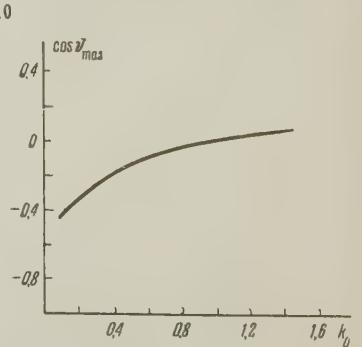

FIG. 1. The dependence on energy of the scattering angle for which the azimuthal anisotropy is maximal.

Figure 1 shows the dependence of ϑ_{max} on k_0, the energy of the primary radiation in units of mc^2.

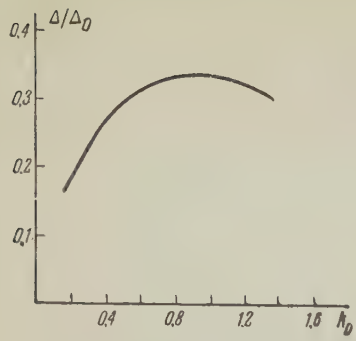

FIG. 2. The dependence on energy of the azimuthal anisotropy for the optimal scattering angle ϑ_{max}.

It is clear from the graph that if the gamma energy is $E_0 > 510$ kev, the optimal scattering angle $\vartheta_{max} < 90°$, but if $E_0 < 510$ kev, then $\vartheta_{max} > 90°$. The dependence of relative anisotropy Δ/Δ_0 for the optimal scattering angle on the energy of the primary gamma quanta is shown in Figure 2. For investigating radiation from Fe^{55} the scattering angle $\vartheta \sim 100°$ was chosen.

b. Source. The Fe^{55} source (~ 50 millicuries) was obtained by irradiating in a reactor target material enriched in the isotope Fe^{54} to 82.8%. Besides the isotope Fe^{55}, the isotopes Fe^{59} and Mn^{54} are formed; the latter is obtained through the reaction $Fe^{54}(n, p)Mn^{54}$. Since the yield of internal bremsstrahlung in K-capture is very small (for Fe^{55} the yield is $\sim 3 \times 10^{-5}$ quantum/decay)[11] the purity of the source is of particular significance. The chemical purification of the source from Mn^{54} was done in the chemical laboratory of the Institute.* The source (iron oxide) was then placed in a Plexiglas container. The measurements were begun 15 months after irradiation, which corresponds to ten Fe^{59} half lives ($T_{1/2} = 45$ days). The experimentally observed spectrum of bremsstrahlung is shown in Fig. 3 (N is the counting rate in arbitrary units).

FIG. 3. Spectrum of internal bremsstrahlung of Fe^{55}.

*Chemical purification was done by N. I. Mertts, to whom the author is grateful.

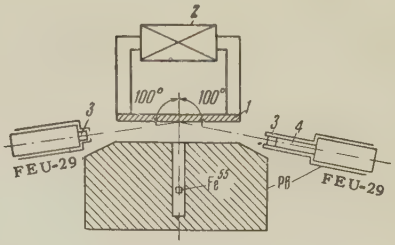

FIG. 4. Schematic diagram 1) permendur scattering disc, 2) magnetizing coil, 3) NaI(Tl) crystals, 4) light pipe.

c. Experimental Setup. Figure 4 shows schematically the experimental setup for measuring the circular polarization of gamma quanta. A disc of permendur which is part of a solid core magnet made of Armco iron serves as the scatterer. The induction in the permendur was 20 000 gauss. The scattered gamma quanta were analyzed by two scintillation spectrometers with FEU-29 photomultipliers and NaI(Tl) crystals. Using two scintillation spectrometers made it possible to increase the collecting power of the equipment by a factor of two. Shielding of the multiplier from the magnetic field of the scatterer was done with a permalloy shield and a three-layered iron shield around the photomultiplier. In addition, a light pipe 10 cm long was installed on one photomultiplier. Sources of Cs^{137} and Hg^{203} were used to check the magnetic shielding. For this a narrow discriminator window was set on the side of the photopeak, and the dependence of the counting rate on the direction of the current in the magnetizing coil was measured. Under these conditions the influence of the magnetic field was less than 0.3%.

d. Measurements and Results. A single-channel discriminator was used to detect a certain region of the spectrum of scattered radiation, and the number of scattered gamma quanta in both spectrometers was measured for opposite directions of the field (which was changed every 5 or 10 minutes). More than 10^5 pulses in each spectrometer were accumulated for the chosen direction of the field in order to obtain each point. The following magnitude was calculated: $\eta = 2(N_1 - N_2)/(N_1 + N_2 - 2N_0)$, where N_1 is the count in the spectrometer when the magnetic field is directed toward the counter, N_2 is the count for the opposite direction of the field, N_0 is the count without the scatterer (including background and direct gamma radiation through the lead shielding). In calculating η, in addition to corrections included in the quantity N_0, it is necessary to correct for scattered radiation caused by Fe^{59}. Since all the measurements take place in the region of soft gamma rays, it is difficult to separate scattered gamma radiation of Fe^{55} from scattered radiation of Fe^{59}. In order to determine the con-

	Energy region of primary gamma quanta, kev	N_1	N_2	Experimental value of η, %	Calculated value of η for 100% polarization, percent
FEU-1	85—110	107128	105886	2.6 ± 1.0	2.57
	110—140	160148	158206	2.9 ± 0.8	2.97
	140—175	119424	117842	3.3 ± 0.9	3.49
	175—220	195051	192054	4.0 ± 0.8	3.95
FEU-2	80—110	129736	128092	2.4 ± 0.7	2.57
	110—140	115960	114215	2.8 ± 0.8	2.98
	130—170	135647	133394	3.6 ± 0.8	3.49
	170—215	145955	143076	3.9 ± 0.8	3.94

tribution of scattering from Fe^{59} to the region of energies under consideration, the iron source was replaced by a Co^{60} source whose gamma-ray spectrum is similar to the Fe^{59} spectrum. In the hard part of the spectrum of scattered radiation where there are no gamma rays from Fe^{55} it is possible to normalize both sources and thus determine the contribution of Fe^{59} in the region of energies that is of interest to us. The results obtained are shown in the table and include corrections which are from 10 to 20% in various parts of the spectrum.

From the table it can be seen that, within the limits of error, the circular polarization does not, in accordance with theoretical expectations, depend on the energy of the radiation under investigation. Averaging all the determinations of P, we obtain $P = 0.98 \pm 0.10$.

The expression for the degree of circular polarization of internal bremsstrahlung accompanying K-capture according to the two-component theory has the following form:[2]

$$P(k) = p(k) \times \frac{\sum_f \{|\langle 1\rangle_{fi}|^2 (|C_V|^2 - |C_S|^2) + |\langle\sigma\rangle_{fi}|^2 (|C_A|^2 - |C_T|^2)\}}{\sum_f \{|\langle 1\rangle_{fi}|^2 (|C_V|^2 + |C_S|^2) + |\langle\sigma\rangle_{fi}|^2 (|C_A|^2 + |C_T|^2)\}},$$

where p(k) is a function depending on energy and is equal to 1 for not too low energies.

The transition under investigation, $Fe^{55} \rightarrow Mn^{55}$ ($3/2^- \rightarrow 5/2^-$), is a transition of the Gamow-Teller type and therefore the last expression reduces to

$$P = (|C_A|^2 - |C_T|^2) / (|C_A|^2 + |C_T|^2).$$

Hence, knowing P, it is possible to determine the admixture of the T variant in beta-decay interaction if we consider that this interaction is primarily axial-vector. From the data the upper limit of the admixture $|C_T|^2/|C_A|^2 \leq 6\%$ is obtained.

In conclusion I wish to take this opportunity to express my sincere gratitude to V. S. Shpinel' for his constant interest in this work.

[1] R. E. Cutkosky, Phys. Rev. **107**, 330 (1957).
[2] P. C. Martin and R. J. Glauber, Phys. Rev. **109**, 1307 (1958).
[3] Herrmannsfeldt, Maxson, Stähelin, and Allen, Phys. Rev. **107**, 641 (1957); Herrmannsfeldt, Burman, Stähelin, Allen, and Braid, Phys. Rev. Letters **1**, 61 (1958).
[4] Goldhaber, Grodzins, and Sunyar, Phys. Rev. **109**, 1015 (1958); Burgy, Krohn, Novey, Ringo, and Telegdi, Phys. Rev. Letters **1**, 324 (1958).
[5] Bernardini, Brovetto, Debenedetti, and Ferroni, Nuovo cimento **7**, 419 (1958).
[6] Mann, Miskel, and Bloom, Phys. Rev. Letters **1**, 34 (1958).
[7] G. Hartwig and H. Schopper, Z. Physik **152**, 314 (1958).
[8] D. B. Beard and M. E. Rose, Phys. Rev. **108**, 164 (1957).
[9] E. G. Beltrametti and S. Vitale, Nuovo cimento **9**, 289 (1958).
[10] H. Schopper, Nuclear Instr. **3**, 157 (1958).
[11] K. Siegbahn, Beta- and Gamma-Ray Spectroscopy (Russ. Transl.), Fizmatgiz, 1959, p 696 [North Holland, Amsterdam, 1955].

Translated by G. Gerhart
10

DEPENDENCE OF THE MAGNETIC STRUCTURE OF A COBALT CRYSTAL ON ITS SIZE

G. S. KANDAUROVA, Ya. S. SHUR, and F. V. MASLENNIKOVA

Ural' State University

Submitted to JETP editor July 17, 1959

J. Exptl. Theoret. Phys. (U.S.S.R.) **38**, 60-63 (January, 1960)

By means of powder patterns, the changes of magnetic structure of a cobalt monocrystal have been observed in the basal plane upon decrease of the crystal thickness from 515 to 15 μ. It has been established that at small thicknesses ($< 200\,\mu$) the domain width varies directly with the square root of the crystal thickness; at larger thicknesses some deviation from this rule is observed.

INTRODUCTION

As is known, the magnetic properties of ferromagnetics in many respects depend on their type of magnetic structure. Change of the type of magnetic structure of ferromagnetics leads to change of their magnetic properties.[1] The type of magnetic structure depends on many factors. In particular, for given physical properties of a ferromagnetic its type of magnetic structure is related to its geometrical dimensions. Upon passage to fine powders or to thin films, the decrease of size of a ferromagnetic leads to a simplification of the type of magnetic structure.[2,3] In very small particles, after attainment of a certain critical dimension, the magnetic structure becomes the simplest of all, transforming to a single-domain structure.

Change of the type of magnetic structure with change of size of the crystal should occur for two reasons: 1) In crystals in which the basic domains[4] pass through the whole thickness of the crystal, there exists the following definite relation between the thickness d of each basic domain and its length L (in the direction along which the magnetization is oriented): $d \sim \sqrt{L}$.[5] Therefore with decrease of L, the thickness of the domains will also decrease. 2) The shape and size of the closure domains is also related to the size of the basic domains. Therefore the structure of the closure domains will change systematically with decrease of size of the basic domains, especially in cases in which, because of the small dimensions of the ferromagnetic, the formation of closure domains is hindered.

The question of the change of magnetic structure with change of size of a ferromagnetic has been specifically studied only in the case of a triaxial ferromagnetic (silicon iron).[2] Similar investigation of magnetically uniaxially ferromagnetics has not been carried out; in the literature there are only fragmentary experimental data,[6-8] from which it is possible to conclude that somewha different magnetic structures are observed in thic and in sufficiently thin crystals of certain magnetically uniaxial materials (manganese-bismuth alloy, barium ferrite).

The object of our work was a study by a visual method (the powder-pattern method) of the chang of magnetic structure of a monocrystal of cobalt o progressive decrease of its thickness.

EXPERIMENTAL METHOD

The investigation was carried out on a monocry talline specimen in the form of a disk of diameter 4 mm and initial thickness 0.52 mm. The surface of the disk was parallel to the basal plane of the c balt crystal. The magnetic structure was observe on this plane by the powder-pattern method. The thickness of the disk-specimen was progressively decreased from 515 to 90 μ by mechanical grinding followed by electrolytic polishing. Further thinnin of the specimen to 15 μ was accomplished by mean of electrolytic etching alone. For electropolishing and etching, a 10% solution of chromic anhydride i orthophosphoric acid, of concentration 85%, was used.

For different thicknesses of the cobalt crystal, comparison was made of the powder-pattern pictures in the middle part of the specimen, where th thickness of the crystal was also determined by means of an optical indicator within an accuracy o 2 μ.

RESULTS OF THE OBSERVATIONS

Figure 1 shows photographs of powder patterns on the basal plane of a cobalt crystal for several specimen thicknesses. When the crystal thickness L is equal to 515 μ (Fig. 1a), there is a compli-

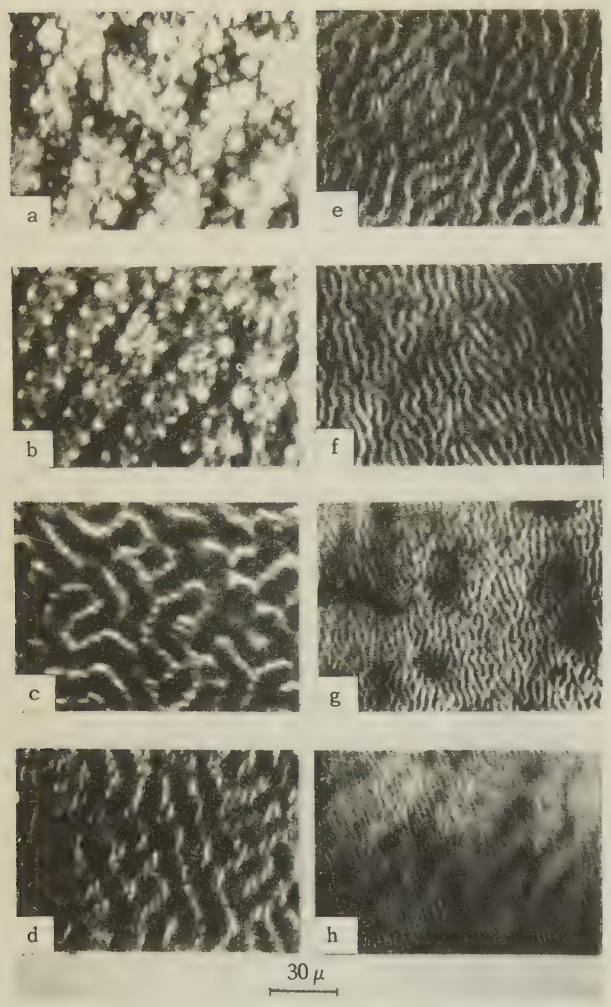

FIG. 1. Magnetic structure of a cobalt monocrystal, observed on the basal plane; crystal thicknesses: a) 515μ; b) 380 μ; c) 210 μ; d) 145 μ; e) 85 μ f) 45 μ; g) 30 μ; h) 15 μ.

cated star-shaped picture of the powder deposition. Coarse and fine stars form integral groups, which in their turn are grouped in labyrinths and zigzags. A similar picture is retained at crystal thickness 380 μ (Fig. 1b). At specimen thicknesses 210 to 85 μ (Fig. 1c, d, e), the basic labyrinth structure is more clearly visible, and also chains of stars. On further thinning of the crystal to 40 to 30 μ (Fig. 1f, g), only a labyrinth structure is observed; the labyrinths become less tortuous, and at thickness 15 μ the picture of the powder deposit is a series of slightly wavy, almost parallel lines (Fig. 1h).

On comparison of the powder-pattern photographs shown, it can be noticed that with decrease of the thickness of the cobalt crystal, the surface magnetic structure on the basal plane of the crystal becomes not only appreciably simpler, but also finer. We may take as a conventional measure of the degree of dispersion of the surface structure the value of d′, the mean width of the labyrinths. From the photographs shown in Fig. 1 it is clear that with thinning of the specimen from 515 to 15 μ, the value of d′ decreases manyfold.

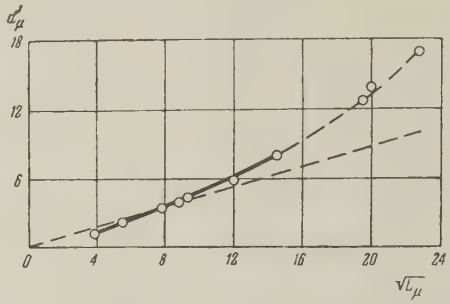

FIG. 2. Dependence of labyrinth width on thickness of a cobalt crystal. o, experimental data; ---, theoretical curve $d'_\mu = 0.43\sqrt{L_\mu}$.

Figure 2 shows the experimentally obtained dependence of the mean width d′ of the labyrinths on $\sqrt{L}$ (curve 1). The experimental curve is well approximated by the $d'_\mu = 0.43\sqrt{L_\mu}$ for thicknesses less than 200 μ.

DISCUSSION OF THE RESULTS OF THE OBSERVATIONS

The observed changes of magnetic structure of a cobalt crystal with decrease of its thickness can be qualitatively understood on the basis of the following considerations.

In the initial state, the magnetic structure of a cobalt monocrystal consists of two types of domain: the basic domains, running through the whole thickness of the crystal, and auxiliary cone-shaped (or wedge-shaped) domains, whose bases are visible in the form of "asterisks" on the basal plane of the crystal. In all domains, both basic and auxiliary, the magnetization is oriented along the hexagonal axis (that is, perpendicular to the specimen surface). The wavy form of the walls between the basic domains near the surface of the crystal[9] and the presence of a large number of wedge-shaped domains, different in form, in depth of penetration, and in size of the wedge base,[10] are apparently responsible for the complicated star-shaped and labyrinthine picture of the powder patterns that we observe on the basal plane of a crystal of thickness 400 to 500 μ (Figs. 1a and 1b). This surface magnetic structure probably differs appreciably from the simpler internal magnetic structure of cobalt.

By analogy with the changes of the magnetic structure observed in transformer iron,[2] where with thinning of the crystal the closure domains disappeared and only the basic domains remained, it may be assumed that in our case also, with diminution of the thickness of the cobalt crystal the

wedge-shaped auxiliary domains first decrease in size and then disappear, so that at certain thicknesses (30 to 15 μ) the lines of the observed labyrinth structure are the terminations of the walls of the basic domains. In addition, according to Goodenough's ideas, on decrease of the crystal thickness there is a decrease of the amplitude of the wavy walls between the basic domains; and at some sufficiently small thicknesses, a configuration of plane-parallel layers will be energetically favorable. These principles apparently determine the observed simplification of the surface magnetic structure with thinning of the cobalt crystal (Fig. 1).

The presence of a magnetic structure with unclosed magnetic flux (complete absence of closure domains), of the plane-parallel layer type, was first predicted by Kittel[11] for very thin plates of cobalt of thickness $\sim 10^{-5}$ cm. Apparently if we take account of the possibility of a decrease of the magnetostatic energy of the crystal by disorientation of the magnetic vectors near the surface,[12] and of the presence of wavy walls not perpendicular to the surface,[9] then in a magnetically uniaxial crystal a magnetic structure without auxiliary wedge-shaped domains will be stable at crystal thicknesses greater than 10^{-5} cm.

As was mentioned above, with decrease of the thickness of a cobalt crystal, the value of the mean width d′ of the labyrinths also decreases sharply. For small thicknesses, as is clear from Fig. 2, the relation between the crystal thickness L and the labyrinth width d′ can be expressed by the quadratic dependence $d'_\mu = 0.43\sqrt{L_\mu}$. This provides the possibility, for sufficiently small crystal thicknesses ($< 200\,\mu$), of taking the value of d′ as the thickness d of the basic domains. For larger thicknesses there is no possibility of directly relating the values of d and d′ because of the complexity of the powder deposit picture.

CONCLUSION

The results of the investigation made and the analysis of them show that on passage to small thicknesses, the magnetic structure of a cobalt crystal, observed on the basal plane of the crystal, rapidly changes. This change of structure expresses itself in the fact that the auxiliary domains disappear and the width of the basic domains decreases. For thicknesses less than 200 μ, the width of the basic domains is proportional to the square root of the crystal thickness.

[1] Shur, Shtol'ts, and Kandaurova, Физика металлов и металловедение (Physics of Metals and Metal Research) **5**, 412 (1957).

[2] Shur, Abel's, and Zaĭkova, Izv. Akad. Nauk SSSR, Ser. Fiz., **21**, 1162 (1957), Columbia Tech. Transl. p. 1149.

[3] Shur, Shtol'ts, Kandaurova, and Bulatova, loc. cit. ref. 1, **5**, 234 (1957).

[4] Ya. S. Shur and V. R. Abel's, Dokl. Akad. Nauk SSSR **104**, 209 (1955).

[5] L. D. Landau and E. M. Lifshitz, Physik. Z. Sowjetunion **8**, 153 (1935).

[6] B. W. Roberts, Trans. Am. Inst. Elec. Engrs. **78**, 192 (1955) [sic!].

[7] Sixtus, Kronenberg, and Tenzer, J. Appl. Phys. **27**, 1051 (1956).

[8] R. F. Pearson, Proc. Phys. Soc. (London) **B70**, 441 (1957).

[9] J. B. Goodenough, Phys. Rev. **102**, 356 (1956).

[10] W. Andrä, Ann. Physik **15**, 135 (1954).

[11] C. Kittel, Phys. Rev. **70**, 965 (1946).

[12] M. Fox and R. S. Tebble, Proc. Phys. Soc. **72**, 765 (1958).

Translated by W. F. Brown, Jr.
11

TEMPERTURE DEPENDENCE OF THE HALL EFFECT OF PURE FERROMAGNETS

N. V. VOLKENSHTEĬN and G. V. FEDOROV

Institute of Metal Physics, Academy of Sciences, U.S.S.R.

Submitted to JETP editor July 27, 1959

J. Exptl. Theoret. Phys. (U.S.S.R.) **38**, 64-68 (January, 1960)

The paper presents results of the measurements of the Hall effects for 99.998% pure iron, nickel, and cobalt, over a wide temperature range from room temperature down to 4.2° K. It is shown that the existing theories are inadequate for a satisfactory explanation of the experimental data obtained for the temperature dependence of R_0 and R_S over a wide temperature range.

MANY papers have been published recently on the Hall effect of ferromagnets.[1-7] In none of these investigations, however, were the Hall effect and the electric resistivity measured in materials of maximum purity and on the same samples, a factor of particular importance at low temperatures.

The Hall effect in ferromagnets is of interest primarily because it differs from the Hall effect in nonferromganetic metals by many "anomalies," due to the presence of spontaneous magnetization. Let us consider the principal of these anomalies.

1. While the Hall emf of nonferromagnetic metals varies linearly with the intensity of the magnetic field H, over a wide range of fields ($e_H = RH$, where R is the Hall constant), experiment shows that in ferromagnets the Hall emf depends not only on the intensity of the external field, but also on the magnetization I of the specimen. The dependence on I is due not to the induction B alone, but also to an added specific dependence on the magnetization. It is usually assumed[1,8] that

$$e_H = R_0 B + R_s 4\pi I,$$

where R_0 and R_S are the ordinary and spontaneous Hall constants, respectively.

2. The absolute values of R_0 do not differ in order of magnitude from the corresponding values of the Hall constants of nonferromagnetic metals (see the table). The spontaneous constant R_S may exceed R_0 in absolute value at room temperature by a factor of two or more (for example, in the case of iron, nickel, and the alloys Fe_3Al and CrTe).*

Nonferromagnetic materials		Ferromagnets		
	R*		R_0	R_S
V	+0.82	Fe	+0.23	+7.22
Mn	+0.84	Ni	−0.46	−6.05
Cu	−0.5	Co	−0.84	+0.6
		Ni_3Mn	−0.56	+155
		Fe_3Al	0.0	+470
		CrTe	—	~ −5000 [9]

*The Hall constants are given in units of 10^{-12} v-cm/amp-gauss.

3. Both R_0 and R_S have a clearly pronounced temperature dependence, that of R_S being greater. It is characteristic that in the region of low temperatures ($T \ll \Theta_f$, where Θ_f is the ferromagnetic Curie point) the temperature dependence of R_0 and R_S can also be not monotonic.

In many theoretical papers the spontaneous Hall constant is associated with the electric resistivity. Some[10] give the relationship $R_S \sim \rho^2$ and others[11] $R_S = a\rho + b\rho^2$. Experimental data[4,5] show, however, that these relations are approximately correct, but only near the Curie point. At lower temperatures (below those of liquid nitrogen) there is no linear relation between $\log R_S$ and $\log \rho$ at all. In the region where a nonmonotonic temperature variation of R_S is observed, the connection between R_S and ρ becomes in general meaningless.

We measured the Hall effect and the specific electric resistivity of pure ferromagnets

$$\text{Fe}\,(\rho_{292°}/\rho_{4.2°} = 11.45), \quad \text{Ni}\,(\rho_{292°}/\rho_{4.2°} = 57.2),$$

$$\text{Co}\,(\rho_{292°}/\rho_{4.2°} = 66.3)$$

in the temperature range from 300° K to 4.2° K using a potentiometer setup and a method de-

*It should be noted that our measurements (see below) show that in the case of cobalt, in which the sign of R_S is reversed, this constant reaches large values at higher temperatures than, for example, in nickel and iron.

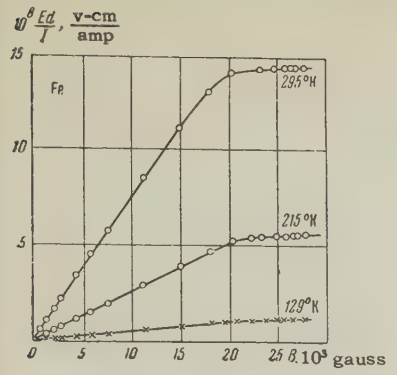

FIG. 1

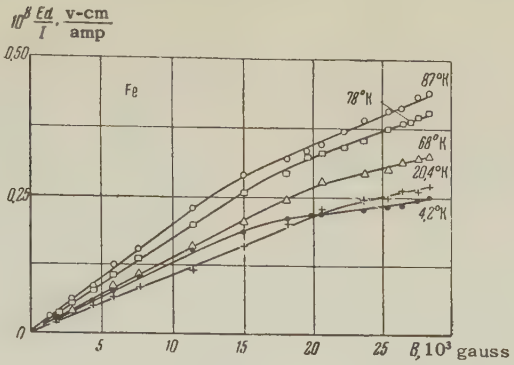

FIG. 2

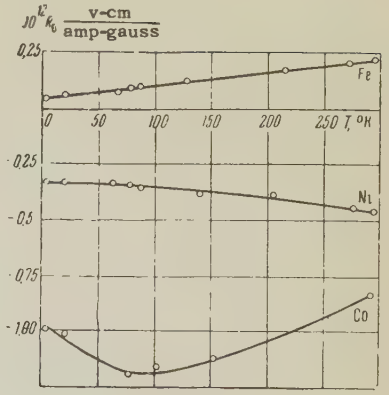

FIG. 3

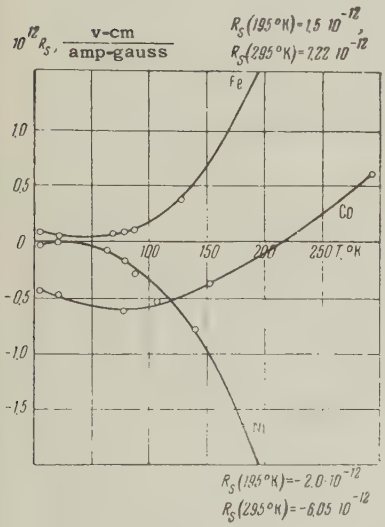

FIG. 4

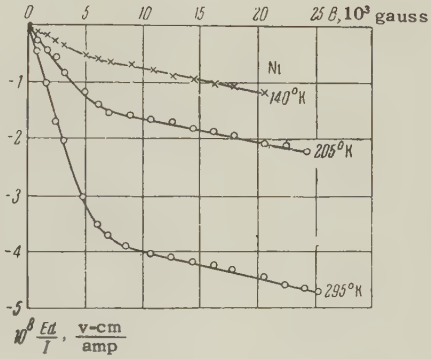

FIG. 5

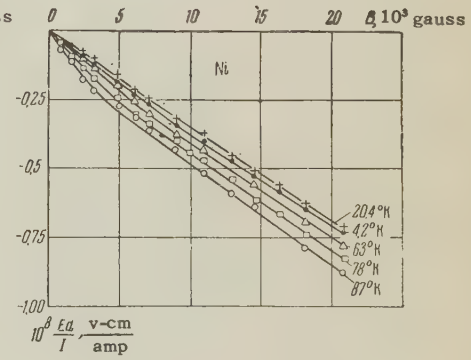

FIG. 6

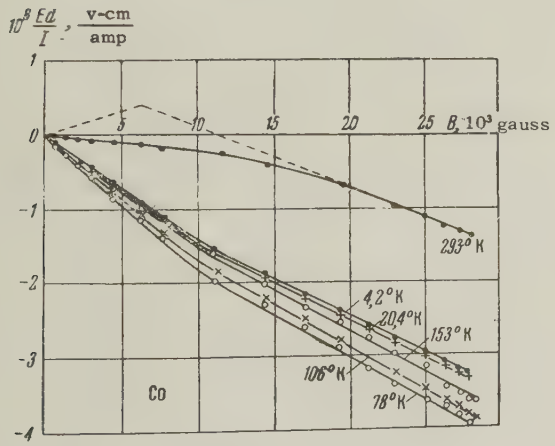

FIG. 7

scribed previously,[12] at the boiling temperatures of liquid nitrogen, hydrogen, and helium, as well as at intermediate temperatures, in a cryostate of the type described in the paper of Borovik-Romanov and Kreĭnes.[13]

We give the measurement results for each of the ferromagnets investigated.

Iron. As can be seen from Figs. 1 — 4, which show the variation of the specific Hall emf $e_H = Ed/I$ (d — thickness of specimen, I — current in the specimen) with the magnetic induction B in the specimen for different temperatures, as well as the temperature dependence of R_0 and R_S. The spontaneous Hall constant $R_S = (de_H/dB)_{B=0} - R_0$, and the ordinary Hall constant $R_0 = (de_H/dB)_{B=H+4\pi I_S}$ are positive over the entire interval of temperatures. R_S diminishes sharply with decreasing temperature, becomes comparable with R_0 at hydrogen temperature, and has an extremum at ~ 40° K.

Nickel. As can be seen from Figs. 3 — 6, R_0 and R_S have the same sign (negative), but in all other respects nickel is analogous to iron in the behavior of the Hall emf and of R_0 and R_S. The extremal value of R_S is reached at ~ 30° K.

Cobalt. The temperature dependence of the Hall emf of cobalt (Figs. 3, 4, and 7) differs substantially from the temperature dependence of e_H observed for iron and nickel. At room temperature R_S is positive and R_0 is negative, the latter having

the greater modulus. At the temperature of liquid nitrogen R_S becomes negative and does not differ much from R_0 in magnitude. The extremal value of R_S is reached at $\sim 80°$ K. The overall variation of the effect, from room temperature down to liquid helium temperature, is considerably less than in iron or nickel.*

An examination of the dependence of R_S on the reduced temperature T/Θ_S, shown in Fig. 8, indicates that the extremum is characteristic of all the investigated ferromagnets, and is observed at reduced temperatures ranging from 0.04 to 0.06.

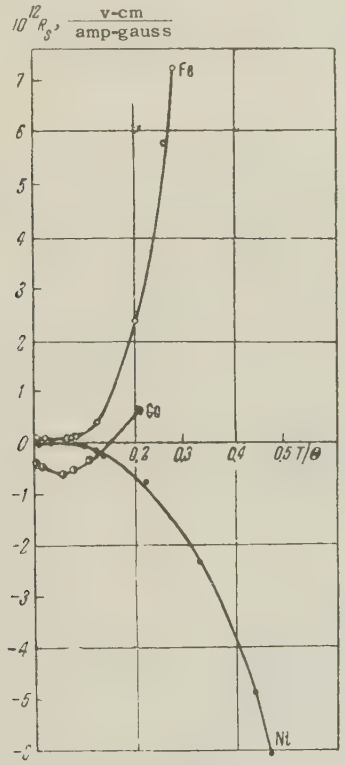

FIG. 8

An analysis of the experimental temperature dependence of the ordinary Hall constant R_0 (see Fig. 3) shows that R_0 changes substantially with temperature for all the investigated ferromagnets, and that in the case of cobalt this dependence is nonmonotonic.

The question of the temperature dependence of R_0 was recently investigated theoretically† and it was shown than an evaluation of the singularities in the energy spectrum and in the carrier scattering mechanism in ferromagnets (polarization of the conduction electrons, scattering by the inhomogeneities of the magnetic moment, etc.) explains qualitatively not only the temperature dependence of $R_0(T)$ at low temperatures, but also its nonmonotonic character.

To gain a better idea of the nature of the Hall constant R_0 in ferromagnets, a more detailed experimental investigation is necessary over an even wider temperature range (from infra-low up to temperatures above the Curie point), along with investigations of single-crystal specimens.

As first noted by Rudnitskiĭ,[14] the spontaneous Hall constant R_S is apparently due to the spin-orbit interaction between the current carriers in the ferromagnets. However, not one of the existing theoretical papers[10,11,14-17] offers a satisfactory explanation of the magnitude and the temperature dependence of the observed effect.

The authors are grateful to S. V. Vonsovskiĭ for continuous interest and attention to this investigation.

*See first footnote of this article.

†See paper by S. V. Vonsovskiĭ, Yu. P. Irkhin, E. A. Turov, and V. G. Shavrov, 6-th All-Union Conference on Low-Temperature Physics, June 1959, Sverdlovsk, and also the paper by Irkhin and Petrova, Conference on the Theory of Metals and Alloys, June 1959, Kiev.

[1] Pugh, Rostoker, and Schindler, Phys. Rev. **83**, 298 (1951).

[2] J. P. Jan, Helv. Phys. Acta **25**, 677 (1952).

[3] A. V. Cheremushkina, Вестн. МГУ, серия мат., мех., (Bull., Moscow State Univ. Math. Mech. Series), No. 1, 121 (1958).

[4] J. P. Jan and H. M. Gijsman, Physica **18**, 339 (1952).

[5] N. V. Volkenshteĭn and G. V. Fedorov, JETP **35**, 85 (1958), Soviet Phys. JETP **8**, 61 (1959).

[6] Belov, Svirina, and Belous, Физика металлов и металловедение (Phys. of Metals and Metal Research) **6**, 621 (1958).

[7] F. P. Beitel and E. M. Pugh, Phys. Rev. **112**, 1516 (1958).

[8] J. Smit, Nuovo cimento Supplement **6**, No. 3, 1177 (1957).

[9] Kikoin, Buryak, and Muromkin, Dokl. Akad. Nauk SSSR **125**, 1011 (1959), Soviet Phys.-Doklady **4**, 386 (1959).

[10] R. Karplus and J. M. Luttinger, Phys. Rev. **95**, 1154 (1954).

[11] N. S. Akulov and A. V. Cheremushkina, Dokl. Akad. Nauk SSSR **98**, 35 (1954).

[12] N. V. Volkenshteĭn and G. V. Fedorov, loc. cit. ref. 6, **2**, 377 (1956).

[13] A. S. Borovik-Romanov and N. M. Kreĭnes, JETP **29**, 790 (1955), Soviet Phys. JETP **2**, 657 (1956).

[14] V. E. Rudnitskiĭ, JETP **9**, 262 (1939).

[15] Vonsovskiĭ, Kobelev, and Rodionov, Izv. Akad. Nauk SSSR, Ser. Fiz. **16**, 569 (1952).

[16] J. M. Luttinger, Phys. Rev. **112**, 739 (1959).

[17] C. Strachan and A. M. Murray, Proc. Phys. Soc. **73**, 433 (1959).

Translated by J. G. Adashko
12

ON THE EXISTENCE OF PARTICLES OF MASS $2m_e \leq \mu \leq 25m_e$

A. N. GORBUNOV, V. M. SPIRIDONOV,* and P. A. CERENKOV

P. N. Lebedev Physics Institute, Academy of Sciences, U.S.S.R.

Submitted to JETP editor July 29, 1959

J. Exptl. Theoret. Phys. (U.S.S.R.) **38**, 69-73 (January, 1960)

Experiments have been carried out with a cloud chamber in a magnetic field with the aim of detecting a possible production of particles of mass $2m_e$ to $25m_e$ in a lead target placed in the bremsstrahlung beam of the 265 Mev synchrotron of the Physics Institute of the Academy of Sciences. It is shown that if particles do exist with masses between $2m_e$ and $25m_e$, spin $\frac{1}{2}$, and a lifetime greater than 10^{-9} sec, then the cross section for their production by electromagnetic interactions is smaller than the expected value by more than two orders of magnitude.

INTRODUCTION

THE question of the existence of light particles of mass equal to several electron masses has been investigated previously in a number of papers. To explain the anomalous scattering of β particles in the neighborhood of radioactive sources, Skobel'tsyn[1-3] proposed the existence of "heavy electrons" of masses (3 to 7) m_e.† In other papers[4-6] on the investigation of penetrating particles in extensive showers in cosmic rays, hypotheses were also introduced on the possible existence of particles of masses (5 to 10) m_e. Although the results of the majority of investigations in the field of cosmic rays left no place for such particles, nevertheless it appeared to us to be useful to set up special experiments, which would enable us to give a definite answer to this question. Since quantum electrodynamics does not place any restrictions on the existence of particles of spin $\frac{1}{2}$ and with masses intermediate between the mass of the electron and the mass of the meson, then, if such particles do exist, they must be produced as the result of a pair-production process with an effective cross section that is inversely proportional to the square of the particle mass. Thus, one might expect that in the case that particles of mass μ do exist, their yield from a target placed in the bremsstrahlung beam of a synchrotron should be, roughly speaking, smaller by a factor of μ^2 than the yield of electron pairs.

As the particle detector we utilized a cloud chamber in a magnetic field, and we identified the particles by their energy losses after passage through lead absorbers.

*Deceased.

†Here and later m_e stands for the electron mass.

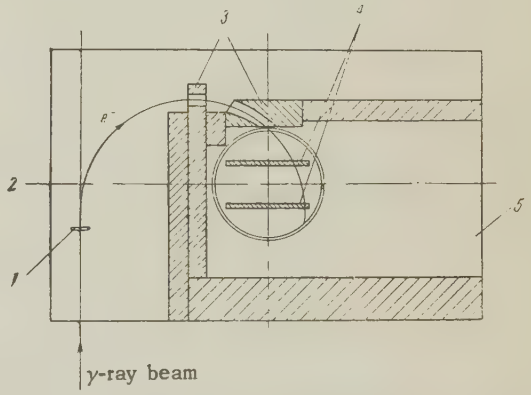

Schematic diagram of the experiment: 1) lead target, 2) cloud chamber, 3) system of diaphragms, 4) plates in the cloud chamber, 5) magnet pole.

DESCRIPTION OF THE EXPERIMENTAL ARRANGEMENT

A schematic diagram of the experiment is shown in the figure. Negative particles produced in the lead target 1 of 1 mm thickness by a bremsstrahlung beam from the 265-Mev synchrotron of the Physics Institute of the Academy of Sciences were deflected by a magnetic field through approximately 180° and were introduced through a "window" sealed by an organic film of 70 μ thickness into the cloud chamber 2 of 30 cm diameter and 8 cm depth, filled to a total pressure of 1.6 atmos by a mixture of helium and argon in the ratio of 50 : 50%. The system of diaphragms 3 placed in the path of the particles, and an appropriate choice of the position of the target 1 enabled us to select for recording those particles which were produced with a momentum of (93 ± 3) Mev/c and emitted at an angle of 3 to 5° to the axis of the bremsstrahlung beam from the synchrotron. In order to identify the particles two

TABLE I. Number of particles that have penetrated the first plate with momenta exceeding $(pc)_I$

$(pc)_I$, Mev	Observed number of particles	Expected total number of electrons and particles of mass μ.									
		m_e	m_e; $2m_e$	m_e; $3m_e$	m_e; $5m_e$	m_e; $8m_e$	m_e; $10m_e$	m_e; $15m_e$	m_e; $20m_e$	m_e; $25m_e$	m_e; $30m_e$
70.6	2	1.5	581	795	449	167	107	38.5	20.5	10.5	6.5
67.4	4	4.9	773	902	469	174	112	41.9	23.9	13.9	9.9
64.2	12	12.5	972	1001	493		119	50	31.5	21.5	17.5
61.0	28	26	1148	1083	517	198	134	63	44.6	34.6	30.6
57.8	44	42	1312	1147	541	215	150	79	60.6	50.6	46.6
54.6	78	72	1497	1246	580	246	181	109	91	81	77
51.4	141	111	1688	1332		286	220	148	130	120	116
48.1	228	164	1865	1420	684	339	274	202	183	173	169
44.9	337	230	2054			405	340	268	249	239	235
41.7	459	314	2243	1631	840	489	424	352	333	323	319
38.5	615	443	2497			617	554	482	462	452	448
35.3	780	590	2742	1957	1118	765	701	628	609	599	595

lead plates (4) each 9.9 mm thick were placed inside the cloud chamber at a distance of 10 cm from each other. The cloud chamber was illuminated by a flash lamp of type IFP-1500 and was photographed by a stereoscopic camera with low-distortion objectives of type Gelios-42 specially designed for taking pictures through a thick glass.

The method of synchronizing the cloud chamber and the synchrotron[7,8] allowed the particles to be introduced into the working volume of the cloud chamber after the expansion in the cloud chamber was completed. This eliminated the distortion of tracks associated with the movement of gas during the expansion period which is particularly noticeable in a cloud chamber which has plates situated within the working volume. The false curvature of the tracks in our chamber did not exceed 0.1 m^{-1}. The cloud chamber was placed in a magnetic field $H = (10.7 \pm 0.1) \times 10^3$ Gauss.

EXPERIMENTAL RESULTS

A total of 20,500 tracks of negative particles of momentum 93 Mev/c incident on the first lead plate was recorded in the cloud chamber. The momenta were measured in the case of those negative particles which passed through the plate and which were not accompanied by positrons (which could be produced as a result of a cascade process in the plate). The numbers of particles which passed through the first plate and retained a momentum greater than $(pc)_I$, are given in Table I (column 2).

A small number of particles which had passed through both lead plates were also recorded. The momenta of these particles after they had emerged from the second plate are given in Table II together with their momenta on leaving the first plate.

TABLE II. Momenta of particles that have penetrated both lead plates

Momentum after the first plate $(pc)_I$, Mev	Momentum after the second plate $(pc)_{II}$, Mev	Momentum after the first plate $(pc)_I$, Mev	Momentum after the second plate $(pc)_{II}$, Mev
61	27.3; 17.7; 9,6	51.4	28.9; 27.3; 25.7;
57.8	22.5; 16.0; 14,5		19.3; 12.8
54.6	14.5; 11.2; 9,6	48.1	19.3; 16; 11.2; 6.4

DISCUSSION OF RESULTS

To estimate the expected number of particles of mass μ incident on the first plate we integrated over the bremsstrahlung spectrum (taken approximately in the form 1/E) the effective cross section for the production of electron pairs, in which in place of m_e we utilized various values of the mass μ from $2m_e$ to $30m_e$. The expected numbers N_μ of particles of mass μ obtained as a result of such an estimate, on the assumption that there exist both electrons and particles with the given value of the mass, are the following ones (the total number of particles recorded before the first plate is equal to 20.5×10^3):

$\mu =$	1	2	3	5	8	10	15	20	25	30
$N_\mu =$	$20.5 \cdot 10^3$	$3.8 \cdot 10^3$	$1.7 \cdot 10^3$	580	180	110	38	19	9	5

We then calculated the probability $W(bl-1, y_0)$ that the particle on passing through the first lead plate will lose just by radiation alone such an amount of energy that $E/E_0 \geq \exp(-y_0)$ (where

TABLE III. Number of particles that have penetrated both lead plates and which have a momentum in excess of $(pc)_I$ after the first plate, and in excess of 19.3 Mev after the second plate

$(pc)_I$	Expected number of particles of mass μ equal to:										Observed number of particles
	1	2	3	5	8	10	15	20	25	30	
65.7	0.35	580	830	450	170	107	37	19	9	5	0
63	0.57	650	860	460	170	107	37	19	9	5	1
61	0.85	720	905	470	170	107	37	19	9	5	2
57.8	1.13	760	930	470	170	107	37	19	9	5	2
54.6	1.2	790	950	470	170	107	38	19	9	5	5

E_0 is the initial, and E is the final energy of the particle). According to Heitler,[9] this probability is given by the following formula

$$W(bl-1, y_0) = (bl-1, y_0)!/\Gamma(bl),$$

where $(bl-1, y_0)!$ is the incomplete Γ function; $b = a\bar{\varphi}N$ (for lead in the case $\mu = m_e$ $b = 2.6\ cm^{-1}$, $a \approx 20.0$); $\bar{\varphi} = z^2r_0^2/137$; N is the number of atoms per cm^3; l is the thickness of the plate in centimeters (in view of the inclination of the plate towards the bottom of the chamber and the angle of incidence of particles on the plate, we obtain in our case $l = 1.13$ cm). The quantity $(bl)_\mu$ for particles of mass μ was chosen in the form

$$(bl)_\mu = (bl)_{m_e}/\mu^2.$$

Table I lists, together with the observed number of particles which have passed through the first plate with momentum greater than $(pc)_I$, also the expected numbers of electrons that have passed through the plate, and also the total expected numbers of electrons and particles of mass μ ($\mu = 2m_e$, $3m_e \ldots$). It is seen from the table that the observed number of particles which have passed through the first plate with small radiation energy losses ($6.6\ Mev \leq \Delta E_{rad} \leq 22.5\ Mev$)* agrees with the expected number of electrons. In the case of higher radiation energy losses ($\Delta E_{rad} > 22.5$ Mev) the observed number of particles that has passed through the first plate becomes greater than the expected number of electrons, with this difference increasing as the radiation losses increase. This difference may be due to the recording of cascade electrons which could occur in the case when the cascade positron did not leave the plate. It is evident that the number of such "false" events will increase as the final particle momentum diminishes.

It can further be seen from Table I that if particles of mass from $2m_e$ to $25m_e$ did exist, then the numbers of recorded particles, particularly in the range of high momenta after the first plate, would have been considerably greater than the observed values.

Even more convincing is the comparison of the observed number of particles which have passed through both plates and which have retained after the second plate a momentum greater than 19.3 Mev with the expected numbers of particles of various masses. The results of such a comparison are given in Table III for different values of the momenta after the first plate. It can be seen from the table that the number of observed particles which have passed through both plates is in satisfactory agreement with the expected number of electrons and contradicts the assumption of the existence of particles with masses in the range from $2m_e$ to $25m_e$.

CONCLUSION

Thus, the results of the experiment show that if there do exist particles of masses between $2m_e$ and $25m_e$ and of spin $\frac{1}{2}$, and having a mean lifetime in excess of several 10^{-9} sec, then the effective cross sections for their production in electromagnetic interactions do not exceed the values shown in Table IV.

TABLE IV

Particle mass in units of m_ec^2	Expected cross section $\bar{\Phi}$ in cm^2	Observed cross section $\bar{\Phi}_{obs}$ in cm^2
2	$9.6\cdot10^{-25}$	$<3\cdot10^{-27}$
3	$4.2\cdot10^{-25}$	$<10^{-27}$
5	$1.5\cdot10^{-25}$	$<6.8\cdot10^{-28}$
8	$6\cdot10^{-26}$	$<7\cdot10^{-28}$
10	$3.8\cdot10^{-26}$	$<7\cdot10^{-28}$
15	$1.7\cdot10^{-26}$	$<0^{-27}$
20	$9.6\cdot10^{-27}$	$<0^{-27}$
25	$6.1\cdot10^{-27}$	$<10^{-27}$

The authors take this opportunity of expressing their gratitude to Academician V. I. Veksler for his interest in this work, to A. G. Gerasimov, V. A. Dubrovina, A. I. Orlova, V. A. Osipova, V. S. Silaeva, Hu Jen-Yu, and Yu. A. Fomin, who

*$(pc)_I = 54.6$ Mev.

took part in obtaining the photographs and in analyzing the results, and also to V. I. Ritus and L. V. Pariĭskaya who have carried out a number of calculations.

[1] D. V. Skobel'tsyn, Izv. Akad. Nauk SSSR, Ser. Fiz. No. 1-2, 75 (1938).

[2] D. V. Skobel'tsyn, Dokl. Akad. Nauk SSSR **21**, 435 (1938).

[3] D. V. Skobel'tsyn, Сб. Памяти Сергея Ивановича Вавилова (Memorial Collection to Sergeĭ Ivanovich Vavilov), U.S.S.R. Acad. Sci., 1952, p. 292.

[4] Auger, Daudin, Freon, and Mase, Compt. rend. **226**, 169 (1918).

[5] L. Jánossy and C. B. A. McCusker, Nature **63**, 181 (1949).

[6] D. Broadbent and L. Jánossy, Proc. Roy. Soc. (London) **192**, 364 (1948).

[7] Gorbunov, Spiridonov, and Cerenkov, Приборы и техника эксперимента (Instrum. and Meas. Engg.) No. 2, 29 (1957).

[8] Gerasimov, Gorbunov, Ivanov, Kutsenko, and Spiridonov, ibid. No. 3, 10 (1957).

[9] W. Heitler, Quantum Theory of Radiation, Oxford, 1954.

Translated by G. Volkoff
13

ON AN EXPERIMENTAL DEMONSTRATION OF THE EXISTENCE OF ADDITIONAL ANOMALOUS LIGHT WAVES IN A CRYSTAL IN THE EXCITON ABSORPTION REGION

M. S. BRODIN and S. I. PEKAR

Physics Institute, Academy of Sciences, Ukrainian S.S.R.

Submitted to JETP editor July 29, 1959

J. Exptl. Theoret. Phys. (U.S.S.R.) 38, 74-81 (January, 1960)

We consider one possible experimental demonstration of the existence of additional waves in a crystal, predicted theoretically in references 1 — 3, in the exciton region of light absorption. We have used the experimental data[4] on the absorption of light in an anthracene single crystal at a temperature of 20° K, which show deviations from the Lambert-Burger law. We give an interpretation of the observed non-exponential dependence of the absorption of light in a crystal plate on its thickness. We show the existence of two identically polarized waves with different refractive indices and absorption coefficients in an anthracene crystal.

1. THEORY

IT has been shown earlier[1-3] that a monochromatic wave incident on a crystal from the vacuum can produce in the exciton absorption region several waves (usually two), which propagate with different velocities. These waves possess the same polarization and we are, therefore, not dealing with double refraction. One of these waves has properties which approximate those of the light wave occurring in normal crystal optics, but the others are essentially anomalous and their amplitudes tend to zero as one moves in the spectrum away either on the red or on the violet side from the exciton absorption region. One must therefore look experimentally for anomalous waves near the exciton absorption region. In the papers mentioned it was also noted that the anomalous waves appear more pronouncedly when the crystal is at a low temperature.

We suggested in reference 2 a number of methods of observing experimentally the existence of the anomalous waves. In the present paper we shall suggest still one more method, which enables us to use already existing experimental data to determine the parameters of both waves ocurring in the crystal. This method reduces to an investigation of the dependence of the intensity of the light transmitted through a plane parallel crystal plate on the plate thickness. One assumes usually that the intensity should decrease exponentially with the plate thickness. If, however, a more complicated dependence is observed in the case of small thicknesses, it is explained by the interference of waves which are multiply reflected from both surfaces of the plate. Such an interference undoubtedly occurs in many cases. In the following, however, we shall be dealing only with cases of strong absorption of the light in the plate, when we can neglect the intensity of the beam that is twice reflected and which passes thrice through the plate as compared with the intensity of the beam that passes once through the plate. In those cases the usual crystal optics predicts a simple exponential decrease in the intensity with thickness and cannot explain the more complicated dependence observed experimentally by Brodin and Prikhot'ko.[4] It will be shown in the following that this more complicated dependence is naturally explained by the generalized crystal optics developed in references 1 — 3.

We shall assume that a monochromatic wave of frequency ω is normally incident from the vacuum onto the plate and that this wave gives rise to two waves in the plate, with complex wave vectors $k_+ = k_+^0 + ik_+'$ and $k_- = k_-^0 + ik_-'$, respectively. One can then show that both waves will move in the plate and will emerge into the vacuum also normally, while the electrical field strength when they emerge from the plate into the vacuum can be written in the form

$$\mathbf{E}e^{-i\omega t} = [\mathbf{a}_+ e^{ik_+^0 l - k_+' l} + \mathbf{a}_- e^{ik_-^0 l - k_-' l}]\, e^{-i\omega t}, \qquad (1)$$

where l is the plate thickness. Different components of the vector $\mathbf{E}$ can, of course, have different complex arguments so that (1) can also describe an elliptically polarized wave. We have assumed that the amplitudes of the waves $\mathbf{a}_+$ and $\mathbf{a}_-$ take into account the reflection of the light from the entrance and exit surfaces (multiple reflections

of the waves are neglected). The light intensity J when emerging from the plate will then be proportional to $|\mathbf{E}|^2$ so that

$$J \sim |\mathbf{E}|^2 = |\mathbf{a}_+|^2 e^{-2k'_+ l} + |\mathbf{a}_-|^2 e^{-2k'_- l} + 2|(\mathbf{a}_+, \mathbf{a}_-^*)| e^{-(k'_+ + k'_-) l} \cos[(k_+^0 - k_-^0) l + \alpha_0]. \quad (2)$$

We have introduced here the notation $(\mathbf{a}_+, \mathbf{a}_-^*) = |(\mathbf{a}_+, \mathbf{a}_-^*)| e^{i\alpha_0}$.

In the case where the + and − waves correspond to the normal double refraction, the amplitudes $\mathbf{a}_+$ and $\mathbf{a}_-$ must be strictly mutually perpendicular, i.e., $(\mathbf{a}_+ \cdot \mathbf{a}_-^*) = 0$. The last term in (2) drops out in that case and the dependence of the intensity of the outgoing light on the plate thickness l must be strictly monotonic. It is represented by the dotted lines in Fig. 1. If, however, the + and − waves are of a different nature, so that $\mathbf{a}_+$ and $\mathbf{a}_-$ are not necessarily perpendicular, the intensity J may, owing to the third term in (2), depend on the thickness l in an oscillatory manner, represented by the full curves of Fig. 1. If the wave with the smaller absorption coefficient has an appreciably larger amplitude, it will dominate over the second wave for all l. One can then in general neglect the latter and obtain in all cases a simple exponential dependence of the intensity on l. The more interesting case is the other one, when the wave with the larger amplitude has the larger absorption amplitude. We have thus depicted in Fig. 1 the case $|\mathbf{a}_-| > |\mathbf{a}_+|$, $k'_- > k'_+$. In that case the − wave dominates for small l; the dependence of ln J on l is described by a straight line of slope $2k'_-$. In the limiting case of large l, on the other hand, the + wave dominates; the dependence of ln J on l is also described by a straight line, but with a smaller slope, which is equal to $2k'_+$. It is thus convenient to determine the absorption coefficients of the two waves in the limiting cases of small and large thicknesses l.

In the region of intermediate thicknesses both terms on the right hand side of (1) may be approximately equal, and the third term in (2) will then also be of the same order as the first two. A sinusoidal oscillation must then take place in the dependence of J on l. The cases when the amplitude of these oscillations is a maximum are depicted in Fig. 1; this takes place when the vectors $\mathbf{a}_+$ and $\mathbf{a}_-$ are parallel (or antiparallel). The maximum possible deviation of the peaks of the oscillations from the dotted curve is equal to ln 2 above and infinite below the curve. Such deviations are, however, realized only if the cosine takes on the values +1 and −1 respectively just for those l for which the absolute magnitudes of the two terms on the right hand side of (1) are exactly equal.

We have plotted Fig. 1 not in l and ln $|\mathbf{E}|^2$, but in dimensionless relative magnitudes, so as to reduce the number of parameters of the family of curves.

One can determine the change in the phase of the wave when it passes through a plane parallel plate, as a function of l, using a normal interference method. For the limiting cases of small and large l this function must be linear, as can be seen from Eq. (1). The slopes of these lines enable us to determine k_-^0 and k_+^0. We can determine $k_+^0 - k_-^0$ also from the period of the oscillations in the dependence of J on l. The oscilla-

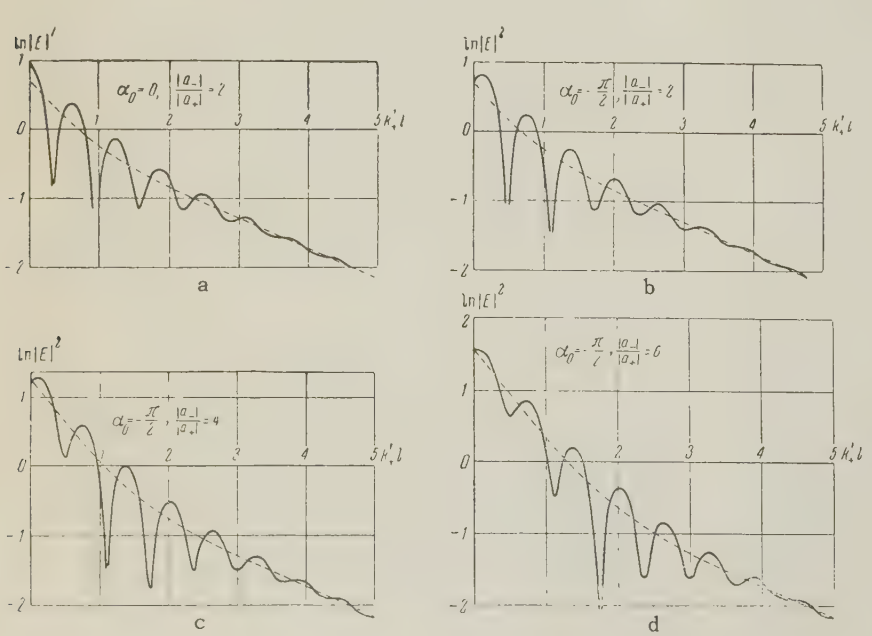

FIG. 1. The dependence of the absolute square of the amplitude of the electrical field of the transmitted wave on the crystal plate thickness; $(k_+^0 - k_-^0)/k'_+ = 10$; $k'_-/k'_+ = 3$.

tions themselves are convincing proof of the fact that the two waves under consideration do not represent double refraction.

The results and conclusions enumerated in the foregoing can be obtained merely from the dependence of the transparency of the plane parallel plate and of the phase shift on the plate thickness. One can obtain additional information about the nature of the two waves from the frequency dependence of the parameters of these waves. If the above-mentioned waves are identical with the ones predicted, in references 1 — 3, the frequency dependence of their parameters considered in reference 2 must be valid. We shall not repeat here the dispersion of the refractive index, which was evaluated there, but only introduce the frequency dependence of the amplitudes $\mathbf{a}_+$ and $\mathbf{a}_-$. The results following below are only valid in the case when there is an isolated exciton absorption band.

Reference 2 was devoted on the whole to an isotropically polarized medium and was applicable to cubic crystals, since we considered waves the wavelength of which was appreciably larger than the crystal constant. The results of that paper are, however, also applicable to some crystals of different symmetry, but only for selected directions of propagation and polarization of the light waves. The expressions for the refractive indices of the + and − waves and the formulae for the transparency of a plane parallel plate [Eqs. (60) and (61)] can, for instance, be obtained for a wider class of crystals. These results and all conclusions derived from them remain valid if the electrical field strength vector of the wave is parallel to one of the principal axes of the tensor a determined by Eq. (14) of reference 1. In those cases where this direction is defined by the symmetry of the crystal itself (as, for instance, for rhombic, tetragonal, or cubic crystals) it is frequency independent. The fact that the electrical field strength is parallel to the principal axis of the tensor a means that the latter can be replaced by a constant factor and after that the calculations take on the same form as in the case of an isotropic medium. We shall restrict ourselves to just such cases in the following.

The transparency of a plane parallel plate is determined by Eqs. (60) and (61) of reference 1. These formulae take automatically into account multiple reflection from both surfaces of the plate. We shall simplify these formulae using the above assumptions about the large absorption of the light in the plate and the possibility to neglect multiple reflection. From this assumption it follows that

$$|e^{2ik_\pm l}| \ll 1, \quad \cot k_\pm l \approx -i, \quad \sin k_\pm l \approx (i/2)e^{-ik_\pm l}. \tag{3}$$

As a result of this Eq. (60) of reference 1 takes the form of Eq. (1) of the present paper with

$$\mathbf{a}_+ = \frac{4\mathbf{A}n_+/(1-q)}{\left(1+\frac{n_+}{1-q}+\frac{n_-}{1-(1/q)}\right)^2}, \quad \mathbf{a}_- = \frac{4\mathbf{A}n_-/[1-(1/q)]}{\left(1+\frac{n_+}{1-q}+\frac{n_-}{1-(1/q)}\right)^2}. \tag{4}$$

Here $\mathbf{A}$ is the electrical field strength amplitude of the incident wave in the vacuum, n_+ and n_- are the complex refractive indices of the + and − waves, and q has the same meaning as in reference 2:

$$q = \frac{n_-^2-\mu}{n_+^2-\mu} \equiv \frac{\vartheta - n_+^2}{\vartheta - n_-^2}, \qquad \mu = \frac{2Mc^2}{\hbar\omega}\left(1-\frac{\mathcal{E}_0}{\hbar\omega}\right), \tag{5}$$

where M is the effective mass of the "transversely polarized" exciton in the direction of propagation of the beam, $\mathcal{E}_0$ is the energy of exciting this exciton in the limit where its quasi-momentum tends to zero, and ϑ the asymptotic value of the square of the refractive index when one goes away from the exciton absorption region either to the red or to the violet.

It follows from Eq. (4) that $\mathbf{a}_+$ and $\mathbf{a}_-$ are parallel. Then

$$\frac{\mathbf{a}_-}{\mathbf{a}_+} \equiv \left|\frac{\mathbf{a}_-}{\mathbf{a}_+}\right| e^{-i\alpha_0} = -q\frac{n_-}{n_+}. \tag{6}$$

If the lifetime of the exciton is sufficiently large and if we can neglect the small imaginary correction to $\mathcal{E}_0$ (see reference 3 for details) we can take the frequency dependence of n_+ and n_- approximately from reference 2. If $M > 0$ one can see from Fig. 1 of reference 2 that in the whole exciton absorption region n_+ is real and n_- purely imaginary and q real and negative. In Eq. (6) we have then $\alpha_0 = -\pi/2$. In the frequency region where $|n_\pm|^2 \gg \vartheta$ we get approximately $q \approx n_+^2/n_-^2$ and $g \equiv |\mathbf{a}_-/\mathbf{a}_+| \approx |n_+/n_-|$; g is a steeply increasing function of ω. The equality $g = 1$ occurs when $\omega \approx \omega_0 = \mathcal{E}_0/\hbar$. Hence $g > 1$ in the frequency region $\omega > \omega_0$ and just in that region one must expect a well defined oscillatory behavior of $\ln J$ vs. l, if $k'_- > k'_+$.

Let us now consider the case $M < 0$. The frequency dependence of n_+ and n_- is given in Fig. 2 of reference 2. Here one must consider separately three frequency regions. In the first (red) region n_+ and n_- are both real and positive, $q > 0$, and the right hand side of Eq. (6) is negative so that $\alpha_0 = \pi$. $g > 1$, but decreases with increasing frequency ω and becomes equal to 1 at the violet limit of this region when $n_+ = n_-$. In the first region the oscillations must thus appear distinctly when $k'_- > k'_+$. In the second region (in-

termediate frequencies) we have according to reference 2 $n_- = -n_+^*$. It follows from this that $|q| = 1$, $g = 1$. If we introduce the quantities k^0 and k' such that $k_+ = k^0 + ik'$, then $k_- = -k^0 + ik'$. Equation (2) then takes the form

$$|E|^2 = 4|a_+|^2 e^{-2k'l} \cos^2(k^0 l + \alpha_0/2). \quad (7)$$

In that case α_0 is a function of ω. The oscillations must thus be observable for all l, and on a plot such as Fig. 1 one will not observe the straight sections at large and small l. We must, however, note that the dependence (7) was obtained assuming the lifetime of the exciton to be infinite. Taking the finite lifetime into account leads to some deviations from Eq. (7).

In the third frequency region (violet) n_+ and n_- are purely imaginary and both must be taken with the plus sign. $q > 0$ so that the right hand side of Eq. (6) is real and negative. Thus $\alpha_0 = \pi$. Moreover, g is a decreasing function of the frequency. $g = 1$ at the red end of the third region, where $n_+ = n_-$. Thus $g < 1$ in the third region. Therefore $|a_-| < |a_+|$ and since k'_- is still greater than k'_+, the + wave will dominate over the − wave. The l-dependence of J must thus be expressed by a simple exponential formula with a damping coefficient k'_+.

We note in conclusion that Eqs. (3) to (6) are applicable for an exciton absorption band isolated in a wide frequency interval, while the qualitative analysis given in the foregoing is valid only for $|n_\pm|^2 \gg \vartheta$, i.e., in a narrow frequency interval near the maximum of the band and only for large exciton lifetimes (which are, for instance, realized at low temperatures).

2. EXPERIMENTAL RESULTS

We chose for the object of our experimental investigation an anthracene crystal at 20° K. The long-wave band of light absorption in the electronic phototransition region was studied. The maximum of this band lies approximately at 25300 cm^{-1}. This absorption is real, since it is very intensive in very pure crystals. The polarization of the absorption and the corresponding luminescence along the crystal axes[5] are some arguments in favor of the idea that this band corresponds to the excitation of a fast moving exciton (with a small effective mass).

Single-crystal layers of anthracene were grown by the method of sublimation from a pure preparation. The most perfect among them, plane parallel and with smooth surfaces, were chosen for the measurements. They were put in optical contact on plane parallel plates of quartz. Because of the strong absorption we chose thin crystals (0.1 − 0.4 μ). The crystal was placed in a cryostat filled with liquid hydrogen for cooling.

The surfaces of the crystal coincided with the crystallographic (a, b) plane. The light was perpendicularly incident upon this surface and the electric field strength vector was parallel to the monoclinic b axis. The direction of b was the second-order crystal axis and coincided therefore with a principal axis of the polarization (and also with a principal axis of the a tensor, mentioned in the first section of this paper). The directions of the incidence of the light and of the polarization were thus just such that the equations of reference 2 were applicable. It is of particular importance to stress that the normal double refraction cannot occur in this case.

Brodin and Prikhot'ko[6] measured the dispersion and absorption in an anthracene plate of well defined thickness. The results of their measurements were evaluated using the formulae of the normal crystal optics. Similar investigations were performed on stilbene toluene, and 1,2-benzene-anthracene. In all four crystals essential deviations were noted from the general Kramers-Kronig dispersion relations[7] between the refractive index and the absorption coefficient.[8] These deviations increased when the crystals were cooled, but in anthracene they were already observed at room temperatures. They could not be explained in the framework of the usual crystal optics.

A little later[4] the absorption of light in an anthracene crystal was measured in more detail and in that case crystals of different thicknesses were used. The results were again evaluated by the usual method. The imaginary part of the refractive index was evaluated using the equation

$$\varkappa = \ln(J_0/J)/2\omega l. \quad (8)$$

The values for κ obtained from crystals of different thicknesses are not reproducible. The Lambert-Bouguer law is this violated. It is impossible to explain this violation by interference phenomena, since one can neglect multiple reflection because of the strong absorption. Indeed, within the absorption band, even away from the maximum and for very thin plates, the intensity of the beam that passes thrice through the plate is some tenths of a per cent of the intensity of the beam passing once through the plate (see the third section of this paper).

The authors decided to evaluate the experimentally obtained results on the absorption, using the generalized theory of exciton absorption,[1-3] as ex-

plained in the first section of the present paper. It was first necessary to consider the dependence upon the plate thickness l of the intensity of the light J which had passed through the crystal. The observed dependence of $\log(J/J_0)$ on l for the frequencies $1/\lambda = 25100$ and $25425\ cm^{-1}$ is given in Fig. 2. The points on the curves are given with their probable experimental errors in the ordinate and abscissa directions. An analysis of the errors

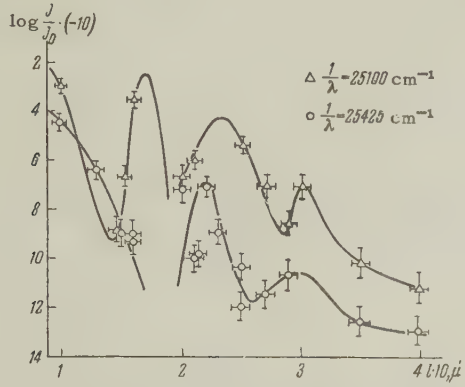

FIG. 2. The dependence of the optical thickness of anthracene crystals on thickness at T = 20°K (the electrical field is parallel to the b axis).

is given in the third section of the paper. The magnitude of J_0 was measured experimentally in relative units, which means the presence of an unknown constant term in the quantity $\log(J/J_0)$; the curves in Fig. 2 may thus possibly be shifted vertically, retaining their form. The accuracy and the number of points is for the time being still insufficiently large. The curves in the figure are therefore tentative. All the same, it seems to us that one can reach the following conclusions from these curves:

a) The Lambert-Bouguer law is violated since it is impossible to fit all the points on one straight line. It is impossible to reduce this violation to a consequence of interference, or to a consequence of the spatial inhomogeneity of the crystal (if the crystal is deformed in an inhomogeneous manner, the dependence on l of $\ln(J/J_0)$ must remain monotonic). It is therefore not clear that this violation can be explained in the framework of the usual theory.

b) The position of the points indicates an oscillatory dependence rather than a scatter. This follows from the fact that the amplitudes of the oscillations here and there exceed by far the errors of the measurements. Apart from this, the oscillations show a systematic character which may be observed in both curves. We have thus obtained qualitatively and approximately an l-dependence such as was predicted theoretically (see Fig. 1) and there is evidence of the existence of two waves in the crystal with different refractive indices and absorption coefficients. The oscillations show that these waves are not double refraction. Double refraction is also excluded by the above mentioned choice of the polarization of the incident wave.

c) According to the first section, the amplitudes of the two waves must be parallel and then the amplitude of the deviation of the curve from the average behavior (see the dotted curve in Fig. 1) on the positive side cannot exceed log 2. It can be seen from Fig. 2 that this is approximately observed. The deviations from the average behavior on the negative side can according to the theory have any value.

The experimental data confirm thus qualitatively the generalized theory of exciton absorption.[1-3] We shall perform shortly more extensive measurements for a larger number of thicknesses. We hope that they will enable us to determine quantitatively the parameters of both waves and their frequency dependence.

3. DESCRIPTION OF THE EXPERIMENTAL SET-UP AND ANALYSIS OF THE ACCURACY OF THE MEASUREMENTS

To measure the optical thickness of crystals we used photoelectric apparatus together with a spectrometer of average dispersion. A block diagram of the optical part of the apparatus is shown in Fig. 3.

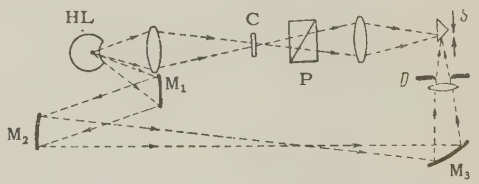

FIG. 3. Block diagram of the optical part of the photoelectric set-up for measuring optical thicknesses.

Two light beams, a direct beam and a comparison beam, emerge from the light source, a hydrogen lamp (H.L.). The first of these is incident upon the crystal C after which it passes through a polarizer P and is focused upon a slit S. The comparison beam is also led to the slit by means of the mirrors M_1, M_2, and M_3 and reflection from a prism. The triangular reflecting prism vibrates with a frequency of 70 cps, letting the direct and comparison beams pass alternately on to the spectrometer slit. A photomultiplier serves as receiver for the light. The intensity of the direct beam was measured by a null method, by comparing it with the intensity of the comparison beam. To compare the intensities we used a variable-

aperture diaphragm D placed along the path of the comparison beam.

There was no need to measure the intensity of the light reflected from the crystal, since the theoretical formulae [in particular, (2) and (4)] express the intensity of the transmitted light, but with account of the reflection of the light from the crystal. The experimental curves of Fig. 2 represent therefore only the intensity of the transmitted light for a comparison with the theory.

Let us now go over to an analysis of the errors of the measurements.

1. The accuracy of the comparison of the intensities of the two beams. The equality of the intensities of the beams is determined by the zero position of the galvanometer pointer. The accuracy of the fixing of this position for a given level of noise depends on the absolute intensities of the beams. In the most unfavorable case of low intensities, the relative error in the measurement of $\log(J/J_0)$ does not exceed 6%, if we disregard the appreciable systematic error connected with the possible inequality of the time during which the basic beam and the comparison beam pass into the spectrograph slit. This systematic error may introduce a constant additive to $\log(J/J_0)$, independent of l, and leads thus to a vertical shift of the curves of Fig. 2 without changing their form. This systematic error will be eliminated in a following paper.

2. The influence of the apparatus function of the spectrometer. The half-width of the spectrometer apparatus function was approximately equal to 1 A. Its influence can therefore be only appreciable at the very steep fall at the red end at the left absorption maximum. As we have chosen points which are situated at least 10 A from the above mentioned red absorption edge for the construction of the l-dependence of $\log(J/J_0)$, we can neglect the influence of the apparatus function.

The crystal thicknesses were measured in two ways: by birefringence using a Berek compensator and a microscope, and by using a Jamin interferometer. The maximum error in the thickness measurement was less than 4%.

There remains the task of estimating the influence of the interference effect due to a possible multiple reflection of the light at the crystal surfaces. Its role changes along the spectrum and depends strongly on the reflection and attenuation coefficients. One can see from Fig. 2 that the majority of the experimental points correspond to values of $\log(J/J_0)$ equal to -0.6 or less. Let us therefore consider the case $\log(J/J_0) = -0.6$ which is far from being very favorable from the point of view of the possibility of neglecting multiple reflection. When the coefficient for reflection of light from the vacuum-anthracene surface is equal to 0.3 and the reflection coefficient from the anthracene-quartz surface equal to 0.1, it turns out that for a beam twice reflected and thrice passing through the crystal the intensity is 0.003 times the intensity of the beam passing once through. We can therefore neglect the multiply reflected beams.

The authors express their gratitude to A. F. Prikhot'ko for his assistance with this experiment and for discussing the results.

Note added in proof (December 14, 1959). A source of appreciable errors may be a break in the light polarized along the a axis of the crystal because of the imperfection of the polarizer and the inaccuracy of its adjustment relative to the crystal. When emerging from the crystal the amplitude of the a-component may turn out to be comparable to the amplitude of the b-component as the first is absorbed much less than the second. To exclude the influence of the a-component we have now introduced measurements with two parallel polarizers, placed before and after the crystal.

[1] S. I. Pekar, JETP **33**, 1022 (1957), Soviet Phys. JETP **6**, 785 (1958).

[2] S. I. Pekar, JETP **34**, 1176 (1958), Soviet Phys. JETP **7**, 813 (1958).

[3] S. I. Pekar, JETP **36**, 451 (1959), Soviet Phys. JETP **9**, 314 (1959).

[4] M. S. Brodin and A. F. Prikhot'ko, Оптика и спектроскопия, (Optics and Spectroscopy) **7**, 132 (1959).

[5] Zhevandrov, Gribkov, and Varfolomeeva, Izv. Akad. Naul SSSR, Ser. Fiz. **23**, 57 (1959), Columbia Tech. Transl., p. 59.

[6] M. S. Brodin and A. F. Prikhot'ko, Оптика и спектроскопия, (Optics and Spectroscopy) **2**, 448 (1957).

[7] Propagation of Short Radio Waves, Ed. D. E. Kerr, Sec. 8.1, New York, 1951.

[8] Brodin, Prikhot'ko, and Soskin, Оптика и спектроскопия, (Optics and Spectroscopy) **6**, 28 (1959).

Translated by D. ter Haar
14

THE PRODUCTION OF ELEMENT 102

G. N. FLEROV, S. M. POLIKANOV,* A. S. KARAMYAN,† A. S. PASYUK, D. M. PARFANOVICH, N. I. TARANTIN, V. A. KARNAUKHOV, V. A. DRUIN, V. V. VOLKOV, A. M. SEMCHINOVA, Yu. Ts. OGANESYAN,* V. I. KHALIZEV, G. I. KHLEBNIKOV, B. F. MYASOEDOV,‡ and K. A. GAVRILOV*

Submitted to JETP editor August 1, 1959

J. Exptl. Theoret. Phys. (U.S.S.R.) **38**, 82-94 (January, 1960)

New experiments for the production of element 102 and the investigation of its nuclear properties are described. Pu^{241} and Pu^{239} targets were bombarded with accelerated O^{16} ions. Nuclear emulsions were used to record the radioactive decay of element-102 atoms. Alpha decay of the new isotope (most probably 102^{253}) was observed, having a half-life between 2 and 40 sec and energy of 8.9 ± 0.4 Mev. Careful analysis of possible background sources indicated that the background level is much lower than the observed effect.

INTRODUCTION

TRANSURANIUM elements have hitherto been produced principally by subjecting uranium and plutonium to prolonged bombardment in nuclear reactors. The atomic number of the target nuclei was gradually increased through successive neutron captures followed by beta decay; elements up to fermium (Z = 100) were produced in this manner. It has thus far not been possible to synthesize still heavier elements in the same way because larger values of Z are accompanied by a rapid reduction of nuclear lifetimes with respect to alpha decay and spontaneous fission, with the consequent sharply reduced probability for the formation of beta-active intermediate products, as a result of whose decay the nuclear charge would be increased.[1]

Further progress became possible with the development of techniques for accelerating multiply-charged ions. These ions can be used to increase the charge of the initial elements by several units at a time, thus avoiding the previously inevitable accumulation of intermediate products. However, even when multiply-charged ions are used the synthesis of new transuranium elements is an extremely difficult experimental task. The fundamental difficulty lies in the fact that the reactions leading to the production of a new element have extremely small cross sections. Fissility increases with the atomic number of the transuranium elements. An excited compound nucleus resulting from the fusion of an accelerated heavy ion with the target nucleus disintegrates principally through a fission process; decay through neutron emission, thus generating atoms of a new element, occurs in only a negligible fraction of the events. The experimenter therefore has only a small number of atoms available to use in identifying the new element and in determining its properties. The short lifetimes of these newly-formed isotopes are a second source of difficulty. Rapid decay hampers and sometimes entirely prevents the identification of a new element through ordinary chemical procedures.

In 1957 and 1958 several laboratories attempted to produce element 102 by using multiply-charged ions. An international group of Swedish, American and British scientists reported the synthesis of the element during the summer of 1957.[2] Among the reaction products of a curium target irradiated with C^{13} ions accelerated in the Stockholm cyclotron an alpha-active isotope was detected which emitted 8.5-Mev alpha particles and possessed a half-life of ~10 min. The total number of alpha particles detected with this energy was only 20. The investigators believed that they had produced element 102 with mass number 253 or 251; however at the University of California Radiation Laboratory these results were not reproduced, in spite of maintenance of identical conditions with much stronger ion beams.[3]

The 150-cm cyclotron of the U.S.S.R. Academy of Sciences Institute of Atomic Energy was used in our work on the synthesis of element 102, the first results being obtained in the autumn of 1957. Targets made of Pu^{241} (100 $\mu g/cm^2$) and of Pu^{239} (300 $\mu g/cm^2$) were irradiated with O^{16} ions ac-

*Joint Institute for Nuclear Research.

†Deceased.

‡Institute for Geochemistry and Analytic Chemistry, Academy of Sciences, U.S.S.R.

celerated to ~100 Mev. Since it was assumed that the half-lives of isotopes of element 102 which might be produced through the reaction of O^{16} ions with plutonium would be very short, we worked out a special physical technique instead of a chemical procedure for identifying the new element.

In the experiments with the Pu^{241} target eighteen 8.5-Mev alpha particles were detected. When Pu^{239} was bombarded 8 energetic particles were observed. The effect was thus smaller by a factor of 7 when converted to identical target thickness and identical bombarding period. After a number of control experiments we concluded that these alpha particles must be associated with the decay of an isotope of element 102, with probable mass number 251 — 253, produced when Pu^{241} was bombarded with O^{16} ions. A short account of these experiments has already been published.[4]

In May, 1958 a group of workers at the University of California published a report of experiments on the production of another isotope of element 102.[5] After Cm^{246} was bombarded with C^{12} ions the American investigators used a radiochemical technique to separate Fm^{250}, which under the given conditions could have resulted from the alpha decay of 102^{254} having a half-life of 3 sec.

The present paper reports further experiments performed at the Institute of Atomic Energy from April to September, 1958. We aimed to determine more precisely the nuclear properties of the produced element-102 isotope and to study the background more thoroughly.*

EXPERIMENTAL PROCEDURE

1. Ion Acceleration

In the present experiments, as previously, the targets were bombarded in the internal beam of the 150-cm cyclotron. Quintuply-charged O^{16} ions were produced directly in a special ion source[6] and were accelerated to 100 Mev. The ion source had been perfected through an improved design of the discharge chamber and enhanced cooling and stability. The power used in the gaseous discharge had been raised to 100 kw. Table I shows the properties of the ion beams which resulted from these improvements.

Since the cyclotron had been designed for work with protons, deuterons and helium ions (m/e = 1 or 2) its employment for the acceleration of quintuply-charged O^{16} ions (m/e = 3.2) required a highly strengthened current in the magnet coils (in order to attain the required magnetic field strength) accompanied by forced cooling. The required magnetic field configuration was obtained by means of additional shims. We know that simultaneously with quintuply-charged ions, singly-charged ions are accelerated at a multiple of the frequency. As a result of the stripping mechanism, the ion beam at the terminal radius contains, in addition to monoenergetic particles, quintuply-charged ions with a continuous energy distribution, produced in the cyclotron out of singly-charged ions. We succeeded in producing a beam in which the monoenergetic component was predominant, having an energy spread of not more than 4%.[7]

TABLE I. Properties of Heavy-Ion Beams

Ions	Charge	Intensity, μamp	Energy, Mev
C^{12}, C^{13}	4	20	94
N^{14}, N^{15}	5	2	110
O^{16}, O^{18}	5	3	102
	6	0.1	130

2. Recoil Technique

The procedure used to separate nuclei of element 102 from the target material was based on the collection of recoil nuclei. When a heavy bombarding particle strikes a target nucleus, the resulting compound nucleus acquires such high momentum that it may be knocked out of a fairly thick target. Ejected nuclei are caught by a suitable technique and are transferred to an emission detector. In this way a small number of the new atoms, which are usually highly radioactive, can be separated from the target material. Another advantage of this procedure is that it permits repeated bombardment of the same target.

The range of the recoil nuclei must be known before a target of optimum thickness can be prepared. In special experiments performed for this purpose thin gold foils with vacuum-deposited layers of aluminum or copper were bombarded with N^{14} ions of known energy. The radon nuclei produced in the reaction $Au^{197}(N^{14}, xn)$ were ejected from the gold and some of them entered a catcher after passing through the aluminum or copper layer. The intensity ratio of alpha-active products in the catcher and in the aluminum and copper layers of different thicknesses indicated the mean ranges for recoil nuclei in these elements. The range for atoms of element 102 produced when Pu^{241} was bombarded with O^{16} ions was estimated by using the experimental results

*A brief account of this work was given in a supplement to the report of G. N. Flerov at the Second International Conference on the Peaceful Uses of Atomic Energy in Geneva.

for the range of radon atoms in conjunction with Firsov's formula

$$R = 0.5 \frac{A_2 (A_1 + A_2)}{A_1} \frac{(Z_1 + Z_2)^{1/3}}{Z_1 Z_2} E, \quad (1)$$

where R is the atomic range in $\mu g/cm^2$; Z_1, A_1 and Z_2, A_2 are the atomic number and mass number of the recoil atom and medium, respectively; E is the kinetic energy of the recoil atom in kev.

Equation (1) was derived for the ranges of atoms with initial velocity $10^7 - 10^8$ cm/sec, taking into account the way in which slowing-down at such velocities is affected by the interaction between electron shells of the colliding atoms.[8] Consideration of the electronic effect showed that in this instance description of the atomic collision required a potential that is inversely proportional to the square of the atomic separation.

While developing a technique for catching recoil nuclei we performed in 1954 qualitative experiments investigating the ranges of radioactive nuclei produced in (n, 2n) and (n, p) reactions when various elements were bombarded with 14-Mev neutrons. The results indicated that the given formula satisfactorily describes the manner in which the ranges of the recoil nuclei depend on E, Z_1, A_1, Z_2 and A_2.

In Table II the experimental mean ranges of nuclei produced in various reactions are compared with the ranges calculated by Eq. (1). In computing the energies of reaction products it was assumed that a compound nucleus is formed, the momentum of the bombarding particle being transferred to the nucleus as a whole. For the recoil effect associated with the ejection of neutrons and protons from the compound nucleus angular isotropy of the emitted particles was assumed. Our data for the range of radon nuclei are in agreement with reference 9.

When the target is made of PuO_2 and the oxygen-ion energy is ~100 Mev a calculation indicates 500 – 600 $\mu g/cm^2$ for the recoil range.

3. Apparatus for Bombarding Targets and Registering Alpha Decay of Reaction Products

Figure 1 shows the experimental setup. An oxygen-ion beam 1 impinged on a plutonium layer 2. Nuclei of element 102 with high momentum were emitted by the target and entered a thin (~2μ) aluminum catcher foil 6. The ion collector 5 behind the catcher of recoil nuclei was connected to the current integrator, which monitored the beam intensity during bombardments and measured the total ion flux traversing the target. The catcher was shifted at regular intervals by means of a kapron thread to a position 2 m from the target and close to photographic plate 8, which served to register alpha decay. All apparatus was located within a brass vacuum tube communicating with the cyclotron chamber. An electric motor located outside of the vacuum system was used to pull the kapron thread through a special vacuum seal. For the purpose of estimating nuclear half-lives, the time during which the catcher remained under the target and close to the photographic plate, and also the time required to transfer it from its position in line with the target, were varied over a broad range. The minimum time required for transfer was 2 sec. An electronic time relay was used to govern the operation of the apparatus.

TABLE II. Experimental Ranges of Recoil Nuclei Compared with Calculations Based on Eq. (1)

Recoil nucleus	Stopping medium	Reaction	E, kev	R_{exp}, $\mu g/cm^2$	R_{calc}, $\mu g/cm^2$
Mg^{27}	Al	Al^{27} (n, p)	550	300 ± 30	280
Al^{28}	SiO_2	Si^{28} (n, p)	500	330 ± 30	185
Cu^{62}	Cu	Cu^{63} (n, 2p)	250	65 ± 10	85
Ag^{106}	Ag	Ag^{107} (n, 2n)	150	35 ± 20	40
Sb^{120}	Sb	Sb^{121} (n, 2n)	150	25 ± 10	30
$Rn^{205-207}$	Al	$Au^{197}(N^{14}, 4-6n)$	6000	240 ± 50	380
$Rn^{205-207}$	Cu	$Au^{197}(N^{14}, 4-6n)$	6000	330 ± 50	490

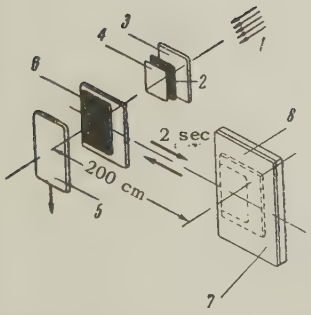

FIG. 1. Experimental setup: 1 – ion beam, 2 – plutonium layer, 3 – backing, 4 – shielding layer, 5 – ion collector, 6, 7 – catcher of recoil nuclei, 8 – photographic plate.

4. Preparation of Plutonium Targets

The targets had to satisfy two basic requirements: 1) sufficiently stable layers of active ma-

terial to withstand prolonged bombardment by an intense oxygen-ion beam; 2) sufficiently thin plutonium layers for the most efficient utilization of the recoil method.

The plutonium was deposited electrolytically or by means of tetraethylene glycol on thin nickel and niobium foils ($1-2\,\mu$). Nickel foils were produced by thermal dissociation of nickel tetracarbonyl on a hot surface; niobium foils were rolled from very pure metal.*

A thin copper film ($\sim 50\,\mu g/cm^2$) was vacuum-deposited on the plutonium layers to prevent damage of the latter. The plutonium-coated foil was clamped in a special brass holder between two well-cooled brass grids with apertures 1 mm in diameter. Satisfactory target stability was indicated by the fact that the target used in the largest number of runs was irradiated ~500 hours by a current of 0.5 μamp with inappreciable damage to the plutonium layers. (Granules of $\sim 0.001\,\mu g$ would easily have been detected on the photogrphic plates.)

Uniformity of the plutonium layers and their total thickness were controlled by special apparatus,[10] consisting of a miniature proportional counter and the target in question separated in a chamber by a distance of 15 cm. This chamber was filled with methane, which served as the working gas of the counter and as the absorber of alpha particles emitted by the target. By varying the gas pressure alpha particles of different energies were admitted to the counter and the target thickness was determined from range straggling. The thickness of the targets was determined to within ~70 $\mu g/cm^2$ of PuO_2. Figure 2 shows the distributions of alpha-particle ranges, which characterize the uniformity and thickness of the target layers. The amount of plutonium in a target varied from 100 to 200 $\mu g/cm^2$ (for 5×10 mm^2 targets), but the presence of inactive material and the copper film resulted in a total equivalent target thickness of $700-900\,\mu g/cm^2$ of PuO_2.

5. Nuclear Emulsion for Registering Alpha Particles

We used the special nuclear emulsion NIKFI-T1,[11] which provides a high degree of discrimination between alpha-particle and proton tracks but is insensitive to beta rays. We used plates without gelatin shielding, in order to provide more precise energy determinations for alpha particles entering the emulsion from the surface. A special technique further improved the discrimination of proton and alpha-particle tracks by means of the partial regression of latent images in water vapor. Processing in water vapor also attenuated the fog of beta and gamma rays.

*A more detailed description of the technique used in preparing the plutonium targets will be given in a separate paper.

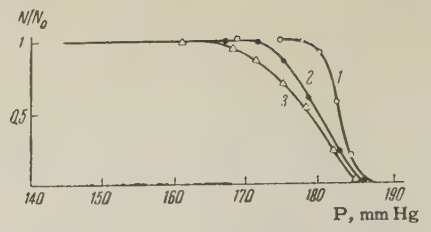

FIG. 2. Integral curves of alpha-particle range in methane for different plutonium targets: 1 – Pu^{239}, total thickness ≈ 250 $\mu g/cm^2$ (of PuO_2); 2 – Pu^{241}, total thickness ~ 750 $\mu g/cm^2$; 3 – Pu^{241}, total thickness ~ 900 $\mu g/cm^2$.

It should be noted that although the catchers were very thin ($\sim 2\,\mu$ aluminum foil) the beta-ray background resulting from activation of the catchers by oxygen ions was so high that NIKFI-Ya or Ilford-E1 emulsions could not be used.

A background resulting from radioactive contamination and cosmic rays accumulates in an emulsion during storage of the plates. For the purpose of removing this background the plates were treated with water vapor a few hours before experimental use until the latent images completely disappeared. The plates were kept in a vacuum before being subjected to bombardment in order to eliminate the danger of radioactive contamination from the air.

Since the plates were only 2 m distant from the targets it was necessary to attenuate the fast neutron flux which might produce an undesirable background of recoil protons and alpha particles from an (n, α) reaction. A shield consisting of 20 cm of copper and 10 cm of paraffin was therefore placed between the cyclotron chamber and the photographic plate. The background resulting from fast neutrons was then negligibly small.

The photographic plates were of considerably larger area than the catchers of recoil nuclei. Scanning of the areas which could not be reached by alpha particles from the catcher permitted direct determination of the background from the (n, α) reaction and from ThC′ under the experimental conditions.

INVESTIGATION OF PLUTONIUM TARGET CONTAMINATION BY BISMUTH AND LIGHTER ELEMENTS

In discussing experiments for the production of element 102 by bombarding plutonium with accelerated O^{16} ions we have stated[4] that bismuth

and lead impurities in the target might to some extent produce an imitative effect. This possibility was based on the fact that the bombardment with oxygen ions could produce "supershell" isotopes of astatine, radon, francium, and radium with lifetimes of a few seconds or minutes, the decay of which would yield alpha particles with energies > 8.5 Mev.

As a control, special experiments were performed to study the alpha-active reaction products produced when oxygen ions impinge on mercury, thallium, lead, and bismuth, using the same technique and conditions as in the experiments for the production of element 102.

1. Bombardment of Mercury and Thallium with Oxygen Ions

Targets consisting of a natural mixture of mercury isotopes were made by using tetraethylene glycol to deposit thin layers ($\sim 100\ \mu g/cm^2$) on niobium foil. Thallium layers of the same thickness were deposited on nickel foil by vacuum evaporation. The targets were bombarded with 98-Mev O^{16} ions. The stationary time of the catcher in the beam and next to the photographic plate was 8 sec, while the transfer time was 3 sec. No alpha particles with energies greater than 8 Mev were detected, but only a group with 6.8 ± 0.2 Mev in the case of mercury and 6.5 ± 0.2 Mev in the case of thallium (Fig. 3). These elements therefore are not subject to the effect in question. Moreover, the alpha-particle groups were so intense that their presence makes it easy to detect even small traces of mercury or thallium in plutonium. It was also determined that the working plutonium targets contained less than $0.01\ \mu g/cm^2$ of these elements, which therefore did not hinder the analysis of the data obtained when plutonium was bombarded with oxygen ions.

2. Bombardment of Bismuth with Oxygen Ions

The bismuth layer was deposited on a nickel backing by means of tetraethylene glycol and was bombarded under the same conditions as the mercury and thallium. The resulting alpha-particle spectrum shown in Fig. 3 reveals two intense groups, with peaks at 6.0 ± 0.2 Mev and 7.5 ± 0.2 Mev. The number of detected alpha particles with ~ 9 Mev was smaller by a factor of about 1000 than the number with ~ 7.5 Mev. From the ratio of these groups in the spectra resulting when plutonium was bombarded with oxygen we can determine the fraction of alpha particles with ~ 9 Mev that is associated with bismuth impurities. In

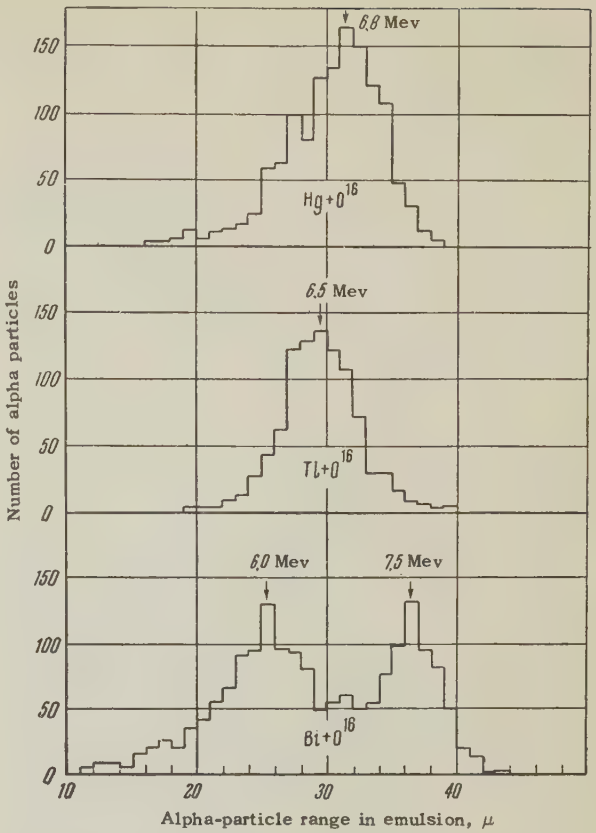

FIG. 3. Spectra of alpha particles from the bombardment of mercury, thallium, and bismuth with O^{16} ions.

the spectra obtained during the autumn of 1957 the 7.5-Mev alpha-particle group is at most 30 times as intense as the 9-Mev group, thus indicating that bismuth impurities in the plutonium target could not have produced a substantial background.

3. Bombardment of Lead with Oxygen Ions

The first experiments with lead indicated that when this element contaminates plutonium targets it may be the principal source of the background. Figure 4 shows the energy spectrum of alpha particles produced when a natural lead target was bombarded with 98-Mev oxygen ions. The reaction products are seen to include isotopes that emit alpha particles with ~ 9 Mev and have a half-life of 35 ± 10 sec.

A relatively large cross section was found for the production of an isotope emitting 9-Mev alpha particles. It was estimated that 1 μg of lead in a plutonium target could imitate the previously observed effect[4] attributed to the decay of element 102.

A sensitive activation method was developed for the precise determination of lead impurities in plutonium targets. When lead is bombarded with carbon or oxygen ions, reactions with large

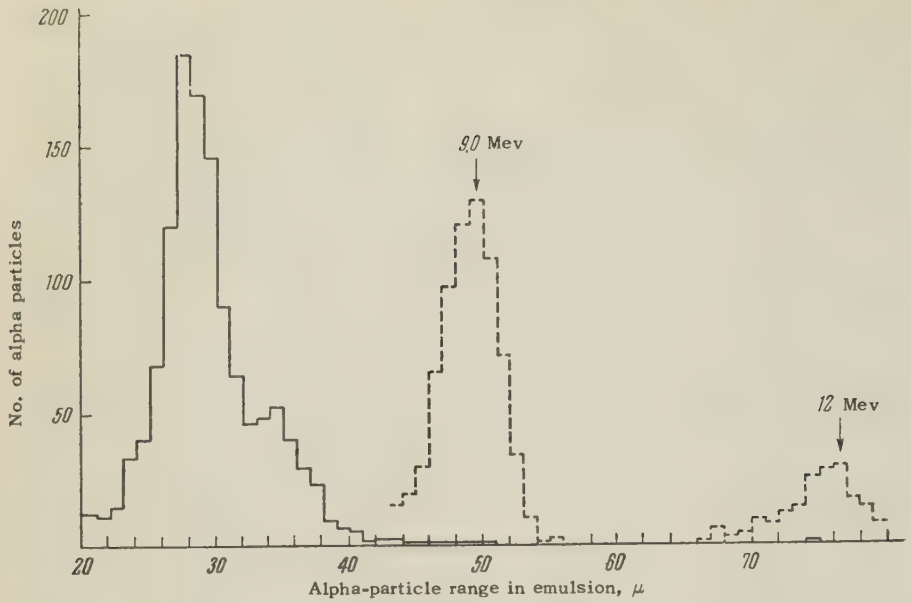

FIG. 4. Spectrum of alpha particles from the bombardment of lead with O^{16} ions. The 9-Mev and 12-Mev alpha-particle groups are shown by means of broken lines, which represent the combined results of several experiments.

cross sections result in the production of Rn^{211}, which is precisely characterized by a half-life of 16 hours and by its equilibrium with Po^{211}, which emits 7.43-Mev alpha particles. The plutonium targets were bombarded with carbon and oxygen ions and the Rn^{211} yield, measured by an ionization chamber, was used to estimate the amount of lead that was present. The technique was sensitive enough to detect as little as 0.01 μg of lead.

Since lead may be concentrated either deep within or on the surface of a plutonium target it was necessary to determine how the ratio of recoil Rn^{211} yield to that of the isotope associated with $E_\alpha = 9$ Mev was dependent on target thickness. Lead targets of different thicknesses were irradiated. Table III gives the ratios of 9-Mev alpha activity to Rn^{211} yield for the lead targets (with the yield ratio for a 215 $\mu g/cm^2$ target taken as unity). The ratio is seen to depend strongly on target thickness. In addition to determining the amount of lead impurities in the plutonium we must therefore know its distribution over the target thickness. For this purpose we compared the relative Rn^{211} yields when plutonium targets were bombarded with oxygen and carbon ions. The same isotope Rn^{211} is produced by both kinds of ions, but since the C^{12} ion transfers considerably less momentum than the oxygen ion to the nucleus the yield for the $(Pb + C^{12})$ reaction depends much more strongly on target thickness. Table III also shows the relative yields of Rn^{211} entering the catcher for the reactions $(Pb + O^{16})$ and $(Pb + C^{12})$, with the ratio for a 215 $\mu g/cm^2$ lead target taken as unity.

TABLE III.

Target thickness, $\mu g/cm^2$	215	520	1160
Yield ratio of 9-Mev alpha activity and Rn^{211} (from $Pb + O^{16}$)	1.00	1.28	1.87
Ratio of Rn^{211} yields for the reactions $Pb + O^{16}$ and $Pb + C^{12}$	1.00	1.15	1.40

By bombarding plutonium targets with oxygen and carbon ions we were thus able to compute their lead content and distribution and thus to determine how much of the 9-Mev alpha-particle background was attributable to lead impurities.

It must be mentioned that when lead was bombarded with oxygen ions additional products were detected which decayed with the emission of 12-Mev alpha particles.[12] This emission was used as an additional control, but because of its low intensity it provides a much less accurate method of determining the lead content than the measurement of the Rn^{211} yield.

BOMBARDMENT OF Pu^{241} AND Pu^{239} WITH OXYGEN IONS: RESULTS AND DISCUSSION

In most of the experiments with Pu^{241}, target No. 1 containing 180 $\mu g/cm^2$ of plutonium was used. This target was bombarded 40 times, in each instance for a period of 3 hours, with the catcher in the beam and near the photographic plate for 8 sec and a transfer time of 3 sec (Fig. 1). As in the earlier work,[4] alpha particles with ranges in the interval $45 - 51\,\mu$ of emulsion were detected. The total number of such particles was 90.

Table IV gives the results of an activation analysis of the targets for lead impurities, for both target No. 1 and target No. 2 made of Pu^{241}, which

TABLE IV.

Target	Pb, 215 $\mu g/cm^2$	Pu^{241}, No. 1	Pu^{241}, No. 2
Yield ratio of 9-Mev alpha activity and Rn^{211} from O^{16}-bombarded targets	1.00	3.5 ± 0.5	7.0 ± 1.0
Ratio of Rn^{211} yields from targets bombarded with O^{16} and C^{12} ions	1.00	1.0 ± 0.2	0.8 ± 0.2

will be discussed below. To make comparison with Table III easy the values for a 215 $\mu g/cm^2$ lead target are taken as unity. The comparison of the tables shows that the lead contamination of plutonium target No. 1 can account for only a fraction of the 9-Mev activity. Comparison of the Rn^{211} yields from bombardment with O^{16} and C^{12} ions indicates that the lead impurities were close to the target surface. Even if it is assumed that the lead is uniformly distributed throughout the target the lead can account for at most 40% of the total number of detected 9-Mev alpha particles.

Approximately the same result, although with considerably lower accuracy, is obtained by using the characteristic 12-Mev alpha rays produced in lead by oxygen ions. For a lead target the ratio of 9-Mev to 12-Mev alpha particles is 4.0 ± 0.5. In the experiments with the Pu^{241} target No. 1 this ratio was 8.0 ± 2.0; this agrees with the fact that 25 — 45% of the 9-Mev alpha particles are attributable to lead impurities.

Scanning of the plate areas that could not be reached by alpha particles from the catcher indicated that the background from the (n, α) reaction and ThC′ contamination did not exceed 5%. The total background unassociated with the production of element 102 was thus not greater than half of the observed effect.

Following further purification of the plutonium to remove lead, target No. 2 containing ~ 100 $\mu g/cm^2$ of Pu^{241} was prepared; the amount of lead was thus considerably smaller than in the first target (Table IV). Figure 5 shows the region of the alpha-particle spectrum above 7.5 Mev resulting from 10 three-hour bombardments of the second target with the recording apparatus functioning exactly as previously. A total of 20 particles was found with ranges in the interval 45 — 51 μ of emulsion, but an activation analysis showed that only 4 of these could be attributed to lead impurities.

Alpha particles with ranges 45 — 51 μ have a mean energy of 8.8 Mev. It must be remembered, however, that the synthesized nuclei are ejected from the target with considerable energy (~ 6 Mev) and penetrate the catcher to a considerable

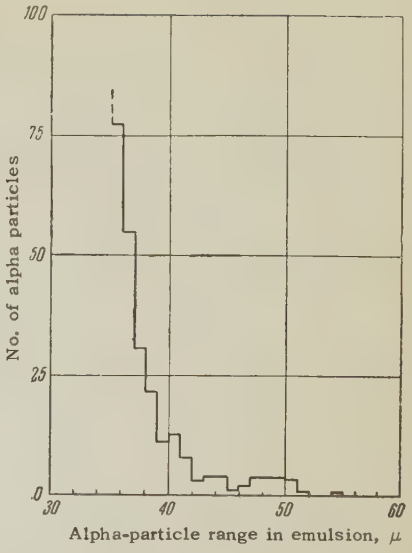

FIG. 5. Spectrum of alpha particles with energies above 7.5 Mev, from Pu^{241} target (No. 2) bombarded with O^{16} ions.

depth. Alpha particles emerging from the catcher have thus lost a portion of their energy, especially when emerging at small angles to the surface. The correction required to account for this effect was determined experimentally by measuring the ranges of alpha particles from Po^{211} produced by oxygen-ion bombardment of lead. When this correction is taken into account the alpha-particle group of present interest has the energy 8.9 ± 0.4 Mev.

The repetition of experiments using oxygen ions and the additional control experiments thus confirm the earlier conclusion[4] that element 102 is produced when Pu^{241} is bombarded with oxygen ions.

In order to determine the half-life of the element-102 isotope we performed a series of 39 three-hour bombardments in which the transfer time of the catcher from the target to the photographic plate was 10, 100, and 250 sec, respectively, with equal lengths of time in the beam and adjacent to the plate. Unfortunately the first target was used; the lead impurities hindered exact determination of the half-life for the activity of interest. It can be stated, however, that all activity with ranges 45 — 51 μ, and therefore the isotope of element 102, decayed with a half-life < 40 sec.

In experiments to determine the lower limit of the half-life the exposure period of the catcher was shortened to 3 sec while the transfer time was 1.5 — 2 sec. The results indicate that the half-life cannot be shorter than 2 sec.

In order to establish the mass number of the new isotope we attempted to determine the dependence of the cross section for its production on the bombarding energy, using 85-, 93-, and

98-Mev oxygen ions. In each instance the effect was too small to provide an exact excitation curve for the alpha activity of interest. It was established that the cross section increases considerably from 85-Mev to 93-Mev but is somewhat reduced above 93 Mev. In consideration of the cross sections for the (O^{16}, 4n) and (O^{16}, 5n) reactions in uranium,[13,14] the foregoing results may be regarded as an indication that the reaction Pu^{241} (O^{16}, 4n) probably took place in our experiments, producing element 102^{253}, although we cannot exclude the possibility that element 102^{254} was produced through a (O^{16}, 3n) reaction. It was shown by the experiments on lighter nuclei (V, Nb) described in reference 15 that this latter reaction possesses considerably greater probability than would follow from the simple theory of nucleon evaporation from a compound nucleus.

The cross section for the production of element 102 can be determined only tentatively since a number of imprecisely determined factors are involved. If we assume that the given isotope is subject only to alpha decay the cross section is of the order 5×10^{-32} cm^2, which is considerably smaller than the cross section obtained by the American investigators for the reaction Cm^{246} (C^{12}, 4n) 102^{254}.

Pu^{239} was also bombarded with oxygen ions. In similar experiments during the autumn of 1957[4] alpha particles with energies > 8.5 Mev were also detected, although their yield for an identical amount of target material was about one-seventh as large as in the case of Pu^{241}. In 20 three-hour bombardments, corresponding to three times as much ion current to the target as in the previous work, we detected only one 8.8-Mev alpha particle. What had been observed previously when Pu^{239} was bombarded was evidently entirely a background effect.

It must be remembered that when multiply-charged ions interact with heavy nuclei, protons or alpha particles may be emitted as well as neutrons. Therefore, when plutonium is bombarded with oxygen ions, mendelevium (Z=101) or fermium (Z=100) can be produced. According to the systematics of alpha-active nuclei, alpha particles with energies greater than 8.5 Mev can be emitted by isotopes of these elements that are lighter than Mv^{250} and Fm^{246}. However, when Pu^{241} is irradiated with O^{16} ions these isotopes can be produced only in reactions involving the emission of seven or more nucleons; this is energetically impossible when 98-Mev oxygen ions are used.

Of course, departures from the systematics might occur in the direction of increasing the alpha-decay energy of Mv and Fm isotopes, i.e., Mv^{251} or Fm^{247} could emit alpha particles having energies greater than 8.5 Mev. There is considerably greater probability that these isotopes will be produced when O^{16} interacts with Pu^{239} than with Pu^{241}. The fact that more rather than fewer alpha particles with higher energy (~ 8.9 Mev) result with Pu^{241} than with Pu^{239} leads us to infer that this emission cannot result from the decay of mendelevium or fermium isotopes.

At the Eighth Mendeleev Congress (in Moscow, March, 1959) A. Ghiorso reported preliminary results from the bombardment of Cm^{244} with C^{13} ions at the University of California. An isotope was produced having a half-life of 10 — 20 sec and emitting alpha particles with 8.8 ± 0.1 Mev, which the American workers attributed to the decay of 102^{253}.

It is the pleasant duty of the authors to thank Academician I. V. Kurchatov for his extreme interest in the present work. We are grateful for the constant assistance rendered by Yu. B. Gerlit, L. I. Guseva, and K. V. Filippova of the Institute for Geochemistry and Analytic Chemistry and by Yu. V. Lobanov, V. L. Mikheev, V. P. Perelygin, A. P. Pleve, and G. M. Ter-Akopyan of the Joint Institute for Nuclear Research, as well as for the valuable aid in matters of technique which was rendered by K. S. Bogomolov and A. A. Sirotinskaya of the Motion Picture and Photography Research Institute, by D. G. Alkhazov of the Leningrad Institute of Physics and Technology and by S. P. Kalinin of the Institute of Atomic Energy.

[1] G. Seaborg, Report at Second International Conference on the Peaceful Uses of Atomic Energy, Geneva, 1958; Атомная энергия (Atomic Energy) **6**, 21 (1959).

[2] Fields, Friedman, Milsted, Atterling, Forsling, Holm, and Aström, Phys. Rev. **107**, 1460 (1957).

[3] Ghiorso, Sikkeland, Walton, and Seaborg, Phys. Rev. Letters **1**, 17 (1958).

[4] Flerov, Polikanov, Karamyan, Pasyuk, Parfanovich, Tarantin, Karnaukhov, Druin, Volkov, Semchinova, Oganesyan, Khalizev, and Khlebnikov, Dokl. Akad. Nauk SSSR **120**, 73 (1958), Soviet Phys.-Doklady **3**, 546 (1958).

[5] Ghiorso, Sikkeland, Walton, and Seaborg, Phys. Rev. Letters **1**, 18 (1958).

[6] Morozov, Makov, and Ioffe, Атомная энергия (Atomic Energy) **3**, 272 (1957).

[7] Yu. Ts. Oganesyan, JETP **36**, 936 (1959), Soviet Phys. JETP **9**, 661 (1959).

[8] O. B. Firsov, Dokl. Akad. Nauk SSSR **91**, 515 (1953).

[9] R. B. Leachman and H. Atterling, Arkiv Fysik **13**, 101 (1958).

[10] V. A. Karnaukhov and V. L. Mikheev, Приборы и техника эксперимента (Instruments and Measurement Engineering), in press.

[11] A. A. Sirotinskaya and K. S. Bogomolov, Тр. Всесоюзного научно-исследовательского кинофотоинститута (Trans. All-Union Motion Picture and Photography Research Institute) **2**, 66 (1958).

[12] Karnaukhov, Khalizev, and Flerov, JETP **37**, 1266 (1959), Soviet Phys. JETP **10**, 901 (1960).

[13] Volkov, Guseva, Tarantin, Myasoedov, and Filippova, JETP **36**, 1207 (1959), Soviet Phys. JETP **10**, 859 (1960).

[14] Perelygin, Donets, and Flerov, JETP **37**, 1558 (1959), Soviet Phys. JETP **10**, 1106 (1960).

[15] Karamyan, Gerlit, and Myasoedov, JETP **36**, 621 (1959), Soviet Phys. JETP **9**, 431 (1959).

Translated by I. Emin
15

(γ, p) REACTION ON Au^{197}

E. D. MAKHNOVSKIĬ

Leningrad Physico-technical Institute, Academy of Sciences, U.S.S.R.

Submitted to JETP editor August 7, 1959

J. Exptl. Theoret. Phys. (U.S.S.R.) **38**, 95-99 (January, 1960)

Energy and angular distributions of protons from irradiation of gold with bremsstrahlung having $E_{\gamma max} = 22.5$ Mev were obtained. The results are compared with calculations based on the statistical theory and on the theory of a direct photoeffect.

PROTON yields from irradiation of heavy elements ($Z > 70$) with bremsstrahlung having $E_{\gamma max} \sim 23$ Mev are 2 or 3 orders of magnitude greater than the yields predicted by the statistical theory of nuclear reactions.[1] The spectra of the photoprotons also contradict this theory. Energy distributions computed from Courant's theory of a direct photoeffect for nuclei like Bi^{209}, Ta^{181}, and Pb^{208} have a shape which is in good agreement with the experimental data of Toms and Stephens.[2] However the yields are 3.3 — 13 times less than the measured yields.

The published data of Dawson[3] on the energy distribution of photoprotons from gold do not agree with either the statistical theory or the direct photoeffect proposed by Courant. His distributions could not be badly distorted by the contribution of deuterons. According to an estimate made in reference 4, this contribution amounted to about 12%. However, the maximum energy of the photon spectrum in reference 3 was set way above the region of the giant resonance — it was equal to 70 Mev. Protons with energies up to 17 Mev were recorded. This could lead to a sizeable contribution of more complex photodisintegrations with emission of protons and, consequently, would make more difficult the analysis of the experimental results.

In the present work, we have measured the energy and angular distribution of photoprotons from irradiation of gold with bremsstrahlung having $E_{\gamma max} = 22.5$ Mev. The results are compared with the statistical theory and with Courant's theory of a direct photoeffect, and also with computations using a theory of direct resonance emission of nucleons, which takes into account the shell structure of the nucleus.[5]

EXPERIMENTAL ARRANGEMENT

The apparatus and the experimental setup have been described in reference 4. The source of γ radiation was the synchrotron of the Physico-technical Institute. A 58 mg/cm^2 gold foil, placed at an angle of 30° to the gamma beam, was irradiated. An area of 1.7×1.5 cm^2 was subjected to the γ radiation. NIKFI-Ya2 nuclear emulsions, with a thickness of 200 μ, recorded the protons at angles of 20, 40, 50, 60, 70, 80, 90, 100, 110, 120, 140, and 160° with respect to the axis of the beam. The mean angle of entry of particles into the emulsions was 8°. The distance from the center of each photoplate to the center of the target was 8.5 cm. The multiplate chamber was shielded with a 10 cm layer of paraffin and a layer of lead of the same thickness.

For the measurements on the photoplates, we selected particle tracks longer than 60 μ, which started from the emulsion surface and were at angles which satisfied the geometrical conditions of the experiment. It was not possible to distinguish singly-charged particles in the emulsion. However the yield of photodeuterons from Au^{197} is an order of magnitude less than the yield of photoprotons. The yield of tritons is still smaller. Because of this, all the selected tracks could be assumed to be proton tracks. The proton energies were determined from their measured range in emulsion and the known range-energy curve. Corrections were made for energy loss in the effective half-thickness of the target.

Deuterons with a range > 60 μ, coming from (γ, d) reactions and recorded as protons, gave a background amounting to ~ 12%.[4] In addition, the interaction of the scattered radiation with the chamber wall material produced a background of protons. These were mainly protons with energies < 4.5 Mev. In the energy range of 7 — 17 Mev, they amounted to about 3%. The background from α particles of acceptable range was < 1%.

RESULTS AND DISCUSSION

The complete energy distribution of the photoprotons over the range 7 — 17 Mev is shown in the histogram of Fig. 1.

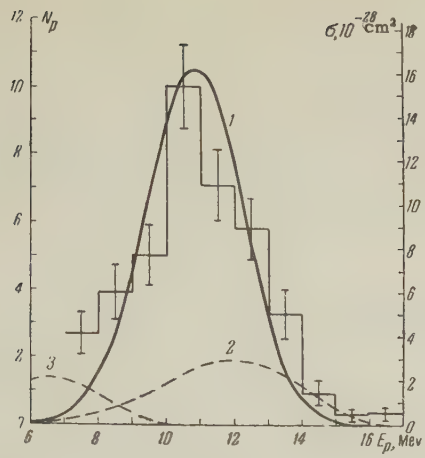

FIG. 1. Proton energy distribution. 1 – energy spectrum from the theory of direct resonance emission of nucleons; 2 – energy spectrum from Courant's theory of a direct photoeffect; 3 – energy spectrum from statistical theory.

The failure of the evaporation model to explain the energy distributions and yields of photoprotons from heavy elements led to the assumption that in this case the (γ, p) reaction goes mainly via a direct photoeffect. In Fig. 1, the solid curve shows the energy distribution of photoprotons computed from the theory of direct resonance emission of nucleons, according to the paper of Wilkinson.[5] In computing this curve we used the scheme of single-particle levels suggested by Klinkenberg.[6] The nuclear radius was taken equal to $1.3 \times 10^{-13} A^{1/3}$ cm.

The penetrabilities of the barriers for protons of various angular momenta and energies were computed by the WKB method. The depth V of the potential well was treated as a parameter. To get agreement between computed and experimental spectra required a value of V equal to ~ 53 Mev. Small changes of well depth had little effect on the location of the maximum, which was at 10.9 Mev. The table lists the proton transitions

Proton transitions	Proton yield, %
$2d_{3/2} \rightarrow 2f_{5/2}$	0.9
$2d_{3/2} \rightarrow 3p_{1/2}$	56.9
$2d_{3/2} \rightarrow 3p_{3/2}$	4.9
$2d_{5/2} \rightarrow 2f_{5/2}$	0.1
$2d_{5/2} \rightarrow 3p_{3/2}$	37.1
$1g_{7/2} \rightarrow 2f_{5/2}$	0.1
	100

in Au^{197} which give significant contributions to the emission of direct resonance photoprotons. The column on the right gives the relative yields of direct resonance photoprotons from these transitions. We see that most of the protons from direct resonance photoemission come from d → p transitions. Curve 1 is normalized so that the area under it in the energy interval 10.2 – 17 Mev is equal to the area under the experimental histogram over the same energy interval. Such a normalization assumes that all protons with energy > 10.2 Mev are due to the direct resonance photoprocess. As we see from the figure, the shape of the theoretical spectrum is quite close to the experimental shape.

The ratios computed by Wilkinson of the cross sections for emission of direct resonance protons to the total cross sections for absorption of bremsstrahlung with $E_{\gamma max} = 23$ Mev in heavy nuclei are in good agreement with experiment.[5] For gold this ratio was equal to approximately 0.14%. If we use the data of reference 7, in which they found essentially the total integral cross section for absorption of γ quanta with this same maximum energy, the integral cross section for the (γ, p) reaction on Au^{197} will be equal to ~ 6.1×10^{-27} Mev-cm². In accordance with this number, we have added an absolute scale of ordinates at the right of Fig. 1.

The dashed curve 2 shows the spectra of protons from the direct photoeffect, obtained using Courant's theory.[8] The shape of the energy distribution was computed from the formula[2,3]

$$I(\varepsilon) \approx f(\varepsilon) \int_{B_p+\varepsilon}^{E_{max}} N_\gamma(E) E^{-3} dE,$$

where $I(\epsilon)$ is the relative number of protons with energy ϵ; $f(\epsilon)$ is the penetrability of the potential barrier;[9] $B_p = 5.72$ Mev is the binding energy of the proton in Au^{197};[1] E_{max} is the maximum energy of the bremsstrahlung; $N_\gamma(E)$ is the number of photons of energy E in the spectrum.

Using the formulas given in reference 8, we computed the absolute cross section for emission of protons with an arbitrarily chosen energy (11.3 Mev). The depth of the potential well and the order of filling of the single-particle levels by protons was assumed to be the same as in the computation using Wilkinson's theory. From the shape of the spectrum and the value at this reference point, the energy distribution was drawn on an absolute scale. The maximum of the spectrum was found to be close to the experimental value. However the area under the curve gives an integral cross section of 1.15×10^{-27} Mev-cm², i.e., approximately five times smaller than Wilkinson's theory.

As a result of collisions with other nucleons in the nucleus, protons which have absorbed a γ quantum are lost to the direct photoprocess. This loss from the direct photoprocess can be taken

into account approximately by introducing into Courant's formula for the total cross section an "escape" coefficient equal to $3\lambda/4R$. Here λ is the mean free path of nucleons in nuclear matter and R is the nuclear radius. For proton energies corresponding to our experiment, λ is $\sim 3.5 \times 10^{-13}$ cm.[10] For Au^{197}, the coefficient is 0.35. If we take account of this probability of "escape" of protons from the nucleus without collision with other nucleons, the integral cross section from Courant's theory becomes 15 times less than that predicted by the theory of direct resonance emission of nucleons.

It should be mentioned that the experimental yields of protons from the (γ, p) reaction ($E_{\gamma max} = 23$ Mev) on Bi^{209}, Ta^{181}, and Pb^{208} are, respectively 3.3, 8, and 13 times greater than the yields computed from Courant's theory.[2]

The dashed curve 3 shows the proton energy distribution computed according to statistical theory, using the formula[3]

$$I(\varepsilon) = \varepsilon\sigma_c(\varepsilon)\, e^{-\varepsilon/T} \int_{B_p+\varepsilon}^{E_{max}} N_\gamma(E)\, \sigma_{\gamma,\,n}(E)\, dE,$$

where $\sigma_c(\epsilon)$ is the cross section for capture of a proton with energy ϵ by the residual nucleus;[9] $\sigma_{\gamma,n}(E)$ is the cross section for the (γ, n) reaction on gold for quantum energy E;[7] T is the temperature of the residual nucleus in Mev.

The curve was normalized so that the area under it in the range 7 — 17 Mev was equal to the difference between the area under the experimental curve and the area under the curve corresponding to Wilkinson's theory. The best agreement with the experimental spectrum was obtained for T = 0.54 Mev. Such a value of T does not contradict existing data on nuclear temperatures for heavy elements. The maximum of the distribution was around 6.5 Mev. Curve 3 shows that the possible contribution from protons caused by an evaporation process is small. It can amount to several percent of the total yield of the (γ, p) reaction. In view of the overlap of the energy regions of protons from the direct photoeffect and from evaporation, it does not appear possible to give a more exact value for this contribution.

According to the theory of the direct photoeffect,[5,8] the angular distribution from transitions of the type $l \to l-1$ has the form

$$d\sigma_{l\to l-1} \sim 1 + \frac{1}{2}\frac{l-1}{l+1}\sin^2\theta,$$

where l is the initial orbital angular momentum of the proton. Computation of the energy spectrum according to the theory of direct resonance emission of nucleons showed that 99% of the protons in direct photoemission are caused by $d \to p$ transitions. For such transitions,

$$d\sigma_{2\to1} \sim 1 + 0.17\sin^2\theta.$$

In other words, an almost isotropic distribution is predicted. In Fig. 2 we show the angular distribution for 197 protons with energies 9 — 15 Mev.

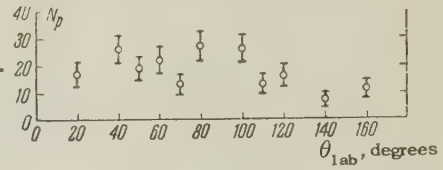

FIG. 2. Proton angular distribution.

The maximum error in determination of solid angles is < 15%. Only the statistical errors are shown on the graph. The observed angular distribution is close to isotropic, and is not in contradiction with expected shape for $d \to p$ transitions.

It is interesting to note that the angular distribution of protons with energies 8 — 11 Mev, obtained by Dawson,[3] was also almost isotropic.

The computations show that the theory of direct resonance emission of nucleons agrees best with our experiment.

The author thanks A. P. Komar and G. M. Shklyarevskiĭ for valuable comments and help with the work, and also the accelerator group for uninterrupted and stable operation of the synchrotron.

Note added in proof (December 15, 1959). After the paper was sent to press, the absolute intensity of the synchrotron beam for $E_{\gamma max} = 22.5$ Mev was measured. It was then possible to compute the yield of protons with energies up to 17 Mev from the (γ, p) reaction on Au^{197}, and this value was found to be $Y = (1.6 \pm 0.9) \times 10^{-5}$ protons/mole-Mev. This value is in good agreement with the results of Dawson,[3] and in poorer agreement with the value obtained by Weinstock and Halpern.[1] The yield of photoprotons from gold, computed by Wilkinson[5] according to the theory of direct resonance emission of nucleons, is in satisfactory agreement with our value.

[1] E. V. Weinstock and I. Halpern, Phys. Rev. **94**, 1651 (1954).

[2] M. E. Toms and W. E. Stephens, Phys. Rev. **98**, 626 (1955); **92**, 362 (1953).

[3] W. K. Dawson, Can. J. Phys. **34**, 1480 (1956).

[4] E. D. Makhnovskiĭ, JETP **36**, 739 (1959), Soviet Phys. JETP **9**, 519 (1959).

[5] D. Wilkinson, Physica **22**, 1039 (1956).

[6] P. E. A. Klinkenberg, Revs. Modern Phys. **24**, 63 (1952).

[7] Montalbetti, Katz, and Goldemberg, Phys. Rev. **91**, 659 (1953).

[8] E. D. Courant, Phys. Rev. **82**, 703 (1951).

[9] J. Blatt and V. Weisskopf, Theoretical Nuclear Physics, Wiley, New York, 1952.

[10] Hayakawa, Kawai, and Kikuchi, Progr. Theor. Phys. **13**, 415 (1955).

Translated by M. Hamermesh
16

ULTRA-HIGH-ENERGY EXTENSIVE AIR SHOWERS

A. T. ABROSIMOV, G. A. BAZILEVSKAYA, V. I. SOLOV' EVA, and G. B. KHRISTIANSEN

Institute of Nuclear Physics, Moscow State University; P. N. Lebedev Physics Institute, Academy of Sciences, U.S.S.R.

Submitted to JETP editor August 15, 1959

J. Exptl. Theoret. Phys. (U.S.S.R.) **38**, 100-107 (January, 1960)

Extensive air showers having from 5×10^6 to 10^8 particles were investigated. Data are presented on the absolute shower intensity, the value spectrum exponent, and on the lateral distributions of the electron-photon component and of the μ mesons of these showers. Data on the electron-photon component indicate either that there is no equilibrium between the electron-photon and the nuclear components in ultra-high-energy showers in the lower layers of the atmosphere, or that the lateral distribution of the electrons on the periphery of the shower is determined not only by the Coulomb scattering, but also by the particle angular divergence in the elementary nuclear-cascade events.

INTRODUCTION

An investigation of ultra-high-energy showers is of particular interest in the determination of the origin of cosmic rays and in the study of the processes that lead to the development of such showers in the atmosphere. There are at present relatively few papers devoted to a study of ultra-high-energy showers. These pertain to the work done by Soviet scientists in 1952-1957 at sea level[1] and on mountains,[2] to the work of Cranshaw, Galbraith, et al.,[3-6] and the work of Clark et al.,[7] reported in 1957-1958 and performed at sea level.

The type of the muon lateral distribution function was determined, not very accurately, with a small hodoscopic array,[1] and the lateral distribution function of all the charged particles was obtained in that experiment from the "separation curve." Cranshaw's group[3-6] investigated in detail showers of the same energy as in reference 1, but the number of particles in each registered shower was not determined, and the data on both the shower particle spectrum and the lateral distribution function were averaged over showers that produced a definite charged-particle density within a circle of a specified radius. The use of luminescent counters has enabled Clark et al.[7] to investigate extensive atmospheric showers most accurately, but they merely verified whether the registered flux densities of all the charged particles satisfied certain lateral distribution functions (with a parameter value s = 1.4, see reference 8).

The present investigation was devoted to a study of showers with 10^6 to 10^8 particles. The work was performed with part of a large array built at the Moscow State University for an all-out investigation of extensive atmospheric showers at sea level. We note that the use of part of the array described in the present paper jointly with part of the array described earlier (see, for example, reference 9) yielded many new data on the energy characteristics of electron-photon and muon components.[10]

DESCRIPTION OF THE EXPERIMENT

The apparatus was mounted on ten laboratory carts. Seven of the carts were located at the center and at the corners of a hexagon inscribed in a circle 150 m in radius, while the remaining three were located on one straight line (Fig. 1) at distances up to 800 m. The carts had light covers made of canvas and glass wool, and the total amount of matter above the counters used to register the shower

FIG. 1. General plan of the installation. The numbers indicate the cart numbers, K – part of the apparatus described in reference 9.

particles did not exceed 1.5 g/cm^2. Charged-particle and penetrating-particle detectors were placed in each cart. The charged-particle detectors were self-quenching Geiger-Müller counters of 330 and 100 cm^2 area. In each cart there were 100 counters of the former type and 24 of the latter. The penetrating-particle detector comprised 24 counters (each of 330 cm^2 area) arranged in one row and surrounded by an absorber made of iron and lead. Figure 2 shows a section through the detector. Each counter of the apparatus was included in a GK-7 hodoscopic cell.

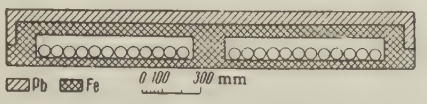

FIG. 2. Section through the penetrating-particle detector.

The apparatus was controlled upon simultaneous operation of four groups of counters, each of 3960 cm^2 area (12 counters of 330 cm^2 area connected in parallel). Each counter in the control groups was also connected to a corresponding hodoscopic cell. Two control counter groups were mounted on cart No. 9, and two on cart No. 10. The control pulses were transmitted to the hodoscopic cell through a high-frequency cable and delay lines, one in each cart. The delay time was chosen such that, during the registration of a shower with a vertical axis, the control pulse should arrive in the middle of the resolution-time interval of the hodoscopic cells. The minimum resolving times of the hodoscopic cells were 13 μsec in carts 1 — 3 and 9 μsec in carts 4 — 10; the resultant mean values were 20 and 15 μsec respectively

The apparatus made it possible to locate the axis and the number of particles of the registered shower, provided the axis was within the limits of the apparatus and the shower had a sufficient number of particles. The density distributions recorded by our apparatus were such that in most cases when the shower axis fell within the hexagon its position could be located accurate to half the distance between measurement points without using any particular type of lateral distribution function. To place the axis position more accurately it was assumed that the lateral distribution function for the investigated showers was the same at distances r up to 250 or 300 m from the axis as for showers with $N \leq 5 \times 10^5$ particles:[11]*

$$\rho(r) = \frac{2 \cdot 10^{-3} N}{r} e^{-r/60}, \qquad r \leqslant 96 \text{ m},$$
$$\rho(r) = \frac{0.60 N}{r^{2.6}}, \qquad r > 96 \text{ m}, \tag{1}$$

*The results given in this reference confirm that the lateral distribution function for the charged particles of the investigated showers is $\sim r^{-2.6}$ at r > 100 m.

where $\rho(r)$ is the particle density at a distance r from the axis.

To find the axis and the number of particles in the shower we used the readings of the carts arranged in a hexagon. From the known formulas

$$\rho = \frac{1}{\sigma} \ln \frac{n}{n-m}, \quad \Delta\rho = \frac{1}{\sigma} \frac{1}{\sqrt{(n/m)\ (n-m)}}$$

we determined the most probable density ρ at the cart location, when m out of the n counters of area σ in the cart operated. The ratio of the particle density at two measurement points and the distance between these points were used to plot the geometric locus of the axis for a specified lateral distribution function. Since the determined density was subject to an error, two curves were plotted for each specified density ratio k, corresponding to $k + \Delta k$ and $k - \Delta k$; the region between these two curves was taken to be the region of most probable axis location. We could choose for our apparatus at least three independent pairs of density registration points and find the intersection of the three regions corresponding to these three independent pairs. The center of the new region thus obtained was taken to be the shower axis.

The average number of shower particles $\overline{N}$ was determined, after finding the shower axis, from the formula

$$\overline{N} = \frac{1}{n} \sum_{i=1}^{n} N_i, \qquad N_i = \rho(r_i)\, \varphi(r_i),$$

where

$$\varphi(r_i) = r_i e^{r_i/60} / 2 \cdot 10^{-3}, \quad r_i \leqslant 96 \text{ m},$$
$$\varphi(r_i) = r_i^{2.6} / 0.60, \qquad r_i > 96 \text{ m},$$

and $\rho(r_i)$ is the density reading of the i-th point, located at a distance r from the axis.

The error in the determination of the axis was 25 m when the axis fell within a circle of 150 m radius centered at cart 8; the error in the determination of the number of particles was not more than 20% for each individual shower.

A total of 1000 showers was recorded by the apparatus after 1420 hrs of observation. To determine the absolute intensity in the lateral distribution functions, we selected for further data reduction those showers in which not less than 30 counters of 330 cm^2 area were operated in each of three carts. This criterion led to a separation, with 100% probability, of showers with more than 0.7×10^7 particles and with an axis within the hexagon. Approximately 300 such showers were selected. It must be noted that in 15% of the 300 showers we could not find the axis position, although the showers had a clearly pronounced charged-particle flux-density gradient within

the limits of our apparatus. In approximately one-third of these showers we could assume, with equal probability, that the shower axis passed either inside or outside the location of our apparatus, and in two-thirds of these showers the distribution of the densities was in sharp contradiction to the lateral distribution function selected by us. We estimated the number of shower particles for the first shower group under the assumption that the axis was located within a circle of 150 m radius. It was found that these showers always had less than 1×10^7 particles. All these showers were excluded from further consideration.*

The probability of registering showers in our apparatus was nearly 100% for $N \geq 1 \times 10^7$. Direct numerical integration has shown that the probability of registering showers with our apparatus within a circle of 150 m radius (with allowance for the dependence of the registration on the angle of inclination of the showers) coincides within 2 — 3% with the registration probability calculated under the assumption that the shower axes are vertical.

We have calculated the vertical shower intensity I_0 ($\geq N$) with more than N particles per unit time, unit area, and unit solid angle, using the following formula

$$I_0(\geqslant N) = \frac{\nu + 2}{2\pi} \frac{1}{T} \int \frac{C(N)\,dN}{\int\limits_S W(N, x, y)\,dx\,dy},$$

where T is the time of registration, S is the area of registration, equal to the area of a circle of 150 m radius, C(N) dN is the number of showers registered with particles ranging from N to N+dN, W(N, x, y) is the probability of registering a shower with a vertical axis passing through the point (x, y), and ν is the exponent of angular distribution of the showers, taken from reference 12.

After 1484 hours of operation we registered, in an area 7×10^4 m^2, 75 showers with $N \geq 10^7$ and 8 showers with $N \geq 3 \times 10^7$, which yields the following absolute intensities:

$$I(\geqslant 10^7) = (1.36 \pm 0.2) \cdot 10^{-6}\ \text{m}^{-2}\text{hr}^{-1}\text{sr}^{-1}$$

$$I(\geqslant 3 \cdot 10^7) = (1.24 \pm 0.43) \cdot 10^{-7}\ \text{m}^{-2}\text{hr}^{-1}\text{sr}^{-1}.$$

On the basis of these data we recalculated the value spectrum exponent γ, using the formula

$$\gamma = \ln [I(N_1)/I(N_2)] / \ln (N_1/N_2)$$

and obtained $\gamma = 2.0 \pm 0.35$.

The results obtained in our apparatus are also used to determine the value spectrum exponent by the method of area variation. Since the control groups of counters represented 12 counters in parallel, each connected in a hodoscopic cell, we could calculate the number of four-fold coincidences of the counter groups with areas 3960 and 1320 cm^2. From this we could calculate the value spectrum exponent on the basis of γ' using the formula

$$\gamma' = \ln [C(\sigma_1)/C(\sigma_2)] / \ln (\sigma_1/\sigma_2),$$

where $C(\sigma)$ is the number of four-fold coincidences of counter groups with area σ. For 1000 four-fold coincidences of groups of 3960 cm^2 counters, 112 four-fold coincidences of 1320 cm^2 counters were registered and we obtained $\gamma' = 2.0 \pm 0.10$. The value spectrum calculated by us indicates that this exponent belongs to the shower interval $(0.3 - 1.2) \times 10^7$ particles.

To construct the lateral distribution functions we used the 200 densest showers with $N \geq 5 \times 10^7$, the axes of which were not farther than 200 m from the center of the hexagon. These showers were used to plot the averaged lateral distribution functions of electrons and muons. The averaging was for four shower groups over the number of particles and over the distance intervals.

The intervals of averaging over N were $0.5 \times 10^7 - 1 \times 10^7$, $1 \times 10^7 - 3 \times 10^7$, $3 \times 10^7 - 7 \times 10^7$, and $7 \times 10^7 - 10^8$. The intervals of averaging over r were: 100 — 130, 130 — 160, 160 — 200, 200 — 250, 250 — 320, 320 — 400, 400 — 500, 500 — 640, 640 — 800, and 800 — 1000 meters. The averaging over N was under the assumption that the flux particle densities were proportional to the number of particles in the shower.

The determined average densities were referred to the center of the interval r and to a shower with $\bar{N} = \Sigma' N_i/n$ particles, where n is the number of showers entering within the interval over which the averaging over r is carried out; N_i is the number of particles in the i-th shower from this interval.

The average value of N for different distances had a spread not greater than 20%. This spread was taken into account by suitable normalization in the construction of the lateral distribution function of the electron component and of the penetrating particles.*

*For the remaining 2/3 of the showers we have also estimated the number of particles in the shower, under the assumption that the axis falls within the hexagon and the function is close to that selected by us. If the indicated estimates are true and the axes actually lie within the hexagon, then the absolute intensity given in the article may be undervalued by 15%.

*In the construction of the lateral distribution function for the muons it was assumed that the number of muons is proportional in first approximation to the number of shower particles N; if the actual dependence, $\sim N^{0.75}$ (reference 6), is taken into account, an insignificant error results.

TABLE I. Values for the exponent n for the electron component

Distances from the axis, m	N				
	$0.7 \cdot 10^7$	$1.7 \cdot 10^7$	$4.6 \cdot 10^7$	$1.1 \cdot 10^8$	$\bar{N} = 2 \cdot 10^7$
80—350	2.66 ± 0.14	2.6 ± 0.1	2.69 ± 0.24	—	$\bar{n} = 2.66 \pm 0.14$
350—1000	3.35 ± 0.8	2.6 ± 0.6	—	2.6 ± 0.6	$\bar{n} = 2.7 \pm 0.5$

TABLE II. Values of the exponent n for mesons

Distances from the axis, m	N				
	$0.7 \cdot 10^7$	$1.7 \cdot 10^7$	$4.6 \cdot 10^7$	$1.1 \cdot 10^8$	$\bar{N} = 2 \cdot 10^7$
350—1000	2.0 ± 0.4	2.4 ± 1.2	2.0 ± 1.2	2.5 ± 1.4	$\bar{n} = 2.3 \pm 0.2$

Random coincidences were accounted for at large distances from the shower axis. The maximal correction, corresponding to a distance of 900 m and showers with $N = 0.7 \times 10^7$ particles amounted to 25% of the registered particle density. In plotting the muon lateral distribution functions it was assumed that the contribution of the nuclear-active particles was negligible at these distances.[5] Each firing of the counter in the detector under the lead was assumed to be due to a muon. Corrections were introduced for δ-electrons. The number of firings of two neighboring counters at distances more than 300 m from the axis was determined experimentally. The number of such events was 10% of the total operating counters under lead at these distances. It was assumed then that 10% of firings under lead were due to δ-electrons. This percentage agrees with estimates of the number of δ-electrons obtained for analogous detectors in other investigations.[11]

We plotted the radial distribution functions for the electron and meson components of the shower. The electron density was determined as a difference between all the charged particles and the mesons with equilibrium electrons, and it was assumed that the equilibrium electrons amount to 30% of the number of muons. The lateral distributions obtained for the electronic and mesonic components were approximated with an r^{-n} law.

Tables I and II give the values of n for showers with different numbers of particles for different distances from the axis. It is seen from the tables that the lateral distribution functions are independent of the number of shower particles within the limits of statistical error. We have therefore averaged further and obtained the lateral distribution functions for showers with $\bar{N} = 2 \times 10^7$, as shown in Figs. 3, 4, and 5. The exponent $\bar{n}$ for the average functions is listed in Tables I and II.

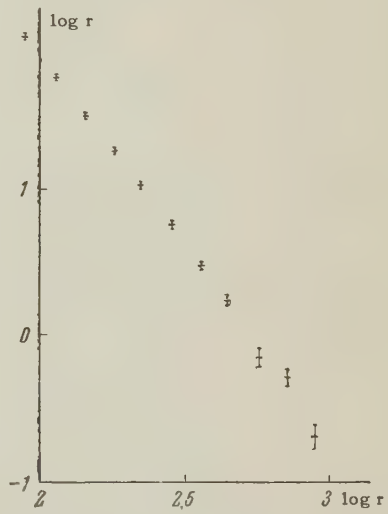

FIG. 3. Lateral distribution of charged particles for $\bar{N} = 2 \times 10^7$.

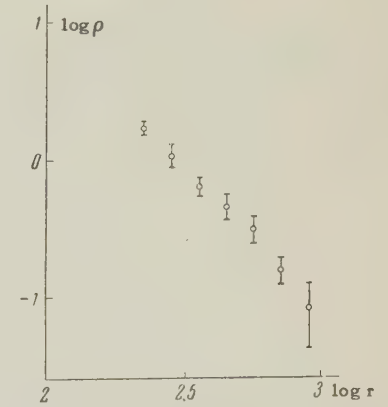

FIG. 4. Lateral distribution of nuons for showers with $\bar{N} = 2 \times 10^7$.

DISCUSSION OF THE RESULTS

The results on the absolute intensities of showers agree, within the limits of errors, with analogous data given in references 5 and 7. According to reference 7, $I (\geq 1 \times 10^7) = (1.95 \pm 0.6)$

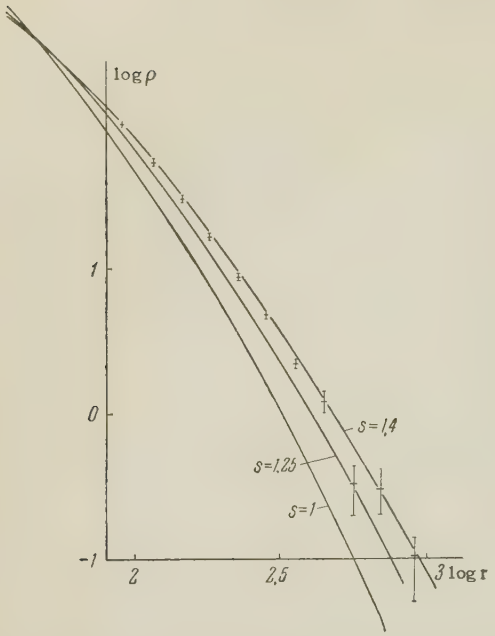

FIG. 5. Lateral distribution of the electron component for showers with $N = 2 \times 10^7$. Curves – theoretical lateral-distribution functions for different values of s. The experimental and theoretical curves were normalized to the total number of particles in a shower at a distance from 10 to 1000 m, and the experimental points for distances less than 100 m were extrapolated in accordance with formula (1).

$\times 10^{-6}\,m^{-2}\,hr^{-1}\,sr^{-1}$. According to reference 5, $I (\geq 1 \times 10^7) = (1.25 \pm 0.3) \times 10^{-6}\,m^{-2}\,hr^{-1}\,sr^{-1}$. It was found in reference 3 that the integral value spectrum exponent experiences a sharp change in the region $N \sim 10^6$. Our data obtained for showers with more than 3×10^6 particles confirm these results.

We have compared our experimental lateral distribution functions for electrons with the results calculated by the electromagnetic cascade theory[8] (Fig. 5). The form of the lateral distribution function is determined by the values of the constants used in the cascade theory formulas, viz: the radiation unit length t_0 and the critical energy β. In many foreign investigations, including those of Nishimura and Kamata,[8] from which we took our theoretical curve for comparison, these constants were $t_0 = 37.7\ g/cm^2$, and $\beta = 84.2$ Mev. But there is more justification for assuming $\beta^* = 72$ Mev and $t_0^* = 32.4\ g/cm^2$.[14] Then, considering that the shapes of the theoretical curves are determined only by the parameter s, we should assign to the curves with parameter s, given by Nishimura and Kamata[8] a parameter $s^* = s \times (0.9 + 0.033\,s)^{-1}$. This follows from the definition[8]

$$s = 3t / [t + 2 \ln (E_0 / \varepsilon_0)].$$

We have plotted the electron lateral distribution functions, taking for r_0 the following value:[15]

$$r_0 = E_s X_0^* T / \beta^* (p - 0.07)\,273 = 80\ m,$$

where $\beta^* = 72$ Mev, X_0^* is the length of one t-unit in meters at the level of observation, p is the pressure in the atmosphere, T is the average absolute temperature during the time of measurements ($T = 290°K$), and E_S is the scattering constant, assumed by us to be 19 Mev in accordance with reference 16. As can be seen from the comparison of the theoretical and experimental curves (Fig. 5), the electron lateral distribution function fits a theoretical curve with a single s.

Nishimura and Kamata have proved[17] that if π^0 mesons are formed only in the axis of the nuclear-cascade shower, and the photons have the same direction as the shower axis, then the structural electron function can be represented by the structural function of a single electron-photon cascade of age s, which is determined by the value of the free absorption path λ of the particles in the shower. In this case, on the basis of the values of λ measured by Cranshaw et al.,[6] one would expect the experimental data for our showers to coincide with the theoretical curves at a parameter $s \geq 1.17$. The equality occurs when the electron component and the nuclear avalanche are balanced. We can therefore conclude from our experimental results that in ultra-high-energy showers there is either no equilibrium between the electron-photon and nuclear components in the lower layers of the atmosphere, or else the electron lateral distribution is determined not by Coulomb scattering alone, but also by the angular divergence of the particles during the acts of the nuclear-cascade process.

In conclusion the authors express their gratitude to S. N. Vernov for the great help in the work, and also to K. I. Solov'ev and Yu. I. Lozin who helped in the performance of the measurements.

[1] Éĭdus, Adamovich, Ivanovskaya, Nikolaev, and Tulyankin, JETP **22**, 440 (1952).

[2] Antonov, Vavilov, Zatsepin, Kutuzov, Skvortsov, and Khristiansen, JETP **32**, 227 (1957), Soviet Phys. JETP **5**, 172 (1957).

[3] T. E. Cranshaw and W. Galbraith, Phil. Mag. **2**, 797 (1957).

[4] Cranshaw, Galbraith, and Porter, Phil. Mag. **2**, 891 (1957).

[5] Cranshaw, de Beer, Galbraith, and Porter, Phil. Mag. **3**, 377 (1958).

[6] Cranshaw, de Beer, Galbraith, and Hillas, Phil. Mag. **3**, 811 (1958).

[7] Clark, Earl, Kraushaar, Linsley, Rossi, and Sherb, Nature **31**, 180, 406, 353 (1957); Nuovo cimento Suppl. **8**, 623 (1958).

[8] J. Nishimura and K. Kamata, Progr. Theor. Phys. **5**, 899 (1950); **6**, 628 (1951); **7**, 185 (1952).

[9] Dmitriev, Kulikov, Massal'skiĭ, and Khristiansen, JETP **36**, 992 (1959), Soviet Phys. JETP **9**, 702 (1959).

[10] Vernov, Dmitriev, Solov'eva, and Khristiansen, JETP **37**, 1481 (1959), Soviet Phys. JETP **10**, 1050 (1960).

[11] Abrosimov, Goryunov, Dmitriev, Solov'eva, Khrenov, and Khristiansen, JETP **34**, 1077 (1958), Soviet Phys. JETP **7**, 746 (1958).

[12] Abrosimov, Goman'kov, Ivanovskaya, and Sarycheva, JETP **33**, 1110 (1957), Soviet Phys. JETP **6**, 856 (1958).

[13] G. V. Kulikov and G. B. Khristiansen, JETP **35**, 635 (1958), Soviet Phys. JETP **8**, 441 (1959).

[14] S. Z. Belen'kiĭ, Лавинные процессы в космических лучах (Cascade Processes in Cosmic Rays), OGIZ, 1948.

[15] G. Cocconi, Nuovo cimento Suppl. **8**, 561 (1958).

[16] B. Chartes and H. Messel, Phys. Rev. **99**, 1604 (1955).

[17] J. Nishimura and K. Kamata, Progr. Theoret. Phys. Suppl. No. 6, 93 (1958).

Translated by J. G. Adashko
17

COMPARISON OF DIFFERENT COORDINATE CONDITIONS IN EINSTEIN'S GRAVITATION THEORY

V. A. FOCK

Leningrad State University

Submitted to JETP editor July 8, 1959

J. Exptl. Theoret. Phys. (U.S.S.R.) 38, 108-115 (January, 1960)

In this paper it is shown that the first-order coordinate conditions actually used by Einstein and Infeld in the problem of the motion of masses coincide with the harmonic ones and define a coordinate system in this order of approximation up to a Lorentz transformation. The difference between the Einstein-Infeld and the harmonic coordinate systems is characterized by the order of smallness of admissible non-Lorentz transformations [Eq. (10)]. These differences may be found explicitly. They are so small that they cannot affect the form of the equations of motion in the first post-Newtonian approximation. On the basis of the results obtained a criticism is given of the general attitude of Einstein and Infeld to the problem of coordinates.

1. INTRODUCTION

THE equations of motion for a system of masses in Einstein's gravitation theory are derived on the assumption that the system is of an insular nature and that at infinity space is Euclidean. Thus, in this problem the specific case is considered when there exists a coordinate system, known as harmonic, which is uniquely defined up to a Lorentz transformation (the existence of such a system follows from the uniqueness theorem for the wave equation). Because of this in the present problem the question of the coordinate system may be easily investigated to the end. Nevertheless this problem is discussed incorrectly in the papers of Einstein and Infeld. The aim of the present note is to establish in an explicit form the relationship between the coordinate systems which are actually used in the papers of Einstein and Infeld and the harmonic coordinate system. This will shed light also on the general principles of the problem under discussion which have been incorrectly dealt with by these authors.

2. COORDINATE CONDITIONS IN THE ZERO-ORDER AND THE FIRST-ORDER APPROXIMATIONS

In the present author's 1939 paper[1] and in all his later papers the harmonic coordinate system is adopted in which the quantities $\mathfrak{g}^{\mu\nu} = \sqrt{-g}\, g^{\mu\nu}$ satisfy the following equations

$$\frac{\partial \mathfrak{g}^{\mu\nu}}{\partial x_\mu} = 0. \tag{1}$$

The time is adopted for the zero coordinate x_0: $x_0 = t$. The following general approximate expressions have been obtained for the quantities $\mathfrak{g}^{\mu\nu}$

$$\mathfrak{g}^{00} = 1/c + 4U/c^3 + 4S/c^5,$$
$$\mathfrak{g}^{0i} = 4U_i/c^3 + 4S_i/c^5,$$
$$\mathfrak{g}^{ik} = -c\delta_{ik} + 4S_{ik}/c^3. \tag{2}$$

Expressions (2) lead to the following equations

$$\mathfrak{g}^{00} - 1/c = O(1/c^3), \qquad \mathfrak{g}^{0i} = O(1/c^3),$$
$$\mathfrak{g}^{ik} + c\delta_{ik} = O(1/c^3), \tag{3}$$

which we shall call the zero-order coordinate conditions. In the zero-order approximation [when the right hand sides of (3) are neglected] relation (1) is satisfied because the main terms in the diagonal elements of $\mathfrak{g}^{\mu\nu}$ are constant and terms of order 1/c are absent in $\mathfrak{g}^{0i}$ and $\mathfrak{g}^{ik}$.

The same zero-order coordinate conditions have been adopted in the papers by Einstein and Infeld.[3-7] The notation in their papers differs somewhat from ours. They have adopted $x_0 = ct$, and the potentials $g_{\mu\nu}$ are expressed in terms of the auxiliary quantities $\gamma_{\mu\nu}$ by means of the formula

$$g_{\mu\nu} = e_\mu \delta_{\mu\nu}(1 - \tfrac{1}{2} e_\alpha \gamma_{\alpha\alpha}) + \gamma_{\mu\nu}, \tag{4}$$

where $e_0 = 1$; $e_1 = e_2 = e_3 = -1$. For the quantities $\gamma_{\mu\nu}$ expansions in powers of the small parameter λ (for which one may take 1/c) are used, viz:

$$\gamma_{00} = \underset{2}{\lambda^2}\gamma_{00} + \underset{4}{\lambda^4}\gamma_{00} + \underset{6}{\lambda^6}\gamma_{00} + \ldots,$$
$$\gamma_{0i} = \underset{3}{\lambda^3}\gamma_{0i} + \underset{5}{\lambda^5}\gamma_{0i} + \ldots,$$
$$\gamma_{ik} = \underset{4}{\lambda^4}\gamma_{ik} + \underset{6}{\lambda^6}\gamma_{ik} + \ldots. \tag{5}$$

The index below the letter γ denotes that this expression is the coefficient of the corresponding power of λ.

In connection with the radiation conditions on the potentials, and also in connection with the requirement of uniform convergence, doubts arise with respect to the justification of the use by Einstein and Infeld of infinite series of the form (5). However, we are interested only in the first terms of these series; therefore we shall here leave this question aside.

From a comparison of formulas (4) and (2) it follows after some calculation that

$$\gamma_{00} = -\frac{4U}{c^2} - \frac{4S - 6U^2}{c^4},$$
$$\gamma_{0i} = \frac{4U_i}{c^3} + \frac{4S_i - 8UU_i}{c^5},$$
$$\gamma_{ik} = \frac{2U^2}{c^4}\delta_{ik} - \frac{4S_{ik}}{c^4}. \qquad (6)$$

It may be easily seen that if $\lambda = 1/c$, then the conditions for the zero-order approximation (3) are algebraically equivalent to the requirement that the first terms of the series for $\gamma_{\mu\nu}$ should be of the form (5), i.e., that the series for γ_{00}, γ_{0i}, and γ_{ik} should begin with terms of order λ^2, λ^3, and λ^4 respectively. This may be written in the form

$$\underset{0}{\gamma_{00}} = 0, \qquad \underset{1}{\gamma_{0i}} = 0, \qquad \underset{2}{\gamma_{ik}} = 0. \qquad (7)$$

Thus, conditions (3) and (7) are equivalent. These conditions follow from an investigation of the approximate expressions for the components of the mass tensor in coordinates close to Cartesian ones. They were obtained in this way both in our paper,[1] and also in the papers by Einstein and his collaborators.[3,5]

It should be noted that although Einstein, Infeld and other authors admit that formulas (3) or (7) are essential for the derivation of the equations of motion, they deny that these formulas represent coordinate conditions. But it is possible to show (cf. Sec. 3) that conditions (3) define (in the approximation under consideration) the coordinate system up to a Lorentz transformation.

The coefficients U, U_i in expressions (2) for g^{00} and g^{0i} enter into the formulation of the coordinate conditions in the next approximation. The quantity U is the Newtonian potential, while the quantities U_i are the components of the vector potential, and the following equation holds

$$\frac{\partial U}{\partial t} + \frac{\partial U_i}{\partial x_i} = 0. \qquad (8)$$

In the given coordinate system the quantities U and U_i are uniquely determined by physical considerations (from a consideration of density and mass flux). Since the coordinate system is fixed in the zero-order approximation* we can likewise regard the quantities U and U_i as being fixed. But then we can make the coordinate conditions (3) more precise by writing them in the following form

$$g^{00} - \frac{1}{c} - \frac{4U}{c^2} = O\left(\frac{1}{c^5}\right); \quad g^{0i} - \frac{4U_i}{c^3} = O\left(\frac{1}{c^5}\right);$$
$$g^{ik} + c\delta_{ik} = O\left(\frac{1}{c^3}\right). \qquad (9)$$

We shall refer to these conditions [together with relation (8)] as the first-order coordinate conditions. We shall see later that these conditions fix the coordinate system (already in the next approximation) up to a Lorentz transformation, so that only a transformation of the following form

$$t' = t + a^0/c^6; \qquad x_i' = x_i + a^i/c^4. \qquad (10)$$

remains a non-Lorentz one.

Our first-order coordinate conditions are also equivalent to those of Einstein. Condition (8) is explicitly given by Einstein and Infeld[5] (although in somewhat different notation) in the following form

$$\left(\frac{1}{c}\frac{\partial \gamma_{00}}{\partial t} - \frac{\partial \gamma_{0i}}{\partial x_i}\right)_{\lambda^3} = 0, \qquad (11)$$

where the subscript λ^3 denotes that the coefficient of λ^3 in the corresponding expression should be taken.

As regards the method of fixing U and U_i (i.e., γ_{00} and γ_{0i} in the notation used by the two authors quoted earlier), this is explicitly dealt with on p. 227 of their article[3] [formulas (10.6) and (10.8)]. There it is directly stated that the values of the potentials U and U_i (in our notation) characterize the problem.

Thus, not only in the zero-order but also in the first-order approximation, the conditions of Einstein and Infeld are equivalent to our conditions which follow from the requirement that the coordinates be harmonic.

3. ADMISSIBLE TRANSFORMATIONS OF COORDINATES

We now examine the extent to which the zero-order and the first-order conditions restrict the coordinate system.

We carry out the following infinitesimal transformation of coordinates

*Without restricting generality we may take the remaining arbitrary Lorentz transformation to be equal to the identity transformation.

$$x'_\alpha = x_\alpha + \eta^\alpha_i (x_0 x_1 x_2 x_3). \tag{12}$$

By considering $g^{\mu\nu}$ as functions of their arguments we easily obtain*

$$\delta g^{\mu\nu} = g^{\mu\alpha}\frac{\partial \eta^\nu}{\partial x_\alpha} + g^{\nu\alpha}\frac{\partial \eta^\mu}{\partial x_\alpha} - \frac{\partial}{\partial x_\alpha}(g^{\mu\nu}\eta^\alpha_i), \tag{13}$$

and, if the initial system was harmonic, then

$$\delta g^{\mu\nu} = \frac{\partial}{\partial x_\alpha}(g^{\mu\alpha}\eta^\nu + g^{\nu\alpha}\eta^\mu - g^{\mu\nu}\eta^\alpha). \tag{14}$$

In the course of the following argument we shall ascribe to the quantities η^ν a definite order of magnitude with respect to $1/c$.

On taking for $g^{\mu\nu}$ approximate expressions which satisfy the zero-order condition we obtain

$$\delta g^{00} = \frac{1}{c}\left(\frac{\partial \eta^0_i}{\partial t} - \frac{\partial \eta^l}{\partial x_l}\right) + O\left(\frac{\eta}{c^3}\right),$$

$$\delta g^{0i} = -c\frac{\partial \eta^0_i}{\partial x_i} + \frac{1}{c}\frac{\partial \eta^i}{\partial t} + O\left(\frac{\eta}{c^3}\right),$$

$$\delta g^{ik} = -c\left(\frac{\partial \eta^k}{\partial x_i} + \frac{\partial \eta^i}{\partial x_k}\right) + c\left(\frac{\partial \eta^0}{\partial t} + \frac{\partial \eta^l}{\partial x_l}\right)\delta_{ik} + O\left(\frac{\eta}{c^3}\right). \tag{15}$$

We examine the consequences for $\delta g^{\mu\nu}$ arising from the zero-order coordinate conditions. It is evident that all $\delta g^{\mu\nu}$ must be of order not smaller than $1/c^3$. On the other hand, even if the quantities η^α should not contain powers of c in the denominator, the terms which we have denoted by $O(\eta/c^3)$ will be of order not smaller than $1/c^3$. By neglecting them and by setting $\delta g^{\mu\nu} = 0$, we obtain for the quantities η^α a system of equations which characterizes an infinitesimal Lorentz transformation.

In particular, if we do not consider translations and spatial rotations, we have

$$\eta^0 = -\frac{1}{c^2}(x_i V_i); \qquad \eta^i = -V_i t. \tag{16}$$

Thus, the zero-order conditions (3) fix the coordinate system up to a Lorentz transformation in which η^i are quantities of zero order† with respect to $1/c$.

Having established this, we may without restriction of generality assume that the Lorentz transformation given above reduces to the identity transformation, and we may proceed to investigate the case when the quantities η^i are of order $1/c^2$ or higher. By repeating the preceding arguments we may easily see that as a result of the first order conditions (9) the same system of equations is obtained for the quantities η^α, and we again obtain a Lorentz transformation in which the quantities V_i may now be of order q^3/c^2, where q is some velocity of zero order with respect to c. (Without a restriction of generality we may regard this Lorentz transformation as also being reduced to the identity transformation.)

We have thus proved that the first-order conditions adopted by Einstein and Infeld firstly coincide with ours and, secondly, define the coordinate system uniquely up to a Lorentz transformation.

The admissible non-Lorentz part of the transformation which does not violate the first-order conditions is equal to

$$\eta^0 = a^0/c^6, \qquad \eta^i = a^i/c^4. \tag{17}$$

where a^0 and a^i are of zero order with respect to $1/c$. It is quite evident that the difference between the two coordinate systems: the harmonic one (t, x_i) and the non-harmonic one (t', x'_i), where

$$t' = t + a^0/c^6, \qquad x'_i = x_i + a^i/c^4, \tag{18}$$

cannot yet affect the equations of motion in the first post-Newtonian approximation.

Thus the fact that the Einstein-Infeld equations coincide with the equations of motion in harmonic coordinates is to be explained not by saying that these equations allegedly do not depend on the coordinate conditions, but simply by the fact that the Einstein-Infeld coordinate system does not differ from the harmonic one in the approximation under discussion.

4. CONNECTION BETWEEN DIFFERENT COORDINATE SYSTEMS IN THE SECOND-ORDER APPROXIMATION

In order to show in the clearest possible way that the Einstein-Infeld coordinate system differs from the harmonic system only by small terms of the form (17), we shall obtain explicit expressions for these terms.

To do this it is necessary to examine the second-order conditions adopted in the papers of Einstein and Infeld and to compare them with the harmonic ones.

The second-order harmonic conditions will be obtained if in Eq. (1) we collect terms of order $1/c^5$ for $\mu = 0$ and terms of order $1/c^3$ for $\mu = 1$. We then have

$$\frac{\partial S}{\partial t} + \frac{\partial S_i}{\partial x_i} = 0, \qquad \frac{\partial U_i}{\partial t} + \frac{\partial S_{ik}}{\partial x_k} = 0. \tag{19}$$

As regards the Einstein-Infeld conditions, we shall write them in two different forms. However, in actual calculations only the second form is utilized.

*Cf., for example, our book,[2] formulas (48.20) and (48.21).

†From this it follows, in particular, that coordinate conditions (3) are sufficient to enable us to write Newton's equations of motion (cf. reference 6).

The first variant can be written in the following form

$$\left(\frac{1}{c}\frac{\partial\gamma_{00}}{\partial t}-\frac{\partial\gamma_{0i}}{\partial x_i}\right)_{\lambda^5}=0, \qquad \left(\frac{1}{c}\frac{\partial\gamma_{i0}}{\partial t}-\frac{\partial\gamma_{ik}}{\partial x_k}\right)_{\lambda^4}=0, \tag{20}$$

and the second variant in the form

$$\left(\frac{1}{c}\frac{\partial\gamma_{00}}{\partial t}-\frac{\partial\gamma_{0i}}{\partial x_i}\right)_{\lambda^5}=0, \qquad \left(\frac{\partial\gamma_{ik}}{\partial x_k}\right)_{\lambda^4}=0. \tag{21}$$

Here the subscripts λ^4 and λ^5 denote that the coefficients of λ^4 and λ^5 should be taken in the corresponding expressions.

If we denote the Einstein and Infeld coordinates by (t', x_i'), then in order to distinguish them from the harmonic coordinates (t, x_i), we ought to insert primes on the independent variables in formulas (20) and (21). However, in the present approximation the distinction between the two sets of coordinates is not significant and the primes may be omitted.

We assume that in the Einstein-Infeld coordinates the quantities S, S_i and S_{ik} in formulas (2) have the values S', S_i', S_{ik}' (while we retain the notation S, S_i and S_{ik} for the same quantities in the harmonic coordinates). As regards U and U_i, in virtue of the first-order coordinate conditions the values of these quantities in the two coordinate systems coincide. In accordance with (6) we now have

$$\gamma_{00}=-\frac{4U}{c^2}-\frac{4S'-6U^2}{c^4},$$
$$\gamma_{0i}=\frac{4U_i}{c^2}+\frac{4S_i'-8UU_i}{c^5},$$
$$\gamma_{ik}=\frac{2U^2}{c^4}\delta_{ik}-\frac{4S_{ik}'}{c^4}. \tag{22}$$

On substituting these expressions into (20), we obtain for the first variant*

$$\frac{\partial S'}{\partial t}+\frac{\partial S_i'}{\partial x_i}=\frac{3}{2}\frac{\partial(U^2)}{\partial t}+2\frac{\partial(UU_i)}{\partial x_i}, \qquad \frac{\partial U_i}{\partial t}+\frac{\partial S_{ik}'}{\partial x_k}=\frac{1}{2}\frac{\partial(U^2)}{\partial x_i} \tag{23}$$

In the second variant the term $\partial U_i/\partial t$ is absent in the left hand side of the second equation of (23). On setting

$$\delta S=S'-S; \qquad \delta S_i=S_i'-S_i; \qquad \delta S_{ik}=S_{ik}'-S_{ik} \tag{24}$$

and on utilizing the harmonic relations (19), we obtain

$$\frac{\partial\delta S}{\partial t}+\frac{\partial\delta S_i}{\partial x_i}=\frac{3}{2}\frac{\partial U^2}{\partial t}+2\frac{\partial(UU_i)}{\partial x_i} \tag{25}$$

in both variants and then

$$\frac{\partial\delta S_{ik}}{\partial x_k}=\frac{1}{2}\frac{\partial(U^2)}{\partial x_i} \quad \text{(1st variant)}, \tag{26}$$

$$\frac{\partial\delta S_{ik}}{\partial x_k}=\frac{1}{2}\frac{\partial(U^2)}{\partial x_i}+\frac{\partial U_i}{\partial t} \quad \text{(2nd variant)}. \tag{27}$$

Keeping in mind the fact that in formula (12) for the transformation of coordinates the quantities

$$\eta^0=a^0/c^6, \qquad \eta^i=a^i/c^4 \tag{28}$$

are so small that their squares may be neglected, we may treat this transformation as an infinitesimal one and calculate the differences (24) with the aid of the formulas

$$4\delta S=c^5\delta g^{00}, \qquad 4\delta S_i=c^5\delta g^{0i}, \qquad 4\delta S_{ik}=c^5\delta g^{ik}, \tag{29}$$

where $\delta g^{\mu\nu}$ have the values (15). On substituting into these equations expressions (17) for η^ν in terms of a^ν, we obtain

$$4\delta S=-\frac{\partial a^i}{\partial x_i}; \qquad 4\delta S_i=\frac{\partial a^i}{\partial t}-\frac{\partial a^0}{\partial x_i},$$
$$4\delta S_{ik}=\delta_{ik}\frac{\partial a^l}{\partial x_l}-\frac{\partial a^i}{\partial x_k}-\frac{\partial a^k}{\partial x_i}. \tag{30}$$

On introducing these expressions into the Einstein-Infeld coordinate conditions we obtain

$$-\Delta a^0=6\frac{\partial(U^2)}{\partial t}+8\frac{\partial(UU_i)}{\partial x_i}, \tag{31}$$

and then in the case of the first variant

$$-\Delta a^i=2\frac{\partial(U^2)}{\partial x_i} \tag{32}$$

and in the case of the second variant

$$-\Delta a^i=2\frac{\partial(U^2)}{\partial x_i}+4\frac{\partial U_i}{\partial t}. \tag{33}$$

Thus, in the transformation formulas (10) the quantities a^ν are determined from the Poisson equations so that if we wish, we can write explicit expressions for them. If we, moreover, require that at infinity the coordinates should go over into Galilean coordinates, then in the expression for a^ν the only undetermined terms will be linear terms corresponding to a Lorentz transformation.

5. CONCLUSION

The general aspect of the problem which we have just discussed of the relation between different coordinate conditions consists of the fact that we have here an obvious illustration of the danger associated with an incorrect application of the concept of relativity, and particularly of the term "general relativity," which does not have an exact meaning, but which often produces some sort of a hypnotic effect.

Einstein and Infeld, and later also some other scientists, have put forward the paradoxical (and incorrect) assertion, that allegedly the equations

*I. Fikhtengol'ts has assisted me in the derivation of some of these formulas.

of motion are not connected with the coordinate conditions or that they are not connected with harmonic coordinate conditions.

This incorrect assertion is repeated in practically every article. Thus, in the 1940 paper[4] it is stated: "We do not make any assumptions in advance with respect to the coordinate system beyond the fact that it is Galilean at infinity." In Sec. 13 of the 1949 paper[5] a similar assertion is repeated (in somewhat more careful form), while in fact zero-order and first-order coordinate conditions are used. In the 1954 paper[6] Infeld, in arguing against me, shows in fact that the form of the Newtonian equations of motion depends only on the zero-order coordinate conditions, but asserts that allegedly "the coordinate conditions have no relation whatsoever to the equations of motion not only in the Newtonian, but also in the next post-Newtonian approximation." This assertion is incorrect even if we say that the zero-order coordinate conditions are not "coordinate conditions," but a "method," as is done by Infeld. The same assertion is repeated in Infeld's 1957 paper.[7]

Starting with the first-order approximation [Eqs. (8) and (9)] Einstein and Infeld begin to use the term "coordinate conditions." But they do not notice that Eqs. (8) and (9), which they are in fact using, define the coordinate system up to transformations of the form (10), and that to this degree of accuracy the coordinate system is harmonic. Moreover, formulas (10) show that the second-order coordinate conditions certainly do not affect the form of the equations of motion in the first post-Newtonian approximation, so that the computations made by various authors in this connection are superfluous. Nevertheless, the whole attention of Einstein, Infeld and other authors is concentrated on the effect of the second-order coordinate conditions, and when after lengthy calculations it turns out that there is no such effect, the authors see in this a confirmation of the idea of "general relativity." But in actual fact the absence of such an effect is a trivial fact, which follows in an obvious way from the elementary formulas (10).

We must assert that in the papers of Einstein and Infeld quoted earlier a point of view predominates which compels them:

a) to deny the existence of coordinate conditions while in fact they have been introduced;

b) to ascribe particular significance to coordinate conditions which cannot affect the form of the equations of motion;

c) to deny that actually in the approximation needed for the formulation of the equations of motion the harmonic, and not any other, coordinate system is used, and, finally,

d) to deny even the fact that the harmonic coordinate system is defined uniquely up to a Lorentz transformation.

It seems to us that there is no doubt that this incorrect point of view is inspired by an incorrect concept of the idea of relativity. We hope that as a result of clarifying this problem our work will turn out to be useful not only because it will make unnecessary many complicated calculations, but also from the point of view of general principles.

---

[1] V. Fock, JETP **9**, 375 (1939). V. Fock, J. Phys. (U.S.S.R.) **1**, 81-116 (1939).

[2] V. Fock, Теория пространства, времени и тяготения (Theory of Space, Time, and Gravitation), Gostekhizdat, Moscow, 1955.

[3] Einstein, Infeld, and Hoffman, Ann. Math. **39**, 65-100 (1938).

[4] A. Einstein and L. Infeld, Ann. Math. **41**, 455-464 (1940).

[5] A. Einstein and L. Infeld, Can. J. Math. **1**, 209-241 (1949).

[6] L. Infeld, Bull. Polish Acad. Sci. Sec. III, **2**, 161-164 (1954).

[7] L. Infeld, Revs. Modern Phys. **29**, 398 (1957).

[8] V. Fock, Revs. Modern Phys. **29**, 325 (1957).

Translated by G. Volkoff
18

CERTAIN SPECIAL FEATURES OF OHMIC HEATING OF ELECTRON GAS IN A PLASMA

A. V. GUREVICH

P. N. Lebedev Physics Institute, Academy of Sciences, U.S.S.R.

Submitted to JETP editor April 17, 1959

J. Exptl. Theoret. Phys. (U.S.S.R.) **38**, 116-121 (January, 1960)

An investigation is made of the heating of the electron gas in a plasma in a constant electric field, taking into account inelastic electron collisions. It is shown that the electron temperature may be in a steady state only for small values of the intensity of the electric field $E < E_k$; in the case $E \geq E_k$ this condition is no longer stable. An investigation is made of the dependence of the field E_k on the degree of ionization of the plasma. A comparison is made with the results of experimental papers.[9,10] An explanation is given of the two modes of heating observed in those papers; good quantitative agreement with their results is obtained.

PREVIOUSLY[1] some peculiarities were pointed out in the behavior of the electron temperature in a strongly ionized plasma, arising as a result of the fact that the frequency of electron-ion collision falls off sharply as the electron velocity increases. It turned out that in a constant electric field the electron temperature may be in a stationary state only for low values of the intensity of the electric field $E < E_k^{el}$. For $E \geq E_k^{el}$ no stationary state exists anymore; in this case the electron temperature increases continuously with time.* The whole investigation is carried out in reference 1 on the assumption that only elastic electron collisions occur. However, it is well known that inelastic collisions usually also play a significant, and even a dominant, role. The object of the present article is to take them into account.

We consider an infinite plasma in an atomic gas situated in a spatially homogeneous constant electric field. When the following conditions are satisfied

$$dT_e/dt \ll \nu_e T_e, \quad Q(T_e) \ll \tfrac{3}{2} kT_e \nu_{eff}, \quad Q(T_e) \ll \tfrac{3}{2} kT_e \nu_e \qquad (1)$$

the main part of the electron distribution function which depends only on the absolute value of the velocity is Maxwellian;† in this case the electron temperature T_e is determined by the following equation

$$\frac{dT_e}{dt} + \frac{2}{3k} Q(T_e) = \frac{2}{3k} \frac{e^2 E^2}{m} \frac{K_\sigma}{\nu_{eff}(T_e)}. \qquad (2)$$

Here, as usual, k is the Boltzmann constant, e and m are the charge and the mass of the electron, E is the intensity of the electric field, ν_e is the electron-electron collision frequency. $\nu_{eff} = \nu_{eff\,i} + \nu_{eff\,n}$, where $\nu_{eff\,i}$ is the effective electron-ion collision frequency and $\nu_{eff\,n}$ is the electron-neutral particle collision frequency; the expressions for $\nu_{eff}(T_e)$ are given, for example, in the book by Al'pert, Ginzburg, and Feĭnberg,[4] and also in reference 5. K_σ is a numerical coefficient whose value depends on the ratio between $\nu_{eff\,i}$ and $\nu_{eff\,n}$; it varies from 1.95 (for $\nu_{eff\,n} \ll \nu_{eff\,i}$) to 1.05 — 1.13 (for $\nu_{eff\,n} \gg \nu_{eff\,i}$).[1,5] Finally, $Q(T_e)$ is the energy lost by the electrons per unit time in collisions with heavy particles:

$$Q(T_e) = \frac{3}{2} k(T_e - T) \delta_{el} \nu_{eff} + \frac{16}{3} \left(\frac{2\pi k T_e}{3m}\right)^{1/2} \frac{e^6}{m\hbar c^3} \times \left(\sum_p Z_p N_{+p}\right) + \sum_l \nu_l \varepsilon_l + \nu_i \left(\varepsilon_i + \frac{3}{2} kT_e\right). \qquad (3)$$

The first term in this expression describes the energy losses by the electron in elastic collisions with heavy particles ($\delta_{el} = 2m/M$), the second term describes bremsstrahlung losses, the third term describes excitation losses, the fourth term describes ionization losses (here ϵ_l is the energy of the l-th level, ν_l is the frequency of its excitation; similarly ϵ_i and ν_i are the ionization energy and frequency).*

*In an alternating electric field this effect depends significantly on its frequency ω; thus, for $\omega \gtrsim \omega_k \approx 0.2\nu_{eff}$ no instability of the electronic apparatus occurs at all. A magnetic field directed at right angles to the electric field also has a similar effect; for example, no instability arises[1] if $eH/mc = \omega_H \gtrsim \omega_k$.

†If the first of conditions (1) is not satisfied, i.e., if the losses are small and the field $E \gtrsim \sqrt{kT_e m \nu_{eff} \nu_e}/e$ [cf. (2)], the velocity distribution of the electrons becomes sharply directed (this case in a fully ionized plasma was investigated by Dreicer[2]). If the second of conditions (1) is not satisfied this also leads to the appearance of a pronounced directed part in the distribution function. When the third condition is not satisfied, the distribution function remains symmetric, but its shape may be significantly altered (cf., for example, reference 3).

*Equation (2) was utilized, in particular, in references 6 and 7 for numerical calculations of plasma heating in the stellarator.

The stationary electron temperature is determined, naturally, by the relation

$$Q(T_e) = e^2E^2K_\sigma/m\nu_{\text{eff}}(T_e). \quad (4)$$

Moreover, it is necessary that the energy given to the electrons by the field should increase with increasing T_e more slowly than the energy loss by collisions. However, it may be easily seen that these conditions are by no means always satisfied. Indeed, the energy given to the electrons by the field increases, as is well known, in the case of a sufficiently high degree of plasma ionization, proportionally to $T_e^{3/2}$ (since $\nu_{\text{eff}\,i} \sim T_e^{-3/2}$). Only the energy lost by the electron through excitation and ionization increases equally rapidly. However, at temperatures of the order of ϵ_i/k the rate of growth of $\nu_i(T_e)$ and $\nu_l(T_e)$ is reduced, while at higher temperatures even a decrease of $\nu_i(T_e)$ and $\nu_l(T_e)$ begins (cf. reference 8). The role played by the remaining terms, which describe the energy lost by the electrons in elastic collisions and by bremsstrahlung, is not very significant under these conditions. Consequently, the electron temperature may be stationary only for $T_e \lesssim \epsilon_i/k$ and at low values of the intensity of the electric field.

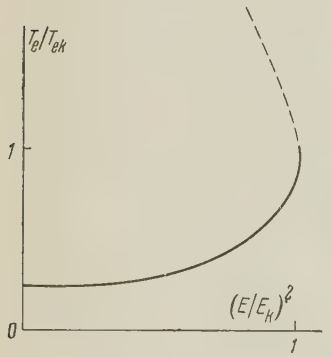

FIG. 1. The dependence of T_e/T_{ek} on E/E_k in a strongly ionized helium plasma.

We now calculate the stationary electron temperature in a helium plasma.* We assume initially that the plasma is strongly ionized ($\nu_{\text{eff}\,i} \gg \nu_{\text{eff}\,n}$), and we take into account in $Q(T_e)$ only the main part of the electron energy losses — the losses due to excitation and ionization of helium atoms, i.e., we neglect initially the effect of losses due to bremsstrahlung, due to excitation and to further ionization of singly ionized helium, and we neglect losses in elastic collisions (they all lead only to a small correction, cf. below). As may be easily seen, in this case the stationary temperature T_e depends on only one parameter. It is shown in Fig. 1; along the vertical axis we have plotted the ratio T_e/T_{ek}, where $T_{ek} \approx 1.03\,\epsilon_i/k$ is the maximum stationary electron temperature; along the horizontal axis we have plotted the ratio $(E/E_k)^2$, where

$$E_k \approx 2.8\left[\frac{e^2N_i\nu_i(\varepsilon_i/k)}{\sqrt{\varepsilon_i/m}}\ln\frac{\varepsilon_i D}{e^2}\right]^{1/2}$$
$$\approx 7.0\cdot 10^{-15}N_{n0}\sqrt{q_i(1-q_i)}\left(1+\frac{1}{45}\ln\frac{kT_i}{2}\right) \quad (5)$$

is the critical field (in v/cm). Here ϵ_i is the ionization energy, D is the Debye radius, $\nu_i(\epsilon_i/k)$ is the frequency of ionization at $T_e = \epsilon_i/k$, $q_i = N_i/N_{n0}$ is the degree of plasma ionization, T_i is the ion temperature (in electron volts), $N_{n0} = 3.52 \times 10^{16}p_0$ is the total gas density (p_0 is the initial pressure).*

It is seen from the diagram that the electron temperature can be stationary (solid curve) only in fields lower than the critical field; however, if $E \geq E_k$, then there exists no stationary state. In this case the electrons have no time to lose the energy communicated to them by the field, and their temperature increases continuously with time.†

The value of the critical field (5) depends significantly on the degree of plasma ionization q_i. Moreover, if $q_i < 0.5$, then E_k increases with increasing q_i, while if $q_i > 0.5$, then E_k decreases. The critical field reaches the maximum value

$$E_{k\,max} \approx 3.5\cdot 10^{-15}N_{n0}\ \text{v/cm}$$

when $q_i = 0.5$. Naturally, in the case when the electric field intensity is greater than $E_{k\,max}$, a stationary condition cannot occur irrespectively of the degree of plasma ionization (since $E > E_{k\,max} \geq E_k$). However, if E is less than $E_{k\,max}$, a stationary state may be realized, if q_i takes on some value in the interval

$$0.5\,(1-\sqrt{1-(E/E_{k\,max})^2}) < q_i < 0.5$$
$$\times(1+\sqrt{1-(E/E_{k\,max})^2}). \quad (6)$$

*For the calculation of $\nu_i(T_e)$, $\nu_l(T_e)$ use was made of effective excitation and ionization cross sections in helium given in reference 8. It should be noted that the corresponding experimental data are not sufficiently complete; moreover, the measured cross sections differ noticeably from values calculated theoretically. As a result of this, the accuracy in the calculation of electron temperature apparently does not exceed 20%.

*The same expression (5) for the critical field E_k will also be obtained in the case of any other atomic gas: only the constant in front of the square root will be altered (it depends on the ratio between the excitation and ionization losses in any given gas).

†When sufficiently high values of T_e are attained the first of conditions (1) is violated, and the electron velocity distribution becomes sharply directed (cf. footnote † on p. 85). We also note that the electron temperature may likewise increase with time in the case of fields $E < E_k$; for this it is necessary that at the time the field is switched on T_e should exceed T_{ek}, with the point T_e/T_{ek} lying above the dotted curve in Fig. 1.

In this case, as the degree of plasma ionization q_i increases, the electron temperature in the stationary state diminishes for $q_i < 0.5$ [since for $q_i < 0.5$ the ratio E/E_k diminishes as q_i increases, and consequently $T_e(E/E_k)$ also diminishes (cf., Fig. 1)], while it increases when $q_i > 0.5$. The minimum value of T_e in the stationary state is given by $T_{e\,min} = T_e(E/E_{k\,max})$. From formula (6) it may also be seen that in the case of fields $E < E_{k\,max}$, the electron temperature likewise becomes nonstationary both in the case of high and low degrees of plasma ionization.

In the case of low degrees of plasma ionization, however, we cannot neglect collisions with neutral particles as was done earlier. Therefore, a suitable calculation was carried out taking into account $\nu_{eff\,n}$, and we also took into account terms describing the energy lost by the electrons in elastic collisions, by bremsstrahlung, and by excitation and ionization of singly ionized helium, which were all neglected previously. The dependence of the electron temperature on the degree of plasma ionization for different values of $(E/E_{k\,max})^2$ obtained as a result of this calculation is given in Fig. 2. It may be seen from the diagram that the instability of electron temperature arises only for high degrees of ionization; in the case of small q_i no such instability occurs. Consequently, it is very important to take into account collisions between electrons and neutral particles at low degrees of ionization, as should be the case.

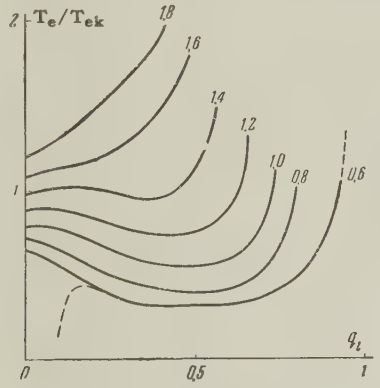

FIG. 2. The dependence of T_e/T_{ek} on q_i. The numbers labelling the curves correspond to different values of $(E/E_{k\,max})^2$.

We now investigate qualitatively the process of plasma heating in a constant electric field E which is smaller than $E_{k\,max}$ or is of the same order of magnitude. In doing this we assume that at the instant of switching on the heating field the electron temperature is lower than T_{ek}, and the degree of plasma ionization is not great. Then in the initial period of heating the electron temperature will increase up to the corresponding stationary value [as is shown by the dotted line in Fig. 2 for the case $(E/E_{k\,max})^2 = 0.6$]. We now take into account the fact that the degree of plasma ionization also increases with time. This means that the electron temperature will subsequently vary in accordance with the stationary state curve, but only up to the point where q_i reaches its critical value, at which point instability occurs. After this the electron temperature again begins to grow sharply (dotted line in Fig. 2). Consequently, in the case of plasma heating in the field $E \lesssim E_{k\,max}$ a "plateau" having a characteristic maximum and minimum may appear in the curve which shows the variation with time of the electron temperature (or of the electron current); this "plateau" corresponds to the region of the stationary state. As may be clearly seen in Fig. 2, the extent of the "plateau" decreases as the intensity of the heating field increases. When $(E/E_{k\,max})^2 > 1.5$ it disappears completely; in this case the electron temperature grows continuously with time.

Thus, when plasma is heated in a constant electric field two modes of heating may occur, depending on the value of the field: with a "plateau" and without a "plateau." The field E_s, which separates these two modes is equal to (in v/cm)

$$E_s \approx \sqrt{1.5}\, E_{k\,max} \approx 4.3 \cdot 10^{-15} N_{n0}. \qquad (7)$$

The ohmic heating of a helium plasma has been investigated experimentally in the case of the stellarator.[9,10] In the experimental paper[9] characteristic curves are given which show the variation with time of the current in the stellarator for various values of the heating field. We note first the good qualitative agreement with the special features of plasma heating described earlier. From the curves shown in the figure given above we may easily determine the field which separates the two modes of heating:

$$E_s \approx (0.083 \pm 0.006) \quad \text{v/cm}. \qquad (8)$$

Formula (7) gives for this case ($N_{n0} = 1.76 \times 10^{13}$) $E_s = 0.076$ v/cm; it is seen that the agreement of the theoretical value with the experimental one (8) is sufficiently good.

Further, in reference 9 the dependence of the maximum current at the current "plateau" (I_{max}) on the electric field intensity has also been measured; these results are shown in Fig. 3, where along the horizontal axis we have plotted the ratio of E/E_s, while along the vertical axis we have plotted the ratio $I_{max}(E)/I_m$ (for $E = E_s$ the maximum and the minimum values of the current, naturally, coincide: $I_{max}(E_s) = I_{min}(E_s) = I_m$). The solid and the dotted curves in the same diagram indicate the possible limits of variation of the current at the current plateau obtained as a

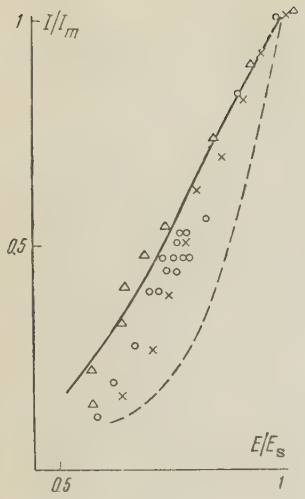

FIG. 3. The dependence of I_{max}/I_m (solid curve) and I_{min}/I_m (dotted curve) on E/E_s; ○, △, × are the experimental results[9] of measuring $I_{max}(E)/I_m$.

result of a theoretical calculation according to the following formula

$$I(E)/I(E_s) = (E/E_p)\nu_{eff}[T_e(E_p)]/\nu_{eff}[T_e(E)];$$

it may be seen from the diagram that they are in good agreement with experiment.*

One might also note a number of qualitative remarks made by the authors of the experimental papers[9,10] which are also in agreement with the results of the present investigation. In particular, the fact that there exists a current "plateau" for a long time (up to 3 millisec) shows that during all this period there exists a considerable number of neutral particles in the plasma (cf. Fig. 2), which is in accord with experimental observations on the luminosity of neutral helium.

*The slope of the curve $I_{max}(E)/I_m$, shown in Fig. 3, may vary somewhat depending on the initial degree of plasma ionization, and also on the initial electron temperature, etc. The minimum value of the current depends on these parameters to a smaller extent.

Consequently, on adding neutral gas to the discharge it is possible to maintain the current and the electron temperature at constant values for long periods of time. By lowering the electric field in a heated and singly ionized gas it is possible, in principle, to achieve similar stationary conditions in the domain of second (or higher) ionization, i.e., at a higher stationary electron temperature.

The author is grateful to V. L. Ginzburg for his interest in this work.

[1] A. V. Gurevich, JETP **35**, 392 (1958), Soviet Phys. JETP **8**, 271 (1959).

[2] H. Dreicer, Proc. of the II Intern. Conf. on the Peaceful Uses of Atomic Energy, Geneva (1958).

[3] A. V. Gurevich, Изв. Высш. шк., Радиофизика (News of Higher Schools, Radiophysics) **2**, 355 (1959).

[4] Al'pert, Ginzburg, and Feĭnberg, Распространение радиоволн (Propagation of Radio Waves), GITTL, Moscow, 1953, §59.

[5] A. V. Gurevich, JETP **30**, 1112 (1956), Soviet Phys. JETP **3**, 895 (1957).

[6] Berger, Bernstein, Frieman, and Kulsrud, Phys. Fluids **1**, 297 (1958).

[7] W. Bernstein and A. Z. Kranz, Phys. Fluids **2**, 57 (1959).

[8] H. Massey and E. Burhop, Electron and Ion Collisions, Oxford, 1952.

[9] Coor, Cunningham, Ellis, Heald, and Kranz, Phys. Fluids **1**, 411 (1958).

[10] Bernstein, Chen, Heald, and Kranz, Phys. Fluids **1**, 430 (1958).

Translated by G. Volkoff
19

EXCITATION OF VIBRATIONAL LEVELS AND COULOMB EXCITATION IN ALPHA DECAY

V. M. STRUTINSKIĬ

Submitted to JETP editor May 7, 1959

J. Exptl. Theoret. Phys. (U.S.S.R.) **38**, 122-133 (January, 1960)

The relative probability of excitation of vibrational levels in the α decay of even-even nuclei is calculated. An expression for the intensity of excitation of the daughter nucleus by α particles of the main (allowed) group is derived in the quasi-classical perturbation theory approximation. The results obtained are applied to an analysis of the experimental data on the fine structure of α decay.

CONSIDERABLE progress has been made recently in the interpretation of the fine structure of the α decay spectra of deformed nuclei.[1-7] These papers are based on the physical fact, first noted by Hill and Wheeler,*[8] that the spatial anisotropy of the potential barrier in nuclei with a nonspherical surface leads to an anisotropy in the angular distribution of the α particles: the intensity of the current in the direction a (see Fig. 1) will be greater than in the direction b owing to the greater penetrability of the Coulomb barrier. Indeed, the particles emitted in the direction a traverse a smaller width of barrier than the particles emitted in the direction b (r^* in Fig. 1 is the radius corresponding to the turning point). In other words, the wave function describing the α decay will contain not only the s wave but also waves with higher angular momentum. We therefore have a mixture of excited states of the daughter nucleus with angular momenta different from that of the initial nucleus. We shall assume that the wave function at the nuclear surface is constant and identical for all fine structure lines belonging to the same rotational band. This is justified qualitatively by the small absorption length of the α particles in the nucleus. The emission of the α particles by the nucleus may be thought of as a local surface process which is not affected by the deformation of the nucleus.

Besides this effect connected with the nonsphericity of the nuclear shape (i.e., with the anisotropy of the nuclear potential), there will always be some interaction between the α particles and the anisotropic component of the Coulomb field of the nucleus. This interaction leads to an additional possibility of energy and momentum exchange between the α particles and the nucleus even after the α particle has passed beyond the range of the nuclear interaction. This mechanism was first noted by Preston,[10] who also calculated its effect.

A close analogy exists between the Coulomb excitation in α decay and the Coulomb excitation of nuclei by passing charged particles. The difference between the two is that the excitation in α decay occurs mainly while the α particle is still beneath the barrier, whereas in the usual excitation the region of classical motion, $r > r^*$, is the more important. Coulomb excitation also occurs in undeformed nuclei; its probability gives the lower limit for the intensity of excitation of the weak lines of the spectrum in an intensive allowed decay. The first of the above-mentioned mechanisms comes into play not only for nuclei with rigid deformation, but also for spherical nuclei in the discussion of the levels connected with deformations of the surface, as, for example, the vibrational levels of the surface oscillations.

The surface effect for spherical nuclei can be calculated rather simply by taking account of the fact that in this case the spatial anisotropy of the Coulomb field of the daughter nucleus can be neglected in first approximation. The problem then consists in the determination of the wave function describing the decay on the sphere S (Fig. 1). In the region outside the sphere S the radial and angular coordinates separate, and the amplitudes of the partial waves at infinity are easily determined in the usual way. To find the wave function on the sphere S we may use the so-called adiabatic approximation. This consists in assuming that the nuclear surface is rigid during the time the α particle passes through the region of greatest interaction, i.e., in our case, through the region between the surface of the nucleus and the sphere S. A precise choice of the radius of this sphere is not important as long as it is sufficiently

*A similar remark was made earlier by Migdal.[9]

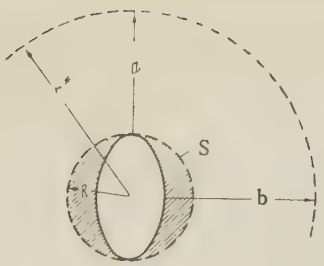

FIG. 1

close to the mean radius of the nucleus so that the change in velocity and the bending of the α particle trajectory can be neglected in the dashed region of Fig. 1.

For the applicability of the adiabatic approximation in this sense it is necessary that the time it takes for the α particle to traverse a distance of the order of the deformation of the nucleus be small compared with the period of oscillation of the surface, i.e., we must require

$$\alpha R\omega/v(R) \ll 1, \tag{1}$$

where $v(r)$ is the velocity of the α particles and αR and ω are the amplitude and the frequency of the surface oscillations. Substituting in (1) the value

$$\alpha \sim \sqrt{\hbar/2B_\lambda\omega} = \sqrt{\hbar\omega_\lambda/2C_\lambda},$$

where B_λ and C_λ are the mass parameter and the deformability for surface oscillations of the type λ, we find the following relation, which is equivalent to the inequality (1):

$$(\hbar\omega KR/2|\mathscr{E}(R)|)\sqrt{\hbar\omega/2C_\lambda} \lesssim 0{,}1 \ll 1,$$

where $\mathscr{E}(r)$ is the kinetic energy of the α particle, $K = \sqrt{2m|\mathscr{E}(R)|}/\hbar$ ($\hbar\omega \approx 0.5$ Mev, $|\mathscr{E}(R)| \approx 15-20$ Mev, $KR \approx 20$).

Fixing the shape of the nuclear surface for the moment, we find for the wave function of the α particle on the surface S the following expression in the quasi-classical approximation:

$$\psi(\mathbf{n})\Big|_S = \text{const}\cdot\exp\left\{-\int_{R(\mathbf{n})}^{r} K(r)\,dr\right\}\Big|_S \approx \text{const}\cdot\exp\left\{KR\sum_{\lambda\mu}\alpha_{\lambda\mu}Y_{\lambda\mu}(\mathbf{n})\right\}, \tag{2}$$

where $\mathbf{n}$ is the direction of the α particle. The surface of the nucleus is given by the equation

$$R(\Omega) = R\left[1 + \sum_{\lambda\mu}\alpha_{\lambda\mu}Y_{\lambda\mu}(\Omega)\right],$$

where $Y_{\lambda\mu}$ is a spherical harmonic.

Formula (2) does not take account of the bending of the trajectory of the α particle, since this effect leads at worst to corrections of the next highest order in α. We now introduce the phonon creation and annihilation operators in expression (2) by replacing α_μ by

$$\sqrt{\hbar/2B_\lambda\omega}\,(b_{\lambda\mu} + (-1)^\mu b^+_{\lambda\mu}),$$

where $b_{\lambda\mu}$ and $b^+_{\lambda\mu}$ are the operators of annihilation and creation of phonons, respectively:

$$b_{\lambda\mu}b^+_{\lambda\mu} = n_{\lambda\mu} + 1, \qquad b^+_{\lambda\mu}b_{\lambda\mu} = n_{\lambda\mu},$$

where $n_{\lambda\mu}$ is the occupation number. The function (2) has now become an operator acting on functions of the occupation numbers $n_{\lambda\mu}$:

$$\psi(\mathbf{n})\Big|_S = \text{const}\cdot\exp\left\{KR\sqrt{\hbar/2B_\lambda\omega} \times\sum_\mu\left[b_{\lambda\mu}Y_{\lambda\mu}(\mathbf{n}) + b^+_{\lambda\mu}Y^*_{\lambda\mu}(\mathbf{n})\right]\right\}. \tag{3}$$

Since the commutator of the operators $\sum_\mu b_{\lambda\mu}Y_{\lambda\mu}$ and $\sum_\mu b^+_{\lambda\mu}Y^*_{\lambda\mu}$ is a c-number (it is equal to $\sqrt{(2\lambda+1)/4\pi}$), we can write the function (3) in the form

$$\psi(\mathbf{n})\Big|_S = \text{const}\cdot\exp(c/2)\exp\left\{KR\sqrt{\hbar/2B_\lambda\omega}\sum_\mu b^+_{\lambda\mu}Y^*_{\lambda\mu}(\mathbf{n})\right\} \times\exp\left\{KR\sqrt{\hbar/2B_\lambda\omega}\sum_\mu b_{\lambda\mu}Y_{\lambda\mu}(\mathbf{n})\right\}, \tag{4}$$

where

$$c = \sqrt{(2\lambda+1)/4\pi}\,(KR\sqrt{\hbar/2B_\lambda\omega})^2$$

is the commutator of the operator $KR\sqrt{\hbar/2B_\lambda\omega}\times\sum_\mu b_\mu Y_{\lambda\mu}$ with its conjugate operator.

The wave function (4) must be expanded in terms of the normalized (to unity) states of the daughter nucleus $\chi^{(n)}_{j,\mu}$ with a given number of phonons n and total angular momentum j, μ. In the case of an even-even nucleus the amplitude of such a state of the daughter nucleus is given by the matrix element of the operator (4) between the state $\chi^{(n)}_{j,\mu}$ and the vacuum state:

$$\langle n; j,\mu|\psi(\mathbf{n})|0;0,0\rangle = \text{const}\cdot\frac{1}{n!}(KR\sqrt{\hbar/2B_\lambda\omega})^n\langle n; j,\mu\Big|\times\Big(\sum_\nu b^+_\nu Y_{\lambda\nu}(\mathbf{n})\Big)^n\Big|0;0,0\rangle = \text{const}\cdot(KR\sqrt{\hbar/2B_\lambda\omega})^n \times\sum_{\nu_1\ldots\nu_n} Q^{j\mu;\,n}_{\lambda\nu_1\ldots\lambda\nu_n}Y^*_{\lambda\nu_1}(\mathbf{n})\ldots Y^*_{\lambda\nu_n}(\mathbf{n}), \tag{5}$$

where we used the following expression for the function $\chi^{(n)}_{j,\mu}$:

$$\chi^{(n)}_{j,\mu} = \sum_{\nu_1\ldots\nu_n} Q^{j\mu;\,n}_{\lambda\nu_1\ldots\lambda\nu_n}b^+_{\lambda\nu_1}\ldots b^+_{\lambda\nu_n}|0;0,0\rangle. \tag{6}$$

The $Q^{\ldots}_{\ldots}$ are numerical coefficients,

$$Q^{j\mu;0}=\delta_{j0}, \quad Q^{j\mu;1}_{\lambda\nu}=\delta_{j\lambda}\delta_{\mu\nu}, \quad Q^{j\mu;2}_{\lambda\nu_1\lambda\nu_2}=\frac{1}{\sqrt{2}}C^{j\mu}_{\lambda\nu_1\lambda\nu_2}, \ldots,$$

and the $C^{c\gamma}_{a\alpha b\beta}$ are Clebsch-Gordan coefficients. In (5) we have

$$\sum_{\nu_1\ldots\nu_n} C^{j\mu;\,n}_{\lambda\nu_1\ldots\lambda\nu_n} Y^*_{\lambda\nu_1}(\mathbf{n})\ldots Y^*_{\lambda\nu_n}(\mathbf{n}) = A^{j,n}_{\lambda} Y^*_{j\mu}(\mathbf{n}).$$

The coefficients $A^{j,n}_{\lambda}$, just like the coefficients $C^{j\mu;n}_{\lambda\nu_1\ldots\lambda\nu_n}$, can be written as linear combinations of Clebsch-Gordan coefficients. For the important values $n = 0, 1, 2$ the coefficients $A^{j,n}_{\lambda}$ are equal to

$$A^{j,0}_{\lambda}=\delta_{j,0}, \quad A^{j,1}_{\lambda}=\delta_{\lambda j}, \quad A^{j,2}_{\lambda}=(2\lambda+1)[8\pi(2j+1)]^{-1/2}C^{j0}_{\lambda0\lambda0}. \tag{7}$$

Taking this into account, we find for the wave function describing the decay of a nucleus with spin zero

$$\psi = \text{const}\cdot\sum_{n=0,1,2} A^{j,n}_{\lambda}(KR\sqrt{\hbar/2B_\lambda\omega})^n G_j(r)(k_j r)^{-1}\sum_{\mu}\chi^{(n)}_{j\mu}Y^*_{j\mu}(\mathbf{n}), \tag{8}$$

where $G_j(r)$ are radial wave functions describing the motion of an α particle with angular momentum $l = j$ and corresponding energy in a spherically symmetric Coulomb field.

According to (8) the amplitudes of the partial waves at infinity are equal to the amplitudes at the surface S multiplied by the corresponding penetration factors for the Coulomb and centrifugal barriers. The probability for α decay with the excitation of a vibrational state with the number of phonons n and angular momentum j, μ is proportional to

$$(2j+1)\,|A^{j,n}_{\lambda}(KR\sqrt{\hbar/2B_\lambda\omega})^n G_j(r\to\infty)|^2. \tag{9}$$

The ratio of the intensity of α decay with excitation of one phonon $(j = \lambda)$ over the intensity of α decay to the ground state is equal to

$$\xi^{(1)}_{\lambda=j}=(2j+1)(KR\sqrt{\hbar/2B_\lambda\omega})^2\frac{P(\mathscr{E}',\,l=\lambda)}{P(\mathscr{E}_0,\,l=0)}, \tag{10}$$

and the relative intensity of the excitation of the two-phonon vibrational state is

$$\xi^{(2)}_{\lambda,\,j}=\frac{(2\lambda+1)^2}{4\pi}(KR\sqrt{\hbar/2B_\lambda\omega})^4 C^{j0}_{\lambda0\lambda0}\frac{P(\mathscr{E}'',\,l=j)}{P(\mathscr{E}_0,\,l=0)}, \tag{11}$$

$P(\mathscr{E}, l)$ denotes the penetrability of the Coulomb barrier for particles with energy $\mathscr{E}$ and orbital angular momentum l:

$$P(\mathscr{E},l)=\exp\left\{-2\int_R^{r^*}|k_l(r)|\,dr\right\}$$

$$\approx\exp\{-2l(l+1)/\varkappa b\}\exp\{-2\varkappa\sqrt{b\gamma}\,\mathscr{E}R/2Ze^2\}, \tag{12}$$

where $b = 2Ze^2/R\mathscr{E}_0$, $\kappa = \sqrt{2m\mathscr{E}_0}\,R/\hbar$, and $\gamma(x)$ is a tabulated function (see, for example, the review article[11]). The quantity $\hbar/2B_\lambda\omega$ entering in (10) and (11) can be expressed in terms of the reduced probability of the radiative transition for a one-phonon excitation:[12]

$$B(E\lambda;\, j=0\to j=\lambda)=(2\lambda+1)\left(\frac{3}{4\pi}ZR_0^\lambda\right)^2\hbar/2B_\lambda\omega. \tag{13}$$

We note that this formula, which expresses the relation between the radiative transition probability and the amplitude of the nuclear surface oscillations, contains the model assumption of irrotational flow of nuclear matter. The degeneracy of the two-phonon state with respect to the angular momentum number existing in the pure harmonic model can be removed by the residual interaction. If, however, the splitting of this level is small in comparison with the resolution of the apparatus, it is meaningful to speak only of the summed intensity of the α decay to the second excited vibrational state. This quantity is obtained by summing (12) over j, where we use the normalization of the Clebsch-Gordan coefficients $\sum_j (C^{j0}_{\lambda_0\lambda_0})^2 = 1$:

$$\xi^{(2)}_{\lambda}=\sum_j\xi^{(2)}_{\lambda,\,j}\approx\frac{(2\lambda+1)^2}{4\pi}(KR\sqrt{\hbar/2B_\lambda\omega})^4\frac{P(\mathscr{E}'',\,l)}{P(\mathscr{E}_0,\,l=0)}, \tag{14}$$

where $P(\mathscr{E}'', l)$ is the average penetrability of the Coulomb barrier for the α particles belonging to the given group of states.

The lowest lying excited states with even parity of the Pb^{206} nucleus ($j = 2$, $E \approx 0.8$ Mev) and of the even isotopes of Po and Rn are possible examples of vibrational levels in the region of α active nuclei. In the table we list the results of the calculations for these nuclei, using formulas (10) to (14). The table also gives the relevant experimental data and the values of the effective radii $R = (r_0A^{1/3} + 2.5)\times10^{-13}$ cm used in the calculations (these values of R are taken from the review article[11]). R_0 in (13) was taken to be equal to $r_0A^{1/3}\times10^{-13}$ cm. The values of $\xi^{(2)}_{\lambda=2}$ in the table were calculated with the help of (14), since it is not excluded that the second excited state of the nuclei is in reality a vibrational state which is threefold degenerate with respect to the spin or a group of close lying levels. This possibility is not in disagreement with the experimental data.

As is seen from the data of the table, there is rather close agreement between the calculated and the experimental values of the quantities B(E2; $0\to2$) or $\xi^{(2)}$, although the calculated value of B(E2) lies somewhat below that obtained from Coulomb excitation. This discrepancy is particularly great in the case of Pb^{206} [B(E2) α decay

Daughter nucleus	Pb^{206}	Po^{214}	Rn^{219}	Rn^{222}
$\mathcal{E}_0$, Mev	5.3	7.13	6.5	4.78
E_2, Mev	0.80	0.61	0.32	0.187
E_1, Mev			0.65	0.447
$10^{-13}R$, cm	$1.42A^{1/3}+2.5$	$1.58A^{1/3}+2.5$	$1.58A^{1/3}+2.5$	$1.54A^{1/3}+2.5$
$\xi^{(1)}$ (experiment)	$1.2\cdot10^{-5}$	$2\cdot10^{-3}$	$4\cdot10^{-2}$	$5.7\cdot10^{-2}$
$\xi^{(2)}$ (experiment)			$8\cdot10^{-5}$	10^{-4}
$10^{-48}B(E2)$, cm^4 (experiment)	0.14	0.60	unknown	unknown
$KR\sqrt{\hbar/2B_2\omega}$ (calculated from $\xi^{(1)}_{exp}$)	0.29	0.33	0.50	0.63
$10^{-48}B(E2)$, cm^4 (calculated from $\xi^{(1)}_{exp}$)	0.022	0.44	1.00	1.20
$\xi^{(2)}$ (calculated from $\xi^{(1)}_{exp}$)			$5\cdot10^{-5}$	$5.5\cdot10^{-5}$

$\approx \frac{1}{7} B(E2)_{Coul}$]. The disagreement even becomes slightly worse if the Coulomb excitation in α decay is taken into account (see below). A possible explanation of this disagreement is that in α decay only the part of the quadrupole moment connected with the deformation of the nuclear surface comes into play. In radiative transitions and Coulomb excitation, on the other hand, the total quadrupole moment of the nucleus enters into the calculation, including also the quadrupole moment of the nucleons in the unfilled shell. Formula (13) involves only the quadrupole moment of the core.

We note that the intensity of the α decay of the even isotopes of Ra to the ground, first, and second excited states of Rn with even parity also agrees with the assumption that these levels have rotational character. The parameter of quadrupole deformation, α, is here assumed to be equal to $0.07-0.09$,[4] which is in qualitative agreement with the magnitude of the moments of inertia of these nuclei. The smallness of the ratio of the energy of the second excited level over the energy of the first excited level $(2.0-2.4)$ may in this case be explained by the circumstance that the rotation of the nucleus is not adiabatic for a small moment of inertia of the nucleus.*

Let us now turn to the discussion of the Coulomb excitation in α decay. For simplicity we consider spherical nuclei, in which case the nonspherical Coulomb field outside the nucleus can be neglected (with the exception of the transition field). In the case of a spherical nucleus the wave function describing the α decay of the nucleus into states with spin I, M = 0 (the result is, of course, independent of the choice of the projection of the angular momentum) can be written in the form

$$\psi_{I,0} = \sum_{lj} r^{-1}a_{lj}(r)\sum_{m\mu} C^{I0}_{lmj\mu}\chi_{j\mu}Y_{lm}(\mathbf{n}) + \sum_{lj} r^{-1}b_{lj}(r)\sum_{m\mu} C^{I0}_{lmj\mu}\bar{\chi}_{j\mu}Y_{lm}(\mathbf{n}), \tag{15}$$

where $\chi_{j\mu}$ and $\bar{\chi}_{j\mu}$ are wave functions describing the internal state of the daughter nucleus in the intensive principal α decay and the state of the nucleus excited by the emitted α particle via the Coulomb interaction, respectively.

The Schrödinger equation satisfied by (15) has the form

$$\left(H(X)-\frac{\hbar^2}{2m}\Delta_r+V_0(\mathbf{r})+V_1(X,\mathbf{r})-E\right)\psi_{I,0}(X,\mathbf{r})=0, \tag{16}$$

where H(X) is the Hamiltonian of the daughter nucleus, and X denotes the internal coordinates of the nucleus. Here

$$V_0=\frac{2Ze^2}{r},$$

$$V_1=\frac{2Ze^2}{r}\sum_{\lambda=1,\ldots}\frac{4\pi}{2\lambda+1}\sum_{i,\nu}(r_i/r)^{\lambda}Y^{*}_{\lambda\nu}(\mathbf{r}_i/r_i)\,Y_{\lambda\nu}(\mathbf{n}),$$

the summation goes over all protons in the nucleus. We can obtain an equation for the functions b_{lj} by multiplying (16) by $\bar{\chi}^{*}_{j\mu}Y^{*}_{lm}(\mathbf{n})$ and integrating the resulting expression over the nuclear variables and the angular coordinates of the α particle. Since we assume that the effect of the transition field is weak, we can neglect the term containing the product of V_1 and b_{lj}. The resulting equation for b_{lj} has the form

$$\left(-\frac{\hbar^2}{2m}\Delta_r^{(l)}+V_0-\mathcal{E}\right)\frac{b_{lj}}{r}C^{I0}_{l-\mu j\mu}=\sum_{l'j'}(a_{l'j'}/r)\times\sum_{m'\mu'}C^{I0}_{l'm'j'\mu'}\int d\mathbf{n}Y^{*}_{lm}(\mathbf{n})<j\mu|V'|j'\mu'>Y_{l'm'}(\mathbf{n}),$$

$$\Delta_r^{(l)}=\frac{1}{r^2}\frac{d}{dr}r^2\frac{d}{dr}-\frac{l(l+1)}{r^2}, \tag{17}$$

where the primes on the indices refer to the principal α decay.

An analogous equation can be written down for the functions $a_{l'j'}$. It is clear, however, that it is

*A different possible explanation of the smallness of the ratio of the second excited level to the energy of the first excited level 2^+ for these nuclei has to do with the asymmetry of their surface shapes (private communication by A. S. Davydov). This possibility is not considered here.

sufficient for the calculation of the b_{lj} in first approximation to know the $a_{l'j'}$ only in the zeroth approximation. This means that we can neglect the inverse transitions from the secondary group to the principal group. In this approximation the functions $a_{l'j'}$ coincide with the functions G introduced earlier.

We write the transition field $<j\mu \mid V_1(X, r) \mid j'\mu'>$ in the form

$$\langle j\mu \mid V_1(X, r) \mid j'\mu' \rangle = \frac{2e^2}{r} \sum_{\lambda=1,\ldots} \frac{4\pi}{2\lambda+1} \sum_{\nu} r^{-\lambda} \langle j\mu \mid \mathfrak{M}^*(\lambda\nu) \mid j'\mu' \rangle Y_{\lambda\nu}, \quad (18)$$

where $\mathfrak{M}(\lambda\nu)$ is the operator for the electric multipole transition (λ, ν):

$$\mathfrak{M}(\lambda\nu) = \sum_i r_i^{\lambda} Y_{\lambda\nu}(\mathbf{r}_i / r_i).$$

The matrix element of the operator $\mathfrak{M}(\lambda\nu)$ can be conveniently expressed in terms of the reduced matrix element $<j \parallel \mathfrak{M}(\lambda) \parallel j'>$, which is defined by

$$\langle j\mu \mid \mathfrak{M}(\lambda\nu) \mid j'\mu' \rangle = (-1)^{\lambda+j-j'} C^{j\mu}_{\lambda\nu j'\mu'} (2j+1)^{-1/2} \langle j \parallel \mathfrak{M}(\lambda) \parallel j' \rangle. \quad (19)$$

The reduced matrix element is related to the reduced transition probability $B(E\lambda; j' \to j)$ in the following way:

$$B(E\lambda; j' \to j) = \sum_{\mu'\nu} |\langle j\mu \mid \mathfrak{M}(\lambda\nu) \mid j'\mu' \rangle|^2 = |\langle j \parallel \mathfrak{M}(\lambda) \parallel j' \rangle|^2 \frac{1}{(2j'+1)}. \quad (20)$$

Substituting (19) in the right hand side of equation (17), we obtain, after summing over the spin projections, the following equation for the $b_{lj}(r)$:

$$\left(-\frac{\hbar^2}{2m}\Delta_r^{(l)} + V_0 - \mathscr{E}_l\right)\frac{b_{lj}}{r} = -\frac{2e^2}{r}\sum_{\lambda l'j'} (-1)^{j-j'} [4\pi(2l'+1)(2j'+1)/(2\lambda+1)]^{-1/2} \times C^{l0}_{l'0\lambda0} B^{1/2}(\lambda; j' \to j)\, r^{-\lambda} W(jj'll'/\lambda I)\, [a_{l'j'}(r)/r], \quad (21)$$

where the $W(abcd \mid ef)$ are Racah coefficients.

The phase of $B^{1/2}(E\lambda)$ in (21) is taken to be that of the matrix element $<j \parallel \mathfrak{M}(\lambda) \parallel j'>$. The angular momenta entering in equation (21) must satisfy the "triangular relations" $(jj'\lambda)$, $(ll'\lambda)$, (jlI), and $(j'l'I)$. These inequalities connecting the magnitudes of the angular momenta have the usual physical interpretation (see Fig. 2).

In place of the functions b_{lj} we introduce new functions $\zeta_{lj}(r)$, which are connected with the b_{lj} by the relation

$$b_{lj}(r) = \zeta_{lj}(r) \exp\{\hbar^{-1} S_{lj}(r)\}, \quad (22)$$

where

$$\hbar^{-1} S_{lj}(r) = \int_R^r |k_{lj}(r)|\, dr,$$

k_{lj} is the wave vector of the α particle [see Eq. (12)]. Substituting (22) in (21), we obtain for the function ζ_{lj} the equation

$$p_{lj}\, d\zeta_{lj}(r)/dr + \tfrac{1}{2}(dp_{lj}/dr)\zeta_{lj}(r) = \frac{2me^2}{\hbar R}\sum_{l'j'} A^{lj}_{l'j'}\left(\frac{R}{r}\right)^{\lambda+1} \times a_{l'j'}(r) \exp\{\hbar^{-1} S_{lj}(r)\} B^{1/2}(\lambda; j' \to j) R^{-\lambda}, \quad p_{lj}(r) = |k_{lj}(r)|. \quad (23)$$

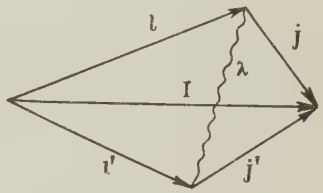

FIG. 2

In (23) we have omitted the term containing the second derivative of the function ζ_{lj}, which is smaller than the other terms by the factor KR, and

$$A^{lj}_{l'j'} = \{4\pi(2l'+1)/(2\lambda+1)\}^{1/2} C^{l0}_{l'0\lambda0} W(jj'll'/\lambda I).$$

The solution of (23) can be written in the form

$$\zeta_{lj}(r) = \zeta^0_{lj'} + (2me^2/\hbar\sqrt{p_{lj}(r)}) \sum_{l'j'} A^{lj}_{l'j'} B^{1/2}(\lambda; j' \to j) R^{-\lambda} \times \int_R^r (R/r')^{\lambda+1}\, d(r'/R)\, [p_{lj}(r')]^{-1/2} \exp\{\hbar^{-1} S_{lj}(r')\}\, a_{l'j'}(r). \quad (24)$$

Here ζ^0_{lj} is the value of the amplitude on the nuclear surface. In our approximation this term corresponds to the nuclear excitation. In the particular case of vibrational levels it corresponds to the above-mentioned "surface" excitation. In this instance ζ^0_{lj} coincides with the amplitude of the "surface" excitation on the sphere S.

For the functions $a_{l'j'}$ we may use the quasiclassical approximation,

$$a_{l'j'}(r) = a^0_{l'j'} [p_{l'j'}(r)]^{-1/2} \exp\{-\hbar^{-1} S_{l'j'}(r)\}, \quad (25)$$

where $a^0_{l'j'}$ is the amplitude of the function a_{lj} on the surface of the nucleus. For $r > r^*$ the function b_{lj} has the form

$$b_{lj}(r) = (2me^2/\hbar\sqrt{p_{lj}(r)}) \times \sum_{l'j'} A^{lj}_{l'j'} B^{1/2} R^{-\lambda} a_{l'j'}(r^*) \exp\{i\hbar^{-1} S_{lj}(r)\} \times \left\{\int_R^{r^*} \left(\frac{R}{r'}\right)^{\lambda+1} d\left(\frac{r'}{R}\right) \exp\left\{\frac{1}{\hbar}[(S_{lj}(r') - S_{lj}(r^*)) - (S_{l'j'}(r') - S_{l'j'}(r^*))]\right\} [p_{lj}(r')\, p_{l'j'}(r')]^{-1/2} + \int_{r^*}^{r} \left(\frac{R}{r}\right)^{\lambda+1} d\left(\frac{r'}{R}\right) \times \exp\left\{\frac{1}{\hbar}[S_{lj}(r') - S_{l'j'}(r')]\right\} [p_{lj}(r')\, p_{l'j'}(r')]^{-1/2}\right\}. \quad (26)$$

To obtain the intensity of the line (l, j) we must multiply the square of (26) by $p_{lj}(r)$ and take the limit of the resulting expression as $r \to \infty$. The intensity of the line corresponding to a level with angular momentum j is obtained by summing over l. The ratio of the intensities is conveniently written in the form

$$\xi_{j'\to j;\ l\to l'} = (4me^2R/\hbar^2 b^\lambda \varkappa)\, B(\lambda;\ j'\to j)\, R^{-2\lambda} \times \left\{ \sum_l \left| \sum_{l'} A^{lj}_{l'j'} a_{l'j'}(r^*)\ (J_1 + J_2) \right|^2 \right\} \Big/ \sum_{l'} |a_{l'j'}(r^*)|^2, \qquad (27)$$

where J_1 and J_2 are, respectively, integrals over the barrier region and over the region of classical motion.

The action function S_{lj} in (26) is now expanded into a sum over the angular momenta and energies of the excited nucleus. The integral J_1 can then be written in the form

$$J_1 = \int_0^{\sqrt{b-1}} dy\,(1+y^2)^{\lambda-1} \exp\{-\sigma_{lj,\,l'j'}(y)\},$$

$$\sigma_{lj,\,l'j'}(y) = c_{ll'}\, y + d_{jj'}\,(y/(1+y^2) + \tan^{-1} y),$$

$$c_{ll'} = [l(l+1) - l'(l'+1)]/\varkappa b, \quad d_{jj'} = \varkappa b\, \Delta\mathscr{E}/2\mathscr{E}.$$

A convenient form of the integral J_2 is

$$J_2 = \frac{1}{2} v_\infty b^\lambda R^\lambda \int_{r^*}^{\infty} r^{-(\lambda+1)} v^{-1}(r) \exp\{-i\omega_{jj'} t(r)\}\, dr,$$

where

$$t(r) = \int_{r^*}^{r} v^{-1}(r)\, dr, \quad \omega_{jj'} = (\mathscr{E}_j - \mathscr{E}_{j'})/\hbar.$$

In the denominators of the integrands of the integrals J_1 and J_2 we neglected the dependence of p_{lj} on l and j. Integrals analogous to J_2 have been computed in the theory of the Coulomb excitation by charged particles.[13,12] The only difference is that the time integration in J_2 goes from 0 to ∞, and not from $-\infty$ to $+\infty$ as in the usual case, i.e., we integrate only over one half of the trajectory of the scattering particle. Furthermore, we neglected in J_2 the dependence of $t(r)$ on the orbital angular momentum. The integral J_2, therefore, corresponds to a head-on collision, i.e., to a classical orbit with eccentricity one.

In a head-on collision the incoming and outgoing branches of the trajectory give the same contribution to the amplitude of electric excitation. This allows us to express the integral J_2 directly in terms of the tabulated integral $I_{\lambda\mu}(\vartheta, \xi)$:[12,14]

$$J_2 = 2^{\lambda-2} I_{\lambda 0}(180°,\ d_{jj'}/2) = 2^{\lambda-2} \int_{-\infty}^{+\infty} \exp\{id_{jj'}(\sinh\omega + \omega)/2\}\,(\cosh\omega + 1)^{-\lambda}\, d\omega,$$

$$d_{jj'} = (2Ze^2/\hbar v_\infty)(\Delta\mathscr{E}/\mathscr{E}).$$

Formula (27) can be simplified considerably in the case of an even-even nucleus. Then $I = 0$, $l = j$, and $l' = j'$. If, moreover, the contribution from the state $l' = j' = 0$ is predominant, which is the case for spherical nuclei, we obtain from formula (27)

$$\xi_{0\to j;\ 0\to 0} = (4me^2R/\hbar b^\lambda \varkappa)[4\pi/(2\lambda+1)]\, B(E\lambda;\ 0\to j) \times R^{-2\lambda}(J_1 + J_2)^2 \delta_{\lambda j}. \qquad (28)$$

In the decay of deformed nuclei several values of l usually have comparable intensity. Besides this, the Coulomb excitation in deformed nuclei is also different in that there exists an appreciable static quadrupole potential outside the nucleus. Nevertheless, even in the calculation of the Coulomb excitation of nonspherical nuclei one can in first approximation neglect the quadrupole field, unless, of course, the quadrupole potential is the transition potential itself.

This circumstance is due to the fact that even the electric quadrupole excitation contributes only little to the intensity of the principal lines of the even group ($j = 0, 2$) (see below, and also reference 4). The electric excitation outside the sphere S is in this approximation also given by formula (27). It is convenient to write this formula in a somewhat different form for deformed nuclei. For this purpose we use a formula which expresses the reduced transition probability through the intrinsic multipole moment of the nucleus in the coordinate system fixed in the nucleus:[12]

$$B^{1/2}(E\lambda;\ j'\to j) = [(2\lambda+1)/4\pi]^{1/2} Q_\lambda^{(0)} C^{jK}_{j'K\lambda 0}.$$

We have

$$\xi_{\Sigma j'\to j;\ 0\to 0} = (4me^2R/\hbar^2 \varkappa b^\lambda)^2 q_\lambda^2 \left| \sum_{l'} \alpha_{l'} (C^{l'0}_{\lambda 0 j 0})^2 (J_1 + J_2) \right|^2,$$

$$q_\lambda = Q_\lambda^{(0)}/R_0^\lambda, \quad \alpha_{l'} = a_{l'}(r^*)/a_0(r^*). \qquad (29)$$

For odd nonspherical nuclei we can use an expression for the transition amplitude which was obtained in the adiabatic approximation (see references 2 and 3):*

$$\alpha_{l'j'} = \alpha_{l'} C^{j'K}_{IKl'0}, \qquad \alpha_{l'j'} = a_{l'j'}(r^*)/a_{0I}(r^*). \qquad (30)$$

Using (29) and (30), we find for an odd nucleus

*In the determination of the wave function in the adiabatic approximation the nucleus is considered at rest and the law of conservation of energy is not observed. The accuracy of the adiabatic approximation is improved considerably, if the conservation of energy is taken into account. The adiabatic approximation in this sense becomes invalid only to the same extent as the nonsphericity of the Coulomb field becomes important. It therefore has quite sufficient accuracy for our purposes.

$$\xi_{\Sigma j' \to j;\, I \to I} = (4me^2R/\hbar^2 \varkappa b^\lambda)\, q_\lambda^2 \left\{ \sum_l \left| \sum_{l'j'} C_{l'j'}^{lj} \alpha_{l'} \times (J_1 + J_2) \right|^2 \right\} \Big/ \sum_{l'} |\alpha_{l'}|^2 (C_{Il'0}^{Il'})^2, \quad (31)$$

where

$$C_{l'j'}^{lj} = (-1)^{j-j'} [(2l'+1) \times (2j'+1)]^{1/2} C_{l'0\lambda 0}^{l0} C_{Il0}^{j'I} C_{j'I\lambda 0}^{jI} W(jj'll'|\lambda I).$$

In formula (31) the projection of the spin on the nuclear axis, K, is set equal to I, since we are considering a transition without change of K, which is equal to I in the initial nucleus.

In those cases where the reduced electromagnetic transition probability is known experimentally (for example, through the lifetime of the state or through the probability of electric Coulomb excitation) the probability of Coulomb excitation of a given state in α decay can be computed directly using formulas (28), (29), and (31). The values of B(E2; $0 \to 2$) are known for the nuclei Pb^{206} and Po^{210} (cf. the table). The integrals $J_1 + J_2$ for these nuclei are equal to 0.2 and 0.77, respectively (the integral J_1 is obtained by numerical integration, the values of the integral J_2 were taken from the above-mentioned tables[12,14]). According to formula (28) we obtain for the relative probability of electric quadrupole excitation for these nuclei the values 2.0×10^{-4}% and 0.03%, respectively. This means that pure Coulomb excitation could explain only approximately $1/6$ to $1/7$ of the observed intensity of the decay to the level 2^+. In order to explain, in the case of Ra^{222}, the observed intensity of the decay to the first excited state 2^+ of the daughter nucleus Rn^{218} (4.5%) by Coulomb excitation alone, one would have to assume that for Rn^{218} one has the value B(E2; $0 \to 2$) = 40×10^{-48} cm^4, which exceeds considerably the expected value (1 to 2×10^{-48} cm^4).

The reduced probability for radiative E2 decay is known also for the odd nucleus Pb^{207} [B(E2; $1/2 \to 5/2$) = 0.028×10^{-48} cm^4]. In the decay of Po^{211} ($9/2^-$), which leads to the formation of this nucleus, we have, besides the intensive transition to the state ($1/2^-$, $l' = 4$), also transitions to the excited states ($5/2^-$) and ($3/2^-$). According to formula (27) we find for the relative intensity of the electric excitation of the level the value 4.5×10^{-5}, which is approximately one hundredth of the experimental value ($l' = 4$, $l = 2$; 4; 6; $J_1 + J_2 = 1.2$; 1.8; 0.8).

Let us now consider the Coulomb excitation of levels with odd parity. In the decay of the even isotopes of Ra we observe, besides the intensive transitions to levels of the same parity, relatively rare transitions to excited states (1^-) of the daughter nuclei Rn ($E_{1^-} \approx 0.6$ Mev). For the decay $Ra^{224} \to Rn^{220}$ we have $J_1 \approx 0.25$ and $J_2 \approx 0.07$. According to formula (29), the observed intensity of the decay ($Ra^{224} \to Rn^{220}$, 1^-) would correspond to the value B(E1; $0^+ \to 1^-$) = $1/50 \times 10^{-24}$ cm^2. For the decay $Ra^{226} \to Rn^{222}$ ($J_1 = 0.10$, $J_2 = 0.02$) we obtain B(E1: $0^+ \to 1^-$) = $1/10 \times 10^{-24}$ cm^2. Both these values are close to the one-particle values of B(E1), but are considerably (10 to 50 times) higher than the value of the reduced probability expected for nuclei with octupole-deformed ("pear-shaped") surfaces.[15]

Decays to levels with odd parity are also observed in heavier even nuclei. Let us take as an example the decay $Th^{228} \to Ra^{224}$. The experimental intensity of the α decay to the level 1^- leads, according to formula (29), to $q_1 = 0.45$ ($\lambda = 1$, dipole excitation) or $q_3 = 9$ ($\lambda = 3$, octupole excitation). This value of q_1 is approximately 10 times larger than the experimental value[16] and the value expected for "pear-shaped" nuclei. According to formula (29), the intensity of the Coulomb excitation of the level 3^- of Ra^{224} amounts to about $1/10$ of the intensity of the decay to the level 1^- for dipole excitation and to $1/3$ of that intensity in the case of octupole excitation (the experimental value is $\sim 1/10$). In the case of Ra^{226}, where the probability for α decay to the level 1^- is relatively smaller than in the decay $Th^{228} \to Ra^{224}$, we find values of q_1 and q_3, which are about one half of the former ones.

Excitation of rotational levels with odd parity is also observed in the decay of Am^{241}:

$$(5/2,\ K = 5/2^+) \to (5/2,\ K = 5/2^-, \quad \text{ground state}).$$

It can be assumed that this decay is the result of electric de-excitation of the daughter nucleus by α particles of the principal group:

$$(5/2,\ 5/2^+) \to (5/2,\ 5/2^+, \quad \text{excited state}).$$

The probability of such an electric dipole process was computed by a different method in reference 11. It appeared that one cannot explain the observed intensity of the decay of Am^{241} to the ground state of Np^{237} by electric dipole excitation: this would require a value for the dipole moment which disagrees with the experimental estimates. Formula (31) leads to the same result. On the other hand, the interpretation of the decay of Am^{241} to the ground state of Np^{237} as an electric octupole excitation would require the value (3 to 4) R^3 for the octupole moment. This is close to the value expected for octupole-deformed nuclei (the calculations were based on formula (31); we included the terms with $j' = 5/2$, $7/2$, $9/2$, $l' = 0.2$, and $l = 1, 3, 5$).

We note that in deformed nuclei only $\frac{1}{8}$ of the observed intensity of α decay to the state 2^+ could be explained by electric quadrupole excitation. The most important effect is the deformation of the nuclear potential.

The above-quoted numerical values of the intensity of the Coulomb excitation of weak lines are true if the Coulomb excitation is the only or the predominant mechanism. In the α decays under consideration this is actually not the case [possible exceptions are the decays of Am^{241} ($\lambda = 3$) and of the even isotopes of Ra ($\lambda = 1$)]. The amplitude of the Coulomb excitation must be added to the amplitude of the nuclear excitation. In the case of vibrational levels we combine the amplitude (8) with the amplitude of the Coulomb excitation (26) and (28), and obtain for the excitation amplitude of the level 2^+:

$$\psi_{\text{Coul.}} + k\psi_{\text{surf. oscill.}}$$

The coefficient k in front of the nuclear excitation amplitude takes account of the circumstance that only part of the total quadrupole momentum can have an effect on the "surface" excitation. Comparing the intensity calculated in this way with the experimental value, we find $k = 0.25$ for Pb^{206} and $k = 0.5$ for Po^{210}. These values of k are close to the values of the coefficients of the quadrupole polarization of the nuclear core as determined by the experimental data on the quadrupole moments of nuclei close to the magic numbers.[17,18]

I express my gratitude to A. G. Zelenkov for valuable comments and help in the analysis of the experimental data.

[1] J. O. Rasmussen and B. Segall, Phys. Rev. **103**, 1298 (1956).

[2] Bohr, Fröman, and Mottelson, Kgl. Danske Videnskab. Selskab, Mat.-Fys. Medd. **29**, Nr. 10 (1955).

[3] V. M. Strutinskiĭ, Report, Acad. Sci. U.S.S.R. (1955).

[4] V. M. Strutinskiĭ, Dokl. Akad. Nauk SSSR **104**, 524 (1955). JETP **32**, 1412 (1957), Soviet Phys. JETP **5**, 1150 (1957).

[5] V. G. Nosov, Dokl. Akad. Nauk SSSR **103**, 65 (1955). JETP **33**, 226 (1957), Soviet Phys. JETP **6**, 176 (1958).

[6] P. O. Fröman, Mat.-Fys. Skr. Dan. Vid. Selsk. **1**, Nr. 3 (1957).

[7] Gol'din, Adel'son-Vel'skiĭ, Birzgal, Piliya, and Ter-Martirosyan, JETP **35**, 184 (1958), Soviet Phys. JETP **8**, 127 (1959).

[8] D. L. Hill and J. A. Wheeler, Usp. Fiz. Nauk **52**, 20 (1954); [Transl. from Phys. Rev. **89**, 1102 (1953)].

[9] A. B. Migdal, Report, Acad. Sci. U.S.S.R. (1948).

[10] M. A. Preston, Phys. Rev. **75**, 90 (1949) and **82**, 515 (1951).

[11] I. Perlman and J. O. Rasmussen, Handbuch d. Phys. **42**, Berlin (1957).

[12] Alder, Bohr, Huus, Mottelson, and Winther, Revs. Modern Phys. **28**, 432 (1956).

[13] K. A. Ter-Martirosyan, JETP **22**, 284 (1952).

[14] K. Alder and A. Winther, Kgl. Danske Videnskab. Selskab, Mat.-Fys. Medd. **31**, Nr. 1 (1956).

[15] V. M. Strutinskiĭ, Атомная энергия (Atomic Energy) **4**, 150 (1956).

[16] A. Bohr and B. Mottelson, Nucl. Phys. **4**, 529 (1957).

[17] M. Goeppert-Mayer and J. H. Jensen, Elementary Theory of Nuclear Shell Structure, Wiley, N.Y. (1955).

[18] S. T. Belyaev, Kgl. Danske Videnskab. Selskab, Mat.-Fys. Medd. **31**, Nr. 11 (1959).

Translated by R. Lipperheide
20

INTEGRAL TRANSFORMATIONS OF THE I. S. SHAPIRO TYPE FOR PARTICLES OF ZERO MASS

L. G. ZASTAVENKO and CHOU KUANG-CHAO

Joint Institute for Nuclear Research

Submitted to JETP editor May 28, 1959

J. Exptl. Theoret. Phys. (U.S.S.R.) **38**, 134-139 (January, 1960)

An expansion in terms of the irreducible representations of the proper Lorentz group is given for the representation which specifies the transformation of the wave function of a particle of zero mass and of arbitrary spin.

THE correspondence

$$\Psi(\mathbf{p},\ \sigma)\xrightarrow{S}\Psi'(\mathbf{p},\ \sigma)=\exp\{i\sigma\varphi(S,\ \mathbf{k})\}\Psi(S^{-1}\mathbf{p},\ \sigma),\quad(1)$$

where S is a transformation belonging to the Lorentz group, $\mathbf{p}$ transforms like the momentum vector of a particle of mass 0, $\mathbf{k}=\mathbf{p}/p$, σ is an integer or a half-integer, and $\varphi(S,\mathbf{k})$ is the angle defined by formula (1.9) in reference 1 (hereafter referred to as I) has, as can be easily seen, the group property.

It defines the transformation law for the wave function of a particle of mass zero, and with spin component σ along the direction of the momentum $\mathbf{p}$, under transformations of the proper Lorentz group.[2]

The object of the present paper is to give an expansion of this representation in terms of the irreducible (ρ, m)-representations (cf. I) of the proper Lorentz group.

1. INTEGRAL TRANSFORMATIONS FOR PARTICLES OF MASS 0

In a manner similar to the way this was done in I we obtain the following system of mutually inverse integral transformations

$$\Psi(\mathbf{p},\ \sigma)=\int d\rho\int d\Omega(\mathbf{n})\,Y_{\rho m\mathbf{n}}(\mathbf{p},\ \sigma)\,f_{\rho m\mathbf{n}},\quad(2)$$

$$f_{\rho m\mathbf{n}}=\sum_{\sigma}\int\frac{d^3\mathbf{p}}{|\mathbf{p}|}\,Y'_{\rho m\mathbf{n}}(\mathbf{p},\ \sigma)\,\Psi(\mathbf{p},\ \sigma),\quad(3)$$

where $f_{\rho m\mathbf{n}}$ transforms according to the irreducible representation (ρ, m) of the proper Lorentz group, and we obtain the following conditions for determining the functions Y and Y':

$$Y_{\rho m S^{-1}\mathbf{n}}(S^{-1}\mathbf{p},\ \sigma)=\exp\{im\varphi(S,\mathbf{n})-i\sigma\varphi(S,\mathbf{k})\}\,[K(\mathbf{n})/K(S^{-1}\mathbf{n})]^{-1-i\rho,2}\,Y_{\rho m\mathbf{n}}(\mathbf{p},\ \sigma),\quad(4)$$

where $K(\mathbf{n})$ is defined by formula (1.9), I. An analogous condition for $Y'_{\rho m\mathbf{n}}(\mathbf{p},\ \sigma)$ is satisfied if we take

$$Y'_{\rho m\mathbf{n}}(\mathbf{p},\ \sigma)=C_{m\rho}\overline{Y}_{\rho m\mathbf{n}}(\mathbf{p},\ \sigma).$$

Both here and later a bar above a letter denotes taking the complex conjugate.

We note that the function

$$Y_{\rho m\mathbf{n}}(\mathbf{p},\ \sigma)=(1/2\pi)\,\delta_{m\sigma}\delta(1-(\mathbf{nk}))\,p^{-1+i\rho/2}\quad(5)$$

satisfies expression (4).

Thus, from (2) — (5) we obtain

$$\Psi(\mathbf{p}\ \ m)=\int d\rho\int d\Omega(\mathbf{n})\,\delta(\mathbf{n}-\mathbf{k})\,p^{-1+i\rho/2}\,f_{\rho m\mathbf{n}},\quad(6)$$

$$f_{\rho m\mathbf{n}}=C_{\rho}\int\frac{d^3\mathbf{p}}{|\mathbf{p}|}\,\delta(\mathbf{n}-\mathbf{k})\,p^{-1-i\rho/2}\,\Psi(\mathbf{p},\ m).\quad(7)$$

Here we have taken into account the fact that $\delta[1-(\mathbf{nk})]=2\pi\delta(\mathbf{n}-\mathbf{k})$.

On substituting (7) into (6) we find that $C_\rho=1/4\pi$ while the integral over ρ in (6) should be taken from $-\infty$ to $+\infty$. Thus, the formulas

$$\Psi(\mathbf{p},\ m)=\int_{-\infty}^{+\infty}d\rho\int d\Omega(\mathbf{n})\,\delta(\mathbf{n}-\mathbf{k})\,p^{-1+i\rho/2}\,f_{\rho m\mathbf{n}},\quad(8)$$

$$f_{\rho m\mathbf{n}}=\frac{1}{4\pi}\int\frac{d^3\mathbf{p}}{|\mathbf{p}|}\,\delta(\mathbf{n}-\mathbf{k})\,p^{-1-i\rho/2}\,\Psi(\mathbf{p},\ m)\quad(9)$$

give a solution of the proposed problem; it turns out to be simpler than in the case of non-zero rest mass.*

2. COMPARISON OF THE RESULTS OBTAINED HERE WITH THOSE OF I

We compare the results obtained here with formulas (4.1), I and (4.2), I for $M=0$ (M is the particle mass). A direct transition to the limit $M\to 0$ in the formulas indicated above is impossible. Instead of this we shall carry out the following formal manipulation of those formulas: we

*In the case $m=0$ the same representation $(\rho, 0)$ is in fact contained twice in the result obtained, since the representations $(\rho, 0)$ and $(0, \rho)$ are equivalent. The transition between these two representations is given by formulas (14) and (15) with $m=0$.

carry out the transition to the limit $M \to 0$ in the factor $R(L_{\mathbf{p}}, \mathbf{n})$, we introduce a new variable of integration $\mathbf{p}/M$ (retaining for it the old notation $\mathbf{p}$) and we replace the factor $\sqrt{1+p^2} - \mathbf{p}\cdot\mathbf{n}$ by $p - \mathbf{p}\cdot\mathbf{n}$. If we now introduce the components of the wavefunction having a definite component of the spin along the direction of the momentum we shall obtain

$$\widetilde{\Psi}(\mathbf{p}, m) = \int_{-\infty}^{0} d\rho \int d\Omega(n) \times [p - \mathbf{pn}]^{-1+i\rho/2} e^{im\theta(\mathbf{p},\mathbf{n})} (-)^{s+m} \widetilde{\varphi}_{-\rho-m\mathbf{n}}, \quad (10)$$

$$\widetilde{\varphi}_{-\rho-m\mathbf{n}} = \frac{p^2 + (2m)^2}{(4\pi)^3} \int \frac{d^3\mathbf{p}}{|\mathbf{p}|} \times [p - \mathbf{pn}]^{-1-i\rho/2} e^{-im\theta(\mathbf{p},\mathbf{n})} (-)^{s+m} \widetilde{\Psi}(\mathbf{p}, m). \quad (11)$$

Here

$$\widetilde{\Psi}(\mathbf{p}, m) = \sum_{\sigma} D^{s}_{\sigma m}(\mathbf{k}) \widetilde{\Psi}'(\mathbf{p}, \sigma), \quad (12)$$

where $\widetilde{\Psi}'(\mathbf{p}, \sigma)$ is the wavefunction utilized in I; the notation $D^{s}_{\sigma m}(\mathbf{k})$ is also explained there. In the derivation of formulas (10) and (11) the following equation was used:

$$[D^{s}(\mathbf{k})^{-1} D^{s}(L_{\mathbf{p}}\mathbf{n}) D^{s}(\mathbf{n})]_{mn} \xrightarrow[M\to 0]{} \delta_{m,-n} (-1)^{s+m} e^{im\theta(\mathbf{p},\mathbf{n})}, \quad (13)$$

where $\theta(\mathbf{p}, \mathbf{n})$ is defined in Appendix B.

We shall compare the expressions (8) and (9), obtained above with (10) and (11).* From the function $f_{\rho m\mathbf{n}}$ which transforms according to the (ρ, m) representation we go over to the function $\varphi_{-\rho-m\mathbf{n}}$, which transforms according to the $(-\rho, -m)$ representation. We make use of the fact that the representations (ρ, m) and $(-\rho, -m)$ are equivalent. Therefore the function $\varphi_{-\rho,-m,\mathbf{n}}$ may be obtained from the function $f_{\rho m\mathbf{n}}$ by the following unitary transformation:

$$\varphi_{-\rho,-m,\mathbf{n}} = \int U_{\rho m}(\mathbf{n}, \mathbf{k}) f_{\rho m\mathbf{k}} d\Omega(\mathbf{k}), \quad (14)$$

$$f_{\rho m\mathbf{k}} = \int \overline{U}_{\rho m}(\mathbf{n}, \mathbf{k}) \varphi_{-\rho,-m,\mathbf{n}} d\Omega(\mathbf{n}), \quad (15)$$

where

$$U_{\rho m}(\mathbf{n}, \mathbf{k}) = \sum_{l \geqslant |m|} \sum_{\alpha=-l}^{l} \frac{2l+1}{4\pi} \times \frac{\Gamma(l+1+i\rho/2)}{\Gamma(l+1-i\rho/2)} \overline{D}^{l}_{\alpha,-m}(\mathbf{n}) D^{l}_{\alpha m}(\mathbf{k}). \quad (16)$$

*It is proved later that (10) and (11) are not equivalent to (8) and (9) (and are therefore incorrect). We emphasize that this by no means indicates that the results of the present paper contradict those of I; it merely means that the formal manipulation which leads to (10) and (11) is not justified.

The function U is discussed in Appendix A and satisfies the following unitarity condition:*

$$\int \overline{U}_{\rho m}(\mathbf{l}, \mathbf{n}) U_{\rho m}(\mathbf{l}, \mathbf{k}) d\Omega(\mathbf{l}) = \delta(\mathbf{n} - \mathbf{k}). \quad (17)$$

On substituting (14) and (15) into (8) and (9) we obtain

$$\varphi_{-\rho,-m,\mathbf{n}} = \frac{1}{4\pi} \int \frac{d^3\mathbf{p}}{|\mathbf{p}|} p^{-1-i\rho/2} U_{\rho m}(\mathbf{n}, \mathbf{k}) \Psi(\mathbf{p}, m), \quad (18)$$

$$\Psi(\mathbf{p}, m) = \int_{-\infty}^{\infty} d\rho \int d\Omega(\mathbf{n}) \overline{U}_{\rho m}(\mathbf{n}, \mathbf{k}) p^{-1-i\rho/2} \varphi_{-\rho,-m,\mathbf{n}}. \quad (19)$$

We substitute into (18) and (19) the following formula derived in Appendix A:

$$U_{\rho m}(\mathbf{n}, \mathbf{k}) = A_{\rho m} [1 - (\mathbf{nk})]^{-1-i\rho/2} Q_m(\mathbf{n}, \mathbf{k}), \quad (20)$$

where

$$A_{\rho m} = 2^{1+i\rho/2} \Gamma(m + 1 + i\rho/2) / 4\pi\Gamma(m - i\rho/2), \quad (21)$$

$$Q_m(\mathbf{n}, \mathbf{k}) = m \sum_{l \geqslant |m|} \sum_{\alpha=-l}^{l} \frac{2l+1}{l(l+1)} \overline{D}^{l}_{\alpha,-m}(\mathbf{n}) D^{l}_{\alpha m}(\mathbf{k}). \quad (22)$$

We then obtain

$$\varphi_{-\rho,-m,\mathbf{n}} = \frac{1}{4\pi} \int \frac{d^3\mathbf{p}}{|\mathbf{p}|} p^{-1-i\rho/2} A_{\rho m} \times [1 - (\mathbf{nk})]^{-1-i\rho/2} Q_m(\mathbf{n}, \mathbf{k}) \Psi(\mathbf{p}, m), \quad (23)$$

$$\Psi(\mathbf{p}, m) = \int_{-\infty}^{\infty} d\rho \int d\Omega(\mathbf{n}) p^{-1+i\rho/2} \overline{A}_{\rho m} \times [1 - (\mathbf{nk})]^{-1+i\rho/2} \overline{Q}_m(\mathbf{n}, \mathbf{k}) \varphi_{-\rho,-m,\cdot}. \quad (24)$$

Since

$$|A_{\rho m}|^2 = \frac{1}{(4\pi)^2} (\rho^2 + 4m^2)$$

and

$$Q_m(\mathbf{n}, \mathbf{k}) = e^{-im\theta(\mathbf{n},\mathbf{k})} (-1)^{s+m} \quad (25)$$

(cf. Appendix C), (23) and (24) differ from (10) and (11) only in that the integral over ρ in (23) and (24) is taken between the limits from $-\infty$ to ∞.

In particular, for $m = 0$ each irreducible representation $(\rho, 0)$ occurs twice in the expansion under consideration in contrast to the case $M \neq 0$.

APPENDIX A

DEFINITION OF THE FUNCTION $U_{\rho m}(\mathbf{n}, \mathbf{k})$

It may be easily shown that from the fundamental relations (14), (15) and the transformation law for $f_{\rho m\mathbf{k}}$ and $\varphi_{-\rho,-m,\mathbf{n}}$ the following functional equation for $U_{\rho m}(\mathbf{n}, \mathbf{k})$ may be obtained:

*In particular, for $m = 0$ we obtain the following simple integral representation for the δ-function:

$$\frac{p^2}{(4\pi)^2} \int [1 - (\mathbf{ln})]^{-1+i\rho/2} [1 - (\mathbf{lk})]^{-1-i\rho/2} d\Omega(\mathbf{l}) = \delta(\mathbf{n} - \mathbf{k})$$

[cf. also formulas (A.4) and (A.6)].

$$U_{\rho m}(S^{-1}\mathbf{n}, S^{-1}\mathbf{k}) = U_{\rho m}(\mathbf{n},\mathbf{k})[K(\mathbf{n})K(\mathbf{k})/K(S^{-1}\mathbf{n})K(S^{-1}\mathbf{k})]^{-1-i\rho/2} \times \exp\{im[\varphi(S,\mathbf{n})+\varphi(S,\mathbf{k})]\} \quad (A.1)$$

(the notations $K(\mathbf{n})/K(S^{-1}\mathbf{n})$ and $\varphi(S,\mathbf{n})$ are defined in I). Since the functions $D^{l}_{\alpha m}(\mathbf{k})$ for $l = |m|, |m|+1, \ldots$ and for fixed m form a complete system, U may be represented in the following form

$$U_{\rho m}(\mathbf{n},\mathbf{k}) = \sum_{l\alpha}\sum_{l'\beta} X_{l\alpha l'\beta}\,\overline{D}^{l}_{\alpha,-m}(\mathbf{n})\,D^{l'}_{\beta m}(\mathbf{k}). \quad (A.2)$$

On taking in formula (A.1) for S the pure rotation $S = R$ we obtain on taking into account formula (1.9b), I,

$$X_{l\alpha l'\beta} = X_l \delta_{ll'}\delta_{\alpha\beta}.$$

Further, we take in (A.1) for S the infinitesimal pure Lorentz transformation L:

$$L^{-1}\mathbf{n} = (\mathbf{n}+\boldsymbol{\varphi})/[1+(\mathbf{n}\boldsymbol{\varphi})].$$

It can then be easily seen that

$$K(L^{-1}\mathbf{n})/K(\mathbf{n}) = 1+(\boldsymbol{\varphi}\mathbf{n}).$$

Since according to (1.9d), I

$$e^{im\varphi(L,\mathbf{k})}D^{l}_{\beta m}(L^{-1}\mathbf{k}) = \sum_{\gamma} D^{l}_{\beta\gamma}(R(L,\mathbf{k}))\,D^{l}_{\gamma m}(\mathbf{k})$$

we obtain from (A.1) and (A.2)

$$\sum X_l \overline{D}^{l}_{\sigma -m}(\mathbf{n})\,D^{l}_{\alpha m}(\mathbf{k}) = [K(\mathbf{n})K(\mathbf{k})/K(L^{-1}\mathbf{n})K(L^{-1}\mathbf{k})]^{1+i\rho/2} \times \sum X_l \overline{D}^{l}_{\alpha\gamma}(R(L,\mathbf{n}))\,\overline{D}^{l}_{\gamma -m}(\mathbf{n})\,D^{l}_{\alpha\delta}(R(L,\mathbf{k}))\,D^{l}_{\delta m}(\mathbf{k}). \quad (A.3)$$

The parameter of the rotation R occurring in the above is defined by formula (A.4), I:

$$D^{l}(R(L,\mathbf{k})) = e^{-i(\mathbf{H}\boldsymbol{\alpha})} \approx 1 - i(\mathbf{H}\boldsymbol{\alpha}), \qquad \boldsymbol{\alpha} = [\mathbf{k}\times\boldsymbol{\varphi}].$$

We then obtain from formula (A.3)

$$\sum X_l \overline{D}^{l}_{\alpha,-m}(\mathbf{n})\,D^{l}_{\alpha m}(\mathbf{k}) = [1-(1+i\rho/2)\boldsymbol{\varphi}(\mathbf{n}+\mathbf{k})] \times \sum X_l \overline{\{[1-i(\mathbf{H}^{l}[\mathbf{n}\times\boldsymbol{\varphi}])]\,D^{l}(\mathbf{n})\}}_{\alpha,-m} \times \{[1-i(\mathbf{H}^{l}[\mathbf{k}\times\boldsymbol{\varphi}])]\,D^{l}(\mathbf{k})\}_{\alpha,m}.$$

Here we must express the cyclic components of the vectors $\mathbf{n}$ and $\mathbf{k}$ in terms of the generalized spherical harmonics $D^{1}_{\alpha 0}(\mathbf{n})$, $D^{1}_{\alpha 0}(\mathbf{k})$, and we must then eliminate products of the D-functions in accordance with the following rule

$$D^{1}_{ab}(\mathbf{n})\,D^{l}_{cd}(\mathbf{n}) = \langle 1lac\,|\,LM\rangle\langle 1l\,bd\,|\,LN\rangle\,D^{L}_{MN}(\mathbf{n}).$$

By equating to zero the coefficient of φ we obtain (in the intermediate steps of the calculation we make use of Racah's rule for combining three Clebsch-Gordan coefficients into one):

$$X_l[l(l+1)-l'(l'+1)-i\rho] + (-)^{l-l'+1}X_{l'}[l'(l'+1) - l(l+1)-i\rho](2l+1)/(2l'+1) = 0.$$

From this it follows that

$$X_l = C(2l+1)\Gamma(l+1+i\rho/2)/\Gamma(l+1-i\rho/2).$$

On utilizing the unitarity condition (17) already mentioned in the main text we obtain, finally, formula (16).

In order to obtain formula (20) we note that the function

$$Q_{\rho m}(\mathbf{n},\mathbf{k}) \equiv [1-(\mathbf{nk})]^{1+i\rho/2}\,U_{\rho m}(\mathbf{n},\mathbf{k}) \quad (A.4)$$

satisfies the same functional equation (A.1) which is satisfied also by $U_{\rho m}(\mathbf{n},\mathbf{k})$, only we must set in it $1+i\rho/2 = 0$. From this it follows that

$$Q_{\rho m}(\mathbf{n},\mathbf{k}) = A_{\rho m}\sum_{l\geqslant|m|}\frac{2l+1}{l(l+1)}\,\overline{D}^{l}_{\alpha -m}(\mathbf{n})\,D^{l}_{\alpha m}(\mathbf{k}).$$

In order to find A_ρ, we set $\mathbf{k} = -\mathbf{n}$ in (A.4).

Since

$$D^{l}(\mathbf{n}) = R_3(\varphi+\pi/2)\,R_1(\theta),$$

$$D^{l}(-\mathbf{n}) = R_3(\varphi+3\pi/2)\,R_1(\pi-\theta),$$

then

$$[D^{l}(\mathbf{n})^{-1}D^{l}(-\mathbf{n})]_{-m,m} = [R_1(-\theta)\,R_3(\pi)\,R_1(\pi-\theta)]^{l}_{-m,m} = [R_1(-\pi)\,R_3(\pi)]^{l}_{-m,m} = e^{-im\pi}(-1)^{2l}(-1)^{l+m}e^{-im\pi}.$$

Since

$$\sum_{l\geqslant|m|}\frac{2l+1}{l(l+1)}(-1)^{l+m} = \sum_{l\geqslant|m|}\left(\frac{1}{l+1}(-1)^{l+m}+\frac{1}{l}(-1)^{l+m}\right) = (-1)^{2m}\frac{1}{m}$$

and, moreover,

$$\sum_{l\geqslant|m|}(-1)^{l+m}(2l+1)\Gamma(l+1+i\rho/2)/\Gamma(l+1-i\rho/2) = \sum_{l\geqslant m}(-1)^{l+m}\left[\frac{\Gamma(l+2+i\rho/2)}{\Gamma(l+1-i\rho/2)}+\frac{\Gamma(l+1+i\rho/2)}{\Gamma(l-i\rho/2)}\right] = (-1)^{2m}\Gamma(m+1+i\rho/2)/\Gamma(m-i\rho/2),$$

the proof of formula (20) is complete.

APPENDIX B

PROOF OF FORMULA (13)

According to formula (1.9b), I,

$$D^{S}(L_{\mathrm{p}}\mathbf{n})\,D^{S}(\mathbf{n}) = D^{S}(L_{\mathrm{p}}^{-1}\mathbf{n})\,R_3(\varphi(L_{\mathrm{p}},\mathbf{n})).$$

Further, from formula (A.2) of Appendix A in I it may be easily seen that

$$L_{\mathrm{p}}^{-1}\mathbf{n} \xrightarrow[M\to 0]{} -\mathbf{k}.$$

Finally, we have,

$$[R(\mathbf{k})]^{-1} R(-\mathbf{k})$$

$$= R_1(-\vartheta) R_3(-\varphi - \pi/2) R_3(\varphi - \pi + \pi/2) R_1(\pi - \vartheta)$$

$$= R_3(-\pi) R_1(\pi),$$

$$[D^S(\mathbf{k})^{-1} D^S(-\mathbf{k})]_{mn} = [R_3(-\pi) R_1(\pi)]^S_{mn} = \delta_{n-m}(-1)^{S+m}.$$

Therefore,

$$\vartheta(\mathbf{p}, \mathbf{n}) = \lim_{M \to 0} \varphi(L_{\mathbf{p}}, \mathbf{n}). \qquad \text{(B.1)}$$

$$S^{-1}\mathbf{k} \to \mathbf{k}, \quad S^{-1}\mathbf{n} \to -\mathbf{k},$$

$$Q_m(S^{-1}\mathbf{n}, S^{-1}\mathbf{k}) \to Q_m(-\mathbf{k}, \mathbf{k}) = (-1)^{S+M}.$$

Thus from (A.5) and (B.1) we obtain formula (25).

APPENDIX C

PROOF OF FORMULA (25)

In formula (A.1) we set $1 + i\rho/2 = 0$, $S = L\mathbf{p}$, with $\varphi(S, \mathbf{k}) = 0$. Further, we let M tend to zero; we then have

Translated by G. Volkoff
21

[1] Chou Kuang-Chao and L. G. Zastavenko, JETP **35**, 1417 (1958), Soviet Phys. JETP **8**, 990 (1959).

[2] Chou Kuang-Chao, JETP **36**, 909 (1959), Soviet Phys. JETP **9**, 642 (1960).

SPACE AND TIME REFLECTIONS IN RELATIVISTIC THEORY

Yu. M. SHIROKOV

Nuclear Physics Institute, Moscow State University

Submitted to JETP editor June 10, 1959

J. Exptl. Theoret. Phys. (U.S.S.R.) **38**, 140-150 (January, 1960)

A complete classification has been obtained for the representations of the inhomogeneous Lorentz group, including space reflections and time reflections of the Wigner type. The question of the values of the squares of the various reflection operations for particles of half-integral spin is investigated in detail. The results are compared with those which are obtained when additional requirements are imposed on the theory, in particular the requirement of locality of the field operators. It is shown that, in addition to mass, spin and parity, elementary particles have still another purely geometrical characteristic, which might be called the symmetry type. The question of the symmetry type for real particles is discussed.

1. INTRODUCTION

THE purpose of this paper is to obtain all possible laws of transformation of wave functions (state vectors) under space and time reflections, which are permitted by the requirements of relativistic invariance, without making use of the property of locality of the field operators. The following postulates are taken as the starting point.

A. Relativistic invariance. The mathematical formulation of this requirement is that[1] the theory must contain operators $M_{\mu\nu}$, p_λ, satisfying the commutation relations

$$[M_{\mu\nu},\ M_{\lambda\sigma}] = i(\delta_{\mu\sigma}M_{\lambda\nu} + \delta_{\mu\lambda}M_{\nu\sigma} + \delta_{\nu\sigma}M_{\mu\lambda} + \delta_{\lambda\nu}M_{\sigma\mu}),$$

$$[M_{\mu\nu},\ p_\lambda] = i(p_\nu\delta_{\mu\lambda} - p_\mu\delta_{\nu\lambda}),\quad [p_\mu,\ p_\nu] = 0 \tag{1}$$

B. The Wigner formulation of the law of time reflection[2] is assumed. According to this formulation, to the operation $t = -t'$ there corresponds the state vector transformation

$$t = -t',\ \Psi = I_t K\Psi', \tag{2}$$

where I_t is a certain linear operator and K is the nonlinear operation of charge conjugation

$$K\Psi' = \Psi'^*. \tag{3}$$

The Schwinger rule for transposition[3] is obtained by substituting (3) into (2). The formulation within the framework of the conventional theory of representations was given earlier.[4]

C. The reflection operations are not assigned explicitly, but are determined from their geometrical properties. Thus the inversion I_s is defined as the operator that transforms the state vector when we reflect the space coordinates

$$\mathbf{x} = -\mathbf{x}',\ \Psi = I_s\Psi'. \tag{4}$$

The time reflection operator was defined in reference 2. It is convenient to introduce still another operator $I_{st}K$, corresponding to the reflection of all four axes:

$$x_\mu = -x'_\mu,\quad \Psi = I_{st}K\Psi'. \tag{5}$$

It is obvious that

$$I_sI_t = I_{st}. \tag{6}$$

Figuratively speaking, the inversion is defined as the operator that relates the state vector to the vector for the state of the same physical system as observed in a mirror.

From these definitions and the fact that the sequences of coordinate transformations

$$x_\mu = x'_\mu + \xi_\mu + \varepsilon_{\mu\nu}x'_\nu,$$
$$x'_\mu = -x''_\mu,\quad x_\mu = -x'''_\mu,\quad x'''_\mu = x''_\mu - \xi_\mu + \varepsilon_{\mu\nu}x''_\nu \tag{7}$$

lead to the same final system, we obtain the commutation relations for the operator I_{st}:

$$p_\mu I_{st} - I_{st}p^*_\mu = 0, \tag{8}$$

$$M_{\mu\nu}I_{st} + I_{st}M^*_{\mu\nu} = 0. \tag{9}$$

The asterisk denotes complex (and not Hermitian) conjugation.* Similarly, we get for I_s the relations

$$[I_s,\ \mathbf{M}] = 0,\ [I_s,\ p_0] = 0,$$
$$I_s\mathbf{p} + \mathbf{p}I_s = 0,\ I_s\mathbf{N} + \mathbf{N}I_s = 0, \tag{10}$$

*The operation of complex conjugation does not affect the imaginary unit in the fourth components of vectors and tensors, so that, for example, $p_4^* = ip_0^*$. This point is not essential, since the use of contravariant vectors with the usual definition of conjugation leads to the same results.

where $N_j = -iM_{j4}$. Each of the reflection operations defined by Eqs. (2) — (5) may or may not contain the charge conjugation. On the other hand, according to (8) and (10), all these operations must be conserved for all interactions.

D. For particles with integral spin, the squares of all reflections are equal to unity. For particles with half-integral spin, the square of each of the reflections I_S, I_tK, $I_{st}K$ may be either plus or minus unity, but they must have the same values for all the half-integral spin particles. In other words, the values of squares of the reflection operators determine the properties of space-time, and not the properties of individual particles. Therefore particles with different values for the square of one of the reflections cannot exist simultaneously,[5] since this would lead to the existence of systems with integer angular momentum and a negative value for the square of the reflection.

As was shown earlier,[4,6] these considerations can be given a geometrical interpretation if we extend the rotation group by adjoining an element $I_{2\pi}$ for the rotation through angle 2π about an arbitrary axis. (Such an extension occurs naturally in treating the topological properties of the parameter space of the rotation group.) Then the square of each of the reflections may be equal to either the identity operator I or to the rotation through 2π, which leads to the following eight groups $G_1 - G_8$:

	G_1	G_2	G_3	G_4	G_5	G_6	G_7	G_8
I_s^2	I	I	$I_{2\pi}$	$I_{2\pi}$	$I_{2\pi}$	$I_{2\pi}$	I	I
$(I_tK)^2 = I_tI_t^*$	I	$I_{2\pi}$	I	$I_{2\pi}$	$I_{2\pi}$	I	$I_{2\pi}$	I
$(I_{st}K)^2 = I_{st}I_{st}^*$	I	$I_{2\pi}$	$I_{2\pi}$	I	$I_{2\pi}$	I	I	$I_{2\pi}$

(11)

Table (11) holds for both integer ($I_{2\pi} = 1$) and half-integral ($I_{2\pi} = -1$) spins. Real space-time transforms according to one of these eight groups, and this fixes once and for all the values of the squares of the reflections for all particles. Thus there exist eight nonequivalent space-time structures. Later we shall show that the difference between these structures is accessible to experimental test.

E. No assumptions whatsoever are made concerning the locality of the field operators, or, in general, concerning the form of the equations of motion. These initial assumptions differ in some ways from those usually made in investigations of this kind (cf., for example, the surveys by Wick and Solov'ev,[7] which give references to the main papers).

The adoption of postulates A and E leads to a great generality and enables us to obtain a number of reflection transformations which satisfy the requirements of relativistic invariance but which do not reduce to local transformations of the Dirac field operators. Postulate C is essentially not new, but it rather restores to the reflection operators their original geometrical meaning. However this point does involve a change in the basic point of view of the investigation of the reflection operations. Usually (cf., for example, reference 7), certain operators (P, CP, T, CT, etc) are defined to act on the field operators, and one investigates the conservation of these operators. Here we impose the requirement that there exist conserved operators I_S, I_t, I_{st}, which correspond to definite coordinate transformations and which satisfy relations (6), (8) — (10), and one of the columns of (11). (Failure to satisfy this requirement is tantamount to denying the Euclidean nature of space-time.) Our problem is to find the explicit form of these operators. The requirements of postulate D are not new (though they contain a somewhat unusual geometrical interpretation), but they are investigated in detail here for the first time. These requirements impose quite rigid limitations (which are different for each of the eight groups) on the possible form of the reflection operators.

2. PARTICLES WITH NONZERO REST MASS

The apparatus of field theory is not suited for investigations which are not based on locality of the theory. We shall therefore make use of the mathematical technique which was used earlier[8] for obtaining the explicit form of the representations of the inhomogeneous Lorentz group. (These representations were first obtained by Wigner.[9]) According to reference 8, the state vector of a free relativistic particle, with mass κ and spin s, can always be brought to the form

$$\Psi^{\kappa s\alpha}_{m_s}(\mathbf{p}), \tag{12}$$

where the kinematical variables are the three-dimensional momentum $\mathbf{p}$ and the spin projection m_S. In addition to mass and spin, the particle may possess other variables (such as charge) which are invariant under four-dimensional rotations and translations; we denote these by the index α. Relativistic invariance is assured by the fact that, for

the state vector (12), we can define[8] operators $M_{\mu\nu}$, $p\lambda$ which satisfy Eqs. (1):

$$\hat{\mathbf{p}} = \mathbf{p}, \quad p_0 = e_p \equiv \sqrt{p^2 + \varkappa^2}, \quad \mathbf{M} = -i\left[\mathbf{p} \times \frac{\partial}{\partial \mathbf{p}}\right] - \mathbf{S},$$

$$\mathbf{N} = ie_p \frac{\partial}{\partial \mathbf{p}} - \frac{[\mathbf{S}\times\mathbf{p}]}{e_p + \varkappa}; \tag{13}$$

$$[S_1, S_2] = iS_3, \ldots, \quad \mathbf{S}^2 = s(s+1). \tag{14}$$

The completeness of the argument is guaranteed by the fact that, to a given pair of values of mass and spin, there corresponds a single irreducible representation of the inhomogeneous Lorentz group, which can always be reduced to the form (13).

For the state vector (12), we must now find operators I_s, I_t, I_{st}, which satisfy (6), (8) – (10), and one of the columns of (11). Let us represent these operators in the form

$$I_s = \lambda_s P, \quad I_t = \lambda_t T, \quad I_{st} = \lambda_{st} PT, \tag{15}$$

where P is an operator which acts only on the variable p and changes the sign of the momentum:

$$P\Psi^{\varkappa s\alpha}_{m_s}(\mathbf{p}) = i^{2s}\Psi^{\varkappa s\alpha}_{m_s}(-\mathbf{p}), \tag{16}$$

while T is an operator which acts on p and m_s (but not on α), and changes the sign of the momentum and the spin projection:

$$T\Psi^{\varkappa s\alpha}_{m_s}(\mathbf{p}) = (-1)^{s-m_s}\Psi^{\varkappa s\alpha}_{-m_s}(-\mathbf{p}). \tag{17}$$

From (16), (17) it follows that

$$P^{-1}\mathbf{p}P = -\mathbf{p}, \quad P^{-1}\mathbf{S}P = \mathbf{S}, \tag{18}$$

$$T^{-1}\mathbf{p}T = -\mathbf{p}, \quad T^{-1}\mathbf{S}T = -\mathbf{S}^* \tag{19}$$

$$P^2 = I_{2\pi}, \quad TT^* = I_{2\pi} = \begin{cases} 1 & \text{(integer spin)} \\ -1 & \text{(half-integer spin)} \end{cases} \tag{20}$$

The operations P and T defined by (16) and (17) are the natural generalization, to the case of arbitrary spin, of the corresponding quantities which are used in the theory of spinor fields. Substituting (13) and (15) in (6), (8) – (10), we obtain, using (18) and (19):

$$\lambda_s\lambda_t = \lambda_{st}; \tag{21}$$

$$[\lambda_s, p_\mu] = 0, \quad [\lambda_s, M_{\mu\nu}] = 0,$$

$$[\lambda_{st}, p_\mu] = 0, \quad [\lambda_{st}, M_{\mu\nu}] = 0. \tag{22}$$

According to (22), the operators λ_s, λ_t, and λ_{st} do not act on the kinematic variables p and m_s; i.e., they are either numbers, or they are matrices with respect to the invariant variable α. According to (11) and (20), for single-valued representations,

$$\lambda_s^2 = 1, \quad \lambda_t\lambda_t^* = 1, \quad \lambda_{st}\lambda_{st}^* = 1 \text{ (integer spin)} \tag{23}$$

and all the factors λ may be numbers. To each value of mass and spin, there correspond two equivalent representations which differ in parity:

$$\lambda_s = 1, \ \lambda_t = 1; \ \lambda_s = -1, \ \lambda_t = 1 \text{ (integer spin)}. \tag{24}$$

(Representations which differ by a phase factor in λ_t are not different, since according to (2) and (3) this factor can be eliminated by multiplying the state vector by an appropriate phase factor.) To obtain the two-valued representations, we must substitute (15) and (20) in (11), and set $I_{2\pi} = -1$. The result is

	G_1	G_2	G_3	G_4	G_5	G_6	G_7	G_8
λ_s^2	−1	−1	1	1	1	1	−1	−1
$\lambda_t\lambda_t^*$	−1	1	−1	1	1	−1	1	−1
$\lambda_{st}\lambda_{st}^*$	−1	1	1	−1	1	−1	−1	1

(25)

If λ_t (or λ_{st}) is a number, the quantity $\lambda_t\lambda_t^*$ (or $\lambda_{st}\lambda_{st}^*$) must necessarily be positive. The factors λ may therefore be numbers only in groups G_2 and G_5. In the other six groups these factors must be two-by-two matrices acting on an additional independent variable, so that the dimensionality of the irreducible representation is double that of the corresponding proper group. One can verify directly that relations (21) and (25) are satisfied by the following sets of factors:

	G_1		G_2		G_3	G_4	G_5		G_6		G_7	G_8
s	i	$-i$	i	$-i$	ρ_1	ρ_1	1	−1	1	−1	$i\rho_1$	$i\rho_1$
λ_t	ρ_2	ρ_2	1	1	ρ_2	ρ_3	1	1	ρ_2	ρ_2	ρ_3	ρ_2
λ_{st}	$i\rho_2$	$-i\rho_2$	i	$-i$	$i\rho_3$	$-i\rho_2$	1	−1	ρ_2	$-\rho_2$	ρ_2	$-\rho_3$

26)

The matrices ρ_1, ρ_2, ρ_3 in (26) have the form of the corresponding Pauli matrices, and act on an additional (charge-type) variable of the state vector. The matrices ρ_1, ρ_2 correspond to an operation of the type of charge conjugation. Because of the presence of the operation of complex conjugation in (2) and (5), the matrices ρ_1 and ρ_2 cannot be transformed into one another by an equivalence transformation if they enter into λ_t or λ_{st}. Table (26) exhausts the irreducible representations for each of the groups $G_1 - G_8$ for the case of half-integral spin.

3. PARTICLES WITH ZERO REST MASS

For zero rest mass, for each value s of the absolute value of the spin, there are two irreducible representations of the proper group, which are one-dimensional in the spin variables, and which differ in the sign of the projection of the spin onto the momentum[9] (spirality). A change in the sign of the momentum changes the sign of the spirality, so that the representations of the group including space reflections must be two-rowed in the spin-like variable for the sign of the spirality. The operators p_μ, $M_{\mu\nu}$ for these representations can be written in the form

$$\hat{p} = p, \quad p_0 = |p|;$$

$$M_1 = -i\left(p_2\frac{\partial}{\partial p_3} - p_3\frac{\partial}{\partial p_2}\right) + s\sigma_3\frac{\cos\varphi}{\sin\vartheta},$$

$$\times M_2 = -i\left(p_3\frac{\partial}{\partial p_1} - p_1\frac{\partial}{\partial p_3}\right) + s\sigma_3\frac{\sin\varphi}{\sin\vartheta},$$

$$M_3 = -i\left(p_1\frac{\partial}{\partial p_2} - p_2\frac{\partial}{\partial p_1}\right);$$

$$N_1 = ip\frac{\partial}{\partial p_1} - s\sigma_3\sin\varphi\cot\vartheta,$$

$$N_2 = ip\frac{\partial}{\partial p_2} + s\sigma_3\cos\varphi\cot\vartheta, \quad N_3 = ip\frac{\partial}{\partial p_3}. \tag{27}$$

Here σ_3 is the Pauli matrix which acts on the variable for the sign of the spirality, and φ, ϑ are the polar angles of the momentum vector.

For integer spin, the operators I_s, I_t, and I_{st} satisfying (6) and (8) — (11) are equal to

$$I_s = \sigma_1 P, \quad I_t = P, \quad I_{st} = \sigma_1 \text{ (integer spin)}. \tag{28}$$

For each absolute value of the spin there is just one irreducible representation.

For half-integral spin, we look for operators I_s, I_t, I_{st} of the form

$$I_s = \lambda_s' P', \quad I_t = \lambda_t' P', \quad I_{st} = \lambda_{st}'. \tag{29}$$

The operation P′ acts on the wave function in the same way as P, i.e., it changes the sign of the momentum, and its square is also equal to -1:

$$P'\Psi(p) = \Psi(-p), \quad (P')^2 = -1, \tag{30}$$

since the eigenfunctions of the operators (27) contain a factor $\exp(\pm i\varphi/2)$, which is multiplied by i when φ is replaced by $\varphi + \pi$. Substituting (29) in (6) and (8) — (10), we find

$$\lambda_s'\lambda_t' = \lambda_{st}', \tag{31}$$

$$\lambda_s'\sigma_3 + \sigma_3\lambda_s' = 0, \tag{32}$$

$$\lambda_t'\sigma_3 - \sigma_3\lambda_t' = 0, \tag{33}$$

$$\lambda_{st}'\sigma_3 + \sigma_3\lambda_{st}' = 0. \tag{34}$$

Relations (32) — (34) express the fact that the projection of the spin along the momentum does not change sign under time reflection, and changes sign under inversion.

Substituting (29) in (11) and using (30), we obtain for the values of the squares of the λ′'s, the table

	G_1	G_2	G_3	G_4	G_5	G_6	G_7	G_8
$(\lambda_s')^2$	−1	−1	1	1	1	1	−1	−1
$\lambda_t'\lambda_t'^*$	−1	1	−1	1	1	−1	1	−1
$\lambda_{st}'\lambda_{st}'^*$	1	−1	−1	1	−1	1	1	−1

(35)

According to (33), the factor λ_t' for the spin variable is either equal to unity or proportional to σ_3. Therefore, in the groups G_1, G_3, G_6 and G_8, where the quantities $\lambda_t'\lambda_t'^*$ are negative, we must introduce an additional discrete variable, so that the representation becomes four-rowed. This doubling is not necessary in the other groups. Relations (31) — (35) are satisfied by the following sets of factors λ′, which exhaust the irreducible representations for the state vectors of particles with zero rest mass and half-integral spin:

	G_1	G_2	G_3	G_4	G_5	G_6	G_7	G_8
λ_s'	$i\sigma_1\rho_3$	$i\sigma_1$	σ_1	σ_1	σ_1	$\sigma_1\rho_3$	$i\sigma_1$	$i\sigma_1$
λ_t'	ρ_2	σ_3	ρ_2	1	σ_3	ρ_2	1	ρ_2
λ_{st}'	$\rho_1\sigma_1$	σ_2	$\sigma_1\rho_2$	σ_1	$-i\sigma_2$	$-i\rho_1\sigma_1$	$i\sigma_1$	$i\sigma_1\rho_2$

(36)

4. SYMMETRY TYPES OF ELEMENTARY PARTICLES

In addition to mass, spin, and parity, elementary particles possess another purely geometric characteristic, which we may call the symmetry

type of the particle. The concept of symmetry type is based on the macroscopically obvious fact that, under each of the reflections $\mathbf{x} \to -\mathbf{x}$, $t \to -t$, $x_\mu \to -x_\mu$, the particle can either go over into itself (symmetry), or into another (anti-particle type) state with the same mass and spin (asymmetry). In the latter case, the transformation of the state vector which is associated with the corresponding reflection must contain an operation C of the type of charge conjugation.

For nonzero rest mass, five types of symmetry are possible:

1. Complete Symmetry. The particle is transformed into itself under all reflections. In this case the operations P (change in signs of momenta) and T (change in signs of momenta and spins) are conserved.

2. T-symmetry. The particle transforms into the antiparticle under space reflections, and is unchanged by time reflection. PC and T are conserved, while P and PT are not. The macroscopic analog of this type of symmetry is the symmetry of a rotating screw-nut.

3. P-symmetry. The particle is unchanged by inversion and changes into the antiparticle under time reflection. P and CT are conserved, while T and PT are not. The macroscopic analog is a rotating weather-vane.

4. PT-symmetry. The particle changes to the antiparticle under inversion, and does not change under reversal of all four coordinates. PC, CT, and PT are conserved, while P, T, and PCT are not. This case contradicts the PCT-theorem, i.e., it is not possible in a local theory. The macroscopic analog is a rotating conical cogwheel.

5. Complete asymmetry. The particle does not change into itself under any of the reflections, i.e., the particle has four different states with the same mass and spin. In this case there are two independent operators C_1 and C_2 of the type of charge conjugation. PC_1, C_2T, and PC_3T (where $C_3 = C_1C_2$) are conserved.

For zero rest mass, we associate with a state of the particle a definite projection of the spin along the momentum, which is invariant with respect to proper transformations but which changes sign under inversion. Thus, for zero mass (and nonzero spin) only T-symmetry (type 2) and complete asymmetry (type 5) are possible.

In some cases (for example, for photons) the operation C does not change the sign of any charge. For this reason we have been careful to call it an operation of the type of charge conjugation.

There are different restrictions on the S-matrix for the various symmetry types. Thus, in cases 3 and 4, the S-matrix is not symmetric, as is usual, but is related to its transposed matrix S^T by $S^T = C^{-1}SC$. The considerations presented here can be presented somewhat differently, by discussing the transformation properties of the physical quantities characterizing the particle. From group-theoretical considerations it follows that the state of a free particle is described by its mass, spin, momentum, spin projection, as well as by other possible variables which must necessarily be invariant under proper transformations.[8] However, these additional variables may be either scalar or pseudoscalar with respect to reflections. If all the additional variables are scalar, the particle belongs to the first type (complete symmetry). If the additional variable is a pseudoscalar with respect to inversion and a scalar with respect to time reflection (for example, the projection of the spin along the momentum in the case of zero mass), the particle has T-symmetry, etc. Thus the investigation of symmetry types of particles is equivalent to the investigation of the behavior under reflections of the quantities characterizing the particle, such as the different charges.

5. THE DIRAC EQUATION

If we impose on the theory the requirement of locality of the field operators, there is an essential change in the final results, which can be followed on the example of the Dirac spinor. Differences occur for three reasons. First of all, the Dirac equation is always a four-component equation, whereas two-component spinors are possible for the groups G_2 and G_5 [cf. Eq. (26)] found in our investigation. Secondly, certain representations are forbidden in a local formulation. Thirdly, certain representations which are equivalent within the framework of the general theory of representations may prove to be inequivalent with respect to local transformations.

Before turning to an investigation of the Dirac equation, let us enumerate all the "physically" inequivalent four-component representations, for a particle with spin $\frac{1}{2}$, which are permissible according to table (26):

	G	λ_s	λ_t	λ_{st}		G	λ_s	λ_t	λ_{st}
1	G_1	i	ρ_2	$i\rho_2$	14	G_5	1	1	1
2		$-i$	ρ_2	$-i\rho_2$	15		-1	1	-1
3	G_2	i	1	i	16		ρ_3	ρ_3	1
4		$-i$	1	$-i$	17		1	ρ_1	ρ_1
5		i	ρ_1	$i\rho_1$	18		-1	ρ_1	$-\rho_1$
6		$-i$	ρ_1	$-i\rho_1$	19		ρ_1	ρ_1	1
7		$i\rho_3$	ρ_3	i	20		ρ_1	1	ρ_1
8		$i\rho_1$	1	$i\rho_1$	21	G_6	1	ρ_2	ρ_2
9		$i\rho_1$	ρ_1	i	22		-1	ρ_2	$-\rho_2$
10	G_3	ρ_1	ρ_2	$i\rho_3$	23	G_7	$i\rho_1$	ρ_3	ρ_2
11		ρ_3	ρ_2	$-i\rho_1$	24		$i\rho_3$	ρ_1	$-\rho_2$
12	G_4	ρ_1	ρ_3	$-i\rho_2$	25	G_8	$i\rho_1$	ρ_2	$-\rho_3$
13		ρ_3	ρ_1	$i\rho_2$	26		$i\rho_3$	ρ_2	ρ_1

(37)

We say that two representations, for example representations 7 and 8, are "physically" inequivalent, even though they are equivalent, if they correspond to different symmetry types. In representation 7, under inversion the particle goes over into itself (conservation of parity), while in 8 the particle under inversion goes over into its antiparticle (conservation of combined inversion).

Now let us consider the possible transformations for the Dirac field operators, which correspond to the addition of the requirement of locality to the invariance requirements (1) and (8) — (10). In the local formulation, these conditions are equivalent to the following requirements: 1) invariance of the equations for the field operators, 2) invariance of the commutation relations, 3) invariance of the definition of the vacuum. Taking account of these requirements, one can show that the following nonequivalent sets of transformations of the Dirac field operator $\psi(\mathbf{x}, t)$ can be associated with the reflection transformations:

	Group	Operators corresponding to coordinate reflections			Number of correspond-representation in (37)
		$x = -x'$	$t = -t'$	$x_\mu = -x'_\mu$	
—	G_1	—	—	—	—
1	G_2	iP	T	iPT	7
2	G_3	PC	iCT	iPT	10
3	G_4	PC	iT	$-iPCT$	12
4		PC	$-iT$	$iPCT$	12
5	G_5	P	T	PT	14
6		$-P$	T	$-PT$	15
7		P	CT	PCT	17
8		P	$-CT$	$-PCT$	17
9		$-P$	CT	$-PCT$	18
10		$-P$	$-CT$	PCT	18
11		PC	CT	PT	19
12		PC	T	PCT	20
13		PC	$-T$	$-PCT$	20
14	G_6	P	iCT	$iPCT$	21
15		$-P$	iCT	$-iPCT$	22
16	G_7	iP	CT	$iPCT$	24
17		iP	$-CT$	$-iPCT$	24
18	G_8	iP	iCT	$-PCT$	26
19		iP	$-iCT$	PCT	26

(38)

In (38) the operations P, T, C are defined in the standard way, with the phase factors

$$P\psi(\mathbf{x},t) = i\gamma_4\psi(-\mathbf{x}, t). \quad (39)$$

$$T\psi(\mathbf{x},t) = \gamma_1\gamma_3\gamma_4\bar{\psi}(\mathbf{x}, -t), \quad (40)$$

$$C\psi(\mathbf{x},t) = \gamma_2\gamma_4\bar{\psi}(\mathbf{x}, t). \quad (41)$$

It can be shown that, with this choice of phase factors, the transformations (39) and (40) on the Dirac field operators are equivalent to the transformations (16) and (17) on the corresponding state vector. For this reason these operations are denoted by the same letters. This equivalence can

be established by means of a Foldy-Wouthuysen transformation[10] of the solutions of the Dirac equation for the field operators, followed by a shift to the configuration representation as in reference 11.

Table (38) exhausts the possible laws for local reflection transformations of Dirac particles. We remind the reader that particles can exist simultaneously only if their operators transform according to representations which belong to the same group, and that all the reflection operations are conserved.

6. DISCUSSION OF RESULTS

Our investigation shows that the known properties of space-time must be fixed in accordance with one of the columns of (11), so that the question arises of determining the group among $G_1 - G_8$ according to which real space-time transforms. To solve this problem, we may use the following differences between the representations of these groups.

a) The pseudoscalar nature of the ground state of positronium. This argument does not depend on whether inversion is or is not accompanied by charge conjugation, since the two-photon system has even charge parity. This requirement eliminates from table (37) the representations $1-6$, 8, 9, 11, 13, 16, 23, and 25, i.e., just those representations which are absent from the local variants (38). Thus the requirement of pseudoscalarity of positronium eliminates the possibility of group G_1, in which the squares of all reflections are equal to unity.

b) The two-component neutrino. If the neutrino is two-component, then, according to (36), the groups G_1, G_3, G_6 and G_8 are not possible.

c) The four-component nature of all known spinor particles with nonzero rest mass. This argument, together with the previous one, makes those representations particularly probable for which the wave function of the spin $-\frac{1}{2}$ particle may be two-component for zero rest mass, but necessarily four-component for particles of finite mass. Groups G_4 and G_7 satisfy this condition.

The following group of arguments is related to non-conservation of the operation of charge conjugation C [ρ_1, ρ_2 in Eq. (37)]. It is to be understood that we are talking about conservation under all interactions, since the problem under discussion involves the geometric properties of space-time itself. Nonconservation of C has the consequence that if, for example, the quantity PC is associated with the transformation $\mathbf{x} = -\mathbf{x}'$ and is therefore conserved, the quantity $PC \cdot C = P$ will not be conserved. On the basis of this remark, we may consider the following additional restrictions on the representations.

d) Conservation of PCT. This requirement is a hypothesis, if the locality condition is not imposed on the theory. Conservation of PCT results in non-conservation of PT, which eliminates representations 3, 4, 7, 9, 10, $14-16$, 19 in (37). Taken together with a), this requirement eliminates groups G_2 and G_3.

e) The hypothesis of conservation of combined parity PC.[12-14] Conservation of PC excludes from (37) the representations $1-7$, 11, 13, $14-18$, 21, 22, 24, and 26. Taken together with point a), this eliminates all the representations of the groups G_1, G_2, G_6, G_7 and G_8.

f) The hypothesis of conservation of T. This excludes from (37) the representations 1, 2, 5, 6, $9-11$, 13, $17-19$, 21, 22, and $24-26$, so that, together with a) it excludes all the representations of groups G_1, G_3, G_6, G_7 and G_8. The locality condition is equivalent to the combined conditions a) and d).

Only representation 12 in (37) satisfies all the requirements enumerated above. This representation belongs to group G_4. In (38) there correspond to it the two locally nonequivalent representations 3 and 4. If we drop requirement c), the remaining conditions will also be satisfied by representation 20 of the group G_5 in (37). In (38) there will correspond to it the two locally nonequivalent representations 12 and 13. In this case, however, it becomes possible to have other particles, whose wave functions transform according to various representations of group G_5, so that the conservation laws d), e) and f) lose their universal character.

Thus, existing experimental data lead to the conclusion that real space-time transforms either according to group G_4 or according to group G_5, the more probable one being group G_4, in which the squares of the inversion and of the reflection of all four axes are equal to unity. (We note that if we treat the reflection as a rotation through angle π about some additional coordinate axis, its square reduces to a rotation through 2π.) It is interesting that such a delicate property of space-time, which is associated with the topology of the parameter space of the rotation group, turns out to be accessible to experimental determination.

In group G_4, all particles must transform according to representation 12 of (37). When we go over to the local formulation, the two representations 3 and 4 in (38), which are non-equivalent under local transformations, will correspond to it. These representations are characterized by

the fact that the transformation properties of the particles they describe are identical, while the field operators transform differently under reflection of all four axes. This difference between the particles will therefore not affect the conditions for invariance of the S-matrix, as determined, for example, according to reference 15. But they will have a marked effect on the composition of the Lagrangian for the interaction which transforms one particle into another.

With regard to actual particles, we may say that the π^0-meson belongs to the completely symmetric type, while the photon and charged particles have T-symmetry. The neutrino has T-symmetry if it is two-component, and is completely asymmetric if it is four-component. One must, however, observe a certain caution in drawing such conclusions. For example, the Wu experiment, strictly speaking, shows only that at least one of the particles participating in the process (for example, the neutrino) does not go over into itself under inversion. On the other hand, if say it should turn out that the quantities P, T and PT are not conserved in proton-proton collisions, this would imply that the proton has four different charge states, in accordance with the initial hypothesis of Lee and Yang.[12] It is of interest to set up a system of experiments necessary for the exact determination of the symmetry types of all known particles.

Usually, in investigating the reflections, one assigns these operations at the start for all the fields being studied, and then investigates the conservation of these operations. Such an approach is, on the one hand, incomplete, and on the other hand mixes up the purely geometrical properties of the reflection operations with the special properties of the operators of the as yet incomplete local theory of fields. The main result of the present paper is the strict separation of the geometrical properties of the reflection operations from the properties of specific equations of motion.

Summarizing, we may say that the investigation of the reflection operations reduces to the answer to three questions: 1) According to which of the groups $G_1 - G_8$ does real space-time transform? 2) According to which representation does each of the particles transform? 3) To which symmetry type does each particle belong? All other questions which arise in studying the reflections either reduce to the ones enumerated or depend essentially on the particular choice of the equations of motion.

[1] V. Bargmann and E. P. Wigner, Proc. Natl. Acad. Sci. U.S. **34**, 211 (1948). P. A. M. Dirac, Revs. Modern Phys. **21**, 392 (1949).

[2] E. P. Wigner, Nachr. Akad. Wiss. Göttingen, Math.-physik. Kl. p. 546-559 (1932).

[3] J. Schwinger, Phys. Rev. **82**, 914 (1951).

[4] Yu. M. Shirokov, JETP **36**, 879 (1959), Soviet Phys. JETP **9**, 620 (1959).

[5] Wick, Wightman, and Wigner, Phys. Rev. **88**, 101 (1952). I. S. Shapiro, Usp. Fiz. Nauk **53**, 7 (1954).

[6] Yu. M. Shirokov, JETP **34**, 717 (1958), Soviet Phys. JETP **1**, 493 (1958).

[7] V. G. Solov'ev, Preprint P-145, Joint Inst. for Nucl. Studies, 1958. G. C. Wick, Ann. Rev. Nuclear Sci. **8**, (1958).

[8] Yu. M. Shirokov, JETP **33**, 861, 1196, 1208 (1957), Soviet Phys. JETP **6**, 664, 919, 929 (1958).

[9] E. P. Wigner, Ann. Math. **40**, 149 (1939).

[10] L. L. Foldy and S. A. Wouthuysen, Phys. Rev. **78**, 29 (1950).

[11] Yu. M. Shirokov, JETP **24**, 129, 135 (1953).

[12] T. D. Lee and C. N. Yang, Phys. Rev. **105**, 1671 (1957).

[13] L. D. Landau, JETP **32**, 405 (1957), Soviet Phys. JETP **5**, 336 (1957).

[14] V. G. Solov'ev, Nucl. Phys. **6**, 618 (1958).

[15] Yu. M. Shirokov, JETP **35**, 1005 (1958), Soviet Phys. JETP **8**, 703 (1959).

Translated by M. Hamermesh
22

THE SECOND MOMENT OF A PARAMAGNETIC ABSORPTION LINE, INCLUDING THE EFFECT OF FINE AND HYPERFINE STRUCTURE

U. Kh. KOPVILLEM

Kazan' State University

Submitted to JETP editor June 16, 1959

J. Exptl. Theoret. Phys. (U.S.S.R.) **38**, 151-156 (January, 1960)

A formula has been obtained for calculating the reduced second moment of a paramagnetic resonance line and the low-frequency paramagnetic absorption, taking into account the electric field within the crystal. A formula is given for calculating the fine structure constants of nuclear and electronic paramagnetic absorption from the experimental value of the second moment of the absorption curve. A study is made of the way in which the spin-spin paramagnetic relaxation time depends on the interaction of the electron magnetic moments with the internal electric field and the nuclear magnetic moments. As an example, the order of magnitude of the spin-spin relaxation time has been estimated for diamagnetic crystals containing Mn^{++} ions as an impurity.

1. INTRODUCTION

THE well-known formulas of Van Vleck (reference 1, Eq. 11) and Broer (reference 2, Eq. 12) for evaluating the reduced second moment $\langle(\Delta\nu)^2\rangle$ of a paramagnetic resonance line $f(\nu)$, and the reduced second moment $\langle\nu^2\rangle$ of a low-frequency paramagnetic absorption line $\varphi(\nu)$, do not take into account the fine and hyperfine structure of the absorption line, and cannot be used to study the internal interactions in many paramagnetic crystals and liquids. After the appearance of Van Vleck's paper,[1] a number of authors derived formulas for calculating $\langle(\Delta\nu)^2\rangle$, taking into account the internal electric field E, but limiting themselves to particular cases. They considered ions[3] with electron spins of $S = 1$, the central line $f(\nu)$ for ions[4] with half-integral spins S, and ions[5] with anisotropic g-factors and with $S = \frac{1}{2}$. As for the $\varphi(\nu)$ lines, Kopvillem[6] in calculating $\langle\nu^2\rangle$ considered the anisotropy of the g-factor and the exchange interaction, and also the interaction $\mathcal{H}_{hfs}$ between the nucleus inside the ion and the magnetic field created at the location of the nucleus by the uncompensated electrons in the ion.

In the present paper a formula is obtained for calculating the reduced second moment of an absorption line for a quantum of constant radio-frequency, for paramagnetic centers which are magnetically equivalent and have an arbitrary spin S, in the following two cases:

a) The field E splits the energy spectrum of the spin system of the paramagnetic material into a series of discrete quasi-continuous bands whose widths depend on the magnetic dipole interaction $\mathcal{H}_d$ and on the exchange interactions $\mathcal{H}_{ex}$ among the paramagnetic centers. In this case the $f(\nu)$ line splits up into a series of fine-structure components $f_{M,M-1}(\nu)$ corresponding to the magnetic dipole transitions $|S, M\rangle \longleftrightarrow |S, M-1\rangle$ between the states $|S, M\rangle$ and $|S, M-1\rangle$ of the paramagnetic centers. (M is the magnetic quantum number.) It should be noted that it is possible to classify the components of the line $f(\nu)$ according to the number M if the static magnetic field H_0 is considerably stronger than the field E, or if the field H_0 is directed along an axis of symmetry of the field E. We shall evaluate the reduced second moment $\langle(\Delta\nu)^2\rangle_{M,M-1}$ for every component $f_{M,M-1}(\nu)$.

b) The energy spectrum of the spin system consists of a single quasi-continuous band whose width depends on the interactions $\mathcal{H}_d$, $\mathcal{H}_{ex}$, $\mathcal{H}_{hfs}$, and the interaction $\mathcal{H}_E$ of the paramagnetic centers with the field E. The condition that the spectrum of the spin system be quasi-continuous is frequently fulfilled in materials such as dielectric crystals and solutions containing ions of the iron group or the rare earths, with electronic configurations corresponding to $3d^5\ {}^6S$ or $4f^7\ {}^8S$. There will be a $\varphi(\nu)$ line under the condition[2] that the frequency ν of the alternating magnetic field H_t is of the order of magnitude of the reciprocal of the paramagnetic spin-spin relaxation time τ_{ss}, and its shape will portray the distribution function for the transition frequencies of the paramagnetic

centers between the levels of the quasi-continuous spectrum of the spin system, arising under the influence of $\mathcal{H}_d$, $\mathcal{H}_{ex}$, $\mathcal{H}_{hfs}$, and $\mathcal{H}_E$. We shall calculate $\langle\nu^2\rangle$ for a $\varphi(\nu)$ line, taking into account all of the interactions enumerated above.

In both of the cases (a) and (b) we shall consider only electron paramagnetic absorption lines. Nevertheless, all the results we obtain may be applied unchanged to the case of nuclear magnetic resonance. For this purpose the operator $\mathcal{H}_E$ would describe the quadrupole and higher-order interactions between atomic nuclei with spins $I > \frac{1}{2}$ and the gradient of the internal electric field E. We shall assume throughout that the spin-lattice interaction is very much smaller than the interaction $\mathcal{H}_1$ within the spin system, and that these spin-spin interactions are the only ones which determine the shape of the paramagnetic absorption line.

2. REDUCED SECOND MOMENT FOR THE FINE-STRUCTURE COMPONENTS OF A PARAMAGNETIC RESONANCE LINE

Let a static magnetic field H_0 be directed along the z axis, which coincides with one of the principal axes of the g-tensor of the paramagnetic ions, and let H_t be parallel to x. We write the Hamiltonian of the spin system in the form

$$\mathcal{H} = \mathcal{H}_0 + \mathcal{H}_1, \quad \mathcal{H}_0 = \mathcal{H}_Z + \mathcal{H}_E, \quad \mathcal{H}_1 = \sum_{i>j}\sum_{\alpha,\gamma} P^{ij}_{\alpha\gamma} S^i_\alpha S^j_\gamma, \quad (1)$$

where $\mathcal{H}_1$ is the perturbation, $\mathcal{H}_Z$ is the Zeeman energy operator of the paramagnetic ions in the field H_0, $\mathcal{H}_E$ is the Stark energy operator of the ions in the field E, $P^{ij}_{\alpha\gamma}$ is a second order tensor describing the internal interactions in the paramagnetic material, i and j are indices distinguishing the ions, and α and γ are indices denoting the coordinate axes. In our case

$$\mathcal{H}_1 = \mathcal{H}_d + \mathcal{H}_{ex}, \quad P^{ij}_{\alpha\gamma} = g_\alpha g_\gamma \beta^2 (r_{ij}^{-3} - 3r_{ij}^{-5}\alpha^{ij}\gamma^{ij}) - n^{ij}_{\alpha\gamma} J^{ij}, \quad (2)$$

where β is the Bohr magneton, g_α is the spectroscopic splitting factor along the axis α, r_{ij} is the radius vector connecting the i-th and j-th ions, α^{ij} is the projection of the vector r_{ij} on the α axis, J^{ij} is the exchange integral[1] for the ions i and j, and $n^{ij}_{\alpha\gamma}$ is a coefficient characterizing the anisotropy of the exchange interaction, due to the influence of the field E.

To calculate $\langle(\Delta\nu)^2\rangle$ we shall use the formula[1]

$$\langle(\Delta\nu)^2\rangle = -h^{-2}\,\mathrm{Sp}\{[\overline{\mathcal{H}_1}, \mathcal{H}_t]^2\}\{\mathrm{Sp}(\mathcal{H}_t^2)\}^{-1}, \quad \mathcal{H}_t = \sum_{i=1}^{N} \overset{+}{S}{}^i_x, \quad (3)$$

where h is Planck's constant, N is the number of paramagnetic ions in the sample, $\overline{\mathcal{H}_1}$ is the portion of the operator $\mathcal{H}_1$ which commutes with $\mathcal{H}_0$, and the notation [,] denotes the formation of the commutator. The operator $\mathcal{H}_t$ describes the effect of the field H_t on the spin system of the paramagnetic material, and its component operators $\overset{+}{S}{}^i_x$ are obtained from S^i_x by removing all matrix elements which do not correspond to the frequency of the field H_t. In our case the field H_t causes transitions between the $|S, M\rangle$ and $|S, M-1\rangle$ states only, and consequently the only non-null matrix elements of the operator S^i_x are of the form $\langle S, M|S^i_x|S, M-1\rangle$ and $\langle S, M-1|S^i_x|S, M\rangle$. Using (1) to (3), we obtain

$$\langle(\Delta\nu)^2\rangle_{M,M-1} = \{h^2(2S+1)\}^{-1}\sum_{i(\neq j)} |Q_1(P^{ij}_{xx} + P^{ij}_{yy})^2 + Q_2 P^{ij2}_{zz} + Q_3 P^{ij}_{zz}(P^{ij}_{xx} + P^{ij}_{yy}) + Q_1(P^{ij}_{xy} - P^{ij}_{yx})^2|,$$

$$Q_1 = \tfrac{1}{16}\{2(S+M)^2(S-M+1)^2 + (S+M+1)^2(S-M)^2 + (S+M-1)^2(S-M+2)^2\},$$

$$Q_2 = \frac{2S+1}{12}\{(2S+1)^2 - 1\},$$

$$Q_3 = -\tfrac{1}{2}(S+M)(S-M+1). \quad (4)$$

If the spin system of the paramagnetic material contains ions i and k which are not equivalent, and paramagnetic resonance occurs in ions of the type k having a spin S′, then the corresponding reduced second moment $\langle(\Delta\nu)^2\rangle_{S'}$ can be calculated with the aid of a formula obtained from (4) by setting $Q_1 = Q_2 = 0$ and substituting S'^k for S^j and k for j. If the paramagnetic centers all have the same spin, but are acted on by different intra-crystalline electric fields E, then the corresponding reduced second moment $\langle(\Delta\nu)^2\rangle_0$ for the fine structure component $f_{1/2,-1/2}(\nu)$ is calculated from formula (14) of reference 4. It should be noted that the quantities $\langle(\Delta\nu)^2\rangle_{M,M-1}$, $\langle(\Delta\nu)^2\rangle_S$, and $\langle(\Delta\nu)^2\rangle_0$ are additive.

3. REDUCED SECOND MOMENT FOR LOW-FREQUENCY PARAMAGNETIC ABSORPTION LINES

The Hamiltonian of the spin system is of the form

$$\mathcal{H} = \mathcal{H}_1,$$

$$\mathcal{H}_1 = \sum_{i>j}^{N}\sum_{\alpha,\gamma} P^{ij}_{\alpha\gamma} S^i_\alpha S^j_\gamma + \sum_{i=1}^{N}\sum_{\alpha} (D^i_\alpha S^{i2}_\alpha + E^i_\alpha S^{i4}_\alpha + A^i_\alpha S^i I^i_\alpha), \quad (5)$$

where (D_α, E_α) and A_α are the elements of tensors characterizing the interactions $\mathcal{H}_E$ and $\mathcal{H}_{hfs}$ respectively (see reference 7). In the present

case $S^i_x = \hat{S}^i_x$, and the operator $\mathcal{H}_t$ has the form

$$\mathcal{H}_t = \beta \sum_{i,\alpha} g^i_{t\alpha} S^i_\alpha, \quad g^i_{t\alpha} = g_\alpha \cos(\alpha, t), \tag{6}$$

where (α, t) is the angle between the direction of the field H_t and the α axis. Using (3) and the expressions (5) and (6) we obtain

$$\langle \nu^2 \rangle = (hg)^{-2} (\langle \nu^2 \rangle_{d+ex} + \langle \nu^2 \rangle_E + \langle \nu^2 \rangle_{hfs}), \tag{7}$$

where subscripts are added in order to distinguish the brackets of the corresponding interactions. The values of the second moments on the right hand side of (7) are given by the following expressions:

$$\langle \nu^2 \rangle_{d+ex} = L \sum_{i(\neq j)} \sum (e_{\theta\psi\pi} e_{\gamma\varepsilon\pi} g^i_{t\varepsilon} g^i_{t\psi} P^{ij}_{\gamma\delta} P^{ij}_{\theta\delta} + e_{\gamma\varepsilon\nu} e_{\theta\psi\delta} g^i_{t\varepsilon} g^j_{t\psi} P^{ij}_{\gamma\delta} P^{ij}_{\nu\theta}), \tag{8}$$

$$\langle \nu^2 \rangle_{hfs} = R \sum e_{\gamma\lambda\nu} e_{\delta\psi\nu} g^i_{t\lambda} g^i_{t\psi} A_{\gamma\theta} A_{\delta\theta}, \tag{9}$$

$$\langle \nu^2 \rangle_E = \sum g^{i2}_{t\beta} \{ e^2_{\alpha\beta\gamma} (v_1 D^{i2}_\alpha + v_2 E^{i2}_\alpha + v_3 D^i_\alpha E^i_\alpha) + e_{\alpha\beta\gamma} e_{\gamma\beta\alpha} (v_1 D^i_\alpha D^i_\gamma + v_4 E^i_\alpha E^i_\gamma + v_3 D^i_\alpha E^i_\gamma) \},$$

$$L = \tfrac{1}{3} S(S+1), \quad R = \tfrac{1}{3} I(I+1), \quad g^2 = \sum g^2_{t\alpha}, \tag{10}$$

where $e_{\alpha\beta\gamma}$ is the unit antisymmetric tensor (with e_{xyz} taken to be unity), and all the indices $\alpha, \beta, \gamma, \theta, \ldots$ are to be summed over the range x, y, z. In formula (9) the index θ is introduced to denote the principal axes of the tensor A. The coefficients v_γ are calculated from the formulas

$$v_1 = b \,\mathrm{Sp}\, \{[S_\alpha, S_\gamma]^2_+\} = \frac{4}{5} S(S+1) - \frac{3}{5},$$

$$v_2 = b \,\mathrm{Sp}\, \{[S^2_\alpha, [S_\alpha, S_\gamma]_+]^2_+\} = \frac{16}{21} S^3 (S+1)^3 - \frac{268}{105} S^2 (S+1)^2 + \frac{112}{35} S(S+1) - \frac{9}{7},$$

$$v_3 = b \,\mathrm{Sp}\{[S_\alpha, S_\gamma]_+ [S^2_\alpha, [S_\alpha, S_\gamma]_+]_+\} = \frac{24}{35} S^2 (S+1)^2 - \frac{38}{35} S(S+1) + \frac{6}{7},$$

$$v_4 = b \,\mathrm{Sp}\, \{[S^2_\alpha, [S_\alpha, S_\gamma]_+]_+ [S^2_\gamma, [S_\alpha, S_\gamma]_+]_+\} = \frac{16}{35} S^3 (S+1)^3 - \frac{4}{7} S^2 (S+1)^2 - \frac{2}{5} S(S+1) + \frac{3}{7},$$

$$b = \left\{ \tfrac{1}{3} S(S+1)(2S+1) \right\}^{-1}, \tag{11}$$

where $\alpha \neq \gamma$; $\alpha, \gamma = x, y, z$; and the symbol $[,]_+$ denotes the formation of the anticommutator. In Eqs. (8) to (10) it is assumed that the mean values derived for the coefficients of the Hamiltonian (5) are determined by the formula

$$\langle A^i_\alpha A^k_\beta \rangle = A_\alpha A_\beta, \tag{12}$$

If the coefficients A^i_α have an arbitrary distribution $\psi(i)$, then

$$\langle A^i_\alpha A^k_\beta \rangle = (N_\alpha N_\beta)^{-1} \sum_{i,k} \psi(i) \psi(k) A^i_\alpha A^k_\beta. \tag{13}$$

In the case (13), the fine and hyperfine structure of the $\varphi(\nu)$ line cannot be resolved by magnetic dilution of the sample, and the coefficients of the Hamiltonian (5) can be found only by comparing the experimental and theoretical moments of the $\varphi(\nu)$ line. It should be mentioned that the coefficients of the Hamiltonian (5) can have different values for magnetically dilute and magnetically concentrated samples. The formulas (8) to (10) which we have obtained can be used to study this question.

In the case of paramagnetic solutions or powders, where the field H_t occurs at arbitrary angles to the x, y, z axes fixed to the molecules or microcrystals, the coefficients $g_{t\alpha} g_{t\beta}$ in expressions (8) to (10) should be replaced by their mean values, found from the formula

$$\langle g_{t\alpha} g_{t\beta} \rangle = \tfrac{1}{3} g_\alpha g_\beta \delta_{\alpha\beta}, \quad \langle g^2 \rangle = \tfrac{1}{3} \sum g^2_\alpha, \tag{14}$$

where $\delta_{\alpha\beta}$ is the Kronecker symbol.

4. REDUCED SECOND MOMENT OF THE $\varphi(\nu)$ LINE FOR $Zn(HCOO)_2 \cdot 2H_2O$ WITH Mn^{++} IMPURITY

As an example of the use of formulas (9) and (10) let us take the case of low-frequency paramagnetic absorption occurring at a Mn^{++} ion in a crystal of $Zn(HCOO)_2 \cdot 2H_2O$. From the experiments of Hadders et al.[8] it is known that for Mn^{++} ions the width $\Delta\nu_{1/2}$ of the $\varphi(\nu)$ line at half-amplitude is determined by the interactions within the spin system. For small concentrations of Mn^{++} ions the order of magnitude of $\langle \nu^2 \rangle$ is determined by the interactions $\mathcal{H}_E$ and $\mathcal{H}_{hfs}$. From (7), (9), and (10) we obtain

$$\langle \nu^2 \rangle = (hg)^{-2} (\langle \nu^2 \rangle_E + \langle \nu^2 \rangle_{hfs}) = (hg)^{-2} \{ g^2_{tx} [v_1 (D_y - D_z)^2 + v_2 (E^2_y + E^2_z) + v_3 (D_y E_y + D_z E_z - D_y E_z - D_z E_y) + v_4 (-2E_y E_z) + R (A^2_{ya_1} + A^2_{ya_2} + A^2_{ya_3} + A^2_{za_1} + A^2_{za_2} + A^2_{za_3})] + g_{tx} g_{ty} [-R (A_{xa_1} A_{ya_1} + A_{xa_2} A_{ya_2} + A_{xa_3} A_{ya_3})] + Q \}, \tag{15}$$

where Q contains terms of the type g^2_{ty}, g^2_{tz}, $g_{tz} g_{tx}$, etc., obtained by permutations of the subscript indices given above.

The tensor elements occurring in (15) can be found by comparing the Hamiltonian (5) with the spin Hamiltonian $\mathcal{H}_S$ for an isolated Mn^{++} ion, as given by Bowers and Owen:[7]

$$\mathcal{H}_S = g\beta (H_z S_z + H_x S_x + H_y S_y) + \frac{a}{6} (S^4_z + S^4_x + S^4_y) + D\left(S^2_z - \frac{35}{12}\right) + E(S^2_x - S^2_y) + A (S_z I_z + S_x I_x + S_y I_y). \tag{16}$$

From (5) and (16) it follows that $E_x = E_y = E_z = a/6$; $D_z = D$, $D_x = E$, $D_y = -E$; $A_{xx} = A_{yy} = A_{zz} = A$; and $g_x = g_y = g_z = g$.

Making these substitutions, we obtain

$$\langle \nu^2 \rangle = h^{-2}\left\{\frac{1}{18}a^2(v_2 - v_4) + 2A^2R + v_1[\cos^2(t, x)(E + D)^2 + \cos^2(t, y)(E - D)^2 + \cos^2(t, z)(E + D)^2]\right\}. \quad (17)$$

Substituting into (17) the numerical values $D = 0.0485\ cm^{-1}$; $g = 1.999$; $E = 0.011\ cm^{-1}$; $a = 0.0009\ cm^{-1}$; $A = 0.0091\ cm^{-1}$; $v_1 = 6.4$, $v_2 = 341.7$, $v_4 = 259.4$, and $R = 2.917$, we obtain

$$\langle \nu^2 \rangle = \{43.72 + 2035[\cos^2(t, x) \cdot \cos^2(t, z)] + 808.2\cos^2(t, y)\} \cdot 10^{16}\ sec^{-2} \quad (18)$$

Using Broer's formula,[2] $\tau_{ss} = (\pi/2\langle \nu^2 \rangle)^{1/2}$, we find from (18) that $\tau_{ssx} = \tau_{ssz} = 2.8 \times 10^{-10}$ sec and $\tau_{ssy} = 4.3 \times 10^{-10}$ sec, where the subscripts x, y, and z are introduced to denote the direction of the field H_t which perturbs the spin system.

5. DISCUSSION OF RESULTS

1. Formula (4) is the generalization of a number of known results. Let $\mathcal{H}_1 = \mathcal{H}_d + \mathcal{H}_{ex}$; then from (4), if (a) $S = 1/2$ and the temperature $T = \infty$, we have formulas (2) to (4) from a paper[5] by the author; (b) adding the condition that the g-factor be isotropic, $g_{\alpha\alpha} = \text{const}$, we get Eq. (11) of Van Vleck's paper[1] for $S = 1/2$; (c) if $S = 1$ and $g_{\alpha\alpha} = \text{constant}$ for the fine structure components $f_{1/2,-1/2}(\nu)$, we obtain equation (8) of Kambe and Ollom.[4]

2. Note the following peculiarities of Eq. (4):

a) The quantity $\langle (\Delta\nu)^2 \rangle_S$, characterizing the local field at the position of the paramagnetic center i, depends on S and is uniform for all the fine-structure components.

b) In the presence of strong intracrystalline electric fields the exchange interaction makes a contribution to $\langle (\Delta\nu)^2 \rangle_{M,M-1}$ and, generally speaking, there are no paramagnetic resonance lines. This is due to the fact that the energy of the paramagnetic centers depends on the orientation of the magnetic moments of the centers with respect to the symmetry axes of the field E.

c) Fine-structure components due to the transitions $|S, M\rangle \longleftrightarrow |S, M-1\rangle$ or $|S, 1-M\rangle \longleftrightarrow |S, -M\rangle$ have the same reduced second moment.

d) The quantity $4(Q_1 + Q_2 - Q_3)/9(2S + 1) = W$, corresponding to the factor $\frac{1}{3}S(S + 1)$ in Van Vleck's formula,[1] is greatest for the transition $|S, 1/2\rangle \longleftrightarrow |S, -1/2\rangle$ and drops off monotonically as the quantity $|M|$ increases.

e) The ratio $10/3 : 1 : 4/9$, relating the reduced second moment $\langle (\Delta\nu)^2 \rangle_\Sigma$ which includes the contributions from all the satellite lines, to $\langle (\Delta\nu)^2 \rangle_{M,M-1}$ and $\langle (\Delta\nu)^2 \rangle_S$ in the case $E = 0$ (see reference 9), is replaced in our case by the formula

$$\langle (\Delta\nu)^2 \rangle_\Sigma : \langle (\Delta\nu)^2 \rangle_{M,M-1} : \langle (\Delta\nu)^2 \rangle_S = {}^{10}/_9 S(S + 1) : W : [4Q_2/9(2S + 1)]$$

which depends on M as well as on S.

3. Let us now return to formulas (8) to (10). When $S = 1/2$, (8) and (9) become identical with (10) and (11) of the author's work in reference 6. If $H_t \parallel x$ and $g_\alpha = \text{constant}$, (8) is identical with Broer's formula (see reference 2). If all the coefficients in the Hamiltonian (5) are zero except E_z and D_z, then (10) agrees with Bersohn's formula (7) (reference 10).

4. The spin-spin paramagnetic relaxation time which we have calculated for a manganese ion agrees in order of magnitude with the results of experiments by Hadders et al.[8] As to the anisotropy of the time τ_{ss}, experimental data are almost entirely lacking. It should be noted that we previously predicted that the time τ_{ss} should depend on the interaction of the electron spins of the paramagnetic ions with the field E surrounding them and with the inner nucleus of the ion (see reference 6), whereas this dependence was first observed experimentally by Townes and his coworkers.[11]

5. Measurements of the quantity $\langle \nu^2 \rangle$ can be made at very low concentrations of paramagnetic centers, where a comparison of the experimental and theoretical results can be made without considering dipole-dipole and exchange interactions between centers. These conditions can be fulfilled conveniently in the case of liquids, where the term $\langle \nu^2 \rangle_{d+ex}$ must be averaged on the basis of some hypothetical assumption as to the nature of the intermolecular motions. A comparison of our results for the manganese ion with the corresponding data for the same ion in aqueous solutions (see reference 12) shows that when crystals containing Mn^{++} ions are dissolved, the field E around the Mn^{++} ion is altered. The coefficients in the Hamiltonian (5) which characterize the field E around a Mn^{++} ion in aqueous solution are several times smaller than the values which we have used in our calculations.

[1] J. H. Van Vleck, Phys. Rev. **74**, 1168 (1948).

[2] L. F. J. van den Broer, Physica **10**, 801 (1943).

[3] Ishiguro, Kambe, and Usui, Physica **17**, 310 (1951).

[4] K. Kambe and J. F. Ollom, J. Phys. Soc. Japan **11**, 50 (1956).

[5] U. Kh. Kopvillem, JETP **34**, 1040 (1958), Soviet Phys. JETP **7**, 719 (1958).

[6] U. Kh. Kopvillem, JETP **35**, 506 (1958), Soviet Phys. JETP **8**, 349 (1959); Изв. Высш. шк., Физика (News of the Universities — Physics), No. 3, 13 (1958).

[7] K. D. Bowers and J. Owen, Rep. Progr. Phys. **17**, 344 (1955).

[8] Hadders, Locher, and Gorter, Physica **24**, 839 (1958); L. C. van der Marel, J. van den Broek, and C. J. Gorter, Physica **24**, 101 (1958).

[9] J. H. Van Vleck, Nuovo cimento Suppl. **6**, 993 (1957).

[10] R. Bersohn, J. Chem. Phys. **20**, 1505 (1952).

[11] Giordmaine, Alsop, Nash, and Townes, Phys. Rev. **109**, 302 (1958).

[12] B. M. Kozyrev, Izv. Akad Nauk SSSR, Ser. Fiz. **21**, 828 (1957), Columbia Tech. Transl. p. 828.

Translated by D. C. West
23

SOME GENERAL RELATIONS IN STATISTICAL QUANTUM ELECTRODYNAMICS

E. S. FRADKIN

The P. N. Lebedev Physics Institute, Academy of Sciences, U.S.S.R.

Submitted to JETP editor June 19, 1959

J. Exptl. Theoret. Phys. (U.S.S.R.) 38, 157-160 (January, 1960)

A number of general relations associated with the gauge invariance of quantum electrodynamics are obtained.

INTRODUCTION

As is well known, the system of equations for the Green's functions of quantum statistics[1,2] differs both in form and in content from the analogous system of equations for the Green's functions of ordinary field theory.

However, as will be shown below, a number of general relations associated with the gauge invariance of quantum electrodynamics hold not only in ordinary quantum electrodynamics[3] but also in statistical quantum electrodynamics.

It is not difficult to convince oneself of the correctness of the relations we shall obtain if one uses perturbation theory and analyzes the simplest Feynman diagrams for quantum statistics, but in this paper a more complete and rigorous proof of these relations is given by means of the exact equations for the Green's functions of quantum statistics.

1. RELATIONS OF THE WARD TYPE FOR QUANTUM STATISTICS

By using results obtained earlier[1] we can get a system of equations for the Green's functions in the presence of a source of the photon field; in the momentum representation this system can be written in the form (the notation is the same as in reference 1)

$$G^{-1}(p,\ p') = [-i\gamma_\nu p_\nu - \gamma_4\mu + m]\,\delta(p-p') - i\epsilon\gamma_\mu \langle A_\mu(p-p')\rangle + \Sigma(p,\ p'), \tag{1}$$

$$[k^2\delta(k-k')\,\delta_{\mu\rho} - \Pi_{\mu\rho}(k,\ k')]\,D_{\rho\nu}(k,\ k') = \delta(k-k')\,(\delta_{\mu\nu} - k_\mu k_\nu/k^2), \tag{2}$$

$$\Pi_{\mu\nu}(k\,k') = \frac{e^2}{(2\pi)^3\beta}\,\mathrm{Sp}\left\{\sum\int \gamma_\mu G(k+s,\ s_1)\,\Gamma_\nu(s_1,\ s_2,\ k')\,G(s_2,\ s)\,d^3s_1 d^3s_2 d^3s\right\}, \tag{3}$$

$$\Sigma(p,\ p') = \frac{e^2}{(2\pi)^3\beta}\sum\int \gamma_\mu G(p+s,\ s_1)\,\Gamma_\nu(s_1,\ p',\ s_2)\,D(s_2,\ s)\,d^3s d^3s_1 d^3s_2, \tag{4}$$

$$\Gamma_\mu(p,\ p',\ k) = -\frac{\delta G^{-1}(p,\ p')}{\delta\langle ieA_\mu(k)\rangle} = \gamma_\mu\delta(p-p'-k) - \frac{\delta\Sigma(p,\ p')}{\delta\langle ieA_\mu(k)\rangle}. \tag{5}$$

In Eqs. (3) and (4) the summations are over all the fourth components of the momenta; these components are, respectively, $2\pi n/\beta$ for photons and $(2n+1)\pi/\beta$ for fermions.* In Eq. (2) the term $k_\mu k_\nu/k^2$ must be understood in the sense of the principal value for the analytic continuation. We note that it is often more convenient to work with a different gauge for the potential A; in particular, we can drop this term.

$$\delta(k-k') = \delta(k-k')\,\delta_{(k_4-k_4')},$$

$$\text{where } \delta_{(k_4-k_4')} = \begin{cases} 1 & \text{for } k_4 = k_4' \\ 0 & \text{for } k_4 \neq k_4' \end{cases}$$

Using Eqs. (1) — (5) and expanding all quantities in series by perturbation theory, we can convince ourselves that the following relation holds:

$$G^{-1}(p+k,\ p') - G^{-1}(p,\ p'-k) = k_\rho\delta G^{-1}(p,\ p')/\delta e\langle A_\rho(k)\rangle. \tag{6}$$

*In the limiting case of zero temperature all the sums over the fourth components go over into integrals. (For $\beta\to\infty$ we get $\frac{1}{\beta}\sum_{p_4}\to\frac{1}{2\pi}\int dp_4$.) In particular, if we further let $\mu\to 0$, we get from (1)–(5) a system of equations equivalent to ordinary quantum electrodynamics, with the following advantages: a) the momentum space has a Euclidean metric, and therefore calculation is considerably simpler than in the usual pseudo-Euclidean space; b) in this system of equations $\mathrm{Im}\,\Pi = \mathrm{Im}\,\Sigma = \mathrm{Im}\,\Gamma = 0$, and thus the number of equations is only half as large as in ordinary quantum electrodynamics. The transition to the quantum theory in the usual representation is accomplished by analytic continuation in the fourth component of the momentum (cf. reference 1), and then all quantities become complex (there is an analogous situation in classical theory, where the dielectric constant for imaginary frequencies becomes a real quantity); c) our Green's functions in the Euclidean parameters do not have poles, and therefore division by D^{-1} and G^{-1} is unique; the poles arise in the analytic continuation of these quantities.

We shall show below that the exact system (1) — (5) (without resort to perturbation theory) also has the relation (6) as one of its consequences.

In fact, according to the left member of (6) we have

$$G^{-1}(p+k,\ p') - G^{-1}(p,\ p'-k) = i\gamma_\rho k_\rho \delta(p+k-p') + \frac{e^2 i}{(2\pi)^3\beta}\sum\!\!\!\!\!\!\int \gamma_\mu \left[G(p+k+s,\ s_1)\frac{\delta G^{-1}(s_1,\ p')}{\delta e\langle A_\nu(s_2)\rangle} - G(p+s,\ s_1)\frac{\delta G^{-1}(s_1,\ p'-k)}{\delta e\langle A_\nu(s_2)\rangle}\right] D_{\nu\mu}(s_2,\ s)\, d^3s d^3s_1 d^3s_2. \quad (7)$$

On the other hand, we get from (1) — (5) for the right member of Eq. (6)

$$k_\rho \frac{\delta G^{-1}(p,\ p')}{\delta e\langle A_\rho(k)\rangle} = -i\gamma_\rho k_\rho \delta(p+k-p') - \frac{e^2 i}{(2\pi)^3\beta} \times \sum\!\!\!\!\!\!\int \gamma_\mu \left[k_\rho \frac{\delta G(p+s,\ s_1)}{\delta e\langle A_\rho(k)\rangle}\frac{\delta G^{-1}(s_1,\ p')}{\delta e\langle A_\nu(s_2)\rangle} - G(p+s,\ s_1)\, k_\rho \frac{\delta^2 G^{-1}(s_1,\ p')}{\delta e\langle A_\rho(k)\rangle\,\delta e\langle A_\nu(s_2)\rangle}\right] \times D_{\nu\mu}(s_2,\ s)\, d^3s d^3s_1 d^3s_2 + \frac{e^2 i}{(2\pi)^3\beta}\sum\!\!\!\!\!\!\int \gamma_\mu G(p+s,\ s_1)\frac{\delta G^{-1}(s_1,\ p')}{\delta e\langle A_\nu(s_2)\rangle} \times k_\rho \frac{\delta D_{\nu\mu}(s_2,\ s)}{\delta e\langle A_\rho(k)\rangle} d^3s d^3s_1 d^3s_2 = R. \quad (8)$$

According to (6), the left members of (7) and (8) are equal. We shall show that indeed the right members of (7) and (8) are identically equal.

Consider the right member of (8). Using the law of the conservation of the four-dimensional current, we have (see Sec. 2)

$$k_\mu \frac{\delta D_{\nu\mu}(s_1,\ s)}{\delta e\langle A_\mu(k)\rangle} = 0.$$

According to Eq. (6)

$$k_\rho \frac{\delta^2 G^{-1}(s_1,\ p')}{\delta e\langle A_\rho(k)\rangle\,\delta e\langle A_\nu(s_2)\rangle} = \frac{\delta G^{-1}(s_1+k,\ p')}{\delta e\langle A_\nu(s_2)\rangle} - \frac{\delta G^{-1}(s_1,\ p'-k)}{\delta e\langle A_\nu(s_2)\rangle}. \quad (6a)$$

After substitution of (6) and (6a) in the right member of (8), we get the following expression:

$$R = -i\gamma_\rho k_\rho \delta(p+k-p') - \frac{e^2 i}{(2\pi)^3\beta}\sum\!\!\!\!\!\!\int \gamma_\mu G(p+s,\ s_3)\left[G^{-1}(s_3+k,\ s_4) - G^{-1}(s_3,\ s_4-k)\right] G(s_4,\ s_1)\frac{\delta G^{-1}(s_1,\ p')}{\delta e\langle A_\nu(s_2)\rangle} \times D_{\nu\mu}(s_2,\ s)\, d^3s d^3s_1 d^3s_2 d^3s_3 d^3s_4 + \frac{e^2 i}{(2\pi)^3\beta}\sum\!\!\!\!\!\!\int \gamma_\mu G(p+s,\ s_1) \times \left[\frac{\delta G^{-1}(s_1+k,\ p')}{\delta e\langle A_\nu(s_2)\rangle} - \frac{\delta G^{-1}(s_2,\ p'-k)}{\delta e\langle A_\nu(s_2)\rangle}\right] D_{\nu\mu}(s_2,\ s)\, d^3s_1 d^3s_2 d^3s. \quad (8a)$$

After the reduction of similar terms in (8a) we find that the right member of (8a) agrees identically with the right member of (7). Thus we have shown that the exact equations for the Green's functions in statistical quantum electrodynamics have the relation (6) as one of their consequences.

The relation (6) is equivalent to an infinite series of relations, which are obtained from (6) by successive differentiations with respect to $\langle A\rangle$, after which one sets $\langle A\rangle = 0$. In particular, we get relations of the type of Ward's identity applicable to quantum statistics:

$$G^{-1}(p) - G^{-1}(p+k) = ik_\rho \Gamma_\rho(p,\ p-k,\ k),$$
$$\frac{\partial G^{-1}(p)}{\partial p_\nu} = -i\lim_{\delta_\nu\to 0}\Gamma_\nu(p,\ p-\delta_\nu,\ \delta_\nu), \quad (9)$$

where δ_ν is a vector which has only its ν-th component different from zero (see footnote †). An analysis of the general proof of the relation (6) enables us, in particular, to indicate for each Feynman diagram of G^{-1} [more exactly, for $\Sigma(p)$] a set of diagrams of the vertex part Γ that assure the fulfillment of the relations (9). This is done in the figure, where the diagrams (up to e^4) are divided into groups a, b, c, within each of which the relations (9) hold.

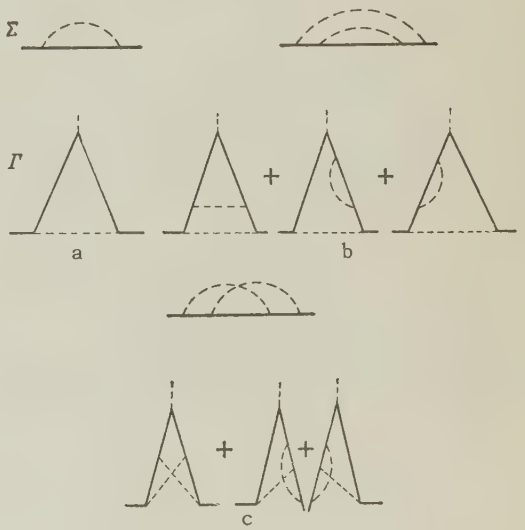

Using the fact that the chemical potential μ appears in $G^{-1}(p)$ in combination with $ie\langle A_4(0)\rangle$, we get

$$\frac{\partial G^{-1}(p)}{\partial ie\langle A_4(0)\rangle} = \frac{\partial G^{-1}(p)}{\partial \mu} = -\Gamma_4(p,\ p,\ 0), \quad (10)$$

where $\Gamma_4(p, p, 0)$ must be understood as the limit of $\Gamma_4(p, p-k, k)$ when $k_4 = 0$ and $k \to 0$.

2. SOME RELATIONS FOR THE POLARIZATION OPERATOR

a) It is not hard to convince oneself that all the odd derivatives of the polarization operator with respect to $\langle A\rangle$ are equal to zero; this means that closed loops with an odd number of fermion

lines are equal to zero (the analog of Furry's theorem for statistics). This can be seen easily if one takes the current in charge-symmetric form (the proof is similar to that carried out in Appendix II of reference 4).

b) The four-dimensional divergence of the polarization tensor $\Pi_{\mu\nu}$ is equal to zero. This holds also when there is an external source of the photon field, so that $\langle A \rangle \neq 0$. In fact, according to (3) and (6), we have

$$k_\nu \Pi_{\mu\nu}(p, k) = \frac{ie^2}{(2\pi)^3\beta} \mathrm{Sp} \left\{ \sum\int \gamma_\mu G(p+s, s_1) [G^{-1}(s_1, s_2 - k) - G^{-1}(s_1 + k, s_2)] G(s_2, s)\, d^3s d^3s_1 d^3s_2 \right\} = 0. \quad (11)$$

Differentiating Eq. (11) with respect to $\langle A \rangle$ and then setting $\langle A \rangle = 0$, we get an infinite sequence of relations equivalent to the operator conservation law for the total charge.

In ordinary quantum electrodynamics it follows from Eq. (11) with $\langle A \rangle = 0$ that the tensor $\Pi_{\mu\nu}$ has the form

$$\Pi_{\mu\nu} = (k_\mu k_\nu - k^2 \delta_{\mu\nu}) \Pi(k^2). \quad (12)$$

In statistics the situation is different. In this case $\Pi_{\mu\nu}(k)$ depends on two vectors: on the argument vector k and on the velocity vector u of the medium. Therefore it follows from Eq. (11) that in the rest system of the medium [in this system the equations (1) — (5) hold] the tensor $\Pi_{\mu\nu}$ has the form

$$\Pi_{\mu\nu} = \left(\frac{k_\mu k_\nu}{\mathbf{k}^2} - \delta_{\mu\nu} \right) A(\mathbf{k}^2, k_4^2) + \Pi_{44} \frac{k_\mu k_\nu}{\mathbf{k}^2} \frac{k_4^2}{\mathbf{k}^2},$$

$$\Pi_{\mu 4} = \Pi_{4\mu} = -\Pi_{44} k_\mu k_4 / \mathbf{k}^2, \text{ where } \nu, \mu = 1, 2, 3. \quad (13)$$

In a coordinate system in which the medium moves with velocity u the tensor $\Pi_{\mu\nu}$ has the following general form†

$$\Pi_{\mu\nu} = \left(\frac{k_\mu k_\nu}{k^2} - \delta_{\mu\nu} \right) A(k^2, (ku)) + \left(\frac{k_\mu k_\nu}{k^2} - \frac{k_\mu k_\nu}{(ku)} - \frac{k_\nu u_\mu}{(ku)} + \frac{u_\nu u_\mu k^2}{(ku)^2} \right) B(k^2, (ku)), \quad (14)$$

where $\nu, \mu = 1, 2, 3, 4$.

In conclusion we remark that by the method of reference 3 one can find in general form the behavior of all the Green's functions under a gauge transformation.

[1] E. S. Fradkin, Dokl. Akad. Nauk SSSR **125**, 311 (1959) Soviet Phys.-Doklady **4**, 347 (1959); JETP **36**, 1286 (1959), Soviet Phys. JETP **9**, 912 (1959).

[2] Abrikosov, Gor'kov, and Dzyaloshinskiĭ, JETP **36**, 900 (1959), Soviet Phys. JETP **9**, 636 (1959).

[3] E. S. Fradkin, JETP **29**, 259 (1955), Soviet Phys. JETP **2**, 361 (1956).

[4] E. S. Fradkin, JETP **29**, 121 (1955), Soviet Phys. JETP **2**, 148 (1956).

Translated by W. H. Furry
24

†The fact that in quantum statistics all quantities have the additional dependence on the timelike vector u of the velocity of the medium has the consequence that for $k \to 0$ we in general get different results depending on the way k goes to zero ($|\mathbf{k}|^2 > k_4^2$ or $|\mathbf{k}|^2 < k_4^2$). For example, from the law of the conservation of the total charge of the system it follows that $\Pi_{44}(k_4, 0) = 0$, whereas by means of the relation (10) one can show that

$$\lim_{k \to 0} \Pi_{44}(0, \mathbf{k}) = \Pi_{44}(0, 0) = e^2 (\partial / \partial \mu) \{ \mathrm{Sp}\, \gamma_4 G(xx) \} = -e^2 \partial \rho / \partial \mu,$$

where ρ is the charge density in the u_ν space. We have thus also shown that Eq. (3.11) of reference 1 for the Debye radius remains valid when all quantum and relativistic corrections are taken into account.

POSSIBLE TRANSMISSION OF ELECTROMAGNETIC WAVES THROUGH A METAL IN A STRONG MAGNETIC FIELD

O. V. KONSTANTINOV and V. I. PEREL'

Leningrad Physico-technical Institute, Academy of Sciences U.S.S.R.

Submitted to JETP editor, June 24, 1959

J. Exptl. Theoret. Phys. (U.S.S.R.) 38, 161-164 (January, 1960)

It is shown that an electromagnetic wave propagating along a magnetic field can penetrate a metal plate perpendicular to the field if the Larmor frequency is higher than the frequency of the propagating wave and much higher than the collision frequency, and if the electron Larmor radius is smaller than the wavelength in the metal.

IT is well known that an electromagnetic wave characterized by a frequency ω which is smaller than the plasma frequency ω_0 cannot propagate through a plasma. Under these conditions the square of the index of refraction of the plasma is negative. If there is a magnetic field the refractive index for the wave which propagates along the field (if $|\omega_c^* \pm \omega|/\nu \gg 1$, where ν is the collision frequency) is given by:

$$N_{0\pm}^2 = 1 - \omega_0^2/\omega(\omega \mp \omega_c^*). \quad (1)$$

Here ω_c^* is the Larmor (cyclotron) frequency of the electron. The symbol $\pm$ denotes the two opposite senses of the circular polarization. It is apparent that when $\omega < \omega_c^*$ the wave that corresponds to N_{0-} can propagate through the plasma. Thus, it is reasonable to assume that a wave characterized by a frequency $\omega < \omega_c^*$, where $(\omega_c^* - \omega)/\nu \gg 1$, can propagate through a metal plate if there is a strong magnetic field perpendicular to the surface of the plate. If a plane-polarized wave strikes the plate at normal incidence (to the surface), a circularly polarized wave is transmitted through the plate; the refractive index (consequently the amplitude of the wave) depends on the magnetic field.

The expression for the refractive index given above holds for a classical electron gas in which spatial dispersion is neglected. For the electron concentrations typical of semi-metals, and even more so in metals, the refractive index for the transmitted wave can be very large, so that effects due to spatial dispersion may be quite significant.

In the present work we investigate the effect of spatial dispersion on transmission of the wave. The analysis is carried out for the simple case of a totally degenerate electron gas characterized by a quadratic isotropic dispersion relation. Collisions are taken into account in approximating the relaxation time; it is assumed that $(\omega_c^* - \omega) \gg \nu$. The analysis indicates that the spatial-dispersion correction is small if the following condition is satisfied:

$$\gamma = (r_0/\lambda)^2 (1 - \omega/\omega_c^*)^{-2} < 1/2.$$

Here r_0 is the Larmor radius of an electron at the Fermi surface and λ is the wavelength in the medium. When $\gamma > 2/3$ there is strong damping due to spatial dispersion and the usual expression for N_- is incorrect. In this case the transmitted wave is attenuated in a distance of several Larmor radii; hence the case $\gamma > 2/3$ is not of interest. When $\gamma < 1/2$ the amplitude of the transmitted wave is determined by the Fresnel formula and the boundary effects associated with the spatial dispersion are not important if the thickness of the plate is greater than several Larmor radii.

The dependence of $\log N_{0-}$ on $\log(\omega_c/\omega - m^*/m)$ is shown in Fig. 1 for a vacuum wavelength of 2 cm and for different electron concentrations (n_0). In this figure m^* is the effective mass of the electron, m is the mass of the free electron* and $\omega_c = eH/mc$. The dashed line denotes $\gamma = 1/2$. The region in which transmission can take place lies below the dashed line. The values of the magnetic field are given on the lower abscissa axis. It is apparent that at concentrations corresponding to those in metals (10^{22} cm^{-3}) transmission can be observed only in extremely high (approximately 3×10^5 oe) magnetic fields; the conditions for transmission are much more favorable at lower concentrations.

*The free electron mass m is introduced here only for convenience in making estimates; obviously the effect depends only on the effective mass m^*.

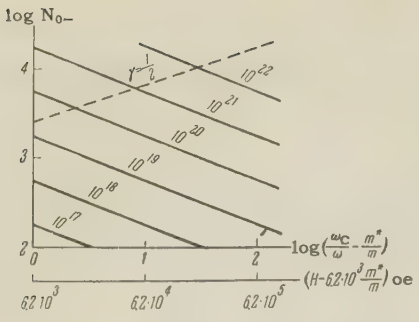

FIG. 1

The imaginary part of the refractive index is given by

$$N'_- = N_{0-}\nu/2\,(\omega_c^* - \omega), \qquad \omega_c^* = eH/m^*c.$$

A ray transmitted at normal incidence through a plate of thickness l, which is perpendicular to a magnetic field, will be attenuated (in power) by a factor $16\,N_0^{-2}\exp\{-2N'_-\omega l/c\}$. If the attenuation is not to be excessive the thickness of the plate must be of order

$$l_0 = \left(\frac{\nu}{\omega_c^* - \omega}\frac{\omega}{c}N_{0-}\right)^{-1} = \lambda\,\frac{\omega_c^* - \omega}{\nu},$$

where λ is the wavelength in the medium.

Taking the values $n_0 = 10^{22}$ cm^{-3}, $H = 3\times10^5$ oe, and $\nu = 3\times10^9$ sec^{-1}, we find $l_0 = 3\times10^{-2}$ m/m* cm. Thus, there are no serious difficulties from this point of view.

The expression for the transmission coefficient given above applies when $l \gtrsim l_0$. If however, $l \ll l_0$, it is necessary to take account of effects due to the interference of waves which are multiply reflected from the boundaries; in this case the expression for the transmission coefficient becomes more complicated. We shall neglect these effects. When the condition $l \gtrsim l_0$ is satisfied the transmission of the wave through each boundary can be considered separately.

We now demonstrate the validity of the statements made above. If an electromagnetic wave is normally incident on the surface of a metal in the presence of a magnetic field perpendicular to the surface, the electric field $E(z)$ associated with the wave inside the metal is given by[1,2]

$$E_-(z) = \frac{E'_-(0)}{\pi}\int_{-\infty}^{\infty}\frac{e^{ikz}dk}{k^2 - \omega^2c^{-2}\varepsilon_-(k,\,\omega)}. \qquad (2)$$

Here, for simplicity it is assumed that the reflection of electrons from the surface of the metal is specular. The z axis is parallel to the magnetic field inside the metal.

$$E_-(z) = E_x(z) - iE_y(z),\ \varepsilon_- = \varepsilon_{xx} - i\varepsilon_{xy},$$

and $E'_-(0)$ is the field derivative at the boundary of the metal

$$\varepsilon_-(k,\,\omega) = 1 + (\varepsilon_0 - 1)\,F(q),$$

$$F(q) = \frac{3}{4}\left[\frac{2}{q^2} + \frac{1}{q}\left(\frac{1}{q^2} - 1\right)\ln\frac{1-q}{1+q}\right];$$

$$q = kv_F/\Omega, \qquad \Omega = \omega_c^* - \omega - i\nu, \quad \varepsilon_0 = 1 + \omega_0^2/\omega\Omega, \qquad (3)$$

where v_F is the electron velocity at the Fermi surface. Using the new variable of integration in (2), we have

$$E_-(z) = \frac{E'_-(0)}{\pi}\int_C \frac{\exp(iq\Omega z/v_F)}{q^2 - \gamma F(q)}\,dq\,\frac{v_F}{\Omega}. \qquad (4)$$

In this treatment the displacement current is neglected. The parameter $\gamma = \epsilon_0(\omega/c)^2(v_F/\Omega)^2$; when $\omega_c^* \gg \omega$, $\gamma = (r_0/\lambda)^2$, where r_0 is the electron Larmor radius and λ is the wavelength in the medium.

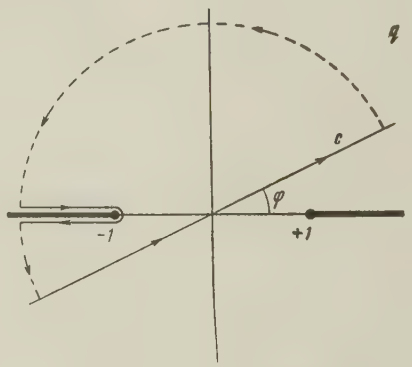

FIG. 2. Path of integration.

The contour C passes through the origin and is inclined to the real axis at an angle $\varphi = \tan^{-1}[\nu/(\omega_c^* - \omega)]$. The function $F(q)$ has branching points at $q = \pm1$. Hence we take cuts along the real axis from $-\infty$ to -1 and from 1 to ∞. It is evident from Fig. 2 that the integral of interest to us can be reduced to the sum of the residues at the poles inside the closed contour which has been indicated and the integral which encloses the left cut. A calculation shows that $|F(q)| < 2$ on the real axis for $q \geq 1$. Hence, when $|\gamma| < 1/2$, in accordance with the Rouché theorem[3], the equation $q^2 - \gamma F(q) = 0$ has two roots in the entire complex plane taken with the cuts. When $|\gamma| < 1/2$ these roots can be found by expanding $F(q)$ in powers of q. These roots are $q_{1,2} = \pm\sqrt{\gamma}$. The root $q_1 = +\sqrt{\gamma}$ lies inside the closed contour. Thus

$$E_-(z) = N^{-1}H_-(0)\exp(iN\omega z/c) + A(z), \qquad (5)$$

where $N = (\omega_0^2/\omega\Omega)^{1/2}$ is the refractive index, $H_-(0) = (ic/\omega)\,E'_-(0)$ is the magnetic field at the

boundary and $A(z)$ is the integral over the contour which goes around the left cut.

When $|\gamma| < 1/2$

$$A(z) \approx \frac{1}{N} H_-(0)\gamma^{3/2}\frac{3}{2}\int_1^\infty \exp\left(iq\frac{\Omega}{v_F}z\right)\frac{1}{q^5}(1-q^2)\,dq.$$

When $z \gg v_F/(\omega_c^* - \omega)$

$$A(z) = \frac{3}{N} H_-(0)\gamma^{3/2}\left(\frac{v_F}{z\Omega}\right)^2 \exp\left(i\frac{\Omega}{v_F}z\right) + O\left[\left(\frac{v_F}{z\Omega}\right)^3\right].$$

Thus, the term $A(z)$, which describes the effect of the boundary, is small when $z \gg v_F/|\Omega|$, i.e., at distances that are much larger than the Larmor radius of the electron (for $\omega_c^* \gg \omega$). The transmitted wave is attenuated by a factor of e in a distance $2v_F/\nu\sqrt{\gamma}$. We may note that the amplitude of the transmitted wave is the same as that given by the Fresnel formulas, while the refractive index is determined by the root of the dispersion equation $k^2 - \omega^2 c^{-2}\epsilon_-(k, \omega) = 0$, as though the medium were homogeneous.

A numerical solution of this equation for $|\gamma| < 2/3$ shows that there are two roots which are in very good agreement with the values of $q_{1,2}$ used above. When $|\gamma| > 2/3$ there are no real roots; the attenuation is large and the wave is not transmitted through the metal.

The above analysis indicates that when the Larmor radius is less than a half wavelength in the medium the effect of spatial dispersion is to distort the field only in the boundary layer, which is several Larmor radii in thickness. Hence, one can neglect spatial dispersion in estimating the effect of deviations of the magnetic field (from the normal to the surface) on transmission. If the wave propagates at an angle φ to the magnetic field (normal to the surface), the refractive index for the transmitted wave is given by the expression $N_- = \omega_0^2/\omega_c^*\omega\cos\varphi$ where $\omega_0 \gg \omega_c \gg \omega$ and $\varphi \ll \pi/2$.

Thus, the accuracy of orientation of the magnetic field is not of great importance.

We may note that an expression for the refractive index which takes account of the anisotropy of the electron mass has been obtained by Gurevich and Ipatova.[4]

The expression for $\epsilon_-(k, \omega)$ in (3) applies when $\hbar\omega_c^* \ll m^* v_F^2/2$. However, the quantum-mechanical expression for $\epsilon_-(k, \omega)$ obtained by the method which has been used by us earlier[5] leads to the expression in (1) for the refractive index for all cases which can be realized in practice, even when $\hbar\omega_c^* \gg m^* v_F^2/2$.

The authors are indebted to L. É. Gurevich, M. Ya. Azbel' and M. I. Kaganov for valuable discussions.

[1] G. E. H. Reuter and E. H. Sondheimer, Proc. Roy. Soc. (London) **A195**, 336 (1948).

[2] M. Ya. Azbel' and M. I. Kaganov, Dokl. Akad. Nauk SSSR **95**, 41 (1954).

[3] B. A. Fuks and B. V. Shabat, Функции комплексного переменного (Functions of a Complex Variable) Gostekhizdat, 1949.

[4] L. É. Gurevich and I. P. Ipatova, JETP **37**, 1324 (1959), Soviet Phys. JETP **10**, 943 (1960).

[5] O. V. Konstantinov and V. I. Perel', JETP **37**, 786 (1959), Soviet Phys. JETP **10**, 560 (1960).

Translated by H. Lashinsky
25

THE BEHAVIOR OF FERMION SPIN IN ELASTIC SCATTERING

A. A. SOKOLOV and M. M. KOLESNIKOVA

Moscow State University

Submitted to JETP editor June 27, 1959

J. Exptl. Theoret. Phys. (U.S.S.R.) 38, 165-171 (January, 1960)

The behavior of spin in the elastic scattering of longitudinally polarized fermions and its dependence on the character of the interaction are investigated. It is shown that in the ultrarelativistic case (or for fermions with zero rest mass) the angle between the spin and the momentum is unchanged in V and A interactions, but the spin flips in S, P, and T interactions.

1. INTRODUCTION

THE motion of a free fermion will be described by a Dirac wave function that takes spin orientation into account,[1,2]

$$\psi = L^{-3/2}\sum_s C_s b_s e^{-i\varepsilon\epsilon Kt + i\mathbf{kr}}, \tag{1}$$

where the quantity $\epsilon = \pm 1$ characterizes the sign of the energy, and $s = \pm 1$ is twice the projection of the spin in the direction of the motion.

We represent the spin matrix b_s in the form

$$b_s = \frac{1}{\sqrt{2}}\begin{pmatrix} A_1 & B_1 \\ A_1 & B_2 \\ A_2 & B_1 \\ A_2 & B_2 \end{pmatrix}. \tag{2}$$

Here the energy K of the fermion is connected with its momentum $\mathbf{k}$ and rest mass k_0 by the well-known relation $K = \sqrt{k^2 + k_0^2}$. The rest of the quantities in (2) are given by

$$A_1 = \sqrt{1 + k_0/\varepsilon K}, \quad A_2 = s\varepsilon\sqrt{1 - k_0/\varepsilon K},$$

$$B_1 = s\cos\theta_s e^{-i\varphi/2} \quad B_2 = s\sin\theta_s e^{i\varphi/2}, \quad \theta_s = \theta/2 - \pi(1-s)/4,$$

where θ and φ are the spherical angles of the vector $\mathbf{k}$.

The polarization properties of the fermions will be characterized by the four-component polarization pseudovector[3]

$$\zeta_\mu = K\int \psi^+\sigma_\mu\psi\, d^3x, \tag{3}$$

where the matrix σ_μ of the spin pseudovector is equal to σ and $\sigma_t = \rho_1$. Substituting (1) in (3) for the components of the polarization pseudovector, we find the values

$$\zeta_3 = Ks_3 = s_0^{-1}K(C_1^+C_1 - C_{-1}^+C_{-1}) \tag{4}$$

for the longitudinal component, directed along the momentum, and

$$\zeta_1 = Ks_1 = s_0^{-1}k_0(C_{-1}^+C_1 + C_1^+C_{-1}) = k_0\cos\delta\sqrt{1-s_3^2},$$
$$\zeta_2 = Ks_2 = s_0^{-1}k_0 i(C_{-1}^+C_1 - C_1^+C_{-1}) = k_0\sin\delta\sqrt{1-s_3^2} \tag{4a}$$

for the transverse components. Here δ is the phase difference between the complex amplitudes C_1^+ and C_{-1}, and the quantity

$$s_0 = C_1^+C_1 + C_{-1}^+C_{-1} \tag{5}$$

inversely proportional to the normalization coefficient. The time component of the polarization is connected with the longitudinal component by the relation $\zeta_t = (k/K)\zeta_3$.

From this it is evident that the polarization properties of free fermions will be determined by two quantities: by the angle δ, characterizing the direction of the spin pseudovector $\mathbf{s}$ in the plane perpendicular to the momentum, where

$$\cos\delta = \zeta_1/\sqrt{\zeta_1^2+\zeta_2^2}, \quad \sin\delta = \zeta_2/\sqrt{\zeta_1^2+\zeta_2^2}, \tag{6}$$

and by the angle α between $\mathbf{s}$ and the direction of the momentum $\mathbf{k}$, where

$$\tan\alpha = \frac{\sqrt{\zeta_1^2+\zeta_2^2}}{\zeta_3} = \frac{k_0}{K}\frac{\sqrt{1-s_3^2}}{s_3}. \tag{7}$$

In investigating the transverse component, Ascoli[4] omitted from an analogous formula the factor k_0/K, since he considered the direction of a 3-component unit spin matrix

$$s_0\left(\frac{K}{k_0}s_1, \frac{K}{k_0}s_2, s_3\right).$$

As can be seen from (4) and (5), the modulus of the vector $\mathbf{s}$ is

$$|s| = \sqrt{s_3^2 + k_0^2K^{-2}(1-s_3^2)}, \tag{8}$$

where $k_0^2/K^2 = 1-\beta^2$, and $c\beta$ is the velocity of the particle.

2. CALCULATION OF THE MATRIX ELEMENTS INCLUDING POLARIZATION EFFECTS

In investigating the transition of an electron from one initial state ($\epsilon = 1$, s, **k**) to some other final state ($\epsilon' = 1$, s', **k'**) we have to calculate matrix elements of the form

$$\gamma'_{\mu\nu} = b'^{+}\gamma_{\mu\nu}b = \tfrac{1}{2}\bar{\rho}_{\mu}(s', s)\,\bar{\sigma}_{\nu}(s', s), \tag{9}$$

where

$$\bar{\rho}_{\mu}(s', s) = (A_1'^{+}A_2'^{+})\,\sigma'_{\mu}\begin{pmatrix}A_1\\A_2\end{pmatrix}, \tag{10}$$

$$\bar{\sigma}_{\nu}(s', s) = (B_1'^{+}B_2'^{+})\,\sigma'_{\nu}\begin{pmatrix}B_1\\B_2\end{pmatrix}, \tag{11}$$

and σ'_{μ}, where $\sigma'_4 = 1$, are the well known two-rowed Pauli matrices. These formulas represent a generalization of the formulas given in reference 2 for the case of not only longitudinal, but also transverse polarization.

Without loss of generality, we can let the initial momentum **k** be directed along the z axis ($\theta = \varphi = 0$) and the final momentum **k'** be localized in the plane xz ($\varphi' = 0$). Then in elastic particle scattering (K' = K) we have

$$\bar{\rho}_{4,3}(s', s) = (1 \pm ss') + \frac{k_0}{K}(1 \mp ss'), \tag{12}$$

$$\bar{\rho}_{2,1}(s', s) = \frac{k}{K}s(1 \mp ss')\begin{pmatrix}-i\\1\end{pmatrix}, \tag{13}$$

$$\bar{\sigma}_{4,n}(s', s) = \tfrac{1}{2}(1 + ss')\begin{pmatrix}\cos(\theta'/2)\\ s(n_x + isn_y)\sin(\theta'/2) + n_z\cos(\theta'/2)\end{pmatrix}$$

$$+ \tfrac{1}{2}(1 - ss')\begin{pmatrix}-s\sin(\theta'/2)\\ (n_x + isn_y)\cos(\theta'/2) - n_z\sin(\theta'/2)\end{pmatrix}, \tag{14}$$

where **n** is some three-component unit vector and θ' is the angle between the momenta **k'** and **k**.

3. THE BEHAVIOR OF FERMION SPIN IN ELASTIC SCATTERING

The interaction of a fermion with a fixed center can be described by the formula

$$U = \gamma u(\mathrm{r}).$$

The matrices $\gamma = \gamma_{\mu\nu}$ determine the character of the interaction (V, A, S, T, P).

We have the following expression for the differential effective cross section, taking polarization effects into account:

$$d\sigma_{s_1' s'} = C'^{+}_{s_1} C'_{s'} \frac{K^2}{4\pi^2 c^2 \hbar^2} |u_{\mathbf{k'k}}|^2 d\Omega, \tag{15}$$

where

$$u_{\mathbf{k'k}} = \int e^{i\mathbf{r}(\mathbf{k}-\mathbf{k'})} u(\mathbf{r})\, d^3x,$$

$$C'_{s'} = b'^{+}(s')\gamma b(s), \qquad C'^{+}_{s_1} = b^{+}(s)\gamma b(s_1'),$$

and in the calculation of the summed (over the spins) differential effective cross section we must put into formula (15)

$$C'^{+}_{s_1} C'_{s'} \to s'_0, \tag{15a}$$

where s'_0 is determined by equality (5).

Let us examine the scattering of longitudinally-polarized fermions. We suppose that before the scattering the spin vector **s** was directed exactly along the particle momentum **k**, that is, $C_{S=1} = 1$, $C_{S=-1} = 0$. We then find what angle the vector **s'** of the scattered fermion will make with the direction of the new momentum **k'**.

The amplitudes characterizing the spin state **s'** of the scattered particle will be respectively

$$C'_1 = b'^{+}\gamma_{\mu\nu}b = \tfrac{1}{2}\bar{\rho}_{\mu}(1, 1)\,\bar{\sigma}_{\nu}(1, 1),$$
$$C'_{-1} = \tfrac{1}{2}\bar{\rho}_{\mu}(-1, 1)\,\bar{\sigma}_{\nu}(-1, 1). \tag{16}$$

It must first be noticed that the representation of the 16 independent Dirac matrices in the form of a product of the matrices ρ_μ and σ_ν (see references 1 and 2) and not in the form of the standard γ matrices is convenient in the sense that the behavior of the spin (especially in the ultrarelativistic case) depends on the ρ_μ matrices.

a) We consider first the interactions proportional to the matrices ρ_1 and ρ_2. They correspond to the time component of the axial vector interaction $A^T = \rho_1\sigma_4$, the spatial component of the vector interaction $V^S = \rho_1\sigma_n$ (describing, for example, the scattering of an electric charge by a magnetic field), the pseudoscalar interaction $P = \rho_2\sigma_4$, and the time (more precisely, the time-space) component of the tensor interaction $T^T = \rho_2\sigma_n$, describing, for example, the scattering of a magnetic moment by an electric field.

As is evident from (14), the interactions V^S and A^T, proportional to the matrix ρ_1, lead to a matrix element that contains the factor $(1+ss')$. In this case, if the momentum vector **k** and the spin vector **s** are parallel (s = 1) before the scattering, then after the scattering the new vectors **k'** and **s'** are still parallel (s' = 1). For the interactions P and T^T, which are proportional to the matrix ρ_2, the matrix element contains the factor $(1-ss')$. Therefore after the scattering the vectors **k'** and **s'** must be antiparallel (s = 1, s' = −1).

For the quantity s'_0 [see (15a)], characterizing the dependence of the summed (over spins) effective cross section, we find, respectively, the following four values, which depend on the character of the interaction (A^T, P, V^S, T^T):

$$s'_0 = \frac{1}{2}\frac{k^2}{K^2}\begin{pmatrix}1 \pm \cos\theta'\\ n^2 \pm N^2\end{pmatrix} \tag{17}$$

where

$$N^2 = 2\sin\theta' n_z n_x - \cos\theta'(n_x^2 + n_y^2 - n_z^2). \tag{18}$$

b) Let us now consider the interactions proportional to the matrices ρ_4 and ρ_3. To them belong the time component of the vector interaction $V^T = \rho_4\sigma_4$ (which describes, for example, the scattering of an electric charge by an electric field), the spatial component of the axial vector interaction $A^S = \rho_4\sigma_n$, the scalar interaction $S = \rho_3\sigma_4$, and the spatial component of the tensor interaction $T^T = \rho_3\sigma_n$ (which describes, for example, the scattering of a magnetic moment by a magnetic field).

In the case of the V^T and S interactions it is easy to show with the help of (4), (4a), and (6) that $\xi_2' = 0$, $\cos\delta' = -1$, i.e., the spin will lie in the plane of the vectors $\mathbf{k}$ and $\mathbf{k}'$ and in the quadrants for which $x' < 0$ (see figure). For

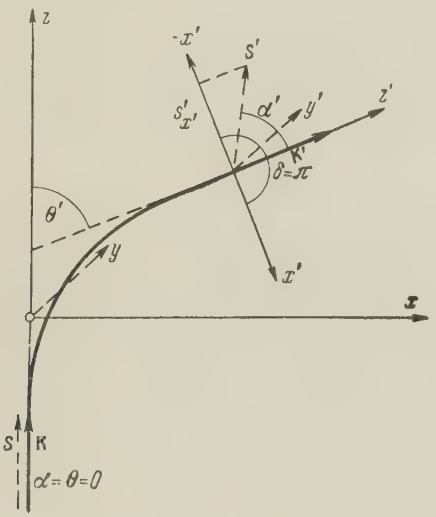

the number s_0' and also for the angle α' between the spin $\mathbf{s}'$ and momentum $\mathbf{k}'$, which is directed along the z' axis, we find correspondingly the values

$$s_0' = C_1'^2 + C_1'^2 + C_{-1}'^2 + C_{-1}'^2 = \tfrac{1}{2}[(1 + k_0^2/K^2) \pm \cos\theta'(1 - k_0^2/K^2)],$$

$$\tan\alpha' = 2\frac{k_0^2 K^{-2}\sin\theta'}{(1 + k_0^2/K^2)\cos\theta' \pm (1 - k_0^2/K^2)}, \qquad (19)$$

where the plus sign corresponds to the vector interaction and the minus sign to the scalar.

In the nonrelativistic case $k_0^2/K^2 = 1$ both interactions, as one might expect, lead to the unique result

$$s_0' = 1, \quad \tan\alpha' = \tan\theta' \quad \text{or} \quad \alpha' = \theta'. \qquad (20)$$

From this, keeping in mind that the spin lies in the quadrants where $x' < 0$, we find, in particular, that for the scattering of an electric charge by an electric field the spin in the nonrelativistic case conserves its original direction (see reference 5), that is, in the specific case mentioned, the direction of the original momentum, $\mathbf{s}' \parallel \mathbf{k}$.

In the ultrarelativistic case $k_0^2K^2 \to 0$, with the help of (19) we find for the V^T interaction

$$\tan\alpha' = \frac{2k_0^2}{K^2}\tan\frac{\theta'}{2}. \qquad (21)$$

For the S interaction we have

$$\tan\alpha' = -\frac{2k_0^2}{K^2}\cot\frac{\theta'}{2}. \qquad (22)$$

From this it follows that as the energy increases the spin in the V^T interaction begins to turn around toward the direction of $\mathbf{k}'$ and coincides with this direction in the limiting case $k_0^2/K^2 = 0$.

In the S interaction, as the energy increases the spin begins to turn toward the direction opposite to that of the momentum, and in the limiting case $k_0^2/K^2 = 0$ the vectors $\mathbf{k}'$ and $\mathbf{s}'$ must be antiparallel ($s' = -1$).

For the A^S and T^S interactions we find

$$s_0' = \tfrac{1}{2}[n^2(1 + k_0^2/K^2) \pm (1 - k_0^2/K^2)N^2], \qquad (23)$$

$$\tan\alpha' = \frac{2k_0^2}{K^2}\frac{\sqrt{n^4 - N^4}}{\pm n^2(1 - k_0^2/K^2) + (1 + k_0^2/K^2)N^2}, \qquad (24)$$

where the plus sign corresponds to A^S and the minus sign to T^S and the number N^2 is determined by the formula (18).

In addition, in this case $\xi_2' = (2k_0^2/s_0'K)n_Z n_Y \neq 0$ and therefore the polarization vector will form some angle with the $(\mathbf{k}\mathbf{k}')$ plane. In the ultrarelativistic case $k_0^2/K^2 = 0$ and therefore the angle α' will tend to zero ($s' = 1$) for the A^S interaction and to 180° for the T^S interaction ($s' = -1$).

In that way, we see that in the very relativistic case, when $k_0^2/K^2 \to 0$, only the V and A interactions, proportional to the matrices ρ_1 and ρ_4 conserve the parallelism of spin and momentum in the scattering process ($s' = s = 1$). In the case of S, T, and P interactions, proportional to ρ_2 and ρ_3, the spin after scattering changes its direction relative to the corresponding momentum to lie opposite ($s' = -s = -1$).

It is possible that this is connected with the fact that in the theory of the spin-oriented neutrino[2,6,7] where a spin reversal relative to the momentum is excluded because it would mean the transition of a neutrino to a nonexistent state, only the V and A variants are allowed.

4. MIXED INTERACTIONS

We want to apply the formulas obtained to the investigation of the scattering of fermions in the presence of a linear combination of interactions

referring to different groups, where in the first group we have the interactions proportional to ρ_1 and ρ_4, and in the second those proportional to ρ_2 and ρ_3. We have such a combination of interactions, for example, in the analysis of the scattering of a particle which has an electric charge e and a "true" magnetic moment μ from a fixed point center having either an electric charge e′ or a magnetic moment μ'.

In this case the interaction energy has the form

$$U = e(\varphi - (\alpha A)) - \mu(\rho_3(\sigma H) + \rho_2(\sigma E)), \qquad (25)$$

where the field created by the point center is determined by the expression

$$\varphi = \frac{e'}{r}, \qquad \mathbf{E} = -\nabla\frac{e'}{r}, \qquad \mathbf{A} = \nabla\times\frac{\mu'}{r},$$

$$\mathbf{H} = \nabla\times\left[\nabla\times\frac{\mu'}{r}\right].* \qquad (26)$$

First we consider the behavior of the spin in the scattering of a particle with an electric charge ($e' \neq 0$, $\mu' = 0$).

Then for the matrix element entering in (15), we find, setting $s = 1$

$$C'_{s'=1} = ee'\cos\frac{\theta'}{2}, \qquad (27)$$

$$C'_{s'=-1} = -e'\left(e\frac{k_0}{K} - 2\frac{k^2}{K}\mu\right)\sin\frac{\theta'}{2}, \qquad (28)$$

from which we get an expression for the effective cross section

$$d\sigma = \frac{d\Omega e'^2}{4\sin^4(\theta'/2)\,k^4c^2\hbar^2}\left[e^2\left(K^2\cos^2\frac{\theta'}{2} + k_0^2\sin^2\frac{\theta'}{2}\right)\right.$$
$$\left. + 4(k^4\mu^2 - k_0 e\mu k^2)\sin^2\frac{\theta'}{2}\right]. \qquad (29)$$

In addition, it is easy to show that the spin vector will lie in the plane of the vectors $\mathbf{k}$ and $\mathbf{k}'$, so that the tangent of the angle which the spin vector will form with the momentum $\mathbf{k}'$, will be given by the expression

$$\tan\alpha' = \frac{k_0\,|(e^2k_0 - 2k^2\mu e)\sin\theta'|}{e^2\cos^2(\theta'/2)K^2 - \sin^2(\theta'/2)(ek_0 - 2k^2\mu)^2}. \qquad (30)$$

It is evident from formulas (29) and (30) that in the nonrelativistic case $k \ll K \sim k_0$ a fundamental role will be played by the Coulomb interaction, i.e., V^T, and that therefore according to (20) the spin should preserve its direction, along the original momentum ($\alpha' = \theta'$). Then in the ultrarelativistic case $k_0 \ll K$, but with $\mu k \ll e$, the spin will turn aside toward the momentum $\mathbf{k}'$. In the case of very large energies $\mu k \gg e$, when the dipole terms, proportional to ρ_2, play a fundamental role, the spin has to continue its turning until it has an orientation opposite to the final momentum $\mathbf{k}'$ ($s' = -1$).

Finally, we consider the spin behavior in the scattering of particles having an electric charge and a magnetic moment (e, μ) on a fixed magnetic moment ($\mu' \neq 0$, $e' = 0$). Here we distinguish two cases:

a) The magnetic moment μ' of the scattering center is parallel to the initial momentum ($\mu'_Z = \mu'$, $\mu'_X = \mu'_Y = 0$). Then

$$C'_1 = -(e + 2\mu k_0)\frac{2k^2\mu'}{K}\sin^2\frac{\theta'}{2}\cos\frac{\theta'}{2}, \quad C'_{-1} = 0, \qquad (31)$$

and for the effective cross section we find the value

$$d\sigma = c^{-2}\hbar^{-2}\mu'^2(e + 2\mu k_0)^2\cos^2(\theta'/2)\,d\Omega', \qquad (32)$$

i.e., in this case the scattering of a magnetic moment μ from a magnetic moment μ' will proceed just as the scattering of a charge $e_1 = 2\mu k_0$ from a magnetic moment μ' without the spin flip relative to the momentum $\mathbf{k}'$. This is connected with the circumstance that the matrix element $\bar{\sigma}_n(-1, 1)$ describing the spin-flip scattering, which should give a basic dipole contribution to the effective cross section at ultrarelativistic energies $k \gg k_0$, goes to zero in the given case.

b) The magnetic moment μ' of the scattering center is perpendicular to the vector $\mathbf{k}$ ($\mu'_Z = 0$, $\mu'^2_X + \mu'^2_Y = \mu'^2 \neq 0$). Then

$$C_1 = -2\frac{k^2}{K}\sin\frac{\theta'}{2}\left[\mu'_x(e + 2\mu k_0)\sin^2\frac{\theta'}{2}\right.$$
$$\left. + i\mu'_y\left(e + 2\mu k_0\sin^2\frac{\theta'}{2}\right)\right],$$
$$C'_{-1} = -4\mu\mu'_y ik^2\sin^2\frac{\theta'}{2}\cos\frac{\theta'}{2}. \qquad (33)$$

From this we find the following values for the effective cross sections without spin flip ($s' = s = 1$):

$$d\sigma_{s'=1} = \frac{\mu'^2_x(e + 2\mu k_0)^2\sin^4(\theta'/2) + \mu'^2_y(e + 2\mu k_0\sin^2(\theta'/2))^2 d\Omega'}{c^2\hbar^2\sin^2(\theta'/2)} \qquad (34)$$

and with spin flip ($s' = -1$)

$$d\sigma_{s'=-1} = 4(\mu/c\hbar)^2\mu'^2_y K^2\cos^2(\theta'/2)\,d\Omega'. \qquad (35)$$

From formula (34) it is evident that in the case $2\mu k_0 \ll e$ the scattering without spin flip at arbitrary energies is basically due to the interaction of the charge e with the magnetic moment μ'.

The dipole terms should appear at higher energies, $\mu K \gg e$, when the scattering of a fermion takes place with spin flip.

Our final formulas may find application in in-

*If we consider a smearing of the scattering center, it is necessary to make a change which takes into account the contact term too[8]

$$\frac{1}{r} \to \frac{1}{r} - \frac{2\pi\overline{r_1^2}}{3}\delta(r)$$

where $\overline{r_1^2}$ is the mean square "smearing." This refinement will not be reflected in the investigation of the behavior of the spin in the scattering.

vestigating the scattering of polarized electrons, which along with the charge e must possess a vacuum, "true" magnetic moment, and also in the scattering of polarized protons or neutrons (e = 0). It should be noted that experimental investigations of spin behavior in the scattering of polarized fermions may help determine the character of the interaction.

[1] A. A. Sokolov, J. Phys. (U.S.S.R.) **9**, 363 (1945).

[2] A. A. Sokolov, Введение в квантовую электродинамику (Introduction to Quantum Electrodynamics) Fizmatgiz, 1958.

[3] Sokolov, Ternov, and Loskutov, JETP **36**, 930 (1959), Soviet Phys. JETP **9**, 657 (1959).

[4] G. Ascoli, Z. Physik **150**, 407 (1958).

[5] H. A. Tolhoek, Revs. Modern Phys. **28**, 277 (1956).

[6] A. A. Sokolov and B. K. Kerimov, Ann. Phys. **2**, 794 (1957).

[7] A. A. Sokolov, Nuclear Phys. **9**, 420 (1959).

[8] E. Salpeter, Phys. Rev. **89**, 92 (1953).

Translated by Wm. Ramsay
26

ELECTROMAGNETIC TRANSITION PROBABILITIES AND STATIC MOMENTS OF ODD-ODD ATOMIC NUCLEI

D. A. VARSHALOVICH

Leningrad Physico-technical Institute, Academy of Sciences, U.S.S.R.

Submitted to JETP editor July 2, 1959

J. Exptl. Theoret. Phys. (U.S.S.R.) **38**, 172-179 (January, 1960)

Formulas are given relating the probabilities of gamma transitions with the static moments of odd-odd and neighboring odd spherical nuclei, assuming multiplet level structure. A rule for the relative intensities of transitions to levels of the same multiplet is given, which is analogous to the rule for relative intensities of transitions to levels of the same rotational band in deformed nuclei. This rule facilitates the determination of the spins and state configurations of odd-odd nuclei. Examples are discussed. The validity of the assumptions made is confirmed by the satisfactory agreement between the experimental and theoretical values of the magnetic dipole moments for a large group of odd-odd nuclei.

1. INTRODUCTION

THE collective model explains in a satisfactory way not only the static, but also the dynamic properties of atomic nuclei. The best quantitative agreement between the experimental and theoretical values of the γ transition probabilities is reached in the transitions associated with the rotational levels of deformed nuclei.[1] This is due to the fact that in the collective model the internal wave functions (describing the internal motion of the nucleons in the nucleus) of states of the same rotational band are identical. Therefore the relative intensities of transitions with the same multipole order to levels of the same rotational band do not depend on the exact form of the wave functions, and the transition probabilities within a given rotational band are determined directly by the static moments μ_1 and q_2.[2]

We shall show that one can obtain analogous relative transition probabilities for spherical nuclei with odd Z and N, since it is possible to separate out those states in the level scheme of these nuclei whose wave functions have in first approximation identical radial dependence and differ only in their angular parts.

The properties of odd-odd nuclei are mainly determined by the quantum states of the last unpaired proton, j_p^π, and neutron, j_n^π, which move in the spherical field of the even-even core. According to the independent particle model, the states (j_p^π, j_n^π) will be degenerate with respect to the total angular momentum $I = j_p + j_n$. The remaining interaction between the unpaired nucleons, i.e., the interaction which does not enter in the self-consistent potential, removes the degeneracy by splitting each such state into $2j_i + 1$ levels ($j_i = \min\{j_p, j_n\}$), corresponding to all possible values of I. A system of levels having the same one-particle configuration (j_p^π, j_n^π) and the same parity $\pi = \pi_p\pi_n$, and differing only by the total spin I, is called a multiplet. The remaining interaction, however, leads to some configuration mixing. Each state $(j_p^\pi, j_n^\pi)\, I^\pi$, described by the wave function

$$\Phi(j_p j_n IM) = \sum_{m_p m_n} C^{IM}_{j_p m_p j_n m_n} \Psi_{j_p m_p}(\mathbf{r}_p)\, \Psi_{j_n m_n}(\mathbf{r}_n) \quad (1)$$

($\Psi_{j_p m_p}$ and $\Psi_{j_n m_n}$ are the wave functions of the unpaired proton and neutron, $C^{IM}_{j_p m_p j_n m_n}$ is a Clebsch-Gordan coefficient) has an admixture of states belonging to other multiplets but possessing the same total angular momentum and parity I^π:

$$\Psi(IM) = \alpha_0 \Phi_0(j_p j_n IM) + \sum_i \alpha_i \Phi_i(j_p' j_n' IM). \quad (2)$$

The mixing of multiplets in odd-odd nuclei is similar to the mixing of rotational bands in deformed nuclei.[3]

We shall consider only those cases in which the residual interaction between p and n is small in comparison with the single-particle energies given by the self-consistent field of the nucleus. The admixture of other configurations is therefore small, $\alpha_i \ll \alpha_0$, and the levels of the odd-odd nuclei can be characterized by the quantum numbers j_p^π and j_n^π. In this classification of states we can divide the γ transitions in odd-odd nuclei into two groups: 1) one- and two-particle transitions between levels

belonging to different multiplets, i.e., transitions in which the state of one or both unpaired nucleons is changed, and 2) transitions between levels of the same multiplet, i.e., transitions in which the states of the two unpaired nucleons remain unchanged.

Below we shall discuss transitions of both groups. The mixing of multiplets must be taken into account in those cases where the ground state configuration is such that the γ transition is forbidden or strongly retarded. The probability of allowed transitions is not appreciably affected by the mixing.

2. TRANSITIONS BETWEEN LEVELS OF DIFFERENT MULTIPLETS

Among the transitions between levels belonging to different multiplets, the single-particle transitions play the most important role. The two-particle transitions are strongly retarded in comparison with the single-particle transitions. In most cases the corresponding states, therefore, do not decay directly, but in cascades via several single-particle transitions.

The reduced probability B of a single-particle transition of the type EL or ML in an odd-odd nucleus, $(j_1, j)\, I_1^{\pi} \rightarrow (j_2, j)\, I_2^{\pi}$, can be expressed in terms of the reduced probability of the corresponding single-proton or single-neutron transition $j_1 \rightarrow j_2$ in the neighboring odd nucleus. It is easily shown with the help of the Racah algebra that for pure configurations

$$B(\sigma L, I_1 \rightarrow I_2) = (2I_2 + 1)(2j_1 + 1) \times W^2(j_1 j_2 I_1 I_2; Lj)\, B(\sigma L, j_1 \rightarrow j_2), \quad (3)$$

where the W(abcd; ef) are Racah coefficients, whose numerical values are given in reference 4. It is seen from the expression (3) that the ratio of the reduced probabilities of single-particle transitions of identical multipole order within the same multiplet, $I_1 \rightarrow I_2$ and $I_1 \rightarrow I_3$, does not depend on the precise form of the wave functions, but is determined only by the angular momenta:

$$\frac{B(\sigma L, I_1 \rightarrow I_2)}{B(\sigma L, I_1 \rightarrow I_3)} = \frac{(2I_2 + 1)\, W^2(j_1 j_2 I_1 I_2; Lj)}{(2I_3 + 1)\, W^2(j_1 j_2 I_1 I_3; Lj)}. \quad (4)$$

Relation (4) is the analog of Alaga's rule for deformed nuclei, which determines the relative intensities of transitions to levels of the same rotational band.[2]

Transitions between levels of different rotational bands in deformed nuclei may be forbidden on account of the quantum number K (the projection of the total angular momentum on the axis of symmetry of the nucleus); in analogy to this, we find that in odd-odd spherical nuclei a considerable number of transitions between levels belonging to different multiplets must be retarded as a consequence of j — forbiddenness:

$$|j_2 - j_1| \leqslant L. \quad (5)$$

Formulas (3) and (4) determine the intensity of the γ transitions and facilitate the identification of the states of odd-odd nuclei. These relations were derived under the assumption of pure configurations. The mixing of multiplets leads to a considerable enhancement of the weak components of the γ spectrum, but has almost no effect on the intensive components. Appreciable deviations from the rule (4) may be caused by direct mixing of the initial and final states of the nucleus for I_1^{π} and I_2^{π}.

It should be noted that relations (3) and (4) permit us to estimate the probabilities not only of the allowed transitions, but also of transitions which are forbidden by the principal quantum number n or by the orbital angular momentum l, whereas the direct calculation using the single-particle model is impossible in these cases.

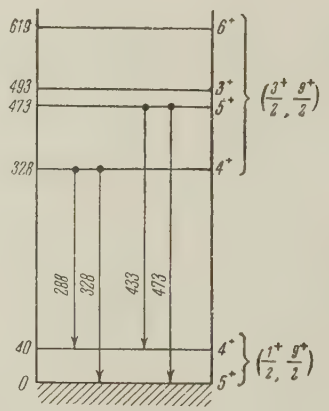

FIG. 1. Level scheme of $_{81}Tl^{208}_{127}$.

For example, in the nucleus $_{81}Tl^{208}$ (reference 5) the γ transitions of the type M1 with energies 288 and 328 kev and the transitions with energies 433 and 473 kev are forbidden by the quantum number l (Fig. 1), since the ground state and the first excited state at 40 kev belong to the configuration $(1/2^+, 3/2^+)$ and the second (328 kev), third (473 kev), fourth (493 kev), and fifth (619 kev) excited states belong to the multiplet $(3/2^+, 3/2^+)$. For the above-mentioned configurations we obtained the following theoretical ratios of the reduced transition probabilities of the type M1:

$$B(M1, 4 \rightarrow 4)/B(M1, 4 \rightarrow 5) = 2.75,$$
$$B(M1, 5 \rightarrow 4)/B(M1, 5 \rightarrow 5) = 0.67.$$

The experimental values for the ratios of these transitions are

$B(288\ \text{kev})\ B(328\ \text{kev}) = 3.30,$

$B(433\ \text{kev})/B(473\ \text{kev}) = 0.34.$

The discrepancy between these figures is due to two factors: firstly, to the presence of an admixture of E2 to the basic radiation of the type M1, and, secondly, to the mixing of states with the same spin and parity. In the case of the first ratio these factors act in opposite directions and compensate each other partially, so that the experimental ratio differs from the theoretical one only by 20%. In the second case both factors lead to a decrease in the ratio, so that the experimental value is about one half of the theoretical value. The comparison of the experimental and theoretical ratios of the intensity of the γ transitions including the effects of the configuration mixing leads to the assignment of the spin 5^+ to the level 328 kev and the spin 4^+ to the level 473 kev.

The rule of relative intensities (4) may be very useful in the analysis of the γ spectra of nuclear reactions with single-particle character, such as the radiative capture processes (n, γ) and (p, γ), and also of the stripping reactions (d, p) and (d, n), since it is easy to determine the configurations of the states of the odd-odd nuclei in these processes.

For example, the capturing state in the capture of a thermal neutron by an odd-proton nucleus has the configuration $(j_p^{\pi}, \frac{1}{2}^+)\, I_1^{\pi}$, where j_p^{π} characterizes the ground state of the target nucleus; the total angular momentum I_1 can have only the two values $j_p \pm \frac{1}{2}$. All intensive γ transitions are single-particle transitions. They are caused by the direct or successive transitions of the neutron captured by the nucleus into the lowest unfilled state. If the configuration and spin of the ground state only of the odd-odd nucleus are known, one can determine which of the two possible values of the spin characterize the capturing state by comparing the intensities of the γ transitions to the ground state and to the neighboring states within the interval of 1 Mev. In many cases it is also possible to identify other intensive transitions. The comparison with the spectrum of the radiative capture of thermal neutrons by the neighboring even-even nucleus is here of great help. In an odd-neutron nucleus the spin and parity of the capturing state are $\frac{1}{2}^+$, so that intensive γ transitions of the type E1 and M1 are possible only to the levels $\frac{1}{2}^{\mp}$ and $\frac{3}{2}^{\mp}$. In the neighboring odd-odd nucleus each of these levels is split up (see Fig. 2). To each intensive component in the spectrum of the odd-neutron nucleus there will thus correspond two or three components of the same multipole order in the spectrum of the odd-odd nucleus. The ratios of the intensities of these components can be calculated theoretically for both possible values of the spin of the odd-odd nucleus in the capturing state $I_1 = j_p \pm \frac{1}{2}$ and all values of j_p. These ratios are listed in the table.

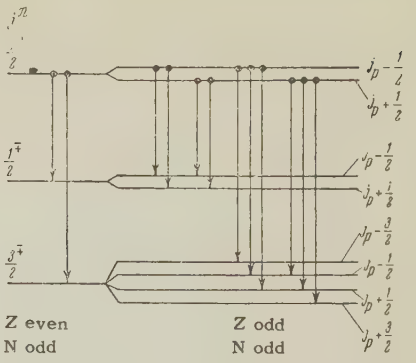

FIG. 2. Scheme of transitions of the type E1(M1) accompanying the capture of thermal neutrons. To each transition in the odd-neutron nucleus correspond several transitions in the neighboring odd-odd nucleus.

Ratios of the reduced probabilities of transitions of the type E1 or M1 to levels of the same multiplet of an odd-odd nucleus in the capture of thermal neutrons*

Initial state	$I_1 = j_p - 1/2$						$I_1 = j_p + 1/2$					
	$j_n = 1/2$		$j_n = 3/2$				$j_n = 1/2$		$j_n = 3/2$			
Final state	$j_p - 1/2$	$j_p + 1/2$	$j_p - 3/2$	$j_p - 1/2$	$j_p + 1/2$	$j_p + 3/2$	$j_p - 1/2$	$j_p + 1/2$	$j_p \mp 3/2$	$j_p - 1/2$	$j_p + 1/2$	$j_p \pm 3/2$
$j_p = 1/2$	0	1	—	—	1	0	0.50	1	—	—	0.20	1
$j_p = 3/2$	0.20	1	0.40	1	1	0	1	1	0	0.07	0.36	1
$j_p = 5/2$	0.29	1	0.77	1	0.80	0	1	0.80	0	0.12	0.43	1
$j_p = 7/2$	0.33	1	0.95	1	0.71	0	1	0.71	0	0.16	0.48	1
$j_p = 9/2$	0.36	1	1	0.94	0.63	0	1	0.67	0	0.19	0.51	1
$j_p = 11/2$	0.39	1	1	0.88	0.56	0	1	0.64	0	0.20	0.53	1

*For large energy differences in heavy nuclei the E2 transitions may be more intensive than the transitions of type M1.

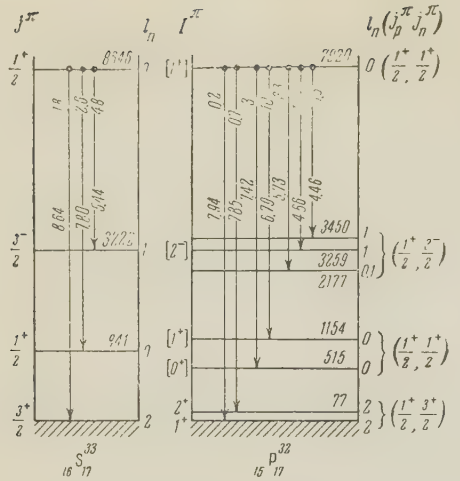

FIG. 3. Scheme of the principal transitions in the reactions $S^{32}(n_{therm}, \gamma)S^{33}$ and $P^{31}(n_{therm}, \gamma)P^{32}$. The values of the spins determined by the relative intensities of the transitions are quoted in square brackets.

Let us consider the spectrum of the γ rays emitted in the reaction $P^{31}(n, \gamma)P^{32}$ and let us compare it with the spectrum of the γ rays in the reaction $S^{32}(n, \gamma)S^{33}$ (reference 6). The nuclei P^{32} and S^{33} have the same number of neutrons. To each intensive transition in the S^{33} nucleus there correspond several transitions in the P^{32} nucleus (Fig. 3). The capturing state of P^{32} has spin and parity 0^+ or 1^+, since for a thermal neutron $j_n^\pi = 1/2^+$ and the ground state of P^{31} is characterized by $j_p^\pi = 1/2^+$. It follows from the level scheme of P^{31} and S^{33}, that the configuration of the ground state and the first excited state at 77 kev of the P^{32} nucleus is $(1/2^+, 3/2^+)$. This is confirmed by the fact that for both states the orbital angular momentum of the neutron is $l_n = 2$, and the spins and parities are 1^+ and 2^+. To the transition 8.64 Mev in the S^{33} nucleus there correspond the transitions 7.94 and 7.85 Mev in the P^{32} nucleus. The experimental ratio of the reduced probabilities of these transitions is $B(7.94) : B(7.85) = 0.30 : 1.00$. It follows from the table that this ratio should be equal to $0.20 : 1.00$ if $I_1 = I^+$ and to $1.00 : 0.00$ if $I_1 = 0^+$ (only transitions of the type M1 are considered). The comparison of the above-mentioned ratios indicates that $I_1 = 1^+$. The slight enhancement of the 7.94 Mev transition is due to the mixing of the initial and final states, since $I_1^\pi = I_2^\pi = 1^+$.

The 7.80-Mev transition in the S^{33} nucleus corresponds to the 7.42 and 6.79 Mev γ transitions to the multiplet $(1/2^+, 1/2^+)$ in the P^{32} nucleus (see Fig. 3). This configuration is confirmed by the fact that for both levels the orbital angular momentum of the neutron is $l_n = 0$. The experimental ratio of the reduced probabilities of these transitions is $B(7.42) : B(6.79) = 0.23 : 1.00$. It is seen from the table that $B(1^+ \to 0^+) : B(1^+ \to 1^+) = 0.50 : 1.00$, i.e., the transition to the level $(1/2^+, 1/2^+)\,1^+$ should be more intensive than the transition to the level $(1/2^+, 1/2^+)\,0^+$. The configuration mixing further enhances the transition $1^+ \to 1^+$. The comparison of the theoretical ratio with the experimental one leads to the assignment of the spin and parity 1^+ to the level 1154 kev of the P^{32} nucleus, and of the spin and parity 0^+ to the 515 kev level.

To the transition of the type E1 with the energy 5.44 Mev in the S^{33} nucleus there corresponds the transition 4.66 Mev or one of the transitions 5.73 or 4.46 Mev in the P^{32} nucleus. It is seen from the table that the most intensive transition for the multiplet $(1/2^+, 3/2^-)$ should be to the level $I_2^\pi = 2^-$. This permits us to assign the spin 2^- to the level 3259 kev of the P^{32} nucleus.

It is evident from the examples of Tl^{208} and P^{32} how the rule of relative intensities (4) allows us to assign spins and parities to the levels of odd-odd nuclei. This relation can be used in an analogous way for the analysis of the γ spectra of the processes (p, γ), (d, p), (d, n), etc. The application of this rule to β decay is less justified, since in the β decay of even-even nuclei to levels of odd-odd nuclei one must take into account the effects of the pair interaction.

3. TRANSITIONS BETWEEN LEVELS OF THE SAME MULTIPLET

Just like the levels of the same rotational band in deformed nuclei, the levels of the same multiplet in odd-odd nuclei have identical parity. Only transitions of the type M1, E2, M3, E4, etc. are possible between such levels. In the case of the rotational band the regular, monotonic sequence of spins has as a consequence that the transitions M3 and of higher multipolarity are suppressed by the transitions of the type M1 and E2. In odd-odd nuclei the sequence of spins is not that simple. It is determined by the spin-dependent part of the residual potential and is different for different quantum states of the proton and the neutron.[7] In a number of cases one therefore observes transitions of the type M3, E4, and even M5 between levels of the same multiplet.

The reduced probabilities B of γ transitions $I_1 \to I_2$ of the type EL or ML between levels of the same multiplet (j_p^π, j_n^π) can be expressed in terms of the static electric or magnetic moments of the same multipolarity m_L^p, m_L^n of the neighboring odd-proton or odd-neutron nuclei. It can be shown with the help of the Racah algebra that, un-

der the assumption of pure configurations,

$$B(\sigma L, I_1 \to I_2) = |am_L^p + bm_L^n|^2. \quad (6)$$

The coefficients a and b have the following form

$$a = \nu_L \sqrt{\frac{(2L+1)(2I_2+1)(2j_p+1)(j_p+1)}{4\pi j_p}} W(j_p j_p I_1 I_2; Lj_n) \quad (7a)$$

$$b = \nu_L \sqrt{\frac{(2L+1)(2I_2+1)(2j_n+1)(j_n+1)}{4\pi j_n}} W(j_n j_n I_1 I_2; Lj_p), \quad (7b)$$

where $\nu_1 = 1$, $\nu_2 = 1/2$, $\nu_3 = -1$, and $\nu_4 = 1$ are chosen such that the definitions of m_L^p and m_L^n agree with the generally accepted definitions of the static magnetic dipole (μ_1), electric quadrupole (q_2), magnetic octupole (μ_3), and electric hexadecapole (q_4) moments of the atomic nuclei.[8]

The static electric and magnetic moments M_L of odd-odd nuclei can also be expressed in terms of the m_L^p and m_L^n of the neighboring odd nuclei:

$$M_L(I) = a' m_L^p + b' m_L^n, \quad (8)$$

where

$$a' = (-1)^{j_p - j_n + I + L} \sqrt{\frac{I(2I+1)(2j_p+1)(j_p+1)}{(I+1) j_p}} \times W(j_p j_p II; Lj_n), \quad (9a)$$

$$b' = (-1)^{j_n - j_p + I + L} \sqrt{\frac{I(2I+1)(2j_n+1)(j_n+1)}{(I+1) j_n}} \times W(j_n j_n II; Lj_p). \quad (9b)$$

Knowing the moments μ_1 and q_2 of the ground states of the odd nuclei, we can thus calculate the probabilities of the transitions M1 and E2 between the levels of the first multiplet of the neighboring odd-odd nucleus (see, for example, reference 9) and its static moments M_1 and Q_2 not only for the ground state, but also for the excited states belonging to this multiplet. On the other hand, knowing two experimental values of $B(\sigma L)$ or M_L which characterize one multiplet of the odd-odd nucleus, one could determine the moments m_L^p and m_L^n, and thus not only μ_1 and q_2, but also μ_3 and q_4. However, in the majority of cases, only one value of $B(\sigma L)$ is known, and the solution of the problem is not unique. We can, therefore, estimate the static moments by this method only in those cases when $a \gg b$ (or $b \gg a$) and the contribution of m_n (or m_p) can be neglected, or when $j_p = j_n$, so that $a = b$ and $B(\sigma L)$ is given directly by the static moment $M_L(I)$ of the same odd-odd nucleus. For $j_p = j_n$ we have

$$B(\sigma L, I_1 \to I_2) = \frac{(2L+1)(I+1)(2I_2+1)\nu_L^2}{4\pi I(2I+1)} \frac{W^2(jjI_1I_2; Lj)}{W^2(jjII; Lj)} |M_L(I)|^2 \quad (10)$$

For example, in the B^{10} nucleus the ground state $I^\pi = 3^+$ and the first excited state at 720 kev, $I^\pi = 1^+$, belong to the multiplet $(3/2^-, 3/2^-)$. The lifetime of the first excited state is $\tau_{1/2} = 1.05 \times 10^{-9}$ sec (reference 5), which corresponds to $B(E2) = 3.94 \times 10^{-4} e^2$ barns^2. With this information we can determine the quadrupole moment for an arbitrary level of the given multiplet. For the first excited state of B^{10} we have $Q_2(1^+) = \pm 0.047$ e barns, and for the ground state $Q_2(3^+) = \pm 0.070$ e barns. The quadrupole moment of the ground state has been measured experimentally and is equal to $Q_2 = +0.074$ e barns (reference 10).

In the same way we can estimate, for example, the moment Q_4 of the Sc^{44} nucleus. The ground state $I^\pi = 3^+$, and the first excited state at 270 kev, $I^\pi = 7^+$, belong to the multiplet $(7/2^-, 7/2^-)$. The lifetime of the first excited state is $\tau_{1/2} = 2.46$ days (reference 5), which corresponds to $B(E4) = 2.1 \times 10^{-5}$ e^2 (barns)^4. From this we find for the ground state of Sc^{44}, $Q_4(3^+) = \pm 2.5 \times 10^{-3}$ e (barns)^2, and for the isomeric state $Q_4(7^+) = \pm 4.5 \times 10^{-2}$ e (barns)^2. These values are 100 to 1000 times smaller than the values of Q_4 determined from the intensities of the decays to levels of the rotational bands in heavy deformed nuclei.[11]

An extensive comparison of the experimental and theoretical values is possible only for the M_1, the static magnetic dipole moments of odd-odd nuclei. Formula (8) for this special case was given in the paper of Schwartz;[12] in the review article of Blin-Stoyle[13] M_1^{exp} and M_1^{theor} were compared in 17 cases. Until now it has been possible to make this comparison for 45 nuclei. Out of the 45 considered cases, 36 are in agreement with experiment with an accuracy of 25%; 4 cases give a discrepancy, but here the sensitivity to small changes in μ_1^p and μ_1^n is very great, so that agreement with experiment could be easily achieved. There is serious disagreement (5 cases) only for those nuclei for which the assumed model is manifestly wrong, that is, for deformed nuclei and for nuclei with configuration levels which cannot be explained by the single-particle scheme of Mayer.[14] The satisfactory agreement between M_1^{exp} and M_1^{theor} indicates that the hypothesis of a multiplet structure of the levels is valid for a large group of odd-odd nuclei.

[1] L. I. Rusinov and D. A. Varshalovich, Атомная энергия (Atomic Energy) **5**, 432 (1958).

[2] A. Bohr and B. Mottelson, Kgl. Danske Videnskab. Selskab, Mat.-Fys. Medd. **27**, Nr. 16 (1953).

Alaga, Alder, Bohr, and Mottelson, Kgl. Danske Videnskab. Selskab, Mat.-Fys. Medd. **29**, Nr. 9 (1955).

[3] A. K. Kerman, Kgl. Danske Vidensk. Selskab, Mat.-Fys. Medd. **30**, Nr. 15 (1956).

[4] Obi, Ishidzu, Horie, Yanagawa, Tanabe, and Sato, Ann. Tokyo Astronom. Observatory, II ser. **4**, Nr. 1 and 2 (1954).

[5] B. S. Dzhelepov and L. K. Peker, Схемы распада радиоактивных ядер (Decay Schemes of Radioactive Nuclei), U.S.S.R. Acad. Sci., 1958.

[6] Groshev, Demidov, Lutsenko, and Pelekhov, Атлас спектров γ-лучей радиационного захвата тепловых нейтронов (Atlas of γ Ray Spectra in the Radiative Capture of Thermal Neutrons), Glavatom, 1958.

[7] A. de Shalit, Phys. Rev. **91**, 1479 (1953).

[8] S. Suekane and Y. Yamaguchi, Progr. Theor. Phys. **17**, 443 and 449 (1957).

[9] A. de Shalit, Phys. Rev. **105**, 1531 (1957).

[10] G. Wessel, Phys. Rev. **92**, 1581 (1953).

[11] Gol'din, Novikova, and Ter-Martirosyan, JETP **36**, 512 (1959), Soviet Phys. JETP **9**, 356 (1959).

[12] H. M. Schwartz, Phys. Rev. **89**, 1293 (1953).

[13] R. J. Blin-Stoyle, Revs. Modern Phys. **28**, 75 (1956).

[14] M. Goeppert-Mayer and J. H. Jensen, Elementary Theory of Nuclear Shell Structure, J. Wiley and Sons, N. Y. (1955).

Translated by R. Lipperheide
27

POLARIZATION OF GAMMA-RAY QUANTA FROM THE INTERNAL COMPTON EFFECT

F. YANOUKH

Institute of Nuclear Physics, Moscow State University

Submitted to JETP editor July 4, 1959

J. Exptl. Theoret. Phys. (U.S.S.R.) **38**, 180-183 (January, 1960)

The circular polarization of the γ-ray quanta from the internal Compton effect is considered. The forms of the angular correlation between the direction of emergence of the β-ray electron and that of a circularly polarized γ-ray quantum are given for transitions of both the magnetic and the electric types.

BECAUSE of parity nonconservation in the weak interactions the γ-ray quanta emitted by a nucleus after β decay are circularly polarized, and there is a correlation between the β-ray electron and the γ-ray quantum.[1] If after β decay there is internal conversion of the γ-ray quanta, the conversion electrons that are emitted will be longitudinally polarized.[2,3] A similar situation will exist also in the case of the so-called internal Compton effect occurring after β decay of a nucleus. Since the internal Compton effect is bremsstrahlung from the conversion electrons, it is clear that in the case of longitudinally polarized electrons the γ-ray quanta will be circularly polarized. It is obvious that there will also be an angular correlation of the β-ray electron and the circularly polarized γ-ray quantum.

Studies of this correlation and of the degree of circular polarization can be useful in some cases for the determination of the values of the nuclear matrix elements or even those of the β-decay constants.

In the present note we consider the circular polarization of γ-ray quanta emitted as the result of internal Compton effect occurring after an allowed β decay, and find the form of the angular correlation between the emission of the β-ray electron and the circularly polarized γ-ray quantum. The calculations have been made in the Born approximation, like the other calculations devoted to this question.[4,5] It is natural to expect that strictly speaking these calculations can apply only for light nuclei, although the results of work by Lindqvist and others[6] on the experimental observation of the internal Compton effect in Ba^{137} are in fair agreement with the theoretical results of Spruch and Goertzel,[4] which were also obtained with the Born approximation.

Suppose that before the β decay the nucleus was in a state with angular momentum j_1, that after the allowed β decay (we consider the V-A interaction) it was in a state with angular momentum j_2, and that after the γ-ray transition it was in a state characterized by the angular momentum j_3. Let the multipole character of the (virtual) γ-ray quantum be l, and let $\Delta \equiv E_{j_1} - E_{j_2}$ be the energy of the γ-ray transition of the nucleus. Then the angular correlation of the β-ray electron with the circularly polarized γ-ray quantum has the usual form

$$w(\theta_\beta) = 1 + \mu \frac{v}{c} \delta \frac{P}{N} \cos\theta_\beta, \qquad (1)$$

where θ_β is the angle between the directions of emission of the β-ray electron and the circularly polarized γ-ray quantum, μ is the sign of the circular polarization ($\mu = \pm 1$), and v is the speed of the β-ray electron. For allowed β transitions we have

$$\delta = \frac{2B\sqrt{j_2(j_2+1)}\,\delta_{j_2 j_1} + D[2 + j_2(j_2+1) - j_1(j_1+1)]}{2\sqrt{j_2(j_2+1)}\,(A\delta_{j_2 j_1} + C)} \times \frac{l(l+1) + j_2(j_2+1) - j_3(j_3+1)}{2\sqrt{j_2(j_2+1)\,l(l+1)}}, \qquad (2)$$

where

$$A = |\langle 1\rangle|^2 (|C_V|^2 + |C'_V|^2),$$
$$B = 2\mathrm{Re}\,\langle 1\rangle\langle\sigma\rangle^* (C_V C'^*_A + C'_V C^*_A),$$
$$C = |\langle\sigma\rangle|^2 (|C_A|^2 + |C'_A|^2), \quad D = |\langle\sigma\rangle|^2 2\mathrm{Re}\, C_A C'^*_A. \qquad (3)$$

Here as usual we have denoted by $\langle 1\rangle$ and $\langle\sigma\rangle$ the matrix elements of the Fermi and Gamow-Teller types. The quantities N and P depend on the multipole character and type of the transition. For transitions of magnetic type with multipole index l we have

$$N^{(M)} = \frac{1}{p'^2}\{k^2 p' + p^2 \Delta \sin^2\theta_{kp}\} + \frac{k^2}{m^2}\left\{p' - \frac{p^2 k}{q^2}\sin^2\theta_{kp}\right\} - \frac{kp^2}{mp'}\frac{\sin^2\theta_{kp}}{q^2}\{kp\cos\theta_{kp} + p^2 + mk\},$$

$$P^{(M)} = \frac{1}{p'^2}\{k^2 p' c_1 + p^2 \Delta c_2\} + \frac{k^2}{m^2}\{p' c_1 - p c_3\} - \frac{m - \varepsilon_p}{mp'}\, pkc_3. \qquad (4)$$

where the quantities appearing in $P^{(M)}$ are

$$c_1 = (-1)^l 2^{1/2}(2l+1)^{3/2}\cdot 4\pi \sum_K \frac{1}{(2K+1)^{1/2}} C^{K0}_{l0l0} X \times (1l1|1l1|11K) h_{1K}(\theta_{kp}),$$

$$c_2 = (-1)^l 5^{-1/2}(2l+1)^{3/2}\cdot 4\pi C^{20}_{l0l0} X \times (1l1|1l1|112) P_{1,1}(\theta_{kp}) P_{2,-1}(\theta_{pq}),$$

$$c_3 = (-1)^{1+l} 2^{-1/2} 3^{1/2}(2l+1)^{3/2}\cdot 4\pi \sum_{K,F} \frac{4-F(F+1)}{(2F+1)^{1/2}(2K+1)^{1/2}} \times C^{K0}_{l0l0} C^{F0}_{1010} X (1l1|1l1|11K) h_{FK}(\theta_{kp}). \quad (5)$$

Somewhat more cumbersome formulas are obtained for transitions of the electric type. In this case

$$N^{(e)} = A_1 + A_2 + A_{12}, \qquad P^{(e)} = B_1 + B_2 + B_{12}, \quad (6)$$

with

$$A_1 = \frac{1}{k^2 p'^2}\left\{(k^2 p' + p^2\Delta\sin^2\theta_{kp})\left[(2l+1)\frac{\Delta^2}{q^2} - l\right] + 2lkp'\left(m - \frac{p^2\Delta}{q^2}\sin^2\theta_{kp} + a_1\right)\right\},$$

$$A_2 = \frac{1}{m^2 k}\left\{kp'\left[(2l+1)\frac{\Delta^2}{q^2} - l\right] - 2l(ma_1 + a_2)\right\},$$

$$A_{12} = \frac{1}{mk^2 p'}\left\{(2k^2 p' + kp^2\sin^2\theta_{kp})\left[(2l+1)\frac{\Delta^2}{q^2} - l\right] - 2k^2 p' a_3 + 2l[(\varepsilon_p - m)a_4 - \Delta a_2 - (m\Delta - kp')a_1 + m(m(m-\varepsilon_p) + kp')]\right\}, \quad (7)$$

where

$$a_1 = -\varepsilon_p + \frac{p\Delta}{q}\cos\theta_{pq},$$

$$a_2 = (m-k)\varepsilon_p - \frac{\Delta}{q}[(m-k)p\cos\theta_{pq} - \varepsilon_p k\cos\theta_{kq}] - \frac{1}{2l}\frac{\Delta^2}{q^2}kp[(l+1)\cos\theta_{kp} + (l-1)\cos\theta_{pq}\cos\theta_{kq}],$$

$$a_3 = \frac{2}{3}\frac{\Delta^2}{q^2}\left[(2l+1) - \frac{(l-1)}{4}(3\cos^2\theta_{kp} - 1)\right],$$

$$a_4 = \varepsilon_q(m-k) + \frac{\Delta}{q}(\varepsilon_q k\cos\theta_{kp} - \varepsilon_q q) - \frac{\Delta^2 k}{2lq}[(l+1)\cos\theta_{kp} + (l-1)\cos\theta_{kp}]; \quad (8)$$

$$B_1 = \frac{1}{k^2 p'^2}\left\{k^2 p' b_2 + 2(\varepsilon_p - m)b_3 + l^{1/2}(l+1)^{1/2}\frac{pk\Delta}{q^2}\sin^2\theta_{kp}(m\Delta + m(\varepsilon_p - m))\right\},$$

$$B_2 = \frac{1}{m^2 k}\left\{kp' b_2 + 2b_1 + l^{1/2}(l+1)^{1/2}\frac{pk^2\Delta}{q^2}\sin^2\theta_{kp}\right\},$$

$$B_{12} = \frac{2}{mk^2 p'}\left\{(m-\varepsilon_p)b_1 + l^{1/2}(l+1)^{1/2}\frac{pk\Delta}{2q^2}\sin^2\theta_{kp} \times ((m-k)(\varepsilon_p - m) + m\Delta - kp')\right\}. \quad (9)$$

Here b_i denote the quantities

$$b_1 = (-1)^{1+l} 3^{1/2} 2^{-3/2}(2l-1)(2l+1)^{3/2} 4\pi\frac{pk\Delta^2}{q^2} \times \sum_{K,F}\frac{4-F(F+1)}{(2F+1)^{1/2}(2K+1)^{1/2}} C^{F0}_{10\,10} C^{K0}_{l-10\,l-10} X \times (1l1-1|1l1-1|11K) h_{FK}(\theta_{kp}),$$

$$b_2 = (-1)^l 2^{1/2}(2l-1)(2l+1)^{3/2} 4\pi\frac{\Delta^2}{q^2}\sum_F (2F+1)^{-1/2} \times C^{F0}_{l-10\,l-10} X (1l1-1|1l1-1|11F) h_{1F}(\theta_{kp}), \quad (10)$$

$$b_3 = (-1)^l 3^{-1/2} 5^{-1/2}(2l-1)(2l+1)^{3/2} 4\pi\frac{p^2\Delta^2}{q^2} \times C^{20}_{l-10\,l-10} X (1l1-1|1l1-1|112) P_{1,1}(\theta_{kp}) P_{2,-1}(\theta_{pq}).$$

The quantities that appear in Eqs. (5) and (10) are given by

$$h_{1K}(\theta_{kp}) = C^{K0}_{10\,10} P_{1,0}(\theta_{kp}) P_{K,0}(\theta_{pq}) - 2C^{K1}_{11\,10} P_{1,1}(\theta_{kp}) P_{K,-1}(\theta_{pq}),$$

$$h_{FK}(\theta_{kp}) = C^{F0}_{10\,10} C^{K0}_{1010} P_{F,0}(\theta_{kp}) P_{K,0}(\theta_{pq}) - 2C^{F1}_{11\,10} C^{K1}_{11\,10} P_{F,-1}(\theta_{kp}) P_{K,+1}(\theta_{pq}). \quad (11)$$

In the expressions (4) – (11) the following notations are used: ϵ_p, $\mathbf{p}$ are the energy and momentum of the electron ejected from the K shell; m is the mass of the electron; k, $\mathbf{k}$ are the energy and momentum of the real γ-ray quantum;

$$\mathbf{q} = \mathbf{p} + \mathbf{k}, \qquad \varepsilon_q = \varepsilon_p + k, \qquad p' = \varepsilon_p - p\cos\theta_{kp};$$

θ_{kp} denotes the angle between the directions of emergence of the conversion electron and the γ-ray quantum; θ_{pq} and θ_{kp} denote respectively the angles between the vectors $\mathbf{p}$ and $\mathbf{q}$ and between $\mathbf{k}$ and $\mathbf{q}$. (It is easy to see that in the final analysis all of these angles can be expressed in terms of the single angle θ_{kp}). The $P_{l,m}$ denote associated Legendre polynomials with the normalization given by Edmonds,[7] and $C^{a\alpha}_{b\beta c\gamma}$ and $X(abc|efg|hik)$ are Clebsch-Gordan and Fano coefficients; their properties and numerical values can be found, for example, in reference 7.

To get an intuitive idea of the value of the degree of circular polarization as a function of the two variables θ_{kp} and k, we have tabulated this function for the γ-ray transition in Co^{60} (transition of type E = 2, Δ = 1.170 Mev). The results of calculations of the dependence of P/N on the energy k of the γ-ray quantum (in units mc^2) and on the angle θ_{kp} are shown in Figs. 1 and 2.

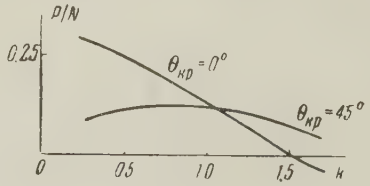

FIG. 1

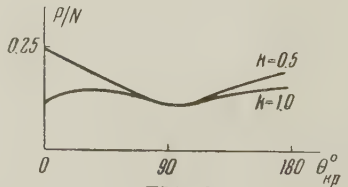

FIG. 2

We note that the degree of circular polarization of the γ-ray quanta for transitions with the same multipole index and transition energy is larger for the magnetic than for the electric transition. This result can be understood easily if we take into ac-

count the fact that in the case of the electric transition there is both longitudinal and also transverse polarization of the conversion electrons, and for small energies of the conversion electron the transverse polarization can even exceed the longitudinal.[2]

In conclusion the writer regards it as his pleasant duty to thank Professor I. S. Shapiro for suggesting the topic and for his interest in the work. The writer is also grateful to E. Naletova for assistance in the numerical calculations.

[1] T. D. Lee and C. N. Yang, Phys. Rev. **104**, 254 (1956). Yu. V. Gaponov and V. S. Popov, JETP **33**, 256 (1957), Soviet Phys. JETP **6**, 197 (1958).

[2] V. B. Berestetskiĭ and A. P. Rudik, JETP **35**, 159 (1958), Soviet Phys. JETP **8**, 111 (1959).

[3] B. V. Geshkenbeĭn, JETP **35**, 1235 (1958), Soviet Phys. JETP **8**, 865 (1959).

[4] L. Spruch and G. Goertzel, Phys. Rev. **94**, 1671 (1954).

[5] É. Melikyan, JETP **31**, 1088 (1956), Soviet Phys. JETP **4**, 930 (1957).

[6] Lindqvist, Petterson, and Siegbahn, Nuclear Phys. **5**, 47 (1958).

[7] A. R. Edmonds, CERN Report 55-26, Geneva, 1955.

Translated by W. H. Furry
28

DAMPING OF OSCILLATIONS OF A DISC IN ROTATING HELIUM II

Yu. G. MAMALADZE and S. G. MATINYAN

Institute of Physics, Academy of Sciences, Georgian S.S.R.

Submitted to JETP editor June 5, 1959

J. Exptl. Theoret. Phys. (U.S.S.R.) 38, 184-187 (January, 1960)

The interaction of an oscillating disc with rotating helium II is examined. An expression is obtained for the torsional moment acting on the surface of the disc, taking into account the presence of vortex lines, mutual friction between the normal and superfluid components, and the possibility of sliding of the vortex lines along the solid surface. A calculation of the damping of oscillations, which neglects sliding and is in linear approximation with respect to the mutual friction coefficients, is in qualitative agreement with the experimental data. It seems that quantitative agreement can only be obtained if sliding is taken into account.

1. The aim of the present work is the explanation of the dependence of the damping of torsional oscillations of a disc on the speed of rotation for helium II,[1,2] which is completely different from the behavior of a classical liquid.[3] A preliminary investigation showed that this dependence cannot be explained by taking account of mutual friction alone.[4] The corresponding effect is less than that observed by at least an order of magnitude.

2. We use Hall's relation[5] to describe the rotating superfluid component

$$\frac{\partial \mathbf{v}_s}{\partial t} + (\mathbf{v}_s\nabla)\mathbf{v}_s + \nu_s\left[\boldsymbol{\omega}\times\operatorname{curl}\frac{\boldsymbol{\omega}}{\omega}\right] = \alpha_n\boldsymbol{\omega}\times[\mathbf{v}_n - \mathbf{v}_s] + \beta_n\left[\frac{\boldsymbol{\omega}}{\omega}\times[\mathbf{v}_n - \mathbf{v}_s]\right] + \nabla\Phi. \quad (1)$$

In this the existence of Onsager-Feynman vortices is taken into account by the additional (third) term which distinguishes this equation from the usual one for the velocity of the superfluid component. In equation (1) $\mathbf{v}_S$ denotes the velocity of the superfluid component, averaged over a volume of linear dimensions considerably greater than the distance between the vortices: $\nu_S = \epsilon/\rho_S\Gamma$, where ϵ is the energy per unit length of vortex line and Γ is the circulation; $\boldsymbol{\omega} = \operatorname{curl}\mathbf{v}_S$; α_n and β_n are the coefficients of mutual friction, related to the coefficients of Hall and Vinen[4] by the equations $\alpha_n = 0.5\,(\rho_n/\rho)\,B'$ and $\beta_n = -0.5 \times (\rho_n/\rho)\,B$; the expression $\nabla\Phi$ contains all gradient terms.*

The normal component is described by the relation

$$\frac{\partial \mathbf{v}_n}{\partial t} + (\mathbf{v}_n\nabla)\mathbf{v}_n = \nu_n\nabla^2\mathbf{v}_n - \alpha_s\boldsymbol{\omega}\times[\mathbf{v}_n - \mathbf{v}_s] - \beta_s\omega^{-1}\boldsymbol{\omega}\times[\boldsymbol{\omega}\times[\mathbf{v}_n - \mathbf{v}_s]] + \nabla\Psi. \quad (2)$$

Here ν_n is the kinematic viscosity of the normal component, $\alpha_S = 0.5\,(\rho_S/\rho)\,B'$, $\beta_S = -0.5\,(\rho_S/\rho)\,B$, and $\nabla\Psi$ contains the gradient terms.

As the relevant effect has been observed at constant temperature, the independent equations of continuity have been used for the superfluid and normal components:

$$\operatorname{div}\mathbf{v}_s = 0, \quad \operatorname{div}\mathbf{v}_n = 0. \quad (3)$$

3. The system (1) — (3) has been linearized for small oscillatory additions to a velocity distribution of the type $\mathbf{v}_S = \mathbf{v}_n = \boldsymbol{\omega}_0 \times \mathbf{r} = \mathbf{v}_0$ ($\boldsymbol{\omega}_0$ is the angular velocity of rotation) and solved for the boundary conditions corresponding to adhesion of the normal component to the surface of the disc. The boundary conditions for $\mathbf{v}_S$ were obtained in the following way.* Equation (1) is rewritten in the form of an equation of conservation of vortices

$$\partial\mathbf{v}_s/\partial t = \mathbf{v}_L\times\boldsymbol{\omega} + \text{gradient terms} \quad (4)$$

where $\mathbf{v}_L$ is the velocity of the vortex lines. It can easily be shown that

$$\mathbf{v}_L\times\boldsymbol{\omega} = \left\{\mathbf{v}_s + \nu_s\operatorname{curl}\frac{\boldsymbol{\omega}}{\omega} - \alpha_n(\mathbf{v}_n - \mathbf{v}_s) - \beta_n\frac{\boldsymbol{\omega}}{\omega}\times[\mathbf{v}_n - \mathbf{v}_s]\right\}\times\boldsymbol{\omega}. \quad (5)$$

The boundary conditions for the r and φ components of $\mathbf{v}_S$ can be found from (5) by substituting the boundary conditions for the φ and r components of $\mathbf{v}_L$. Taking account of partial sliding of

*L. D. Landau has shown that (1) follows from the laws of conservation of energy and momentum. The value of η_S, equal to $dE/d\omega$ (where E is the energy per unit volume of rotating helium), is related to ν_S by the relation $\eta_S = \rho_S\nu_S$.

*This method of obtaining the boundary conditions for $\mathbf{v}_S$ is due to L. D. Landau.

the vortex lines along the surface of the disc, we obtain*

$$w_{sr}(0) - 2\omega_0\varphi_0 = \frac{a}{i\Omega}(dw_{sr}/dz)_{z=0},$$

$$w_{s\varphi}(0) = \frac{a}{i\Omega}(dw_{s\varphi}/dz)_{z=0}. \qquad (6)$$

In these equations $\mathbf{w}_S(z)$ denotes $(\mathbf{v}_S - \mathbf{v}_0)/r \times \exp(i\Omega t)$; Ω and φ_0 are the frequency and amplitude of the oscillations and a is the coefficient of sliding. We assume that the z axis is in a direction at right angles to the surface of the disc, which corresponds to z = 0. We have, finally, the natural boundary condition

$$w_{sz}(0) = 0. \qquad (7)$$

4. If we consider the oscillation of an infinite disc in an unbounded liquid, the solution of the system (1) — (3) consists of the sum of four plane waves with wave numbers determined by the relations

$$k_{1,2}^2 = \tfrac{1}{2}(k_{n0}^{(+)2} + k_{s0}^{(+)2} + q_1^{(+)} + q_2^{(+)}) \pm \tfrac{1}{2}[(k_{s0}^{(+)2} - k_{n0}^{(+)2} + q_1^{(+)} - q_2^{(+)})^2 + 4q_1^{(+)}q_2^{(+)}]^{1/2},$$

$$k_{3,4}^2 = \tfrac{1}{2}(k_{n0}^{(-)2} + k_{s0}^{(-)2} + q_1^{(-)} + q_2^{(-)}) \pm \tfrac{1}{2}[(k_{s0}^{(-)2} - k_{n0}^{(-)2} + q_1^{(-)} - q_2^{(-)})^2 + 4q_1^{(-)}q_2^{(-)}]^{1/2};$$

$$k_{n0}^{(\pm)2} = -i(\Omega \pm 2\omega_0)/\nu_n, \qquad k_{s0}^{(\pm)2} = \mp(\Omega \pm 2\omega_0)/\nu_s,$$

$$q_1^{(\pm)} = \mp 2\omega_0 i(\beta_n \mp i\alpha_n)/\nu_s, \qquad q_2^{(\pm)} = 2\omega_0(\beta_s \mp i\alpha_s)/\nu_n. \qquad (8)$$

The penetration depths corresponding to these wave numbers are sufficiently small for the walls of the beaker to be considered to be located at infinity.† In addition to the boundary conditions already given, there must then be no oscillatory addition to $\mathbf{v}_0$ at infinity.

5. The moment of the force, acting on the surface of the disc is given by the formula‡

$$M = \pi R^4[\eta_n(dw_{n\varphi}/dz)_{z=0} + \eta_s(dw_{sr}/dz)_{z=0}]\exp(i\Omega t), \qquad (9)$$

with the values

$$\frac{2}{\varphi_0}\left(\frac{dw_{n\varphi}}{dz}\right)_{z=0} = \frac{\Omega(\varkappa_1 k_2 - \varkappa_2 k_1) + 2\omega_0 q_2^{(+)}(k_2 - k_1) + ak_1k_2(\varkappa_2 - \varkappa_1)}{\varkappa_2 - \varkappa_1 - a(\varkappa_2 k_2 - \varkappa_1 k_1)/\Omega}$$

$$+ \frac{\Omega(\varkappa_3 k_4 - \varkappa_4 k_3) - 2\omega_0 q_2^{(-)}(k_4 - k_3) + ak_3k_4(\varkappa_4 - \varkappa_3)}{\varkappa_4 - \varkappa_3 - a(\varkappa_4 k_4 - \varkappa_3 k_3)/\Omega},$$

$$\frac{2}{\varphi_0}\left(\frac{dw_{sr}}{dz}\right)_{z=0} = i\frac{2\omega_0(\varkappa_2 k_2 - \varkappa_1 k_1) - \Omega q_1^{(+)}(k_2 - k_1)}{\varkappa_2 - \varkappa_1 - a(\varkappa_2 k_2 - \varkappa_1 k_1)/\Omega}$$

$$+ i\frac{2\omega_0(\varkappa_4 k_4 - \varkappa_3 k_3) + \Omega q_1^{(-)}(k_4 - k_3)}{\varkappa_4 - \varkappa_3 - a(\varkappa_4 k_4 - \varkappa_3 k_3)/\Omega}. \qquad (10)$$

In (10) we have introduced the notation

$$\varkappa_{1,2} = -k_{1,2}^2 + k_{n0}^{(+)2} + q_2^{(+)}, \qquad \varkappa_{3,4} = -k_{3,4}^2 + k_{n0}^{(-)2} + q_2^{(-)}. \qquad (11)$$

6. In view of the unwieldiness of (10) for making comparison with experimental data, we will only consider the case a = 0 (perfectly rough surface) and carry out the calculation to linear approximation with respect to the mutual friction coefficients (which is justifiable for relatively small values of ω_0). The results of this calculation are shown in the figure together with the experimental results. The ordinate is $\Delta = \delta - \Omega_0\delta_0/\Omega$, where δ and δ_0 are the logarithmic decrements in helium and in vacuum respectively, and Ω and Ω_0 are the corresponding frequencies of oscillation. We are now carrying out the calculations without the restrictions mentioned.

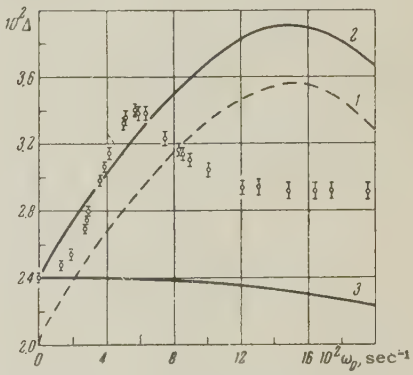

Dependence of Δ on the speed of rotation of helium II. 1 — Result calculated from Eq. (9) with the coefficients corresponding to T = 1.78°K, not taking account of sliding; 2 — The same with a correction for edge effects to first order [Eq. (9)];[3] 3 — Damping due to the viscosity of the normal component; the experimental points were obtained at 1.78°K with a "heavy" disk ($\Omega \approx \Omega_0$), the surface of which was covered with granules.[6]

The authors thank L. D. Landau for his valuable advice and suggestions, É. L. Andronikashvili for his interest in the work and L. P. Pitaevskiĭ for fruitful discussion.

[1] Andronikashvili, Tsakadze, Mamaladze, and Matinyan, 5th All-Union Conference on the Physics of Low Temperatures, Tbilisi, 1958.

*The physical interpretation of the boundary conditions imposed on $\mathbf{v}_L$ is that the difference in velocity between a vortex line and the surface is proportional to the force exerted on the vortex: $\mathbf{F} = \varepsilon\sigma$, σ is the tangential unit vector of the vortex line at the point of contact with the surface of the disk.

†There are, therefore, no resonance effects connected with the accommodation of a whole number of half wavelengths into the distance between the disk and the top or bottom of the beaker.

‡Equation (9) is derived by using the expression for the flow momentum tensor, given by L. D. Landau in the derivation of (1), which has already been mentioned. To explain the physical meaning of the second term of (9) we point out that it can be obtained by a direct consideration of the force acting on the surface of the disk by the vortex lines attached to it, which have a tension ε.

[2] É. L. Andronikashvili and D. S. Tsakadze, Сообщения АН ГрузССР (Reports, Acad. Sci. Georgian S.S.R. **20**, 667 (1958).

[3] Yu. G. Mamaladze and S. G. Matinyan, Физика металлов и металловедение (Phys. of Metals and Metal Res.) in press.

[4] H. E. Hall and W. F. Vinen, Proc. Roy. Soc. **A238**, 215 (1956).

[5] H. E. Hall, Proc. Roy. Soc. **A245**, 546 (1958).

[6] É. L. Andronikashvili and D. S. Tsakadze, JETP **37**, 322 and 562 (1959), Soviet Phys. JETP **10**, 227 and 397 (1960).

Translated by R. Berman
29

GALVANOMAGNETIC CHARACTERISTICS OF METALS WITH OPEN FERMI SURFACES. II

I. M. LIFSHITZ and V. G. PESCHANSKIĬ

Physico-technical Institute, Academy of Sciences, Ukrainian S.S.R.; Khar'kov State University

Submitted to JETP editor July 7, 1959

J. Exptl. Theoret. Phys. (U.S.S.R.) **38**, 188-193 (January, 1960)

On the basis of a theory developed earlier of galvanomagnetic phenomena,[1,2] detailed calculations have been carried out for certain concrete types of Fermi surfaces, a particular case of which is, for example, the open surface constructed by Pippard for copper. It is shown that the stereographic projection of the resistances obtained for an open surface of this type agrees well with experimental data for gold (Alekseevskiĭ and Gaĭdukov). The peculiarities of galvanomagnetic phenomena have been studied for a surface of the "corrugated" plane type. The possibility of a new type of angular singularities has been indicated, connected with the sharp change in the direction of the open trajectories on approaching the field direction perpendicular to the corrugated plane. Possibilities are discussed of a more complete determination of the energy spectrum according to the galvanomagnetic characteristics of the metal.

METALS with open Fermi surfaces are characterized by a sharp anisotropy of the resistance and the Hall field in the region of strong magnetic field; this anisotropy increases with increase in the magnetic field.[2] As was explained earlier,[1,2] the basic character of the angular dependence of the resistance and of the Hall field is determined by the topological structure of the Fermi surfaces. In particular, it is very important to make clear whether the open trajectories of the motion of an electron in momentum space (ϵ = const, p_z = const) exists for a given direction of the magnetic field or whether such are absent.* In these two cases the asymptotic character of the tensors of conductivity σ_{ik} and resistivity ρ_{ik} in strong magnetic fields is quite different.

The general method of observation of galvanomagnetic phenomena in metals with an arbitrary Fermi surface (closed or open) was investigated in the papers mentioned. In the present communication concrete types of Fermi surfaces are considered which are of particular interest. Some of these were discovered recently by Alekseevskiĭ and Gaĭdukov.

1. By measuring the surface resistance of a single crystal of copper in a high frequency variable electromagnetic field, Pippard made it clear that the Fermi surface for copper in all probability is open.[3] The surface constructed by him can be described with a great deal of accuracy by an analytic expression containing only the first harmonics in the Fourier expansion of $\epsilon(\mathbf{p})$. This fact was noted by Moliner[4] who made the assumption that for all metals with a face-centered cubic lattice (metals of the copper group) the Fermi surface could be represented by an analytic expression of the form

$$\varepsilon(\mathbf{p}) = \lambda\{3 - \cos(ap_x/2\hbar)\cos(ap_y/2\hbar) - \cos(ap_z/2\hbar)\cos(ap_x/2\hbar) - \cos(ap_y/2\hbar)\cos(ap_z/2\hbar) + \beta[3 - \cos(ap_x/\hbar) - \cos(ap_y/\hbar) - \cos(ap_z/\hbar)]\} = \zeta_0, \quad (1)$$

a = lattice constant, $\hbar$ = Planck's constant, ζ_0 = Fermi energy. For $\beta \approx 0.1$ and $\zeta_0/\lambda \approx 3.6$, the experimental points of Pippard lie on the surface (1) with accuracy up to 1 percent.

A somewhat more general form of the expansion of $\epsilon(\mathbf{p})$, which is also suitable for simple and body-centered cubic lattices,

$$\varepsilon(\mathbf{p}) = \alpha\{3 - \cos(ap_x/\hbar)\cos(ap_y/\hbar) - \cos(ap_x/\hbar)\cos(ap_z/\hbar) - \cos(ap_y/\hbar)\cos(ap_z/\hbar) + \beta[3 - \cos(ap_x/\hbar) - \cos(ap_y/\hbar) - \cos(ap_z/\hbar)] + \delta[1 - \cos(ap_x/\hbar)\cos(ap_y/\hbar)\cos(ap_z/\hbar)]\} = \zeta_0, \quad (1a)$$

leads, as analysis will show, to the same possible types of topological structure of the surfaces as (1).

We now investigate the galvanomagnetic properties of metals whose isoenergetic surfaces are de-

*The trajectories of the motion of the electrons in the usual coordinate space are obtained from the trajectories of motion in momentum space by a rotation through the angle $\pi/2$ with a similarity coefficient eH/c. All the notation is consistent with that of reference 1.

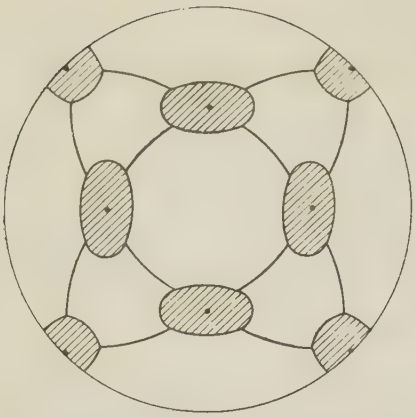

FIG. 1. Stereographic projection of the directions of the magnetic field (shaded regions and continuous lines), which lead to open trajectories $\varepsilon = \text{const}$, $p_z = \text{const}$ for a Fermi surface consisting of corrugated cylinders directed along the three-dimensional diagonals of the cell of the reciprocal lattice.

scribed by the expression (1a) and (1) with arbitrary values of the parameters δ, ζ_0/α and β.

For fixed values of α, β and δ, the region of possible values of ζ_0 is limited ($\epsilon_{\min} \leq \zeta_0 \leq \epsilon_{\max}$; $\epsilon_{\min} = 0$). If $\zeta_0 = \epsilon_{\min}$ or $\zeta_0 = \epsilon_{\max}$, Eq. (1a) describes a set of isolated points. When $\zeta_0 - \epsilon_{\min}$ is not large or is close to its maximum value, the surface (1a) is a small closed surface (sphere), whose dimensions increase in proportion to the departure of ζ_0 from its minimum or maximum possible value. For intermediate values of ζ_0, the Fermi surface (1a) can be either closed or open.

For $2\alpha(\beta+2) < \zeta_0 < 4\alpha(\beta+1)$, $\delta \ll 1$, the surface (1a) is an open surface of the type "three-dimensional grid," consisting of "corrugated" cylinders, directed along the principal crystallographic axes [100], [010], [001]. For $\zeta_0 > 4\alpha(\beta+1)$, the surface (1a) again represents closed regions located around the centers of the cubic cells of the reciprocal lattice. Quasiparticles with such values of the energy behave as positively charged particles — "holes." (For simplicity we consider $\alpha > 0$ and $\beta > 0$.)

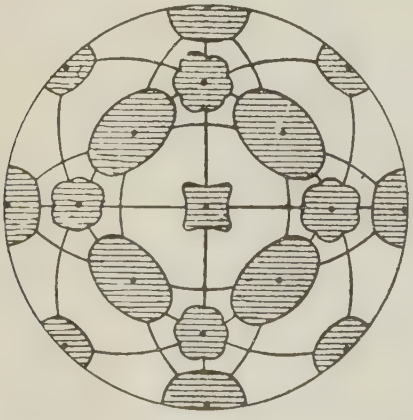

FIG. 3. Stereographic projection of the directions of the magnetic field (shaded region and continuous lines), which lead to the appearance of open plane intersections of surfaces consisting of corrugated cylinders whose axes are parallel to the three-dimensional diagonals and the diagonals of the boundaries of the cubic lattice.

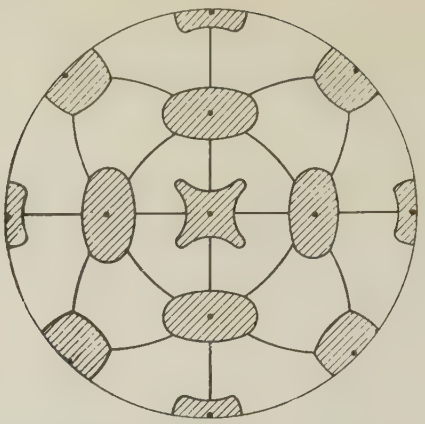

FIG. 2. Stereographic projection of the directions of the magnetic field (shaded regions and continuous lines), for which open plane intersections exist for surfaces formed by corrugated cylinders whose axes are directed along the three-dimensional diagonals and the principal crystallographic axes.

For $\beta < 1$,

$$\zeta_0/\alpha > [3(1+\beta/2)^2 + \delta(1+\beta^3/8)] \qquad (1a')$$

the surface (1a) is a "three-dimensional grid" of corrugated cylinders whose axes can be parallel to the three-dimensional diagonals, the diagonals of the boundaries and the edges of the cubic cell of the reciprocal lattice.[5] For values of ζ_0/α close to

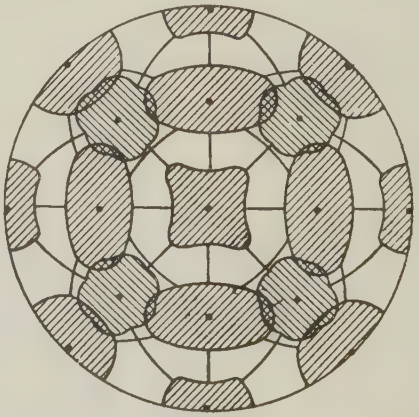

FIG. 4. Stereographic projection of the directions of the magnetic field (shaded regions and continuous lines), which lead to the appearance of open plane intersections of an isoenergetic surface of the type "three-dimensional grid," formed from corrugated cylinders whose axes have thirteen different directions (the three-dimensional diagonals, the diagonals of the boundaries and edges of the cell). The doubly shaded regions are the directions of the magnetic field for which the layers of open trajectories with different average directions exist.

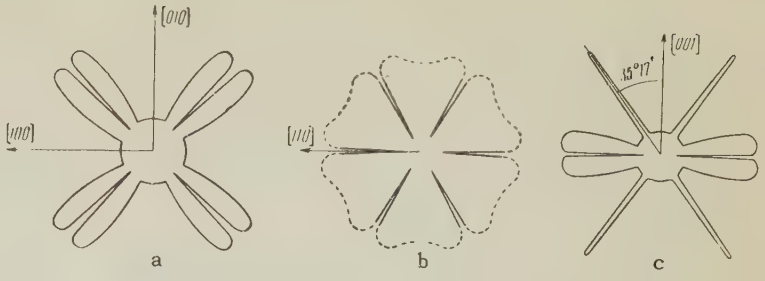

FIG. 5. Angular dependence of the resistivity $\rho = \rho(\vartheta)$ (diagram of rotation of $\mathbf{H} \perp \mathbf{j}$) of metals with a Fermi surface consisting of corrugated cylinders directed along the three-dimensional diagonals of the cubic cell: a – electric current j directed along the [001] axis, b – electric current j directed along the [111] axis, c – j directed along the [110] axis.

the maximum value, the surface (1a) again consists only of closed regions distributed about the centers of the walls ($\beta < \delta$) or the middle of the edges ($\beta > \delta$) of the cells of the reciprocal lattice. [As before, we shall take $\alpha > 0$ for simplicity. The case $\alpha < 0$ does not lead to any new qualitative singularities of the open surfaces of (1).]

Thus, in all, five different types of open surfaces are possible.[5] The simplest topological case of an open surface (1a) ("three-dimensional grid") of corrugated cylinders whose axes are parallel to the principal crystallographic axes [100], [010], [001] has been studied in detail previously. The stereographic projections of the directions of the magnetic field which lead to open plane intersections $\epsilon = \text{const}$, $p_z = \text{const}$ with the remaining four varieties of open surfaces of (1a) are shown in Figs. 1 – 4. For surfaces described by Eq. (1), Fig. 3 takes place for $-1/4 < \beta < 0$, $3 + 6\beta < \zeta_0/\lambda < 3 + 4\beta$, while Fig. 4 holds for $0 < \beta < 1$, $\zeta_0/\lambda > 3(1 + 2\beta)$.

The stereographic projections of particular directions of the magnetic field for gold and silver constructed experimentally by Alekseevskiĭ and Gaĭdukov[6] are very close to the sterographic projections shown in Fig. 3. Figure 5 shows polar diagrams ($\mathbf{H} \perp \mathbf{j}$) of the angular dependence of the resistance of metals whose Fermi surface is an open surface of the type "three-dimensional grid" formed from corrugated cylinders whose axes are directed along the three-dimensional diagonals of the cell of the reciprocal lattice. Figure 6 shows polar diagrams for the resistance of metals with an open Fermi surface consisting of corrugated cylinders whose axes are parallel to the three-dimensional diagonals, the diagonals of the walls and the edges of the cells of the reciprocal lattice. (For the stereographic projection, see Fig. 4.) The Fermi surface for copper has a very similar topological structure.

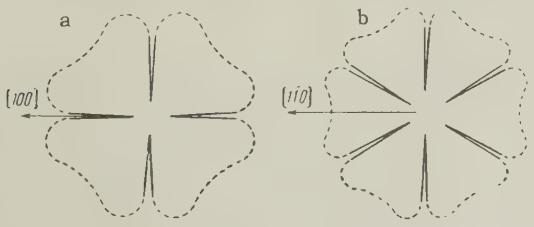

FIG. 6. Angular dependence of the resistivity $\rho(\vartheta)$ (diagram of rotation $\mathbf{H} \perp \mathbf{j}$) of metals with a Fermi surface formed from corrugated cylinders whose axes have thirteen different crystallographic directions: a – j directed along the [001] axis, b – j directed along the [111] axis.

2. As a second example, let us consider an open Fermi surface of the type "corrugated plane" (see Figs. 3 and 5 of reference 2 and Fig. 7 of the present paper) which can evidently exist for metals with hexagonal, tetragonal, and rhombic crystallographic lattices. For such a surface, open trajectories exist for any direction of the magnetic field. Their average direction p_x, generally speaking, coincides with the lines of intersection of the plane $p_z = \text{const}$ and the plane $\nu\xi$, tangent to the Fermi surface (ν, ξ, ζ are coordinate axes connected with the crystallographic axes of the reciprocal lattice). When these planes (plane $\nu\xi$ and the plane $p_z = \text{const}$) are parallel to each other, i.e., the direction of the magnetic field coincides with the ζ axis, the thickness of the layer of open trajectories vanishes (for metals with hexagonal and tetragonal crystallographic lattices), or these trajectories have a perfectly definite direction ξ, determined exclusively by the symme-

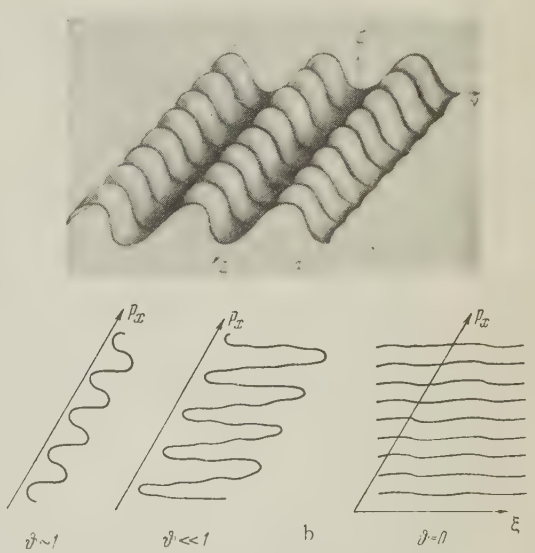

FIG. 7. a – constant energy surface of the type "corrugated plane," b – its intersection with the plane $p_z = \text{const}$.

try of the corrugated surface (for metals with rhombic crystallographic lattice). In particular, this takes place if the "ripples" on the surface have the form of parallel waves (see Fig. 7). (The ν axis is the preferred direction of the corrugation. In the direction of the ξ axis, the surface is weakly corrugated.)

For this surface particular interest is attached to the case in which the direction of the magnetic field is close to the ζ axis. For $\vartheta \lesssim \gamma_0$ (ϑ is the angle between the direction of the magnetic field and the axis ζ), the open trajectories are greatly extended in the direction of the ξ axis, although their average direction evidently coincides with the p_x axis. For $\vartheta = 0$, the direction of the open trajectories changes over from the p_x axis to the ξ axis (see Fig. 7b). It is clear that for $\vartheta \sim \gamma_0$, it is not possible to make use of the solution of the kinetic equation in powers of $\gamma_0 = H_0/H$ for the determination of the asymptotic value of the tensor σ_{ik} (see reference 1), since the average value $\overline{v}_x$ over a time of the order of the time of the mean free path of the electron ($\Delta\tau \sim 1/\gamma_0$) can turn out to be materially different from zero, whereas on all trajectories $\overline{v}_x = 0$.

A similar situation arises in the case of a surface of the "corrugated cylinder" type, when the direction of the magnetic field is almost perpendicular to the axis of the cylinder (see reference 1). In the simplest case, when the x and ξ axes are orthogonal, we obtain the following expression for σ_{ik} ($\eta = \gamma_0/\vartheta$):

$$\sigma_{ik} = \begin{pmatrix} a_{xx}(\eta) & \gamma_0 a_{xy}(\eta) & a_{xz}(\eta) \\ \gamma_0 a_{yx}(\eta) & \gamma_0^2 a_{yy}(\eta) & \gamma_0 a_{yz}(\eta) \\ a_{zx}(\eta) & \gamma_0 a_{zy}(\eta) & a_{zz}(\eta) \end{pmatrix}. \qquad (2)$$

$a_{ik}(\eta)$ can be represented by the following extrapolated formulas which characterize the behavior of σ_{ik} for $\eta \ll 1$ and $\eta \gg 1$:

$$a_{ik}(\eta) = (\alpha_{ik}^{(0)} + \alpha_{ik}^{(1)}\eta + \alpha_{ik}^{(2)}\eta^2)/(\beta_{ik} + \eta^2),$$
$$\alpha_{xx}^{(0)} = \alpha_{xx}^{(1)} = \alpha_{xz}^{(0)} = \alpha_{zx}^{(0)} = \alpha_{yy}^{(1)} = \alpha_{yz}^{(1)} = 0,$$
$$\beta_{yy} = \beta_{yz} = \beta_{zy} = 0. \qquad (3)$$

All $a_{ik}(\eta)$ tend to finite values $a_{ik}(\infty) = \alpha_{ik}^{(2)}$ as $\eta \to \infty$.

The transverse resistivity ρ in the limiting cases $\vartheta \ll \gamma_0$ and $\vartheta \gg \gamma_0$ has the following form:

$$\rho = b(H/H_0)^2 \cos^2\alpha + A; \quad \vartheta \gg \gamma_0$$
$$\rho = (H/H_0)^2 [b_1 \cos^2(\alpha + \varphi) + b_2\vartheta^2 \cos^2\alpha] + A_1; \quad \vartheta \ll \gamma_0, \qquad (4)$$

where α is the angle between the direction of the electric current and the x axis; φ is the angle between the x and ξ axes; b_1, b_2, b, A, A_1 are constants of approximately the same order. (For $\vartheta \ll \gamma_0 \ll 1$, the z axis virtually coincides with the ζ axis.)*

It can easily be seen from Eq. (4) that the transverse resistivity increases quadratically with increase in magnetic field over the whole polar diagram $\rho(\vartheta)$ if the direction of the electric field lies in the $\nu\xi$ plane and does not coincide with the ν axis. When the electric current is directed along the ζ axis, the transverse resistivity in strong magnetic fields reaches saturation independently of the orientation of the direction of the magnetic field, since all the open trajectories are perpendicular to the direction of the electric current. In all remaining cases two sharp minima exist on the polar diagram of $\rho(\vartheta)$ for the resistivity (at the point of a minimum, $\rho \approx$ const); the width of the minimum decreases with decrease in the magnetic field as 1/H. As Alekseevskiĭ and Gaĭdukov have shown,[6] the Fermi surface of gallium has evidently a similar topological structure.

In conclusion, we note that by means of polar diagrams obtained experimentally for different orientations of the electric field, it is not only possible to determine the region of the direction of the magnetic field for which there are open trajectories ϵ = const, p_z = const, but also to construct a stereographic projection of the direction of these trajectories. In certain cases, very interesting information on the Fermi surface can be obtained by an investigation of the Hall effect. For example, if at a given direction of the magnetic field, there is a layer of open trajectories ϵ = const, p_z = const with different average directions, then the Hall "constant" decreases with increase of magnetic field as $1/H^2$. Simultaneous investigation of the anisotropy of the resistivity and the Hall effect permits a more detailed study of the topological structure of the Fermi surface.

We thank N. E. Alekseevskiĭ and Yu. P. Gaĭdukov for acquainting us with their experimental results before publication.

[1] Lifshitz, Azbel', and Kaganov, JETP **31**, 63 (1956); Soviet Phys. JETP **4**, 41 (1957).

[2] I. M. Lifshitz and V. G. Peschanskiĭ, JETP **35**, 1251 (1958), Soviet Phys. JETP **8**, 875 (1959).

[3] A. B. Pippard, Phil. Trans. Roy. Soc. (London) **A250**, 325 (1957).

*In a rectangular crystal lattice the orientations of the corresponding axes in real and reciprocal space are identical.

[4] F. G. Moliner, Phil. Mag. **3**, 207 (1958).
[5] V. G. Peschanskiĭ, Dissertation, Kharkov State University, 1958.
[6] N. E. Alekseevskiĭ and Yu. P. Gaĭdukov, JETP **36**, 447 (1959), Soviet Phys. JETP **9**, 311 (1959); Yu. P. Gaĭdukov, JETP **37**, 1281 (1959), Soviet Phys. JETP **10**, 913 (1960).

Translated by R. T. Beyer
30

THE TWO-CENTER MODEL AND THE HYDRODYNAMICAL THEORY OF THE MULTIPLE PRODUCTION OF PARTICLES

A. A. EMEL'YANOV and I. L. ROZENTAL'

The P. N. Lebedev Physics Institute, Academy of Sciences, U.S.S.R.

Submitted to JETP editor July 9, 1959

J. Exptl. Theoret. Phys. (U.S.S.R.) **38**, 194-197 (January, 1960)

It is pointed out that when there are fluctuations of the initial volume or the final temperature the hydrodynamical theory of collisions of high-energy particles can lead to kinematics similar (but not identical) to that predicted by the two-center model.

RECENTLY a large number of papers have appeared (cf., e.g., references 1 — 3) giving analyses of showers registered in photographic emulsions and showing a sharply marked two-cone structure in the center-of-mass system. The kinematics of such showers can be described approximately by means of the following model: after the collision two quasi-independent systems ("fire balls") are formed, which then disintegrate isotropically in their own coordinate systems into real particles. It is well known, however, that the hydrodynamical theory of the multiple production of particles[4] is based on the existence of a single system at the instant of the collision. Therefore the question can arise of the necessity of placing these two models in opposition to each other. Without entering here into the question of the relative statistical reliability of the conclusion that two centers exist in a collision,* we would like to point out that in principle the hydrodynamical theory can lead to a kinematics of collisions which is close to that corresponding to the two-center model. The main argument against this assertion has been the difference between the angular distributions of the secondary particles as observed experimentally in these particular showers and as theoretically predicted by the hydrodynamical theory. Whereas it was previously supposed that in the center-of-mass system the theoretical maximum of the angular distribution lies in the range of angles around $\pi/2$ (if one plots as abscissa the quantity $\eta = -\ln \tan \vartheta$), experimentally one sometimes observes a minimum in this range of angles, which has a natural explanation in the two-center model. Figures 1 and 2 show as examples the angular distributions of two showers. One of them (Fig. 1) is characterized by a single maximum and is well described by the hydrodynamical theory; the other has a "two-hump" structure which corresponds approximately to the kinematics of the two-center model.

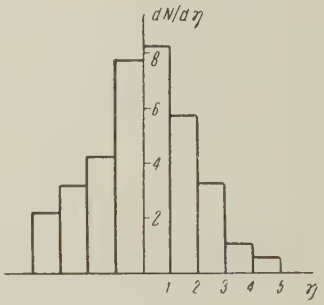

FIG. 1. Angular distribution of secondary particles in a case with a single maximum.[5] Type of interaction $1+0+37\alpha$, $\eta = -\ln \tan \vartheta$.

In the present paper we put forward the proposition that in some cases the collision kinematics predicted by the hydrodynamical theory can be close to such a "two-hump" distribution, and consequently it can simulate the kinematics of two independent centers. We begin our argument with the statement that some such "two-hump" character always exists, but cannot in practice manifest itself. Our arguments will be based on the consideration of the simple wave in the hydrodynamical solution of the problem of the separation of particles, which has not previously been taken into account in the analysis of "two-humped" showers. In fact, the particles that arise in the disintegration of the simple wave (cf., references 6, 7) have the following properties:

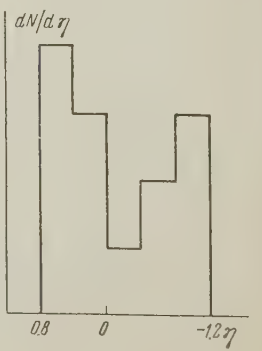

FIG. 2. Angular distribution of secondary particles in a case with two maxima.[1] Type of interaction 0 + 13p.

*The showers that give evidence of the existence of two centers are as a rule obtained as the result of a very severe selection.

with neglect of the thermal motion and for a definite primary energy the angular distribution of these particles is given by a δ function. Therefore, strictly speaking, there must be δ functions at both ends of angular distributions, and consequently the curve should theoretically have maxima at the ends and a drop in the middle. Under ordinary conditions, however, the influence of the δ-function term on the distribution is very small. In fact, the fraction Δ of the particles in the simple wave is given by the ratio

$$\Delta = T_f/2T_0, \qquad (1)$$

where T_0 is the initial and T_f the final temperature. Assuming that $T_f = \mu c^2$ (μ is the mass of the π meson),[8,9] and calculating T_0 for the initial uncompressed volume taken to be a sphere of radius $\hbar/\mu c$, we can find that there is less than one particle in each of the two simple waves, and naturally this has little effect on the total distribution. Figure 3a shows the angular distribution of the secondary particles for primary energy $E_0 = 10^{12}$ ev with the simple waves included. Here, however, the angular distribution of the secondary particles in the simple wave is represented not as a δ function, but spread out so as to take into account the thermal motion. We have approximated its effect by a Gaussian curve with $T_f = \mu c^2$.

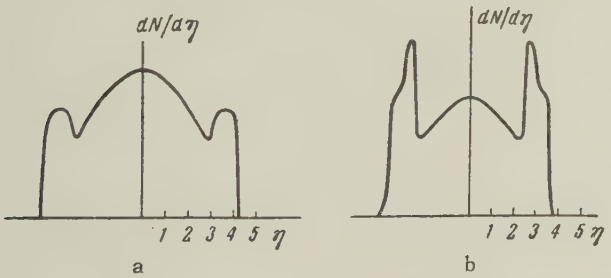

FIG. 3. Theoretical angular distribution for nucleon-nucleon interaction with $E_0 = 10^{12}$ ev: a – interaction radius $\hbar/\mu c$; b – interaction radius $2\hbar/\mu c$.

It follows from Eq. (1) that Δ depends essentially on the ratio T_f/T_0. Therefore we may suppose that to get an explanation of the "two-humped" behavior within the framework of the hydrodynamical theory we should change the value of this ratio. Some physical effects can be named that could in principle lead to an increase of this ratio. For example, it is very likely that the quantity T_f can fluctuate from shower to shower (of course in such a way that we still have $\overline{T}_f = \mu c^2$). Another cause of an increase of this ratio could be a change of the nature of the elementary act (for example, the "degree of peripherality,"[7,10] which brings with it a change of the size of the initial volume*).

Figure 3b shows the angular distribution of the secondary particles for $E_0 = 10^{12}$ ev and a doubled radius of the interaction volume. A still larger part can be played by the simple wave if the experimental indications[11] that there are showers with very small energy losses ($\sim 0.15\ E_0$) are confirmed. Such collisions can be crudely interpreted (although such an interpretation is to a considerable extent arbitrary) as resulting from collisions of "quasi-real" π mesons. In this case there is an even larger increase of the value of Δ. Figures 4a and b show

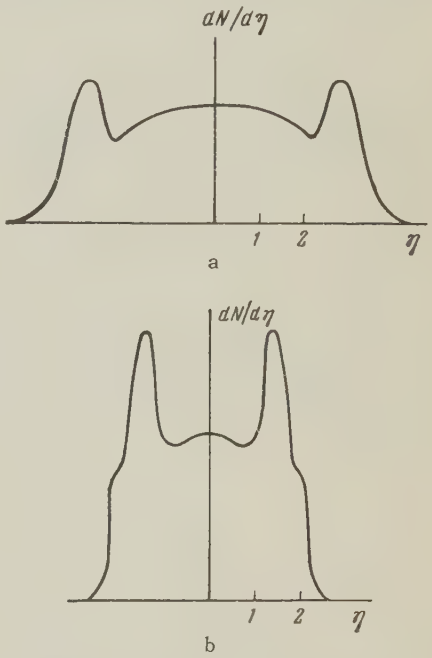

FIG. 4. Theoretical angular distribution for nucleon-nucleon interaction with energy $E_0 = 10^{12}$ ev: a – interaction radius $\hbar/\mu c$; b – interaction radius $2\hbar/\mu c$. The interaction is interpreted as a $\pi\pi$ collision.

angular distributions of the secondary particles produced in collisions of nucleons with energy $E_0 = 10^{12}$ ev. The collisions are interpreted as collisions of two π mesons moving with the same velocities as the nucleons. Furthermore it helps the explanation to note that because of the thermal motion the particles will spread apart isotropically in the coordinate system associated with the simple wave, and this simulates the effect of separate centers.

In conclusion we must state how differences can appear between the two models. First of all, if we do not assume an increase of the volume V_0 with

*In cases in which there is a fluctuation of the decay temperature and $T_f > \mu c^2$ (for the region of the simple wave) the transverse momentum of the particles will be larger than for $T_f = \mu c^2$; besides this, the fraction of K mesons among the secondary particles is increased.

the energy, then already for $E_0 > 10^{13}$ ev the "two-humped" character based on arguments from the hydrodynamical theory must disappear.*

At the present time, however, on the basis of the available experiments one cannot distinguish with certainty between the models based on the assumption of a single system and of two systems. The two models can lead to similar (though not identical) kinematics. The fact that the characteristics of individual, rarely occurring, showers may disagree quantitatively (but not qualitatively) with the curves shown in Figs. 3b and 4b is by no means a refutation of these curves. In fact, each of the "humps" of these curves contains on the average 2 to 4 particles. Furthermore there can be very large fluctuations acting to change these numbers. The problem of the quantitative testing of the present arguments (and also of any other theory describing the "two-humped" showers) can be solved only after thorough statistical analysis of experimental data.

*More exactly, this is true for the "two-humped" character arising from Eq. (1); as has been pointed out by G. A. Milekhin (private communication), if we resort to a more radical revision of the hydrodynamical theory (renouncing the equation of state $p = \varepsilon/3$) the "two-humped" behavior may become much more pronounced.

[1] Ciok, Coghen, Gierula, Holyński, Jurak, Miesowicz, and Saniewska, Nuovo cimento **10**, 741 (1958).

[2] G. Cocconi, Phys. Rev. **111**, 1699 (1958).

[3] K. Niu, Nuovo cimento **10**, 994 (1958).

[4] L. D. Landau, Izv. Akad. Nauk SSSR, Ser. Fiz. **17**, 51 (1953).

[5] Gramenitskiĭ, Zhdanov, Zamchalova, and Shcherbakova, JETP **32**, 936 (1957), Soviet Phys. JETP **5**, 763 (1957).

[6] N. M. Gerasimova and D. S. Chernavskiĭ, JETP **29**, 372 (1955), Soviet Phys. JETP **2**, 344 (1956).

[7] I. L. Rozental', JETP **31**, 278 (1956), Soviet Phys. JETP **4**, 217 (1957).

[8] Z. Koba, Prog. Theoret. Phys. **15**, 461 (1956).

[9] G. A. Milekhin and I. L. Rozental', JETP **33**, 197 (1957), Soviet Phys. JETP **6**, 154 (1958).

[10] Vernov, Grigorov, Zatsepin, and Chudakov, Izv. Akad. Nauk SSSR, Ser. Fiz. **19**, 493 (1955), Columbia Tech. Transl. p. 445.

[11] Edwards, Losty, Perkins, Pinkau, and Reynolds, Phil. Mag. **3**, 237 (1958).

Translated by W. H. Furry
31

GREEN'S FUNCTION IN THE FIXED-SOURCE MODEL OF CHARGED SCALAR MESONS

B. M. BARBASHOV and G. V. EFIMOV

Joint Institute for Nuclear Research

Submitted to JETP editor July 9, 1959

J. Exptl. Theoret. Phys. (U.S.S.R.) **38**, 198-200 (January, 1960)

The calculation of the Green's function for a static nucleon, interacting with charged scalar mesons is given as an example of a new method of solution which is different from the perturbation method.

We consider a system with a Hamiltonian of the form

$$H = m(\psi^+\psi) + \frac{1}{2}\sum_{i=1}^{2}\int d\mathbf{x} : [\pi_i^2(\mathbf{x}) + (\nabla\varphi_i(\mathbf{x}))^2 + \mu^2\varphi_i^2(\mathbf{x})] :$$
$$+ g\sum_{i=1}^{2}\int d\mathbf{x}\,(\psi^+\tau_i\psi)\,\varphi_i(\mathbf{x})\,\rho(\mathbf{x}). \qquad (1)$$

Here ψ^+ and ψ are nucleon field operators, $\pi_i(\mathbf{x})$ and $\varphi_i(\mathbf{x})$ are meson field operators, $\rho(\mathbf{x}) = \sum v(k)\,e^{i\mathbf{k}\cdot\mathbf{x}}$ is the nucleon form factor, and the τ_i are the isotopic spin-$\frac{1}{2}$ matrices.

On the basis of results from references 1 – 3, it can be shown that the nucleon Green's function in our case can be represented as a functional integral of the following form:

$$G(t-t_0) = \langle 0|T\{\psi(t)\psi^+(t_0)S\}|0\rangle / \langle 0|S|0\rangle$$
$$= \frac{1}{C}\int\!\!\int \delta\Lambda_1\delta\Lambda_2\widetilde{G}(t-t_0;\,\Lambda_1,\,\Lambda_2)$$
$$\times\exp\left\{\frac{i}{2}\int_{t_0}^{t}\int_{t_0}^{t} ds_1 ds_2\Delta^{-1}(s_1-s_2)\,\Lambda_j(s_1)\,\Lambda_j(s_2)\right\}. \qquad (2)$$

Here $\Delta^{-1}(s_1-s_2)$ is determined by the relation

$$\int_{t_0}^{t}\Delta^{-1}(s_1-s_2)\,\Delta(s_2-s_3)\,ds_2 = \delta(s_1-s_3),$$

where

$$i\delta_{kl}\Delta(s_1-s_2) = \langle 0\left|T\left\{\hat{\varphi}_k(s_1)\hat{\varphi}_l(s_2)\right\}\right|0\rangle$$
$$= \delta_{kl}\sum\frac{v^2(k)}{2\omega_k}\exp\left\{-i\omega_k|s_1-s_2|\right\},$$

$$\hat{\varphi}_l(s) = \sum\frac{v(k)}{\sqrt{2\omega_k}}(a_{lk}e^{-i\omega_k s} + a_{lk}e^{+i\omega_k s}),$$

C is the normalization constant, and $\Lambda_j(s)$ are real scalar functions. $\widetilde{G}(t-t_0;\,\Lambda_1,\,\Lambda_2)$ is a nucleon Green's function in an external classical field $\Lambda_j(s)$ and obeys the equation

$$[i\partial/\partial t - m - g(\tau_1\Lambda_1(t) + \tau_2\Lambda_2(t))]\widetilde{G}(t-t_0;\,\Lambda_1,\,\Lambda_2)$$
$$= i\delta(t-t_0),$$
$$\widetilde{G}(t-t_0;\,\Lambda_1,\,\Lambda_2)|_{t<t_0} = 0. \qquad (3)$$

Therefore the problem of finding the nucleon Green's function reduces to the solution of (3) and to the functional integration of the solution found with the weight function

$$\exp\left\{\frac{i}{2}\int_{t_0}^{t}\int_{t_0}^{t} ds_1 ds_2\Delta^{-1}(s_1-s_2)\,\Lambda_j(s_1)\,\Lambda_j(s_2)\right\}.$$

To solve (3) we write $\widetilde{G}$ in the form

$$\widetilde{G}(t-t_0;\,\Lambda_1,\,\Lambda_2) = \theta(t-t_0)\,e^{-im(t-t_0)}\,Y(t-t_0;\,\Lambda_1,\,\Lambda_2).$$

Then $Y(t-t_0;\,\Lambda_1,\,\Lambda_2)$ will obey the following equation:

$$i\frac{\partial}{\partial t}Y(t-t_0;\,\Lambda_1,\,\Lambda_2)$$
$$= g(\tau_1\Lambda_1(t) + \tau_2\Lambda_2(t))\,Y(t-t_0;\,\Lambda_1,\,\Lambda_2),$$
$$Y(t-t_0;\,\Lambda_1,\,\Lambda_2)|_{t=t_0} = I. \qquad (4)$$

Methods of solving matrix equations like (4) were developed by Lappo-Danilevskiĭ.[4] Making use of them, one can find the integral matrix of (4) as an entire function of the matrices I and τ_i.

$$Y(t-t_0;\,\Lambda_1,\,\Lambda_2)$$
$$= \Phi_0(t-t_0;\,\Lambda_1,\,\Lambda_2)\,I + \sum_{i=1}^{3}\Phi_i(t-t_0;\,\Lambda_1,\,\Lambda_2)\,\tau_i. \qquad (5)$$

If we introduce the notation

$$p^{(m)}(t-t_0;\,\Lambda_1,\,\Lambda_2) = (i\sqrt{2}\,g)^m\int_{t_0}^{t} d\xi_1\int_{t_0}^{\xi_1} d\xi_2$$
$$\ldots\int_{t_0}^{\xi_{m-1}} d\xi_m\Lambda_1(\xi_1)\,\Lambda_2(\xi_2)\,\Lambda_1(\xi_3)$$
$$\ldots\exp\left\{ig\int_{t_0}^{t}\rho^{(m)}_{\xi_1\xi_2\ldots\xi_m}(s)\,[\Lambda_1(s)-\Lambda_2(s)]\,ds\right\},$$

where

$$\rho^{(m)}_{\xi_1\xi_2\ldots\xi_m}(s) = \begin{cases} 1 & \xi_{2k} < s < \xi_{2k+1} \\ -1 & \xi_{2k+1} < s < \xi_{2k} \end{cases},$$

the functions Φ_0 and Φ_i can be written in the form

$$\Phi_0(t-t_0;\ \Lambda_1, \Lambda_2) = \frac{1}{2}\sum_{n=0}^{\infty}\{p^{(2n)}(t-t_0;\ \Lambda_1, \Lambda_2) + p^{(2n)}(t-t_0;\ \Lambda_2, \Lambda_1)\};$$

$$\Phi_1(t-t_0;\ \Lambda_1, \Lambda_2) = \Phi_2(t-t_0;\ \Lambda_2, \Lambda_1) = \frac{1}{2}\sum_{n=0}^{\infty}\{p^{(2n)}(t-t_0;\ \Lambda_1, \Lambda_2) - p^{(2n)}(t-t_0;\ \Lambda_2, \Lambda_1) - \sqrt{2}\,p^{(2n+1)}(t-t_0;\ \Lambda_1, \Lambda_2)\},$$

$$\Phi_3(t-t_0;\ \Lambda_1, \Lambda_2) = \frac{1}{2}\sum_{n=0}^{\infty}\{-p^{(2n)}(t-t_0;\ \Lambda_1, \Lambda_2) + p^{(2n)}(t-t_0;\ \Lambda_2, \Lambda_1) - \sqrt{2}\,p^{(2n+1)}(t-t_0;\ \Lambda_1, \Lambda_2) + \sqrt{2}\,p^{(2n+1)}(t-t_0;\ \Lambda_2, \Lambda_1)\}.$$

Further on, it is shown that having solution (5) one can carry out the functional integration (2), since there arise integrals of the Gaussian type, which can be calculated by a method given by Feynman.[1] Omitting a long computation, we write down the final expression for the Green's function

$$G(t-t_0) = \theta(t-t_0)\,e^{-im(t-t_0)}\Big[\exp\Big\{-\frac{ig^2}{2}\int_{t_0}^{t}\int_{t_0}^{t}\Delta(s_1-s_2)\,ds_1 ds_2\Big\} + (-ig^2)\int_{t_0}^{t}dt_1\int_{t_0}^{t_1}dt_2\,\Delta(t_1-t_2)\exp\Big\{-\frac{ig^2}{2}\int_{t_0}^{t}\int_{t_0}^{t}\rho^{(2)}_{t_1t_2}(s_1) \times \Delta(s_1-s_2)\,\rho^{(2)}_{t_1t_2}(s_2)\,ds_1 ds_2\Big\} + \ldots + (-ig^2)^n\int_{t_0}^{t}dt_1\int_{t_0}^{t_1}dt_2\ldots\int_{t_0}^{t_{2n-1}}dt_{2n} \times [P\Delta(t_1-t_2)\,\Delta(t_3-t_4)\ldots\Delta(t_{2n-1}-t_{2n})] \times \exp\Big\{-\frac{ig^2}{2}\int_{t_0}^{t}\int_{t_0}^{t}\rho^{(2n)}_{t_1,t_2,\ldots t_{2n}}(s_1)\,\Delta(s_1-s_2)\,\rho^{(2n)}_{t_1,t_2,\ldots t_{2n}} \times (s_2)\,ds_1, ds_2\Big\} + \ldots\Big], \qquad (6)$$

where P is a symmetrization operator on the variables $t_1, t_2, \ldots t_{2n}$, for example

$$P\Delta(t_1-t_2)\,\Delta(t_3-t_4) = \Delta(t_1-t_2)\,\Delta(t_3-t_4) + \Delta(t_1-t_3)\,\Delta(t_2-t_4) + \Delta(t_1-t_4)\,\Delta(t_2-t_3).$$

We note that the method used allows us to write down the n-th term in the series (6), in contrast to perturbation theory. The first term in the series (6) is the exact Green's function for a nucleon interacting with scalar neutral mesons.[3] On expanding in terms of g^2, our series goes over to the perturbation theory result. For series (6) there exists the bounding function

$$\exp\Big\{-\frac{ig^2}{2}\int_{t_0}^{t}\int_{t_0}^{t}\Delta(s_1-s_2)\,ds_1 ds_2\Big\}\Big(1+\exp\Big\{\frac{g^2t^2}{2}\sum\frac{v^2(k)}{2\omega_k}\Big\} + \exp\Big\{\frac{g^2t^2}{4}\sum\frac{v^2(k)}{2\omega_k}\Big\}\Big).$$

In that way, with v(k) for which the sum $\sum v^2(k)/2\omega_k$ is finite, the series (6) converges absolutely and uniformly for arbitrary finite values of t and g^2.

Questions of renormalizing the Green's functions obtained require further investigation.

In ending, we express our deep gratitude to Prof. D. I. Blokhintsev and Academician N. N. Bogolyubov for valuable discussions, and also to Yu. L. Obukhov for his consideration of mathematical questions.

[1] R. P. Feynman, Phys. Rev. **84**, 108 (1951).

[2] N. N. Bogolyubov and D. V. Shirkov, Введение в теорию квантованных полей, (Introduction to the Theory of Quantum Fields), Gostekhizdat, 1957.

[3] S. F. Edwards and R. E. Peierls, Proc. Roy. Soc. (London) **224**, 24 (1954).

[4] I. A. Lappo-Danilevskiĭ, Применение функций от матриц к теории линейных систем обыкновенных дифференциальных уравнений, (The Application of Functions of Matrices to the Theory of Linear Systems of Ordinary Differential Equations), Gostekhizdat, 1957.

Translated by W. Ramsay
32

SCATTERING OF GAMMA-RAY QUANTA BY NUCLEONS NEAR THE THRESHOLD FOR MESON PRODUCTION

L. I. LAPIDUS and CHOU KUANG-CHAO

Joint Institute for Nuclear Research

Submitted to JETP editor July 9, 1959

J. Exptl. Theoret. Phys. (U.S.S.R.) 38, 201-211 (January, 1960)

The elastic scattering of γ-ray quanta near the threshold for single meson production is treated by means of dispersion relations. It is shown that when one takes into account meson production in the s state there are appreciable departures from monotonic variation with energy of the scattering amplitudes, cross sections, and other observable quantities near the threshold of the reaction. On definite assumptions about the analysis of photoproduction in the range of γ-ray energies up to 220 Mev, calculations are made of the scattering amplitude and the differential and total cross sections for elastic scattering of polarized and unpolarized γ-rays by protons, and also of the polarization of the recoil protons above the photoproduction threshold.

1. The study of the scattering of γ-ray quanta by nucleons is especially interesting near the threshold for single meson production. The region near the photoproduction threshold is of interest not only for comparisons with the predictions of dispersion relations, but also in particular in connection with the studies of departures from monotonic variation with the energy of the cross-sections (and polarizations) near the threshold of the reaction.[1] From this latter point of view the scattering of γ-ray quanta by nucleons and nuclei near the threshold for meson production is of especial interest as an example of a process going with a comparatively small cross section and being strongly perturbed above threshold by the process of intense meson production. Thus marked effects can be expected in the region near the threshold. It is clear that a sufficiently accurate experimental study of the anomalies near the threshold can be useful in understanding the process of pion production near threshold.

As a more detailed examination shows, the polarization effects are especially sensitive to the parameters characterizing the photoproduction of pions. Our main purpose here is a detailed examination of the effect of meson production on the cross section, the polarization of the recoil nucleons, and the polarization of the γ rays near the photoproduction threshold.

Phenomenological analysis and dispersion relations are used to obtain formulas useful for the analysis of experimental data. The results of the numerical calculations, which are based on definite assumptions about the analysis of the photoproduction, must be regarded as preliminary. In making the numerical estimates we have completely neglected fine-structure effects associated with the mass difference of the mesons (and of the nucleons).

There are many well known papers in which the scattering of γ-ray quanta by nucleons has been treated by various methods (see literature references in our previous paper[2]). In the present paper we have tried to manage with a minimum number of assumptions, without resorting to approximate methods, whose use is hard to justify. We consider not only the scattering cross sections for unpolarized γ rays, but also the polarization effects in the scattering. In this connection we have also considered the polarization of the γ rays.

2. Let us represent the transition matrix in the form

$$\mathcal{M} = \sum_{\mu\nu} e'_\mu N_{\mu\nu} e_\nu \equiv (\mathbf{e'Ne}).$$

Let us choose two coordinate systems x, y, z and x′, y′, z′ in which the z and z′ axes are parallel to the initial and final momenta of the photon, and the y and y′ axes are in the same direction. In these coordinates the functions for the spin eigenstates of the photon with the eigenvalues $S_z = \pm 1$ have the following form:

$$\zeta_1 = -(\mathbf{h} - i\mathbf{j})/\sqrt{2}, \qquad \zeta_{-1} = (\mathbf{h} + i\mathbf{j})/\sqrt{2},$$
$$\zeta'_1 = -(\mathbf{h}' - i\mathbf{j})/\sqrt{2}, \qquad \zeta'_{-1} = (\mathbf{h}' + i\mathbf{j})/\sqrt{2}, \qquad (1)$$

where $\mathbf{h}$, $\mathbf{j}$, and $\mathbf{k}$ are unit basis vectors directed along these coordinate axes. In the general

case the polarization state of the photon will be a linear combination, i.e.,

$$\mathbf{e} = c_1\zeta_1 + c_{-1}\zeta_{-1}, \tag{2}$$

where c_1 and c_{-1} are the respective probabilities (sic) of the photon states with $S_Z = +1$ and $S_Z = -1$.

Using the spin eigenstates as the basis of the representation, we can write the transition matrix in the form

$$\mathcal{M} = \begin{pmatrix} (\zeta_1'^{*}\mathbf{N}\zeta_1) & 0 & (\zeta_1'^{*}\mathbf{N}\zeta_{-1}) \\ 0 & 0 & 0 \\ (\zeta_{-1}'^{*}\mathbf{N}\zeta_1) & 0 & (\zeta_{-1}'^{*}\mathbf{N}\zeta_{-1}) \end{pmatrix}. \tag{3}$$

Let us further introduce the density matrix of the photon in the form

$$\rho = \begin{pmatrix} c_1c_1^{*} & 0 & c_1c_{-1}^{*} \\ 0 & 0 & 0 \\ c_{-1}c_1^{*} & 0 & c_{-1}c_{-1}^{*} \end{pmatrix}. \tag{4}$$

The density matrix ρ_f of the final state is connected with the density matrix ρ_{in} of the initial state by the relation

$$\rho_f = \mathcal{M}\rho_{in}\mathcal{M}^{+}. \tag{5}$$

Although in Eqs. (3) and (4) the transition matrix and the density matrix are written as three-rowed matrices, they have only four independent nonzero elements. Consequently we can represent them by means of two-rowed matrices and use the well known apparatus of the Pauli matrices.[3]

$$\mathcal{M} = \begin{pmatrix} (\zeta_1'^{*}\mathbf{N}\zeta_1) & (\zeta_1'^{*}\mathbf{N}\zeta_{-1}) \\ (\zeta_{-1}'^{*}\mathbf{N}\zeta_1) & (\zeta_{-1}'^{*}\mathbf{N}\zeta_{-1}) \end{pmatrix} = A + \mathbf{B}\sigma_\gamma, \tag{6}$$

$$\rho = \begin{pmatrix} c_1c_1^{*} & c_1c_{-1}^{*} \\ c_{-1}c_1^{*} & c_{-1}c_{-1}^{*} \end{pmatrix} = \frac{1}{2}(1 + \sigma_\gamma\mathbf{P}), \tag{7}$$

where P_X, P_Y, and P_Z are the Stokes parameters. Nonvanishing P_X and P_Y correspond to linear polarization of the photons along the x and y axes, while $P_Z \neq 0$ corresponds to circular polarization of the photon.

From Eq. (6) it is not hard to get

$$\begin{aligned} 2A &= (\zeta_1'^{*}\mathbf{N}\zeta_1) + (\zeta_{-1}'^{*}\mathbf{N}\zeta_{-1}) = \mathrm{Sp}\,\mathcal{M}, \\ 2B_z &= (\zeta_1'^{*}\mathbf{N}\zeta_1) - (\zeta_{-1}'^{*}\mathbf{N}\zeta_{-1}) = \mathrm{Sp}(\sigma_\gamma^z\mathcal{M}), \\ 2B_x &= (\zeta_1'^{*}\mathbf{N}\zeta_{-1}) + (\zeta_{-1}'^{*}\mathbf{N}\zeta_1) = \mathrm{Sp}\,(\sigma_\gamma^x\mathcal{M}), \\ 2iB_y &= (\zeta_1'^{*}\mathbf{N}\zeta_{-1}) - (\zeta_{-1}'^{*}\mathbf{N}\zeta_1) = i\,\mathrm{Sp}\,(\sigma_\gamma^y\mathcal{M}) \end{aligned} \tag{8}$$

where the spurs (traces) are taken over the photon variables. The quantities A and B_i can be connected with the quantities $R_1, \ldots, R_6$, which were introduced in reference 2 (hereafter referred to as I) and which determine the matrix $\mathcal{M}$ [cf. Eq. (I, 15)]:

$$\begin{aligned} 2A &= (R_1 + R_2)(1 + \cos\theta) - i(R_3 + R_4)\sin\theta(\sigma\mathbf{n}), \\ 2B_z &= (R_3 + R_4)\,\sigma(\mathbf{k} + \mathbf{k}') + (1 + \cos\theta)(R_5 + R_6)\,\sigma(\mathbf{k} + \mathbf{k}'), \\ 2iB_y &= [R_3 - R_4 - (1 - \cos\theta)(R_5 - R_6)]\,\sigma(\mathbf{k} - \mathbf{k}'), \\ 2B_x &= (R_1 - R_2)(1 - \cos\theta) + i(R_3 + R_4)\sin\theta\,(\sigma\mathbf{n}), \end{aligned} \tag{9}$$

where $\mathbf{n}\sin\theta = \mathbf{k}\times\mathbf{k}'$, $\cos\theta = \mathbf{k}\cdot\mathbf{k}'$.

It is easy to calculate the density matrix of the final state:

$$\begin{aligned} \rho_f &= \tfrac{1}{2}(A + \sigma_\gamma\mathbf{B})(1 + \sigma_\gamma\mathbf{P})(A^{+} + \sigma_\gamma\mathbf{B}^{+}) \\ &= \tfrac{1}{2}\{AA^{+} + \mathbf{BB}^{+} + (A\mathbf{B}^{+} + \mathbf{B}A^{+})\mathbf{P} - i([\mathbf{BB}^{+}]\mathbf{P})\} \\ &+ \tfrac{1}{2}\sigma_\gamma\{A\mathbf{B}^{+} + \mathbf{B}A^{+} + i[\mathbf{BB}^{+}] + (AA^{+} - \mathbf{BB}^{+})\mathbf{P} + [\mathbf{B}(\mathbf{PB}^{+}) \\ &+ (\mathbf{BP})\mathbf{B}^{+}] + iA[\mathbf{PB}^{+}] - i[\mathbf{PB}]A^{+}\}. \end{aligned} \tag{10}$$

By means of the expression (10) one can calculate all observable quantities. For the interaction of unpolarized γ rays and nucleons the differential cross section will have the form

$$d\sigma/do \equiv I_0(\theta) = \tfrac{1}{2}\,\mathrm{Sp}\,(AA^{+} + \mathbf{BB}^{+}), \tag{11}$$

where the spur is taken over the nucleon variables. Substituting Eq. (9) in Eq. (11), we get

$$\begin{aligned} 4I_0(\theta) &= |R_1 + R_2|^2(1 + \cos^2\theta) + |R_1 - R_2|^2(1 - \cos\theta)^2 \\ &+ |R_3 + R_4|^2(3 - \cos^2\theta + 2\cos\theta) \\ &+ |R_3 - R_4|^2(3 - \cos^2\theta - 2\cos\theta) \\ &+ 2|R_5 + R_6|^2(1 + \cos\theta)^3 + 2|R_5 - R_6|^2(1 - \cos\theta)^3 \\ &+ 4\mathrm{Re}\,(R_3 + R_4)^{*}(R_5 + R_6)(1 + \cos\theta)^2 \\ &- 4\mathrm{Re}\,(R_3 - R_4)^{*}(R_5 - R_6)(1 - \cos\theta)^2. \end{aligned} \tag{12}$$

The expression for the polarization of the nucleon after the interaction of an initially unpolarized photon and nucleon can be represented in the form*

$$\begin{aligned} 2I_0(\theta)\langle\sigma\rangle_f &= \sin\theta\,\mathbf{n}\,\mathrm{Im}\,[(R_3 + R_4)(R_1 + R_2)^{*}(1 + \cos\theta) \\ &- (R_3 - R_4)(R_1 - R_2)^{*}(1 - \cos\theta)] \\ &= 2i[\mathbf{k}\times\mathbf{k}']\{R_1R_4^{*} - R_1^{*}R_4 + R_2R_3^{*} - R_2^{*}R_3 \\ &+ [R_1R_3^{*} - R_1^{*}R_3 + R_2R_4^{*} - R_2^{*}R_4]\cos\theta\}. \end{aligned} \tag{13}$$

The well known fact that the cross section $I_0(\theta)$ does not change when one replaces electric transitions by magnetic appears in the fact that Eq. (12) is invariant under the simultaneous interchanges:

$$R_1 \rightleftarrows R_2, \qquad R_3 \rightleftarrows R_4, \qquad R_5 \rightleftarrows R_6. \tag{14}$$

It can be seen from Eq. (13) that the expression for the polarization of the recoil nucleon also remains unchanged by this transformation.

3. Let us now establish the relations between the Stokes parameters and the statistical tensor moments. As is well known, the statistical tensor moments are defined by the relations

*Eqs. (19), (23), and (24) in reference 4 contain errors.

$$T_{00}=1/\sqrt{3},\quad T_{10}=S_z/\sqrt{2},\quad T_{20}=\sqrt{\tfrac{2}{3}}\left(\tfrac{3}{2}S_z^2-1\right),$$
$$T_{22}=\tfrac{1}{2}[S_x^2-S_y^2+i(S_xS_y+S_yS_x)],$$
$$T_{2-2}=\tfrac{1}{2}[S_x^2-S_y^2-i(S_xS_y+S_yS_x)]. \quad (15)$$

They are normalized so that

$$\mathrm{Sp}\, T_{JM}T^{+}_{J'M'}=\delta_{JJ'}\delta_{MM'}. \quad (16)$$

By means of these tensor moments the density matrix can be represented in the form

$$\rho_f=\rho_{00}T_{00}+\rho_{10}T_{10}+\rho_{20}T_{20}+\rho_{22}T_{22}+\rho_{2-2}T_{2-2}. \quad (17)$$

Here $\rho_{00}=2^{1/2}\rho_{20}=3^{-1/2}$. The parameters ρ_{JM} are connected with the Stokes parameters:

$$\rho_{10}=\sqrt{2}P_z,\quad \rho_{22}=P_x-iP_y,\quad \rho_{2-2}=P_x+iP_y. \quad (18)$$

In virtue of time-reversal invariance,[5,4] the expression for the cross section $I(\theta,\varphi)$ for scattering of a polarized γ-ray beam by unpolarized protons can be put in the form

$$I(\theta,\varphi)=I_0(\theta)[1+2\langle T_{22}\rangle_i\langle T_{22}\rangle_f\cos 2\varphi], \quad (19)$$

where

$$2I_0(\theta)\langle T_{22}\rangle_f=\sin^2\theta(|R_1|^2+|R_4|^2-|R_2|^2-|R_3|^2), \quad (20)$$

$\langle T_{22}\rangle_i$ is the initial polarization of the γ-ray beam. We note that the expression (20) changes sign under the transformation (14).

4. For practical calculations we use the results of reference 2. The deviations from monotonic variation of the cross-section for scattering of γ rays in the immediate neighborhood of the meson-production threshold are due to the production of mesons in the s state. According to the available experimental data, the cross section for production of π^+ mesons in the s state is much larger than the cross section for production of π^0 mesons in this state. Difficult experiments had to be done even to establish the fact that π^0 mesons indeed are produced in the s state.

The energy ν of a photon in the laboratory system (l.s.) and the energy ν_c in the center-of-mass system (c.m.s.) are connected by the well known relation

$$\nu_c=\nu/\sqrt{1+2\nu/M}.$$

Using the expression for the total energy of the meson in the c.m.s.

$$\omega_c=(\nu+m_\pi^2/2M)/\sqrt{1+2\nu/M}$$

we find without difficulty that the expression for the square of the momentum of the meson produced

$$q_c^2=\omega_c^2-m_\pi^2=(\nu-\nu_0)(\nu+\nu_0-m_\pi^2/2M)/(1+2\nu/M);$$
$$\nu_0=m_\pi(1+m_\pi/2M)$$

can with some accuracy (better than 7.5 percent) be replaced by

$$q_c^2\approx(\nu^2-\nu_0^2)/(1+2\nu/M). \quad (21)$$

This then gives

$$q_c/\nu_c=(\nu^2-\nu_0^2)^{1/2}/\nu.$$

Because there is a mass difference between neutron and proton and between π^+ and π^0 mesons, the effects near threshold in the scattering of γ rays by nucleons have a "fine structure." To make reliable numerical calculations one would need a much more detailed analysis of the data on photoproduction than we now have available. Wishing to get an idea of the scale of size of the effects near threshold, we shall confine ourselves mainly to a consideration of π^+-meson production. The quantities E_1, E_{33}, and M_{33} are taken from the analysis of Watson and others.[6] The production of π^0 mesons is taken into account only in the resonance state (through M_{33}). The connection of the photoproduction amplitudes with the π-N scattering phase shifts is well known (cf., e.g., references 6, 7).* In the range of energies where we can neglect the difference between the $\nu_0(\pi^0)$ and $\nu_0(\pi^+)$ thresholds, when we sum the contributions from π^+ and π^0 mesons the terms containing the π-N scattering phase shifts cancel each other. For example

$$|M_3^+|^2+|M_3^0|^2=6|M_{33}|^2+\tfrac{3}{4}|M_{13}^{(1)}-2\delta M_{13}^{(1)}|^2\approx 6|M_{33}|^2.$$

We have calculated the dispersion integrals by using simple expressions to interpolate the energy dependence of $|E_1|^2$ and $|M_{33}|^2$ and then integrating directly. Setting $\nu_0=150$ Mev, and hereafter measuring energies in terms of ν_0, in the range $1\le\nu\le\nu_1=2.20$ we approximate the energy dependence of $|E_1|^2$ by the following expression:

$$|E_1|^2\approx|E_1^+|^2=A\sqrt{\nu^2-1}/\nu,$$
$$A=(3.3\cdot 10^{-15}\,\mathrm{cm/sr}^{1/2})^2\nu_0=0.54\ e^2/M. \quad (22)$$

It is just the contribution E_1^2 in the dispersion integrals that leads to the nonmonotonic behavior in the energy dependence of the real parts of the amplitudes. As can be seen from (I, 42), the contribution of $|E_1|^2$ is characterized by two integrals

$$\frac{2\nu^2}{\pi}\int_1^{\nu_1}\frac{|E_1|^2}{\nu'^2-\nu^2}d\nu',\qquad \frac{2\nu^3}{\pi}\int_1^{\nu_1}\frac{|E_1|^2\,d\nu'}{\nu'(\nu'^2-\nu^2)}. \quad (23)$$

Substitution of Eq. (22) in the expression (23) gives

*In the more general form of the problem[4] one requires the parametrization of a three-rowed S matrix, which describes both the photo-production and scattering of π mesons and also the scattering of γ rays by nucleons. For the scattering of γ rays effects of deviations from isotopic invariance can give additions to the scattering phase shifts (and to the mixing coefficients) that are by no means small.

$$\frac{2\nu^2}{\pi}\int_1^{\nu_1}\frac{|E_1|^2}{\nu'^2-\nu^2}d\nu' = \frac{2}{\pi}A\times\begin{cases}\tan^{-1}(\nu_1^2-1)^{1/2} - \dfrac{(\nu^2-1)^{1/2}}{2}\ln\left|\dfrac{(\nu_1^2-1)^{1/2}+(\nu^2-1)^{1/2}}{(\nu_1^2-1)^{1/2}-(\nu^2-1)^{1/2}}\right|, & \nu>1\\ \tan^{-1}(\nu_1^2-1)^{1/2} - (1-\nu^2)^{1/2}\tan^{-1}\sqrt{\dfrac{\nu_1^2-1}{1-\nu^2}}, & \nu<1\end{cases} \quad (24)$$

and

$$\frac{2}{\pi}\nu^3\int_1^{\nu_1}\frac{|E_1|^2}{\nu'(\nu'^2-\nu^2)}d\nu' = \frac{2}{\pi}A\nu\times\begin{cases}\left(\dfrac{\nu_1^2-1}{\nu_1^2}\right)^{1/2} - \dfrac{(\nu^2-1)^{1/2}}{2\nu}\ln\left|\dfrac{\nu(\nu_1^2-1)^{1/2}+\nu_1(\nu^2-1)^{1/2}}{\nu(\nu_1^2-1)^{1/2}-\nu_1(\nu^2-1)^{1/2}}\right|, & \nu>1\\ \left(\dfrac{\nu_1^2-1}{\nu_1^2}\right)^{1/2} - \left(\dfrac{1-\nu^2}{\nu^2}\right)^{1/2}\tan^{-1}\sqrt{\dfrac{\nu^2(\nu_1^2-1)}{\nu_1^2(1-\nu^2)}}, & \nu<1.\end{cases} \quad (25)$$

From Eqs. (24), (25), (22), (I, 42), and (I, 32) it can be seen that at the meson-production threshold the derivatives of the quantities R_1 and R_3 go to infinity (approaching threshold from the side $\nu > 1$), and the derivatives of the real parts of these quantities also go to infinity (on the side $\nu < 1$), whereas on the other side of threshold the derivatives are finite. This result is very general. Thus the dispersion relations turn out to contain specific effects near the reaction threshold like those discussed and analyzed without use of the dispersion relations by Wigner, Baz', Okun', Breit, Capps, Newton, and others.*

The use of dispersion relations makes it possible to examine in more detail the effect on the elastic scattering (or on the reaction) of the inelastic processes that occur in a certain energy range. Moreover, the interesting effects that occur in the immediate neighborhood of the reaction threshold ("local effects" which could be discussed when one does not use the method of analytic continuation given by the dispersion relations) are only a part of the total effect of the inelastic processes on the energy dependences of the quantities that characterize the elastic scattering.

From the example of the scattering of γ rays by protons we can see how the presence of the inelastic process of meson photoproduction in the energy range $\nu > 1$ affects the characteristics of the elastic scattering, including also effects for $\nu < 1$ (deviation from the Powell formula, or from Eq. (I.16) for $\gamma < 1$). The deviation from monotonic variation in Eqs. (24) and (25) is characterized by a sharp drop from the value of the function at $\nu = 1$ in the region $\nu < 1$ (with an infinite derivative at $\nu = 1$) and a slow drop in the region $\nu > 1$ (with a finite derivative at $\nu = 1$).

5. In the range of energies 330 – 500 Mev ($2.2 < \nu < 3.34$) the quantity $|E_1|^2$ is represented in the form

$$|E_1|^2 = 1.27(1-0.175\nu)^2 e^2/M. \quad (26)$$

The contribution from this energy range to the values of the real parts of the amplitudes is small, if for the scattering of the γ rays we consider the energy near and below the threshold.

The analysis of the photoproduction made previously, and particularly the results of Akiba and Sato, indicate that

$$|M_3|^2 = 6|M_{33}|^2 \approx |E_2|^2 \approx \mathrm{Re}(E_2^* M_3). \quad (27)$$

For our estimates we adopt Eq. (27). The polarization of the recoil nucleons is especially sensitive to this assumption. In the energy range $1 < \nu < 2$ the quantity $|M_{33}|^2$ can be approximated by the expression

$$|M_{33}|^2 = B_0\nu(\nu^2-1)^{3/2}, \qquad B_0 = 0.009e^2/M. \quad (28)$$

Consequently,

$$|M_3|^2 = 6|M_{33}|^2 = B\nu(\nu^2-1)^{3/2}, \qquad B = 0.054e^2/M,$$

and the contribution of this expression, which describes the production of mesons in the p state, to the dispersion relations is given by the integrals

$$\frac{2\nu^2}{\pi}\int_1^{\nu_1}\frac{|E_2|^2}{\nu'^2-\nu^2}d\nu' = \frac{2B}{\pi}\nu^2\left[\frac{1}{3}(\nu_1^2-1)^{3/2}+(\nu_1^2-1)^{1/2}(\nu^2-1)\right] + \frac{2B}{\pi}\nu^2\begin{cases}-\frac{1}{2}(\nu^2-1)^{3/2}\ln\left|\dfrac{(\nu_1^2-1)^{1/2}+(\nu^2-1)^{1/2}}{(\nu_1^2-1)^{1/2}-(\nu^2-1)^{1/2}}\right|, & \nu>1\\ (1-\nu^2)^{3/2}\tan^{-1}\sqrt{(\nu_1^2-1)/(1-\nu^2)}, & \nu<1\end{cases} \quad (29)$$

and

$$\frac{2\nu^3}{\pi}\int_1^{\nu_1}\frac{d\nu'}{\nu'}\frac{|E_2|^2}{\nu'^2-\nu^2} = \frac{B}{\pi}\nu^3\left[\nu_1(\nu_1^2-1)^{1/2}+(\nu^2-3/2)\ln\left|\frac{\nu_1+(\nu_1^2-1)^{1/2}}{\nu_1-(\nu_1^2-1)^{1/2}}\right|\right] - \frac{B}{\pi}\nu^3(\nu^2-1)\begin{cases}\sqrt{\dfrac{\nu^2-1}{\nu^2}}\ln\left|\dfrac{\nu(\nu_1^2-1)^{1/2}+\nu_1(\nu^2-1)^{1/2}}{\nu(\nu_1^2-1)^{1/2}-\nu_1(\nu^2-1)^{1/2}}\right|, & \nu>1\\ 2\sqrt{\dfrac{1-\nu^2}{\nu^2}}\tan^{-1}\dfrac{\sqrt{(\nu_1^2-1)/\nu_1^2}}{\sqrt{(1-\nu^2)/\nu^2}}, & \nu<1\end{cases} \quad (30)$$

which have the characteristic feature that the second derivative with respect to the energy goes to infinity (again on the side $\nu < 1$).

*The writers plan to turn to the application of dispersion relations to this problem in another paper.

In the energy range $2 < \nu < 3.34$

$$6|M_{33}|^2 = 2.17(1 - 0.244\nu)^2 e^2/M. \quad (31)$$

The contributions of the expressions (28) and (31) are given by integrals of the forms

$$J_1(\nu) = \frac{2\nu^3}{\pi}\int_{\nu_1}^{\nu_2}\frac{\alpha+\beta\nu'+\gamma\nu'^2}{\nu'(\nu'^2-\nu^2)}d\nu'$$

$$= \frac{\nu}{\pi}\ln\left\{\left(\frac{\nu_2-\nu}{\nu_1-\nu}\right)^{\alpha+\beta\nu+\gamma\nu^2}\left(\frac{\nu_2+\nu}{\nu_1+\nu}\right)^{\alpha-\beta\nu+\gamma\nu^2}\left(\frac{\nu_1}{\nu_2}\right)^{2\alpha}\right\}, \quad (32)$$

$$J_2(\nu) = \frac{2\nu^2}{\pi}\int_{\nu_1}^{\nu_2}\frac{d\nu'(\alpha+\beta\nu'+\gamma\nu'^2)}{\nu'^2-\nu^2}$$

$$= \frac{\nu}{\pi}\left\{2\gamma\nu(\nu_2-\nu_1)+(\alpha+\gamma\nu^2)\ln\left(\frac{\nu_2-\nu}{\nu_1-\nu}\frac{\nu_1+\nu}{\nu_2+\nu}\right)\right.$$

$$\left.+\beta\nu\ln\left(\frac{\nu_2^2-\nu^2}{\nu_1^2-\nu^2}\right)\right\} \quad (33)$$

6. The energy dependences of the real parts of the amplitudes $R_1, \ldots, R_6$ (in the l.s.), calculated by means of dispersion relations, are shown in Fig. 1, a, b. The half-widths of Re (R_1) and Re (R_2)

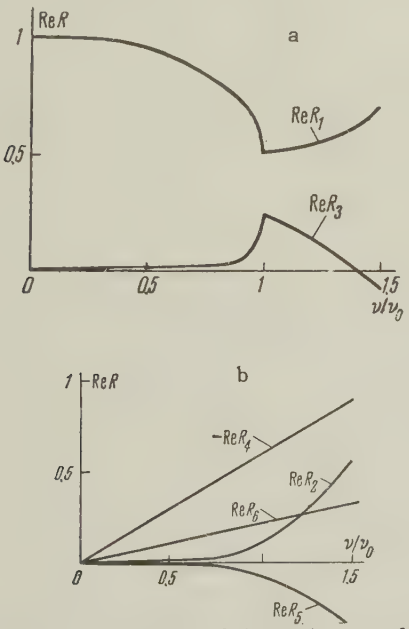

FIG. 1. Energy dependences of the real parts of the amplitudes R_1 and R_3 (a) and R_2, R_4, R_5, and R_6 (b) (the values of the functions are expressed in terms of e^2/M as a unit).

are $\nu_0/10$ and $\nu_0/20$, respectively, and are mainly due to the square of the ratio of the real part to the coefficient A in Eq. (22):

$$\varepsilon = 1 - \nu = \tfrac{1}{8}(\mathrm{Re}\,R)^2/A^2. \quad (34)$$

In a general analysis of the nonmonotonic behavior near the threshold A. I. Baz' has given for the width of the peak restrictions of the form $r_0(1-\nu^2)^{1/2} \ll 1$ (where r_0 is the interaction radius). The more detailed treatment of the present paper has automatically given the more accurate criterion (34). The effect of the inelastic processes on Re (R_3) is very strong, although the contribution of Re (R_3) to the observable quantities is small, so that the experimental study of the energy dependence of Re (R_3) is a difficult problem. The energy dependence of Re (R_4) and Re (R_6) is given with great accuracy by the general relation (I,18). The departure from zero of Re (R_2) and Re (R_5) is entirely due to inelastic processes, but the production of mesons in the s state does not contribute to these quantities.

The differential scattering cross section (in the c.m.s.) (12) can be written in the form

$$I_0(\theta, \nu) = A_0(\nu) + A_1(\nu)\cos\theta + A_2(\nu)\cos^2\theta + A_3(\nu)\cos^3\theta. \quad (35)$$

The results of calculations for the scattering angles 90° and 0° are shown in Figs. 2 and 3. We at once note the marked difference between the energy dependences of the cross sections at $\theta = 0$ and at 90°.

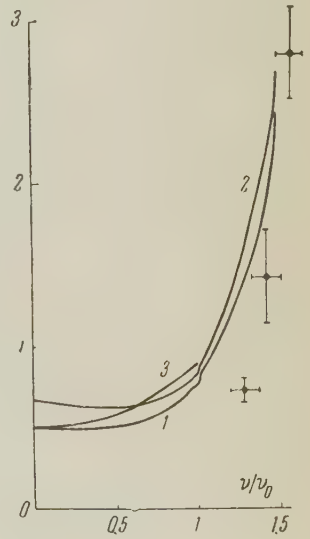

FIG. 2. Energy dependences of the differential cross section $I_0(90°)$ (curve 1), the total scattering cross section (curve 2), and the differential cross section with the dispersion part not taken into account (curve 3) (the values of the functions are expressed in terms of $(e^2/M)^2$ as a unit). Experimental data from reference 9.

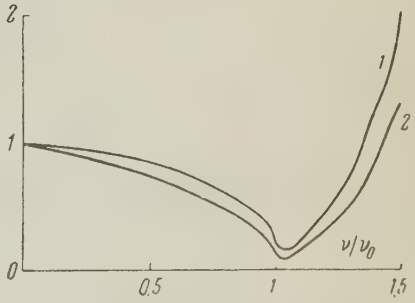

FIG. 3. Energy dependence of the differential cross section $I_0(0°)$: curve 1 is for the cross section in the l.s.; curve 2, for the c.m.s. (values of the functions in units $(e^2/M)^2$.

The function $I_0(0°, \nu)$ has been calculated earlier by Cini and Stroffolini.[8] We have improved the accuracy in the region near the threshold. Outside this region there is good agreement between the two calculations. Our results relating to $I_0(90°, \nu)$ in the energy region near 200 Mev also agree with other published calculations.[9] A new

contribution is the careful treatment of the region near threshold, in which there are effects not discussed previously.

Figure 2 shows the energy dependence of the total cross section for elastic scattering, and also shows for comparison the energy dependence of the cross section calculated from Eqs. (16) and (18). The effects near threshold are practically imperceptible, but the difference between the two curves shows the general effect of inelastic processes on the elastic-scattering cross section.

The local effects are much more prominent if we calculate the difference

$$\sigma_s/4\pi - I_0(90°, \nu)$$

or the dependence of A_2 on the energy ν (Figs. 4 and 5). To get experimental data on A_2 one

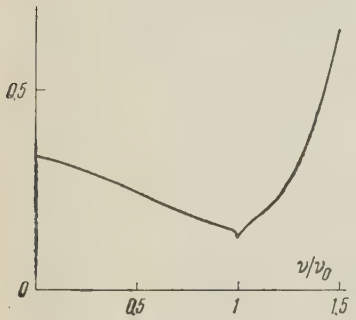

FIG. 4. Energy dependence of $2[\sigma_s/4\pi - I_0(90°)]$ (in units $(e^2/M)^2$).

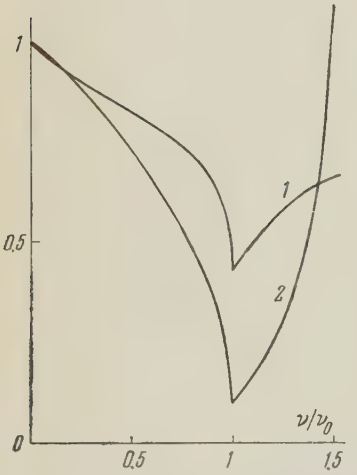

FIG. 5. Energy dependences: 1 – of the photon polarization $2\langle T_{22}(90°)\rangle$; 2 – of twice the coefficient $A_2(\theta)$ of the $\cos^2\theta$ term in the cross section (values of functions in units $(e^2/M)^2$).

needs only to study the cross sections $I_0(\theta, \nu)$ at $\theta = 45°$, 90°, and 135° with sufficient accuracy to find the energy dependence of the difference

$$I_0(45°) + I_0(135°) - I_0(90°).$$

It is interesting to note the energy dependence of the polarization of the recoil nucleon. Below the meson-production threshold the imaginary parts of the quantities $R_1, \ldots, R_6$ vanish in the e^2 approximation, the right member of Eq. (13) is zero, and there is no polarization of the recoil nucleon. Below threshold, in virtue of invariance under time reversal, the cross section for scattering by polarized protons does not differ from $I_0(\theta)$. Above the threshold for production of π mesons there is a nonvanishing polarization of the recoil nucleons. The values of the imaginary parts of the amplitudes above threshold are shown in Fig. 6. The results of calculations on the dependence of the polarization at $\theta = 90°$ (angle in c.m.s.) on the photon energy (in the l.s.) are shown in Fig. 7. It can be seen that over a rather wide range of energies, 180 – 220 Mev, the polarization reaches 20 to 25 percent.

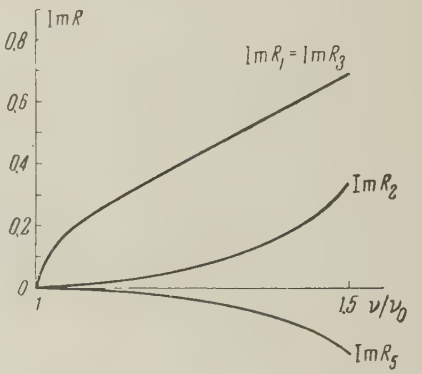

FIG. 6. Energy dependence of the imaginary parts of the amplitudes (in units e^2/M).

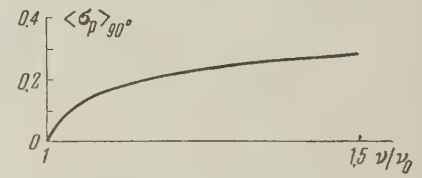

FIG. 7. Energy dependence of the polarization of the recoil protons at $\theta = 90°$.

The values of the polarization are rather sensitive to the assumptions made in the analysis of the photoproduction data, and in particular to the assumption (27). Consequently, the experimental study of the polarization of the recoil nucleons could give valuable information about the photoproduction of mesons.

In the expression (20), as compared with $I_0(\theta)$, there is a decided decrease of the contribution of $|R_4|^2$, and $|R_3|^2$ occurs with the negative sign, so that the dips near the threshold are particularly marked in the energy dependence of $\langle T_{22}(90°)\rangle$ (Fig. 5).

7. A detailed examination of the scattering of γ rays by nucleons in the region near the meson-production threshold, made by the use of dispersion relations, has made it possible to see what effect the production of mesons in the s state has on the anomalies near the threshold. The scattering of γ rays by nucleons and by nuclei is an example of the sort of process in which the energy dependence of the amplitudes is especially strongly affected by inelastic processes and the effects extend over a wide range of energies. In γ-N scattering the local effects on a number of observable

quantities are quite appreciable, but rather severe requirements are imposed on the procedures for experimental studies, expecially as regards resolution in energy, since the widths of the dips in question are of the order of 5 to 10 Mev.

The treatment given in the present paper shows that the effects near threshold are sometimes masked by the strong energy dependence of the scattering amplitudes. Therefore it seems that the most favorable conditions for the experimental study of such effects should be found at small energies, and also for the interaction of particles with small spins.

In the case of γ-N scattering, besides the contribution of the "peak" amplitudes R_1 and R_3, there are large effects from other amplitudes, particularly from R_4. The effects of these "smearing-out" factors may be smaller in the scattering of γ rays by helium nuclei (or other spinless nuclei), since in this case the transition matrix will have the form

$$M = R_1'(\mathbf{ee}') + R_2'(\mathbf{ss}').$$

A treatment of the scattering of γ-ray quanta by deuterons near the threshold for the photodisintegration of the deuteron, where local effects will evidently be large, will be presented in another paper.

From the point of view of the general effect of some processes on others it is interesting to analyze the photodisintegration of the deuteron in the energy range near and below the threshold for meson production. Noting the results of the calculations on the γ-N scattering, we can evidently suppose that the well known "resonance" energy dependence of the cross section for the photodisintegration of the deuteron is due to meson-production processes above threshold and can be treated by a method using dispersion relations.

It is commonly assumed that at quite high γ-ray energies the γ-N scattering cross sections will be almost entirely due to inelastic processes, i.e., to the imaginary parts of the amplitudes. In this connection it may be very interesting to study γ-N scattering, and especially the polarization of the recoil nucleons, near the thresholds of reactions of the production of new particles, such as

$$\gamma + N \rightarrow Y + K,$$

and a number of other processes. In this case the difficulties associated with the size of the cross section and the low energy of the recoil nucleon may very probably be smaller.

The writers are deeply grateful to B. Pontecorvo and Ya. Smorodinskiĭ for helpful discussions.

[1] E. Wigner, Phys. Rev. **73**, 1002 (1948). A. I. Baz', JETP **33**, 923 (1957), Soviet Phys. JETP **6**, 709 (1958). G. Breit, Phys. Rev. **107**, 1612 (1957). A. I. Baz' and L. B. Okun', JETP **35**, 757 (1958), Soviet Phys. JETP **8**, 526 (1958). R. K. Adair, Phys. Rev. **111**, 632 (1958).

[2] L. I. Lapidus and Chou Kuang-Chao, JETP **37**, 1714 (1959), Soviet Phys. JETP **10**, 1213 (1960).

[3] H. A. Tolhoek, Revs. Modern Phys. **28**, 277 (1956).

[4] L. I. Lapidus, JETP **34**, 922 (1958), Soviet Phys. JETP **7**, 638 (1958).

[5] L. Wolfenstein and J. Ashkin, Phys. Rev. **85**, 947 (1952). L. Wolfenstein, Ann. Rev. Nuclear Sci. **6**, 43 (1956).

[6] Watson, Keck, Tollestrup, and Walker, Phys. Rev. **101**, 1159 (1956).

[7] E. Fermi, Suppl. Nuovo cimento **2**, 17 (1955). (Russian Transl., IIL, 1956).

[8] M. Cini and A. Stroffolini, Nuclear Phys. **5**, 684 (1958).

[9] T. Akiba and J. Sato, Progr. Theoret. Phys. **19**, 93 (1958). G. Chew, Proc. Annual Internat. Conf. on High Energy Physics at CERN, 1958, p. 93.

Translated by W. H. Furry
33

ON THE THEORY OF ULTRASONIC ABSORPTION BY METALS IN A STRONG MAGNETIC FIELD

É. A. KANER

Institute of Radio-physics and Electronics, Academy of Sciences of the Ukrainian S.S.R.

Submitted to JETP editor July 11, 1959

J. Exptl. Theoret. Phys. (U.S.S.R.) **38**, 212-218 (January, 1960)

The ultrasonic absorption coefficient α is calculated for metals in strong magnetic fields, where $r \ll \lambda \ll l$ (r and l are the characteristic orbital radius and the free path of the electrons, and λ is the length of the acoustic wave in the metal). Closed electron orbits are considered, with an arbitrary law of electron dispersion. It is shown that in a strong field the quantity α becomes saturated regardless of whether $n_1 = n_2$ or $n_1 \neq n_2$. For $\mathbf{k} \perp \mathbf{H}$ ($\mathbf{k}$ being the wave vector, $\mathbf{H}$ the magnetic field, and n_1 and n_2 the number of "electrons" and "holes" respectively) the saturation value is $kl \gg 1$ times larger than its value α_0 for $H = 0$; otherwise $\alpha \sim \alpha_0$. Comparison of theory with experiment[3] shows good agreement.

1. INTRODUCTION

EXPERIMENTAL study of ultrasonic absorption in metals located in a constant magnetic field at low temperatures[1-3] has led to the observation of fluctuations in the coefficient of sound absorption as a function of the magnetic field $\mathbf{H}$. Pippard's qualitative theory of the phenomenon[4] and the more detailed calculations of V. Gurevich[5] have shown that the magnetic fluctuations of the absorption coefficient are related to an unusual "spatial resonance" when an extremal diameter of the electron orbit in the direction perpendicular to the vectors $\mathbf{k}$ and $\mathbf{H}$ ($\mathbf{k}$ being the wave vector of the sound wave and $\mathbf{k} \perp \mathbf{H}$) becomes an integral multiple of the acoustic wavelength λ. From an experimental study of the anisotropy of the fluctuations it is possible to determine the extremal diameters of the Fermi surface for the electrons in the metal, and in certain simple cases to establish its shape completely.

The fluctuations in the absorption coefficient occur in a range of relatively weak magnetic fields, where $1 \lesssim kr \ll kl$. It is of some interest to discover which of the properties of the Fermi surface can be determined by a study of the absorption in a strong magnetic field. The present paper is devoted to this question.

2. STATEMENT OF THE PROBLEM. THE BASIC EQUATIONS

In this paper we limit ourselves basically to the consideration of closed Fermi surfaces only. More precisely, we shall determine the contribution made to the absorption coefficient by the closed electron trajectories. We shall assume that the vectors $\mathbf{k}$ and $\mathbf{H}$ are mutually perpendicular, and that the magnetic field is sufficiently strong that $kr \ll 1$ and $\gamma = r/l \ll 1$. At the same time we consider that the magnetic field is not so large that it is necessary to take into account the "skin effect," i.e., the non-uniformity of the alternating electromagnetic field. The latter condition reduces to the requirement that the "skin depth," i.e., the length δ of the corresponding electromagnetic wave in the metal, with the same frequency ω as the acoustic wave, should be the smallest parameter with the dimensions of a length in the problem.*

The absorption coefficient α is found from the quotient

$$\alpha = |Q| / \mathcal{E}, \tag{2.1}$$

where Q is the dissipative function and $\mathcal{E} = \frac{1}{4}\rho\omega^2 |\mathbf{u}_0^2|$ is the energy density in the sound wave. ρ is the density of the metal, and $\mathbf{u}(\mathbf{r}, t) = \mathbf{u}_0 \exp(i\omega t - i\mathbf{k}\cdot\mathbf{r})$ is the displacement vector in the sound wave.

$$Q = -T \frac{d}{dt} \int \frac{2}{h^3} d\tau_p \{(1-f)\ln(1-f) + f \ln f\}, \tag{2.2}$$

where T is the electron temperature in energy units, the integral represents the entropy of the

*$\delta = c/(2\pi\omega\sigma)^{1/2}$, where, in calculating the electrical conductivity σ, the effect of the magnetic field and the spatial dispersion are taken into account.

electrons in the metal, $f(\mathbf{r}, \mathbf{p}, t)$ is the electron distribution function, $d\tau_p$ is the volume element in momentum space, and h is Planck's constant.

The function f satisfies the kinetic equation

$$\frac{\partial f}{\partial t}+\left(\frac{\partial \varepsilon}{\partial \mathbf{p}}+\dot{\mathbf{u}}\right)\nabla f-\left(e\mathbf{E}+\frac{e}{c}\left[\frac{\partial \varepsilon}{\partial \mathbf{p}}+\dot{\mathbf{u}}\right]\times\mathbf{H}+\nabla\varepsilon\right)\frac{\partial f}{\partial \mathbf{p}}+\left(\frac{\partial f}{\partial t}\right)_{st}=0, \tag{2.3}$$

where e, ϵ, and $\partial\epsilon/\partial\mathbf{p}$ are the charge, energy and velocity of the electron and c is the speed of light. Following the work of Akhiezer, Kaganov, and Lyubarskiĭ[6] we consider that the energy of an electron in the field of the acoustic wave is equal to

$$\varepsilon(\mathbf{r}, \mathbf{p}, t)=\varepsilon_0(\mathbf{p})+\lambda_{ik}\partial u_i/\partial x_k, \tag{2.4}$$

where $\lambda_{ik}(\mathbf{p})$ is some tensor of the second rank which will, generally speaking, not be symmetrical in the indices i and k.

The second term in (2.4) is connected with the assumption that the frequency ω is much smaller than the collision frequency ν, so that at every instant of time there exists a thermal equilibrium, in which the electrons acquire some additional energy proportional to the tensor $\partial u_i/\partial x_k$. ϵ_0 is the energy of the electron in the absence of the sound. A change in electron energy leads to a change in the chemical potential $\mu=\mu_0+\mu'$ and in the temperature. The latter, as has been shown in reference 6, can be neglected because $T \ll \mu_0$.

In order to determine the rotational part of the electric field it is necessary to use Maxwell's equations, which upon elimination of the alternating magnetic field take the form

$$\nabla^2 E_\beta=(4\pi i\omega/c^2)\,j_\beta, \tag{2.5}$$

where the index β refers to the y and z axes (the Ox axis is chosen along $\mathbf{k}$, and Oz along $\mathbf{H}$). In order to find the longitudinal components of the field it is necessary to make use of the vanishing of the space charge density, which by virtue of Maxwell's equations is equivalent to the equation

$$j_x=0, \tag{2.6}$$

In the case where the length δ of the electromagnetic wave in the metal is small compared with all the other dimensions, equation (2.5) reduces to $j_\beta=0$, which, together with (2.6), leads to the equation

$$\mathbf{j}=0, \tag{2.7}$$

from which the electric field vector is determined.

Let us now linearize the kinetic equation (2.3):

$$f=f_0(\varepsilon-\mu)-\chi\partial f_0/\partial\varepsilon,$$

$$f_0(\varepsilon-\mu)=[\exp\{(\varepsilon-\mu)/T\}+1]^{-1}, \tag{2.8}$$

where χ is a new unknown function. After some simple calculations we obtain

$$Q=-\mathrm{Re}\,\frac{1}{h^3}\int\frac{\partial f_0}{\partial\varepsilon}\chi^*\left(\frac{\partial\chi}{\partial t}\right)_{st}d\tau_p; \tag{2.9}$$

$$\frac{\partial\chi}{\partial t}+(\mathbf{v}\nabla)\chi+\Omega\frac{\partial\chi}{\partial\tau}+\left(\frac{\partial\chi}{\partial t}\right)_{st}=\lambda_{ik}\frac{\partial\dot{u}_i}{\partial x_k}-\dot{\mu}'-e\mathbf{E}^*\mathbf{v}, \tag{2.10}$$

where τ is the dimensionless time of the orbital motion of the electrons in the magnetic field;[7] $\Omega=eH/mc$ is the frequency of revolution of an electron in its orbit; $m=(2\pi)^{-1}\partial S(\epsilon_0, p_z)/\partial\epsilon_0$ is the effective mass, $S(\epsilon_0, p_z)$ is the area of the intersection of the surface $\epsilon_0(\mathbf{p})=\text{const}$ with the plane $p_z=\text{const}$, and

$$\mathbf{v}=\partial\varepsilon_0/\partial\mathbf{p}; \quad e\mathbf{E}^*=e\mathbf{E}+\frac{e}{c}[\dot{\mathbf{u}}\times\mathbf{H}]+\nabla\mu'.$$

Averaging (2.9) over the angle in momentum space, and making use of the conservation law for the total number of particles, we obtain

$$\mu'=\langle\lambda_{ik}\rangle\frac{\partial u_i}{\partial x_k}-\left(\int f_0 d\tau_p\Big/\int\limits_{\varepsilon_0=\mu_0}\frac{dS}{v}\right)\mathrm{div}\,\mathbf{u},$$

$$\langle\lambda_{ik}\rangle=\int\limits_{\varepsilon_0=\mu_0}\frac{dS}{v}\lambda_{ik}\Big/\int\limits_{\varepsilon_0=\mu_0}\frac{dS}{v}. \tag{2.11}$$

The current density is

$$\mathbf{j}=\frac{2e}{h^3}\int d\tau_p\frac{\partial f_0}{\partial\varepsilon}\chi\mathbf{v}. \tag{2.12}$$

Noting that all the quantities in (2.10) depend on time and the coordinates in the manner $\exp(i\omega t-i\mathbf{k}\cdot\mathbf{r})$, and assuming that it is possible to introduce a relaxation time* $t_0(\mathbf{p})=1/\nu(\mathbf{p})$, we shall re-write equation (2.10) in the following final form:

$$(i\omega-ik\mathbf{v}+\nu)\chi+\Omega\partial\chi/\partial\tau=\Delta\lambda_{ik}\partial\dot{u}_i/\partial x_k-e\mathbf{E}^*\mathbf{v}, \tag{2.13}$$

where

$$\Delta\lambda_{ik}=\lambda_{ik}-\langle\lambda_{ik}\rangle+\delta_{ik}\int f_0 d\tau_p\Big/\int\frac{ds}{v}\quad(\langle\chi\rangle=0).$$

The solution of equation (2.13) which is periodic in τ has the form

$$\chi(\tau)=\frac{1}{\Omega}\int\limits_{-\infty}^{\tau}d\tau_1\left[\Delta\lambda_{ik}(\tau_1)\frac{\partial\dot{u}_i}{\partial x_k}-e\mathbf{E}^*\mathbf{v}(\tau_1)\right]\exp\left(\int\limits_{\tau}^{\tau_1}\frac{\nu-ik\mathbf{v}+i\omega}{\Omega}d\tau_2\right) \tag{2.14}$$

and gives the expression for χ which is valid for

*This assumption does not affect the qualitative nature of the results.

arbitrary magnetic fields. Let us consider the behavior of χ in the strong-field region. Making use of the fact that the function preceding the exponent in the integral (2.14) is periodic in τ, it can easily be shown[8] that $\chi(\tau)$ is equal to

$$\chi(\tau) = \left\{\Omega\left[1 - \exp\left(-\frac{2\pi\bar{\nu} - 2\pi i\bar{\mathbf{k}\mathbf{v}}}{\Omega}\right)\right]\right\}^{-1} \times \int_{\tau-2\pi}^{\tau} d\tau_1 \left(\Delta\lambda_{ik}(\tau_1)\frac{\partial \dot{u}_i}{\partial x_k} - e\mathbf{E}^*\mathbf{v}(\tau_1)\right) \exp\left(\int_{\tau}^{\tau_1} \frac{\nu - i\mathbf{k}\mathbf{v}}{\Omega} d\tau_2\right) \quad (2.15)$$

(we have neglected the small quantity ω in comparison with ν in all the exponents). In equation (2.15) the bar denotes the average over a period 2π in τ:

$$\bar{\varphi} = (1/2\pi)\oint \varphi(\tau)\, d\tau.$$

In the case which we are considering (a closed Fermi surface, and $\mathbf{k} \perp \mathbf{H}$), we have $\mathbf{k}\cdot\bar{\mathbf{v}} = 0$ because[7]

$$v_x = \frac{1}{2\pi}\oint \frac{1}{m}\frac{dp_y}{d\tau} d\tau \equiv 0.$$

Noting that the quantities ν and $|\mathbf{k}\cdot\mathbf{v}|$ are $\ll \Omega$, we may expand all the exponentials in series, obtaining as a result

$$\chi = \frac{1}{2\pi\bar{\nu}} \int_{\tau-2\pi}^{\tau} d\tau_1 \left(\Delta\lambda_{ik}(\tau_1)\,\partial\dot{u}_i/\partial x_k - e\mathbf{E}^*\mathbf{v}\right) \times \left(1 - \int_{\tau}^{\tau_1} \frac{\nu - i\mathbf{k}\mathbf{v}}{\Omega} d\tau_2 + \frac{1}{2}\left[\int_{\tau}^{\tau_1} \frac{\nu - i\mathbf{k}\mathbf{v}}{\Omega} d\tau_2\right]^2\right). \quad (2.16)$$

Finally, in order to find the non-equilibrium contribution to the distribution function it is necessary to calculate the electric field $\mathbf{E}^*$ from equation (2.7).

3. DETERMINATION OF THE ELECTRIC FIELD

There is a fundamental difference in the forms of the function χ in the two cases $n_1 \neq n_2$ and $n_1 = n_2$, where n_1 (or n_2) is the number of electrons (or holes) in the definite volume bounded by the surface $\epsilon(\mathbf{p}) = \mu_0$ within which the energy is less (greater) than μ_0 (see reference 7).

Let us first consider the case $n_1 \neq n_2$. Substituting (2.16) into formula (2.12) for the current density, we obtain

$$j_i = \sigma_{ik}E_k^* - j_i', \quad (3.1)$$

where the electrical conductivity tensor is equal to

$$\sigma_{ik} = \frac{2e^2}{h^3}\int dp_z \frac{m}{2\pi\bar{\nu}}\oint d\tau v_i(\tau) \int_{\tau-2\pi}^{\tau} d\tau_1 v_k(\tau_1) \times \left\{1 + \int_{\tau}^{\tau_1}(\gamma - iq)\, d\tau_2 + \frac{1}{2}\left[\int_{\tau}^{\tau_1}(\gamma - iq)\, d\tau_2\right]^2\right\}, \quad \gamma = \nu/\Omega, \quad q = kv_x/\Omega, \quad (3.2)$$

and the expression for j_i' is obtained from $\sigma_{ik}E_k^*$ by replacing $eE_k^*v_k(\tau_1)$ in (3.2) by the quantity $\Delta\lambda_{ik}(\tau_1)\,\partial\dot{u}_i/\partial x_k$.

The field $\mathbf{E}^*$ is found from (2.7):

$$E_i^* = \rho_{ik}j_k', \quad (3.3)$$

where $\rho_{ik} = (\sigma^{-1})_{ik}$ is the electrical resistivity tensor.

When the resistivity tensor is evaluated, it leads to the following results:

$$\sigma_{ik} = \begin{pmatrix} \gamma_0^2 a_{xx} & \gamma_0 a_{xy} & \gamma_0 a_{xz} \\ \gamma_0 a_{yx} & q_0^2 a_{yy} & \gamma_0 a_{yz} + q_0^2 a'_{yz} \\ \gamma_0 a_{zx} & \gamma_0 a_{zy} + q_0^2 a'_{zy} & a_{zz} \end{pmatrix}. \quad (3.4)$$

Here $\gamma_0 = H_0/H \ll 1$; H_0 is the field for which the characteristic radius r_0 of the orbit is equal to the characteristic free path; $q_0 = kr_0 \ll 1$ although $q_0 \gg \gamma_0$, but q_0^2, generally speaking, may be comparable with γ_0 (this is why two terms have been retained in the σ_{yz} and σ_{zy} components).

The expansion of the quantities a_{ik} in γ_0 and q_0 begins with terms which do not depend on the magnetic field, and whose form, generally speaking, depends on the nature of the collisions. The exceptions to this are the components $\sigma_{yx} = -\sigma_{xy} = ecH^{-1}(n_1 - n_2)$, which do not depend upon the collision integral because they are due to the drift of particles across the magnetic field (Hall current). The quantities a_{ik} are of the order of σ_0, the static conductivity of the metal when $H = 0$.

The "deformation" current $\mathbf{j}'$ is equal to

$$j_x' = \frac{ikc^2}{eH^2}\frac{2}{h^3}\int\frac{dS}{v}\left\{\frac{1}{2}p_y^2 - \frac{1}{\bar{\nu}}\overline{p_y\nu}p_y + \frac{1}{2}\frac{1}{\bar{\nu}}\overline{p_y^2\nu}\right\}\Delta\lambda_{ik}\frac{\partial\dot{u}_i}{\partial x_k},$$

$$j_y' = \frac{ikc}{H}\frac{2}{h^3}\int\frac{dS}{v}\frac{1}{\bar{\nu}}\overline{v_x p_x}\Delta\lambda_{ik}\frac{\partial\dot{u}_i}{\partial x_k},$$

$$j_z' = -\frac{ikc}{H}\frac{2}{h^3}\int\frac{dS}{v}\frac{1}{\bar{\nu}}(p_y\bar{v}_z - \overline{p_y v_z})\,\Delta\lambda_{ik}\frac{\partial\dot{u}^i}{\partial x_k}. \quad (3.5)$$

The matrix of the resistivity tensor σ_{ik} has the form

$$\rho_{ik} = \begin{pmatrix} q_0^2\gamma_0^{-2}b_{xx} & \gamma_0^{-1}b_{xy} & b_{xz} + q_0^2\gamma_0^{-1}b'_{xz} \\ \gamma_0^{-1}b_{yx} & b_{yy} & b_{yz} \\ b_{zx} + q_0^2\gamma_0^{-1}b'_{zx} & b_{zy} & b_{zz} \end{pmatrix}, \quad (3.6)$$

where all components of the tensor b_{ik}, with the exception of $\rho_{yx} = -\rho_{xy} = H/ec(n_1 - n_2)$, depend on the collision integral and are of the order of σ_0^{-1}.

Substituting ρ_{ik} from (3.6) into (3.3) for the electric field, we obtain

$$E_x^* = \rho_{xy}j_y' \sim (q_0/\gamma_0 ev_0)\,\Delta\lambda_{ik}\partial\dot{u}_i/\partial x_k,$$
$$E_y^* = \rho_{yk}j_k' \sim (q_0/ev_0)\,\Delta\lambda_{ik}\partial\dot{u}_i/\partial x_k,$$
$$E_z^* = \rho_{z\beta}j_\beta' \sim (q_0/ev_0)\,\Delta\lambda_{ik}\partial\dot{u}_i/\partial x_k. \quad (3.7)$$

Upon substituting E^* into the expression (2.16) for χ, it is easy to verify that the terms containing the electric field can be neglected, since at most they are $1/q_0 \gg 1$ times smaller than the terms containing $\Delta\lambda_{ik}\partial\dot{u}_i/\partial x_k$.

Thus, in the case where $n_1 \neq n_2$,

$$\chi = (1/\bar{\nu})\,\overline{\Delta\lambda_{ik}}\,(\partial\dot{u}_i/\partial x_k). \tag{3.8}$$

In the case where $n_1 = n_2$ an analogous treatment, taking into account the electric field (to which the component E_y^* makes the chief contribution) leads to the following result:

$$\chi = \frac{1}{\bar{\nu}}\left\{\overline{\Delta\lambda_{ik}} - \frac{S}{m}\sum\langle S\overline{\Delta\lambda_{ik}}\bar{\nu}^{-1}/m\rangle\left(\sum\langle S^2\bar{\nu}^{-1}/m^2\rangle\right)^{-1}\right\}\frac{\partial\dot{u}_i}{\partial x_k}, \tag{3.9}$$

where

$$S_j(\mu_0,\ p_z) = \oint p_x dp_y,\quad m = (2\pi)^{-1}\frac{\partial S_j}{\partial\mu_0}$$

is the area of the section of the j-th surface $\epsilon_j(p) = \mu_0$ by the plane $p_z = \text{const}$. The sign of the area depends on the direction of the contour path:[7] for surfaces bounded by states of lower energy ("electrons"), $S > 0$; for "holes," $S < 0$. The summation extends over the entire surface $\epsilon_j = \mu_0$, and m is the effective mass.

4. THE ABSORPTION COEFFICIENT. SOME REMARKS

When the function χ is known, it is easy to find the dissipation function, and with it the coefficient of ultrasonic absorption also. In the case $n_1 \neq n_2$,

$$|Q| = \frac{1}{h^3}\sum\int_{\varepsilon_j=\mu_0}\frac{dS}{v}\,|\overline{\Delta\lambda_{ik}}(\partial\dot{u}_i/\partial x_k)|^2\frac{1}{\bar{\nu}}. \tag{4.1}$$

When $n_1 = n_2$,

$$|Q| = \frac{1}{h^3}\sum\int_{\varepsilon_j=\mu_0}\frac{dS}{v}\frac{1}{\bar{\nu}}\left|\overline{\Delta\lambda_{ik}}\frac{\partial\dot{u}_i}{\partial x_k} - \frac{S}{m}\sum\langle S\overline{\Delta\lambda_{ik}}\bar{\nu}^{-1}/m\rangle\left(\sum\langle S^2\bar{\nu}^{-1}/m^2\rangle\right)^{-1}\frac{\partial\dot{u}_i}{\partial x_k}\right|^2. \tag{4.2}$$

In both cases the absorption coefficient α is of the order of magnitude

$$\alpha \sim N\mu_0\omega^2 t_0/\rho s^2, \tag{4.3}$$

where s is the speed of sound in the metal and $N \sim n_1$.

The expression (4.3) for α agrees in form with the absorption coefficient in the absence of a magnetic field, in the frequency and temperature range where $kl \ll 1$ (cf. reference 6). When $kl \gg 1$ the absorption coefficient is kl times smaller in the absence of the magnetic field. Consequently the ultrasonic absorption coefficient saturates in strong magnetic fields, while at the same time the magnitude of the absorption under saturation conditions is considerably larger than the absorption in the absence of a field. This conclusion agrees qualitatively with the experiments of Galkin and Korolyuk[3] on ultrasonic absorption by single crystals of lead in strong magnetic fields.

In this connection, however, a few qualifying remarks are necessary. The fact is that the experiments mentioned above showed a strong anisotropy in the absorption in strong fields. The absorption coefficient α varied by a factor of 5 or 6 for different orientations of $\mathbf{H}$ with respect to the crystal axes. This difference may be due to the existence of open electron trajectories, over which the mean value of the velocity component v_x does not reduce to zero.

This would lead to the appearance of $\bar{\nu} - (ik\bar{v}_x/\Omega)$ instead of $\bar{\nu}$ in the denominator of the expression for χ, the second term being much larger than the first.

In the case where the direction of an open trajectory* is perpendicular to the vectors $\mathbf{k}$ and $\mathbf{H}$ (or inclined at a small angle $\vartheta \ll \gamma_0$), the contribution to the absorption coefficient from the open (or extremely elongated) trajectories turns out to be considerably smaller than the contribution from the closed trajectories. For example, in the case of a Fermi surface in the shape of a smooth cylinder, the absorption coefficient is kl times smaller than when the trajectories are closed, and its order of magnitude is the same as that of the zero-field absorption coefficient ($H = 0$). The asymptotic value of the absorption coefficient depends greatly on the nature of the open surface and on the angle between the magnetic field and the direction of the open trajectory. A study of the peculiarities of strong-field ultrasonic absorption by metals with open Fermi surfaces will be published in a separate paper.

For the same reason, an analogous reduction in the acoustic absorption coefficient should also take place for closed trajectories, when the wave vector $\mathbf{k}$ is not perpendicular to $\mathbf{H}$ ($\cos\vartheta \gg 1$, where ϑ is the angle between $\mathbf{k}$ and $\mathbf{H}$).

In conclusion I should like to thank M. I. Kaganov for valuable advice and comments.

*For example, in the case of a Fermi surface of the "fluted cylinder" type, the direction of the cylinder axis; in the case of a "three-dimensional grid" type of surface, the line of intersection of the plane perpendicular to $\mathbf{H}$ with the nearest crystallographic plane.

[1] H. E. Bömmel, Phys. Rev. **100**, 758 (1955).
[2] Morse, Bohm, and Gavenda, Phys. Rev. **109**, 1394 (1958).
[3] A. A. Galkin and A. P. Korolyuk, JETP **36**, 1307 (1959) and **37**, 310 (1959), Soviet Phys. JETP **9**, 925 (1959) and **10**, 219 (1960).
[4] A. B. Pippard, Phil. Mag. **2**, 1147 (1957).
[5] V. L. Gurevich, JETP **37**, 71 (1959), Soviet Phys. JETP **10**, 51 (1960).
[6] Akhiezer, Kaganov, and Lyubarskiĭ, JETP **32**, 837 (1957), Soviet Phys. JETP **5**, 685 (1957).
[7] Lifshitz, Azbel', and Kaganov, JETP **31**, 63 (1956), Soviet Phys. JETP **4**, 41 (1957).
[8] M. Ya. Azbel' and É. A. Kaner, JETP **32**, 896 (1957), Soviet Phys. JETP **5**, 730 (1957).

Translated by D. C. West
34

COLLECTIVE PROPERTIES OF Si^{30}, Si^{31}, *AND* Ne^{23}, *AND REDUCED WIDTHS IN STRIPPING REACTIONS*

V. G. SUKHAREVSKIĬ

Institute for Nuclear Physics, Moscow State University

Submitted to JETP editor July 15, 1959

J. Exptl. Theoret. Phys. (U.S.S.R.) 38, 219-221 (January, 1960)

Within the framework of the unified model with strong coupling, we investigate the collective properties of Si^{30}, Si^{31} and Ne^{23}, by analyzing the experimentally observed reduced widths for neutron capture in (d, p) stripping reactions. The analysis shows that Si^{31} apparently has an oblate shape with a Nilsson parameter $\delta < 0$, but it is not possible to establish the shape of the deformation for Ne^{23}, though it does confirm that this nucleus is highly deformed. The result for Si^{30} does not agree with the theoretical estimates, which raises doubts concerning the applicability of the strong coupling scheme to this nucleus.

IT is known that the low-lying levels of light nuclei in the region up to $A = 40$ in many cases show a well developed rotational structure, which is describable by the uniform model of the nucleus[1] in the form proposed by Nilsson.[2] Analyses within the framework of this model have been made of the experimental data for Al^{25} and Mg^{25},[3] Si^{29},[4] for nuclei in the region $4 < A < 32$,[5] etc. In particular, it was shown[4] that Si^{29} apparently has an oblate shape, with deformation parameter $\delta \approx -0.15$, although the question of the existence of oblate nuclei remains an open question. It therefore seems desirable to further investigate the collective properties of light nuclei. In this paper we consider the possibility of experimental confirmation of the deformation of the nuclei Si^{30}, Si^{31} and Ne^{23}, which have been studied in stripping reactions,[6,7] by using the measured values of the reduced widths for neutron capture.

The expressions for the reduced widths for capture into rotational states of deformed nuclei were calculated by Satchler.[8] In the case of strong coupling with the surface, the motion of the odd nucleon in the spheroidal potential is described by the single-particle wave function $\chi_\Omega = \Sigma_j C_j \psi_j$, where j is the angular momentum of the external nucleon and Ω its projection on the symmetry axis of the nucleus. The coefficients C_j were computed by Nilsson. Because of the orthogonality of the single-particle wave functions, the reduced widths γ^2, in the reaction A(d, p)B, for capture of the neutron into an orbit with definite j, l will be proportional to $|C_j|^2$:

$$\gamma^2 \sim [(2I_A + 1)/(2I_B + 1)] \Sigma_j |\langle I_A j K_A \Omega | I_B K_B \rangle|^2 |C_j|^2.$$

For an even-odd initial nucleus,

$$|C_j|^2 \sim (2I_B + 1)\gamma^2 \delta_{j, I_B} \delta_{\Omega, K_B},$$

where δ is the delta function, and K is the projection of the total angular momentum of the nucleus on the symmetry axis.

The nucleus Si^{31} has $j = 3/2$ in its ground state, and is a convenient example for investigating the sign of the deformation, since in the uniform model the potential energy of a nucleus with an odd particle having angular momentum $j = 3/2$ is degenerate, with values $\Omega = 3/2$, $\delta < 0$, and $\Omega = 1/2$, $\delta > 0$. Within the framework of this model, the sign of the deformation for Si^{31} can be established from knowledge of the value of $\Omega = K$. Analysis[1] of the l-forbidden β transition $Si^{31} \rightarrow P^{31}$ gives $j = \Omega = 3/2$ for the state of the external nucleon in Si^{31}. The value of $\Omega = K$ can also be determined from the quantum numbers of the sequence of levels in the rotational band, as predicted by the uniform model. Unfortunately, the spins and parities are known only for the ground and first excited states of Si^{31}. The determination of the quantum numbers of the next two levels at 1.70 and 2.32 Mev would give still another possibility for determining the sign of the deformation in Si^{31}. A direct comparison of the experimental values of reduced widths from the $Si^{30}(d, p)Si^{31}$ reaction with the values of $|C_j|^2$ does no good in this case, since the reaction was studied at a deuteron energy of 4.3 Mev, which is almost equal to the Coulomb barrier for this nucleus, so that the values of γ^2 are greatly reduced by Coulomb and nuclear interactions.[6] For this reason, the table compares the ratios of reduced widths, multiplied by appropriate

Nucleus	Level energy, Mev	$I_B = j, \pi$	γ^2 Mev cm $\times 10^{-13}$	$\lvert\delta\rvert$	$\frac{\gamma^2(2I_B+1)}{\gamma'^2(2I'_B+1)}$	$\delta < 0$	$\delta > 0$
Si^{31}	0	$^3/_2{}^+$	0.031*	0.15	3.7—5.2	$\frac{\lvert C_j\rvert^2_{K=3/2}}{\lvert C_j\rvert^2_{K'=1/2}} = 5.2$	$\frac{\lvert C_j\rvert^2_{K=1/2}}{\lvert C_j\rvert^2_{K'=1/2}} = 1.8$
Si^{31}	0.76	$^1/_2{}^+$	0.017*				
Ne^{23}	0	$^5/_2{}^+$	0.023	0.30	4.0—6.4	$\frac{\lvert C_j\rvert^2_{K=5/2}}{\lvert C_j\rvert^2_{K'=1/2}} = 6.2$	$\frac{\lvert C_j\rvert^2_{K=5/2}}{\lvert C_j\rvert^2_{K'=5/2}} = 6.2$
Ne^{23}	0.98	$^1/_2{}^+$	0.017				
Si^{30}	0	0^+	0.087*	0.15	0.3—0.2		
Si^{30}	2.24	2^+	0.057*				

*Because of a numerical error, incorrect values of γ^2 (and of θ^2) were given in reference 6. However, this does not change the conclusions of the paper.

statistical factors, with the ratios of the coefficients $|C_j|^2$ for the Nilsson orbits for the ground and first excited states, for the cases $\delta < 0$ and $\delta > 0$ (columns 7 and 8 of the table). $\Omega = K = 3/2$ corresponds to the eighth Nilsson orbit, while $\Omega = K = 1/2$ is the eleventh orbit. The absolute values of the equilibrium deformation $|\delta|$ given in column 5 are taken from reference 5. Column 4 of the table gives the values of γ^2 computed omitting and including the isotropic part of the angular distributions. The ratio of the $|C_j|^2$'s for $\delta < 0$ is just bracketed by these values. A similar situation occurs for Ne^{23}, which was studied in the reaction $Ne^{22}(d, p)Ne^{23}$. For this nucleus, $j = 5/2$ (the fifth Nilsson orbit), but the ratio of the $|C_j|^2$'s no longer determines the sign of the deformation, though it is known that in the region $A = 20 - 25$ the nuclei are deformed and have a prolate shape ($\delta > 0$). It is possible that, in both cases, part of the isotropic angular distribution, which is usually attributed to a reaction which proceeds via compound nucleus formation, may be caused by the stripping mechanism. Thus the analysis of reduced widths from stripping shows that the nucleus Si^{31} apparently has an oblate shape with deformation parameter $\delta < 0$, but it is not possible to establish the sign of the deformation for Ne^{23}, although it is confirmed that this nucleus is highly deformed.

In the case of even-even final nuclei, the probabilities of capture to levels of the rotational band differ only in their statistical factors and the corresponding Clebsch-Gordan coefficients $\langle I_B\Omega | I_A j I_A \Omega - I_A\rangle$.[8] For $_{14}Si^{30}$ the experimental ratio of reduced widths from the reaction $Si^{29}(d, p)Si^{30}$, multiplied by the corresponding statistical factors, is equal to 0.3 to 0.2, whereas the theory gives 1 for the case of strong coupling. In the experiment[6] it was not possible to separate completely the proton groups corresponding to the transition to the 2.24 Mev level of Si^{30}, and to the ground state of Si^{29} from the reaction on Si^{28} which is present as an impurity in the target. As a result the ratio of the reduced widths is apparently reduced by 25 — 30%. However, this cannot explain all of the difference between the experimental and theoretical values. It may be that, for Si^{30} as for certain other nuclei in the region $28 \leq A \leq 32$, the strong coupling scheme is not valid. To clarify this question it will be necessary to determine the spins and parities of higher excited states of Si^{30}.

Very recently doubts have been raised concerning the validity of using reduced widths for analysis of nuclear structure,[9] since in addition to the usual stripping reaction there may be other direct reactions, such as the ejection of a proton by the deuteron with capture of the deuteron. However, when the usual stripping process is allowed, the cross section for other direct processes, especially when the deuteron energy is around the value of the Coulomb barrier for the target nucleus, will be probably much smaller than the stripping cross section. The use of reduced widths for analysis therefore seems to be justified.

[1] A. Bohr and B. Mottelson, Kgl. Danske Videnskab. Selskab, Mat.-fys. Medd. **27**, No. 16 (1953).

[2] S. G. Nilsson, Kgl. Danske Videnskab. Selskab, Mat.-fys. Medd. **29**, No. 16, 1-68 (1955).

[3] Litherland et al., Can. J. Phys. **36**, 378 (1958).

[4] Bromley, Gove, and Litherland, Can. J. Phys. **35**, 1057 (1957).

[5] Gonchar, Inopin, and Tsitko, Тезисы доклада на VIII ежегодном совещании по ядерной спектроскопии.

(Reports to the 8th Annual Conference on Nuclear Spectroscopy) Leningrad, U.S.S.R. Acad. Sci. 1958, p. 13.

[6] V. G. Sukharevskiĭ, JETP **36**, 52 (1959), Soviet Phys. JETP **9**, 37 (1959).

[7] V. G. Sukharevskiĭ, JETP **36**, 1377 (1959), Soviet Phys. JETP **9**, 981 (1959).

[8] G. R. Satchler, Ann. Phys. **3**, 275 (1958).

[9] Belyaev, Zakhar'ev, and Neudachin, Атомная энергия (Atomic Energy) in press.

Translated by M. Hamermesh
35

GREEN'S FUNCTION FOR ODD NUCLEI

Yu. T. GRIN', S. I. DROZDOV, and D. F. ZARETSKIĬ

Submitted to JETP editor July 17, 1959

J. Exptl. Theoret. Phys. (U.S.S.R.) **38**, 222-228 (January, 1960)

The techniques of many-body theory are applied to a study of pair correlations in finite systems with an odd number of particles. The Green's function is found, and perturbation theory developed.

PROPERTIES of low-excited states of Fermi systems with an even number of particles differ essentially from those of systems with an odd number of particles. If one considers the application of many-body theory to nuclei, then one encounters the problem of finding the Green's function for odd systems in order to calculate the moments of inertia, magnetic moments, excitation spectra and electromagnetic transition probabilities in odd nuclei. Migdal[1] developed techniques for studying pair correlations between particles in finite systems with an even number of particles. In the present work, the extension of these techniques to finite systems containing an odd number of particles is considered. The Green's function is calculated for such systems and perturbation theory is formulated.

For our purposes, it is convenient to write Gor'kov's system of equations[2,1] separately for the Green's functions $G^+(x_1, x_2)$ and $G^-(x_1, x_2)$ respectively for $\tau = t_1 - t_2 > 0$ and $\tau < 0$.

$$(i\partial/\partial\tau - H)\,G^+ - i\Delta F^+ = 0,\quad (i\partial/\partial\tau + H^* - 2\mu)\,F^+ + i\Delta^* G^+ = 0, \tag{1}$$

$$(i\partial/\partial\tau - H)\,G^- - i\Delta F^- = 0,\quad (i\partial/\partial\tau + H^* - 2\mu)\,F^- + i\Delta^* G^- = 0.$$

$$\Delta^* = \gamma F(\mathbf{r}_1, \mathbf{r}_2, \tau)|_{\tau=0}, \tag{2}$$

where

$$G^+(x_1, x_2) = -i(\Phi_0^N,\ \psi(x_1)\psi^+(x_2)\Phi_0^N),$$

$$G^-(x_1, x_2) = i(\Phi_0^N,\ \psi^+(x_2)\psi(x_1)\Phi_0^N),$$

$$F^+(x_1, x_2) = (\Phi_0^{N+2},\ \psi^+(x_1)\psi^+(x_2)\Phi_0^N),$$

$$F^-(x_1, x_2) = -(\Phi_0^N,\ \psi^+(x_2)\psi^+(x_1)\Phi_0^{N-2}). \tag{3}$$

Here Φ_0^N is the wave function for the ground state of the N-particle system; $\psi(x)$, $\psi^+(x)$ are particle annihilation and creation operators in the Heisenberg representation. At $t = 0$, one has the usual commutation relations for $\psi(\mathbf{r}, t)$

$$\{\psi(\mathbf{r}_1),\ \psi^+(\mathbf{r}_2)\} = \delta(\mathbf{r}_1 - \mathbf{r}_2),$$
$$\{\psi(\mathbf{r}_1),\ \psi(\mathbf{r}_2)\} = \{\psi^+(\mathbf{r}_1),\ \psi^+(\mathbf{r}_2)\} = 0. \tag{4}$$

The chemical potential is defined by

$$\mu = {}^1/_2\,[E_0(N+2) - E_0(N)],$$

where $E_0(N)$ is the ground-state energy of the N-particle system. The parameter γ characterizes the effective interaction which leads to the pairing. We will assume Δ to be constant in our system.

We are interested in comparing properties of systems of different parity in particle number; therefore, we neglect everywhere differences in properties of neighboring systems of the same parity. Boundary conditions on G and F can be written, using their definitions (3) and commutation relations (4), in the form

$$i\,[G^+ - G^-]_{\tau=0} = \delta(\mathbf{r}_1 - \mathbf{r}_2);\quad [F^+ - F^-]_{\tau=0} = 0. \tag{5}$$

We expand G and F in terms of eigenfunctions of the single-particle Hamiltonian H

$$G^\pm(\mathbf{r}_1,\ \mathbf{r}_2,\ \tau) = \sum_{\lambda\lambda'} G^\pm_{\lambda\lambda'}(\tau)\,\varphi^*_\lambda(\mathbf{r}_1)\,\varphi_{\lambda'}(\mathbf{r}_2),$$
$$F^\pm(\mathbf{r}_1, \mathbf{r}_2, \tau) = \sum_{\lambda\lambda'} F^\pm_{\lambda\lambda'}(\tau)\,\varphi^*_\lambda(\mathbf{r}_1)\,\varphi_{\lambda'}(\mathbf{r}_2),$$

where $H\varphi_\lambda = \epsilon_\lambda\varphi_\lambda$. If Δ is constant, only the diagonal terms remain in these expansions.[1] Therefore, instead of Eqs. (1), (2), and (5) we obtain

$$(i\partial/\partial\tau - \varepsilon_\lambda)\,G^\pm_\lambda - i\Delta F^\pm_\lambda = 0,\quad (i\partial/\partial\tau + \varepsilon_\lambda - 2\mu)\,F^\pm_\lambda + i\Delta^* G^\pm_\lambda = 0; \tag{6}$$

$$\Delta^* = \gamma\sum_\lambda F_\lambda(0)\,\varphi^*_\lambda(\mathbf{r})\,\varphi_\lambda(\mathbf{r}); \tag{7}$$

$$i\,[G^+_\lambda(0) - G^-_\lambda(0)] = 1,\quad F^+(0) - F^-_\lambda(0) = 0. \tag{8}$$

The solution of (6) has the form

$$G^\pm_\lambda(\tau) = C^\pm_{1\lambda}\exp\{i(E_\lambda - \mu)\tau\} + C^\pm_{2\lambda}\exp\{-i(E_\lambda + \mu)\tau\}; \tag{9a}$$

$$F^\pm_\lambda(\tau) = \frac{i\Delta}{E_\lambda - \varepsilon_\lambda}C^\pm_{1\lambda}\exp\{i(E_\lambda - \mu)\tau\} - \frac{i\Delta}{E_\lambda + \varepsilon_\lambda}C^\pm_{2\lambda}\exp\{-i(E_\lambda + \mu)\tau\}. \tag{9b}$$

In (9b) and in the following, ϵ_λ is measured from μ as origin.

Using the initial conditions, Eqs. (8), it is possible to eliminate two constants:

$$C^+_{1\lambda} = C^-_{1\lambda} - i(E_\lambda - \varepsilon_\lambda)/2E_\lambda,\ C^+_{2\lambda} = C_{2\lambda} - i(E_\lambda + \varepsilon_\lambda)/2E_\lambda.$$

In order to determine two other constants, we compare the solution obtained with the exact expression for the Green's function of the N-particle system. We consider a nucleus in which there are N_a particles with positive projection of angular momentum $(+\lambda)$ and N_b particles with negative projection $(-\lambda)$. An exact expression for the diagonal part of the Green's function can be put in the form:[3]

$$G^+_\lambda = i\sum_s |(a^+_\lambda)_{s0}|^2 \times \exp\{-i[E_s(N_a+1, N_b) - E_0(N_a, N_b)]\tau\},$$

$$G^-_\lambda = -i\sum_s |(a_\lambda)_{s0}|^2 \times \exp\{i[E_s(N_a-1, N_b) - E_0(N_a, N_b)]\tau\},$$

$$G^+_{-\lambda} = i\sum_s |(a^+_{-\lambda})_{s0}|^2 \times \exp\{-i[E_s(N_a, N_b+1) - E_0(N_a, N_b)]\tau\},$$

$$G^-_{-\lambda} = -i\sum_s |(a_{-\lambda})_{s0}|^2 \times \exp\{i[E_s(N_a, N_b-1) - E_0(N_a, N_b)]\tau\}, \quad (10)$$

where $E_s(N\pm1)$ is the energy of the s-th state of the system of $N\pm1$ particles. We use the notation $2E_0(N_a+1, N_b) - E_0(N_a+1, N_b+1) - E_0(N_a, N_b) = 2\tilde{\Delta}$. Comparing exponents in (9a) and (10) for G^+_λ and $G^+_{-\lambda}$, we obtain

$$E_\lambda + \tilde{\Delta} = -\varepsilon^{(1)}_s(N_a+1, N_b), \quad (11a)$$

$$E_\lambda - \tilde{\Delta} = \varepsilon^{(2)}(N_a+1, N_b), \quad (11b)$$

$$E_\lambda + E_0(N_a, N_b+1) - E_0(N_a+1, N_b) + \tilde{\Delta} = -\varepsilon^{(3)}_s(N_a, N_b+1), \quad (11c)$$

$$E_\lambda - E_0(N_a, N_b+1) + E_0(N_a+1, N_b) - \Delta = \varepsilon^{(4)}_s(N_a, N_b+1). \quad (11d)$$

Comparison of exponents for G^-_λ and $G^-_{-\lambda}$ gives equations coinciding with Eqs. (11). The quantity $\epsilon_s(N_a, N_b) = E_s(N_a, N_b) - E_0(N_a, N_b)$ is positive by definition. We will show that the condition $\epsilon_s \geq 0$ sets definite restrictions on the solutions of Eqs. (9a) and (9b).

We define the ground state of a system with particle number $N+1 = (N_a+1, N_b)$, setting $\epsilon^{(2)}_s = E_{\lambda_0} - \tilde{\Delta} = 0$, where λ_0 is a state near to the Fermi surface. Then the conditions Eqs. (11) take the form

$$E_\lambda + E_{\lambda_0} = -\varepsilon^{(1)}_s(N_a+1, N_b), \quad (12a)$$

$$E_\lambda - E_{\lambda_0} = \varepsilon^{(2)}_s(N_a+1, N_b), \quad (12b)$$

$$E_\lambda + E_0(N_a, N_b+1) - E_0(N_a+1, N_b) + E_{\lambda_0} = -\varepsilon^{(3)}_s(N_a, N_b+1), \quad (12c)$$

$$E_\lambda - E_0(N_a, N_b+1) + E_0(N_a+1, N_b) - E_{\lambda_0} = \varepsilon^{(4)}_s(N_a, N_b+1). \quad (12d)$$

The quantity $E_0(N_a, N_b+1) - E_0(N_a+1, N_b) = \Delta E$ can be considered to be the excitation energy of the nucleus (N_a+1, N_b). Then the conditions (12a) and (12c) cannot be satisfied for any λ. In accordance with Eq. (12b) we set $\Delta E = 0$. Then the conditions (12b) and (12d) coincide, and are satisfied for arbitrary λ. Therefore, in Eqs. (9a) and (9b) we should set

$$C^+_{1\pm\lambda} = 0,\ C^-_{2\pm\lambda} = 0.$$

The functions G and F become

$$G^+_{\pm\lambda}(\tau) = -i\frac{E_\lambda + \varepsilon_\lambda}{2E_\lambda}\exp\{-i(E_\lambda + \mu)\tau\},$$

$$G^-_{\pm\lambda}(\tau) = i\frac{E_\lambda - \varepsilon_\lambda}{2E_\lambda}\exp\{i(E_\lambda - \mu)\tau\},$$

$$F^+_{\pm\lambda}(\tau) = -\frac{\Delta}{2E_\lambda}\exp\{-i(E_\lambda + \mu)\tau\},$$

$$\times F^-_{\pm\lambda}(\tau) = -\frac{\Delta}{2E_\lambda}\exp\{i(E_\lambda - \mu)\tau\}. \quad (13)$$

Since $-iG^-_\lambda(0) = \rho_\lambda$ is the density matrix of the particles, it is easy to see that the solution found corresponds to an even system $(\rho_\lambda = \rho_{-\lambda})$. At the same time, from Eq. (12b) we determine the excitation spectrum for odd nuclei:

$$\varepsilon_s = E_\lambda - E_{\lambda_0},$$

where the quantities E_λ, E_{λ_0} contain the Δ of the even system.

In a Fourier representation for τ, the functions G_λ and F_λ take the form

$$G_\lambda(\omega) = \frac{(E_\lambda + \varepsilon_\lambda)/2E_\lambda}{\omega - E_\lambda + i\delta} + \frac{(E_\lambda - \varepsilon_\lambda)/2E_\lambda}{\omega + E_\lambda - i\delta}, \quad (14)$$

$$F_\lambda(\omega) = -\frac{i\Delta}{2E_\lambda}\left[\frac{1}{\omega - E_\lambda + i\delta} - \frac{1}{\omega + E_\lambda - i\delta}\right]. \quad (15)$$

An analogous result is obtained if we determine the ground state of the $N+1$ particle system from Eq. (11c).

We now consider another possibility. Let the ground state of the $N+1$ particle system be determined from the relation

$$-\varepsilon^{(1)}_s(N_a+1, N_b) = E_{\lambda_0} + \tilde{\Delta} = 0.$$

Then the conditions [Eqs. (11)] take the form

$$E_\lambda - E_{\lambda_0} = -\varepsilon^{(1)}_s(N_a+1, N_b), \quad (16a)$$

$$E_\lambda + E_{\lambda_0} = \varepsilon^{(2)}_s(N_a+1, N_b), \quad (16b)$$

$$E_\lambda + E_0(N_a,\ N_b+1) - E_0(N_a+1,\ N_b) - E_{\lambda_0} = -\varepsilon_s^{(3)}(N_a,\ N_b+1), \tag{16c}$$

$$E_\lambda - E_0(N_a,\ N_b+1) + E_0(N_a+1,\ N_b) + E_{\lambda_0} = \varepsilon_s^{(1)}(N_a,\ N_b+1). \tag{16d}$$

Condition (16a) is satisfied only for $\lambda = \lambda_0$, and condition (16b), for all λ. The quantity $\Delta E = E_0(N_a, N_b+1) - E_0(N_a+1, N_b)$ corresponds to the minimum excitation energy of the nucleus (N_a+1, N_b). Therefore, in accordance with Eq. (16b), $\Delta E = E_{\lambda_0} + E_{\lambda_1}$, where λ_1 is a state near in energy to the state λ_0. Then Eq. (16c) is not satisfied for any λ, and Eq. (16d) becomes

$$E_\lambda - E_{\lambda_1} = \varepsilon_s(N_a,\ N_b+1).$$

In deformed nuclei, the energy levels are doubly degenerate, and this relation is satisfied for all $\lambda \neq \lambda_0$. Therefore, in the solutions to Eqs. (9a) and (9b) we should set

$$C_{1\lambda}^{+} = C_{2-\lambda}^{-} = 0,\ \lambda \neq \lambda_0,$$
$$C_{1-\lambda}^{+} = C_{2\lambda}^{-} = 0,\ C_{2-\lambda_0}^{+} = C_{1\lambda_0}^{-} = 0.$$

In this case, G and F take the form

$$G_\lambda^{+}(\tau) = -i\frac{E_\lambda - \varepsilon_\lambda}{2E_\lambda}\delta_{\lambda\lambda_0}\exp\{i(E_\lambda-\mu)\tau\} - i\frac{E_\lambda+\varepsilon_\lambda}{2E_\lambda}(1-\delta_{\lambda-\lambda_0})\exp\{-i(E_\lambda+\mu)\tau\}$$

$$G_\lambda^{-}(\tau) = i\frac{E_\lambda - \varepsilon_\lambda}{2E_\lambda}(1-\delta_{\lambda\lambda_0})\exp\{i(E_\lambda-\mu)\tau\} + i\frac{E_\lambda+\varepsilon_\lambda}{2E_\lambda}\delta_{\lambda-\lambda_0}\exp\{-i(E_\lambda+\mu)\tau\},$$

$$F_\lambda^{+}(\tau) = \frac{\Delta}{2E_\lambda}\delta_{\lambda\lambda_0}\exp\{i(E_\lambda-\mu)\tau\} - \frac{\Delta}{2E_\lambda}(1-\delta_{\lambda-\lambda_0})\exp\{-i(E_\lambda+\mu)\tau\},$$

$$F_\lambda^{-}(\tau) = -\frac{\Delta}{2E_\lambda}(1-\delta_{\lambda\lambda_0})\exp\{i(E_\lambda-\mu)\tau\} + \frac{\Delta}{2E_\lambda}\delta_{\lambda-\lambda_0}\exp\{-i(E_\lambda+\mu)\tau\}. \tag{17}$$

In calculating the density matrix ρ_λ, we see that $\rho_\lambda = \rho_{-\lambda}$ $(\lambda \neq \pm\lambda_0)$, $\rho_{\lambda_0} = 0$, $\rho_{-\lambda_0} = 1$. Thus, the solution obtained corresponds to a nucleus with an odd number of particles where the odd particle is in state $-\lambda_0$ with probability 1, and the corresponding state λ_0 is empty. If we determine the ground state of the system from Eq. (11c), then we obtain an analogous result with the odd particle in state λ_0. Equation (16b) gives the excitation spectrum of the even system

$$\varepsilon_s = E_\lambda + E_{\lambda_0}.$$

It should be noted that in this case the Δ of the odd system enters into E_λ and E_{λ_0}. Therefore, Δ of the odd nucleus can be determined, knowing the value of the energy gap in the excitation spectra of the neighboring even-odd nucleus.

Calculating $F_\lambda(0)$, we obtain from Eq. (7) the equation for Δ of the odd system given earlier in reference 1:

$$1 = -\gamma\sum_\lambda \frac{1-\delta_{\lambda\lambda_0}-\delta_{\lambda-\lambda_0}}{2E_\lambda}\varphi_\lambda^*(\mathbf{r})\varphi_\lambda(\mathbf{r}). \tag{18}$$

In the Fourier representation for τ, the Green's function of the odd system with the odd particle in state λ_0 has the form

$$G_\lambda(\omega) = \frac{(E_\lambda+\varepsilon_\lambda)/2E_\lambda}{\omega - E_\lambda + i\delta\theta_{\lambda\lambda_0}} + \frac{(E_\lambda-\varepsilon_\lambda)/2E_\lambda}{\omega + E_\lambda - i\delta\theta_{\lambda-\lambda_0}}, \tag{19}$$

$$F_\lambda(\omega) = -\frac{i\Delta}{2E_\lambda}\left(\frac{1}{\omega - E_\lambda + i\delta\theta_{\lambda\lambda_0}} - \frac{1}{\omega + E_\lambda - i\delta\theta_{\lambda-\lambda_0}}\right), \tag{20}$$

where

$$\theta_{\lambda\lambda_0} = \begin{cases} 1, & \lambda \neq \lambda_0. \\ -1, & \lambda = \lambda_0. \end{cases}$$

The case of spherical nuclei needs separate consideration. In this case the levels are multiply degenerate, and, consequently, $E_\lambda = E_{\lambda_0}$ for all states λ corresponding to a given energy level. Then Eqs. (16d) and (16a) are satisfied for any of these λ. Therefore, in order to fill in the missing supplementary condition, it is necessary to turn to considerations connected with conservation of the total angular momentum of the system

$$J_z = \sum_\lambda (j_z)_\lambda \rho_\lambda.$$

Assuming that the nucleons pair off into states of zero angular momentum, we find $J_Z = 0$ for even systems and $J_Z = (j_Z)_{\lambda_0}$ for odd ones. From this it follows that $\rho_{\lambda_0} = 1$ and, consequently, $G_{\lambda_0}^{+}(0) = 0$. Therefore, if one exponent is missing in $G_{\lambda_0}^{+}$, then, on account of the initial condition, the other one will also be absent. From the condition $\rho_\lambda = \rho_{-\lambda}$ for all $\lambda \neq \pm\lambda_0$, it follows that the coefficient in front of the exponential, according to condition (16a), is zero. Then the expressions (19) and (20) can also be applied to the case of spherical nuclei.

Migdal[1] showed that for small, time-independent perturbations, corrections to the functions G and F take the form

$$G'_{\lambda\lambda'} = G_\lambda V_{\lambda\lambda'} G_{\lambda'} + F_\lambda V^*_{\lambda\lambda'} F_{\lambda'} + iG_\lambda \Delta'_{\lambda\lambda'} F_{\lambda'} + iF_\lambda \Delta'^*_{\lambda\lambda'} G_{\lambda'}, \tag{21}$$

$$F'_{\lambda\lambda'} = -D_\lambda V^*_{\lambda\lambda'} F_{\lambda'} + F_\lambda V_{\lambda\lambda'} G_{\lambda'} + iF_\lambda \Delta'_{\lambda\tilde{\lambda}'} F_{\lambda'} - iD_\lambda \Delta'^*_{\lambda\lambda'} G_{\lambda'}; \tag{22}$$

$$\Delta'^*(\mathbf{r}) = \gamma\sum_{\lambda\lambda'} F'_{\lambda\lambda'}\varphi_\lambda(\mathbf{r})\varphi^*_{\lambda'}(\mathbf{r}). \tag{23}$$

For an odd nucleus, G and F are determined by (19) and (20), and D is

$$D_\lambda = \frac{(E_\lambda - \varepsilon_\lambda)/2E_\lambda}{\omega - E_\lambda + i\delta\theta_{\lambda\lambda_0}} + \frac{(E_\lambda + \varepsilon_\lambda)/2E_\lambda}{\omega + E_\lambda - i\delta\theta_{\lambda-\lambda_0}}. \tag{24}$$

Substituting (19) and (20) in (21), and integrating over ω, we obtain the correction to the density matrix:

$$\rho'_{\lambda\lambda'} = \frac{V_{\lambda\lambda'}(\varepsilon_\lambda\varepsilon_{\lambda'} - E_\lambda E_{\lambda'}) - \Delta^2 V^*_{\lambda\lambda'} + \Delta(\varepsilon_\lambda \Delta'_{\lambda\lambda'} + \varepsilon_{\lambda'}\Delta'^*_{\lambda\lambda'})}{2E_\lambda E_{\lambda'}(E_\lambda + E_{\lambda'})} + \delta_{\lambda'-\lambda_0}\frac{V_{\lambda\lambda'}(E_{\lambda'} - \varepsilon_\lambda)(\varepsilon_{\lambda'} - E_{\lambda'}) + \Delta^2 V^*_{\lambda\lambda'} + \Delta[\Delta'^*_{\lambda\lambda'}(E_{\lambda'} - \varepsilon_{\lambda'}) + \Delta'_{\lambda\lambda'}(E_{\lambda'} - \varepsilon_\lambda)]}{2E_{\lambda'}(E^2_\lambda - E^2_{\lambda'})}$$

$$+ \delta_{\lambda'\lambda_0}\frac{V_{\lambda\lambda'}(E_{\lambda'} + \varepsilon_\lambda)(E_{\lambda'} + \varepsilon_{\lambda'}) - \Delta^2 V^*_{\lambda\lambda'} + \Delta[\Delta'^*_{\lambda\lambda'}(E_{\lambda'} + \varepsilon_{\lambda'}) + \Delta'_{\lambda\lambda'}(E_{\lambda'} + \varepsilon_\lambda)]}{2E_{\lambda'}(E^2_{\lambda'} - E^2_\lambda)}$$

$$+ \delta_{\lambda-\lambda_0}\frac{V_{\lambda\lambda'}(E_\lambda - \varepsilon_\lambda)(\varepsilon_{\lambda'} - E_\lambda) + \Delta^2 V^*_{\lambda\lambda'} + \Delta[\Delta'^*_{\lambda\lambda'}(E_\lambda - \varepsilon_{\lambda'}) + \Delta'_{\lambda\lambda'}(E_\lambda - \varepsilon_\lambda)]}{2E_\lambda(E^2_{\lambda'} - E^2_\lambda)}$$

$$+ \delta_{\lambda\lambda_0}\frac{V_{\lambda\lambda'}(E_\lambda + \varepsilon_\lambda)(E_\lambda + \varepsilon_{\lambda'}) - \Delta^2 V^*_{\lambda\lambda'} + \Delta[\Delta'^*_{\lambda\lambda'}(E_\lambda + \varepsilon_{\lambda'}) + \Delta'_{\lambda\lambda'}(E_\lambda + \varepsilon_\lambda)]}{2E_\lambda(E^2_\lambda - E^2_{\lambda'})}$$

for $E_\lambda \neq E_{\lambda'}$;

$$\rho'_{\lambda\lambda'} = \frac{\varepsilon_\lambda\Delta(\Delta'_{\lambda\lambda'} + \Delta'^*_{\lambda\lambda'}) - \Delta^2(V_{\lambda\lambda'} + V^*_{\lambda\lambda'})}{4E^3_\lambda} + (\delta_{\lambda'-\lambda_0} + \delta_{\lambda\lambda_0})\frac{\Delta^2(V_{\lambda\lambda'} + V^*_{\lambda\lambda'}) + \Delta[\Delta'^*_{\lambda\lambda'}(E_\lambda - \varepsilon_\lambda) - \Delta'_{\lambda\lambda'}(E_\lambda + \varepsilon_\lambda)]}{8E^3_\lambda}$$

$$+ (\delta_{\lambda'\lambda_0} + \delta_{\lambda-\lambda_0})\frac{\Delta^2(V_{\lambda\lambda'} + V^*_{\lambda\lambda'}) + \Delta[\Delta'_{\lambda\lambda'}(E_\lambda - \varepsilon_\lambda) - \Delta'^*_{\lambda\lambda'}(E_\lambda + \varepsilon_\lambda)]}{8E^3_\lambda} \tag{25}$$

for $E_\lambda = E_{\lambda'}$.

Analogously, we find the correction to the function F:

$$F'_{\lambda\lambda'} = \frac{\Delta(\varepsilon_{\lambda'}V_{\lambda\lambda'} + \varepsilon_\lambda V^*_{\lambda\lambda'}) - \Delta'^*_{\lambda\lambda'}(E_\lambda E_{\lambda'} + \varepsilon_\lambda\varepsilon_{\lambda'}) + \Delta^2\Delta'_{\lambda\lambda'}}{2E_\lambda E_{\lambda'}(E_\lambda + E_{\lambda'})} + \delta_{\lambda'-\lambda_0}\frac{\Delta[(E_{\lambda'} - \varepsilon_{\lambda'})V_{\lambda\lambda'} - (E_{\lambda'} + \varepsilon_\lambda)V^*_{\lambda\lambda'}] - \Delta'^*_{\lambda\lambda'}(E_{\lambda'} + \varepsilon_\lambda)(E_{\lambda'} - \varepsilon_{\lambda'}) - \Delta^2\Delta'_{\lambda\lambda'}}{2E_{\lambda'}(E^2_{\lambda'} - E^2_{\lambda'})}$$

$$+ \delta_{\lambda'\lambda_0}\frac{\Delta[(E_{\lambda'} + \varepsilon_{\lambda'})V_{\lambda\lambda'} - (E_{\lambda'} - \varepsilon_\lambda)V^*_{\lambda\lambda'}] + \Delta'^*_{\lambda\lambda'}(E_{\lambda'} - \varepsilon_\lambda)(E_{\lambda'} + \varepsilon_{\lambda'}) + \Delta^2\Delta'_{\lambda\lambda'}}{2E_{\lambda'}(E^2_{\lambda'} - E^2_\lambda)}$$

$$+ \delta_{\lambda-\lambda_0}\frac{\Delta[(E_\lambda - \varepsilon_{\lambda'})V_{\lambda\lambda'} - (E_\lambda + \varepsilon_\lambda)V^*_{\lambda\lambda'}] - \Delta'^*_{\lambda\lambda'}(E_\lambda + \varepsilon_\lambda)(E_\lambda - \varepsilon_{\lambda'}) - \Delta^2\Delta'_{\lambda\lambda'}}{2E_\lambda(E^2_{\lambda'} - E^2_\lambda)}$$

$$+ \delta_{\lambda\lambda_0}\frac{\Delta[(E_\lambda + \varepsilon_{\lambda'})V_{\lambda\lambda'} - (E_\lambda - \varepsilon_\lambda)V^*_{\lambda\lambda'}] + \Delta'^*_{\lambda\lambda'}(E_\lambda - \varepsilon_\lambda)(\varepsilon_{\lambda'} + E_\lambda) + \Delta^2\Delta'_{\lambda\lambda'}}{2E_\lambda(E^2_\lambda - E^2_{\lambda'})}$$

for $E_\lambda \neq E_{\lambda'}$;

$$F'_{\lambda\lambda'} = \frac{\Delta\varepsilon_\lambda(V_{\lambda\lambda'} + V^*_{\lambda\lambda'}) - \Delta'^*_{\lambda\lambda'}(E^2_\lambda + \varepsilon^2_\lambda) + \Delta^2\Delta'_{\lambda\lambda'}}{4E^3_\lambda} + (\delta_{\lambda'-\lambda_0} + \delta_{\lambda\lambda_0})\frac{\Delta(E_\lambda - \varepsilon_\lambda)(V_{\lambda\lambda'} + V^*_{\lambda\lambda'}) + (E_\lambda - \varepsilon_\lambda)^2\Delta'^*_{\lambda\lambda'} - \Delta^2\Delta'_{\lambda\lambda'}}{8E^3_\lambda}$$

$$+ (\delta_{\lambda'\lambda_0} + \delta_{\lambda-\lambda_0})\frac{-\Delta(E_\lambda + \varepsilon_\lambda)(V_{\lambda\lambda'} + V^*_{\lambda\lambda'}) + (E_\lambda + \varepsilon_\lambda)^2\Delta'^*_{\lambda\lambda'} - \Delta^2\Delta'_{\lambda\lambda'}}{8E^3_\lambda} \tag{26}$$

for $E_\lambda = E_{\lambda'}$.

Substituting (26) in (23) and using the equality

$$\Delta'^*(\mathbf{r}) = -\gamma\sum_{\lambda\lambda'}\Delta'^*_{\lambda\lambda'}\varphi_\lambda(\mathbf{r})\varphi^*_{\lambda'}(\mathbf{r})\frac{1 - \delta_{\lambda\lambda_0} - \delta_{\lambda-\lambda_0}}{2E_\lambda} = -\gamma\sum_{\lambda\lambda'}\Delta'^*_{\lambda\lambda'}\varphi_\lambda\varphi^*_{\lambda'}\frac{1 - \delta_{\lambda'\lambda_0} - \delta_{\lambda'-\lambda_0}}{2E_{\lambda'}},$$

we obtain an integral equation for $\Delta'(\mathbf{r})$:

$$\sum_{\lambda\lambda'}\varphi_\lambda(\mathbf{r})\varphi^*_{\lambda'}(\mathbf{r})\frac{\Delta'^*_{\lambda\lambda'}[2\Delta^2 + (\varepsilon_\lambda - \varepsilon_{\lambda'})^2] + 2\Delta^2\Delta'_{\lambda\lambda'} + 2\Delta(\varepsilon_{\lambda'}V_{\lambda\lambda'} + \varepsilon_\lambda V^*_{\lambda\lambda'})}{2E_\lambda E_{\lambda'}(E_\lambda + E_{\lambda'})} + \sum_{\substack{\lambda \\ (E_\lambda \neq E_{\lambda_0})}}\frac{1}{E_{\lambda_0}(E^2_{\lambda_0} - E^2_\lambda)}\{\varphi_{\lambda_0}(\mathbf{r})\varphi^*_\lambda(\mathbf{r})[2\Delta(E_{\lambda_0} + \varepsilon_\lambda)V_{\lambda_0\lambda}$$

$$- 2\Delta(E_{\lambda_0} - \varepsilon_{\lambda 0})V^*_{\lambda_0\lambda} + 2\Delta^2\Delta'_{\lambda_0\lambda} + \Delta'^*_{\lambda_0\lambda}2(E_{\lambda_0} + \varepsilon_\lambda)(E_{\lambda_0} - \varepsilon_{\lambda_0}) + \Delta'^*_{\lambda_0\lambda}(E^2_\lambda - E^2_{\lambda_0})] + \varphi_\lambda(\mathbf{r})\varphi^*_{\lambda_0}(\mathbf{r})[2\Delta(E_{\lambda_0} + \varepsilon_{\lambda_0})V_{\lambda\lambda_0}$$

$$- 2\Delta(E_{\lambda_0} - \varepsilon_\lambda)V^*_{\lambda\lambda_0} + 2\Delta^2\Delta'_{\lambda\lambda_0} + \Delta'^*_{\lambda\lambda_0}2(E_{\lambda_0} - \varepsilon_\lambda)(E_{\lambda_0} + \varepsilon_{\lambda_0}) + \Delta'^*_{\lambda\lambda_0}(E^2_\lambda - E^2_{\lambda_0})]\} + \sum_{\substack{\lambda \\ (E_\lambda \neq E_{\lambda_0})}}\frac{1}{2E^3_{\lambda_0}}\{\varphi_{\lambda_0}(\mathbf{r})\varphi^*_\lambda(\mathbf{r})$$

$$\times[\Delta(E_{\lambda_0} - \varepsilon_{\lambda_0})(V_{\lambda_0\lambda'} + V^*_{\lambda_0\lambda}) - \Delta^2\Delta_{\lambda_0\lambda} - \Delta'^*_{\lambda_0\lambda}(2E_{\lambda_0}\varepsilon_{\lambda_0} + \Delta^2)] + \varphi_\lambda(\mathbf{r})\varphi^*_{\lambda_0}(\mathbf{r})[-\Delta(E_{\lambda_0} + \varepsilon_{\lambda_0})(V_{\lambda\lambda_0} + V^*_{\lambda\lambda_0})$$

$$- \Delta^2\Delta'_{\lambda\lambda_0} + \Delta'^*_{\lambda\lambda_0}(2E_{\lambda_0}\varepsilon_{\lambda_0} - \Delta^2)]\} = 0. \tag{27}$$

As a check, Eqs. (25) — (27) were also obtained by using Eq. (1) without going to the Fourier representation.

In the present work, a theorem about the form of the Green's function of a nonspherical nucleus was proved. It turned out that, in spite of the effect of pair correlations, the odd particle was in a definite state with probability 1, and that the conjugate state was completely empty. However, the pairing of particles in the nucleus leads to the excitation spectrum of the nucleus differing essentially from that of the usual one-particle one connected with excitations of the odd particle: $\epsilon_s = E_\lambda - E_{\lambda_0}$, $E_\lambda = \sqrt{\Delta^2 + \epsilon_\lambda^2}$. It is easy to see that for small excitations ($|\epsilon_\lambda| < \Delta$) the density of levels of the odd nucleus turns out to be roughly $2\Delta/|\epsilon_\lambda|$ times larger than in the one-particle model. The formulae (25) — (27) obtained from perturbation theory at the end of the article are essential for application of the theory considered. They make it possible to calculate effects connected with the influence of the odd particle, e.g., moments of inertia of odd nuclei, or magnetic moments.

The authors would like to express their gratitude to A. B. Migdal, V. M. Galitskiĭ and S. T. Belyaev for valuable advice and discussion.

[1] A. B. Migdal, JETP **37**, 249 (1959), Soviet Phys. JETP **10**, 176 (1960).

[2] L. P. Gor'kov, JETP **34**, 735 (1958), Soviet Phys. JETP **7**, 505 (1958).

[3] V. M. Galitskiĭ and A. B. Migdal, JETP **34**, 139 (1958), Soviet Phys. JETP **7**, 96 (1958).

Translated by G. E. Brown
36

PERIPHERAL INTERACTION OF 9 Bev NUCLEONS

I. M. DREMIN and D. S. CHERNAVSKIĬ

P. N. Lebedev Physics Institute, Academy of Sciences, U.S.S.R.

Submitted to JETP editor July 18, 1959

J. Exptl. Theoret. Phys. (U.S.S.R.) **38**, 229-232 (January, 1960)

The peripheral interaction of two nucleons (E_L = 9 Bev) arising in the exchange of one pion is considered. The cross section for such processes is estimated. It is found that excited nucleons in such peripheral interactions are in states with isospin $^3/_2$.

THE following features were observed[1] in the interaction of 9 Bev nucleons: 1) in the case of collision of two protons (to be referred to as p-p interaction), the distribution of secondary particles was anisotropic in the center-of-mass system (c.m.s.); 2) in the case of neutron-proton collisions, the distribution of secondary charged particles was asymmetrical; namely, in the majority of cases the secondary proton is emitted in the initial direction ("the proton conserves its charge").

Tamm has shown[2] that all of these facts can be explained by assuming that in peripheral interactions of the two nucleons, both nucleons are simultaneously excited to the isobaric state with isospin $^3/_2$ and mass $\mathfrak{M} = 1.3m$ (m is the mass of the nucleon).

We shall investigate here the peripheral interaction in the exchange of one meson by two nucleons of energy E_L = 9 Bev. We shall concentrate mainly on the question as to how well justified the assumption (made by Tamm in reference 2) about simultaneous isobaric excitation of both nucleons is, and what the cross section for such a process is. It should be noted, that the calculation of peripheral collisions of two nucleons where both nucleons are excited should be carried out in perturbation theory (see reference 3); the Weizsäcker-Williams method gives incorrect results in this case.

The calculation was carried out, starting from Feynman diagrams (see the figure). Using the general rules, the expression for the probability of the process can be written in the form

$$dw = (2\pi)^4 \sum_{n,n'} \left| \frac{M_1(p_0, -k)\, M_2(q_0, k)}{k^2 + \mu^2} - \frac{M_1(p_0, -k')\, M_2(q_0, k')}{k'^2 + \mu^2} \right|^2 \times \delta\Big(\sum_i^n p_i + \sum_j^{n'} q_j - p_0 - q_0\Big) \prod_i^n \frac{d^3 p_i}{(2\pi)^3} \prod_j^{n'} \frac{d^3 q_j}{(2\pi)^3}, \qquad (1)$$

where p_0 and q_0 are the 4-momenta of the colliding nucleons, p_i and q_j are the momenta of the secondary particles, $k = p_0 - \sum p_i = p_0 - P_1$;

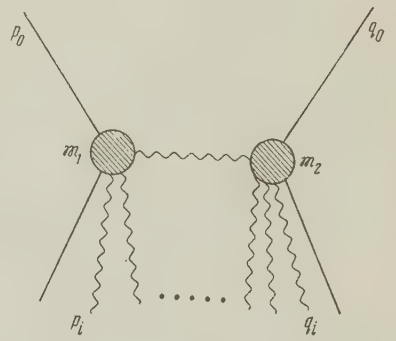

$k' = p_0 - \sum q_j$; $k^2 = \mathbf{k}^2 - k_0^2$; M_1 and M_2 are the matrix elements corresponding to the first and second vertices of the diagram.

It should be noted that the denominator of the first term is small only in the region of small angles $\vartheta \sim \mu/p_0$ (ϑ is the angle between $\mathbf{p}_0$ and $\mathbf{P}_1$); the denominator of the second term is small in the region $\vartheta \sim \pi - \mu/p_0$. It can be shown that the square of the first term in the region $\vartheta \sim \mu/p_0$ has the same absolute value as the square of the second term in the region $\vartheta \sim \pi - \mu/p_0$. The interference term is small compared with these terms and is of comparable size only in the region $\vartheta \sim \pi/2$, where all three terms are small.* Because of this, the interference term can be neglected, and the interaction probability can be written as

$$dw = \sum_{n,n'} \frac{2(2\pi)^4}{(k^2 + \mu^2)^2} |M_1|^2 |M_2|^2 \delta \times \Big(\sum_i^n p_i + \sum_j^{n'} q_j - p_0 - q_0\Big) \prod_i^n \frac{d^3 p_i}{(2\pi)^3} \prod_j^{n'} \frac{d^3 q_j}{(2\pi)^3}.$$

Calculation of the matrix elements M_1 and M_2 requires knowledge of operators for the angular

*In integrating over the angles ϑ, the contribution from the interference term is smaller by a factor of p_0^2/μ^2 than the contributions from the squares of the first or second term, if the angular dependence is assumed to be determined by the denominator.

parts, which is not known at these energies. Therefore, it is more convenient to use known results about the magnitude of the pion-nucleon interaction cross section. Noting that the probability of interaction of a π meson (with 4-momentum k) with a nucleon (of momentum q_0) is equal to

$$w_\pi(k) = \sum_{n'} \int \frac{(2\pi)^4}{2\omega} |M(q_0, k)|^2 \delta\left(\sum_j^{n'} q_j - q_0 - k\right) \prod_j^{n'} \frac{d^3 q_j}{(2\pi)^3},$$

$$\omega = \sqrt{k^2 + \mu^2}, \qquad (2)$$

it is possible to rewrite the expression for the cross section for peripheral collision of nucleons $\sigma(q_0, p_0)$ as

$$E_1 E_2 J \sigma(p_0, q_0) = \frac{8}{(2\pi)^4} \int \frac{d^4 P_1}{(k^2 + \mu^2)^2} E_1 \omega J_\pi^{(1)} \sigma_1(\omega) E_2 \omega J_\pi^{(2)} \sigma_2(\omega), \qquad (3)$$

where E_1 and E_2 are the energies of the colliding nucleons (they are equal in the c.m.s., $E_1 = E_2 = E_0$); ω is the energy of the π meson, $\sigma(\omega)$ is the cross section for pion-nucleon interaction; J_π is the relative current of π mesons, so that $J_\pi \sigma(\omega) = \omega_\pi$.

The quantity $\omega E J_\pi \sigma(\omega)$ is invariant with respect to Lorentz transformations and can depend only on invariant combinations of the momenta p_0 and k. It should be noted that the momentum of the virtual π meson enters into these invariant combinations; however, the degree of its "virtualness" in peripheral interactions is small: $k^2 + \mu^2 \sim \mu^2$.

In the future we neglect any differences in these expressions from those for the interaction of a real π meson with a nucleon. This neglect is equivalent to the assumption that $\omega E J_\pi \sigma(\omega)$ depends less on the angle ϑ between p_0 and P_1 than does the denominator $(k^2 + \mu^2)$. In fact, it is easy to see that for small imaginary values $\vartheta \sim i\mu/E_0$, the "virtualness" $k^2 + \mu^2 = 0$ and the quantity $\omega E J_\pi \sigma(\omega)$ coincide with the expression for real π mesons. Extrapolating this value into the region of real small angles (considering the dependence of $\omega E J_\pi \sigma(\omega)$ on angle to be both analytical and small), we find that in the region of real angles this expression is near to that for real π mesons. In this case, the quantities $\omega E_1 J_\pi^{(1)} \sigma_1(\omega)$ and $\omega E_2 J_\pi^{(2)} \sigma_2(\omega)$ depend only on the quantities m^2 and μ^2 (μ is the meson mass), and also on the quantities $\mathfrak{M}_1^2$ and $\mathfrak{M}_2^2$ ($\mathfrak{M}_1^2 = -P_1^2 = -|\sum_i^n p_i|^2$ and $\mathfrak{M}_2^2 = -|\sum_j^{n'} q_j|^2$) which can conveniently be introduced since they represent masses of excited nucleons which then rapidly decay into secondary particles.* The differential $d^4 P_1$ can be expressed as

$$d^4 P_1 = \frac{P_1}{2E_0} \mathfrak{M}_1 d\mathfrak{M}_1 \mathfrak{M}_2 d\mathfrak{M}_2 \, 2\pi d(\cos\vartheta). \qquad (4)$$

The cross section can then be put into the form

$$\sigma(E_0) = \frac{2}{(2\pi)^3 E_0^2} \int dz \int dy \int d(\cos\vartheta) \times \frac{\sqrt{z^2 - m^2\mu^2}\sqrt{y^2 - m^2\mu^2}}{[\mu^2 + \varkappa^2 + 2p_0^2(1 - \cos\vartheta)]^2} \sigma_\pi(z) \sigma_\pi(y), \qquad (5)$$

where $z = (\mathfrak{M}_1^2 - m^2 - \mu^2)/2$, $y = (\mathfrak{M}_2^2 - m^2 - \mu^2)/2$

$$\varkappa^2 = zy/E_0^2 + (z + y)[2zy + m^2(z + y)]/4E_0^4.$$

From this expression it can be seen that the angular distribution of excited particles is anisotropic in the c.m.s. and concentrated in the region of small angles $\vartheta^2 \sim (\mu^2 + \kappa^2)/p_0^2$. As will be seen from the following, $\kappa^2 \sim \mu^2$ and, consequently, the angles ϑ are $\sim \mu/p_0$, in agreement with the generally accepted picture[4] that $p_\perp \sim \vartheta p_0 \sim \mu$.

Integrating over angles, we obtain the total cross section as

$$\sigma(E_0) = \frac{1}{(2\pi)^3 E_0^2} \int_{m\mu}^{z_{max}} dz \int_{m\mu}^{y_{max}} dy \frac{\sqrt{z^2 - m^2\mu^2}\sqrt{y^2 - m^2\mu^2}}{(\mu^2 + \varkappa^2)[(\mu^2 + \varkappa^2)\vartheta_{max}^{-2} + p_0^2]} \times \begin{cases} \frac{10}{9}\sigma_{3/2}\sigma_{3/2} + \frac{16}{9}\sigma_{3/2}\sigma_{1/2} + \frac{1}{9}\sigma_{1/2}\sigma_{1/2} & \text{for p-p interactions} \\ \frac{14}{9}\sigma_{3/2}\sigma_{3/2} + \frac{8}{9}\sigma_{3/2}\sigma_{1/2} + \frac{5}{9}\sigma_{1/2}\sigma_{1/2} & \text{for p-n interactions} \end{cases} \qquad (6)$$

Here $\sigma_{3/2}$ and $\sigma_{1/2}$ enter separately; they are the cross sections for pion-nucleon interaction in states with isospin $3/2$ and $1/2$.

In accordance with the above, we used experimental values for the pion-nucleon cross section for $\sigma(z/m)$ and $\sigma(y/m)$.

In order to evaluate the cross section, it is necessary to integrate (6) numerically, since the values of $\sigma(z/m)$ and $\sigma(y/m)$ are given numerically. The main contribution to the integral comes from the region $\mathfrak{M}_1^2 - m^2 \sim \mathfrak{M}_2^2 - m^2 \sim 2E_0\mu$ ($\kappa^2 \sim \mu^2$), since the denominator increases rapidly with larger values of $\mathfrak{M}_1$ and $\mathfrak{M}_2$.

It should be noted that in our case, where $E_L = 9$ Bev and $E_0 = 2.3$ Bev, this region coincides with the region of maximum cross section $\sigma_{3/2}(z/m)$, so that $\sigma_{3/2}$ makes the overwhelming contribution in all expressions.

We give now the results of calculations.†

*We note that here and in the following calculations, the masses $\mathfrak{M}_1$ and $\mathfrak{M}_2$ are considered to be variables which can take on arbitrary values and are not yet set equal to the mass of the isobar.

†Experimental data on the cross section for pion-nucleon interactions up to π-meson energy $\omega = 1.9$ Bev[5] was used in the calculations. The maximum angle was taken equal to $\vartheta_{max} = 3\mu/p_0$.

The quantity $\sigma_{3/2,3/2}(E_0)$ — the cross section for the process in which both excited nucleons are in the state with isospin $3/2$ — is equal to

$$\sigma_{3/2,\,3/2}(E_0) \approx \begin{cases} 2.9 \text{ mb for p-p interactions} \\ 4 \text{ mb for p-n interactions} \end{cases} \quad (7)$$

The quantity $\sigma_{3/2,1/2}(E_0)$ is the cross section for the process in which one of the excited nucleons has isospin $3/2$ and the other $1/2$:

$$\sigma_{3/2,\,1/2}(E_0) \approx \sigma_{3/2,\,3/2}(E_0) \times \begin{cases} 0.48 \text{ mb for p-p interactions} \\ 0.17 \text{ mb for p-n interactions.} \end{cases} \quad (8)$$

Further,

$$\sigma_{1/2,\,1/2}(E_0) \approx \sigma_{3/2,\,3/2}(E_0) \times \begin{cases} 0.01 \text{ mb for p-p interactions} \\ 0.05 \text{ mb for p-n interactions.} \end{cases}$$

From this it follows that the main process is that with two isobars.

It should be noted that Eq. (6) does not include processes in which at least one of the mesons remains unexcited. The contribution from these processes can be estimated, assuming that the angular operator in this process is equal to γ_5. This contribution turns out to be equal to

$$\sigma_0(E_0) \sim 10^{-2}\sigma_{3/2,\,3/2}(E_0). \quad (9)$$

From this it can be seen that it is negligible in comparison with (7) and (8) and has no effect on the conclusions drawn above.

In conclusion we note that (6) can be employed at higher energies and in cases where the nucleons are excited differently.

In the high-energy region it gives more complete information than either the Weizsäcker-Williams method or the expression in reference 3, obtained under rougher approximations, for peripheral interactions.

In conclusion, the authors would like to thank Academician I. E. Tamm, Academician V. I. Veksler, and Professor E. L. Feĭnberg for fruitful discussions.

[1] Gramenitskiĭ, Podgoretskiĭ, et al. See V. I. Veksler, Nucleon-Nucleon and Pion-Nucleon Interactions. Report to the Conference on High-Energy Physics, Kiev, 1959 (preprint, p. 16).

[2] I. E. Tamm, Report to the Conference on High-Energy Physics, Kiev, 1959.

[3] Yu. A. Romanov and D. S. Chernavskiĭ, JETP, in press.

[4] O. Minakawa and Y. Nischimura, Observation of High-Energy Jets with Emulsion Chambers, Univ. of Tokyo, Preprint, 1958.

[5] O. Piccioni, Proc. of Conference on High-Energy Physics at CERN, 1958, p. 65.

Translated by G. E. Brown
37

ON THE NONLINEAR THEORY OF STATIONARY PROCESSES IN AN ELECTRON PLASMA

F. M. NEKRASOV

Khar'kov State University

Submitted to JETP editor July 17, 1959

J. Exptl. Theoret. Phys. (U.S.S.R.) **38**, 233-238 (January, 1960)

We have used a transport equation without a collision integral to consider nonlinear problems of oscillation modes of an electron plasma and of the interaction between plasma beams. We have obtained relations between the wavelength and the frequency and the amplitude of the oscillations. We determine the maximum field for which periodic processes are possible in a plasma. We have found the conditions for the propagation of large amplitude waves both for a plasma at rest and for a plasma of moving beams.

THE Boltzmann-Vlasov transport equation,[1] which is based upon a model of particles that interact through a self-consistent field, is a good approximation to describe an electron plasma. The field describes the so-called long-range collisions of the particles, i.e., the interaction of the particles which is connected with the slow decrease of the Coulomb forces. The short-range interaction is described by the collision integral.

This paper is devoted to a study of stationary processes in an electron plasma using this equation. We consider in the paper the propagation of electrostatic waves with a constant phase velocity both in a plasma at rest and in a plasma of moving beams in the nonlinear approximation. Similar nonlinear problems have been solved earlier by a number of authors;[2-4] they considered the interaction of beams in the hydrodynamic approximation[2] and the interaction of a hydrodynamic beam with a plasma described by a transport equation.[3,4]

For the sake of simplicity, we consider in this paper an unbounded plasma. We assume that all quantities depend on one coordinate x only. The ion motion and effects of short-range collisions both with charged and with neutral particles are not taken into account. The first neglect is based upon the large difference in mass between ions and electrons, and the second one can be assumed to be fulfilled if we consider a high temperature plasma with a high degree of ionization.

To consider solutions of the type of moving waves we shall go over to a system of coordinates in which the wave is at rest. Under the above assumptions the electron plasma is described in this system of coordinates by the equations

$$\frac{\partial f}{\partial x} + \frac{e}{m}\frac{d\varphi}{dx}\frac{\partial f}{\partial v} = 0, \qquad \frac{d^2\varphi}{dx^2} = 4\pi e\left\{\int\limits_{(v)} f(x, v)\,dv - n_0\right\}, \quad (1)$$

where $f(x, v)$ is the electron distribution function in configuration space, $\varphi(x)$ the self-consistent field potential, e and m the electronic charge and mass, and n_0 the constant positive charge density. We must say a few words about the domain of integration over the velocities in the Laplace equation. One usually integrates between the limits $-\infty < v < +\infty$, i.e., one assumes that at every point in space there are particles with zero kinetic energy. We shall consider an electron plasma in which there are no bound particles, i.e., where there are no particles for which the region of motion is limited on two or on one side by the electrostatic potential barrier. The limits of integration are in that case determined as follows.

Let $\mathcal{E}_0$ be the total energy of that plasma particle at $x = x_0$ which possesses a minimum energy. The other particles at that point will then satisfy the relation

$$mv^2/2 - e\varphi(x_0) \geqslant \mathcal{E}_0.$$

Since the particle with minimum energy performs an infinite motion during which its energy is conserved, the relation

$$mv^2/2 - e\varphi(x) \geqslant \mathcal{E}_0$$

must be valid for all particles at any point x. This relation determines the domain of integration over the velocities.

A particle may be captured if it loses energy through an interaction that is not connected with the self-consistent field. The capture of a particle leads to a decrease of the depth of the potential well of the self-consistent field. This is the normal mechanism of damping of the field when short-range Coulomb collisions and collisions with neutral atoms

are taken into account. These processes are not taken into account in the present paper, since we have assumed that the interaction takes place only through the self-consistent field $E(x)$.

The presence of captured particles is connected with the character of the establishment of a stationary state in the plasma. In the present paper we assume that it occurs without capture of particles. For waves whose phase velocity is much larger than the average thermal velocity of the electrons, this assumption is well justified.

Let us find the electrical field distribution in the plasma in its dependence on the form of the distribution function and the magnitude of this field in an arbitrary point $x = 0$; i.e., let us solve the Cauchy problem for Eq. (1) under the following initial conditions:

$$\varphi(0) = 0, \quad -d\varphi(0)/dx = E_0,$$
$$f(0, v) = A\exp\{-m(v - v_{ph})^2/2T\} \quad \text{if} \quad mv^2/2 \geqslant mv_0^2/2,$$
$$f(0, v) = 0 \quad \text{if} \quad mv^2/2 < mv_0^2/2, \tag{2}$$

where $\frac{1}{2}mv_0^2$ is the minimum energy at the point $x = 0$, v_{ph} the constant phase velocity of the wave, T the electron temperature in ergs, and A is determined from the normalization condition

$$A\int\limits_{v^2 \geqslant v_0^2} \exp\{-m(v - v_{ph})^2/2T\}\, dv = n_0. \tag{3}$$

The form of $f(0, v)$ and the normalization condition are chosen in such a way that the electron velocity distribution in the laboratory system of coordinates goes over into the Maxwell distribution for $E(x) \to 0$.

The quantities v_0^2 and E_0 are connected with the character of the establishment of the self-consistent field. One may assume for the oscillations of a free plasma that the field E_0 is caused by the density fluctuations of the electrons. In the following we shall assume that $v_0^2 \neq 0$. Analysis shows that if $v_0^2 = 0$ a perturbation connected with the density fluctuations of the electrons will be concentrated in a bounded region. Its dimensions are determined by the perturbing field. The detailed problem of the choice of v_0^2 is considered later on.

The distribution function satisfying the transport equation and the initial conditions is as follows

$$f(x, v) = \begin{cases} A\exp\left[-\frac{m}{2T}\left(\pm\sqrt{v^2 - \frac{2e\varphi}{m}} - v_{ph}\right)^2\right] \\ \text{if} \quad \frac{mv^2}{2} - e\varphi \geqslant \frac{mv_0^2}{2} \\ 0 \quad \text{if} \quad mv^2/2 - e\varphi < mv_0^2/2 \end{cases} \tag{4}$$

The $\pm$ signs in front of the radical correspond to $v > 0$ and $v < 0$.

It is convenient for the following to introduce the dimensionless quantities

$$mv^2/2T = u^2, \; e\varphi/T = z, \; x\sqrt{4\pi e^2 n_0/T} = x/\lambda_D = \zeta,$$
$$mv_0^2/2T = u_0^2; \; mv_{ph}^2/2T = u_{ph}^2. \tag{5}$$

The Laplace equation takes on the following form in this notation

$$\frac{d^2z}{d\zeta^2} = \frac{\int\limits_{u_0}^{\infty}\{\exp[-(t-u_{ph})^2] + \exp[-(t+u_{ph})^2]\}(t^2+z)^{-1/2}\, t\, dt}{\int\limits_{u_0}^{\infty}\{\exp[-(t-u_{ph})^2] + \exp[-(t+u_{ph})^2]\}\, dt} - 1. \tag{6}$$

Here $u_0 = +\sqrt{u_0^2}$. Integrating this equation twice and taking the initial conditions into account gives

$$\zeta = \int\limits_0^z dz/\sqrt{E_0^2 - 2V(z)}, \tag{7}$$

where

$$\tilde{E}_0^2 = (dz(0)/d\zeta)^2 = E_0^2/4\pi n_0 T,$$

$$V(z) = z - 2\frac{\int\limits_{u_0}^{\infty}\{\exp[-(t-u_{ph})^2] + \exp[-(t+u_{ph})^2]\}(\sqrt{t^2+z} - t)\, t\, dt}{\int\limits_{u_0}^{\infty}\{\exp[-(t-u_{ph})^2] + \exp[-(t+u_{ph})^2]\}\, dt}, \tag{8}$$

$V(z)$ is defined in the interval $-u_0^2 \leq z < \infty$. $V(z)$ decreases monotonically in the section $-u_0^2 \leq z \leq 0$, and increases monotonically in the section $0 \leq z < \infty$. The point $z = 0$ is a minimum of $V(z)$. It is well known (see, for instance, reference 5) that (7) defines z as a periodic function of ζ for those z which satisfy the condition

$$2V(z) \leqslant \tilde{E}_0^2. \tag{9}$$

This relation, however, defines for $Z = -u_0^2$ the maximum field strength $\tilde{E}_{0,\max}$ for which stationary processes are possible in a plasma which is described by Eq. (1).

The period $\tilde{\lambda}$ of the function z is determined by the usual expression

$$\tilde{\lambda} = 2\int\limits_{z_1}^{z_2} \frac{dz}{\sqrt{\tilde{E}_0^2 - 2V(z)}}, \tag{10}$$

where z_1 and z_2 are the roots of the equation

$$\tilde{E}_0^2 - 2V(z) = 0. \tag{11}$$

The difference $z_2 - z_1$ determines the amplitude of the self-consistent field potential in its dependence on the magnitude of $\tilde{E}_0$.

Equations (7) – (11) solve the given problem

about the propagation of electrostatic waves of constant phase velocity in an electron plasma. All required results can in the general case be obtained by numerical integration of the corresponding equations.

We need an explicit expression for $\tilde{E}$ and u_0 for further evaluations. One can see from (8) that $\tilde{E}_0$ is determined by the ratio of the energy density of the electrostatic field to the average kinetic energy density of the electrons. For fields which are caused by fluctuation processes this quantity is of the order of unity. We shall choose u_0^2 from thermodynamic considerations, assuming that an electron plasma in its equilibrium state is a perfect gas described by the distribution function

$$f(u)\,du = \pi^{-1/2}\exp\{-(u-u_{ph})^2\}\,du. \qquad (12)$$

The factor $\pi^{-1/2}$ corresponds to a normalization to one particle. The most probable value of u_0^2 will be the average value $\overline{u^2}$. One can then write

$$u_0^2 = \overline{u^2} - \Delta u^2, \qquad (13)$$

where Δu^2 is of the same order of magnitude as the average fluctuations in energy $\sqrt{\overline{(\Delta u^2)^2}}$. From the physics of the problem, u_0^2 corresponds to the minimum energy so that we must take for Δu^2 a quantity somewhat larger than $\sqrt{\overline{(\Delta u^2)^2}}$, or,

$$\Delta u^2 = A\sqrt{\overline{(\Delta u^2)^2}},\quad A \geqslant 1.$$

From these considerations, however, it follows that we must choose the minus sign in front of Δu^2. From (12) we get

$$\overline{u^2} = {}^1/_2 + u_{ph}^2,\quad \sqrt{\overline{(\Delta u^2)^2}} = \sqrt{\overline{u^4} - (\overline{u^2})^2} = \sqrt{2u_{ph}^2 + {}^1/_2}. \qquad (14)$$

We see from (13) and (14) that if $u_{ph}^2 \lesssim 1$ the magnitude of u_0^2 is basically determined by fluctuation processes, i.e., for phase velocities less than or of the order of the thermal velocities, the oscillations have a purely fluctuation character. In that case $u_0^2 \ll 1$. Calculation shows that the frequencies of these oscillations are much less than the Langmuir frequency $\omega_0 = (4\pi n_0 e^2/m)^{1/2}$, their wavelength much less than the Debye screening radius λ_D and the energy density of the electrostatic field much less than the energy density of the thermal motion of the electrons. When $u_{ph} \gg 1$ we get from (13)

$$u_0^2 \approx u_{ph}^2(1 - A/u_{ph}). \qquad (15)$$

The coefficient for the fluctuation correction is dropped since the magnitude of A is defined up to a factor of that order.

One can linearize Eq. (6) when $E_0 \ll 1$. It goes over into the equation for harmonic oscillations with a dispersion relation

$$\omega^2 = \omega_0^2(1 + 3T/mv_{ph}^2),$$

which is practically the same as the well known results of the linear theory. For the maximum field we get from (8) and (9)

$$E_{0\,max}^2/8\pi \approx n_0 mv_{ph}^2/2. \qquad (16)$$

The ratio of the terms omitted in the last equation to those retained is of the order of magnitude $(T/mv_{ph}^2)^{1/4}$.

Electrostatic waves of large amplitude (the term "large amplitude" must here and in the following be taken in the sense of $E_0^2/n_0T \gg 1$) can thus be propagated in a plasma if the phase velocity of the wave is much larger than the thermal velocity of the electrons. One can neglect the influence of fluctuation processes on these waves. Physically this result is completely understandable. For processes which take place with velocities larger than the thermal velocity of the electrons, one can consider the plasma as a collective medium, the behavior of which is completely determined by the average value of the density n_0, the temperature T and the law of interaction between the particles.

It is not difficult to generalize this to the case of the propagation of waves in a plasma of moving beams. We shall again give our considerations in the system of coordinates in which the wave is at rest. We shall assume for the sake of simplicity that the temperatures of the beams are the same. We take as the equilibrium distribution functions of the beams Maxwell distributions. The statement of the problem and the solutions of the transport equations for the beams are exactly the same as before.

The Laplace equation in dimensionless quantities is of the form

$$d^2z/d\zeta^2 = \alpha_1\int_{u_0}^{\infty} F_1(t)(t^2+z)^{-1/2}t\,dt \Big/ \int_{u_0}^{\infty} F_1(t)\,dt + \alpha_2\int_{u_0}^{\infty} F_2(t)(t^2+z)^{-1/2}t\,dt \Big/ \int_{u_0}^{\infty} F_2(t)\,dt - 1,$$

$$F_{1,2}(t) = \exp[-(t-u_{1,2})^2] + \exp[-(t+u_{1,2})^2] \qquad (17)$$

and together with the notation (5) we have introduced the new symbols

$$\alpha_1 = n_1/n_0,\ \alpha_2 = n_2/n_0,\ u_{1,2}^2 = m(v_{1,2} + v_{ph})^2/2T,$$

where n_1 and n_2 are the equilibrium densities of the first and the second beam; v_1 and v_2, there average velocities in the laboratory system of coordinates. Positive values of v_1 and v_2 correspond to a motion of the beams against the wave, i.e., u_1 and u_2 characterize the relative phase

velocities for the first and the second beam.

The condition for the existence of stationary solutions of Eq. (7) is the condition for electrical neutrality of the plasma: $\alpha_1 + \alpha_2 = 1$. Integrating (17) twice leads to

$$\zeta = \int_0^z \frac{dz}{\sqrt{\tilde{E}_0^2 - 2W(z)}}, \tag{18}$$

$$W(z) = z - 2\alpha_1 \int_{u_0}^{\infty} F_1(t)\,(\sqrt{t^2+z} - t)\,t\,dt \Big/ \int_{u_0}^{\infty} F_1(t)\,dt$$
$$- 2\alpha_2 \int_{u_0}^{\infty} F_2(t)\,(\sqrt{t^2+z} - t)\,t\,dt \Big/ \int_{u_0}^{\infty} F_2(t)\,dt. \tag{19}$$

We shall put, as before, the quantity u_0^2 equal to the sum of the average value $\overline{u^2}$ and a fluctuation correction for a particle described by the distribution function

$$f(u)\,du = [\alpha_1 \pi^{-1/2} \exp\{-(u-u_1)^2\}$$
$$+ \alpha_2 \pi^{-1/2} \exp\{-(u-u_2)^2\}]\,du, \tag{20}$$

i.e.,

$$u_0^2 = \overline{u^2}\,(1 - A\sqrt{\overline{(\Delta u^2)^2}}/\overline{u^2}).$$

We get from (20)

$$\overline{(\Delta u^2)^2} = \tfrac{1}{2} + 2\alpha_1 u_1^2 + 2\alpha_2 u_2^2 - \alpha_1^2 u_1^4 - \alpha_2^2 u_2^4 + \alpha_1 u_1^4$$
$$+ \alpha_2 u_2^4 - 2\alpha_1\alpha_2 u_1^2 u_2^2. \tag{21}$$

Solutions describing stationary processes of large amplitude with characteristics that depend weakly on the fluctuations are of interest. For them the conditions

$$\overline{u^2} \gg 1, \qquad \sqrt{\overline{(\Delta u^2)^2}}/\overline{u^2} \ll 1 \tag{22}$$

must be satisfied. We shall assume that $\alpha_1 \neq 0$, $\alpha_2 \neq 0$, and $v_1 \neq v_2$. These cases go over into the one considered earlier. Let $\alpha_1 u_1^2$ be the larger of the quantities $\alpha_1 u_1^2$ and $\alpha_2 u_2^2$; we can then write the conditions (22), using (21), in the form

$$\alpha_1 u_1^2 \gg 1, \qquad \sqrt{\alpha_2/\alpha_1}\,|1 - u_2^2/u_1^2| \ll 1. \tag{23}$$

For beams with equal density we obtain the following conditions for the propagation of large amplitude waves:

$$m(v_1 - v_2)^2/2T \gg 1, \quad v_{ph} \approx -(v_1 + v_2)/2. \tag{24}$$

In particular, there can exist a standing wave with large amplitude in two beams going in opposite directions with the same velocity. If the densities in the beams are very different there is only one condition for propagation:

$$m(v_1 + v_{ph})^2/2T \gg 1,$$

where v_1 is the velocity of the denser beam.

The maximum field for which stationary processes are possible can be determined from (19). An estimate for $u_1 \gg 1$ and $u_2 \gg 1$ gives

$$E_{0\,max}^2/8\pi = \tfrac{1}{2} n_1 m (v_1 + v_{ph})^2 + \tfrac{1}{2} n_2 m (v_2 + v_{ph})^2. \tag{25}$$

The character of the stationary processes occurring in a plasma at rest or in motion is thus determined by the relative phase velocity. If the latter is equal to zero the field of a perturbation is screened by the electrons of low energy and is localized in a bounded region of space (in our considerations this corresponds to $u_0 = 0$ and $u_{ph} = 0$). When the phase velocity increases the number of electrons which can screen the field of the wave diminishes and for phase velocities much larger than the thermal velocities the screening action of the electrons can in general be neglected. The maximum fields which can then occur are determined by the relative phase velocity of the wave. The order of their magnitude is given by (16) and (25).

In a plasma of two beams of comparable density with different velocities there exist waves of two kinds. One has a phase velocity equal to the arithmetic mean of the values of the beam velocities. It is propagated along the faster beam. The condition for its propagation is a large relative velocity of the beams. The phase velocity of the second beam must be much larger than the velocity of either beam. With regard to this wave the beams may be considered to be a plasma at rest.

For small fields, waves with a large phase velocity have a harmonic character and their frequency is practically the same as the plasma frequency ω_0, while the dispersion law of these waves is determined by the well-known relation from the linear theory.

In conclusion the author expresses his sincere gratitude to Ya. B. Faĭnberg for suggesting the topic and for valuable discussions and to A. F. Popov for a discussion of the results.

[1] A. A. Vlasov, JETP **8**, 291 (1938).

[2] H. K. Sen, Phys. Rev. **97**, 849 (1955).

[3] Akhiezer, Lyubarskiĭ, and Faĭnberg, Ученые записки ХГУ (Scientific papers of the Khar'kov State University) **6**, 73, (1955).

[4] Faĭnberg, Kurilko, and Nekrasov, Proceedings of the Geneva Conference on Accelerators, 1959, in press.

[5] L. D. Landau and E. M. Lifshitz, Механика (Mechanics), Fizmatizdat, 1958.

Translated by D. ter Haar
38

ON THE STRUCTURE OF THE PHOTON GREEN'S FUNCTION

D. A. KIRZHNITS, V. Ya. FAĬNBERG, and E. S. FRADKIN

P. N. Lebedev Physics Institute, Academy of Sciences, U.S.S.R.

Submitted to JETP editor July 22, 1959

J. Exptl. Theoret. Phys. (U.S.S.R.) **38**, 239-242 (January, 1960)

It is shown that the so-called Redmond procedure is not unambiguous. This conclusion is not changed when the requirements of renormalization invariance are taken into account.

ATTENTION has recently been called to the possibility of using dispersion relations (d.r.) for the elimination of the fictitious pole of the boson Green's function in quantum field theory.[1] A simple analysis (see Sec. 1) shows, however, that this procedure does not possess the necessary property of uniqueness. As can be seen from the results of Sec. 2, this conclusion remains valid also when one takes into account the requirements of renormalization invariance.

1. ON THE AMBIGUITY OF THE REDMOND PROCEDURE

We confine ourselves to a consideration of quantum electrodynamics. It is not hard to show that if the Källén-Lehmann d.r.

$$d(z) = 1 + \frac{z}{\pi}\int_0^\infty \frac{\operatorname{Im} d(\zeta)\, d\zeta}{\zeta(\zeta - z - i\varepsilon)}, \qquad (1)$$

holds, where

$$(k_\mu k_\nu - z\delta_{\mu\nu})\, d(z) = -D_{\mu\nu}(k)\, z^2, \quad z \equiv k_0^2 - \mathbf{k}^2,$$

then an analogous dispersion relation also holds for the polarization operator

$$\Pi(z) = \frac{z}{\pi}\int_0^\infty \frac{\operatorname{Im}\Pi(\zeta)\, d\zeta}{\zeta(\zeta - z - i\varepsilon)},$$

$$d^{-1}(z) = 1 + \Pi(z). \qquad (2)$$

For the proof it suffices to note that, because of the condition $\operatorname{Im} d(z) \leq 0$, the function $d(z)$ has no zeroes either in the complex z plane or on the negative semiaxis $\operatorname{Re} z < 0$.

An important point is that in general the converse proposition is not true: for the d.r. (2) for $\Pi(z)$ to have as a consequence the d.r. (1), we have as the necessary and sufficient condition

$$\frac{1}{\pi}\int_0^\infty \frac{\operatorname{Im}\Pi(\zeta)}{\zeta}\, d\zeta \leqslant 1. \qquad (3)$$

In fact, as can be seen from Eq. (2), and also from the condition $\operatorname{Im}\Pi = -\operatorname{Im} d/|d|^2 \geq 0$, the inequality (3) assures the absence of poles of the function $d(z)$ outside the semiaxis $\operatorname{Re} z > 0$.

It is important to emphasize that the condition (3) is entirely identical with the well known inequality (8) of the paper of Lehmann, Symanzik, and Zimmermann.[2] The function $F(z)$ contained in that inequality is connected with $\Pi(z)$ by the relation $F(z) = 2z \operatorname{Im}\Pi(z)$. Though it does satisfy the d.r. (2), the asymptotic expression for $d(z)$ obtained in the "three-gamma" approximation (cf., e.g., reference 3) is nevertheless in contradiction with the condition (3) [$\operatorname{Im}\Pi(z) = \pi\alpha$, $\alpha = e^2/3\pi$]. Therefore a fictitious pole appears in $d(z)$ and the d.r. (1) is violated.

The recently proposed procedure,[1] having as its purpose the removal of this difficulty, consists in using a summation of the "main" terms of the perturbation-theory series to calculate only the quantity $\operatorname{Im} d(z)$. The function $d(z)$ itself is reconstructed by means of the relation (1). By what has been said, the d.r. (2) and the condition (3) then hold, as can also be verified directly. This procedure, however, is not unambiguous. In fact, any function $\operatorname{Im}\Pi$ that satisfies (3) and goes over for $\alpha \to 0$ into the corresponding expression of perturbation theory (to a given order in α) can be used to reconstruct the photon Green's function by means of Eq. (2). The function so obtained will obey the d.r. (1) and agree with perturbation theory.

As an example let us consider the following expression:

$$\operatorname{Im}\Pi(z) = \pi\alpha/(1 + z/z_0), \qquad (4)$$

where by the condition (3) $z_0 \leq m^2 \exp(1/\alpha)$. Simple manipulations give

$$d^{-1}(z) = 1 - \frac{\alpha}{z + z_0}\left\{z_0 \ln\left(1 - \frac{z}{m^2}\right) + z \ln\frac{z_0}{m^2}\right\}; \quad z_0 \gg m^2. \qquad (5)$$

For correspondence with perturbation theory it is enough to require that as α decreases z_0 increase faster than any finite power of α^{-1}. If, in particular,

we set $z_0 = m^2 \exp(\alpha^{-1/2})$, we arrive at an expression that has no resonance properties and does not lead to strong coupling $(d^{-1}(\infty) = 1 - \alpha^{1/2})$.

In the removal of this ambiguity a large part could be played by general requirements of causality and unitarity of the theory. In this connection it is important to emphasize that the conditions expressed by the d.r. (1) are only necessary, but by no means sufficient to secure causality and unitarity.

A treatment of this circle of questions is impossible, however, in the language of one-particle Green's functions; it is necessary to bring into the argument Green's functions of higher orders, in terms of which $\operatorname{Im}\Pi(z)$ is expressed. It cannot be excluded that the expression obtained for the Green's function in reference 1, which has its real part nonanalytic in α and its imaginary part analytic in α, may be in contradiction with the conditions of unitarity and causality, which closely relate the real and imaginary parts of matrix elements.

2. ON THE RENORMALIZATION INVARIANCE OF THE PHOTON GREEN'S FUNCTION

The condition of renormalization invariance (r.i.) of the photon Green's function $d(z, \lambda, \alpha_\lambda)$ is of the form[4]

$$\alpha_\lambda d(z, \lambda, \alpha_\lambda) = \alpha_{\lambda'} d(z, \lambda', \alpha_{\lambda'}), \tag{6}$$

where λ is the square of the normalized momentum $[d(\lambda, \lambda, \alpha_\lambda) = 1]$, $z = k_0^2 - |\mathbf{k}|^2$, and $\alpha_\lambda = e_\lambda^2/3\pi$ is the corresponding coupling constant.

Starting with Eq. (6) and assuming that for $z \gg m^2$ the function d depends only on z/λ and α_λ (the perturbation-theory series has this property), it has been proved[5,4] that the renormalized d function, i.e., the function corresponding to $\lambda = 0$, must have the form

$$d(z, \alpha_0) = \alpha_0^{-1} F(\ln(z/m^2) + \varphi(\alpha_0)). \tag{7}$$

Here F and φ are mutually inverse functions. From this a number of important conclusions have been drawn: that the shape of the effective charge distribution of the electron is independent of α_0, that the value of the bare charge is independent of α_0 and strong coupling inevitably appears (in the case of a finite charge renormalization), and so on. We would like to emphasize that these conclusions do not have the force of inevitability, being connected not only with the requirement of r.i., but also with definite assumptions about the structure of the Green's function.

In themselves these propositions are by no means obligatory (particularly in the case of finite charge renormalization). Thus the use of the dispersion relations in finding the photon Green's function[1,6] leads to the appearance of terms nonanalytic in α, which change decidedly the behavior of the d function in the high-momentum region. Although even in this case the perturbation-theory series depends for $z \gg m^2$ on the combination z/λ only, the exact expression $d(z, \lambda, \alpha_\lambda)$ does not have this property.

It is therefore important to ascertain whether the requirement of r.i. by itself imposes any limitations on the structure of the d function. For this purpose we turn to the general solution of the functional equation (6). It is easily verified that this equation can be written in the form

$$\alpha_\lambda d(z, \lambda, \alpha_\lambda) = \alpha_0(\alpha_\lambda, \lambda)\, d(z, \alpha_0(\alpha_\lambda, \lambda)), \tag{8}$$

where the renormalization-invariant (unchanged by a change of λ) function $\alpha_0(\alpha_\lambda, \lambda)$ is given by the relation*

$$\alpha_0^{-1} = \alpha_\lambda^{-1} + \ln(-\lambda/m^2). \tag{9}$$

It is obvious that the function $d(z, \alpha_0)$ that appears here is identical with the renormalized Green's function.

Thus from any given expression for the renormalized Green's function one can reconstruct a renormalization-invariant expression $d(z, \lambda, \alpha_\lambda)$ that for $\lambda \to 0$ goes over into the original expression. According to Eqs. (8) and (9) this task reduces simply to the introduction of the factor α_0/α_λ and the replacement of α_0 by an invariant combination of α_λ and λ.†

In particular we get a renormalization-invariant expression for the Green's function (5) considered above. Confining ourselves for simplicity to the region $m^2 \ll |\lambda| \ll z_0$, we have from Eq. (9)

$$\alpha_0^{-1} = \alpha_\lambda^{-1} + \ln(-\lambda/m^2). \tag{10}$$

Using Eq. (8), we get ($z \gg m^2$ throughout)

$$d^{-1}(z, \lambda, \alpha_\lambda) = 1 - \frac{\alpha_\lambda}{z - z_0}\left(z_0 \ln\left(\frac{z}{\lambda}\right) + z \ln\left(-\frac{z_0}{\lambda}\right)\right), \tag{11}$$

From here on we must express z_0 and α_0 in terms of α_λ and λ by means of Eq. (10). In particular, setting $z_0 = m^2 \exp(1/\alpha_0^{1/2})$, we get

$$d^{-1}(z, \lambda, \alpha_\lambda) = \frac{1 - \alpha_\lambda \ln(z/\lambda) + (\alpha_\lambda/\alpha_0)(1 - \sqrt{\alpha_0})(z/z_0)}{1 + z/z_0}. \tag{12}$$

*The relations (8) and (9) are in complete agreement with the results of Ovsyannikov.[7]

†In the general case the requirement of r. i. imposes one relation on the arguments of $d(z, \lambda, \alpha_\lambda)$. Therefore the function $d(z, \alpha_0)$ is, generally speaking, an arbitrary function of two arguments.

This expression is in contradiction with Eq. (7), and at the same time satisfies the requirement of r.i. and the Källén-Lehmann equation and goes over into the perturbation-theory series for $\alpha \to 0$. Only for the special choice $z_0 = Cm^2 \exp(1/\alpha_0)$, $(C \leq 1)$ does one get an expression consistent with Eq. (7).

Summarizing, we can say that the requirement of r.i. does not in itself impose any restrictions on the renormalized Green's function. Even the further requirement that for $\alpha \to 0$ the function must go over into the perturbation-theory series does not lead with necessity to the relation (7).

[1] P. Redmond, Phys. Rev. **112**, 1404 (1958). Bogolyubov, Logunov, and Shirkov, JETP **37**, 805 (1959), Soviet Phys. JETP **10**, 574 (1960).

[2] Lehmann, Symanzik, and Zimmermann, Nuovo cimento **2**, 425 (1955).

[3] L. D. Landau, in collection Niels Bohr and the Development of Physics, New York, 1955 (reference to p. 75 in Russian Transl., IIL 1958).

[4] N. N. Bogolyubov and D. V. Shirkov, Введение в теорию квантованных полей (Introduction to the Theory of Quantized Fields), Gostekhizdat, 1957.

[5] M. Gell-Mann and F. Low, Phys. Rev. **95**, 1300 (1954).

[6] V. Ya. Faĭnberg, JETP **37**, 1361 (1959), Soviet Phys. JETP **10**, 968 (1960).

[7] L. V. Ovsyannikov, Doklady Akad. Nauk SSSR **109**, 1112 (1956).

Translated by W. H. Furry
39

ON MESON-NUCLEON SCATTERING IN LARGE ORBITAL ANGULAR MOMENTUM STATES

A. D. GALANIN

Submitted to JETP editor July 22, 1959

J. Exptl. Theoret. Phys. (U.S.S.R.) **38**, 243-247 (January, 1960)

The πn phase shifts for scattering in large orbital angular momentum states are described in terms of the $\pi\pi$-interaction coupling constant. If the results obtained can be extended to the $l = 2$ case and if the assumption is made that the $\pi\pi$ scattering amplitude exhibits no resonance at low energies, then a disagreement with experiment is obtained.

As was shown by Okun' and Pomeranchuk,[1] πn scattering in large orbital angular momentum states is dominated by the diagram shown in the figure. This diagram contains the πn scattering amplitude and the $\pi\pi$ scattering amplitude. Consequently experimental data on πn scattering phase shifts in large orbital angular momentum states may in principle yield information about the magnitude of $\pi\pi$ scattering.

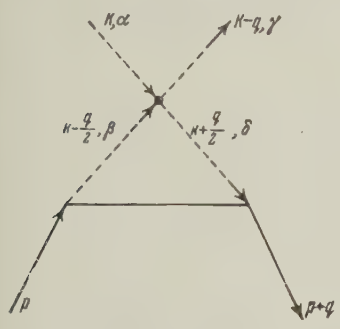

Principal diagram for πn scattering in large orbital angular momentum states.

The scattering phase shifts in large angular momentum states are determined by the value of the amplitude in the vicinity of the nearest singularity in the momentum transfer q^2. In the case under consideration the nearest singularity occurs at $q^2 = 4\mu^2$ and the next one at $q^2 = 16\mu^2$. The large interval between the two nearest singularities encourages the speculation that the indicated diagram for πn scattering will also be dominant for not very large angular momenta.

The general expression for the $\pi\pi$ scattering amplitude is given by

$$\Gamma_{\alpha\beta\gamma\delta}(p_1, p_2, p_3, p_4) = A\delta_{\alpha\beta}\delta_{\gamma\delta} + B\delta_{\alpha\gamma}\delta_{\beta\delta} + C\delta_{\beta\gamma}\delta_{\alpha\delta}, \quad (1)$$

where A, B, C are functions of the momenta p_i. We have here the following symmetry conditions: $p_1 \to p_2$, $B \to C$; $p_2 \to p_3$, $A \to B$; $p_1 \to p_3$, $A \to C$. Using the notation indicated in the figure we get $p_1 = K$, $p_2 = k - q/2$, $p_3 = -K + q$, $p_4 = -k - q/2$ and to the substitution $k \to -k$ corresponds $A \to C$.

The general expression for the πn scattering amplitude is given by

$$f_{\alpha\beta}(p_1, p_2, p_3, p_4) = (\bar{u}_{-p_4}|\delta_{\alpha\beta}\left[L^{(1)} + \tfrac{1}{2}(\hat{p}_3 - \hat{p}_1)M^{(1)}\right] - i\varepsilon_{\alpha\beta\gamma}\tau_\gamma\left[L^{(2)} + \tfrac{1}{2}(\hat{p}_3 - \hat{p}_1)M^{(2)}\right]|u_{p_2}) \quad (2)$$

and we have the symmetry conditions (p_1, p_3 — meson momenta, p_2, p_4 — nucleon momenta) $p_1 \to p_3$, $L^{(2)} \to -L^{(2)}$, $M^{(1)} \to -M^{(1)}$. In the notation of the figure: $p_1 = -k + q/2$, $p_2 = p$, $p_3 = k + q/2$, $p_4 = -p - q$ and for $k \to -k$ we have

$$L^{(2)} + \hat{k}M^{(2)} \to -(L^{(2)} + \hat{k}M^{(2)}).$$

The amplitude corresponding to the diagram in the figure may be written as follows:

$$M_{\alpha\gamma}(q^2) = \frac{1}{2\pi i}\int \Gamma_{\alpha\beta\gamma\delta}\left(K, k - \frac{q}{2}, -K + q, -k - \frac{q}{2}\right) \times f_{\beta\delta}\left(-k + \frac{q}{2}, p, k + \frac{q}{2}, -p - q\right)\Delta(k, q)\, d^4k,$$

$$\Delta(k, q) = [(k - q/2)^2 - \mu^2]^{-1}[(k + q/2)^2 - \mu^2]^{-1} \quad (3)$$

or, after substitution of (1) and (2), as follows:

$$M_{\alpha\gamma}(q^2) = \frac{1}{2\pi i}\int [\delta_{\alpha\gamma}(A + C + 3B)(\bar{u}_{p+q}|\, L^{(1)} + \hat{k}M^{(1)}|\, u_p) - i\varepsilon_{\alpha\gamma\sigma}\tau_\sigma(A - C)(\bar{u}_{p+q}|\, L^{(2)} + \hat{k}M^{(2)}|\, u_p)]\Delta(k, q)\, d^4k. \quad (4)$$

When calculating scattering phase shifts in large angular momentum states values of q^2 near $4\mu^2$ and small values of the variable of integration k in (4) are of importance. An estimate of the effective values of k^2 may be obtained by considering the integral ($q^2 = -2\mathbf{p}^2(1 - \cos\theta)$ with θ the scattering angle and $\mathbf{p}$ the momentum in the c.m.s.)

$$I_l = \int_{-1}^{+1} M(\vartheta) P_l(\cos\vartheta)\, d(\cos\vartheta),$$

in the same way as was done previously[2] for the nn scattering amplitude. Such an estimate leads to

$$|k^2_{\text{eff}}| \approx \mu^2/L, \quad (5)$$

$$L = (l + 1)\xi/\sqrt{1 + \xi^2}, \quad \xi = \mu/|\mathbf{p}|; \quad (6)$$

it is assumed that the inequality $L \gg 1$ holds.

Since $A + C + 3B$ and $L^{(1)} + \hat{k}M^{(1)}$ are even functions of k, and $A - C$ and $L^{(2)} + \hat{k}M^{(2)}$ are

odd functions of k one may, accurate to first order terms in 1/L, omit in (4) the term proportional to $\epsilon_{\alpha\gamma\sigma}\tau_\sigma$. Thus, for $L \gg 1$, the πn scattering amplitude is independent of isotopic spin indices:

$$M_{\alpha\gamma}(q^2) = M(q^2)\,\delta_{\alpha\gamma},$$

$$M(q^2) = \frac{1}{2\pi i}\int (A + C + 3B) \times (\bar{u}_{p+q}|\, L^{(1)} + \hat{k}M^{(1)}\,|\, u_p)\,\Delta(k, q)\, d^4k. \quad (7)$$

If A + C + 3B is a sufficiently smooth function of k inside the region (5) it can be taken out from under the integral sign in (7):

$$M(q^2) = -\frac{5\lambda}{2\pi i}\int (\bar{u}_{p+q}|\, L^{(1)} + \hat{k}M^{(1)}\,|\, u_p)\,\Delta(k, q)\, d^4k, \quad (8)$$

where we have set $-5\lambda = (A + C + 3B)_{k=0}$

The dependence of the scattering phase shifts on the mechanical spin variables can be obtained without a knowledge of the explicit form of $L^{(1)}$ and $M^{(1)}$. As a matter of fact $L^{(1)}$ and $M^{(1)}$ are functions of the vectors p, q and k. In carrying out the k-integration in Eq. (8) we will obtain either $(\bar{u}_{p+q}|\hat{q}\,|\,u_p)$ or $(\bar{u}_{p+q}|\hat{p}\,|\,u_p)$ in place of $(\bar{u}_{p+q}|\hat{k}\,|\,u_p)$. But $(\bar{u}_{p+q}|\hat{q}\,|\,u_p) = 0$ and $(\bar{u}_{p+q}|\hat{p}\,|\,u_p) = m(\bar{u}_{p+q}u_p)$. It then follows that the spin dependence of M is contained in the factor $(\bar{u}_{p+q}u_p)$, i.e.,

$$M(q^2) = (\bar{u}_{p+q}u_p)\,F(q^2), \quad (9)$$

where the function $F(q^2)$ depends on the precise form of $L^{(1)}$ and $M^{(1)}$.

Passing from the four-component spinors u to the two-component v we obtain

$$M(q^2) = (v'^*|\, m^{-1}(E + \omega)(f + i\sigma[\mathrm{K}\times\mathrm{K}']\varphi)\,|\, v), \quad (10)$$

where

$$f = \frac{m + E}{2(\omega + E)}\left[1 - \frac{p^2 t}{(E + m)^2}\right]F(q^2),$$

$$\varphi = \frac{F(q^2)}{2(E + \omega)(E + m)} \quad (11)$$

($t = \cos\theta$, ω = meson energy, E = nucleon energy).

We next expand the amplitudes f and φ in Legendre polynomials (see, e.g., reference 2):

$$f = (2i|\,p\,|)^{-1}\sum_l [(l+1)\exp(2i\delta_l^+) + l\exp(2i\delta_l^-) - 2l - 1]\,P_l(t)$$
$$\approx |\,p\,|^{-1}\sum_l [(l+1)\,\delta_l^+ + l\delta_l^-]\,P_l(t), \quad (12)$$

$$\varphi = (2i|\,p\,|^3)^{-1}\sum_l (\exp(2i\delta_l^+) - \exp(2i\delta_l^-))\,dP_l(t)/dt$$
$$\approx -(|\,p\,|^3\sqrt{1-t^2})^{-1}\sum_l (\delta_l^+ - \delta_l^-)\,P_l^{(1)}(t), \quad (13)$$

where $\delta_l^\pm$ are the scattering phase shifts in states of orbital angular momentum l and $j = l \pm \frac{1}{2}$.

Consequently*

$$[(l+1)\,\delta_l^+ + l\delta_l^-]/(2l+1) = \frac{(m+E)\,|\,p\,|}{4(E+\omega)}\int_{-1}^{+1}\left[1 - \frac{p^2 l}{(E+m)^2}\right]F(q^2)\,P_l(t)\,dt, \quad (14)$$

$$\delta_l^+ - \delta_l^- = -\frac{|\,p\,|^3}{4(E+m)(E+\omega)}\,\frac{2l+1}{l(l+1)} \times \int_{-1}^{+1}(1-t^2)\,\frac{dF(q^2)}{dt}\,P_l(t)\,dt. \quad (15)$$

For $L \gg 1$ the following formula holds:[2]

$$\int_{-1}^{+1} F(q^2)\,P_l(t)\,dt = \frac{4\xi^2}{\pi i}\,Q_l(1 + 2\xi^2)\int_0^\infty e^{-Ls^2}(\Delta F)\,ds, \quad (16)$$

where Q_l is the Legendre function of the second kind;

$$s = \sqrt{1 - q^2/4\mu^2} = \sqrt{1 + (1-t)/2\xi^2}, \quad (17)$$

and (ΔF) is the jump in the function $F(q^2)$ across the cut in the complex s-plane running from $s = 0$ to $s = \infty$.

Taking into account the fact that $dF/dt = -(4\xi^2 s)^{-1}\,dF/ds$, as well as that $(\Delta F) = 0$ at $s = 0$ we obtain [for $s \ll 1$: $t = 1 + 2\xi^2$, $1 - t^2 = -4\xi^2(1 + \xi^2)$]

$$[(l+1)\,\delta_l^+ + l\delta_l^-]/(2l+1) = -c_1 b Q_l(2 + 2\xi^2), \quad (18)$$
$$\delta_l^+ - \delta_l^- = -c_2 b Q_l(1 + 2\xi^2), \quad (19)$$

where

$$c_1 = \frac{\mu\xi}{m}\,\frac{E+m}{E+\omega}\left(1 - \frac{p^2 + 2\mu^2}{(E+m)^2}\right),$$

$$c_2 = \frac{2l+1}{l}\,\frac{2\mu^3\sqrt{1+\xi^2}}{m(E+m)(E+\omega)},$$

$$b = -\frac{m}{\pi i}\int_0^\infty e^{-Ls^2}(\Delta F)\,ds. \quad (20)$$

It is obvious that $c_2 \ll c_1$. In the nonrelativistic approximation for the nucleons when $|\,p\,| \ll m$, but $|\,p\,| \sim \mu$, the ratio c_2/c_1 is of the order of $\sqrt{2} \times (\mu/m)^2 \approx 0.03$. It then follows that δ_l^+ and δ_l^- are almost equal. This conclusion is a consequence of the assumption that A + C + 3B is a sufficiently smooth function within the region (5), i.e., that the $\pi\pi$ scattering amplitude has no resonances for low meson energy. If this assumption is not justified then in addition to the matrix element $(\bar{u}_{p+q}u_p)$, M will also contain the matrix element $(\bar{u}_{p+q}|\,\hat{K}\,|\,u_p)$ and the sign dependence of M may be substantially altered.

*We make use of

$$\int_{-1}^{+1} P_l^{(1)}(t)\,P_{l'}^{(1)}(t)\,dt = \delta_{ll'}\,\frac{2l(l+1)}{2l+1}; \quad dP_l(t)/dt = -\frac{1}{\sin\theta}\,P_l^{(1)}(t),$$

$$d[(1-t^2)\,F(q^2)]/dt \approx (1-t^2)\,dF/dt \text{ for } L \gg 1.$$

According to the experiments of Mukhin and Pontecorvo[3] $\delta_2^+ \approx -\delta_2^-$, which disagrees with (18) and (19). Thus, if it is true that the two-pion interaction (see figure) is already dominant for $l = 2$, the discrepancy with experiment would indicate the existence of a resonance in the $\pi\pi$ scattering amplitude at low energies (about the $\pi\pi$ resonance see also references 4 and 5).

For a quantitative determination of the πn scattering phase shifts for $L \gg 1$ it is necessary to evaluate $F(q^2)$ and b. We obtain

$$f_{\alpha\gamma} = \frac{\alpha}{m}\delta_{\alpha\gamma} + \tau_\alpha\tau_\gamma \frac{-\hat{k}}{(k+q/2)^2 + 2p(k+q/2)} + \tau_\gamma\tau_\alpha \frac{\hat{k}}{(k-q/2)^2 - 2p(k-q/2)},$$

(which is in agreement with Galanin et al.[2,6]) from where, making use of the results obtained in reference 6, we deduce

$$F(q^2) = \frac{5g^2\lambda}{8m}\left[(\alpha - 1)s + \frac{\varepsilon}{2}\ln(\varepsilon + 2s)\right],$$

where $\epsilon = \mu/m$ and $\alpha = 1.2$. Carrying out the s-integration in Eq. (20) we get (see reference 6; it is assumed that $-5\lambda = (A+C+3B)_{k=0}$ is independent of q^2):

$$b = (5g^2\lambda/16\sqrt{\pi}L^{3/2})\left[\alpha - 1 + \sqrt{\pi}\zeta\left(1 - \frac{2}{\sqrt{\pi}}\zeta\right)\right],$$

where it was assumed that $1 \ll L \ll 4m^2/\mu^2$ and $\zeta = \epsilon\sqrt{L}/2 \ll 1$, and terms quadratic in ζ were taken into account.

In this way the values of πn scattering phase shifts for sufficiently large l provide an opportunity for obtaining λ which determines the $\pi\pi$ interaction. The qualitative discrepancy with the experimental data (indicated above) on the signs of the D-wave phases, due either to a $\pi\pi$ amplitude resonance or to the fact that an orbital angular momentum two is not sufficiently large for the considerations here outlined to be valid even as an order of magnitude estimate,* precludes the use of the Mukhin and Pontecorvo data[3] on the D phase shifts for a determination of the constant λ.

The author expresses his indebtedness to I. Ya. Pomeranchuk, B. L. Ioffe and L. B. Okun' for useful advice and discussions.

[1] L. B. Okun' and I. Ya. Pomeranchuk, JETP **36**, 300 (1959), Soviet Phys. JETP **9**, 207 (1959).

[2] Galanin, Grashin, Ioffe, and Pomeranchuk, JETP **37**, 1663 (1959), Soviet Phys. JETP **10**, 1179 (1960).

[3] A. I. Mukhin and B. Pontecorvo, JETP **31**, 550 (1956), Soviet Phys. JETP **4**, 373 (1957).

[4] W. R. Frazer and J. R. Fulco, Phys. Rev. Lett. **2**, 365 (1959).

[5] G. F. Chew and S. Mandelstam, Preprint.

[6] Galanin, Grashin, Ioffe, and Pomeranchuk, JETP **38**, 475 (1960), Soviet Phys. JETP **10**, in press.

Translated by A. M. Bincer
40

*Lowest order perturbation theory gives D phase shifts of opposite sign and gives a δ^+ phase (which is determined more reliably experimentally) amounting to a significant part of its experimental value. This circumstance indicates that $l = 2$ is apparently too small to apply the theory developed above. The author is grateful to Prof. Chew for indicating this possibility.

Letters to the Editor

POSSIBLE OCCURRENCE OF A SECOND-ORDER PROCESS IN INELASTIC SCATTERING OF DEUTERONS BY NUCLEI

V. A. EDAKOVA, V. G. NEUDACHIN, and E. A. ROMANOVSKIĬ

Institute for Nuclear Physics, Moscow State University

Submitted to JETP editor June 8, 1959

J. Exptl. Theoret. Phys. (U.S.S.R.) **38**, 248-250 (January, 1960)

In many papers, in calculating cross sections for various "direct" nuclear reactions at low and medium energies, the authors use perturbation theory, the applicability of which is not justified (because of the absence of a small parameter). However the results of the computations appear to be in good agreement with the experimental data (for inelastic scattering of protons,[1] and for the stripping reaction), probably because in these reactions higher-order processes do not produce any special features in the angular distribution. Nevertheless, the study of processes associated with the appearance of "higher-order effects" is of fundamental interest.

Apparently the most favorable reaction for studying the role of second-order effects should be the inelastic scattering of deuterons. In this case, the first-order process is process a, as a result of which the neutron or the proton in the deuteron interacts with the nuclear surface and transfers part of its energy to it.[2,3] According to Huby and Newns,[2] at low and medium energies the maximum in the angular distribution, for $l \geq 2$ (where l is the angular momentum transferred by the deuteron to the nucleus), occurs at medium angles. But because of the low binding energy of the deuteron, one of the second order processes, the process b of "double stripping" (for example d—p—d′) should give a maximum in the angular distribution at zero degrees, if the orbital angular momenta of the neutrons which are transferred from the deuteron to the nucleus (l_i) and back (l_f) are small.

In many cases the experimental angular distributions show, in addition to the maximum associated with the first order process, a maximum at an angle close to zero.[4] A maximum at zero degrees cannot be explained by the "focusing" properties of the nucleus[5] (since the transparency for deuterons is much less than for protons,[6] and the angular distribution has a shape different from that given by the "focusing" properties of the nucleus), or by the effect of Coulomb excitation of the nucleus, since at these energies the angular distribution from Coulomb excitation is practically isotropic (for low energy transfer) and the cross section is many times less than that observed in experiment.

Process b was first treated theoretically by Fairbairn,[7] using the method of "matching" the wave functions at the nuclear boundary. However, no direct comparison of the formula with experiment could be made. In the present work, to calculate the differential cross section $d\sigma/d\Omega$ for inelastic scattering (process b), we use the results of the general theory of scattering.[8] In the Born approximation, the reaction cross section is given by the square of the matrix element of the transition:

$$I \sim \int \Psi^*_{k'd}(\mathbf{r}_p\mathbf{r}_n)\Psi^*_f(\xi)\,V_{np}(\mathbf{r}_p\mathbf{r}_n)\left\{\int g(\mathbf{r}_p\mathbf{r}'_p;\ \mathbf{r}_n\mathbf{r}'_n;\xi,\xi')V_{np}(\mathbf{r}'_p\mathbf{r}'_n)\right.$$
$$\left.\times\exp[ik_d(\mathbf{r}'_p+\mathbf{r}'_n)/2]\,\chi(|\mathbf{r}'_p-\mathbf{r}'_n|\,\Psi_i(\xi)\,d\mathbf{r}'_n d\mathbf{r}'_p d\xi'\right\} d\mathbf{r}_p d\mathbf{r}_n\,d\xi, \quad (1)$$

where $\Psi_{k'd}$ is the wave function of the initial deuteron wave, $\Psi_i(\xi)$ and $\Psi_f(\xi)$ are the wave functions of the ground state and final state of the nucleus, $V_{np} = V_0\delta(\mathbf{r}_p - \mathbf{r}_n)$ is the neutron-proton interaction potential, $\chi(|\mathbf{r}_p - \mathbf{r}_n|)$ is the internal wave function of the deuteron, $g(\mathbf{r}_p\mathbf{r}'_p;\ \mathbf{r}_n\mathbf{r}'_n;\ \xi,\ \xi')$ is the Green's function for the (d, p) reaction. Writing the wave functions of the intermediate system as a product of the wave function of the initial (even-even) nucleus and the wave function of the captured nucleon, we perform an expansion of the plane waves into spherical partial waves and sum the resulting expressions over the magnetic quantum numbers of the initial and final state, using Levinson's method.[9]

The computation was carried out for the reaction $Mg^{24}(d, d')Mg^{24*}$ (with $\Delta E = 1.37$ Mev, $E_0 = 15$ Mev). The summation over states of the intermediate nuclei (I_N) was limited to the lowest levels of Mg^{25} and Al^{25}, having spins of $5/2^+$, $1/2^+$, and $3/2^+$. The transitions $I_i \rightarrow I_N$ occur via the transfer of an s-nucleon or via the transfer of an s- or d-nucleon; the transitions $I_N \rightarrow I_f$ involve the transfer by the nucleus to the free nucleon of an s-nucleon or a d-nucleon. The results of the computation are shown in the figure together with the experimental data[4] and the value of $d\sigma/d\Omega$ for process a. By normalizing curves a and b, we can apparently explain the experimental angular distribution.

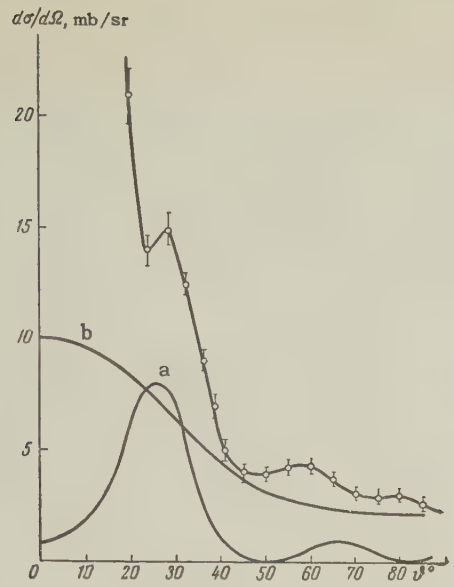

The maximum value $(d\sigma/d\Omega)_{max}$ for process a depends weakly on E_d. With increasing E_d, the first maximum shifts toward smaller ϑ, but does not go beyond zero, since $m_d = m_{d'}$ and $|\mathbf{k}_d - \mathbf{k}'_d| \to 0$ for increasing E_d. According to Eq. (1), for process b the dependence of $(d\sigma/d\Omega)_{max}$ on E_d should be stronger, since even for ordinary stripping $(d\sigma/d\Omega)_{max}$ depends on E_d approximately as E_d^{-2}, while the first maximum in the angular distribution is shifted, for large E_d, to the left of zero angle (since $|\mathbf{k}_p - \mathbf{k}_d|$ for a given ϑ varies approximately as $E_d^{1/2}$). Apparently these qualitative conclusions are in agreement with the presently available experimental data on excitation of first excited levels by inelastic scattering of deuterons on Mg^{24} (references 4 and 10), Be^9 (references 4 and 11), and Mg^{24} with excitation of the 4^+ level.[10] In the last case, the absence of a maximum at $\vartheta \sim 0$ is explained by the fact that to excite the level it is necessary that l_i and l_f be large (for example, $l_i = l_f = 2$). With increasing l_i and l_f, the reaction amplitude drops if E_d is not very large, while the peak in the angular distribution is shifted toward large scattering angles.

In the scattering of deuterons by nuclei with different external shells, different intermediate states give the main contribution to process b. Thus, in the scattering of deuterons by C^{12}, apparently the 1p-state is most important, for Mg^{24} the main contribution is from the 1d+2s states, and possibly the 2p states, for Ca^{40}, the 2p states.

In conclusion the authors express their gratitude to G. S. Tyurikov for aid in carrying out the numerical computations.

[1] C. Levinson and M. Banerjee, Ann. Phys. **2**, 471 (1957).

[2] R. Huby and H. Newns, Phil. Mag. **42**, 1442 (1951).

[3] A. G. Sitenko, Usp. Fiz. Nauk **67**, 377 (1959), Soviet Phys. Uspekhi **2**, 195 (1959).

[4] J. Haffner, Phys. Rev. **103**, 1398 (1956).

[5] N. Austern and S. Butler, Phys. Rev. **109**, 1402 (1958).

[6] O. D. Cheishvili, JETP **32**, 1240 (1957), Soviet Phys. JETP **5**, 1009 (1957).

[7] W. M. Fairbairn, Proc. Roy. Soc. (London) **A238**, 448 (1957).

[8] E. Gerjuoy, Phys. Rev. **91**, 645 (1953).

[9] I. B. Levinson, Papers of the Phys. Tech. Institute, Academy of Sciences, Lithuanian SSR **2**, No. 17, 31 (1957); Papers of the Academy of Sciences, Lithuanian SSR, **B4**, 3 (1957); I. B. Levinson and V. V. Vanagas, Оптика и спектроскопия (Optics and Spectroscopy) **2**, 10 (1957).

[10] Hinds, Middleton, and Parry, Proc. Phys. Soc. **A70**, 900 (1957).

[11] R. G. Summers-Gill, Phys. Rev. **109**, 1591 (1958).

Translated by M. Hamermesh
41

COMPETITION BETWEEN NEUTRON EVAPORATION AND FISSION IN THE REACTIONS OF MULTIPLY CHARGED IONS WITH HEAVY NUCLEI

N. I. TARANTIN

Submitted to JETP editor June 23, 1959

J. Exptl. Theoret. Phys. (U.S.S.R.) **38**, 250-252 (January, 1960)

In this work we use certain experimental results[1-3] to estimate the relative importance of two competing processes — neutron evaporation and fission — in the de-activation of the compound nuclei formed when heavy elements are bombarded by multiply charged ions.

As is well known, the reaction cross section σ_{xn} for the evaporation of x neutrons when a particle interacts with a nucleus can be written

$$\sigma_{xn}(E) = \sigma_c(E)\,\bar{G}_n^x P(E, x).$$

We used this relation to approximate the experimental values of the cross section for neutron evaporation. $\sigma_c(E)$ is the cross section for formation of the compound nucleus and was calculated

	Reaction	"Mean" intermediate nucleus	Γ_n/Γ_f	T, Mev
1	Th^{232} (C^{12}, 4n) Cm^{240}	$Cm^{242.5}$	0.22	1.3
2	Th^{232} (C^{13}, 5n) Cm^{240}	Cm^{243}	0.27	1.5
3	U^{238} (C^{12}, 4n) Cf^{246}	$Cf^{248.5}$	0.21	1.3
4	U^{238} (C^{12}, 5n) Cf^{245}	Cf^{248}	0.24	1.3
5*	U^{238} (C^{13}, 5n) Cf^{246}	Cf^{249}	0.29	1.5
6*	U^{238} (C^{13}, 6n) Cf^{245}	$Cf^{248.5}$	0.29	1.6
7	Pu^{241} (C^{13}, 4n) Fm^{250}	$Fm^{252.5}$	0.12	1.3
8	U^{238} (O^{16}, 4n) Fm^{250}	$Fm^{252.5}$	0.09	1.4
	From the comparison			
9	reactions 2 and 1	Cm^{245}	0.81	
10	reactions 5 and 3	Cf^{251}	0.89	
11	reactions 6 and 4	Cf^{251}	1.00	

*In approximating the data for these reactions, we took into account the fact, demonstrated by supplementary experiments, that the energies of the C^{13} ions quoted in reference 1 were 2 Mev too high.

using the experimental results in reference 4 and the formula obtained by Maksimov.[5] P(E, x) is the probability that the nucleus de-excites itself by the emission of x neutrons and was calculated on the basis of Jackson's model,[6] as modified for fissionable nuclei.[7] The calculations were carried out for various nuclear temperatures T so as to obtain the best possible fit to the experimentally measured position of the maximum for the reaction. $\bar{G}_n^x$ is the ratio $\frac{\Gamma_n}{\Gamma_n + \Gamma_f}$, averaged over the compound and intermediate nuclei, and was chosen so as to give a best fit to the absolute values of the cross section. The results are shown in the table. In rows 1 to 8 are given average values of Γ_n/Γ_f, obtained from the relation $\Gamma_n/\Gamma_f = \bar{G}_n/(1-\bar{G}_n)$, while rows 9 to 11 give values of Γ_n/Γ_f for individual nuclei.

It is interesting to compare the values of Γ_n/Γ_f so obtained with values of Γ_n/Γ_f for the same nuclei obtained in a different way: for example, with He^4 ions. Such a comparison is of interest because in the interaction of heavy ions with nuclei, states of very high excitation and angular momentum can be formed, and such states are particularly likely to fission.[8] The figure shows Γ_n/Γ_f as a function of A for the nuclei Cm, Cf, and Fm, the solid circles (●) corresponding to heavy ion reactions and the open circles (○) to He^4 ions. Data for reactions initiated by He^4 were taken from references 9 to 11. From the figure it follows that values of Γ_n/Γ_f obtained with ions C^{12}, C^{13}, and O^{16} agree fairly well with values obtained for He^4 as the bombarding particle. The values of Γ_n/Γ_f from heavy ion reactions do tend to be somewhat smaller but by an amount within experimental errors. There seems to be no evidence for some effect associated with the heavy ions. Thus in-

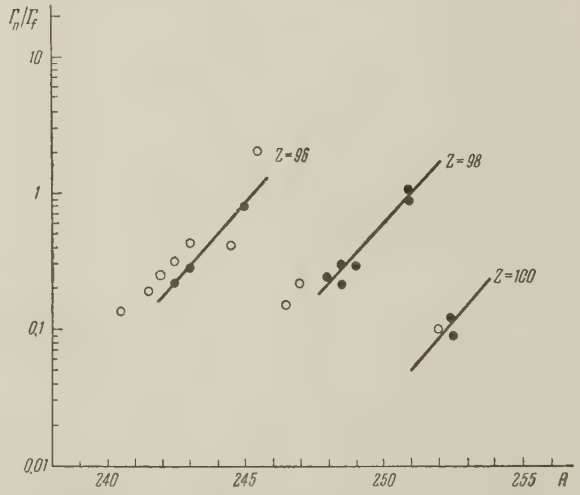

creasing the angular momentum of the compound nucleus from 25 ħ (reactions initiated by 44 Mev He^4 ions) to 45 ħ (reactions initiated by 80 Mev C^{12} and C^{13} ions, and by 95 Mev O^{16} ions) does not significantly decrease Γ_n/Γ_f. This is a very important fact for the synthesis of new elements using accelerated heavy ions.

In conclusion, the author would like to express his gratitude to Prof. G. N. Flerov for discussion of these results.

[1] Volkov, Guseva, Pasyuk, Tarantin, and Filippova, JETP 36, 762 (1959), Soviet Phys JETP 9, 536 (1959).

[2] Guseva, Myasoedov, Tarantin, and Filippova, JETP 37, 973 (1959), Soviet Phys. JETP 10, 694 (1960).

[3] Volkov, Guseva, Myasoedov, Tarantin, and Filippova, JETP 37, 1207 (1959), Soviet Phys. JETP 10, 859 (1960).

[4] V. A. Druin and S. M. Polikanov, Ядерные реакции при малых и средних энергиях (Nuclear Reactions at Low and Intermediate Energies) Moscow 1958, p. 507.

[5] M. Z. Maksimov, JETP **33**, 1411 (1957), Soviet Phys. JETP **6**, 1085 (1958).

[6] J. D. Jackson, Can. J. Phys. **34**, 767 (1956).

[7] Vandenbosch, Thomas, Vandenbosch, Glass, and Seaborg, Phys. Rev. **111**, 1358 (1958).

[8] G. A. Pik-Pichak, loc. cit. ref. 4, p. 525.

[9] Glass, Carr, Cobble, and Seaborg, Phys. Rev. **104**, 434 (1956).

[10] Chetham-Strode, Choppin, and Harvey, Phys. Rev. **102**, 747 (1956).

[11] Amiel, Chetham-Strode, Choppin, Ghiorso, Harvey, Holm, and Thompson, Phys. Rev. **106**, 553 (1957).

Translated by R. Krotkov
42

EFFECT OF CONDUCTIVITY ANISOTROPY IN A MAGNETIC FIELD ON THE STRUCTURE OF A SHOCK WAVE IN MAGNETOGASDYNAMICS

S. A. KAPLAN

L'vov State University

Submitted to JETP editor June 27, 1959

J. Exptl. Theoret. Phys. (U.S.S.R.) **38**, 252-253 (January, 1960)

A systematic study of shock waves in a magnetized plasma must also take account of its anisotropic properties. Such a study is very difficult because of the cumbersome character of the initial equations, and can be carried out only by numerical integration. However, one can obtain a quantitative estimate of the thickness of the shock front in the plasma in a quite elementary way, and study the qualitative peculiarities of the effect of conduction anisotropy on the structure of shock waves.

We shall begin with the induction equation for an anisotropic plasma, which for the stationary case can be written in the form[1]

$$-\operatorname{curl}[\mathbf{u}\times\mathbf{H}] = \frac{c^2}{4\pi\sigma}\left\{\nabla^2\mathbf{H} - \frac{\omega\tau}{H}\operatorname{curl}[\operatorname{curl}\mathbf{H}\times\mathbf{H}]\right\} \quad (1)$$

Here $\sigma = \tau ne^2/m$ is the electrical conductivity, $\omega = eH/mc$ is the Larmor frequency for electrons, and τ is the time of free flight; the remaining notation is standard. We assume that the plane of the front coincides with the coordinate plane $x = 0$. In passage through the front of an oblique shock, the conditions of conservation of mass flow $j = \rho u_x$ = const, of momentum flux (we need only the tangential components $u_{y,z} = H_x H_{y,z}/4\pi j$), and also H_x = const. Taking it into account that all the parameters in our case change only with x, Eq. (1), written in components with account of the conservation conditions, can be integrated once. We get

$$H_z(u_x - H_x^2/4\pi j) = \frac{c^2}{4\pi\sigma}(H_z' - \omega\tau H_x H_y'/H) + \text{const},$$

$$H_y(u_x - H_x^2/4\pi j) = \frac{c^2}{4\pi\sigma}(H_y' + \omega\tau H_x H_z'/H) + \text{const}, \quad (2)$$

and the x component of Eq. (1) vanishing identically. If the dependence of u_x and $\omega\tau H_x/H$ on the coordinates is not taken into account, integration of (2) gives

$$H_y \pm iH_z \sim \exp\left\{x\frac{4\pi\sigma}{c^2}\left(u_x - \frac{H_x^2}{4\pi j}\right)\frac{1 \pm i\omega\tau H_x/H}{1 + (\omega\tau H_x/H)^2}\right\}. \quad (3)$$

In the perpendicular wave $H_x = 0$, (2) reduces to equations already considered (see, for example, reference 2). The thickness of the front here is of the order $\Delta x = c^2/4\pi\sigma u_x$. Thus the conduction anisotropy has no effect on the structure of the perpendicular shock wave.

In an oblique gasmagnetic shock wave, $H_x \neq 0$. It then follows from (3) that the vector $\{0, H_y, H_z\}$ inside the front rotates about the x axis with period

$$p \approx \frac{2\pi c^2}{4\pi\sigma}\frac{1 + (\omega\tau H_x/H)^2}{(u_x - H_x^2/4\pi j)\,\omega\tau H_x/H} \simeq \frac{c^2}{2\sigma}\frac{\omega\tau\cos\varphi}{u_x - H_x^2/4\pi j}.$$

This effect can be considered as a generalization to nonlinear motion of the well known rotation of the plane of polarization of waves in an isotropic medium. An appreciable change in the absolute value takes place at distances of the order

$$\Delta x \approx \frac{c^2}{4\pi\sigma}\frac{1 + (\omega\tau H_x/H)^2}{u_x - H_x^2/4\pi j} \approx \frac{c^2}{4\pi\sigma}\frac{(\omega\tau\cos\varphi)^2}{u_x - H_x^2/4\pi j},$$

which must be considered in the thickness of an oblique shock front in an anisotropic magnetized plasma. Here φ is the angle of inclination of the front to the magnetic field. Thus the conduction anisotropy leads to a very great increase in the front thickness of oblique gasdynamic shocks. It should be noted that the front thickness of oblique gasmagnetic shock waves is proportional to the square of the magnetic field intensity.

[1] B. N. Gershman and V. L. Ginzburg, Уч. Зап. Горьковского уи-та (Sci. Notes, Gorkiĭ Univ.) **50**, 3 (1956).

[2] G. S. Golitsyn and K. P. Stanyukovich, JETP **33**, 1517, Soviet Phys. JETP **6**, 1171 (1958).

Translated by R. T. Beyer
43

ENERGY DISTRIBUTIONS OF PRODUCTS OF REACTIONS IN WHICH SEVERAL PARTICLES ARE EMITTED

V. V. KOMAROV and A. M. POPOVA

Institute for Nuclear Physics, Moscow State University

Submitted to JETP editor June 27, 1959

J. Exptl. Theoret. Phys. (U.S.S.R.) **38**, 253-255 (January, 1960)

In studying the energy distributions of products of reactions in which several particles emerge, which occur via a direct interaction with subsequent decay of the residual nucleus, it is necessary to take into account the interaction of the decay products in the final state. The question of the effect of final-state interaction on the shape of the energy spectra of reaction products was first considered by Migdal,[1] and later by various other authors.[2] The effect of interaction of the reaction products in the final state is that, independently of the mechanism of the decay itself, the interaction of the products from the decay of a system changes the magnitude and shape of the effective cross section, and the energy and angular distributions of the decay products. The final state interaction is assumed to be strong, of short range, and to affect the wave functions of the reaction products until they go beyond the range of the nuclear forces. For this treatment it is essential that the energies of the particles interacting in the final state be small.

In the present note it is shown that the spectra of products of a reaction from which several particles emerge can be explained quite well by computing in the Born approximation and taking account of the interaction of the particles in the final state. The wave function describing the relative motion of the particles interacting in the final state depends on their separation ρ, and must have a different form inside ($\rho < \rho_0$) and outside ($\rho > \rho_0$) the range of the nuclear forces. The parameters determining the nuclear interaction of the particles in the final state are found by matching the wave functions for $\rho < \rho_0$ and $\rho > \rho_0$ at the boundary of the region of action of the nuclear forces.[3]

As an example, we calculated the energy distributions of He^3 nuclei from the reaction T + d $\rightarrow$ He^3 + n + n for various angles, for a deuteron energy of 12 Mev, taking into account the interaction of the neutrons in the final state. This reaction can be regarded as a direct interaction accompanied by the decay of the residual system, since two neutrons cannot form a bound state. In writing the matrix element it was assumed that the reaction proceeds via a direct process of temporary capture, i.e., the deuteron pulls a proton out of the triton and there is a δ-function interaction between this proton and each of the nucleons in the deuteron. Evidence that the reaction proceeds via a direct process comes from the anisotropic angular distribution of the He^3 nuclei, which are ejected preferentially forward.[4]

The computation of the energy distributions of the He^3 nuclei for different angles of emergence was made using the formula

$$d\sigma/dEd\vartheta \sim |H_{ba}|^2 f(E),$$

where $f(E)$ is the density of states of He^3, while H_{ba} is the matrix element for the transition including the interaction of the two neutrons in the final state, which was taken to have the form of a square well with radius $\rho_0 = 2.8 \times 10^{-13}$ cm.

The wave function describing the internal state of the potentially scattering neutrons, has the form

$$\psi(\rho) = e^{iq\rho} + f(\theta)\, e^{-iq\rho}/\rho,$$

for $\rho > \rho_0$, where q is the wave vector of the relative motion of the two neutrons and $f(\theta)$ is the amplitude of the scattered wave. For an incident deuteron energy of 12 Mev, the energy of relative motion of the two neutrons does not exceed 1.6 Mev, so that the only contribution to the differential cross section comes from the S-wave part of the partial wave expansion of the wave function for the relative motion of the two neutrons. The spin function for two neutrons must be antisymmetric ($s = 0$) because of the Pauli principle. For the S-state, the radial wave function of the relative motion of the two neutrons for $\rho > \rho_0$ has the form

$$\psi^{(1)}(\rho) = \frac{i\sqrt{\pi}}{q\rho}(e^{-iq\rho} - e^{iq\rho}) + \sqrt{4\pi}a\rho^{-1}e^{-iq\rho},$$

where $a = -(\alpha - iq)^{-1}$ is the neutron-neutron scattering length in an S-state. The interaction energy of the neutrons in our case is 70 kev. Inside the region of interaction, $\rho < \rho_0$, the radial part of the wave function for the relative motion of the two neutrons has the form $\psi^{(2)}(\rho) = A \sin k'\rho$, where A is an arbitrary constant and k' is the wave vector of the relative motion of the two neutrons within the region of action of the nuclear forces. A and k' are found by matching the functions $\psi^{(1)}$ and $\psi^{(2)}$ at the boundary of the region of action of the nuclear forces.

The figure shows the energy distributions of He^3 nuclei at angles of 25 and 75° in the center-of-

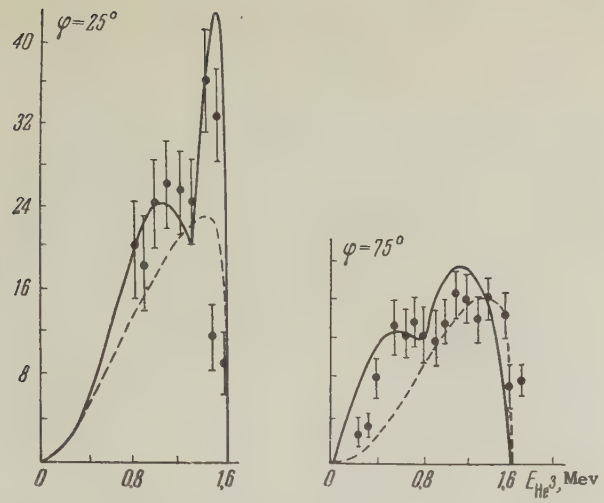

mass system, computed including (solid curve) and omitting (dashed curve) the interaction of the neutrons in the final state, and the experimental energy distribution[4] of the He^3 nuclei (the points on the figure). As one sees from the figure, the energy distributions of He^3 nuclei, computed including the potential scattering of the neutrons in the final state, give a good description of the experimental results.

In conclusion it should be mentioned that, on the basis of these considerations, one can not only explain the energy distributions of products of reactions which lead to emission of several particles, but one also gets a value for the parameters of the interaction of these particles in the final state.

[1] A. B. Migdal, JETP **28**, 3 (1955), Soviet Phys. JETP **1**, 2 (1955).

[2] K. Brueckner, Phys. Rev. **82**, 598 (1951); K. M. Watson, Phys. Rev. **88**, 1163 (1952).

[3] V. V. Komarov and A. M. Popova, JETP **36**, 1574 (1959), Soviet Phys. JETP **9**, 1118 (1959).

[4] Brolley, Hall, Rosen, and Stewart, Phys. Rev. **109**, 1277 (1958).

Translated by M. Hamermesh
44

ISOTHERMAL DISCONTINUITIES IN MAGNETOHYDRODYNAMICS

V. I. TSEPLYAEV

Moscow State University

Submitted to JETP editor July 8, 1959

J. Exptl. Theoret. Phys. (U.S.S.R.) **38**, 255-256 (January, 1960)

In magnetohydrodynamics, under the condition that

$$\beta_m/\beta_T \ll \gamma M_m^2 u_2 [(1/\gamma M_1^2 + 1/2\, M_m^2 + 1)\, u_2 + 3/2\, M_m^2]/(\gamma+1), \quad (1)$$

the principal role in the diffusion of the shock front is played by thermal conductivity, while magnetic viscosity can be neglected. Here and below we use the dimensionless quantities

$$u = v/v_1, \quad M_1^2 = v_1^2/a_1^2, \quad M_m^2 = v_1^2/a_m^2;$$

$$\beta_m = \nu_m/v_1 l_1, \quad \beta_T = \chi/v_1 l_1$$

where

$$a_m^2 = H_1^2/4\pi\rho_1, \quad a_1^2 = \gamma p_1/\rho_1.$$

Here, $\nu_m = c^2/4\pi\sigma$ is the magnetic viscosity, χ the coefficient of temperature conductivity, and l the mean free path of the ion. The system of coordinates moves with the velocity of the wave in the direction of its propagation (for example, from right to left). The remaining notation is universal in magnetohydrodynamics.

Account of thermal conductivity alone leads to the appearance of an isothermal discontinuity. It is well known that in the absence of a magnetic field, a gradual change in the hydrodynamic quantities takes place only at gas velocities smaller than $u_2 = (\gamma+1)/(3\gamma-1)$ by $+\infty$, whereas in this case $M_1^2 = (3\gamma-1)/\gamma(3-\gamma)$ (see, for example, reference 1). We call the velocity $u_2 = u_l$, for which the isothermal discontinuity appears, the limiting velocity. If the magnetic field is not equal to zero, then the limiting velocity can vary from $u_l = (\gamma+1)/(3\gamma-1)$ to 1, depending on the values of M_1^2 and M_m^2. These three quantities are related in the following fashion:

$$M_1^2 = 2[\gamma - (2-\gamma)u_l]/\gamma[(5\gamma-7)u_l^2 + (5-\gamma)u_l - (3\gamma-1)u_l^3 - (\gamma-1)],$$

$$M_m^2 = [\gamma - (2-\gamma)u_l]/u_l^2[(3\gamma-1)u_l - \gamma - 1]. \quad (2)$$

The region in front of the isothermal discontinuity is especially clearly seen in the diagram of M_1^2, M_m^2. The connection between u_2, M_1^2 and M_m^2 has the form

$$M_m^2 = (\gamma u_2 + 2 - \gamma)/[(\gamma+1)u_2^2 - (\gamma-1)u_2 - 2u_2/M_1^2]. \quad (3)$$

In shock waves with parameters taken from the shaded region, the changes of all variables take

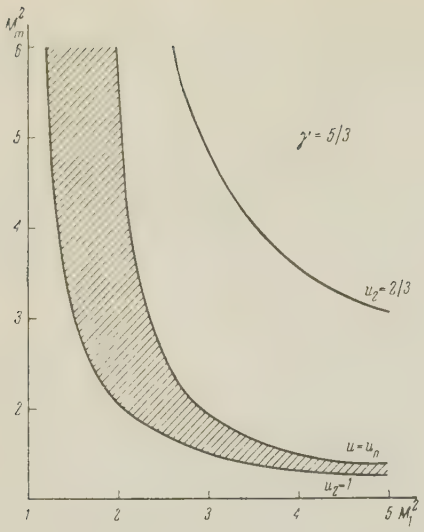

place smoothly. The drawing shows that the magnetic field creates more favorable conditions for the formation of an isothermal discontinuity: the isothermal discontinuity appears for smaller amplitudes of the waves the larger the field in the medium.

It is easy to obtain values of quantities characterizing the wave directly in front of the jump. For example, the velocity is

$$u = 1/2\{1/\gamma M_1^2 + 1/2 M_m^2 + 1 - u_2 + [(1/\gamma M_1^2 + 1/2 M_m^2 + 1 - u_2)^2 + 2/u_2 M_m^2]^{1/2}\}. \quad (4)$$

I thank K. P. Stanyukovich for discussions.

[1] L. D. Landau and E. M. Lifshitz, Механика сплошных сред (Mechanics of Continuous Media) (Gostekhizdat, 1954).

Translated by R. T. Beyer
45

NUMBER OF EXTENSIVE ATMOSPHERIC SHOWERS OF COSMIC RAYS NEAR SEA LEVEL

S. I. MISHNEV and S. I. NIKOL'SKIĬ

P. N. Lebedev Physics Institute, Academy of Sciences, U.S.S.R.

Submitted to JETP editor July 18, 1959

J. Exptl. Theoret. Phys. (U.S.S.R.) 38, 257-258 (January, 1960)

THE frequency of extensive atmospheric showers with different numbers of charged particles was investigated by many researchers at different altitudes.[1] The most widely used research method consists of measuring the dependence of the number of multiple coincidences of discharges in counters on the effective area of the counters (the so called "density spectrum"). The value spectrum of extensive atmospheric showers can be obtained from the density spectrum by using the well known lateral distribution function of particles in the shower (in the particular case when this function is independent of the number of particles in the shower) and under the assumption that the value spectrum of the showers obeys a power law with a constant or slowly-varying exponent (see the paper by Migdal[2]). The latter assumption is connected with the fact that the axes of the registered showers may pass at varying distances from the particle flux-density detector; when counters are used it is also connected with the random character of the registration of the shower particle flux density.

With the development of methods for the registration and investigation of individual extensive atmospheric showers, direct data have appeared on the value spectrum of showers.[3,5] However, when the number of shower particles is small, it becomes difficult to register individual showers and determine subsequently the number of particles by comparing the particle flux density at certain points at the level of observation. In this connection we used a modification of the method of measuring the density spectrum of extensive atmospheric showers. The modification consisted of registering only the fourfold coincidences of counter discharges which were not accompanied by threefold coincidences in any of the three groups of counters in the same area, located ~ 6 m from the center of the array (Fig. 1). The counter area σ in all the registration channels, including the anticoincidence channels, was changed simultaneously ($\sigma = 0.4\,m^2$; $0.2\,m^2$, $990\,cm^2$, $330\,cm^2$, and $165\,cm^2$). This method of registration, while not differing in principle from the measurement of the density spectrum, makes it possible to reduce substantially the difference between the number of particles in the showers causing operation of the setup at a given counter area. This is

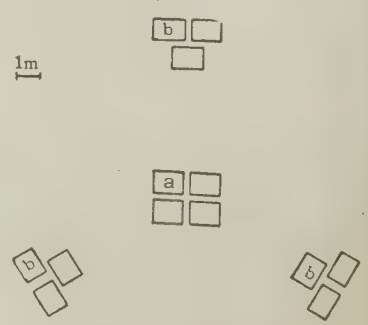

FIG. 1. Plan of the array: a – group of counters connected for fourfold coincidence, b – group of counters connected for threefold coincidence.

due to the fact that the probability of registering showers whose axes pass outside the center group of the counters of the array is considerably reduced, because of the conditions of anticoincidence of the discharges in the central group of counters with the discharges in any peripheral group.

Numerical calculations of the number of registered showers were performed under the assumption that the integral spectrum of extensive atmospheric showers has the form $f(>N) = A/N^{1.45}$, and the function of lateral distribution of the charged particles does not depend on the number of particles in the shower and corresponds to the experimental data of Abrosimov, Goryunov, et al.[6] The results of calculations for the counter areas $\sigma = 0.4\,m^2$ are given in Fig. 2. To reconcile the calculated number of showers with the experimentally observed one (H = 200 m above sea level) it is necessary to assume in the foregoing spectrum a value $A = 9 \times 10^4\,m^{-2}hr^{-1}$, which differs somewhat from the corresponding value given by Norman[7] ($1.15 \times 10^5\,m^{-2}hr^{-1}$), but is in better agreement with the data obtained by individual investigations of extensive atmospheric showers.[3]

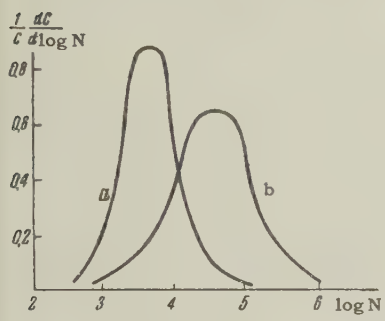

FIG. 2. a – shower spectrum by number of particles N, registered by the array at $\sigma = 0.4\,m^2$; b – number of showers causing coincidence of discharges in counters of the same area.

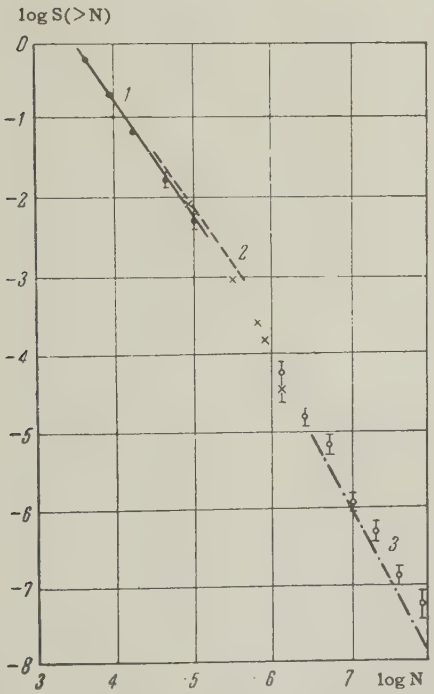

FIG. 3. Intensity of extensive atmospheric showers S (in $m^{-2}hr^{-1}$) with different number of particles N: 1 – data of present investigation (H = 200 m), 2 – data of reference 7 (H = 60 m), 3 – data of reference 5 (H = 60 m), × – data of reference 3 (H = 200 m), ○ – data of reference 4 (H = 180 m).

Comparison of the shower spectrum by number of particles which we obtained with data of other authors is given in Fig. 3.

The authors express their sincere gratitude to N. S. Il'ina for help in the measurements.

[1] K. Greisen, Progr. in Cosmic Ray Physics **3**, Amsterdam, 1956.

[2] A. B. Migdal, JETP **15**, 313 (1945).

[3] G. V. Kulikov and G. B. Khristiansen, JETP **35**, 635 (1958), Soviet Phys. JETP **8**, 441 (1959).

[4] Clark, Earl, Kranshaar, Linsley, Rossi, and Scheib, Nature **180**, 406 (1957).

[5] Cranshaw, de Beer, Galbraith, and Porter, Phil. Mag. **3**, 377 (1958).

[6] Abrosimov, Goryunov, Dmitriev, Solov'eva, Khrenov, and Khristiansen, Izv. Akad. Nauk SSSR, Ser. Fiz. **19**, 666 (1955), Columbia Tech. Transl. p. 605.

[7] R. J. Norman, Proc. Phys. Soc. **A69**, 804 (1956).

Translated by J. G. Adashko
46

INVERSE DISPERSION RELATIONS FOR PHOTOPRODUCTION OF PIONS ON NUCLEONS

N. F. NELIPA and V. A. TSAREV

P. N. Lebedev Physics Institute, Academy of Sciences, U.S.S.R.

Submitted to JETP editor July 18, 1959

J. Exptl. Theoret. Phys. (U.S.S.R.) **38**, 259-260 (January, 1960)

IT has been emphasized by Blank and Shirkov[1] that it is inconvenient to use conventional ("direct") dispersion relations when the imaginary part of the amplitude for some process becomes larger than the real part since one then deals with a small integral of a large (and generally speaking, alternating in sign) quantity. To overcome this difficulty Blank and Shirkov proposed "inverse" dispersion relations and derived them explicitly for the pion-nucleon scattering process. In contrast to direct

dispersion relations the inverse relations express the imaginary part of the amplitude in terms of a Cauchy integral over the real part of the same amplitude.

The aim of this note is the construction of inverse dispersion relations for pion photoproduction on nucleons.* Direct dispersion relations for pion photoproduction on nucleons were obtained by several authors.[4-8] In the following we make use of the notation and the results of Logunov, Tavkhelidze and Solov'ev.[8]

Using the same method as Blank and Shirkov did, we obtain inverse dispersion relations in the following form (for the case when the nonphysical region is contiguous with the continuous spectrum region):

$$A_j^i(E,\mathbf{p}^2) = \frac{1}{\pi}\ln\frac{E+E_n}{E-E_n}D_j^i(E,\mathbf{p}^2) - \frac{2}{\pi}\,\mathrm{P}\int_{E_n}^{\infty}\frac{dE'\eta'_{ij}}{E'^2-E^2}\left\{D_j^i(E',\mathbf{p}^2) + \frac{1}{\pi}A_j^i(E',\mathbf{p}^2)\ln\frac{E'+E_n}{E'-E_n}\right\} - \frac{1}{E^2-E_p^2}(\eta'_{ij})_p\ln\frac{E_n+E_p}{E_n-E_p}\frac{M}{p_0}\frac{2}{\pi}\varepsilon_{ij}. \qquad (1)$$

Here

$$(\eta'_{ij})_p = \begin{vmatrix} E & E & E_p & E \\ E & E & E_p & E \\ E_p & E_p & E & E_p \end{vmatrix},$$

$$\|\varepsilon_{ij}\| = \begin{vmatrix} \frac{f}{\mu}\frac{e}{2p_0E_p} & \frac{f}{\mu}(\mu'_p-\mu_n) & -\frac{f}{\mu}(\mu'_p-\mu_n) & -\frac{ef}{4\mu}-\frac{Mf}{2\mu}(\mu'_p-\mu_n) \\ \frac{f}{\mu}\frac{e}{2p_0E_p} & \frac{f}{\mu}(\mu'_p+\mu_n) & -\frac{f}{\mu}(\mu'_p+\mu_n) & -\frac{ef}{4\mu}-\frac{Mf}{2\mu}(\mu'_p+\mu_n) \\ \frac{f}{\mu}\frac{e}{2p_0E_p} & -\frac{f}{\mu}(\mu'_p-\mu_n) & \frac{f}{\mu}(\mu'_p-\mu_n) & \frac{ef}{4\mu}+\frac{Mf}{2\mu}(\mu'_p-\mu_n) \end{vmatrix},$$

$$p_0 = \sqrt{\mathbf{p}^2+M^2}, \qquad \mathbf{p}^2 = \mu^2M/4(M+\mu), \qquad E_n = (\mathbf{p}^2+\mu^2/4)/p,$$

e, f are the electromagnetic and mesonic coupling constants; μ'_p, μ_n are the anomalous magnetic moments of the proton and neutron; M, μ are the nucleon and meson masses. Although the large function A appears under the integral sign in the right hand side of the expression (1) its contribution to the integral (for high energy photons) should generally speaking be small because it is multiplied by the logarithm.† Unfortunately at this time the experimental data needed to carry out a detailed estimate are not available.

For practical purposes it is convenient to have the inverse dispersion relations expressed in the barycentric frame of reference. We shall not write them out since they can easily be obtained from the direct dispersion relations.

Inverse dispersion relations for pion photoproduction may be written in another form[9] which differs from the preceding in that the imaginary part does not appear under the integral sign.

For the case when the nonphysical region is contiguous with the continuous spectrum region they are given by

$$\mathrm{Im}\left[\frac{t_j^i(E,\mathbf{p}^2)}{\sqrt{E^2-E_n^2}}\right] = -\frac{2}{\pi}\,\mathrm{P}\int_{E_n}^{\infty}\frac{\mathrm{Re}\,t_j^i(E',\mathbf{p}^2)\,\eta_{ij}dE'}{(E'^2-E^2)\sqrt{E^2-E_p^2}} - \frac{2}{E_p^2-E^2}(\eta_{ij})_p\varepsilon_{ij}\frac{M}{p_0}\frac{1}{\sqrt{E_n^2-E_p^2}}. \qquad (2)$$

In order to obtain these relations in the barycentric frame[8] from the direct dispersion relations it is necessary to multiply the one-nucleon term by

$$[(2M+1)(2M+1-4M\nu_1)]^{-1/2}$$

and replace in the left hand side $\mathrm{Re}\,U_j^i(W,\nu_1)$ by

$$\frac{-\{\mathrm{Im}\,U_j^i(W,\nu_1)\}}{\sqrt{W^2-(M+1)^2}\sqrt{W^2-M^2+2M+1-4M\nu_1}}$$

and under the integral signs $\mathrm{Im}\,U_j^i(W',\nu_1)$ by

$$\frac{\{\mathrm{Re}\,U_j^i(W',\nu_1)\}}{\sqrt{W'^2-(M+1)^2}\sqrt{W'^2-M^2+2M+1-4M\nu_1}}.$$

Lastly we observe that in expression (2), in contrast to expression (1), there appears under the integral sign a factor $\sim 1/E$. This circumstance may turn out to be useful if it is necessary to discard the high energy part of the integral.

*For the analysis of experimental data on pion photoproduction using direct dispersion relations, see references 2 and 3.

†An analogous situation also occurs for inverse dispersion relations for pion-nucleon scattering[1] where estimates indicate that the contribution of A to the integral does not exceed 20%.

[1] V. Z. Blank and D. V. Shirkov, JETP **33**, 1251 (1957), Soviet Phys. JETP **6**, 962 (1958).

[2] E. L. Goldwasser, 7-th Rochester Conference 1957, p. 50.

[3] Lazarus, Panofsky, and Tangherlini, Preprint.

[4] E. Corinaldesi, Nuovo cimento **4**, 1384 (1956).

[5] A. A. Logunov and B. M. Stepanov, Dokl. Akad. Nauk SSSR **110**, 368 (1956), Soviet Phys.-Doklady **1**, 552 (1957).

[6] Logunov, Stepanov, and Tavkhelidze, Dokl. Akad. Nauk SSSR **112**, 45 (1957), Soviet Phys.-Doklady **2**, 12 (1957).

[7] Chew, Goldberger, Low, and Nambu, Phys. Rev. **106**, 1345 (1957).

[8] Logunov, Tavkhelidze, and Solov'ev, Nuclear Physics **4**, 427 (1957).

[9] W. Gilbert, Phys. Rev. **108**, 1078 (1957).

Translated by A. M. Bincer
47

GALVANOMAGNETIC PHENOMENA IN INDIUM AND ALUMINUM

E. S. BOROVIK and V. G. VOLOTSKAYA

Physico-technical Institute, Academy of Sciences, Ukrainian S.S.R.

Submitted to JETP editor July 22, 1959

J. Exptl. Theoret. Phys. (U.S.S.R.) **38**, 261-262 (January, 1960)

THE existing data on galvanomagnetic phenomena in indium and aluminum[1-7] refer to specimens in which the resistivity decreases less than a thousand-fold between room temperature and 4.2° K. We had at our disposal metals of appreciably greater purity which enabled us to reach a region of larger effective fields[8] than in previous investigations. Besides increasing the range, a study of aluminum in large effective fields is of interest in connection with the results of Lüthi and Olsen.[7]

The indium specimen was a single crystal, 1.84 mm in diameter and 12.55 mm between the potential leads. The aluminum specimen was a polycrystalline strip, 0.27 mm thick, 3 mm broad, and 36 mm between the leads. The temperature dependence of resistivity is shown in the table.

The measurements were made with the current normal to the magnetic field. A rotation diagram was taken for indium of the resistance change and Hall effect, and the measurements showed that the Hall constant is isotropic and is independent of field in the range $10 - 28 \times 10^3$ oe; its value is

T, °K	$[r_0(T)/r_0(273)1] \cdot 10^4$	
	In	Al
20.4	0.8	9.6
4.2		4.3
2.2		4.3

$R = 1.5 \times 10^{-3}$ cgs magnetic units. The ratio of Hall field, E_y, to the field in the current direction, E_x, increases linearly with magnetic field, as is shown in Fig. 1 (curve 1). The Hall field is nearly 20 times greater than the field in the current direction at the largest magnetic fields.

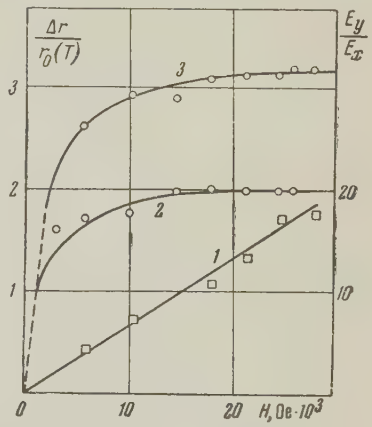

FIG. 1. Hall effect and magnetoresistance in In, T = 4.2°K. Curve 1 – E_y/E_x; Curve 2 – $\Delta r/r$ for the direction corresponding to the minimum effect; Curve 3 – $\Delta r/r$ for the direction for maximum effect.

The anisotropy of the relative change of resistance was found to be small, the greatest difference from the mean value not exceeding 25%. Curves 2 and 3 of Fig. 1 show the resistance change in a magnetic field for directions which show the maximum and minimum effects. It can be seen that in high fields the resistance tends to a limiting value. The results agree with those of other authors.[2,3,4]

The results for aluminum are shown in Fig. 2.

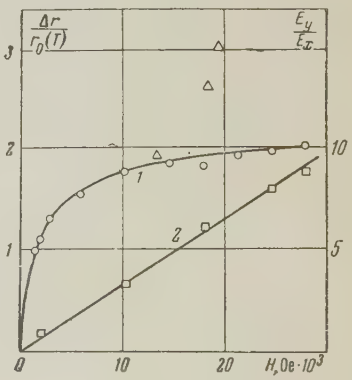

FIG. 2. Hall effect and magnetoresistance in Al, T = 4.2°K. Curve 1 – $\Delta r/r$; Curve 2 – E_y/E_x; Δ – data of Lüthi and Olsen.

Here again we have a linear increase of E_y/E_x (curve 2) with increasing magnetic field and the resistance (curve 1) tends to a limiting value.

The Hall constant in high fields is constant and equal to 9.4×10^{-4}. This agrees with the results of E. S. Borovik.[5] (We should point out that in this paper the value given for R was incorrectly an order of magnitude greater).

The data of Lüthi and Olsen[7] are represented by the triangles in Fig. 2. Köhler's rule has been used to reduce the effective fields to our scale. Clearly, there is disagreement for large fields and we are inclined to regard Olsen's results as in error. The source of error could be the incorrect neglect of the Hall field on the results for the resistance change. It can be seen from Fig. 2 (curve 2) that the Hall field is nearly 10 times greater than the field in the current direction. We found an upward trend to the curve, as in Lüthi and Olsen's work, when the potential leads for the measurement of resistance were not mounted on the same current line. The effect we found was weaker and started in larger fields (21,000 oe). The source of the error found for such a disposition of potential leads has been elucidated by Alekseevskiĭ, Brandt, and Kostina.[10]

The results obtained for indium — the absence of anisotropy in the Hall coefficient and the small anisotropy of magnetoresistance — enable us to state that indium belongs to the group of metals with closed Fermi surfaces.[11] The form of the dependence of resistance and E_y/E_x on field shows that indium is a metal with unequal numbers of holes and electrons.[8]

From the relations obtained for the Hall effect and magnetoresistance in high fields, ignoring Olsen's results, we may suppose that aluminum also belongs to the same type of metals, but measurements on a single crystal would be necessary to make sure of this.

As has been shown by Lifshitz, Azbel', and Kaganov,[11] the difference between the concentrations of electrons and holes can be derived rigorously from the Hall constant in high fields by the formula $R = 1/nec$ (where n is the concentration difference). We have derived this from the data given above. For indium $n = 4.2 \times 10^{22}$ and for aluminum $n = 6.7 \times 10^{22}$. These values are in agreement with earlier determinations.[8]

[1] E. Justi and H. Sheffers, Phys. Z. **39**, 105 (1928).

[2] Foroud, Justi, and Kramer, Phys. Z. **41**, 113 (1940).

[3] E. S. Borovik, Dokl. Akad. Nauk SSSR **69**, 767 (1949).

[4] E. S. Borovik, Dokl. Akad. Nauk SSSR **75**, 639 (1950).

[5] E. S. Borovik, JETP **23**, 83 (1952).

[6] G. B. Yntema, Phys. Rev. **91**, 1388 (1953).

[7] B. Lüthi and J. L. Olsen, Nuovo cimento **3**, 840 (1956).

[8] E. S. Borovik, Izv. Akad. Nauk SSSR, Ser. Fiz. **19**, 429 (1955), Columbia Tech. Transl. p. 383.

[9] M. Köhler, Ann. Physik **32**, 211 (1938).

[10] Alekseevskiĭ, Brandt, and Kostina, JETP **34**, 1339 (1958), Soviet Phys. JETP **7**, 924 (1958).

[11] Lifshitz, Azbel', and Kaganov, JETP **31**, 63 (1956), Soviet Phys. JETP **4**, 41 (1957).

Translated by R. Berman
48

POSSIBLE MODE OF OSCILLATION FOR A CHARGE IN CROSSED FIELDS

Yu. N. BARABANENKOV

Moscow State University

Submitted to JETP editor July 23, 1959

J. Exptl. Theoret. Phys. (U.S.S.R.) **38**, 263 (January, 1960)

WE consider the motion of a charge in mutually perpendicular uniform electric and magnetic fields. It is assumed that a damping force $m\gamma(v)\mathbf{v}$ acts on the charge. The z axis is taken in the direction of the magnetic field, the y axis is in the direction of the electric field, and we assume that $v_z \equiv 0$. We convert from the variables v_x and v_y to the new variables a and ψ, using the relations

$$v_x = v_x^0 + a\cos\psi, \quad v_y = v_y^0 - a\sin\psi,$$

$$v_x^0 = \frac{cE/H}{1+\gamma^2(v_0)/\omega_H^2}, \quad v_y^0 = \frac{\gamma(v_0)/\omega_H}{1+\gamma^2(v_0)/\omega_H^2}\frac{cE}{H}. \qquad (1)$$

It is apparent that $\mathbf{v}^0(v_x^0, v_y^0)$ is the drift velocity while a and ψ are the amplitude and phase of the Larmor rotation of the charge. If the damping is linear (γ independent of v) the Larmor rotation disappears in the course of time and only the drift motion remains.

The situation is changed, however, if the damping is nonlinear. Here we have the analog of a self-oscillating system of the Thomson type, with the Larmor rotation of the charge acting as the "tank circuit." The amplitude of this rotation does not vanish in the course of time, but approaches a

constant stable value, given by the relation

$$\frac{1}{\pi}\int_0^{\pi}(a+v_0\cos\psi)\,\gamma\left(\sqrt{v_0^2+a^2+2v_0 a\cos\psi}\right)d\psi=0. \quad (2)$$

The drift motion remains and is determined by the relations in Eq. (1).

Equation (2) has a root $0 < a < v_0$ if the condition

$$\frac{1}{\gamma(v_0)}\left(\frac{d\gamma}{dv_0}\right)_{v_0} < -\frac{2}{v_0}, \quad (3)$$

which is the oscillation excitation condition, is satisfied.

The theorem proposed applies if the parameter γ/ω_H is small, and can be verified by averaging[1] the equations for a and ψ. It will be apparent from the expression for $\gamma(v)$ given in reference 2 that a charge in a plasma can oscillate. In this case the excitation condition (3) is given approximately by $cE/H > v_T$. Here v_T is the thermal velocity of the charges which surround the charge and damp its motion.

In conclusion we wish to thank Ya. P. Terletskiĭ for discussion of the present work.

[1] N. N. Bogolyubov and Yu. A. Mitropol'skiĭ, Асимптотические методы в теории нелинейных колебаний (Asymptotic Methods in the Theory of Nonlinear Oscillations) 2nd ed., Fizmatizdat, 1958.

[2] L. Spitzer, Physics of Fully Ionized Gases, Interscience, New York 1956, Russ. Transl. IIL, 1956, p. 93.

Translated by H. Lashinsky
49

DIRECT ELECTRON-POSITRON PAIR PRODUCTION BY ELECTRONS

V. A. TUMANYAN

Submitted to JETP editor August 6, 1959

J. Exptl. Theoret. Phys. (U.S.S.R.) **38**, 264-265 (January, 1960)

IN this note we follow the terminology used in the paper by Tumanyan et al.,[1] in which 25 cases of production of visible tridents were analyzed in the experimental part. Up to this time 29 additional visible tridents have been registered as a result of a study of the photon component of two high energy ($\gtrsim 10^{13}$ ev) nuclear interactions* and a study of three isolated electron-photon showers.

The energies of the electron-positron pairs created by the photon component were determined from measurements of relative multiple scattering. In the isolated electron-photon showers the energy of the primary electron-positron pairs was also determined from the characteristics of the longitudinal development of the electromagnetic cascade.[2]

In a total length of electron track of 107.5 radiation length units 54 visible tridents were observed, which should be referred to an average electron energy of 20 Bev. The true number of tridents obtained with the help of the results of a Monte Carlo calculation[1] turned out to be 19.6. Our results on the determination of the mean free path λ, together with the results of other authors, are shown in the figure (taken from the paper by Weill et al.[3] which contains references to the literature for the appropriate sources; our data are represented by the star and the crosshatched cell). The curves show the theoretical dependence of λ on the electron

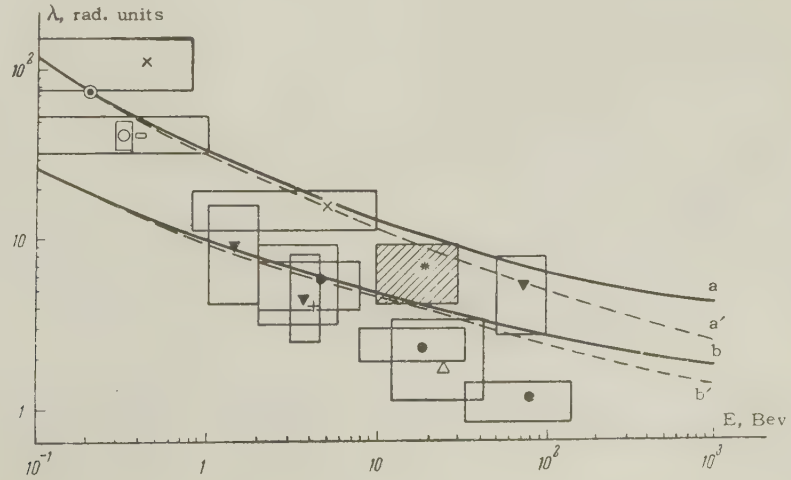

energy. The upper curves a′ and a correspond to the calculations by Bhabha[5] as corrected by Block, King, and Wada[4] for the cases of no screening (a′) and complete screening (a). The two lower curves b′ and b (b′ — no screening, b — complete screening) were calculated by us from the results of Murota, Ueda, and Tanaka,[6] whose calculation is more exact than Bhabha's.

As can be seen from the figure, the totality of the experimental results on the determination of λ for an energy interval of primary electrons 1 — 100 Bev is in satisfactory agreement with the theory of Murota et al. A certain disagreement between experiment and the predictions of the above mentioned theory for electrons in the energy interval 0.1 — 1 Bev is apparently due to an illegitimate extrapolation into the indicated energy region of the correction calculated by Koshiba and Kaplon[7] for the number of false tridents, which should lead to a substantial underestimate of the true number of tridents.

Thus the experimental results on the determination of the cross section for direct electron-positron pair production by electrons should apparently be considered as being in agreement with the predictions of quantum electrodynamics up to 100 Bev energies for the primary electrons.

I am grateful to Prof. I. I. Gurevich for valuable advice received in the course of this work.

*These events were found by A. A. Varfolomeev's group.

[1] Tumanyan, Stolyarova, and Mishakova, JETP **37**, 355 (1959), Soviet Phys. JETP **10**, 253 (1960).
[2] K. Pinkau, Nuovo cimento **3**, 1285 (1956).
[3] Weill, Gaillond, and Rosselet, Nuovo cimento **6**, 413 (1957).
[4] Black, King, and Wada, Phys. Rev. **96**, 1627 (1954).
[5] H. J. Bhabha, Proc. Roy. Soc. **A152**, 559 (1935).
[6] Murota, Ueda, and Tanaka, Progr. Theor. Phys. **16**, 482 (1956).
[7] M. F. Kaplon and M. Koshiba, Phys. Rev. **97**, 193 (1955).

Translated by A. M. Bincer
50

CYCLOTRON ABSORPTION OF ELECTROMAGNETIC WAVES IN A PLASMA

K. N. STEPANOV

Physico-Technical Institute, Academy of Sciences, Ukrainian S.S.R.

Submitted to JETP editor August 12, 1959

J. Exptl. Theoret. Phys. (U.S.S.R.) **38**, 265-267 (January, 1960)

THE propagation of electromagnetic waves in a magnetoactive plasma at frequencies ω, close to $m\omega_H^{e,i}$ ($m = 1, 2, \ldots$; where ω_H^e is the gyromagnetic frequency of the electron and ω_H^i is the gyromagnetic frequency of the ion) is characterized by strong absorption; this absorption is due to the thermal motion of the electrons and ions (cyclotron absorption)[1-5] and is of interest in connection with problems of microwave diagnostics and radiofrequency heating of plasmas.

The damping of waves characterized by $\omega \approx m\omega_H^e$, $m = 2, 3, \ldots$, is especially pronounced in the case of a double resonance, i.e., when $m\omega_H \approx \omega_+$, where ω_+ is the frequency given by the condition

$$A = 1 - u_e - v_e + u_e v_e \cos^2\theta = 0,$$

$$u_e = (\omega_H^e/\omega)^2,\ v_e = (\Omega_e/\omega)^2,$$

Ω_e is the electron Langmuir frequency, and θ is the angle between the direction of propagation of the wave and the direction of the magnetic field. As is well known,[2,6] when $\omega \approx \omega_+$ the index of refraction for the extraordinary wave n_2 become very large and a plasma wave can appear. When $\omega \approx m\omega_H^e \approx \omega_+$ and $m = 3, 4$ the complex indices of refraction for these waves, determined from the dispersion equation which has been reported earlier,[2] are

$$n' = n_{2,3} + i\varkappa_{2,3},$$

where

$$n_{2,3}^2 = \{-A_0 \pm (A_0^2 - 4\beta_e^2 B_0 A_1)^{1/2}\}/2\beta_e^2 A_1 \gg 1,$$

$$\varkappa_{2,3} = \sigma_m^e \sin^2\theta\,(1-u_e)\,n_{2,3}^3\,(2B_0 + A_0 n_{2,3}^2)^{-1},$$

$$B_0 = (2-v_e)\,u_e - 2\,(1-v_e)^2 - u_e v_e \cos^2\theta,$$

$$A_1 = -v_e\{3\cos^4\theta\,(1-u_e) + \cos^2\theta\sin^2\theta\,(6 - 3u_e + u_e^2) \times (1-u_e)^{-2} + 3\sin^4\theta\,(1-4u_e)^{-1}\},$$

$$\sigma_m^e = \frac{\sqrt{\pi}\,m^{2m-2}\sin^{2m-2}\theta\,\Omega_e^2}{2^{m+1/2}m!\cos\theta\,\omega_H^{e2}}\,(\beta_e n_{2,3})^{2m-3}\exp(-z_m^{e2}),$$

$$z_m^e = (1 - m\omega_H^e/\omega)\,(\sqrt{2}\,\beta_e n_{2,3}\cos\theta)^{-1},\qquad \beta_e = (T_e/m_e c^2)^{1/2}, \tag{1}$$

T_e is the temperature of the electron gas and m_e is the mass of the electron. If, however, $\omega \approx 2\omega_H^e \approx \omega_+$,

$\mathrm{Re}\, n' \sim \mathrm{Im}\, n' \sim \beta_e^{-1/3}$ for $|1 - 2\omega_H^e/\omega| \lesssim \beta_e^{2/3}$, $|A_0|^3 \lesssim \beta_e^2$.

We now consider cases of ion cyclotron resonance. If $\omega \approx \omega_H^i$, the indices of refraction for the ordinary and extraordinary waves (when $\beta_i c \ll V_A \ll c$) are given by the expressions

$$n_1^2 = N_+^2 = \frac{1+\cos^2\theta}{\cos^2\theta}\,\frac{c^2/V_A^2}{u_i - 1}, \quad n_2^2 = N_-^2 = \frac{c^2/V_A^2}{1+\cos^2\theta}, \qquad (2)$$

where $c^2/V_A^2 = (\Omega_i/\omega_H^i)^2$ (the subscript i used in the quantity f_i denotes the quantity f_e with the electron mass replaced by the ion mass m_i and the temperature of electron gas replaced by the ion temperature T_i). The expression for n_1 given in (2) applies when $|1 - \omega_H^i/\omega| \gg \beta_i N_+ \cos\theta$; in this case the cyclotron damping of the ordinary wave is exponentially small. When $|1 - \omega_H^i/\omega| \ll \beta_i N_+ \cos\theta$ however, this wave is highly damped:

$$n_1' = n_1 + i\varkappa_1 = \frac{\sqrt{3}+i}{2}\left\{\sqrt{\frac{\pi}{8}}\,\frac{c^2(1+\cos^2\theta)}{V_A^2\beta_i\cos^3\theta}\right\}^{1/3}. \qquad (3)$$

The extraordinary wave also experiences cyclotron absorption:

$$\varkappa_2 = \beta_i N_-^2 \cos\theta \sin^4\theta \exp(-z_1'^2)/\sqrt{8\pi}\,|w(z_1')|^2(1+\cos^2\theta)^2, \qquad (4)$$

where

$$z_1' = (1 - \omega_H^i/\omega)(\sqrt{2}\,\beta_i N_- \cos\theta)^{-1},$$

$$w(z) = e^{-z^2}\left(1 + \frac{2i}{\sqrt{\pi}}\int_0^z e^{t^2}dt\right).$$

The extraordinary wave is weakly damped: $\kappa_2 \ll N_-$ since $\beta_i N_- \ll 1$. When $\beta_i c \sim V_A$ propagation of both waves is impossible because of the strong damping: $n_{1,2} \sim \kappa_{1,2} \sim 1/\beta_i$ if $\omega \sim \omega_H^i$.

In the case of multiple resonances

$$\omega \approx m\omega_H^i, \qquad m = 2, 3, \ldots, \qquad n_{1,2}' = N_\pm + i\varkappa_{1,2},$$

where

$$N_\pm^2 = \{\varepsilon_{11}(1+\cos^2\theta) \mp [\varepsilon_{11}^2(1+\cos^2\theta)^2 - 4\cos^2\theta(\varepsilon_{11}^2 + \varepsilon_{12}^2)]^{1/2}\}/2\cos^2\theta, \qquad (5)$$

$$\varkappa_{1,2} = \sigma_m^i N_\pm \{(1+\cos^2\theta)N_\pm^2 - 2\varepsilon_{11} - 2i\varepsilon_{12}\}\{2\cos^2\theta N_\pm^4 - \varepsilon_{11}(1+\cos^2\theta)N_\pm^2\}^{-1}, \qquad (6)$$

$$\sigma_m^i = \frac{\sqrt{\pi}\,m^{2m-2}\sin^{2m-2}\theta c^2}{2^{m+3/2}m!\cos\theta V_A^2}(\beta_i N_\pm)^{2m-3}\exp(-z_m'^2),$$

$$z_m^i = (1 - m\omega_H^i/\omega)(\sqrt{2}\,\beta_i N_\pm \cos\theta)^{-1}, \quad \varepsilon_{11} = 1 - v_i/(1-u_i),$$

$$\varepsilon_{12} = -iv_i/\sqrt{u_i}(1-u_i).$$

If $|z_m^i| \lesssim 1$, then $\kappa_{1,2}/N_\pm \sim (\beta_i N_\pm)^{2m-3}$.

Waves characterized by frequencies $\omega \sim \omega_H^i$ (ω not necessarily close to $m\omega_H^i$) are also damped as a consequence of absorption in the electron gas (Landau damping). The refractive indices for these waves are given by Eq. (5) and the damping coefficients are

$$\varkappa_{2,3}/N_\pm = \mathrm{Im}\left\{\frac{1}{\varepsilon_{33}}[\varepsilon_{11}\sin^2\theta N_\pm^4 + (2\varepsilon_{12}\varepsilon_{23}\cos\theta\sin\theta - \varepsilon_{23}^2\cos^2\theta - (\varepsilon_{11}^2 + \varepsilon_{12}^2)\sin^2\theta)N_\pm^2 + \varepsilon_{11}\varepsilon_{23}^2] + \varepsilon_{22}'(\varepsilon_{11} - \cos^2\theta N_\pm^2)\right\} \times \{2\varepsilon_{11}(1+\cos^2\theta)N_\pm^2 - 4\cos^2\theta N_\pm^4\}^{-1}, \qquad (7)$$

where

$$\varepsilon_{23} = -i\tan\theta v_i(1 + i\sqrt{\pi}z_0^e w(z_0^e))/\sqrt{u_i},$$

$$\varepsilon_{22}' = i\,2\sqrt{\pi}(m_e/m_i)\sin^2\theta v_i z_0^e w(z_0^e)\beta_e^2 N_\pm^2/u_i,$$

$$\varepsilon_{33} = (2m_i/m_e)\,v_i(z_0^e)^2(1 + i\sqrt{\pi}z_0^e w(z_0^e)),$$

$$z_0^e = (\sqrt{2}\,\beta_e N_\pm \cos\theta)^{-1}.$$

The damping (7) is small; $\kappa_{2,3} \ll N_\pm$. Even if $|z_0^e| \lesssim 1$, i.e., $V_A \sim \beta_e c$, we find $\kappa_{2,3}/N_\pm \sim m_e/m_i$.

[1] V. P. Silin, Тр. ФИАН СССР (Proc. Inst. Phys. Acad. Sci. U.S.S.R.) **6**, 199 (1955).

[2] A. G. Sitenko and K. N. Stepanov, JETP **31**, 642 (1956), Soviet Phys. JETP **4**, 512 (1957).

[3] K. N. Stepanov, JETP **35**, 283 (1958), Soviet Phys. JETP **8**, 195 (1959).

[4] R. Z. Sagdeev and V. D. Shafranov, (Proceedings of the Second International Conference on the Peaceful Uses of Atomic Energy) Vol. I, Moscow, 1959, p. 202.

[5] V. D. Shafranov, Физика плазмы и проблема управляемых термоядерных реакций (Plasma Physics and the Problem of a Controlled Thermonuclear Reaction), Acad. Sci. U.S.S.R., 1958, Vol. IV, p. 426.

[6] V. N. Gershman, JETP **24**, 659 (1953).

Translated by H. Lashinsky
51

CURVES FOR THE PHOTOPROTON YIELD FROM THE C^{12} NUCLEUS

E. B. BAZHANOV

Leningrad Physico-technical Institute, Academy of Sciences, U.S.S.R.

Submitted to JETP editor August 14, 1959

J. Exptl. Theoret. Phys. (U.S.S.R.) **38**, 267-269 (January, 1960)

A previously described[1] scintillation telescope was used to investigate the depencence of the photo-

proton yield from the C^{12} nucleus on the peak energy of bremsstrahlung γ rays. Yield curves were simultaneously obtained for three proton energy intervals: 18.6 — 24.2 Mev, 24.2 — 29.9 Mev, and 29.9 — 38.7 Mev with average energies of 21.4, 27.0, and 34.3 Mev respectively. All the measurements were made with an angle $\theta = 57.5°$ with respect to the direction of the γ beam, and the maximum angular resolution of the telescope was $\pm 6.0°$. The target, 150 mg/cm^2 thick, was placed perpendicular to the beam. The absolute doses of the γ rays that had passed through the target for each peak γ energy were measured with a thick-walled copper ionization chamber, which had been calibrated with a calorimeter.[2] The sensitivity of the ionization chamber to bremsstrahlung γ rays was practically independent of the peak γ energy within the energy interval used.

Figures 1, 2, and 3 present the experimental results for the average proton energies given above. Smooth curves (labeled a) were plotted through the experimental points, and after a preliminary procedure to smooth out the original variations, the Penfold-Leiss[3] method was used to convert them into cross section curves (labeled b). The statistical accuracy of the experiment was insufficient to prove the existence of a second maximum in the cross section curve in Fig. 1. However, since the yield curve is seen to rise generally right up to the largest energies, it appears altogether probable that there is a long "tail" like the one indicated in Fig. 3. The curves labeled c represent Dedrick's calculations[4] based on a quasi-deuteron mechanism of γ-nucleus interaction. It must be noted that agreement with the experiment for high energies is entirely satisfactory. Similar agreement has been observed[5] in the case of photoprotons with an average energy of 37 Mev. The arrows to the right along the abscissa indicate the minimum γ energies necessary for the formation of protons with a minimum energy for the corresponding interval. These energies were obtained from the known kinematical relation, which is based on the conservation laws for the interaction between γ quanta and a quasi-deuteron in the nucleus:

$$E_\gamma = \frac{2E_p}{1 - E_p'/M + p' \cos\theta / M},$$

$$E_p = E_{p\,min,} + \frac{1}{2} E_{\text{binding}}(\gamma, pn).$$

In our opinion the wide maximum observed in the case of comparatively low γ energies is to a considerable extent due to a contribution by the $C^{12}(\gamma p)B^{11}$ reaction. In favor of this view is the good correspondence which exists between the experimental thresholds for the reaction and those predicted on the basis of the relation

$$E_{\gamma\,min} = E_{p\,min} + E_{\text{binding}}(\gamma p)),$$

where $E_{\text{binding}}(\gamma p) = 16$ Mev (the arrows to the left). Shklyarevskiĭ[6] has used the harmonic oscillator potential to investigate the interaction of γ quanta with any individual nucleon in a nucleus or with the remaining non-participating nucleons on the basis of an independent particle model. The shaded areas in the figures represent the contribution by $(1p)^4$ and $(1s)^2$ shells as determined by Shklyarevskiĭ's formulae. The parameter $\epsilon = \hbar\omega_0$, which represents the separation between the shells, is assumed to be equal to 15.5 Mev on the basis of Hofstadter's data.[7] The dependence of the well depth, V_0, on the proton energy[8] was also taken into consideration. The effective well depth was computed from the following relation:

$$V^l_{\text{eff}} = V_0(E_p) - \overline{V}^l, \qquad \overline{V}^l = \int_0^\infty \varphi^*_{nlm}(r)\, V(r)\, \varphi_{nlm}(r)\, dr,$$

where $\varphi_{nlm}(r)$ is the oscillator wave function. When $l = 0$, $\overline{V^0} = \frac{3}{4}\epsilon$; when $l = 1$, $\overline{V^1} = \frac{5}{4}\epsilon$. The

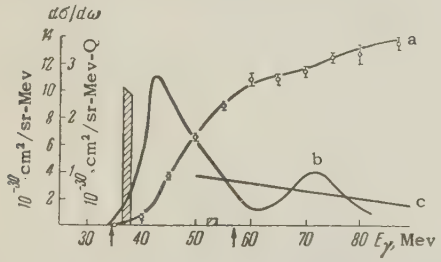

FIG. 1. Photoproton yield and cross section curves for C^{12} with $\overline{E}_p = 21.4$ Mev. The right ordinate scale refers to curve a and the left to curves b and c and the shaded areas. The errors are statistical.

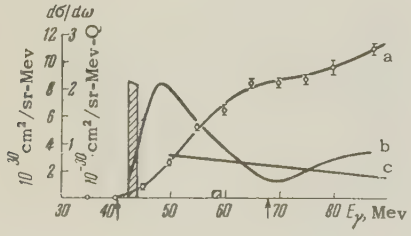

FIG. 2. The same as in Fig. 1, but for photoprotons with $\overline{E}_p = 27.0$ Mev.

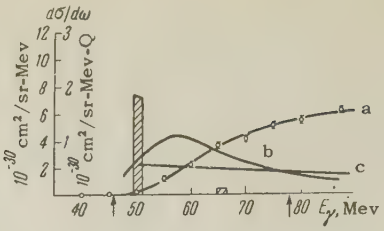

FIG. 3. The same as in Fig. 1, but for photoprotons with $\overline{E}_p = 34.3$ Mev.

contribution from the $(1s)^2$ shell does not exceed 6% of the contribution from the $(1p)^4$ shell in all cases.

Shown below for comparison are the integral cross sections computed with the Shklyarevskiĭ formulae and those obtained experimentally:

Interval of proton energy, Mev	18.6 – 24.2	24.2 – 29.9
Integration interval of experimental data, Mev	34 – 63	42 – 70
Integral cross section obtained experimentally, 10^{-30} cm² Mev/sr	135.2 ± 20.6	120.6 ± 18.9
Computed integral cross section, 10^{-30} cm² Mev/sr	10.5	8.8

The difference by a factor of ten should be considered too large, even making allowances for the approximate nature of the theoretical computations, as well as for the fact that a quasi-deuteron interaction mechanism may also introduce a certain contribution to the experimental integral cross section. The 5 — 7 Mev shift toward high γ energies of the experimental maximum that can be seen in all the graphs relative to the computed contribution from the $(1p)^4$ shell can be explained by the fact that all of Shklyarevskiĭ's calculations are based on the assumption that the final nucleus remains in the ground state, which, of course, is hardly probable.

The author wishes to thank Prof. A. P. Komar and his laboratory associates for their interest in this paper and also L. E. Lazarev for kindly making possible the use of the tables[3] for computing the cross section curves.

[1] Bazhanov, Volkov, and Kul'chitskiĭ, JETP **35**, 322 (1958), Soviet Phys. JETP **8**, 224 (1958).

[2] S. P. Kruglov, J. Tech. Phys. (U.S.S.R.) **28**, 2310 (1958), Soviet Phys.-Tech. Phys. **3**, 2120 (1958).

[3] A. S. Penfold and J. E. Leiss, Analysis of Photo Cross Sections, University of Illinois (1958).

[4] K. G. Dedrick, Phys. Rev. **100**, 58 (1955).

[5] Whitehead, McMurray, Aitken, Middlemas, and Collie, Phys. Rev. **110**, 941 (1958).

[6] G. M. Shklyarevskiĭ, JETP **36**, 1492 (1959), Soviet Phys. JETP **9**, 1057 (1959).

[7] R. Hofstadter, Ann. Rev. Nuclear Sci. **7**, 231 (1957).

[8] A. E. Glassgold, Revs. Modern Phys. **30**, 419 (1958).

Translated by A. Skumanich
52

MAGNETIC ANISOTROPY OF THE DISORDERED ALLOY Ni_3Mn *AT HELIUM TEMPERATURES*

N. V. VOLKENSHTEĬN and M. I. TURCHINSKAYA

The Metal Physics Institute, Academy of Sciences, U.S.S.R.

Submitted to JETP editor August 28, 1959

J. Exptl. Theoret. Phys. (U.S.S.R.) **38**, 270-271 (January, 1960)

FOR polycrystalline specimens of the alloy Ni_3Mn in the disordered state, a number of workers[1-3] have shown that the reversible magnetization curves taken at liquid helium temperatures lie significantly below the curves taken at liquid hydrogen temperature and do not attain saturation at tens of thousands of oersteds. Magnetization curves of this type could be due to a rapid temperature variation of the magnetic anisotropy. To resolve this question a study is required on single crystals — the magnetization curves being taken in various crystallographic directions. We have performed such a study.

From a large single crystal of the alloy Ni_3Mn with face-centered cubic lattice in the disordered state, specimens of prismatic shape ($1.2 \times 1.2 \times 18$ mm³) were cut, the long axes of which were parallel respectively to the three crystallographic directions: [111], [110], [100]. The reversible magnetization curves of these specimens were taken at room temperature and at liquid nitrogen, hydrogen, and helium temperatures.

The results are given in the figure. From the curves it is seen that at room temperature for all crystallographic directions there is a linear dependence of induction on field, and there is no anisotropy.

On going to nitrogen temperature the character of the curves undergoes a marked change. Firstly, the curves $4\pi I(H)$ assume a form typical of a ferromagnet. Secondly, magnetic anisotropy appears; it increases on lowering the temperature to liquid-hydrogen temperature, but does not change essentially on further cooling to liquid-helium temperature. The crystallographic direction [100] remains the difficult, [111] the easy, and [110] the intermediate direction throughout the temperature interval studied (from 77.8 to 4.2°K). In spite of the fact that the magnetic anisotropy (a measure of which is the area included between the curves for the [100] and [111] axes) does not in-

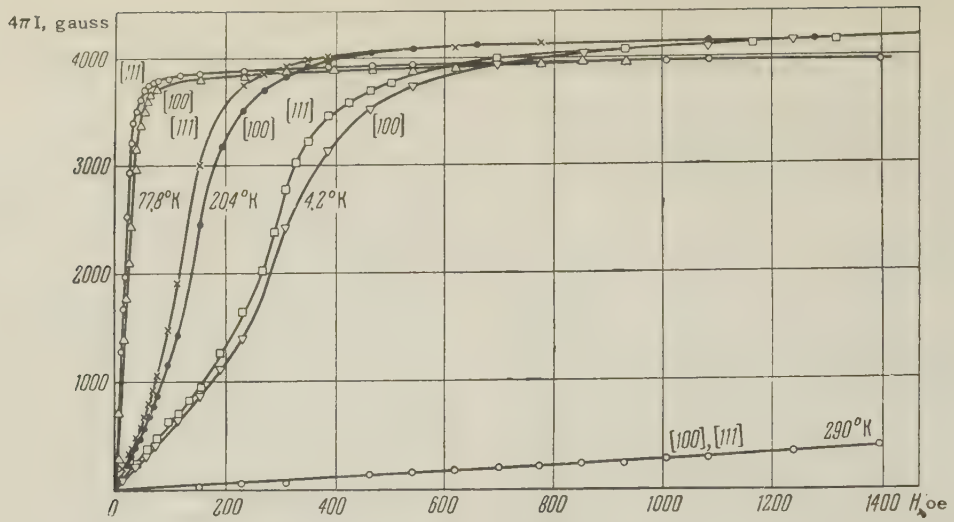

crease significantly on changing the temperature from 20.4 to 4.2° K, the curves for the easy and difficult directions at 4.2° K lie considerably below the curves at 20.4° K and magnetic saturation requires large fields.

It should be remarked that the saturation fields at all temperatures are much smaller than the saturation fields obtained earlier[1,2] in polycrystalline specimens. Measurements of the coercive force H_c show that at nitrogen temperature for all crystallographic directions it is fractions of an oersted, but at hydrogen temperature it is of the order of oersteds. This data differs greatly from the data obtained on polycrystalline specimens in which we obtained for H_c more than a hundred oersted at nitrogen temperature and a thousand oersted at hydrogen temperature. The main explanation for this probably resides in the fact that, because various types of structural distortions are present, polycrystalline specimens are much harder magnetically than single-crystal specimens of the same material.

An analysis of the results obtained shows that the increase of saturation field with decreasing temperature — even for the easy direction of magnetization (see curves for the [111] axis at 77.8, 20.4, and 4.2° K) — cannot be due to an increase in the magnetic anisotropy when the ferromagnetic alloy studied is cooled to a low temperature. A more reasonable assumption is that, at temperatures below nitrogen in the disordered alloy Ni_3Mn, a transition is possible from a ferromagnetic to an antiferromagnetic state with comparatively low critical fields ($\leq 10^3$ oe) at which magnetic saturation is attained (parallel magnetizations of the magnetic sublattices).

From what has been said follows the necessity for neutron diffraction studies and detailed measurements of the temperature dependence of the magnetic anisotropy constant, in order to resolve definitely the unusual magnetic properties of Ni_3Mn alloys in the disordered state at low temperatures.

The authors are grateful to Dr. R. Bozorth and Dr. K. Williams for kindly providing the single crystal for the investigation.

[1] Volkenshteĭn, Turchinskaya, and Galoshina, JETP **35**, 1312 (1958), Soviet Phys. JETP **8**, 916 (1959).

[2] Kouvel, Graham, and Jacobs, International Conference on Magnetism in Grenoble, June 2 — 6, 1958.

[3] Kouvel, Graham, and Becker, J. Appl. Phys. **29**, 518 (1958).

Translated by K. F. Hulme
53

ASYMMETRY OF URANIUM FISSION AT HIGH PROTON ENERGIES

A. I. OBUKHOV

Radium Institute, Academy of Sciences, U.S.S.R.

Submitted to JETP editor August 28, 1959

J. Exptl. Theoret. Phys. (U.S.S.R.) **38**, 271-273 (January, 1960)

AT low bombarding-particle energies, the fission of uranium is mostly asymmetrical. The mass curve of the fission product yield has two maxima with a deep trough between them. As the particle

energy increases, the contribution of symmetrical fissions increases and at a certain energy the curve becomes a single-hump one (see, for example, the survey article by Lavrukhina[1]). At the same time, a certain broadening of the mass curve takes place.[1-3] When uranium is bombarded with 660-Mev protons, a relative increase is observed in the number of fission events which are asymmetrical in range with increasing nuclear excitation energy.[4]

We have investigated the asymmetry of the ranges of fission fragments of uranium in P-9 (ch) nuclear emulsions at proton energies of 460 and 660 Mev. The asymmetry in the ranges of the fission fragments corresponds in general to the asymmetry in the masses.

Figure 1 shows the distribution of fission events as a function of the ratio of the ranges of the light and heavy fragments. The figure shows also the corresponding distribution for the case of fission of U^{235} by thermal neutrons.[4] A comparison of the distributions shows that as the proton energy is increased from 460 to 660 Mev, the fissions that are strongly asymmetrical in range make a relatively larger contribution.

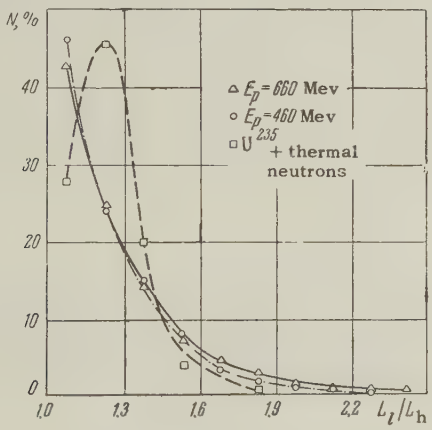

FIG. 1

According to the liquid-drop model, the lowest barrier for uranium fission is possessed by the symmetrical form of fission.[5] Calculations based on this model give a difference of ~ 6 Mev in the value of the energy of deformation for the asymmetrical uranium fission (with dimensional asymmetry of 1.5) and the symmetrical form.[6] If $\Delta E = E_a - E_s$ is the difference in the activation energies for the asymmetrical and symmetrical forms of fission, then, according to statistical theory, the ratio of their probabilities is

$$W = \sigma_s/\sigma_a \sim \exp(\Delta E/T), \qquad (1)$$

where T is the temperature of the nucleus.

As the temperature of the nucleus increases, the relative contribution of fissions which are asymmetrical in mass will increase at $\Delta E > 0$, in accordance with (1). We employ this expression to explain the increase in the contribution of the product of asymmetrical (A = 67) and approximately symmetrical (A = 115) disintegrations in the bombardment of uranium by protons of 70 — 340 Mev.[7] We assume that these are all the fission products prior to the evaporation of the nucleons, since the yields of these products are vanishingly small at low excitation energies. We use as the nuclear fission temperature the temperature corresponding to average excitation energy of the nuclei. The average excitation energy was calculated on the basis of the laws of conservation of energy and momentum and the assumption that the momentum of the cascade particles is carried away by a single particle in the direction of the incident protons. The values of the front component of the nuclear momentum necessary for this purpose were determined by interpolating the known experimental values at certain proton energies. According to (1), log W should depend linearly on 1/T at ΔE = const. Figure 2 shows the experimental values of σ_{115}/σ_{67} vs. 1/T in a semilogarithmic scale.

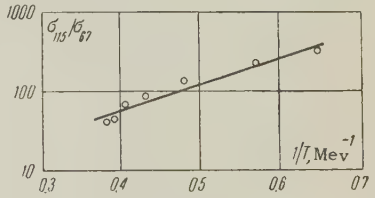

FIG. 2

It was assumed that $T = 2.92\sqrt{U/A}$, where U is the excitation energy and A the mass number of the fissioning nucleus. If a straight line is drawn through the points, the slope of the line determines the difference in the activation energies. For the selected products, $\Delta E \approx 8$ Mev. As the excitation energy is increased, this fission asymmetry will correspond to products with lower mass numbers. If A = 67 and 115 is invariably used for the fission products at the given asymmetry, this analysis will lead to approximately double the value of ΔE. Consequently, and also in view of the roughness with which the nuclear temperature has been determined for symmetrical and asymmetrical fissions from the average excitation energy and in view of the possible contribution due to fission after emission of a certain number of nucleons, the value given for ΔE is only tentative.

At high particle energies the mass curve is a

result of superposition of fission products of uranium nuclei before and after evaporation of the nucleons. The fission asymmetry of nuclei with small excitation energy is determined by the influence of certain factors, among which the shell effect can play a large role. At large excitation energy the influence of these factors apparently does not manifest itself during the instant of fission. If it is assumed that fission asymmetry of such nuclei is determined by Eq. (1), so that the most probable is symmetrical fission, and that the relative contribution of the asymmetrical form of fission increases with increasing excitation energy, then the change in shape of the mass curve of the fission products of uranium with increasing particle energy becomes understandable. Fairhall et al.[8] have shown that nuclear fission near bismuth at excitation energies up to ~40 Mev occurs prior to neutron evaporation. The increase in the fraction of asymmetrical fission with increasing temperature, in accordance with (1), agrees qualitatively with the observed broadening of the mass curves of the fission products of bismuth with increasing excitation energy.[4,9] The broadening of the mass curve of the fission products with increasing atomic number of the target, found in bombardment by 450-Mev protons,[10] may be, in particular, the result of the increase in the average excitation energy with increasing atomic number of the target.

Among the experiments performed up to now on the fission of nuclei, two groups can be segregated. In accordance with the experiments of the first group, the fission of nuclei near uranium competes successfully with the evaporation of neutrons over a broad range of excitation energies.[11,12] The investigations of the second group[13] are evidence that the fission of uranium bombarded with high energy protons occurs essentially after the excitation energy has been removed by nucleon evaporation. The "cold" nucleus can have a large angular momentum. Consequently, and also as a result of the change in the composition of the nucleons, the fission characteristics of such a nucleus, including the asymmetry, may differ from the characteristics of nuclear fission in the case of small particle energies.

In conclusion, the author expresses his gratitude to Prof. N. A. Perfilov for interest in this work.

[1] A. K. Lavrukhina, Usp. Khimii **27**, 517 (1957).

[2] Sugihara, Drevinsky, Troianello, and Alexander, Phys. Rev. **108**, 1264 (1957).

[3] Bunney, Scadden, Abriam, and Ballou, Second UN Intern. Conf. on the Peaceful Uses of Atomic Energy, 1958, P-643.

[4] V. P. Shamov and O. V. Lozhkin, JETP **29**, 286 (1955), Soviet Phys. **2**, 111 (1956).

[5] S. Frankel and N. Metropolis, Phys. Rev. **72**, 914 (1947).

[6] D. R. Inglis, Ann. Phys. **5**, 106 (1958).

[7] Stevenson, Hicks, Nervik, and Netheway, Phys. Rev. **111**, 886 (1958).

[8] Fairhall, Jensen, and Neuzil, Second UN Intern. Conf. 1958, P-677.

[9] A. W. Fairhall, Phys. Rev. **102**, 1335 (1956); Murin, Preobrazhenskiĭ, and Titov, Izv. Akad. Nauk SSSR, OkhN **4**, 577 (1955); L. G. Jorda and N. Sugarman, Phys. Rev. **99**, 1470 (1955).

[10] P. Kruger and N. Sugarman, Phys. Rev. **99**, 1459 (1955).

[11] Butler, Bowles, and Brown, Second UN Intern. Conf., 1958, P-6.

[12] Vandenbosch, Thomas, Vandenbosch, Glass, and Seaborg, Phys. Rev. **111**, 1358 (1958); B. D. Pate, Canad. J. Chem. **36**, 1707 (1958).

[13] V. P. Shamov, Физика деления атомных ядер (Physics of Fission of Atomic Nuclei), Atomizdat, M, 1957, p. 129; G. N. Harding and F. J. Farley, Proc. Phys. Soc. **A69**, 853 (1956).

Translated by J. G. Adashko
54

ON THE CROSS SECTION FOR COMPOUND NUCLEUS FORMATION IN THE INTERACTION OF ATOMIC NUCLEI

V. V. BABIKOV

Joint Institute of Nuclear Research

Submitted to JETP editor September 18, 1959

J. Exptl. Theoret. Phys. (U.S.S.R.) **38**, 274-276 (January, 1960)

THE available data[1] on the nuclear reactions induced by multiply charged ions indicate that one of the basic processes in these reactions is the formation of a compound nucleus with high energy of excitation and its subsequent decay.

The cross section for compound nucleus formation, $\sigma(E)$, can be calculated on the basis of a model in which the colliding nuclei have a sharp

spherical boundary and are completely absorptive for particles entering the sphere of nuclear interaction.

The fact that the problem contains the large parameter* $\eta = Z_1Z_2e^2/\hbar v \gg 1$ indicates that in this model the cross section $\sigma(E)$ must be close to the classical value $\sigma(E) = \pi R^2(1 - B/E)$ for ion energies above the Coulomb barrier $B = Z_1Z_2e^2/R$ ($R = R_1 + R_2$ is the radius of the region of nuclear interaction). The condition of quasi-classical motion for an ion with angular momentum $l\hbar$ near the boundary $r = R$, $|d\lambda\!\!\!^{-}_l(r)/dr| \ll 1$, can be written in the form (we take advantage of the fact that in reactions induced by multiply charged ions the parameter $\rho = R/\lambda\!\!\!^{-}(\infty) \gg 1$)†

$$1 - \beta - \gamma_l^2 \geqslant \left(\frac{2-\beta}{9\rho}\right)^{2/3}, \qquad \beta = \frac{2\eta}{\rho}, \qquad \gamma_l = \frac{l+1}{\rho}. \quad (1)$$

According to the classical model of a black sphere the values of l satisfying condition (1) with an equality sign give the following contribution to the cross section:

$$\sigma = \pi R^2\left[1 - \beta - \left(\frac{2-\beta}{9\rho}\right)^{2/3}\right]. \quad (2)$$

The contribution from angular momenta which do not satisfy condition (1) can be calculated for arbitrary values of β with the help of a simple quantum mechanical model close to the classical model.‡ In view of the large excitation energy and, hence, of the high level density of the compound nucleus it is appropriate to use the resonanceless theory with a nuclear potential in the form of a square well with radius R. The depth U plays practically no role in reactions with multiply charged ions. Since the nucleons in the ion are bound more strongly than the nucleons in the ground state of the compound nucleus (for target nuclei with $A > 50$), part of the kinetic energy of the ion is used for the "unpacking," i.e., the lowest bound state level in the well lies above zero. Therefore $U/E < \pi^2/4\rho^2 \ll 1$, and the well depth can be neglected in comparison with the energy E.

Keeping this remark in mind, we now consider the known[2] expression for the partial reaction cross section in this model:

$$\sigma_l = \pi\lambda\!\!\!^{-2}(2l+1)\,4\,s_l\rho/[\Delta_l^2 + (s_l+\rho)^2]. \quad (3)$$

The quantities s_l and Δ_l are expressed in terms of the Coulomb functions $G_l(\rho)$ and $F_l(\rho)$ and their derivatives $G_l'(\rho)$ and $F_l'(\rho)$. The presence of the large parameters ρ and η in the problem allows us to obtain simple analytic expressions for s_l and Δ_l and, hence, for σ_l in the form of asymptotic expansions in terms of inverse powers of these parameters. We use contour integral representations[3] in the complex plane for G_l and F_l and shift the parameter η to the exponent under the integral. By the method of steepest descent we then obtain

$$\left.\begin{aligned} s_l &= \frac{\pi 3^{1/3}(2-\beta)^{1/3}}{\Gamma^2(1/3)}\rho^{2/3}[1 + O(\rho^{-1/3})], \\ \Delta_l &= -\frac{\pi(2-\beta)^{1/3}}{3^{1/3}\Gamma^2(1/3)}\rho^{2/3}[1 + O(\rho^{-1/3})], \end{aligned}\right\} |1 - \beta - \gamma_l^2| \ll \left(\frac{2-\beta}{9\rho}\right)^{2/3};$$

$$s_l = \rho a\left[\frac{(a+\gamma_l)^2+1}{(a-\gamma_l)^2+1}\right]^{1/2}\exp\left[-\rho\left(\gamma_l \ln\frac{(a+\gamma_l)^2+1}{(a-\gamma_l)^2+1} + \beta\tan^{-1}\frac{2a}{2-\beta} - 2a\right)\right][1 + O(\rho^{-1/2})], \quad (4)$$

$$\Delta_l = -\rho a[1 + O(\rho^{-1})], \quad a = \gamma_l^2 + \beta - 1 \geqslant \left(\frac{2-\beta}{9\rho}\right)^{2/3}. \quad (5)$$

Summing over all l with the corresponding extrapolation to the values l determined by the equalities

$$1 - \beta - \gamma_l^2 = \pm\left(\frac{2-\beta}{9\rho}\right)^{2/3},$$

we find** for the different regions of the ion energy ($\beta = B/E$, terms $\sim \rho^{-4/3}$ are neglected)

$$\sigma = 2\pi R^2\rho^{-1/3}\exp\left[-\rho\left(\beta\tan^{-1}\frac{2\sqrt{\beta-1}}{2-\beta} - 2\sqrt{\beta-1}\right)\right], \quad \beta - 1 \geqslant \left(\frac{2-\beta}{9\rho}\right)^{2/3};$$

$$\sigma = 2\pi R^2\rho^{-1}\left\{\exp\left(-\frac{4}{27}\right) + \frac{2\pi}{3\Gamma^2(1/3)}\left[1 + \left(\frac{2-\beta}{9\rho}\right)^{-2/3}(1-\beta)\right]\right\}, \quad |1-\beta| \leqslant \left(\frac{2-\beta}{9\rho}\right)^{2/3};$$

$$\sigma = \pi R^2\left[1 - \beta - \left(\frac{2-\beta}{9\rho}\right)^{2/3} + \frac{2(2-\beta)}{\rho}\left(\exp\left(-\frac{4}{27}\right) + \frac{4\pi}{3\Gamma^2(1/3)}\right)\right], \quad 1 - \beta \geqslant \left(\frac{2-\beta}{9\rho}\right)^{2/3}. \quad (6)$$

The comparison of the cross sections (6) with the experimental data of Druin and Polikanov[4] on the fission cross sections of bismuth bombarded by the ions of carbon, nitrogen, and oxygen, which practically coincide with the corresponding cross sections for the formation of a compound nucleus, leads to good agreement (see the figure) for the following choices of the parameter R:

C^{12}, $R = 1.17 \cdot 10^{-12}$ cm;
N^{14}, $R = 1.24 \cdot 10^{-12}$ cm;
O^{16}, $R = 1.27 \cdot 10^{-12}$ cm.

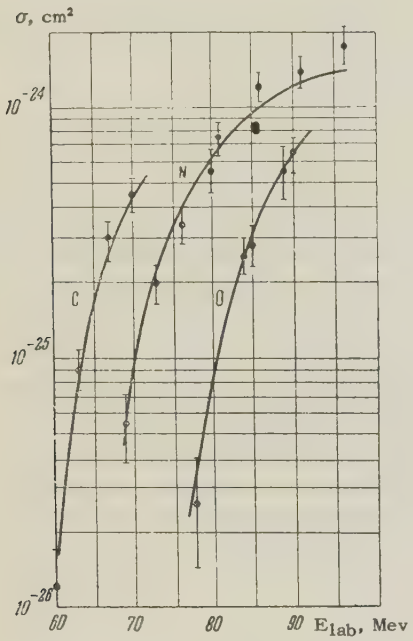

Thomas[5] and Piliya[6] also considered the cross section for compound nucleus formation caused by heavy ions. Thomas calculated the cross sections numerically for several ions and target nuclei, using formula (3) with a definite choice of the nuclear potential parameters R and U, which makes it difficult to use his results in the case of arbitrary nuclei (see also footnote‡). The results of Piliya are quite different from those quoted above, since he made use of an incorrect asymptotic expansion.

In conclusion I express my gratitude to G. N. Flerov for his interest in this work and also to G. N. Vyalov and S. M. Polikanov for fruitful remarks.

*The whole discussion is in the center-of-mass system of the colliding nuclei.

†Condition (1) differs from $|d\lambda(R)/dR| \ll 1$ by a coefficient ~ 1 which was introduced to be used in connection with condition (4).

‡The condition of complete absorption at the nuclear boundary in the quantum mechanical description (only incoming waves in the region $r < R$) is different from the analogous condition in the classical model. The use of the quantum description for all angular momenta would lead to a smaller cross section which does not go over into the classical result for $\hbar \to 0$ ($\rho \to \infty$).

**In the same way we can obtain expressions for the average moment of inertia of the nucleus.

[1] G. N. Flerov, Report at the II International Conference on Peaceful Uses of Atomic Energy in Geneva, vol. 1, Atomizdat, p. 272 (1959).

[2] J. Blatt and V. Weisskopf, Theoretical Nuclear Physics, Wiley, N.Y. (1952).

[3] N. F. Mott and H. S. W. Massey, The Theory of Atomic Collisions, Oxford (1952).

[4] V. A. Druin and S. M. Polikanov, JETP **36**, 744 (1959), Soviet Phys. JETP **9**, 522 (1959).

[5] T. D. Thomas, The Cross Section for Compound Nucleus Formation in Heavy Ion Induced Reactions (preprint).

[6] A. D. Piliya, JETP **37**, 583 (1959), Soviet Phys. JETP **10**, 413 (1960).

Translated by R. Lipperheide
55

*PHOTOPRODUCTION OF POSITIVE PIONS IN HYDROGEN NEAR THRESHOLD**

É. G. GORZHEVSKAYA, V. M. POPOVA, and F. R. YAGUDINA

P. N. Lebedev Physics Institute, Academy of Sciences, U.S.S.R.

Submitted to JETP editor September 19, 1959

J. Exptl. Theoret. Phys. (U.S.S.R.) **38**, 276-278 (January, 1960)

EXPERIMENTS on photoproduction of pions from nucleons near threshold play an essential role in testing the meson theory based on dispersion relations. In particular, there is great interest in the behavior of the square of the matrix element for the photoproduction of positive pions near threshold, since according to the theory the direct interaction of the photon with the meson current leads to an increase in the square of the matrix element as the photon energy decreases. Besides this, a comparison of the π^+ photoproduction cross section for hydrogen near threshold with the π^- photoproduction cross section for neutrons[1,2] allows us to match the experimental data with the predictions of meson theory about the quantity σ^-/σ^+ near threshold. Our work is devoted to clarifying these questions.

The differential cross section for positive pion photoproduction was measured for the proton energy intervals 152.9 — 158.3 and 158.3 — 161 Mev. It was convenient to measure the energy in a given region by the CH_2—C subtraction method. The Coulomb fields present in the nucleus strongly decrease the possibility of the formation of low-energy positive pions from carbon.† In addition, such a method gives the possibility of using thin targets, which allow the detection of low-energy mesons and free us from the necessity of introducing corrections for energy loss and the scattering of mesons in the target.

The mesons formed in the polyethylene and carbon targets (by the action of a gamma ray beam from the synchrotron of the Joint Institute for Nuclear Research with a maximum energy of 263 Mev) were detected by photographic plates. The plates were subjected to a double scanning. In this, the effectiveness of discovering mesons was 90%, on an average. Those π-μ decays found in the emulsions were chosen whose muon tracks ended in the emulsion.

The experimental geometry was such that mesons with energies from 0.5 to 6 Mev at angles of 60° and 120° to the proton beam in the laboratory system were detected in the plates.

To find the cross sections in the center-of-mass system, all the events were broken down by energy and angular intervals. The cross section was taken as the weighted average of all the values obtained.

The values of the cross sections $d\sigma^+/d\Omega$ for 120° and the square of the matrix element $(d\sigma^+/d\Omega)\pi/w$ are given below, where w is the ordinary kinematic factor

$$\omega = \eta_i\omega/(1+\omega/M)(1+\nu/M);$$

η, ω, and ν are respectively the momentum, total meson energy, and photon energy in the center-of-mass system, and M is the proton mass. Here we give the values of the square of the matrix element, calculated according to the formula

$$\frac{d\sigma^+}{d\Omega}\frac{\pi}{\omega} = \frac{2e^2f^2}{\mu^2\nu\omega}\left[1-\frac{\eta_i^2}{2\nu^2}\frac{\sin^2\theta}{(1-\eta_i\cos\theta)^2}-\frac{g_n+g_p}{M}\left(1-\frac{\eta^2}{2}\right)\right].$$

The coupling constant f^2 is taken as 0.08.

Photon energy E_γ, Mev (lab.)		155.6	159.6
$10^{30}\frac{d\sigma^+}{d\Omega}$, $\frac{cm^2}{sr}$ (c.m.)		3.4±0.6	4.2±1.7
$10^{28}\frac{d\sigma^+}{d\Omega}\frac{\pi}{\omega}$, $\frac{cm^2}{sr}$ (c.m.)	experiment	0.6±0.1	0.5±0.2
	theory	0.621	0.577

It should be noted that the value of the π^+ photoproduction cross section for hydrogen at E_γ = 160 Mev given in the recently published work of Barbaro et al.[3] agrees well with our data.

The figure‡ comparing the theoretical dependence of the square of the matrix element on the photon energy with experimental data from various authors, shows that the increase in the squared matrix element actually takes place up to threshold, and confirms the correctness of taking into account the direct interaction of the photon with the meson beam in the extrapolation to threshold.

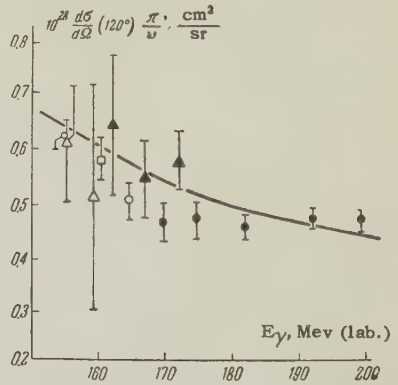

The dependence of the square of the matrix element of pion photoproduction on the energy of the photons. The curve was calculated from dispersion theory. △ — data from our work, □ — data from reference 3, ● — from reference 4, ○ — from reference 5, ▲ — data of Adamovich, Larionova, and Kharlamov (private communication).

The value of the ratio σ^-/σ^+, calculated on the basis of our data and of data on the photoproduction of pions in the same energy interval[1,2] is $\sigma^-/\sigma^+ = 1.3 \pm 0.3$, which agrees well with the predictions of meson theory.

The authors express thanks to Academician V. I. Veksler for directing the work and to M. I. Adamovich for his interest in the work and his participation in examining the results.

*The results in the present letter were given in the summary report of Bernardini at the Kiev conference on high energy physics, July, 1959.

†It is interesting to note that the cross section for positive pion photoproduction from one proton of carbon is ~ 0.1 of the cross section for hydrogen.

‡The figure is taken from the report of Bernardini at the conference on high energy physics at Kiev, 1959.

[1] Adamovich, Kuzmicheva, Larionova, and Kharlamov, JETP **35**, 27 (1958), Soviet Phys. JETP **8**, 21 (1959).

[2] A. Baldin, Nuovo cimento **8**, 569 (1958).

[3] Barbaro, Goldwasser, and Carlson-Lee, Bull. Am. Phys. Soc. **4**, 23 (1959).

[4] Beneventano, Bernardini, Carlson-Lee, Stoppini, and Tau, Nuovo cimento **4**, 323 (1956).

[5] Leiss, Robinson, and Penner, Phys. Rev. **98**, 201 (1955).

Translated by W. Ramsay
56

QUASISTABLE STATES WITH LARGE ISOTOPIC SPIN IN LIGHT NUCLEI

Ya. B. ZEL'DOVICH

Institute of Theoretical and Experimental Physics, Academy of Sciences U.S.S.R.

Submitted to JETP editor September 24, 1959

J. Exptl. Theoret. Phys. (U.S.S.R.) **38**, 278-280 (January, 1960)

We consider an odd nucleus A with one excess neutron, with a minimum value of isotopic spin $T = \frac{1}{2}$ in the ground state, and with a neutron binding energy Q. The excited states of the nucleus A* with excitation energy $E > Q$ have as a rule a rather large probability of neutron emission, i.e., a large width Γ_n of the process $A^* \rightarrow B + n$, where B is an even nucleus.

Let the ground state of the nucleus B have $T = 0$, and let the state B* with $T = 1$ have an excitation energy Δ. We assume that the nucleus A has an excited state A_3^* with $T = \frac{3}{2}$ and excitation energy E_3 such that $Q < E_3 < Q + \Delta$. The decay of A_3^* to $B^* + n$ is energetically impossible, while the decay of A_3^* into $B + n$ proceeds via a change in isotopic spin and should therefore have an anomalously small width Γ_n. The state A_3^* is quasistable and should appear in a unique manner in the scattering of neutrons by nuclei B, and also in the photoeffect $A + \gamma = B + n$.

When n is scattered by B the isotopic spin of the system in the initial state is $T = \frac{1}{2}$, and it is usually assumed that states with $T = \frac{3}{2}$ should make only a small contribution to the scattering cross section. However, if a quasistate exists, then sharp scattering resonance takes place at a neutron energy $E_n = E_3 - Q$, with a maximum cross section

$$4\pi\lambda^2(2J + 1)/(2S + 1).$$

The low probability of the process, connected with the disturbance of the isotopic spin, manifests itself not in a reduction in the scattering cross section, but in a reduction of the width of the resonance scattering. Therefore observation of resonance is quite possible if the neutrons are sufficiently monochromatic.

At resonance the increase in the scattered cross section will be accompanied by an increased probability of the process B(n, γ)A, since $\sigma_{n,\gamma}/\sigma_{sc} = \Gamma_\gamma/\Gamma_n$ and an anomalously small Γ_n should give* an anomalously large Γ_γ/Γ_n. Incidentally, the inequality $\Gamma_\gamma/\Gamma_n \ll 1$ remains in force, since $\Gamma_n \sim e^2$, when the isotopic spin is disturbed by the Coulomb interaction, like Γ_γ, which contains, however, other small factors, $(v/c)^u$, $(R/\lambda\!\!\!^{-})^v$, and $(\hbar/Mc\lambda\!\!\!^{-})^w$ in degrees that depend on the type of transition (for E1: u = 2, v = 2, and w = 0; for M1: u = v = 0, and w = 2, etc).

The existence of a quasistable A_3^* should lead to a narrow resonance in the reverse process† A(γ, n)B and also to resonant scattering of γ by A. Incidentally, owing to the inequality $\Gamma_\gamma/\Gamma_n \ll 1$, the latter process can apparently not be observed.

The state A_3^* forms an isotopic multiplet with the ground state of the nucleus with three excess neutrons, and, by introducing a known Coulomb correction, it is possible to determine the expected position of the quasistable level. Thus, knowing the masses[1] of the boron isotopes B^{12} and B^{13}, it is possible to determine the energies of the corresponding states of C_2^{12*} ($T = 1$) and C_3^{13*} ($T = \frac{3}{2}$). The result (in our notation) is $E_3 = 11.2$ Mev at $Q = 4.95$ Mev and $\Delta = 11.54$ Mev. Consequently, the level C_3^{13*} should be quasistable, since its energy is insufficient for decay into $C_2^{12*} + n$.

One should expect a narrow resonance in the scattering of n by C^{12} at $E_n = 11.2 - 4.95 = 6.25$ Mev, corresponding to a neutron energy of 7.20 Mev in the laboratory system.

From the similarity between C^{13} in the state with $T = \frac{3}{2}$ and the ground state of B^{13} one expects C_3^{13*} to be in the state $\frac{3}{2}^-$, which leads to a scattering of neutrons in the state $P_{3/2}$ on C^{12}, with a cross section

$$4\pi\lambda^2(2J + 1)/(2S + 1) = 0.8 \text{ b}.$$

A relatively narrow resonance was observed experimentally[2] at $E_n = 6.30$ Mev, along with a superposition of two resonances at $E_n = 7.4$ and 8.7 Mev.

The state of interest to us can be investigated by studying the angular distribution and polarization of the scattered neutrons. On the other hand, at least in principle, there is a possibility of ascertaining the existence of the unknown isobars by resonance in the scattering of neutrons by stable nuclei. Thus, narrow resonance in neutron scattering on Be^{10} or C^{14} could denote the existence of stable (with respect to emission of neutrons) nuclei Li^{11} or B^{15}.

I take this opportunity to express my gratitude to V. I. Gol'danskiĭ for a discussion.

*$A_s \rightarrow A + \gamma$ is allowed, Γ_γ has a normal value.

†It is possible that the best method of observing the quasi-stable level is to let the reaction proceed against the continuous spectrum of bremsstrahlung and to determine the maxima in the spectrum of the emitted neutrons from the time of flight, using a pulsed γ source.

[1] F. Ajzenberg-Selove and T. Lauritsen, Nucl. Phys. 11, 5 (1959).

[2] Bondelid, Dunning, and Talbott, Phys. Rev. 105, 193 (1957).

Translated by J. G. Adashko
57

(d, t) REACTIONS ON MEDIUM AND HEAVY NUCLEI

N. A. VLASOV, S. P. KALININ, A. A. OGLOBLIN, and V. I. CHUEV

Submitted to JETP editor September 27, 1959

J. Exptl. Theoret. Phys. (U.S.S.R.) **38**, 280-282 (January, 1960)

THE study of triton spectra from (d, t) reactions on light nuclei[1,2] has shown that mainly hole levels, corresponding to the ripping out of a neutron from the nucleus, are excited in this reaction. It is of interest to investigate the hole levels of medium and heavy nuclei, which differ in that they have a complex structure and a large number of filled shells. The neutron would be expected to be ripped out of various shells, with the excitation of hole levels with differing excitation energies, corresponding to the binding energies of the neutron in these shells.

In the present work, the spectra of tritons from (d, t) reactions in Fe, Zr, In, Au, and Bi were measured. Deuterons were accelerated in the cyclotron up to an energy of 20 Mev. The triton spectra were measured as previously[1-3] from the activity of tritium collected in stacks of foil.

Since the energies of tritons emitted from heavy nuclei depend only weakly on angle, tritons were collected in stacks of foil subtending a rather wide angular interval. There was one angular interval, 15 — 40°, for the targets of iron and indium, and two angular intervals, 8.5 — 23° and 24.5 — 39° for zirconium and gold. The maxima of distributions corresponding to practically all angular momenta l of the removed neutron lie within these angular intervals, with the exception of $l = 0$. The angular distribution of the tritons was measured for the bismuth target.

The measured triton spectra are given in Fig. 1. Along the abscissa are marked the excitation energies of the residual nucleus formed as a result of the reaction on the main isotope (Fe^{56} — 92%, Zr^{90} — 51%, In^{115} — 96%, Au^{179} — 100%, Bi^{209} — 100%). The magnitude of the energy resolution for each of the spectra is shown as a horizontal dash in the region of the main group. The magnitudes of the cross sections for Fe^{56}, Zr^{90}, and In^{115} were calculated from the atoms in a naturally occurring mixture of isotopes.

In all spectra, an intense group of tritons, which usually had two peaks, was observed corresponding to an excitation energy of 0 — 2 Mev. Excitation of states of the residual nucleus of energy higher than 2 Mev proceeds with substantially smaller probability. This means that in all of the nuclei studied, the main process is removal of the most weakly bound neutron, apparently out of the same outer (filled or unfilled) shell. The width of the group (1.5 — 2 Mev) is characterized by the spread in binding energies of the removed neutrons.

The character of the angular distributions, following from comparison of intensities of groups in the two angular intervals, agrees with known data on the character of that from outer shells.[4] In Zr^{90}, the outer neutrons are in $1g_{9/2}$ states; therefore the angular momentum of the removed neutron should be $l = 4$. The intensities of the first maxima in the Zr^{90} (d, t) spectrum are almost the same for the angular intervals 8.5 — 23° and 24.5 — 39°, in complete agreement with what one would expect for a large value of l.

On the other hand, the intensity of the group of tritons from reactions in the isotopes $Zr^{91,92,94}$ drops by a factor of 4 or 5 in going from the first to the second angular interval, in agreement with neutrons filling the $2d_{5/2}$ state above the closed shell.

In the spectrum of Au^{197}, both lines are more intense in the angular interval 24.5 — 39° than in the interval 8.5 — 23°. According to shell theory, the state of outer neutrons, $1i_{13/2}$, corresponds to a large value of the angular momentum $l = 6$. It should be noted that a reliable determination of angular momenta for medium and heavy nuclei cannot be made, since there is, up to now, no possibility of reliably calculating the effect of the Coulomb interaction on the angular distribution.

In Fig. 2 are shown angular distributions of three groups of tritons from the reaction

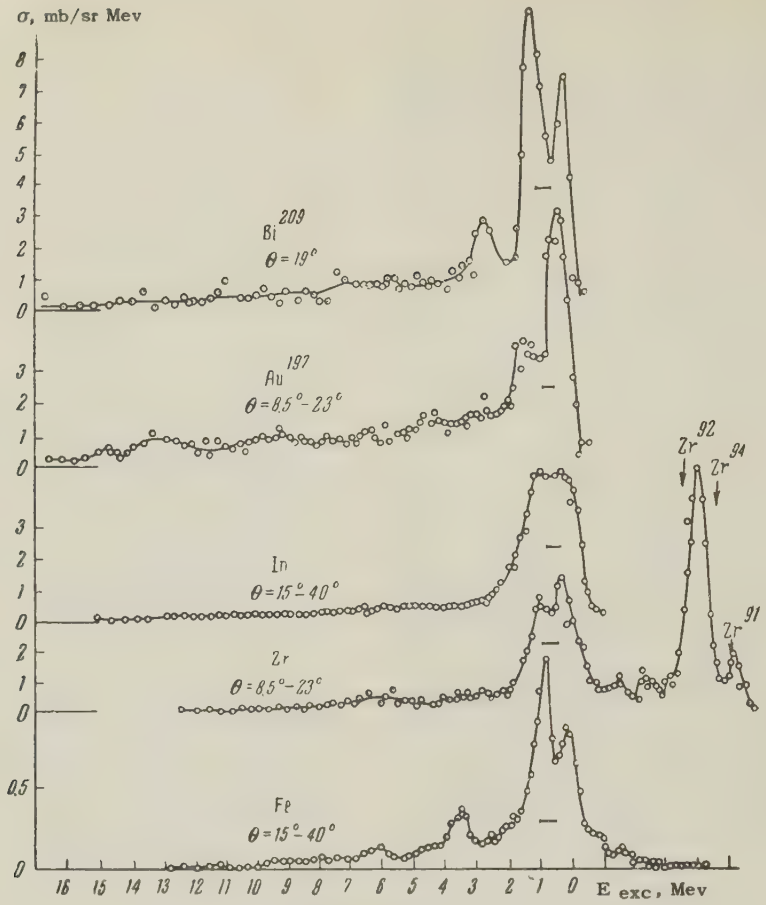

FIG. 1

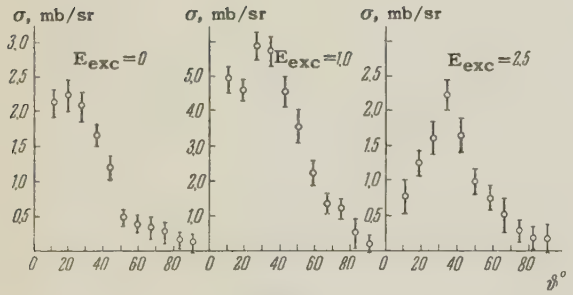

FIG. 2

Bi^{209} (d, t) Bi^{208}. One can assign the values of l (1, 1+3, 3) to them on the basis of available data[4] on the configuration of the levels of Pb^{207} (ground, $p_{1/2}$; 0.57 Mev, $f_{5/2}$; 0.90 Mev, $p_{3/2}$; 1.63 Mev, $i_{13/2}$; 2.35 Mev, $f_{7/2}$).

The most interesting characteristic of the measured spectra is their great similarity, manifesting itself in the fact that they all show at maximum triton energy a wide group with two more or less clear maxima, about 1 Mev apart. This is in spite of the fact that the target nuclei are completely different, both in the number of outer neutrons and with respect to the configuration being filled by these neutrons. The approximate equality of the absolute values of differential cross sections (with the exception of Fe) is of interest.

The authors are grateful to their colleagues in the cyclotron laboratory for carrying out the irradiations.

[1] N. A. Vlasov and A. A. Ogloblin, JETP **37**, 54 (1959), Soviet Phys. JETP **10**, 39 (1960).

[2] Vlasov, Kalinin, Ogloblin, and Chuev, JETP **37**, 1187 (1959), Soviet Phys. JETP **10**, 844 (1960).

[3] N. A. Vlasov and A. A. Ogloblin, Сб. трудов конференции по ядерным реакцям при малых и средних энергиях (Conference on Nuclear Reactions at Low and Medium Energies), Moscow, 1958.

[4] J. P. Elliott and A. M. Lane, Handbuch der Physik **39**, 241 (Springer, 1957).

Translated by G. E. Brown
58

THE GAMMA SPECTRUM OF La^{140} *IN THE ENERGY RANGE 2300–3900 kev*

B. S. DZHELEPOV, B. A. EMEL'YANOV, K. P. KUPRIYANOVA, and Yu. N. PODKOPAEV

Leningrad State University

Submitted to JETP editor September 28, 1959

J. Exptl. Theoret. Phys. (U.S.S.R.) **38**, 282-284 (January, 1960)

MANY investigations have been devoted to the study of the γ spectrum of La^{140}. The hardest γ rays observed until now in the radiation of La^{140} have an energy $h\nu \sim 2920$ kev. According to references 1 and 2 the mass difference $La^{140} - Ce^{140}$ amounts to ~ 3800 kev. Consequently, one can assume that the decay of La^{140} excites states of Ce^{140} with energies up to ~ 3800 kev, and transitions from higher excitation levels to the ground state can be observed.

Using the γ hodoscope of the Physics Research Institute of the Leningrad State University, a description of which was published elsewhere,[3,4] we investigated the hard γ radiation from La^{140}. Four series of measurements were carried out with different sources and at different values of the magnetic field intensity H. In series I and IV (H = 1159 and 1226 oe, respectively), the sources were two different La_2O_3 compounds, in which the isotope La^{140} was obtained from the reaction (n, γ). The activity of each source did not exceed 50 mC at the beginning of the measurements. In series II and III (H = 1011 and 1159 oe), the source was a mixture of Ba^{140} and La^{140} in equilibrium (activity not more than 25 mC at the start of the measurements).

Resolution of the spectrum into components, with allowance for the dependence of the instrument line shape on $h\nu$ and H in each series of measurements, has made it possible to separate four γ lines with the following energies (averaged over four series) 2530 ± 30, 2915 ± 30 (these lines are already known[5]), 3110 ± 50, and 3380 ± 70 kev; the latter two were observed by us for the first time.

The diagram shows the form of the γ spectrum of La^{140} after eliminating the background from the first series of measurements (dotted lines — resolution of the spectrum into components). The relative intensities of the γ transitions with $h\nu$ = 2915, 3110, and 3380 kev, determined from the areas of the lines of this series, amount to 1.0, 0.42 ± 0.07, and 0.019 ± 0.006 respectively. The errors in the determination of the relative intensities are due to the inaccuracy in the knowledge of the spectral sensitivity, the statistical measurement errors, and the inaccuracy of the resolution of the spectrum into components. If it is assumed that the intensity of the 2915-kev γ transition is 7×10^{-4} quantum per decay,[5] then the intensity of the 3110 and 3380 kev transitions is respectively 2.9×10^{-4} and 1.3×10^{-5} quantum per decay.

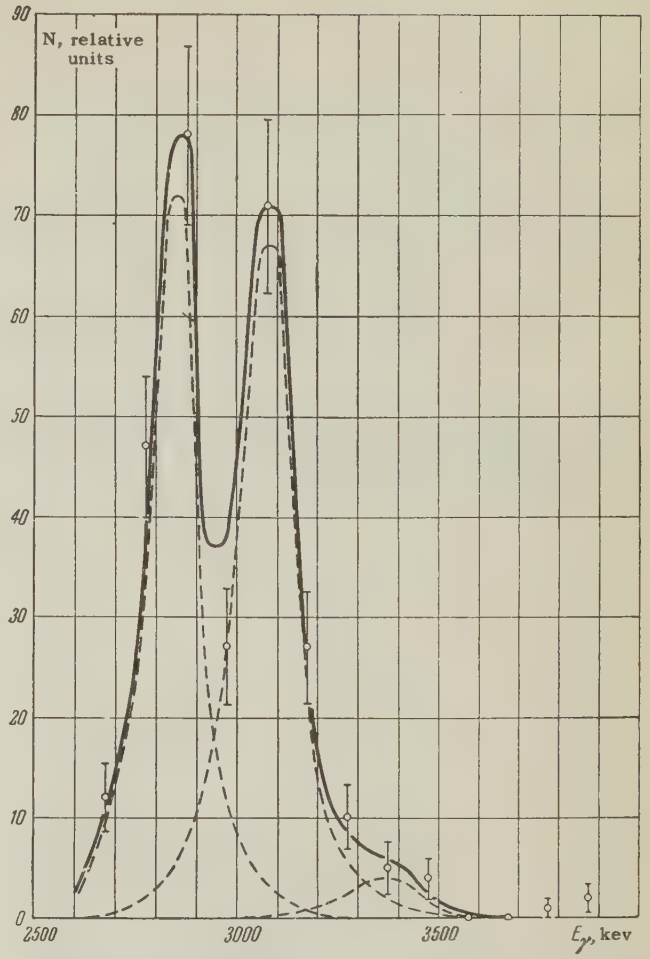

Experimental spectrum of γ rays from La^{140} in the range 2600 – 3900 kev. At H = 1159 oe, the probability of registration is optimum for $h\nu$ = 3705 kev; the observed 2915, 3110, and 3380 kev lines are attenuated by factors of 54, 2.4, and 1.4 respectively; the line $h\nu$ = 2530 kev is not registered at all under these conditions.

The 3110 and 3380 kev γ rays found by us are produced during transitions from the corresponding excited levels of Ce^{140}, heretofore unknown, to the ground state. We observed no harder γ rays in the radiation of La^{140}.

We consider it our duty to express deep gratitude to O. V. Chubinskiĭ for furnishing us with data on the spectral sensitivity of the instrument, to N. D. Novosil'tseva for providing us with sources, and to L. V. Gustova for help with the measurements.

[1] B. S. Dzhelepov and L. K. Peker, Схемы распада радиоактивных ядер (Decay Schemes of Radioactive Nuclei), U.S.S.R. Acad. Sci., M-L, 1958.

[2] J. Riddell, A Table of Levy's Empirical Atomic Mass, Chalk River, Ont., 1057.

[3] B. S. Dzhelepov, Izv. Akad. Nauk SSSR, Ser. Fiz. **21**, 1580 (1957), Columbia Tech. Transl. p. 1569.

[4] O. B. Chubinskiĭ, Izv. Akad. Nauk SSSR, Ser. Fiz. **21**, 1583 (1957), Columbia Tech. Transl. p. 1572.

[5] V. P. Prikhodtseva and Yu. V. Khol'nov, Izv. Akad. Nauk SSSR, Ser. Fiz. **22**, 176 (1958), Columbia Tech. Transl. p. 173.

Translated by J. G. Adashko
59

ANISOTROPIC DISTRIBUTION OF INTERNAL BREMSSTRAHLUNG IN K CAPTURE BY POLARIZED NUCLEI

S. F. TIMASHEV and V. A. KAMINSKIĬ

Institute of Nuclear Physics, Moscow State University

Submitted to JETP editor September 28, 1959

J. Exptl. Theoret. Phys. (U.S.S.R.) **38**, 284-285 (January, 1960)

ANISOTROPY in the angular distribution of internal bremsstrahlung in K capture by polarized nuclei occurs if parity is not conserved in weak interactions. Experimental investigation of this phenomenon yields in principle the same information on the constants of the β-decay interaction as do experiments on the angular distribution of electrons in the β decay of polarized nuclei. From the experimental point of view the measurement of anisotropy of internal bremsstrahlung in K capture by polarized nuclei can be more convenient since in this case the observed effect is less dependent on the thickness of sources in which scattering of the radiation involved can take place. We also note that the anisotropy coefficient of internal bremsstrahlung does not depend on the energy of the γ quanta.

We calculated this effect for allowed transitions according to the usual method of the Born approximation in the Coulomb field of the nucleus. The angular distribution has the form

$$W = 1 + P\alpha\cos\theta, \tag{1}$$

where $P = \langle J_Z\rangle/J$ is the polarization of the nucleus, J and J_Z are respectively the spin and the projection of the spin of the nucleus in the ground state, and θ is the angle between the direction of polarization of the nucleus and the momentum of the bremsstrahlung. For interactions of the general type S + T + V + A the anisotropy coefficient is given by the formulas:

$J \to J$ (no) transition

$$\alpha = \frac{\frac{1}{J+1}[(g_T g_T'^* + g_T' g_T^*) - (g_A g_A'^* + g_A' g_A^*)]\langle\|\sigma\|\rangle^2 + \frac{2J}{\sqrt{J(J+1)}}\mathrm{Re}\{[(g_S g_T'^* + g_S' g_T^*) - (g_V g_A'^* + g_V' g_A^*)]\langle\|1\|\rangle\langle\|\sigma\|\rangle\}}{[(|g_S|^2 + |g_S'|^2) + (|g_V|^2 + |g_V'|^2)]\langle\|1\|\rangle^2 + [(|g_T|^2 + |g_T'|^2) + (|g_A|^2 + |g_A'|^2)]\langle\|\sigma\|\rangle^2}, \tag{2}$$

$J \to J - 1$ (no) transition

$$\alpha = \frac{(g_I g_I'^* + g_I' g_T) - (g_A g_A'^* + g_A' g_A^*)}{(|g_T|^2 + |g_T'|^2) + (|g_A|^2 + |g_A'|^2)}, \tag{3}$$

$J \to J + 1$ (no) transition

$$\alpha = \frac{J}{J+1}\,\frac{-(g_T g_T'^* + g_T' g_T) + (g_A g_A'^* + g_A' g_A^*)}{(|g_T|^2 + |g_T'|^2) + (|g_A|^2 + |g_A'|^2)}. \tag{4}$$

Here $\langle\|1\|\rangle$ and $\langle\|\sigma\|\rangle$ are the nuclear matrix elements for the Fermi and Gamow-Teller parts of the interactions.

For the (V-A) interaction, with strict invariance under time reversal and with two-component neutrinos (polarized with spin opposite to the momentum direction in K capture) we have

$J \to J - 1$ (no) $\quad \alpha = +1,$ (5)

$J \to J + 1$ (no) $\quad \alpha = -J/(J+1),$ (6)

$J \to J$ (no)

$$\alpha = \left[\frac{1}{J+1}R^2B^2 - \frac{2J}{\sqrt{J(J+1)}}RB\right] \Big/ (1 + B^2R^2), \tag{7}$$

where[1] $R = |g_A/g_V| = 1.19 \pm 0.02$; $B = \langle\|\sigma\|\rangle/\langle\|1\|\rangle$.

Since experiments on K-capture radiation are best done with nuclei which decay directly to the ground state so that the background of nuclear γ rays does not interfere with the investigation of the bremsstrahlung, we list below values of the anisotropy coefficient α_{VA} for several such nuclei:[2]

V^{49}	$^7/_2^- \to {}^7/_2^-$	$J \to J$ (no)	$\alpha_{VA} = (0.32B^2 - 2.1B)/(1 + 1.42B^2)$
Fe^{55}	$^3/_2^- \to {}^5/_2^-$	$J \to J+1$ (no)	$\alpha_{VA} = -0.6$
Ge^{71}	$^1/_2^- \to {}^3/_2^-$	$J \to J+1$ (no)	$\alpha_{VA} = -0.33$
Mo^{93}	$^7/_2^+ \to {}^9/_2^+$	$J \to J+1$ (no)	$\alpha_{VA} = -0.78$
Cs^{131}	$^5/_2^+ \to {}^3/_2^+$	$J \to J-1$ (no)	$\alpha_{VA} = +1$

In conclusion we wish to express our gratitude to V. S. Shpinel' who drew our attention to this effect, and to I. S. Shapiro for his valuable advice and leadership.

[1] Sosnovskiĭ, Spivak, Prokof'ev, Kutikov, and Dobrynin, JETP **36**, 1012 (1958), Soviet Phys. JETP **9**, 717 (1959).

[2] B. S. Dzhelepov and L. K. Peker, Схемы распада радиоактивных ядер (Decay Schemes of Radioactive Nuclei), Acad. Sci. U.S.S.R., 1958.

Translated by Genevra Gerhart
60

ELASTIC SCATTERING OF PROTONS BY CHROMIUM ISOTOPES AT 5.40 Mev

A. P. KLYUCHAREV and N. Ya. RUTKEVICH

Physico-technical Institute, Academy of Sciences, Ukrainian S.S.R.

Submitted to JETP editor September 29, 1959

J. Exptl. Theoret. Phys. (U.S.S.R.) **38**, 285-287 (January, 1960)

WE have investigated the angular distribution of protons scattered elastically by the chromium isotopes Cr^{52} and Cr^{53}. Protons accelerated in a linear accelerator were energy-analyzed by a magnetic field giving a deflection of 24° and sent through a collimation system with a diaphragm opening 2.3 mm in diameter onto a target located in the scattering chamber. The target consisted of thin metallic foils 4 μ thick in the case of Cr^{52} and 0.7 μ thick in the case of Cr^{53}. The protons scattered by the target were recorded in photoemulsion pellicles 100 μ thick at angles of 20 — 160° every 10°. In the angular region 20 — 70° the plates were placed at distances $r = \text{const}/\sin^2(\theta/2)$, which made it possible to protect the emulsion from the intense "illumination" by protons scattered at small angles by the Coulomb field of the nucleus.

Figure 1 shows the energy spectrum of protons scattered by the nuclei under investigation at an angle of 130°. It is readily seen that the inelastic group of protons is easily distinguishable and that the number of elastically-scattered protons can be counted readily at any angle. We note that the inelastically scattered protons corresponding to the 540-kev level of Cr^{53} are relatively few, which is evidence that this level is weakly excited, while the number of protons corresponding to the 970-kev level is considerable.

The angular distribution of the elastically-scattered protons is shown in Fig. 2. The difference in the scattering is seen to be not only quantitative, but also qualitative. The intensity of the protons scattered by Cr^{52} is 2.5 times as large

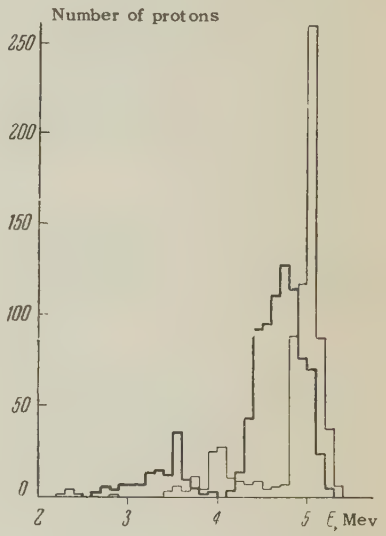

FIG. 1. Proton energy spectrum: heavy line — Cr^{52}, 893 tracks; thin line — Cr^{53}, 729 tracks.

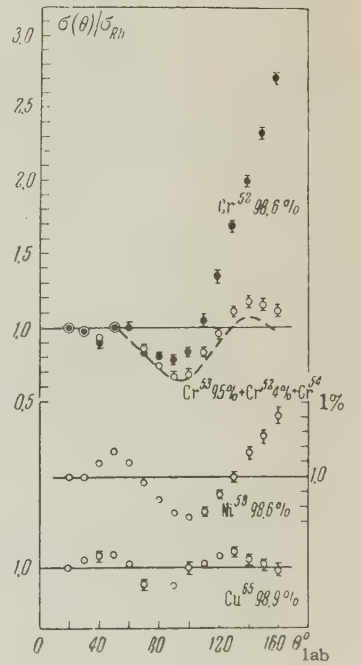

FIG. 2. Ratio of the measured cross section to the Rutherford cross section as a function of the angle of observation in the laboratory system; the dashed curve was obtained from a recalculation of the measured ratio for pure Cr^{53}.

as that for Cr^{53} in the large-angle region, and, moreover, in the case of the former, it increases rapidly and practically linearly with the angle, beginning from the minimum, while for Cr^{53} the curve passes through a maximum in the angular region 140 — 150°. There is also a visible difference in the depth of the minimum of the curves in the region of 90°. The region of small angles has to be investigated more carefully.

Shown for comparison in Fig. 2 are measurements we have made of the angular dependence of 5.45-Mev protons scattered elastically from Cu^{65} and Ni^{58}.[1] From the comparison it follows that the even-even Cr^{52} scatters protons, just like the even-even Ni^{58} and other even-even nuclei [Ni^{60}, Ni^{62} (reference 1), Fe, Ti (reference 2)]. The shape of the angular dependence for even-odd Cr^{53} is similar to the shape for odd-even Cu^{65}.

The results obtained by us are evidence of the fact that a change of one in the number of nucleons in the atomic nucleus, independently of the charge state of the nucleus, essentially changes the interaction between the nucleon and the nucleus. It is possible that the change is the result of a change in the spin of the nucleus in passing from even-even nuclei with spin zero to even-odd or odd-even nuclei with half-integer spin.

In addition, the decrease in the relative cross section for Cr^{53}, in comparison with Cr^{52}, in the large-angle region, apparently can be considered as an increase in the absorption at the boundary of the nucleus, owing to the diffuse surface of the Cr^{53} nucleus due to the addition of an odd neutron.

[1] Rutkevich, Gorlovnaya, Val'ter, and Klyucharev, Dokl. Akad. Nauk SSSR, (in press).

[2] Kondo, Yamazaki, Toi, Nakasimi, and Yamabe, J. Phys. Soc. Japan **13**, 231 (1958).

Translated by E. Marquit
61

ANGULAR DISTRIBUTION OF PROTONS FROM THE REACTION $Ca^{40}(d, p)Ca^{41}$

N. I. ZAIKA, O. F. NEMETS, and V. S. PROKOPENKO

Joint Institute of Nuclear Research

Submitted to JETP editor September 30, 1959

J. Exptl. Theoret. Phys. (U.S.S.R.) **38**, 287-289 (January, 1960)

THE theories of stripping reactions[1,2] give a surprisingly good overall agreement with many experiments, in spite of the fact that they do not take into account the Coulomb and nuclear interactions of the deuteron and proton with the nucleus, and compound-nucleus formation. In addition, the calculations have been carried out in the Born approximation, which can hardly be justified at low and medium deuteron energies. In a series of cases, substantial deviations from the predictions of the simple stripping theory have been observed. In some of these cases, these deviations are connected with effects of the Coulomb and nuclear interactions,[3] and in others, with the difference of reaction mechanism from that of pure stripping.[4,5] Therefore, it is of interest to obtain data making it possible to see the effects of the factors mentioned on the angular distributions.

We studied the angular distribution of protons from the reaction $Ca^{40}(d, p)Ca^{41}$ leading to the ground, first, and third excited states, for a deuteron energy of 13.6 Mev. The nucleus Ca^{40} was chosen for the measurements, since one might expect a small probability of compound-nucleus formation owing to the closed neutron and proton shells. In addition, at small deuteron energies, strong nuclear interaction is observed,[6,7] and it is of interest to carry out the measurements at higher energies.

The measurements were carried out with the external beam of the cyclotron of the Institute of Physics of the Academy of Sciences, Ukrainian S.S.R. The geometry of the experiment was the same as in previous work.[8] The only difference in the method was that a polystyrene absorber was placed before the entrance to the ionization chamber. It completely stopped deuterons, substantially relieving the amplifier of the chamber, and making it possible to increase the beam on the target. This also led to a complete elimination of background in d-p reactions from deuterons undergoing elastic scattering in the target for values $Q > 2.7$ Mev. The energy resolution was not significantly decreased by this. The target was prepared by vacuum coating and had a thickness of 3 mg/cm^2.

In Figs. 1, 2, and 3 we give the experimental and theoretical (solid lines) angular distributions of protons corresponding to the ground and excited states at 1.95 and 2.42 Mev. The total cross sections for these were in the ratios 1 : 7.5 : 2.5. In

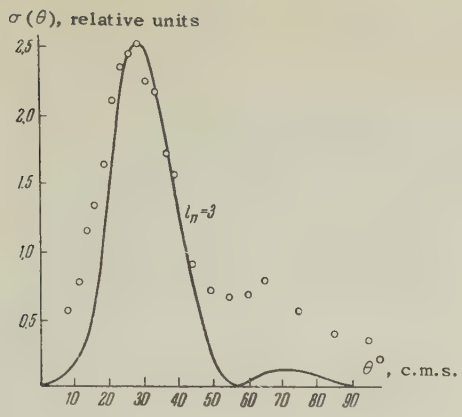

FIG. 1

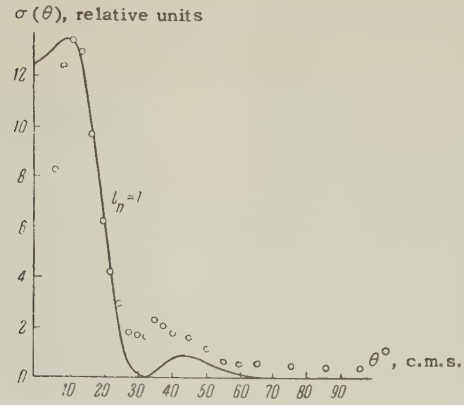

FIG. 2

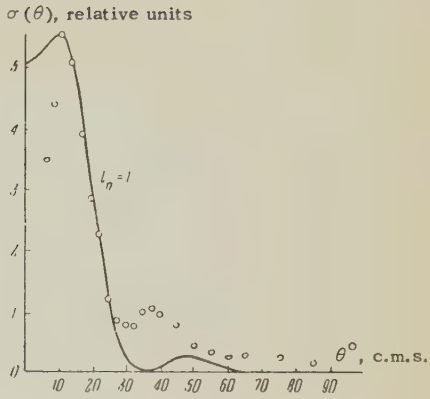

FIG. 3

calculating the angular distributions the interaction radius was chosen to be 6×10^{-13} cm. The values found for the spin and parity of the ground state, and also for the energies, spins and parities of the excited states are in agreement with data of previous works.[9,10]

The narrowing of the peaks of the experimental angular distributions in Figs. 2 and 3 can be related to the effect of nuclear interaction. The displacement of the peaks towards smaller angles, required in this case by the theory and observed by Teplov and Yur'ev[6] at low deuteron energies, becomes completely insignificant already for deuteron energies $E_d = 7$ Mev[10] and 8 Mev,[9] and it may be expected that it will be even smaller at higher energies. At the same time, for deuteron energies of 8 Mev, the experimental distribution of the group with $l_n = 1$ turned out to be the same as the theoretical one in the small-angle region.[9]

It should be noted that the "background" (isotropic part of the angular distribution) is less at 13.6 Mev than at 7 and 8 Mev, indicating the growing role of direct interaction with increasing energy.

In conclusion, the authors would like to express their gratitude to Prof. M. V. Pasechnik for his constant interest in the work, Yu. A. Bin'kovskiĭ for preparation of the targets, and also to the personnel of the cyclotron crew who made possible the continuous operation of the cyclotron.

[1] S. T. Butler, Proc. Roy. Soc. **A208**, 559 (1951).

[2] Bhatia, Huang, Huby, and Newns, Phil. Mag. **43**, 485 (1952).

[3] W. Tobocman and M. H. Kalos, Phys. Rev. **97**, 132 (1955).

[4] L. Madansky and G. E. Owen, Phys. Rev. **99**, 1608 (1955).

[5] D. H. Wilkinson, Phys. Rev. **105**, 666 (1957).

[6] I. B. Teplov and B. A. Yur'ev, JETP **33**, 1313 (1957), Soviet Phys. JETP **6**, 1011 (1958).

[7] L. L. Lee, Jr. and J. P. Schiffer, Phys. Rev. **107**, 1340 (1957).

[8] N. I. Zaika and O. F. Nemets, Izv. Akad. Nauk SSSR, Ser. Fiz. **23**, No. 12 (1959), Columbia Tech. Transl., in press.

[9] J. R. Holt and T. N. Marsham, Proc. Phys. Soc. **A66**, 565 (1953).

[10] C. K. Bockelman and W. W. Bueckner, Phys. Rev. **107**, 1366 (1957).

Translated by G. E. Brown
62

CROSS SECTION FOR THE FORMATION OF Ω^- PARTICLES IN THE REACTIONS $\pi^- + p \rightarrow \Omega^- + 3K$ AT 8 Bev AND $p + \bar{p} \rightarrow \Omega + \bar{\Omega}$ AT 4 Bev

HSIEN TING-CH'ANG

Joint Institute for Nuclear Research

Submitted to JETP editor September 30, 1959

J. Exptl. Theoret. Phys. (U.S.S.R.) **38**, 289-290 (January, 1960)

ACCORDING to the Gell-Mann scheme, a hyperon can exist with strangeness -3 and isotopic spin zero.[1] We take the lower bound of its mass to be $M_\Xi + M_\pi$, and the upper bound to be $M_\Xi + M_K$, that is, its mass is located between 1.58 and 1.93 M_N. In this note, the cross section for the formation of Ω^- particles in the collisions of π^-p at 8 Bev and $p\bar{p}$ at 4 Bev is estimated in the statistical model.

According to the statistical model of multiple production of particles, the probability of the formation of n particles in the final state is[2]

$$S_n = [V/(2\pi)^3]^{n-1} f_{TS} W \quad (E_0), \qquad (1)$$

where V is the spatial volume in which the par-

ticles are produced; f_{TS} is the statistical weight, taking account of the spin and isotopic spin of the particles in the final state; $W(E_0)$ is the phase-space volume for a total center-of-mass energy E_0. For comparison with experiment we use Barashenkov's hypothesis[3] that the pions and baryons are formed in the volume V_π, but that the K mesons are produced in a smaller volume V_K ($\xi = V_K/V_\pi = 0.0232$). If there are k K mesons in the final state and $-l$ ($k+l=n$) pions and baryons, then V^{n-1} in (1) must be replaced by V_1^{n-1}:

$$V_1^{n-1} = \frac{(k+l\xi)\,\xi^{k-1}}{n} V^{n-1}. \qquad (2)$$

From (1) and (2) we obtain the following relations between the cross sections for 8 Bev pions:

$$(\pi^- + p \to \Omega^- + 3K)/(\pi^- + p \to 2K + \overline{K} + \Sigma) = 3.3\cdot 10^{-2}, \quad (3)$$

$$(\pi^- + p \to \Omega^- + 3K)/(\pi^- + p \to \Xi + 2K) = 4.3\cdot 10^{-3}, \quad (4)$$

$$(\pi^- + p \to \Omega^- + 3K)/(\pi^- + p \to \pi + N) = 0.86\cdot 10^{-4} \quad (5)$$

and for 4-Bev antiprotons

$$(p + \bar{p} \to \Omega + \bar{\Omega})/(p + \bar{p} \to \Xi + \bar{\Xi}) = 0.43. \qquad (6)$$

It is assumed in the calculation that the particles in the final state are nonrelativistic. Since the results in the statistical theory depend strongly on the choice of the volume V, the calculated ratio (3) is more reliable, since it does not depend on V.

If we use the experimental data on the cross section of the reaction $\pi^- + p \to \pi + N$ for π^- energies $\sim$ 8 Bev ($\sigma \sim 6$ mb),[4] we get for the reaction $\pi^- + p \to \Omega^- + 3K$ at the same energy $\sigma \sim 0.5\ \mu b$.

The cross section for $\pi^- + p \to \Xi + 2K$ is obtained as $\sigma \sim 120\mu b$. This value is significantly larger than the experimental one,[5] which has $\sigma = 2.3^{+3.5}_{-1.6}\ \mu b$ for 5 Bev negative pions. It is possible, therefore, that the absolute values of the cross sections calculated above for the production of Ω^- particles are overestimates. Since at present only two cases of Ξ^- obtained in an accelerator are known, it seems natural from (4) that the Ω^- particle has not yet been observed, if indeed it even exists.

On the basis of formula (6), searches for Ω^- and other possible heavier hyperons can be usefully made in reactions involving nucleon-antinucleon collisions.

The author thanks Prof. M. A. Markov for setting up the problem and Chou Kuang Chao and V. S. Barashenkov for valuable remarks.

[1] M. Gell-Mann, Report to the Conference on Elementary Particles at Pisa, 1955.

[2] E. Fermi, Progr. Theoret. Phys. Japan **5**, 570 (1950). Belen'kiĭ, Maksimenko, Nikishov, and Rozental', Usp. Fiz. Nauk **62**, 1 (1957).

[3] Barashenkov, Barbashev, and Bubelev, Nuovo cimento **7**, Suppl. **1**, 117 (1958).

[4] O. Piccioni, Proceedings, Annual International Conference on High Energy Physics, p. 65, CERN (1958).

[5] Fowler, Powell, and Shonle, Nuovo cimento **11**, 428 (1959).

Translated by W. Ramsay
63

MEASUREMENT OF THE ANGULAR CORRELATIONS OF 298 — 880 kev AND 298 — 966 kev GAMMA CASCADES OF Dy^{160}

M. V. KLIMENTOVSKAYA and G. CHANDRA*

Institute of Nuclear Physics, Moscow State University

Submitted to JETP editor September 30, 1959

J. Exptl. Theoret. Phys. (U.S.S.R.) **38**, 290-291 (January, 1960)

THE decay of Tb^{160} and the decay scheme of the Dy^{160} nucleus have repeatedly been investigated by various methods, with particular detail in references 1 — 6.

It can be assumed that the sequence of the most intense γ transitions and the spins and parities of the normal and excited states of Dy^{160} with energies 86, 283, 966 kev (the figure shows the corresponding part of the decay scheme of Dy^{160}) have been reliably established. The information on the spins and parities of the other levels is contradictory. To the level with energy 1264 kev there is assigned a spin 3^-,[1,2] 4,[3] and 2^-.[4-6]

Bertolini and his co-workers[3] measured the an-

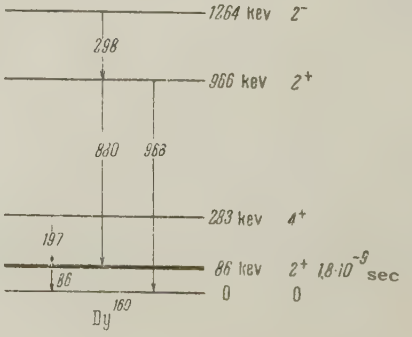

gular correlations between the γ transitions with energy 298 kev and with energy above 750 kev. Ofer[5] measured the angular correlation separately for a number of γ cascades and particularly for the 298 — 880 kev and 298 — 966 kev cascades. The obtained results, especially for the 298 — 966 kev cascade, show that the 1264-kev level has the characteristic 2^- and dipole transition with energy 298 kev; the possible admixture of quadrupole radiation is less than 1/1000. The data for the 298 — 880 kev cascade obtained in the same paper lead to the transition sequence 2(D), 2(D+Q)2 for $\delta^2 = 3600$, i.e., the intensity of the quadrupole radiation is 3600 times that of the dipole. There are no indications in the paper, however, of any correction for the contribution of the angular correlation of the 298 — 966 kev cascade in measuring the angular correlation of the 298 — 880 kev cascade.

We have measured the angular correlation of the 298 — 966 kev and 298 — 880 kev γ cascades with the apparatus previously described.[7]† To prevent false coincidences due to Compton scattering from one crystal to another, the crystal used to count the 880 and 966 kev photons was screened with a lead filter 5 mm thick on the front and 4 mm on the side surface. For measurements at 90 and 135°, a lead screen 5 mm thick was interposed between the crystals. After introducing corrections for the variations of the single loadings in the counters and for the finite angular resolution of the detectors, the angular correlation function of the 298 — 966 kev cascade was found to be

$$W(\theta) = 1 + (0.23 \pm 0.03) P_2(\cos\theta),$$

corresponding to the sequence of transitions 2(D+Q)2(Q)0 if the mixture ratio $\delta^2 = I(Q)/I(D)$ in the 298-kev transition is less than 1/1000. The obtained result entirely agrees with the measurement of the angular correlation of this cascade by Ofer.[5] By a suitable adjustment of the window of the pulse-height analyzer, the 966-kev γ line was practically completely separated from the 880-kev γ line.

In measuring the angular correlation of the 298 — 966 kev cascade corrections were made for the contribution of the angular correlation of the 298 — 966 kev cascade, for the variation of the single loadings in the counters, and for the finite angular resolution of the detectors. As a result, the following angular correlation function was obtained for the 298 — 880 kev cascade:

$$W(\theta) = 1 - (0.116 \pm 0.037) P_2(\cos\theta).$$

If account is taken of the results obtained for the 298 — 966 kev cascade, this correlation function agrees best with the transition sequence 2(D)2(D+Q)2, where the mixture ratio δ^2 in the 880-kev γ transition should be ≈ 56 ($\delta < 0$), i.e., the intensity of the dipole radiation (M1) in the the 880-kev γ transition should constitute (1.8 ± 1.5)% and the intensity of the quadrupole radiation (E2) should be (98.2 ± 1.5)%. This result differs from the result of Ofer,[5] who found the 880-kev transition to be practically pure Q.

From our work it follows that the spin of the 1264-kev energy level is 2.

The authors wish to thank Professor V. S. Shpinel' for discussion of the results.

*Tata Institute for Fundamental Research, Bombay, India.

†We take this opportunity to correct an error made in reference 7. On page 1364, line 9 from the bottom should read "spin ⁹⁄₂" (instead of ³⁄₂), line 7 from the bottom should read "spin ³⁄₂" (instead of ⁹⁄₂).

[1] Grigor'ev, Dzhelepov, Zolotavin, Kraft, Kratsik, and Peker, Izv. Akad. Nauk SSSR, Ser. Fiz. **22**, 191 (1958), Columbia Tech. Transl. p. 188.

[2] Grigor'ev, Zolotavin, and Kratsik, Izv. Akad. Nauk SSSR, Ser. Fiz. **23**, 191 (1959), Columbia Tech. Transl. p. 183.

[3] Bertolini, Bettoni, and Lazzarini, Nuovo cimento **3**, 754, 1162 (1956).

[4] O. Nathan, Nucl. Phys. **4**, 125 (1957).

[5] S. Ofer, Nucl. Phys. **5**, 331 (1958).

[6] Bäckström, Lindskog, Bergman, Bashandy, and Bäcklin, Arkiv f. Fysik **15**, 121 (1959).

[7] M. V. Klimentovskaya and P. I. Shavrin, JETP **36**, 1360 (1959), Soviet Phys. JETP **9**, 967 (1959).

Translated by M. Chaucey
64

CRITICAL CURRENTS IN SUPERCONDUCTING TIN FILMS

N. E. ALEKSEEVSKIĬ and M. N. MIKHEEVA

Institute for Physical Problems, Academy of Sciences, U.S.S.R.

Submitted to JETP editor October 9, 1959

J. Exptl. Theoret. Phys. (U.S.S.R.) **38**, 292-293 (January, 1960)

THE most interesting measurements of critical currents in superconducting films are those on films of such geometry that the magnetic field

due to the current can be calculated and compared with theory. Since measurements on such films have either been made with continuous current[1,2] or with long period pulses (0.1 — 0.01 sec)[3] there was the danger that the small values of critical current are a consequence of Joule heating of the film. It therefore seemed of interest to extend the measurements to the region of shorter pulses. In the present work we have measured the critical currents in tin films by a pulse method, with the time of rise varying between $\tau = 0.1$ and $\tau = 0.0001$ sec.

As before,[3] the film was a flat disk with a central current lead and a radial distribution of current flow. The measurements showed that the critical current depends appreciably on the time τ, increasing as it decreases (Fig. 1). For example, for a film of thickness $d = 2.0 \times 10^{-5}$ cm the critical currents for $\tau = 0.01$ and $\tau = 0.0001$ sec differ by a factor of two. We should note that when the temperature is reduced by 0.3 — 0.4° K below the critical temperature, the critical current increased to 10 amp for $\tau = 0.0001$ sec.

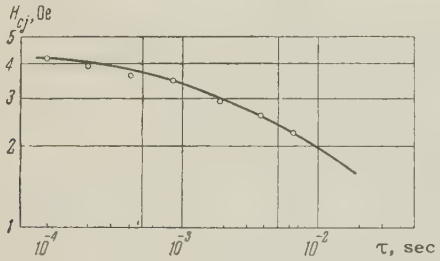

FIG. 1. Dependence of the magnetic field of the critical current, H_{cj}, on the time of rise of the current pulse for a tin film of thickness $d = 2.03 \times 10^{-5}$ cm.

If the critical field due to the current, H_{cj}, is plotted against τ, it is seen that H_{cj} tends to a constant value as τ is reduced. By extrapolating to τ equal to zero, the critical current is almost the same (5 — 10%) as the experimental value for $\tau = 0.0001$ sec. The experimental data discussed below refer to measurements made with the shortest pulses.

Our results show that near the critical temperature the form of the H_{cj} vs. ΔT curve ($\Delta T = T_c - T$) depends appreciably on the temperature of the substrate at the time of deposition of the film. For films obtained by evaporating the metal in vacuum onto a substrate cooled to liquid nitrogen temperature (78° K) and then warmed up to room temperature, the temperature dependence of H_{cj} can be roughly represented by the relation $H_{cj} = a\Delta T$ (see Fig. 2). Films obtained by evaporation at room temperature show a temperature dependence of critical current field near T_c close to that predicted by the Ginzburg-Landau theory[4,5] (see Fig. 3), although such films are

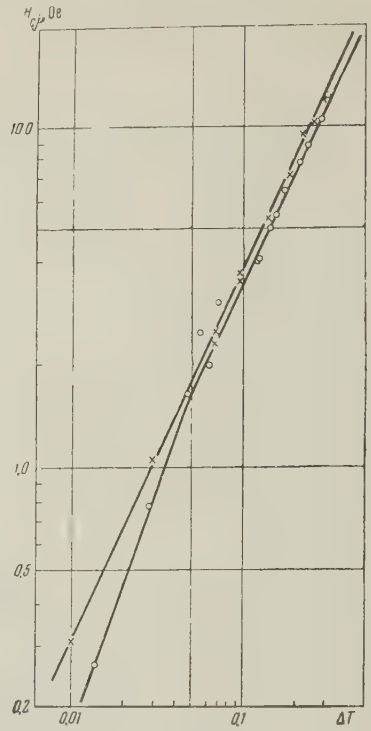

FIG. 2. Dependence of the field of the critical current on temperature (ΔT) for a tin film of thickness $d = 2 \times 10^{-5}$ cm. × — film deposited on a substrate cooled by liquid nitrogen, and the measurements made with current pulses for which the time of rise was $\tau = 4 \times 10^{-4}$ sec; o — film deposited on a substrate at room temperature, $\tau = 2.5 \times 10^{-4}$ sec.

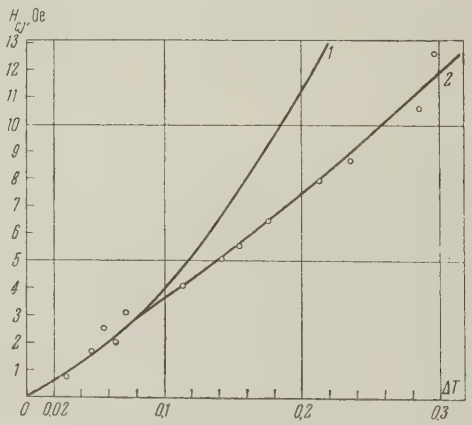

FIG. 3. Temperature dependence of field of the critical current for a tin film of thickness $d = 2 \times 10^{-5}$ cm, $\tau = 0.00025$ sec. Curve 1 is theoretical, calculated from Eq. (1); curve 2 is experimental. The film was deposited on a substrate at room temperature.

less reliable than films condensed at liquid nitrogen temperature. For these films there is a change in slope of the curves in the range $\Delta T = 0.05 - 0.1$° K. After the break, the form of the temperature dependence of H_{cj} for these films is the same as for films condensed at T = 78° K.

The calculated values of H_{cj} near T_c are, in both cases, close to the theoretical values calculated from the relation

$$H_{cj}/H_{cm} = (\sqrt{2}/3\sqrt{3})\, d/\delta, \qquad (1)$$

where d is the film thickness; δ_0 is taken as 6.5×10^{-6} cm, as follows from Zavaritskiĭ's work.[6]

[1] L. A. Feĭgin and A. I. Shal'nikov, Dokl. Akad. Nauk SSSR **108**, 823 (1956), Soviet Phys.-Doklady **1**, 377 (1957).

[2] N. I. Ginzburg and A. I. Shal'nikov, JETP **37**, 399 (1959), Soviet Phys. JETP **10**, 285 (1960).

[3] N. E. Alekseevskiĭ and M. N. Mikheeva, JETP **31**, 951 (1956), Soviet Phys. JETP **4**, 810 (1957).

[4] V. L. Ginzburg and L. D. Landau, JETP **20**, 1064 (1950).

[5] V. L. Ginzburg, Dokl. Akad. Nauk SSSR **118**, 464 (1958), Soviet Phys.-Doklady **3**, 102 (1958).

[6] N. V. Zavaritskiĭ, Dokl. Akad. Nauk SSSR 78, 665 (1951).

Translated by R. Berman
65

THE SUPERCONDUCTIVITY OF ELECTROLYTICALLY DEPOSITED COPPER-BISMUTH ALLOYS

N. E. ALEKSEEVSKIĬ, V. V. BONDAR', and Yu. M. POLUKAROV

Institute of Physical Problems, Academy of Sciences, U.S.S.R.

Submitted to JETP editor October 9, 1959

J. Exptl. Theoret. Phys. (U.S.S.R.) **38**, 294-295 (January, 1960)

WHILE studying the phase structure of electrolytically deposited copper-bismuth alloys, it was found that, depending upon the value of the overvoltage at the cathode, alloys could be obtained containing both mixtures of copper and bismuth crystals (in agreement with the equilibrium diagram of this system) and non-equilibrium phases.[1] Alloys consisting of non-equilibrium phases occurred at high overvoltages at the cathode in the form of dense silver-colored deposits in the composition range 40 to 90 wt % bismuth.

Data obtained by thermal analysis and x-ray studies allowed the supposition that these alloys contained a non-equilibrium phase, the decomposition of which occurred at a temperature of about 120° C. In alloys containing between 40 and 60 wt % bismuth, on the basis of thermal analysis data, we succeeded in discovering, as well as the non-equilibrium phase mentioned, yet another unstable phase, the decomposition of which started at a temperature of about 60° C. The absence in x-ray photographs of reflections from this phase prevented the establishment of its nature.

The existence of superconductivity has been shown in unstable compounds of bismuth with rhodium and various other metals;[2,3] it was, therefore, of interest to explore the possibility that superconductivity might appear also in the copper-bismuth alloys described above. Electrolytic deposits of copper-bismuth alloys were obtained from a solution of the following composition: 1N $Cu(ClO_4)_2$, 4N $Bi(ClO_4)_3$, 4N $HClO_4$. The deposits were obtained with current densities of from 80 to 250 ma/cm^2. The amount of bismuth in the alloys varied from 25 to 90 wt %. For the measurements specimens in the form of copper plates $30 \times 3 \times 0.05$ mm were used, on both sides of which the copper-bismuth alloy was deposited electrolytically. Measurements on such specimens in liquid helium showed that on lowering the temperature their electrical resistivity fell sharply (see Figure; Cu-Bi alloy with 20% Cu). The resistance drop usually occurred close to 2° K, and changed slightly on changing the amount of copper in the alloy.

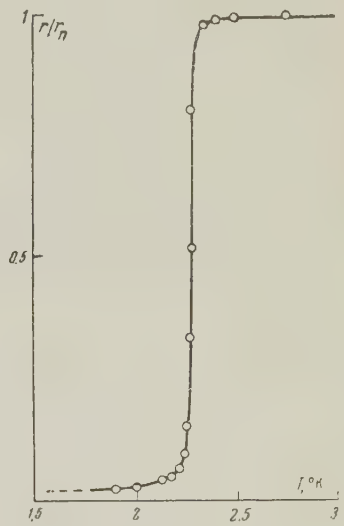

If the specimens were annealed at 120° C, the resistance drop was not observed on re-measuring down to 1.5° K. It should be noted, however, that if the anneal was at 80° C, the resistance drop did not disappear. The sharp decrease of specimen resistance was naturally considered as due to the transi-

tion of the Cu-Bi alloy into the superconducting state. This supposition was supported by the fact that switching on a magnetic field, at a temperature lower than the temperature of the drop, caused an increase of resistance, i.e., destroyed the superconductivity. Measurements on one specimen gave $dH_c/dT \approx 1000$ oe/deg.

On the basis of the results obtained, it can be concluded that a non-equilibrium phase formed at high overvoltages at the cathode undergoes a transition into a superconducting state at a temperature of about 2.2° K. An anneal at 120° C causes the decomposition of this phase, as a result of which superconductivity disappears. When the anneal is performed at a lower temperature (80° C), causing the decomposition of the second non-equilibrium phase, superconductivity is preserved. Thus, the second non-equilibrium phase is not responsible for the appearance of superconductivity in copper-bismuth deposits.

X-ray investigations of the copper-bismuth alloys obtained showed that unannealed specimens gave only weak diffuse rings, which can be taken as due to either high internal stresses or to the absence of long-range order in the system. An anneal at 120° C causes the decomposition of the non-equilibrium phase and the appearance on the x-ray photograph of reflections corresponding to the lattices of pure copper and bismuth. Further investigations will probably allow a more detailed explanation of the nature of the new non-equilibrium phase in the copper-bismuth system; however, it can be seen even now that the electrolytic method of obtaining metals under conditions of high overvoltage at the cathode allows phases to be obtained which are very far from equilibrium and which possess a number of new properties, amongst which, as follows from the account given, the appearance of superconductivity is possible.

We express gratitude to S. Ya. Berkovich for help in the measurements.

[1] Yu. M. Polukarov and V. V. Bondar', Dokl. Akad. Nauk SSSR **123**, 720 (1958).

[2] Alekseevskiĭ, Zhuravlev, and Lifanov, JETP **27**, 125 (1954).

[3] Alekseevskiĭ, Zhdanov, and Zhuravlev, JETP **28**, 237 (1955), Soviet Phys. JETP **1**, 99 (1955).

Translated by K. F. Hulme
66

FORMATION OF THE ISOMER Cd^{115m} BY THE FISSION OF GOLD UNDER THE ACTION OF HEAVY IONS

S. M. POLIKANOV and Yu. T. CHUBURKOV

Submitted to JETP editor October 15, 1959

J. Exptl. Theoret. Phys. (U.S.S.R.) **38**, 295-296 (January, 1960)

COMPOUND nuclei with large angular momentum are formed by the irradiation of the nuclei of the heavy ions C, N, and O. In the event of nuclear fission, their rotation causes an anisotropic angular distribution of the fission fragments,[1] and the degree of anisotropy increases with increasing angular momentum of the compound nucleus. Besides this, apparently, the increase of the angular momentum of the nucleus must influence the isomer yield of the fission fragments. It is of interest to determine, if only qualitatively, the dependence of the yields of some isomers among the fission fragments on the magnitude of the total angular momentum of the fissioning nucleus.

The dependence of the production cross sections of Cd^{115m} ($T_{1/2}$ = 43d, $I = 1/2$) and of the isomer Cd^{115m} ($T_{1/2}$ = 43d, $I = 11/2$) on the energy of incident particles was investigated by some workers in the fission of different nuclei by neutrons, protons, deuterons, and alpha particles.[2] A general tendency for increased isomer yield was observed with increased energy of the incident particle. But a more rigorous comparison of these data is difficult because of the necessity of accounting for the nuclear cascade in reactions with light fast particles.

The purpose of the present work has been the determination of the emission ratio of Cd^{115} and Cd^{115m} in the irradiation of gold by C^{12}, N^{14}, and O^{16} ions. The experiments were carried out with the 150 cm cyclotron at the Institute of Atomic Energy of the U.S.S.R. Academy of Sciences. The target was a gold foil 13 μ thick. The target was irradiated within the cyclotron chamber at radii of 67 and 61 cm, which correspond to 102 and 85 Mev for oxygen or 78 and 64 Mev for carbon. The target was irradiated with nitrogen ions at a radius of 67 cm (89 Mev). The ion current was 0.2 — 0.5 μa. The duration of irradiation was 2 — 3 hours. After irradiation, the foil was dissolved in aqua regia. To this were added carriers of cadmium, actinium, rubidium, silver, and iron in amounts of 15 mg. The CdS was separated from the solution. The chemical yield was determined by the weight

Reactions	$Au^{197} + O^{16}$		$Au^{197} + N^{14}$	$Au^{197} + C^{12}$	
Ion energies, Mev	102	85	89	78	64
l^2_{max}	2700	760	2060	1750	530
Emission ratio of Cd^{115} and Cd^{115m}	0.43	0.50	0.47	0.55	0.64

method after careful purification. The purity of the solution of cadmium was monitored by the β-particle half-life and energy. The measurement of the radiation intensity was taken by an end-window Geiger counter (MSG-17). The thickness of the CdS layer deposited from the filter paper onto a backing was ~ 10 mg/cm^2. The variation of the thickness of the layer of CdS from experiment to experiment, $2-3$ mg/cm^2, need not have a considerable effect on the scattering and self-absorption of β radiation.[3] It is also necessary to note that in all our experiments, apparently, a considerable quantity of Ag^{115} ($T_{1/2} = 20$ min.) was formed, which decays 90%[4] to Cd^{115} by β emission. After irradiation, the foil was kept intact for a sufficiently long time for the full decay of Ag^{115}. Additional experiments showed that approximately 30% of Cd^{115} was formed as a result of Ag^{115} decay.

The results of the principal experiments are presented in the table (the given data are uncorrected for the formation of Cd^{115} from Ag^{115}).

The table lists also the computed l^2_{max} for the corresponding reactions (l^2_{max} is the maximum orbital momentum of the ion at which fusion of the impinging nuclei arises). It is apparent that with a change of l^2_{max} from 500 to 3000, the emission ratio of Cd^{115} and Cd^{115m} changes very slightly.

In conclusion we consider it our pleasant duty to thank corresponding member of the Academy of Sciences U.S.S.R. G. N. Flerov for guidance in this present work.

[1] V. M. Strutinskiĭ, Атомная энергия (Atomic Energy) **6**, 508 (1957).

[2] P. Kruger and N. Sugarman, Phys. Rev. **99**, 1468 (1955).

[3] H. G. Hicks and R. S. Gilbert, Phys. Rev. **120**, 1286 (1958).

[4] Hollander, Perlman, and Seaborg, Revs. Modern Phys. **25**, 534 (1953).

Translated by M. Wilson
67

LATERAL DISTRIBUTION FUNCTION OF THE FLUX OF CHARGED PARTICLES IN AN INDIVIDUAL EXTENSIVE ATMOSPHERIC SHOWER

S. N. VERNOV, N. N. GORYUNOV, V. A. DMITRIEV, G. V. KULIKOV, Yu. A. NECHIN, and G. B. KHRISTIANSEN

Institute of Nuclear Physics, Moscow State University

Submitted to JETP editor October 14, 1959

J. Exptl. Theoret. Phys. (U.S.S.R.) **38**, 297-298 (January, 1960)

THE apparatus in operation at the Moscow State University for an all-out investigation of extensive atmospheric showers (EAS) makes it possible to investigate the individual characteristics of each recorded shower. In this note we report experimental data on the lateral distribution functions of the flux density of charged particles up to 25 meters from the shower axis. To obtain these data, we used a hodoscope with a large number of Geiger-Müller counters and a core detector consisting of ionization chambers arranged in two rows.[1] The first row of ionization chambers, shielded with lead, is used to determine the distribution of the energy flux carried by the electron-photon component near the shower axis. A direct examination of the distribution of the energy flux in the first row of ionization chambers makes it possible to determine the position of the shower axis for showers with a sufficient number of particles, with accuracy on the order of the chamber dimensions (25 cm). The hodoscopic counters were used to determine the flux density of the charged particles at different distances from the shower axis. To investigate the lateral-distribution functions of the flux density of the charged particles in an individual shower, we selected 26 of the densest showers (with $N \geq 10^5$), whose axes fall in the first row of the ionization chambers, for only in such showers can the charged-

No.	S							
	0.8	0.9	1.0	1.1	1.2	1.3	1.4	1.5
1	0.4	0.1						
2	≪0.01	0.05	≪0.01					
3	0.01	0.7	0.4					
4		0.2	0.6	0.15				
5		0.01	0.1	0.01				
6		0.05	0.5	0.05				
7			0.01	0.15	0.01			
8			0.01	0.5	0.02			
9			0.1	0.3	0.1			
10			≪0.01	0.5	0.1			
11				0.15	0.9	0.2		
12				0.01	0.25	0.05		
13				0.35	0.75	0.15		
14				<0.01	0.15	<0.01		
15				0.03	0.15	<0.01		
16				0.05	0.25	<0.01		
17					<0.01	0.4	<0.01	
18					0.15	0.6	0.01	
19					0.15	0.9	0.01	
20					0.15	0.45	<0.01	
21					0.01	0.1	0.01	
22					0.15	0.4	0.02	
23					0.1	0.5	0.05	
24					≪0.01	0.2	0.1	
25						0.3	0.8	0.1
26						<0.01	0.4	0.02

particle flux density be investigated in this range of distances with good accuracy.

The experimental charged-particle lateral distribution functions obtained for each of the selected showers were compared with the theoretical functions, calculated by Nishimura and Kamata[2] for various values of the cascade parameter S. The theoretical curves were normalized here to the number of particles experimentally observed in a circle of radius 25 m. The Pierson matching criterion was used to choose the theoretical curve corresponding to the experimental data. The results [the Pierson function $P(\chi^2)$] are listed in the table, which shows which values of the parameter S characterize the charged-particle flux density lateral distribution functions in the registered showers with different particle numbers N.

The experimental data given indicate the existence of extensive atmospheric showers of various ages near sea level.

[1] Vernov, Goryunov, Zatsepin, Kulikov, Nechin, Strugal'skiĭ, and Khristiansen, JETP **36**, 669 (1959), Soviet Phys. JETP **9**, 468 (1959).

[2] J. G. Wilson, ed. Progress in Cosmic Ray Physics, (Russ. Transl.), vol. 3, 1959, p. 7.

Translated by J. G. Adashko
68

A MEASUREMENT OF THE SURFACE TENSION AT THE BOUNDARY BETWEEN THE SUPERCONDUCTING AND NORMAL PHASES OF INDIUM

Yu. V. SHARVIN

Institute of Physical Problems, Academy of Sciences, U.S.S.R.

Submitted to JETP editor October 21, 1959

J. Exptl. Theoret. Phys. (U.S.S.R.) **38**, 298-300 (January, 1960)

THE value of the surface tension σ_{ns} at the boundary between the superconducting and normal phases of indium has been measured by a method described previously.[1]

A single-crystal disc with diameter 50 mm and thickness 2.06 mm, fabricated of indium with impurity content ~0.002%, was placed in a magnetic field directed at an angle of 15° to the specimen surface. The structures observed were completely analogous to those observed in tin[1] at the same values of H/H_c. The period of the structure was measured for various fields and temperatures and the quantity $\Delta(T) = \sigma_{ns}(8\pi/H_c^2)$ was calculated.*

In the figure are given the results of measurements on Δ made in the range 2.11 to 3.245° K with an accuracy of 8 — 10%. In this range the results can be described within the limits of error by the relationship

$$\Delta_{In} = 3.3 \cdot 10^{-5} (1 - T/T_c)^{-1/2} \text{ cm}$$

(where $T_c = 3.40°$ K), to which the curve in the figure corresponds.

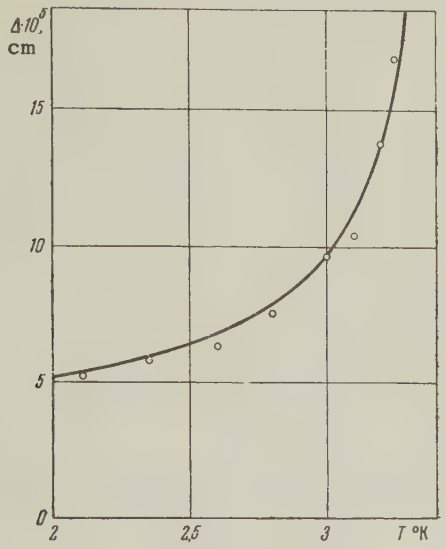

We did not attempt to study the anisotropy of Δ by the method described. Trial measurements with various positions of the disc relative to the magnetic field showed that the anisotropy is small and lies within the limits of accuracy quoted above.

The values of Δ close to T_c can be compared with other quantities characterizing the superconductor by means of a relationship from the phenomenological Ginzburg-Landau theory.[2,3] In reference 1 a marked discrepance was pointed out between the experimental value of Δ and that calculated from the G.-L. theory using the quantities δ and H_c; the latter exceeds by a factor of about 1.5. Recently Gor'kov[4] showed, however, that the charge entering into the relationship of the G.-L. theory is two electronic charges and not one, as was assumed previously. This correction changed the relationship between Δ and δ in the required direction, but a small discrepancy of the opposite sign now appeared. In the table are given values of the constant C_Δ occurring in the asymptotic law $\Delta = C_\Delta (1 - T/T_c)^{-1/2}$ for $T \to T_c$, the values of the analogous constant C_δ for the penetration depth, the limiting values of the quantity H_{c1}/H_c for $T \to T_c$, where H_{c1} is the supercooling field, and also the results of calculating these quantities following G.-L. (see references 2 — 5). In the last column are given the values of $C_H = (dH_c/dT)\,T_c$ used in the calculations.

The values of C_δ for tin are quite reliable, since the measurements of δ were made by a number of investigators sufficiently close to T_c (down to $T_c - T = 0.017°$ in reference 6). Measurements on δ for single-crystal indium were recently made by Dheer[7] for $T_c - T \geq 0.46$. Thus, extrapolation of this data in order to obtain C_δ is less reliable than for tin. However, the values of C_δ and the data from supercooling agree with one another surprisingly well, as they do also for tin (columns 6 and 7 of the table). The discrepancy between Δ and δ for both metals amounts to 25 — 30% in terms of C_Δ (or 15 — 20% in terms of C_δ).

In the last row of the table are given data for aluminum obtained by Faber and Pippard.[8-10] The values of C_δ here are in general less satisfactory, since in this case δ should be studied with $T_c - T \sim 0.001°$ (see reference 11), but the existing measurements[8] were only made down to $T_c - T = 0.12°$. Comparison of the data on Δ and H_{c1}/H_c can be made also in the case of aluminum.[11] Here the relationship of the data is the opposite of that observed for tin and indium (see columns 3 and 4 or 6 and 7). The supercooling obtained experimentally is much larger than follows from the data for Δ.

It seems to us that the difference in this respect of the data for aluminum from the results for tin and indium is associated with some inaccuracy in the method used by Faber[10] for determining Δ. The use of the complicated meandering

	$C_\delta \cdot 10^6$, cm expt1	$C_\Delta \cdot 10^6$, cm from δ	$C_\Delta \cdot 10^6$, cm expt1	$C_\Delta \cdot 10^6$, cm from H_{c1}/H_c	$\varkappa$ *** from δ	$\varkappa$ *** from Δ	$\varkappa$ *** from H_{c1}/H_c	H_{c1}/H_c	C_H, oersted
	1	2	3	4	5	6	7	8	
Sn	2.55 *	1.63	2.3	1.6	0.16	0.108	0.164	0.232[9]	570
In	2.25 **	2.44	3.3	2.38	0.108	0.076	0.112	0.158[9]	495
Al	(2.46) [8]	(6.5)	9[10] (12—14)	10.3	(0.054)	0.032 (0.02— —0.015)	0.0257	0.0363[9]	206

*Value averaged from references 6, 8, 12, and 13.

**The value taken for the calculation was averaged over the angle α between the current and the tetragonal axis of indium using Dheer's data[7] ($C_\delta = 2.35$ for $\alpha = 90°$, $C_\delta = 2.11$ for $\alpha = 0°$).

*** $\varkappa$ is the dimensionless parameter of the G.-L. theory; $H_{c1}/H_c = \sqrt{2}\varkappa$.

structure of the intermediate state in Faber's method is less reliable than the use of the inclined field method, in which one is able to observe the simplest layer structure. Faber also presents data obtained at one temperature using the inclined field method (see reference 10, Fig. 10), which, however, he does not use in the final results. Approximate treatment of this data using our formulae leads to the value $C_\Delta \times 10^5 = 12 - 14$, which is given in the table in brackets. The relationship between Δ and the value of the supercooling is then close to the case of Sn and In.

It is difficult at present to propose definite reasons for this small but systematic discrepancy. However, it would be stretching matters to ascribe it to accidental experimental errors.

I express my sincere gratitude to Acad. P. L. Kapitza for interest in the work, and to A. I. Shal'nikov and L. P. Gor'kov for detailed discussion of the results.

*During the calculation we attempted to estimate the effect of the specimen edges, i.e., the difference between the specimen and an infinite plate. The values of Δ, calculated using the formula for an ellipsoid inscribed in the specimen, are approximately 10% smaller than those obtained using the formula for an infinite plate (see reference 1). The true values will apparantly lie somewhere inside this range. Because accurate calculation is difficult for a disc, we used for calculation the formula for a flat ellipsoid of rotation having the same volume as our specimen (with axes 2.06 and 61.2 mm). The difference from the infinite case amounted in this instance to 8%. Introducing this correction into the results of reference 1, we obtained for tin

$$\Delta_{Sn} = 2.3 \cdot 10^{-5} (1 - T/T_c)^{-1/2} \text{ cm for } 2.16° < T < 3.5°.$$

[1] Yu. V. Sharvin, JETP **33**, 1341 (1957), Soviet Phys. JETP **6**, 1031 (1958).

[2] V. L. Ginzburg and L. D. Landau, JETP **20**, 1064 (1950).

[3] V. L. Ginzburg, JETP **30**, 593 (1956), Soviet Phys. JETP **3**, 621 (1956).

[4] L. P. Gor'kov, JETP **36**, 1918 (1959), Soviet Phys. JETP **9**, 1364 (1959).

[5] V. L. Ginzburg, JETP **31**, 541 (1956), Soviet Phys. JETP **4**, 593 (1957).

[6] Yu. V. Sharvin, JETP **22**, 367 (1952).

[7] P. N. Dheer, Superconductivity, Conf. Roy. Soc. Mond Laboratory, Cambridge, (1959).

[8] T. E. Faber and A. B. Pippard, Proc. Roy. Soc. **A231**, 336 (1955).

[9] T. E. Faber, Proc. Roy. Soc. **A241**, 531 (1957).

[10] T. E. Faber, Proc. Roy. Soc. **A248**, 460 (1958).

[11] V. L. Ginzburg, JETP **36**, 1930 (1959), Soviet Phys. JETP **9**, 1372 (1959).

[12] E. Laurmann and D. Shoenberg, Proc. Roy. Soc. **A198**, 560 (1949).

[13] A. L. Schawlow and G. E. Devlin, Phys. Rev. **113**, 120 (1959).

Translated by K. F. Hulme
69

SEVERAL POSSIBLE APPLICATIONS FOR THE RESONANT SCATTERING OF GAMMA RAYS

I. Ya. BARIT, M. I. PODGORETSKIĬ, and F. L. SHAPIRO

P. N. Lebedev Physics Institute, U.S.S.R. Academy of Sciences

Submitted to JETP editor November 4, 1949

J. Exptl. Theoret. Phys. (U.S.S.R.) 38, 301-302 (January, 1960)

BECAUSE of recoil during the emission of a gamma quantum by a free nucleus, the energy of the quantum is always less than the difference between the energy levels of the radiating nucleus. An analogous shift occurs in the absorption of a gamma quantum. This circumstance greatly hinders the observation of resonant scattering of gamma rays, which must occur with a large probability if this shift is absent or compensated.

Recently, however, Mössbauer[1,2] and others[3] have shown that at low temperatures the entire crystal takes up the recoil momentum in an observable fraction of the emissions and absorptions of low-energy gamma quanta. Under the indicated conditions the displacement of the gamma lines (as also the Doppler broadening) practically disappears, which makes possible the direct observation of resonant absorption. This was particularly clearly demonstrated by Mössbauer[2] and by Craig et al.,[3] who observed the dependence of the resonant-absorption cross section on the rate of change of the distance between source and absorber (Doppler effect). The experiments were performed with the 129-kev gamma rays of Ir-191. The lifetime of the excited state was shown to be equal to about 10^{-10} sec, which corresponds to a width $\Gamma = 10^{-5}$ ev and to a fractional width of about 10^{-10}. The influence of the Doppler effect manifests itself already at velocities of the order of 1 cm/sec.

In the work of Mössbauer[2] the described method is proposed for measuring the widths of gamma

lines, and also for studying gamma-ray cascades since the resonant absorption can be observed only for transitions to the ground state of the nucleus. To us it appears possible to use resonant absorption also for investigating a diverse family of shifts and splittings of nuclear levels.* As an example we point out the transverse Doppler effect, the nuclear Zeeman effect,† and the shift in a gravitational field predicted by the general theory of relativity. The investigation of the first two effects is possible in the observation of shifts of the order of 10^{-7} to 10^{-8} ev. As for the shifts in a gravitational field, for a difference of about 10 m in the elevations of source and absorber, the relativistic shift will be about 10^{-15}, which for a quantum energy of 100 kev corresponds to an absolute shift of about 10^{-10} ev.

For observing such small shifts, it is necessary to work under conditions where the natural width of the gamma line is less than the shift being studied or is close to it and where the line is not broadened by incidental effects.‡ Preliminary estimates show, that the latter condition is attainable for a line with a width $\Gamma \sim 10^{-7}$ to 10^{-8} ev, and, perhaps, is attainable for $\Gamma \sim 10^{-10}$ ev, which corresponds to a lifetime of $\sim 10^{-5}$ sec.

Among the known isomeric states of stable nuclei there is one with a fractional width $\Gamma/E \sim 10^{-15}$ — the 92-kev level of Zn^{67} ($\tau = 9.3 \times 10^{-6}$ sec), excited as the result of K capture[4] by 78-hour Ga^{67}. In principle, the 92-kev gamma transition in Zn^{67} can be used for the observation of the above mentioned gravitational effect.**

At the present time, an experimental investigation of the possibilities indicated above by use of the resonant scattering of gamma rays appears to be expedient.

The authors thank T. Vishka and V. Ogievetskiĭ for helpful discussions.

*As has become known to us, analogous considerations were expressed by W. E. Lamb at the Conference on Quantum Electronics, held 14-16 October, 1959 in the USA, and by Alikhanov.

†We wish to point out, that the use of the nuclear Zeeman effect may afford the possibility of investigating the gamma transitions of polarized nuclei and the interactions with polarized gamma quanta.

‡Examples of such incidental effects are the Doppler broadening due to vibration of the source or absorber, and washed out or split lines due to magnetic or electric fields.

**In experiments it may be convenient to produce a shift of known magnitude with the aid of the Doppler effect (relatively large shifts) or of the nuclear Zeeman effect (small shifts).

[1] R. L. Mössbauer, Z. Physik **151**, 124 (1958).

[2] R. L. Mössbauer, Z. Naturforsch **14a**, 211 (1959).

[3] Craig, Dash, McGuire, and Nagle, Bull. Am. Phys. Soc. **4**, 373 (1959).

[4] B. S. Dzhelepov and L. K. Peker, Схемы распада радиоактивных ядер (Decay Schemes of Radioactive Nuclei) (1958).

Translated by J. Heberle
70

POSSIBLE MAGNETIC EFFECTS FROM HIGH-ALTITUDE EXPLOSIONS OF ATOMIC BOMBS

O. I. LEĬPUNSKIĬ

Submitted to JETP editor, November 26, 1959

J. Exptl. Theoret. Phys. (U.S.S.R.) **38**, 302-304 (January, 1960)

LET us consider an atomic explosion at such an altitude that the explosion products expand practically into a vacuum (e.g., an "Argus" explosion at an altitude of 500 km). In the explosion the bomb materials are heated to many ev and thus form a dense plasma, which then expands from the explosion center at the rate of several hundreds of kilometers per second. Thus, the plasma volume will be increased and the ion concentration correspondingly reduced. The expansion of the plasma through the magnetic field will cease as soon as the kinetic pressure of the plasma (or its "head"), which will be falling off as the expansion progresses because of the decrease in ion concentration, equals the magnetic pressure. Because of the diamagnetism of the plasma, the earth's magnetic field will be decreased in the volume occupied by the plasma and if the ion concentration is sufficient, it will be eliminated altogether. For the present purpose, this weakening or elimination of the field inside the plasma can be represented as the result of the establishment within the plasma volume of an effective magnetic dipole whose field within the plasma is opposite to the magnetic field of the earth. Once this effective dipole has appeared, it will create a noticeable magnetic field at great distances from the explosion center, and this field will be registered as the appearance of a magnetic disturbance ("storm") whose leading edge will have a rise time corresponding to the period of plasma expansion. As the plasma expands in the magnetic field, magnetohydrodynamic fluctuations may also be excited.

Besides the magnetic disturbance due to the appearance of a plasma in the vicinity of the explosion, disturbances may exist due to the subsequent movement of the plasma along the field line in a magnetic trap, i.e., in regions remote from the explosion site. The nearest approach of the plasma to the earth should be expected at the magnetic conjugate points or at the extremities of the trap (i.e., at the reflection points) where an increase in plasma concentration can be expected. For these reasons one may expect to find an intensification of the magnetic disturbance at the sub-conjugate points or sub-mirror points and around these.

The effective magnetic moment M of the plasma is equal to

$$M \sim W/H, \tag{1}$$

where W is the energy of the explosion and H is the magnetic field at the explosion point. At the sub-burst point of an explosion occurring at altitude h, the amplitude of magnetic disturbance H′ is

$$H' \sim M/h^3 \sim W/Hh^3 \sim 10^{-26} W (1 + R_3/h)^3 \tag{2}$$

(10^{26} being the magnetic moment of the earth and R_3 being the earth's radius). For an "Argus" explosion (h = 500 km, W = 10^3 tons = 4.2×10^{19} erg) H′ should be $\sim 100 \times 10^{-5}$ oe. At a distance L from the explosion H′ is

$$H' \sim W/HL^3. \tag{2'}$$

The rise time τ of the leading edge of the magnetic disturbance is equal to the expansion time of the plasma with a mass Q to some final volume V:

$$\tau \sim Q^{1/3}/H^{2/3}W^{1/3}, \text{ sec.} \tag{3}$$

The frequency of the magneto-acoustic oscillations can be determined from the expression

$$\nu \sim r/4c \sim 1/4\tau, \text{ sec}^{-1}. \tag{4}$$

with $c = H/\sqrt{4\pi Q/V}$ as the Alvén speed of the magneto-acoustic wave; $r = (3V/4\pi)^{1/3}$ the characteristic size of the plasma; and $V \simeq 4\pi W/H^2$. The rise time of the leading edge is seen to depend only slightly on the energy of the explosion and increases as the altitude of the explosion is increased. In the case of an "Argus" explosion τ should be ~ 0.5 sec and $\nu \sim \frac{1}{2}$ sec (where we have substituted in (3) and (4) Q = 5×10^5 g, H = 0.5 oe, W = 4×10^{19} erg). For explosions at altitudes of 6,000 and 60,000 km, respectively $\tau \simeq 2$ and 50 sec.

Penetration of the earth's magnetic field by individual volumes of plasma from the sun could present a similar picture, since this plasma moves at a rate close to the expansion speed of the explosion plasma. However, these phenomena would probably have their own peculiarities due to the slowing down of the solar plasma at a great distance from the earth.

Should an explosion occur in the polar regions, where the mirror is practically open on one side, the possibility of an effect cannot be ruled out, since the plasma could reach the mirror point situated below the explosion.

Equations (2) and (2′) can be used to evaluate H′ in the region of the conjugate points, once W is replaced by Wk, with k representing the portion of plasma ions reaching the conjugate point. In the case of the mechanism set forth here, it is essential that the rate of expansion of the magnetic disturbance be equal to the speed of light. Disturbances are also possible due to magneto-acoustic oscillations propagating through the ionosphere. The recording of these oscillations should show a lag in conformance with the lower speed of the disturbance (Alvén speed). This fact provides a direct criterion for distinguishing them from disturbances of the type described above. The fields of these disturbances are smaller than the values given by Eq. (2).

Papers recently published[1,2] have indicated that the "Argus" explosions produced periodic magnetic disturbances with a period of 1 — 2 sec.[2] We note that this period is close to the value of 2 sec predicted by Eq. (4). At the sub-burst point the amplitude of the disturbance amounted to 10×10^{-5} oe,[1] rather than 100×10^{-5} oe as predicted by Eq. (2). However, the measurements were made with instruments whose sensitivity was impaired in the region of the measured frequencies, so that the true value of H′ should have been greater than 10×10^{-5} oe.

The values for H′ were measured at distances of from 5,000 to 10,000 km from the explosion (the coordinates of the explosions being −38°/12°WG; −50°/8°WG, and −50°/10°WG). The various measured values of H′ exceed those predicted by Eq. (2′) by 5 to 100 times. It may be that at some stations (e.g., Paris) the recorded disturbance was from a plasma that had moved along a field line toward the conjugate point (the Azores) and that therefore happened to be nearer the observation site when recorded than at the instant of the explosion. Unfortunately, the time service was too crude to permit an accurate comparison of the detection and explosion times.

Another possible reason for the partial enhance-

ment is the influence of geological conditions (electrical conductivity), which as geophysical experience has shown can alter the amplitude of a magnetic disturbance at a recording station by several magnitudes.

The enhancement of the measured magnetic disturbance over the maximum amplitude predicted by the magnetostatic model forces one to seek a different concept of the propagation of the disturbance. Ya. A. Al'pert has suggested that a disturbance propagates in the space between two conductive layers, i.e., the ionosphere and earth. The disturbance therefore is only slightly weakened with distance. It travels from the explosion point to this spherical layer in the form of a magnetohydrodynamic wave in the ionosphere and is propagated along magnetic field lines with slight absorption.

The author is grateful to Ya. A. Al'pert, V. L. Ginzburg, A. S. Kompaneets, M. A. Leontovich, and D. A. Frank-Kamenetskiĭ for discussions of this article.

[1] P. Newman, J. Geophys. Research **64**, 923 (1959).

[2] E. Selzer, Compt. rend., Paris **249**, 1133 (1959).

Translated by A. Skumanich
71

THE $d + d \rightarrow \pi^0 + He^4$ REACTION AT 400 Mev DEUTERON ENERGY

Yu. K. AKIMOV, O. V. SAVCHENKO, and L. M. SOROKO

Joint Institute for Nuclear Research

Submitted to JETP editor November 13, 1959

J. Exptl. Theoret. Phys. (U.S.S.R.) **38**, 304-306 (January, 1960)

UP till now all experimental investigations in testing the principle of charge invariance in the formation process of π mesons were carried out by comparing two charges of coupled reactions, the cross sections of which have to be in a given relation while preserving the full isotopic spin. This refers to the reactions $p + p \rightarrow d + \pi^+$ and $n + p \rightarrow d + \pi^0$, which were investigated at 400 and 600 Mev, and also to the reactions $p + d \rightarrow t + \pi^+$ and $p + d \rightarrow He^3 + \pi^0$, which were compared at 340,[5] 450,[6] and 600 Mev.[7]

However, a more direct method of checking the principle of charge invariance, which is free from any systematic errors, consists of establishing the degree of forbidenness as a consequence of the preservation of the isotopic spin in the process of meson formation. Thus, for instance, forbidenness due to this principle should take place in the reaction[8]

$$d + d \rightarrow \pi^0 + He^4. \quad (1)$$

By this process it is also possible to check the hypothesis, advanced by Baldin,[9] of the existence of the isotopically scalar π^0 mesons, to eliminate the contradiction between the data covering the photoproduction of π mesons near threshold and the Panofsky relation.

A description follows here of the first data of the reaction (1), obtained in the synchrocyclotron of the Joint Institute for Nuclear Research at 400 Mev deuteron energy. The measurements were made with an extracted beam of deuterons having an intensity of about 3×10^{10} sec^{-1}. The secondary charged particles formed in the targets of heavy polyethylene and carbon were separated by a brass collimator placed at an angle of 5.6° to the deuteron beam, were deflected by a magnetic field at an angle of 27°, and passed through a steel collimator in the shielding concrete wall. They were then recorded by a telescope consisting of six scintillator counters. The identification of the charged particles knocked out of the target was carried out by effective momentum, specific ionization, and range. The separation of particles with a given momentum was carried out with the aid of an electromagnet, the poles of which had been given a special shape to improve resolving power. The separation of the particles with regard to the extent of the specific ionization was made independently in each of the five telescope counters. This method[10] made it possible to separate reliably the rare processes of the emission of particles with a high degree of ionization against the background of the extraneous radiation of lower ionization. The particle range was determined by retarding filters, which were arranged before the fifth and the sixth telescope counter, the latter being connected in anticoincidence with the first five so as to separate the particles in the given range interval. In the first five telescope counters scintillators were used with foils 0.5 mm thick, which enabled the recording of the α particles starting with 60 Mev energy. The discriminator scale was calibrated in a beam of α particles at 800, 700, 460, and 370 Mev. The general control of the apparatus and the calibration of the electromagnet scale were carried out by recording the He^3

nuclei originating from the reaction $d + d \rightarrow He^3 + n$.

The α-particle yield from heavy polyethylene and carbon with an effective momentum 635 Mev/c, corresponding to the α particles of reaction (1), was measured under an angle of 5.6° in the laboratory system, to which an isotropic angle $[\theta = a \times \cos^{-1}(1/\sqrt{3})]$ corresponds approximately in the c.m.s. The absolute cross sections were determined under the same conditions, by recording the deuterons from the reaction $p + p \rightarrow d + \pi^0$, the cross section of which is well known[11] at present. The results of the first measurements have shown that, with a reliability of 90%, the total cross section of reaction (1) is

$$\sigma_t(d + d \rightarrow \pi^0 + He^4) < 1 \cdot 10^{-31} \text{ cm}^2$$

The estimate obtained proves that the cross section of reaction (1) surpasses only a few times the cross section of the electromagnetic process $d + d \rightarrow \gamma + He^4$, which according to the data of the reverse reaction[12] $\gamma + He^4 \rightarrow d + d$ amounts to about 10^{-32}, whereas in the absence of forbiddenness in reaction (1) the cross sections of these two processes may differ by a factor of 10^2.

Since, under the conditions of the given experiments, the α particles resulting from the reaction $d + d \rightarrow \pi_0^0 + He^4$, in which the formation of the isotopically scalar π^0-meson takes place may also be recorded, the estimate of the total cross section received for reaction (1) may be looked upon as an indication that isotopically scalar π^0 mesons are not present in large quantities in the (135^{+15}_{-35}) Mev interval.

We also measured the differential cross section of the reaction $d + d \rightarrow He^3 + n$ for the angle 5.6° in the laboratory system, and found it to be equal, in the center-of-mass system, to

$$\frac{d\sigma}{d\Omega}(15.5^\circ) = (3.8 \pm 0.5) \cdot 10^{-29} \text{ cm}^2/\text{sr}.$$

[1] A. Rosenfeld, Phys. Rev. **96**, 139 (1954).

[2] R. Hildebrand, Phys. Rev. **89**, 1090 (1953).

[3] C. Cohn, Phys. Rev. **105**, 1582 (1957).

[4] Flyagin, Dzhelepov, Kiselev, and Oganesyan, JETP **35**, 854 (1958), Soviet Phys. JETP **8**, 592 (1959).

[5] Bandtel, Frank, and Moyer, Phys. Rev. **106**, 802 (1957).

[6] Crewe, Garmin, Ledley, Lillethum, March, and Marcowitz, Phys. Rev. Letters **2**, 269 (1959).

[7] Harting, Kluyver, Kusumegi, Rigopaulos, Sacks, Tibbell, Vanderhaeghe, and Weber, Phys. Rev. Letters **3**, 52 (1959).

[8] L. I. Lapidus, JETP **31**, 865 (1956), Soviet Phys. JETP **4**, 740 (1957).

[9] A. M. Baldin and P. Kabir, Dokl. Akad. Nauk SSSR **122**, 361 (1958), Soviet Phys.-Doklady **3**, 956 (1959).

[10] Akimov, Komarov, Savchenko, and Soroko, Приборы и техника эксперимента (Instrum. and Meas. Engg.), in press.

[11] M. G. Meshcheryakov and B. S. Neganov, Dokl. Akad. Nauk SSSR **100**, 677 (1955).

[12] A. N. Gorbunov and V. M. Spiridonov, JETP **33**, 21 (1957), Soviet Phys. JETP **6**, 16 (1958).

Translated by J. Brady
72

ON THE PROBLEM OF PERIPHERAL COLLISIONS OF NUCLEONS WITH HIGH ENERGIES

V. M. MAKSIMENKO

P. N. Lebedev Physics Institute, Academy of Sciences, U.S.S.R.

Submitted to JETP editor November 4, 1959

J. Exptl. Theoret. Phys. (U.S.S.R.) **38**, 306-307 (January, 1960)

TAMM[1] has recently developed a model for the interaction of fast nucleons with large impact parameters, according to which the interaction is due to the exchange of one π meson, whereby one or both nucleons are excited to an isobaric state which subsequently decays.

Together with the excitation of the isobar $(3/2, 3/2)$ (which we shall denote by the symbol X in the following), an interaction with the isotopic spin $1/2$ is also possible. The latter can be interpreted as the excitation of the second isobaric level of the nucleon.[2] This second isobar (which we denote by the symbol Y) can decay according to the following schemes:

1) $Y \rightarrow N + \pi$, $\omega_1 = 0{,}324$;
2) $Y \rightarrow X + \pi$, $\omega_2 = 0{,}418$;
3) $Y \rightarrow N + 2\pi$, $\omega_3 = 1 - \omega_1 - \omega_2 = 0{,}258$.

The probabilities, ω, for these decays can be estimated by the statistical weights, assigning to the isobar Y the mass $1.64\,M_{nucl}$, the isotopic spin $1/2$, and linear dimensions of the order $\hbar/\mu c$. We

neglect the possibility of decays leading to the formation of strange particles.

In peripheral interactions of this type the directions of motion of the isobar and of its decay products in the center of mass system do not differ much from the direction of motion of the nucleons before the interaction. According to the criterion chosen in reference 3 for the selection of such peripheral collisions (the presence of a slow proton in the laboratory system), we consider in the following only those "stars" in which there is a proton flying in the backward direction in the center of mass system. Taking this into account and making use of isotopic invariance, we can calculate with the help of the Clebsch-Gordan coefficients the probabilities W_{mn} for the observation of stars in which (in the center of mass system) m charged particles are emitted in the forward direction and n charged particles (including the proton) in the backward direction.

For p-p collisions we find

$$W_{11} = \tfrac{4}{15}\sigma_{pp}(X, X) + \tfrac{1}{16}(1 + \omega_1 + \tfrac{1}{27}\omega_2)\sigma_{pp}(X, Y) + \tfrac{1}{12}(1 - \omega_1 - \tfrac{1}{9}\omega_2)(1 + \omega_1 - \tfrac{1}{3}\omega_2)\sigma_{pp}(Y, Y),$$

$$W_{02} = \tfrac{1}{5}\sigma_{pp}(X, X) + \tfrac{1}{16}(1 + \omega_1 + \tfrac{1}{3}\omega_2)\sigma_{pp}(X, Y),$$

$$W_{22} = \tfrac{1}{5}\sigma_{pp}(X, X) + \tfrac{1}{16}(7 + \omega_1 - \omega_2)\sigma_{pp}(X, Y)$$

(we do not give the expressions for W_{13}, W_{31}, and W_{33}, since these cases were neglected in the analysis of the experiment[3]). For p-n collisions we find

$$W_{01} = \tfrac{2}{63}\sigma_{pn}(X, X) + \tfrac{1}{18}(1 + \omega_1 + \tfrac{1}{3}\omega_2)\sigma_{pn}(X, Y) + \tfrac{2}{15}(1 + \omega_1 + \tfrac{1}{3}\omega_2)^2\sigma_{pn}(Y, Y),$$

$$W_{21} = \tfrac{1}{63}\sigma_{pn}(X, X) + \tfrac{1}{72}(11 - \omega_1 - \tfrac{1}{3}\omega_2)\sigma_{pn}(X, Y) + \tfrac{1}{45}(5 - \omega_1 - \tfrac{1}{3}\omega_2)(1 + \omega_1 + \tfrac{1}{3}\omega_2)\sigma_{pn}(Y, Y),$$

$$W_{12} = \tfrac{2}{21}\sigma_{pn}(X, X) + \tfrac{1}{8}(1 + \omega_1 - \tfrac{7}{27}\omega_2)\sigma_{pn}(X, Y) + \tfrac{1}{30}(1 + \omega_1 - \tfrac{1}{3}\omega_2)^2\sigma_{pn}(Y, Y),$$

where $\sigma_{pp}(X, X)$ is the cross section for formation of two isobars in p-p collisions, etc.

For a more rigorous choice of cases of peripheral collisions of this type, those cases in reference 3 were selected in which there is a fast proton in addition to the slow one. We denote the corresponding probabilities by $W_{mn}^{(p)}$:

$$W_{11}^{(p)} = \tfrac{8}{45}\sigma_{pp}(X, X) + \tfrac{1}{36}(1 + \omega_1 + \tfrac{1}{3}\omega_2)\sigma_{pp}(X, Y) + \tfrac{1}{36}(1 + \omega_1 + \tfrac{1}{3}\omega_2)^2\sigma_{pp}(Y, Y),$$

$$W_{22}^{(p)} = \tfrac{1}{5}\sigma_{pp}(X, X) + \tfrac{1}{4}(1 + \omega_1 - \tfrac{1}{3}\omega_2)\sigma_{pp}(X, Y).$$

Dremin and Chernavskiĭ[4] recently made a quantitative estimate of the cross sections for these processes. Using their data and substituting the values of ω_i quoted above, we obtain characteristic numbers (see column a in the table) which can be compared with the results of the experiment.[3] In column b of the table we list for comparison the results of the calculation under the assumption that always only 2X are formed.

	Experiment	Calculation	
		a	b
$W_{22}/(W_{11}+W_{02})$	0.47	0.73	0.43
$-2W_{02}/(W_{11}+W_{02})$	—0.56	—0.88	—0.86
W_{02}/W_{11}	0.39±0.13	0.79	0.75
$W_{11}^{(p)}/W_{22}^{(p)}$	14/8=1.75±0.77	0.60	0.89
$(W_{21}-W_{12})/(W_{21}+W_{12})$	0.33	—0.46	—0.71
W_{12}/W_{21}	1.3	2.6	6

In conclusion I express my deep gratitude to I. E. Tamm and I. L. Rozental' for discussing this paper and also to D. S. Chernavskiĭ, I. M. Dremin, and the authors of reference 3 for providing me with the results of their work before publication.

[1] I. E. Tamm, Материалы конференции по физике высоких энергий в г. Киеве (Materials of the High Energy Conference at Kiev, 1959).

[2] G. Bernardini, ibid.

[3] Wang Shu-Fen, Vishki, Gramenitskiĭ, Grishin, Dalkhazhav, Lebedev, Nomofilov, Podgoretskiĭ, and Strel'tsov, ibid.

[4] I. M. Dremin and D. S. Chernavskiĭ, ibid.

Translated by R. Lipperheide
73

ON GAUGE TRANSFORMATIONS IN QUANTUM ELECTRODYNAMICS

Yu. A. GOL' FAND

P. N. Lebedev Physics Institute, Academy of Sciences, U.S.S.R.

Submitted to JETP editor July 18, 1959

J. Exptl. Theoret. Phys. (U.S.S.R.) **38**, 308-309 (January, 1960)

INVARIANCE of a quantum-mechanical theory with respect to a particular group of transformations is ordinarily associated with the existence

of corresponding constants of the motion. For example, for a system with central symmetry there is conservation of the components of the angular momentum M, which generate the rotation group. Gauge transformations with a constant phase are generated by the charge operator $\hat{Q}$. Such constants of the motion do not exist, however, for the general group of gauge transformations,

$$\psi \to e^{i\Lambda}\psi, \qquad A_\mu \to A_\mu - \partial\Lambda/\partial x_\mu . \tag{1}$$

We shall show that by the introduction of additional variables into the Hamiltonian one can construct an infinite set of constants of the motion, which generate the transformations (1), and thus can include the gauge transformations in the general scheme of canonical transformations.

Let us write the Hamiltonian of quantum electrodynamics in the form

$$H = \sum_{p,\sigma} E_p (a^+_{p\sigma}a_{p\sigma} + b^+_{p\sigma}b_{p\sigma}) + \sum_k \omega\,(c^+_{1k}c_{1k} + c^+_{2k}c_{2k} - c^+_{3k}c_{1k} - c^+_{4k}c_{3k}) + \sum_k \sum_{\lambda=1}^{4} \frac{e}{\sqrt{2\omega}} \{c_{\lambda k}(e^\lambda j^+_k) + c^+_{\lambda k}(e^\lambda j_k)\}; \tag{2}$$

$$j_k \equiv (\rho_k,\ \mathbf{j}_k) = \int \bar{\psi}\gamma_\mu \psi e^{-i\mathbf{kx}}\, d^3x, \tag{3}$$

where a and b are the operators of the electron-positron field, and c are the operators of the electromagnetic field; $\mathbf{j}_k$ are the Fourier components of the current vector. The integral in Eq. (3) is taken over unit volume. The polarization vectors e^λ are chosen in the following way: e^1 and e^2 are unit space vectors perpendicular to $\mathbf{k}$, and

$$e^3 = (1, \mathbf{k}/\omega)/\sqrt{2}, \qquad e^4 = (1, -\mathbf{k}/\omega)/\sqrt{2}.$$

For the photons one introduces an indefinite metric. In accordance with this, the operators c satisfy the commutation relations

$$[c^+_{3k}, c_{4k'}] = [c^+_{4k}, c_{3k'}] = \delta_{kk'}, \qquad [c^+_{3k}, c_{3k'}] = [c^+_{4k}, c_{4k'}] = 0$$

(the remaining commutation relations are the usual ones). We now introduce "supplementary" variables α_k and β_k, which satisfy the commutation relations

$$[\alpha^+_k, \beta_{k'}] = [\beta^+_k, \alpha_{k'}] = \delta_{kk'}, \quad [\alpha^+_k, \alpha_{k'}] = [\beta^+_k, \beta_{k'}] = 0 \tag{4}$$

and commute with all the other quantities, and add to the Hamiltonian (2) the quantity

$$H_{\alpha\beta} = -\sum_k \omega\,(\alpha^+_k\beta_k + \beta^+_k\alpha_k).$$

It is easy to verify that the "total" Hamiltonian $H + H_{\alpha\beta}$ commutes with the quantities

$$R_k = \alpha^+_k(e\rho_k/2\omega^{3/2} - c_{4k}), \qquad R^+_k = \alpha_k(e\rho^+_k/2\omega^{3/2} - c^+_{4k}). \tag{5}$$

In terms of the operators (5) the gauge transformations (1) can be expressed in the form of a unitary operator

$$U_\Lambda = \exp\left\{i\sum_k \left(\lambda_k R_k + \lambda^+_k R^+_k\right)\right\}, \tag{6}$$

where λ_k are arbitrary numbers. The function $\Lambda(x)$ for the transformation (6) is

$$\Lambda(x) = \sum_k \frac{1}{2\omega^{3/2}}(\lambda_k\alpha_k \exp\{i(\mathbf{kx} - \omega t)\} + \lambda^+_k\alpha^+_k \exp\{-i(\mathbf{kx} - \omega t)\}),$$

and in virtue of the relations (4) $\Lambda(x)$ can be regarded as a numerical function.

In our representation the supplementary condition $(\partial A_\mu/\partial x_\mu)\,\Phi = 0$ can be written in the form

$$(c_{4k} - e\rho_k/2\omega^{3/2})\,\Phi = 0, \qquad (c^+_{4k} - e\rho^+_k/2\omega^{3/2})\,\Phi = 0. \tag{7}$$

Comparing Eqs. (7) and (5), we see that for the allowed states the quantities R_k and R^+_k are equal to zero:

$$R_k\,\Phi = R^+_k\,\Phi = 0. \tag{8}$$

Obviously the conditions (8) single out the Maxwellian electrodynamics from among all the theories described by the Hamiltonian (2).

The variables α and β are of the nature of two additional components of the electromagnetic field. Since these components do not interact with charges, this scheme is entirely equivalent to the usual electrodynamics.

Translated by W. H. Furry
74

THE RELATIVISTIC PHOTOEFFECT IN THE L SHELL

M. GAVRILA

Parhon University, Bucharest

Submitted to JETP editor July 14, 1959

J. Exptl. Theoret. Phys. (U.S.S.R.) **38**, 309-311 (January, 1960)

THE problem of a theory of the nonrelativistic photoeffect in the L shell was solved a long time ago.[1,2] The relativistic aspects of this problem, however, have only been remarked upon. In view of the successful development of β-ray spectrom-

$h\nu/mc^2$	0	1/8	1/4	1/2	1	4	∞
$\sigma^{nr}_{L_I}/\sigma_{L_I}$	1	0.95	0.91	0.79	0.54	0.07	0
$\sigma^{nr}_{L_{II}+L_{III}}/\sigma_{L_{II}+L_{III}}$	1	0.72	0.61	0.38	0.16	0.007	0
$\sigma_{L_{II}}/\sigma_{L_{III}}$	0.500	0.535	0.546	0.558	0.531	0.366	0.281

etry in recent years it becomes now desirable to make a more careful analysis of the contribution of the L shell to the photoelectric absorption at high energies.[3,4] As it is impossible to obtain exact analytic expressions for the relativistic cross sections, we attempt to find their approximate form for the light elements.* Thus we determine the cross sections for the L_I subshell which are accurate up to and including the first order of αZ; in the case of the L_{II} and L_{III} subshells we only obtained approximations of zeroth order in αZ.

As usual, the calculation is based on the central Coulomb field approximation for the different electrons, with Z changed to $Z_S = Z - 4.5$ (see reference 1, §69 α). The spinor corresponding to the final state of the electron is treated in the Born approximation. The integration in the matrix elements is performed in momentum space. The calculations are analogous to those in the case of the K shell, described earlier by the author.[5] To find the differential cross section for one of the L subshells, we must sum the contributions from all electrons of this subshell, taking into account the two possible spin orientations in the final state. Mathematically this involves very laborious calculations of traces.

As a result we obtain for the differential cross sections the expressions

$$d\sigma_{L_I} = \tfrac{1}{8}(d\sigma_K)_S, \tag{1}$$

$$\begin{aligned} d\sigma_{L_{II}} = {} & \tfrac{1}{24}\lambda_0^2\alpha^8 Z_S^7(\gamma^2-1)^{1/2}\gamma^{-4}(\gamma-1)^{-5} \\ & \times\Big\{\tfrac{1}{4}(3\gamma+1)\Theta^{-4} - \tfrac{1}{16}\gamma(9\gamma^2+30\gamma-7)\Theta^{-3} \\ & + \tfrac{1}{8}\gamma^2(\gamma^3+6\gamma^2+11\gamma-2)\Theta^{-2} \\ & - \tfrac{1}{16}\gamma^3(\gamma-1)(\gamma+7)\Theta^{-1} + \sin^2\theta\cos^2\varphi(\gamma+1)\gamma^{-1}\big[2\Theta^{-5} \\ & - 2\gamma\Theta^{-4} - \tfrac{1}{8}\gamma^2(3\gamma+1)(\gamma-1)\Theta^{-3}\big]\Big\}\,d\omega, \end{aligned} \tag{2}$$

$$\begin{aligned} d\sigma_{L_{III}} = {} & \tfrac{1}{12}\lambda_0^2\alpha^8 Z_S^7(\gamma^2-1)^{1/2}\gamma^{-4}(\gamma-1)^{-5}\Big\{-\tfrac{1}{4}(3\gamma-1)\Theta^{-4} \\ & + \tfrac{1}{2}\gamma(3\gamma^2-1)\Theta^{-3} + \tfrac{1}{2}\gamma^2(\gamma^3-2\gamma^2+2\gamma+1)\Theta^{-2} \\ & - \tfrac{1}{4}\gamma^3(\gamma-2)(\gamma-1)\Theta^{-1} + \sin^2\theta\cos^2\varphi(\gamma+1)\gamma^{-1}[2\Theta^{-5} \\ & - \gamma(3\gamma-1)\Theta^{-4} + \gamma^2(\gamma-1)\Theta^{-3}]\Big\}\,d\omega, \end{aligned} \tag{3}$$

where $(d\sigma_K)_S$ is given by formula (92) of reference 5, with Z replaced by Z_S, the angles θ and φ are determined in reference 5, and

$$\gamma = 1/(1-\beta^2)^{1/2}, \quad \Theta = 1 - \beta\cos\theta, \quad \lambda_1 = \hbar/mc.$$

The corresponding total cross sections are

$$\sigma_{L_I} = \tfrac{1}{8}(\sigma_K)_S, \tag{4}$$

$$\begin{aligned} \sigma_{L_{II}} = {} & \tfrac{1}{256}\alpha^6 Z_S^7\varphi_0\frac{(\gamma^2-1)^{1/2}}{(\gamma-1)^5} \\ & \times\Big\{9\gamma^3-5\gamma^2+24\gamma-16-\frac{\gamma^2+3\gamma-8}{(\gamma^2-1)^{1/2}}\ln[\gamma+(\gamma^2-1)^{1/2}]\Big\}, \end{aligned} \tag{5}$$

$$\begin{aligned} \sigma_{L_{III}} = {} & \tfrac{1}{32}\alpha^6 Z_S^7\varphi_0\frac{(\gamma^2-1)^{1/2}}{(\gamma-1)^5} \\ & \Big\{4\gamma^3-6\gamma^2+5\gamma+3-\frac{\gamma^2-3\gamma+4}{(\gamma^2-1)^{1/2}}\ln[\gamma+(\gamma^2-1)^{1/2}]\Big\}, \end{aligned} \tag{6}$$

where σ_K is given by formula (98) of reference 5. The formulas for the cross sections are valid for light nuclei, since we must fulfill the condition $(\pi\alpha Z_S/\beta)^2 \ll 1$ for the L_I subshell and the condition $\pi\alpha Z_S/\beta \ll 1$ for the L_{II} and L_{III} subshells.

In the extreme relativistic limit $\beta \to 1$ we easily find that the total cross sections (4) to (6) are proportional to $mc^2/h\nu$. In the limiting case of small energies we can show by neglecting terms of order β^2 that the angular distributions given by formulas (1) to (3) go over into the corresponding nonrelativistic expressions of Schur (see reference 1, §72 β). The value of the ratio $(d\sigma_{L_{II}}/d\sigma_{L_{III}})_{nr} = 1/2$ is equal to the ratio of the number of electrons in these subshells.

Formulas (4) to (6) predict a slower decrease of the total cross sections with increasing photon energy than the nonrelativistic formulas. In the case of the light elements this can be seen from the table, in which we list the ratios of the relativistic (σ) over the nonrelativistic (σ^{nr}) cross sections (to lowest order in αZ_S). There we also give the values of the relativistic ratio $\sigma_{L_{II}}/\sigma_{L_{III}}$. It can be assumed that the error associated with the ratios given in the table is of order $(\alpha Z_S)^2$.

In conclusion the author expresses his grati-

tude to Acad. S. Titeica for his interest in this work and to Prof. R. H. Pratt for clarifying comments on a number of questions touched upon in this paper.

*Recently Pratt calculated the total cross section up to terms of order αZ in the extreme relativistic case.

[1] H. A. Bethe and E. Salpeter, Handbuch der Physik **35**, Part I, Berlin (1957).

[2] H. Hall, Revs. Modern Phys. **8**, 358 (1936).

[3] E. P. Grigor'ev and A. V. Zolotavin, JETP **36**, 393 (1959), Soviet Phys. JETP **9**, 272 (1959).

[4] Novakov, Hultberg, and Andersson, Arkiv Fysik **13**, 117 (1958).

[5] M. Gavrila, Phys. Rev. **113**, 514 (1959).

Translated by R. Lipperheide
75